INSIGHTS IN TOXOPLASMA BIOLOGY AND INFECTION - 15TH BIENNIAL MEETING ON TOXOPLASMA BIOLOGY AND TOXOPLASMOSIS

EDITED BY: Jorge Enrique Gómez Marín, Jeroen P. J. Saeij and Alejandra De La Torre
PUBLISHED IN: Frontiers in Cellular and Infection Microbiology

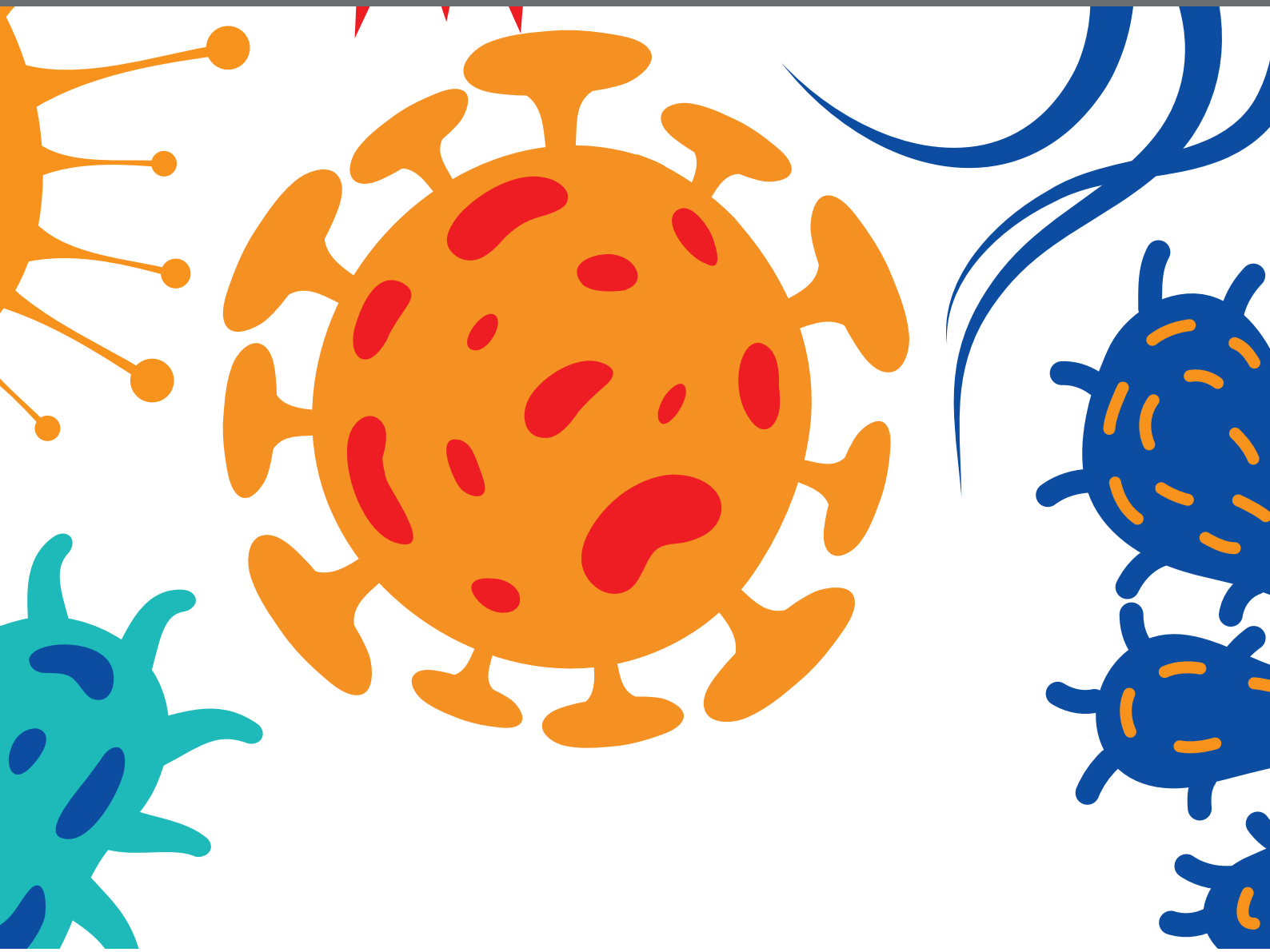

frontiers Research Topics

frontiers

ISSN 1664-8714
ISBN 978-2-88966-721-5
DOI 10.3389/978-2-88966-721-5

About Frontiers

Frontiers is more than just an open-access publisher of scholarly articles: it is a pioneering approach to the world of academia, radically improving the way scholarly research is managed. The grand vision of Frontiers is a world where all people have an equal opportunity to seek, share and generate knowledge. Frontiers provides immediate and permanent online open access to all its publications, but this alone is not enough to realize our grand goals.

Frontiers Journal Series

The Frontiers Journal Series is a multi-tier and interdisciplinary set of open-access, online journals, promising a paradigm shift from the current review, selection and dissemination processes in academic publishing. All Frontiers journals are driven by researchers for researchers; therefore, they constitute a service to the scholarly community. At the same time, the Frontiers Journal Series operates on a revolutionary invention, the tiered publishing system, initially addressing specific communities of scholars, and gradually climbing up to broader public understanding, thus serving the interests of the lay society, too.

Dedication to Quality

Each Frontiers article is a landmark of the highest quality, thanks to genuinely collaborative interactions between authors and review editors, who include some of the world's best academicians. Research must be certified by peers before entering a stream of knowledge that may eventually reach the public - and shape society; therefore, Frontiers only applies the most rigorous and unbiased reviews.
Frontiers revolutionizes research publishing by freely delivering the most outstanding research, evaluated with no bias from both the academic and social point of view. By applying the most advanced information technologies, Frontiers is catapulting scholarly publishing into a new generation.

What are Frontiers Research Topics?

Frontiers Research Topics are very popular trademarks of the Frontiers Journals Series: they are collections of at least ten articles, all centered on a particular subject. With their unique mix of varied contributions from Original Research to Review Articles, Frontiers Research Topics unify the most influential researchers, the latest key findings and historical advances in a hot research area! Find out more on how to host your own Frontiers Research Topic or contribute to one as an author by contacting the Frontiers Editorial Office: frontiersin.org/about/contact

INSIGHTS IN TOXOPLASMA BIOLOGY AND INFECTION - 15TH BIENNIAL MEETING ON TOXOPLASMA BIOLOGY AND TOXOPLASMOSIS

Topic Editors:
Jorge Enrique Gómez Marín, University of Quindío, Colombia
Jeroen P. J. Saeij, University of California, Davis, United States
Alejandra De La Torre, Rosario University, Colombia

Citation: Marín, J. E. G., Saeij, J. P. J., De La Torre, A., eds. (2021). Insights in Toxoplasma Biology and Infection - 15th biennial meeting on Toxoplasma Biology and Toxoplasmosis. Lausanne: Frontiers Media SA.
doi: 10.3389/978-2-88966-721-5

Table of Contents

frontiers in Cellular and Infection Microbiology

EDITORIAL
published: 09 March 2021
doi: 10.3389/fcimb.2021.652637

Editorial: Insights in *Toxoplasma* Biology and Infection—15th Biennial Meeting on *Toxoplasma* Biology and Toxoplasmosis

Jorge Enrique Gomez-Marin[1*†] *and Alejandra de-la-Torre*[2†]

[1] *Grupo de Estudio en Parasitología Molecular (GEPAMOL), Centro Investigaciones Biomédicas, Facultad de Ciencias de la Salud, Universidad del Quindío, Armenia, Colombia,* [2] *Escuela de Medicina y Ciencias de la Salud, Grupo NeURos, Centro de Neurociencia (NeuroVitae), Universidad del Rosario, Bogotá, Colombia*

Keywords: ***Toxoplasma gondii*, toxoplasmosis, drug design, *in vivo* model, ocular toxoplasmosis, immune response**

OPEN ACCESS

Edited by:
Tania F. De Koning-Ward,
Deakin University, Australia

Reviewed by:
Daniel Gold,
St. Edward's University, United States

****Correspondence:***
Jorge Enrique Gomez-Marin
gepamol2@uniquindio.edu.co

†ORCID:
Jorge Enrique Gomez-Marin
orcid.org/0000-0001-6472-3329
Alejandra de-la-Torre
orcid.org/0000-0003-0684-1989

Specialty section:
This article was submitted to Parasite and Host, a section of the journal Frontiers in Cellular and Infection Microbiology

Received: *12 January 2021*
Accepted: *15 February 2021*
Published: *09 March 2021*

Citation:
Gomez-Marin JE and de-la-Torre A (2021) Editorial: Insights in Toxoplasma Biology and Infection—15th Biennial Meeting on Toxoplasma Biology and Toxoplasmosis. Front. Cell. Infect. Microbiol. 11:652637. doi: 10.3389/fcimb.2021.652637

Editorial on the Research Topic

Insights in Toxoplasma Biology and Infection—15th Biennial Meeting on Toxoplasma Biology and Toxoplasmosis

INTRODUCTION

The 15th Biennial Meeting on *Toxoplasma* Biology and Toxoplasmosis was held between 19–22 June 2019 in Colombia. The Scientific Committee of this event (**Figure 1**) organized a program that gathered worldwide experts discussing new knowledge advancements regarding the protozoa and the infection caused by it. Numerous topics were addressed, including not only basic parasite-biology mechanisms, but also immune response, diagnostic tools, development of new therapies and public health aspects of *T. gondii* infection. Eleven articles and 118 authors are part of this special Research Topic published in Frontiers in Cellular and Infection Microbiology, which offers a comprehensive view of relevant work presented during the global conference. In this Editorial, we will comment briefly the main aspect addressed for these works and how they improve our current knowledge for this important zoonotic infection.

One basic mechanism of *Toxoplasma* biology is the process by which centromeres are held in position at the nuclear envelope and keep track of the position of their chromosomes, without condensing their chromatin during division. The work published on this Research Topic showed that centromere-associated protein interacts with chromatin and that chromatin binding factors at the centromeres mediate the maintenance of their localization at the periphery of the nucleus (Francia et al.). This data shed light about how Apicomplexa coordinates chromosomes during division. Another basic aspect is how *T. gondii* influences host cell's biological processes. The work reported by Vieira et al. showed the disruptive effects of this parasite in one murine myoblast cell line, where *T. gondii* established a pro-inflammatory environment extended to neighboring cells and damaged their response to myogenic stimuli. Additional evidence of the modulation of *T. gondii* on inflammatory host signal pathway was provided by the transcriptome analysis by Li et al., which analyzed how *Toxoplasma*-ROP18 virulent factor altered the expression of 750 genes (467 upregulated genes and 283 downregulated genes) in HEK293T cells. This data provided new understanding into how ROP18 may influence these processes by altering the expression of genes, transcription factors and pathways, laying the foundations for future *in vitro* and *in vivo* studies.

FIGURE 1 | Scientific Committee of the XVth Biennal *Toxoplasma* Biology meeting from left to right: Sebastian Lourido, David Roos, Jeroen Saeij, Karen Shapiro, Jorge Gomez-Marin, Aurelien Dumetre, Fabiana Lora- Suarez and Alejandra de-la-Torre.

Immune response in animal models others than mouse was analyzed by Rahman et al., which showed how pigs can serve as an interesting model for studying the *T. gondii* infection kinetics in the gut. The results suggest that upon ingestion the parasite first enters the host at the duodenum and then disseminates to other tissues. This is associated with the activation of IFN γ secreting immune cells. These findings lay a foundation for further study on the early stages of *T. gondii* intestinal infection and might inform strategies aimed at preventing initial invasion of the host by this parasite (Rahman et al.).

Considering the epidemiological factors of this zoonosis, Blaizot et al. described the investigation of a toxoplasmosis outbreak in a remote Amerindian community. This work highlighted the probable multifactorial origin of this infection, underscoring new life habits among an indigenous population which live in close contact with the Amazon rainforest. Sedentary settlements had been built in the last few decades without providing safe water sources, increasing the risk of parasite circulation in cases of dangerous new habits such as cat domestication. The authors recommended the pursuit of a "One Health" strategy of research involving medical anthropology, veterinary medicine, and public health, for a better understanding of the transmission routes and the presence of this zoonotic disease.

Studies in human cells about the immune response to the parasite modified by parasite virulent proteins ROP18 and ROP16 were reported by Hernandez-de-los-Rios et al. The research group studied infecting cells with knockout parasite for each of these proteins, and how the secretion by peripheral blood polymorphic mononuclear cells of proinflammatory cytokines was influenced by the host's polymorphisms in the cytokine genes. The findings suggest that the immune response to the parasite in humans does not only depend on the presence of parasite virulence factors like ROP16 and ROP18, but also on the host genetic susceptibility to the infection (Hernández-de-los-Ríos et al.).

One major aspect of human toxoplasmosis is the retinal involvement. An interesting review by de Campos et al. analyzed the available evidence of the effects that congenital TORCH (**T**oxoplasmosis – **O**ther – **R**ubella – **C**ytomegalovirus - **H**erpes) infections may cause to the developing retina and the cellular and molecular aspects of these diseases, with special emphasis on congenital ocular toxoplasmosis. While some

questions remain unanswered, this work gives an insight in which key factors are implicated on retinal damage during *in utero* infection, for further research in the pathophysiology of congenital ocular toxoplasmosis (Campos et al.). Again, in relation to ocular toxoplasmosis, Nakashima et al. investigated the correlation of serum IgG anti-*T. gondii* antibody concentrations with Nested PCR. This work was developed considering that the influence of IgG anti-*T. gondii* antibodies in molecular analysis carried out in peripheral blood remain unclear and considering that blood transfusion and organ transplantation represent different forms for *T. gondii* transmission, apart from food and water-borne sources. Results from chronically infected healthy blood donors showed that variations in the serum IgG anti-*T. gondii* antibody concentrations do not correlate to the parasitemia detected by Nested PCR. Similarly, Murata et al. compared serological methods such as ELISA and ELFA, as well as molecular cPCR, Nested PCR and qPCR, for the diagnosis of ocular *T. gondii* infection. The authors showed that the combined use of certain tests along with clinical evaluation and follow up could be useful for the correct diagnosis of *T. gondii* infection (Murata et al.).

A new strategy that is promising for diagnosis is the aptamer assay that uses short, single-stranded oligonucleotides that bind to targets with high affinity and specificity by folding into tertiary structures. The detection of the virulent protein *Toxoplasma* ROP18 protein in human serum with aptamer, signaled that detection of this protein was related with more severe forms of congenital toxoplasmosis suggesting its use as prognostic biomarker (Vargas-Montes et al.).

Finally, one major finding reported in this Research Topic is the development of a powerful tetrahydroquinolone, JAG21, which can eliminate apicomplexan parasites in tissues (McPhillie et al.). This is an extraordinary achievement in *in vivo* models because, until now, there are no drugs that can eliminate tissue cysts of the parasite responsible of reactivations during the host's period of life. The authors created a next generation lead compound with high *in vitro* and *in vivo* efficacy against *T. gondii* tachyzoites, bradyzoites and established encysted organisms (McPhillie et al.). This compound is promising and deserves further development through preparation of advanced formulations and testing in further studies of pharmacokinetics, efficacy, and safety.

In summary, this Research Topic shows significant advances made in the study of *T. gondii* using *in-vitro*, *in-vivo* and animal models. The results presented here will illuminate the pathway to create an effective clinical response to this public health key issue.

AUTHOR CONTRIBUTIONS

JG and AT drafted and edited the editorial. All authors contributed to the article and approved the submitted version.

Conflict of Interest: The authors declare that the research was conducted in the absence of any commercial or financial relationships that could be construed as a potential conflict of interest.

frontiers in Cellular and Infection Microbiology

ORIGINAL RESEARCH
published: 13 November 2019
doi: 10.3389/fcimb.2019.00386

Enzyme-Linked Aptamer Assay (ELAA) for Detection of *Toxoplasma* ROP18 Protein in Human Serum

Monica Vargas-Montes[1], *Nestor Cardona*[1,2], *Diego Mauricio Moncada*[3], *Diego Alejandro Molina*[1], *Yang Zhang*[4]* and *Jorge Enrique Gómez-Marín*[1]*

[1] Centre for Biomedical Research CIBM, University of Quindío, Armenia, Colombia, [2] Dentistry Faculty, University Antonio Nariño, Armenia, Colombia, [3] Department of Pediatrics, Emory University, Atlanta, GA, United States, [4] College of Science, Harbin Institute of Technology, Shenzhen, China

Toxoplasma gondii engenders the common parasitic disease toxoplasmosis in almost all warm-blooded animals. Being a critical secretory protein, ROP18 is a major virulence factor of *Toxoplasma*. There are no reports about ROP18 detection in human serum samples with different clinical manifestations. New aptamers against ROP18 protein were developed through Systematic Evolution of Ligands by Exponential enrichment (SELEX). An Enzyme-Linked Aptamer Assay (ELAA) platform was developed using SELEX-derived aptamers, namely AP001 and AP002. The ELAA was used to evaluate total antigen from *T. gondii* RH strain (RH Ag) and recombinant protein of ROP18 (rROP18). The results showed that the ELAA presented higher affinity and specificity to RH Ag and rROP18, compared to negative controls. Detection limit of rROP18 protein in serum samples was measured by standard addition method, achieving a lower concentration of 1.56 μg/mL. Moreover, 62 seropositive samples with different clinical manifestations of toxoplasmosis and 20 seronegative samples were tested. A significant association between ELAA test positive for human serum samples and severe congenital toxoplasmosis was found ($p = 0.006$). Development and testing of aptamers-based assays opens a window for low-cost and rapid tests looking for biomarkers and improves our understanding about the role of ROP18 protein on the pathogenesis of human toxoplasmosis.

Keywords: ROP18 protein, aptamer, SELEX, ELAA, toxoplasmosis, human serum

OPEN ACCESS

Edited by:
Tiago W. P. Mineo, Federal University of Uberlandia, Brazil

Reviewed by:
Fatemeh Ghaffarifar, Tarbiat Modares University, Iran
Cosme Alvarado-Esquivel, Universidad Juárez del Estado de Durango, Mexico

***Correspondence:**
Yang Zhang
zhangyang07@hit.edu.cn
Jorge Enrique Gómez-Marín
jegomez@uniquindio.edu.co

Specialty section:
This article was submitted to Parasite and Host, a section of the journal Frontiers in Cellular and Infection Microbiology

Received: *31 August 2019*
Accepted: *28 October 2019*
Published: *13 November 2019*

Citation:
Vargas-Montes M, Cardona N, Moncada DM, Molina DA, Zhang Y and Gómez-Marín JE (2019) Enzyme-Linked Aptamer Assay (ELAA) for Detection of Toxoplasma ROP18 Protein in Human Serum. Front. Cell. Infect. Microbiol. 9:386. doi: 10.3389/fcimb.2019.00386

INTRODUCTION

Toxoplasma gondii (*T. gondii*) is an intracellular parasite with cosmopolitan distribution that infects the majority of warm-blooded animals (Jones and Dubey, 2012). Nearly one third (~25%) of the world's human population may be chronically infected with *T. gondii* (Pappas et al., 2009). Infection in humans can cause severe ocular, neurologic, and sometimes systemic disease, especially in immunocompromised and congenitally infected individuals (Cardona et al., 2011; Pfaff et al., 2014). Transmission of the parasite has been demonstrated in humans by the consumption of meat, vegetables and contaminated water (Lora-Suárez et al., 2007; Franco-Hernandez et al., 2016; Triviño-Valencia et al., 2016). For all these reasons, Food and Agriculture Organization (FAO) and World Health Organization (WHO) declared toxoplasmosis as a foodborne parasite infection disease of global concern (Robertson et al., 2013).

Globally, the serological prevalence of toxoplasmosis is highly variable, ranging from 10 to 15% in the United States, to >60% in South and Central America (Gilbert et al., 2008). Additionally, it

has been reported that South America is the continent with the highest burden of the disease, with congenital and ocular toxoplasmosis frequently associated with more severe symptoms (de-la-Torre et al., 2007; De-la-Torre et al., 2009; Torgerson and Mastroiacovo, 2013). The high rate of ocular toxoplasmosis in Colombia is likely attributable to exposure to more-virulent strains of *T. gondii* (Ajzenberg, 2012), even if other factors, such as inoculum exposure or the genetic background of the host, may be involved (de-la- Torre et al., 2013). Therefore, there are some indications that disease outcomes in humans can be influenced by the variability of the infecting *T. gondii* strain (Grigg et al., 2001; Reese et al., 2011; McLeod et al., 2012; Sánchez et al., 2014).

Experimental crosses between *T. gondii* strains with different virulence patterns allowed the identification of several polymorphic genes coding for secreted factors of the parasite, associated with differences in the virulence in mice (Saeij et al., 2006; Taylor et al., 2006; Talevich and Kannan, 2013). These key virulence factors include proteins from the rhoptry family (ROP kinases) that exert kinase or pseudokinase activities (Hunter and Sibley, 2012) contributing to disarm innate immunity and promote survival of the parasite (Hakimi et al., 2017). ROP18 is one of the major virulence factors of *T. gondii*, identified as a serine/threonine kinase secreted into the parasitophorous vacuole (PV) and host cytosol (Taylor et al., 2006; Talevich and Kannan, 2013). A recent study shows that ROP18 is a conserved virulence factor in genetically diverse strains from North and South America (Behnke et al., 2015). Furthermore, there is a report that demonstrates the presence of virulent alleles that code for ROP18 in humans with ocular toxoplasmosis in Colombia, who presents a more severe inflammatory reaction in the eye (Sánchez et al., 2014). Currently, there is only one study that indicates the presence of specific IgM and IgG antibodies against ROP18 in sera from humans with toxoplasmosis (Gatkowska et al., 2015). However, there are not any reported methods that allow the direct detection of this protein in human serum. ROP18 protein identification in human serum would be of great importance in order to ascertain a possible correlation between the presence of this virulent factor and the severity of the disease.

To perform the identification and quantification of protein biomarkers in serum, DNA and RNA aptamers have been used (Drolet et al., 1996; Gold et al., 2010). Aptamers are short, single-stranded oligonucleotides, that bind to targets with high affinity and specificity by folding into tertiary structures (Ellington and Szostak, 1990; Tuerk and Gold, 1990). These molecules have promising roles in clinical diagnostics and as therapeutic agents (Zhang et al., 2019), showing some advantages compared to antibodies, such as shorter generation time, lower costs of manufacturing, no batch-to-batch variability, higher modifiability, better thermal stability and higher target potential (Zhou and Rossi, 2017). Due to these characteristics, aptamers could be used as molecular recognition agents alternative to antibodies in enzyme linked immunosorbent (ELISA) assays, hence its application has given rise to the ELAA assay (Enzyme-Linked Aptamer Assay), in which aptamers are the recognition agents (Toh et al., 2015). This ELAA assay has been used to recognize *Leishmania infantum* proteins, like H2A histones (Ramos et al., 2007; Martin et al., 2013) and also for detecting *Mycobacterium tuberculosis* culture filtrate protein and secreted antigen in sputum samples from tuberculosis patients (Rotherham et al., 2012).

Although aptamer research in the area of parasitology is still in the early stages, promising results have been obtained for the main protozoan parasites, including *Trypanosoma* spp., *Plasmodium* spp., *Leishmania* spp., *Entamoeba histolytica,* and *Cryptosporidium parvuum.* These aptamers have been used to detect and treat the parasitic infections caused by these parasites in human beings (Ospina-Villa et al., 2018). For *T. gondii*, only one work with DNA aptamers has been reported for the detection of anti-*Toxoplasma* IgG antibodies (Luo et al., 2013).

There are no aptamer-based methods for the detection of *T. gondii* proteins in serum. Therefore, we developed specific aptamers against ROP18 protein by SELEX. Those newly identified aptamers were utilized in a direct or a sandwich ELAA test to detect total antigen from *Toxoplasma* and recombinant ROP18 protein. Moreover, human serum samples with rROP18 protein were analyzed, as well as the seropositive samples from individuals with toxoplasmosis were evaluated with this novel ROP18-ELAA platform (**Figure 1**). The newly developed aptamer-based sensing platform for ROP18, will enhance our understanding about the role of virulence factors on the pathogenesis of toxoplasmosis in humans.

MATERIALS AND METHODS

Human Clinical Samples and Definition of Clinical Manifestations

Human serum samples for the ELAA test were obtained from 62 individuals with toxoplasmosis, 20 seronegative for the infection and 5 from individuals with a different infection as a control of specificity. Most of the samples ($n = 67$) were collected at the Center for Biomedical Research (CIBM) at the University of Quindío and some of them with ocular toxoplasmosis ($n = 20$) were recruited at the "Clínica Barraquer" in Bogotá-Colombia, with the previous signature of the informed consent. We included 18 serum samples from patients with toxoplasmic lymphadenitis (IgM and IgG anti-*Toxoplasma* positive) with avidity <50%; 13 from individuals with chronic-asymptomatic infection without eye injury (IgM anti-*Toxoplasma* negative and IgG anti-*Toxoplasma* positive); 21 from patients with ocular toxoplasmosis diagnosed by indirect ocular fundoscopy, with antibody levels positive in serum/aqueous humor (index <2), with PCR for *Toxoplasma* B1 sequence positive and based on the criteria previously described (De La Torre and López-Castillo, 2009); and 10 serum samples with congenital toxoplasmosis (IgG anti-*Toxoplasma* positive) confirmed as described by the European Network in congenital toxoplasmosis (Lebech et al., 1996). In the same way, we included 20 serum samples from seronegative individuals (IgM and IgG anti-*Toxoplasma* negative) as the negative control of the assay. Additionally, five serum samples from IgM Dengue-positive individuals (Diagnosed by an IgG capture ELISA for Dengue, Vircell Ref. M1018, carried out in the CIBM), were included to evaluate the cross-reactivity of previously standardized ELAA.

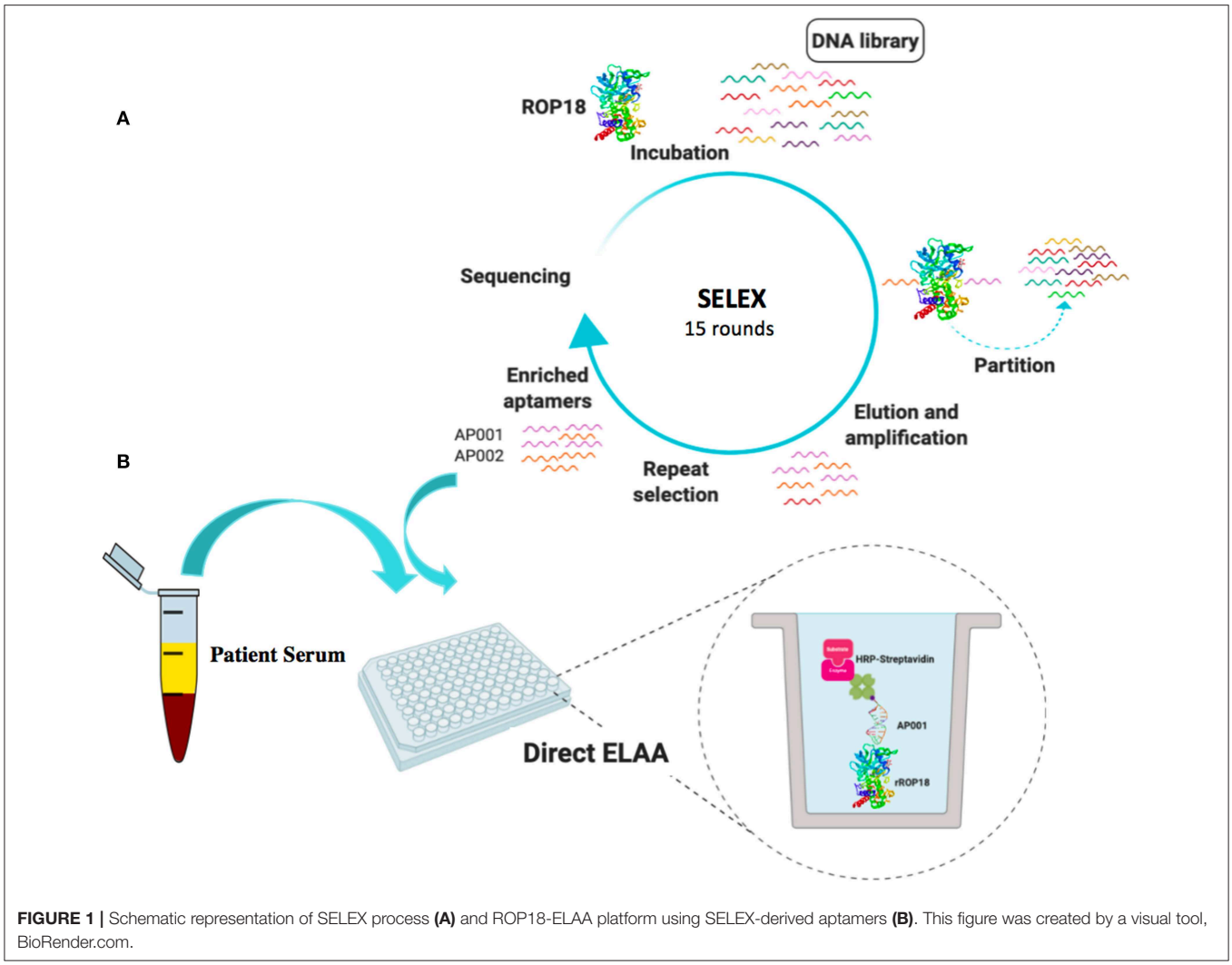

FIGURE 1 | Schematic representation of SELEX process **(A)** and ROP18-ELAA platform using SELEX-derived aptamers **(B)**. This figure was created by a visual tool, BioRender.com.

In vitro Selection of Aptamers Against *T. gondii* ROP18

Two nanomoles ssDNA library (5′-ATCCAGAGTGACGCAG CA-40N-TGGACACGGTGGCTTAGT-3′) were dissolved in 350 μL binding buffer (a solution of DPBS containing 5 mM $MgCl_2$, 0.1 mg/mL tRNA, 1 mg/mL BSA), mixed and heated at 95°C for 5 min, then snap cooled on ice to create folded ssDNA.

The snap-cooled DNA library was brought to room temperature and incubated with 400 pmol GST-rROP18 protein that was conjugated with Glutathione Sepharose beads at RT with rotation for 1 h. After incubation, the supernatant containing unbound sequences was removed and the beads were washed three times with 1 mL washing buffer (a solution of DPBS containing 5 mM $MgCl_2$). The ssDNA-protein-bead complexes were suspended in DNase-free water for PCR amplification of ROP 18-bound sequences by using forward primer (5′-ATCCAGAGTGACGCAGCA-3′) and reverse primer with biotinylated 5′ end (5′-biotin-ACTAAGCCACCGTGTCCA-3′). PCR product was then passed three times through the DNA synthesis column loaded with streptavidin sepharose beads. The beads were washed again with 2.5 mL of PBS. 500 μL of 200 mM NaOH was added to elute the ssDNA. The eluted ssDNA was added into a NAP5 column pre-washed with 15 mL of deionized water for desalting. 1,000 μL of DNase-free water was allowed to pass through the column to elute the ssDNA. The concentration of ssDNA was determined by UV absorbance at 260 nm and concentrated by using a DNA Speedvac dryer. Precipitated ssDNA was resuspended in binding buffer for subsequent round of selection. After 15 rounds of selection, the final enriched libraries were PCR-amplified and cloned into pJET1.2/blunt cloning vector using the CloneJET PCR Cloning Kit (Thermo Fisher Scientific) according to the manufacturer's instructions. One hundred fifty Colonies from the 15th round of selection were picked and analyzed by Sanger sequencing.

Aptamer and Antibody Anti-ROP18

Two top enriched DNA aptamers with biotin labeled were used as recognition agents. Those aptamers are AP001 with the sequence 5′-TCCTGGCAGCGCTTTTGCTTGTTTGCTC

TCGTACCTGTCC-3' and AP002 with the sequence 5′-CGCA CCGATCCGGTGTTAATCTCGACGTCCCTTAAGTTTG-3'. In addition, a rabbit anti-ROP18 polyclonal antibody (a gift from the Dr. L. D. Sibley from the University of Washington, Saint Louis, United States of America).

Toxoplasma lysate antigen from the RH strain (RH Ag) was used as positive control, because it expresses the ROP18 protein (**Supplementary Figure S1**). RH Ag was prepared as previously reported (Torres-Morales et al., 2014) with some modifications. Briefly, *T. gondii* tachyzoites from the RH strain were maintained *in vitro* in human fibroblasts (HFF) at 37°C and 5% CO_2. The antigen was obtained after recovering the tachyzoites from the culture and centrifuged at 3,000 rpm for 5 min in RPMI medium, the tachyzoites pellet was resuspended in saline and subjected 5 times to freeze-thawing and to breakage by sonication 8 times a 20 W for 20 s. Subsequently, the lysis of the parasite was verified by microscopy. Finally, 1x protease inhibitor cocktail (dilution 1:100) was added to the antigen (Ref. I3786, Sigma-Aldrich, St. Louis, USA), the aliquots were performed and stored at −80°C. The protein quantification was performed by the Bicinchoninic Acid Protein Assay (Ref. 23227, Thermo Scientific, Rockford, IL) by using the spectrophotometer EPOCH (BioTek Instruments, Winooski, VT, USA) at 280 nm. The RH Ag, was evaluated at different concentrations (from 200 to 6.25 μg/ml) in order to determine the detection limit for each assay.

In addition to RH Ag, the recombinant protein ROP18 (rROP18) of *T. gondii* RH strain produced in our lab was also used as positive control in the last steps of the standardization. In the same way, three negative controls were included: the recombinant protein Disulfide isomerase of *T. gondii* (PDI); Lucifensin-CPD, a recombinant protein from the fly *Lucilia sericata* (LucGT), both produced in our lab, and bovine serum albumin (BSA) (AMRESCO), these controls were used at a concentration of 6.25 μg/mL. Likewise, a lysate antigen from a Knockout strain for ROP18 (KOROP18, a gift from the Dr. Sibley, St. Louis, USA) of *T. gondii* was used as another negative control of the assay, this antigen was prepared similar to RH Ag.

Enzyme-Linked Aptamer Assay (ELAA) Standardization

For standardization of the ELAA assay, two different configurations were evaluated: direct and sandwich ELAA (Toh et al., 2015), in order to determine which configurations allowed to reach a higher detection limit of RH Ag and rROP18 protein in human serum. Initially, all the conditions for direct ELAA were standardized and based on these conditions we performed the sandwich ELAA, in which the only additional step was the anti-ROP18 antibody, added at the beginning of the assay.

To standardize the general protocol, the antigens (Ag RH, rROP18, PDI, LucGT, BSA, and KOROP18) were immobilized in 96-well microtiter plates (NUNC) diluted in 0.1 M carbonate buffer at a pH of 9.6 (Na_2CO_3, 0.159 g/100 mL; $NaHCO_3$, 0.293 g/100 mL) and adding 100 μL per well. The antigen incubation was evaluated for 1 h at 37°C, or overnight at 4°C as previously reported (Rotherham et al., 2012; Luo et al., 2013). After coating, we performed 5 washes with 0.01 M phosphate buffered saline (PBS) (pH 7.4) plus 0.05% Tween 20 (PBS-T), previously used in other studies (Martin et al., 2013; García-Recio et al., 2016). Then, three different conditions were included for the blocking step: 1% BSA (AMRESCO) diluted in PBS-T (Luo et al., 2013), 5% skimmed milk (Rotherham et al., 2012) in PBS-T and no blocking, as reported in other studies (Martin et al., 2013; García-Recio et al., 2016). Each well was blocked with 300 μL of the blocking solution by 1 h at 37°C. After washing three times, biotinylated aptamers (200 nM) against ROP18 were added to each well, these oligonucleotides were diluted in binding buffer (PBS, 0.5% glucose, 0.1% albumin and 1 M $MgCl_2$) and incubated for 1 h at 37°C. Then, 5 washes were performed and 100 μL of streptavidin-horseradish peroxidase conjugate (ThermoFisher) was added, evaluating three previously reported dilutions, 1:10,000 (Murphy et al., 2003), 1:15,000 (Rotherham et al., 2012), and 1:20,000 (Balogh et al., 2010) diluted in PBS and 1% BSA for 1 h at 37°C. Finally, after five washes, horseradish peroxidase activity was detected by using TMB for 15 min at room temperature and stopped by adding a 5% of sulfuric acid (H_2SO_4). The absorbance at 450 nm was read in an Epoch 2 spectrophotometer (BioTek Instruments, Winooski, VT, USA). All the samples were processed in triplicate.

Aptamer Concentration and Binding Affinity of AP001 and AP002

In order to study the binding affinity of aptamers AP001 and AP002, 50 μg/mL (5 μg/well) of RH Ag expressing ROP18 protein were plated in coating buffer and incubated in a 96-well microtiter plate overnight at 4°C. Then, the wells were washed 5 times in PBS-T and then blocked 1 h with 1% BSA in PBS. Afterwards, three washes were performed and biotin-labeled aptamers were diluted in binding buffer at concentration between 50 and 500 nM, and then incubated at 37°C for 1 h. Next, 100 μL of streptavidin-HRP (1:10,000 dilution) were added to the individual wells and developed using TMB solution as above. Data were analyzed using non-linear regression with an equation $y = (x \times Bmax) / (x + Kd)$, where Bmax is the maximal binding and Kd is the concentration of ligand required to reach half-maximal binding.

Detection Limit of rROP18 Protein by Direct ELAA

To identify the detection limit of the rROP18 protein in serum, concentrations from 50 to 1.56 μg/mL of the antigen were evaluated. RH Ag and KOROP18 Ag were included at a concentration of 50 μg/mL (the maximum concentration used for rROP18). All the antigens were diluted in a serum sample from a seronegative individual (IgM and IgG *Toxoplasma* negative). To select the serum dilution we analyze results of absorbance after performing ELAA protocol with 1:2, 1:5, and 1:10 dilutions of serum from one seronegative individual (IgM and IgG *Toxoplasma* negative) that was artificially spiked with 2.5 μg of recombinant ROP18 protein. The 1:10 serum dilution was the only one that allowed to differentiate between the absorbance levels of rROP18 and KOROP18 Ag ($p = 0.022$) and between rROP18 and serum without antigen ($p = 0.023$). The direct ELAA

was performed with the general protocol previously standardized and only with one of the selected aptamers (AP001).

Aptamer-Antibody Assay: Sandwich ELAA

The aptamer-antibody assay binding was performed using the direct ELAA described above with minor modifications. The anti-ROP18 polyclonal antibody was coated onto a 96-well microtiter plate overnight, diluted 1:500 in carbonate buffer and incubated overnight at 4°C. After washing five times with PBS-T, unspecific ligand sites were then saturated with 300 μL of 1% BSA diluted in PBS for 1 h at 37°C. After 3 washes, the samples were included: rROP18 was added at concentrations from 50 to 1.56 μg/mL, in order to identify a new detection limit, RH Ag and KOROP18 Ag were included again at a concentration of 50 μg/mL. All the antigens were diluted in the seronegative serum sample previously indicated and were diluted 1:10 in carbonate buffer. The samples were incubated by 2 h at 37°C with shaking. The biotinylated aptamer was then added at 300 nM in binding buffer, followed by the HRP-conjugated streptavidin (1:10,000). The detection limit obtained from this assay was compared with that obtained in the direct ELAA, with the aim to analyze if the detection limit of the protein was affected in the presence of the antibody.

ROP18-ELAA in Human Serum Samples

The standardized direct ELAA was applied for ROP18 detection in all the serum samples previously described ($n = 87$). The 20 serum samples from seronegative individuals (IgM and IgG anti-*Toxoplasma* negative) were used to calculate the cut-off point of the test (Cut off: average absorbance plus two standard deviations). In order to normalize the data and establish a Reactivity index (RI) for each serum, the mean absorbance of each sample was divided by the cut-off point of the test. Serum samples with IR> 1 were considered positive (Caballero-Ortega et al., 2014). The serum samples were processed in duplicate and two tests were performed per sample. The inter- and intra-assay coefficient of variation [CV = (standard deviation of the RI/arithmetic mean of the RI) * 100] was calculated.

Bioethical Aspects

This study was conducted according to the tenets of the Declaration of Helsinki, strictly following the Guide for Good Laboratory Procedures. Informed written consent, according to the regulation 008430 of 1993 of the Ministry of Health in Colombia was obtained from all people that accepted to participate in the study. The protocol was approved by the Institutional Ethical Committee (Reference numbers: 5–14-1 from Universidad Tecnológica de Pereira and 030314 from Escuela Superior de Oftalmología Instituto Barraquer de América) approved the study.

Statistical Analysis

Data from ELAA standardization were expressed as means ± SEM. Differences in means were compared by the Student *t* test or a by non-parametric test if values were not normally distributed. Kruskal Wallis test and the Dunn test, were used for multiple comparisons between the standardization conditions. Spearman correlation test was performed to evaluate associations between quantitative variables of the population and the Reactivity index from the ELAA test. These data were analyzed using Graph Pad Prism 6.0 software (San Diego, CA, USA).

Differences in proportions between groups of patients were analyzed using the Fisher exact test. In addition, the association between the test positivity and different clinical characteristics related to the severity of ocular and congenital toxoplasmosis were evaluated. Epi-Info software 7.0 (Centers for Disease Control and Prevention, Atlanta, Georgia) was used to perform these analysis (available at: http://www.cdc.gov/epiinfo/). A $p < 0.05$ was considered to be statistically significant.

RESULTS

In vitro Selection of ROP18 Aptamers by SELEX

A random ssDNA library was used to select aptamers binding to rROP18. GST-rROP18 protein conjugated with Glutathione Sepharose beads was used as the target. Following incubation, the bound aptamers were separated from unbound ones, and target-bound ssDNA were eluted and enriched at each round of selection by amplification using PCR. A total of 15 rounds of repeated separation-amplification cycles were completed in order to receive high affinity and specificity of DNA aptamers against ROP18 protein. Cloning and sequencing of aptamer pools from the 15 rounds of cycles identified several aptamer candidates (**Figure 1A**). Aptamers AP001 with the sequence 5′-TCCTGGCAGCGCTTTTGCTTGTTTGCTCTCGTACCT GTCC-3' and AP002 with the sequence 5′-CGCACCGATCCG GTGTTAATCTCGACGTCCCTTAAGTTTG-3' were the top enriched sequences, representing 14.42% and 13.46% of the final enriched population. These two novel ROP18 aptamers were labeled with biotin and utilized as biorecognition elements to construct a ELAA sensing platform. Biotin-streptavidin strategy was used for signal production (**Figure 1B**).

Direct ELAA Standardization

Direct ELAA has been reported as one of the simplest and fastest methods, in which the antigen is immobilized on the surface of the platform, followed by a blocking step, addition of biotinylated aptamers, then streptavidin conjugated with HRP enzyme and the TMB substrate (Toh et al., 2015). To start with, we first developed a direct ELAA for total antigen from *Toxoplasma*. PDI, LucGT, and BSA proteins were used as negative controls. The optimal conditions of this direct ELAA test were obtained by evaluation of conditions, including time and temperature of antigen incubation, blocking solution, streptavidin dilution and aptamers concentration.

Firstly, we found that incubation of RH Ag overnight at 4°C allowed to reach a higher detection limit in the direct ELAA (**Figure 2**). Initially, antigen incubation for 1 h at 37°C was evaluated, showed that the AP001 and AP002 aptamers reached a significant antigen detection limit of 25 μg/mL compared to the negative controls ($p < 0.05$) (**Figures 2A,B**). Subsequently, antigen incubation was analyzed overnight at 4°C (**Figure 2**). We found that detection limit improved for the condition of 4°C

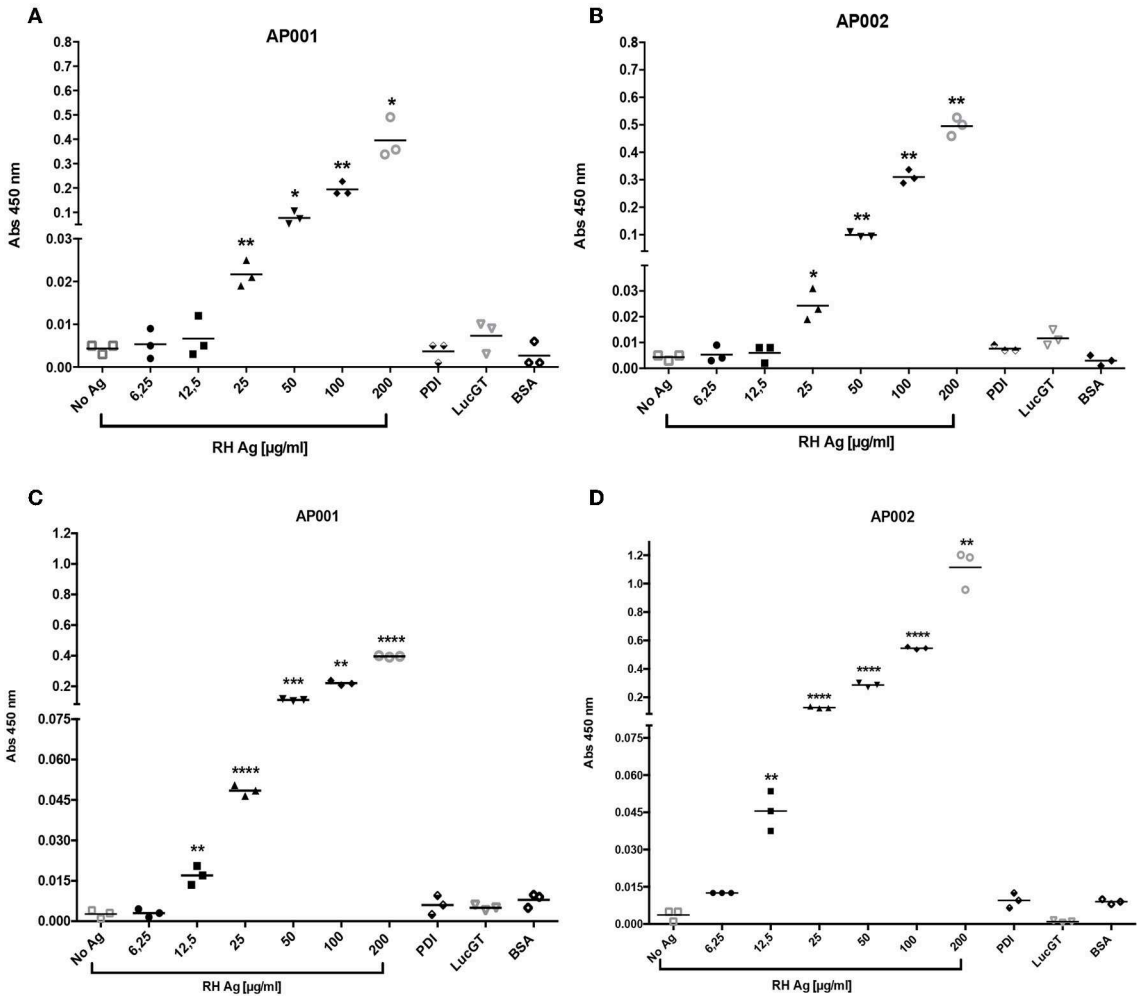

FIGURE 2 | Detection limit of RH antigen according time and temperature. The ELAA assays were performed with AP001 **(A,C)** and AP002 **(B,D)** anti-ROP18 aptamers. We evaluated incubation 1 h at 37°C **(A,B)** and 4°C overnight **(C,D)**. Different concentrations of *T. gondii* total antigen of the RH strain (RH Ag) were evaluated and three negative controls, PDI, LucGT, and BSA were included. The data are represented with the mean of each sample evaluated in triplicate. Welch's *t*-test. $^{*}p < 0.05$, $^{**}p < 0.01$, $^{***}p < 0.001$, $^{****}p < 0.0001$ vs. controls without antigen (No Ag).

overnight, reaching a detection limit of 12.5 µg/mL ($p < 0.01$) with both aptamers (**Figures 2C,D**). Overnight incubation at 4°C probably allowed more antigen adherence to the plate. Many other studies using the same incubation conditions were reported (Ramos et al., 2007; Rotherham et al., 2012; García-Recio et al., 2016).

Regarding the blocking solution, we found that 1% BSA was more effective compared to the other conditions (**Figure 3**). For AP001 ELAA, all negative controls showed significantly lower absorbance levels for the 1% BSA condition ($p < 0.05$) (**Figure 3A**). In the case of AP002, lower absorbance values were detected for the negative controls with 1% BSA, although significant differences were only found for the blank condition and the negative control with albumin (**Figure 3B**) ($p = 0.019$ and $p = 0.028$ respectively). Regarding the positive control (RH Ag), 1% BSA and the no blocking condition allowed to reach significantly higher levels of absorbance compared to 5% skim milk condition ($p = 0.05$ and $p = 0.03$ for AP001 and AP002, respectively), indicating a higher sensitivity of the assay. However, the no blocking condition was not selected due to the non-specificity generated for the negative controls. This could explain why BSA is more effective for biotin-streptavidin systems, as it contains only one purified protein without endogenous biotin (Alegria-Schaffer et al., 2009), thus avoiding background interferences or non-specific interactions. That's probably the reason why other studies also reported the use of BSA as blocking agent for ELAA tests with biotinylated aptamers (Vivekananda and Kiel, 2006; Balogh et al., 2010; Luo et al., 2013). Therefore, we continued working with 1% BSA as a blocking agent.

Related to streptavidin dilution, we found that 1:10,000 dilution allowed to reach higher absorbance levels in the positive controls of the assay (**Figures 3C,D**). In AP001 ELAA, only

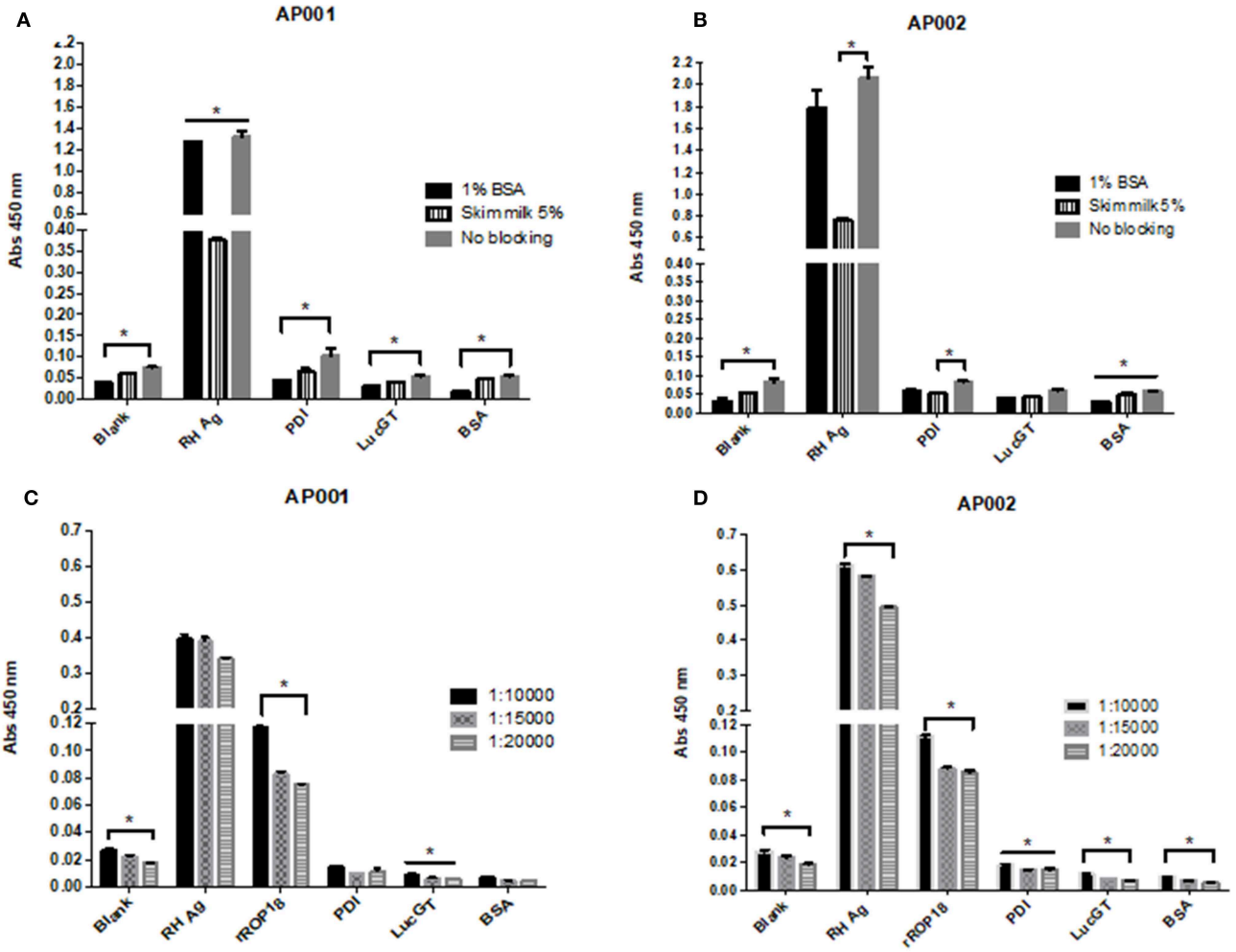

FIGURE 3 | Evaluation of different blocking conditions and streptavidin dilutions for AP001 **(A,C)** and AP002 **(B,D)** ELAA test. Different blocking conditions were evaluated: 1% bovine serum albumin, 5% skim milk and no blocking **(A,B)**. Three different dilutions of streptavidin (1: 10,000, 1: 15,000 and 1: 20,000) were evaluated **(C,D)**. RH Ag was used as a positive control (50 μg/ml) for both experiments. rROP18 (25 μg/ml) was also used as positive control for streptavidin experiment. Three negative controls were included, PDI, LucGT, and BSA. The data are represented by the mean ± SEM. Kruskal Wallis. *$p < 0.05$.

the absorbance levels for rROP18 were significantly higher for 1:10,000 dilution ($p = 0.021$) (**Figure 3C**); whereas in the ELAA test with AP002, the absorbance was significantly higher for both, the RH Ag and rROP18 for 1:10,000 dilution compared to 1:20,000 dilution ($p = 0.013$ and $p = 0.040$, respectively). Regarding the negative controls, although differences between evaluated dilutions were found, mainly for AP002 (**Figure 3D**), the absorbance levels obtained were very low for all controls with all dilutions, with mean values of OD that ranged between 0.005 and 0.028. Therefore, considering that 1:10,000 dilution favored the sensitivity of the experiment, it was selected for the subsequent trials. This result agrees with other studies using biotinylated aptamers (Murphy et al., 2003; Rotherham et al., 2012; Stoltenburg et al., 2016).

It is worth noting that both aptamers showed a minimal recognition profile toward three negative control proteins (PDI, LucGT, and BSA), compared to the positive control (RH Ag). The significantly lower absorbance levels in negative controls suggested a higher specificity of the ELAA test.

Aptamer Concentration and Binding Affinity of AP001 and AP002

A direct ELAA including all the previous standardized conditions was performed to analyze the optimal aptamer concentration. Aptamer concentrations were analyzed from 50 to 500 nM. We found that recognition of RH Ag was concentration-dependent, therefore, the absorbance levels increased as the aptamer concentrations increased ($r = 1$; $p = 0.003$; Spearman correlation test) (**Figures 4A,B**). The same pattern has also been found in other studies (Martin et al., 2013; García-Recio et al., 2016). Based on these results, we concluded that it was possible to continue working with an intermediate aptamer concentration (300 nM) in the subsequent ELAA tests, since it allowed an appropriate detection of the antigen, with acceptable absorbance

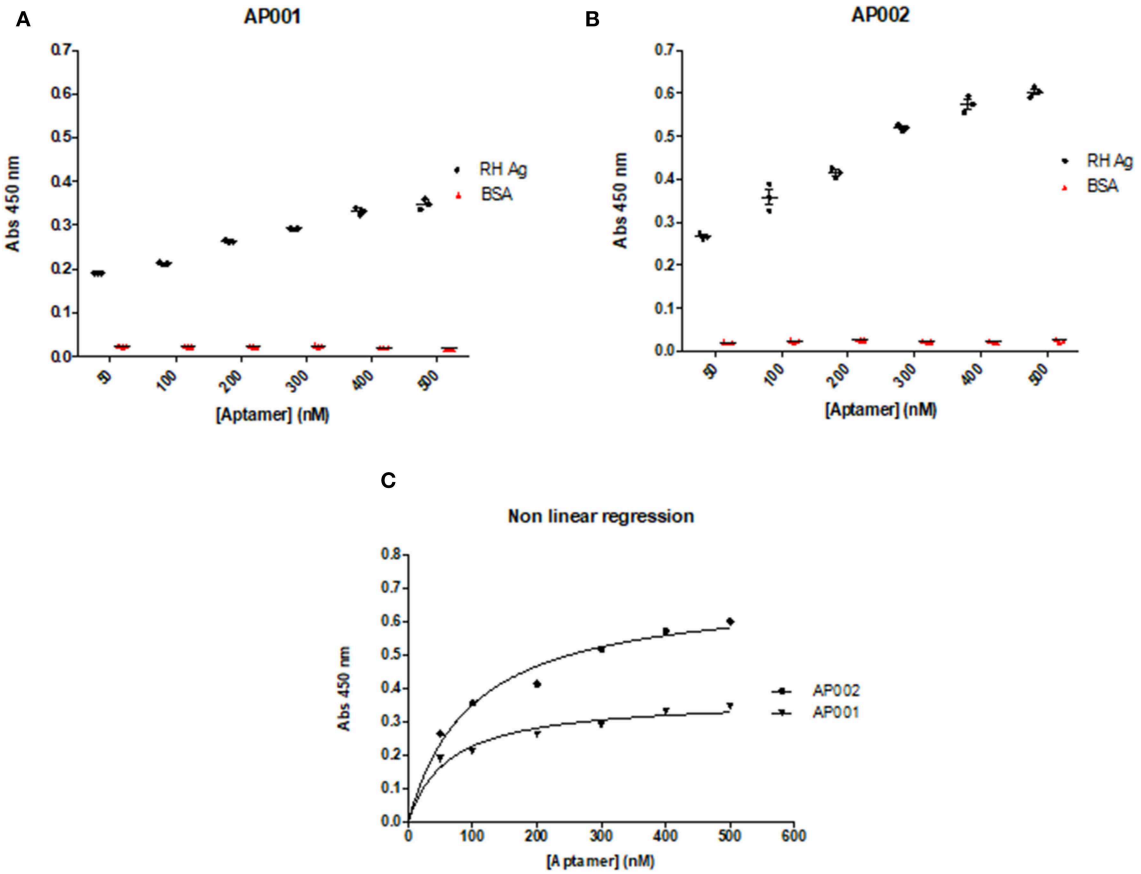

FIGURE 4 | Concentration and Binding affinity of AP001 **(A)** and AP002 **(B)** aptamers. Ag RH was used as a positive control and different concentrations of each aptamer (from 50 to 500 nM) were used. BSA was used as a negative control. The dissociation constant (Kd) was calculated through a non-linear regression to define the affinity of aptamers to the RH Ag, obtaining a Kd of 62.7 nM for AP001 and a Kd of 97.7 nM for AP002 **(C)**.

levels (OD: 0.3–0.5) and thus allowing a moderate use of the capture reagent.

Additionally, to determine the binding affinity, we used the absorbance and concentration data from this experiment to calculate the dissociation constant (Kd). The data were analyzed using a non-linear regression, where Kd is the concentration of ligand (aptamer) required to reach half of the maximum bond, finding that a lower value of Kd will be obtained by the aptamer with greater affinity toward the antigen. Regarding this analysis, we found that aptamer AP001 showed a higher affinity with a Kd value of 62.7 ± 17.27 nM; whereas the aptamer AP002 showed a Kd of 97.7 ± 22.20 nM (**Figure 4C**); these results suggested that it was feasible to continue working with AP001 aptamer in subsequent trials with human serum samples.

Detection Limit of rROP18 Protein in Serum Samples by Direct ELAA and Sandwich ELAA

In order to identify the detection limit of direct ELAA with serum samples, rROP18 protein concentrations from 50 to 1.56 μg/mL were evaluated by standard addition method. The recombinant ROP 18 protein was added in the seronegative human serum sample and then diluted 1:10 in coating buffer. Total Ag of the RH strain was included as a positive control and total antigen of the KOROP18 strain was used as a negative control. The results indicated that recognition of the ROP18 protein was concentration-dependent and AP001 was able to detect rROP18 protein in serum since the minimum concentration (1.56 μg/mL), showing significant differences compared to the serum sample without antigen KOROP18 ($p = 0.028$) (**Figure 5A**).

In comparison, we also performed a sandwich ELAA using an anti-ROP18 polyclonal antibody as a capture agent and the aptamer AP001 as a detection agent. The data showed that sandwich ELAA allowed the detection of rROP18 protein since a concentration of 3.12 μg/mL (**Figure 5B**) in the serum. These results indicated that the sensitivity of sandwich ELAA was lower than the direct ELAA (1.56 μg/mL). We also found that absorbance levels obtained for sandwich ELAA were reduced, presenting OD values between 0.054 ± 0.002 for the minimum and 0.059 ± 0.001 for the maximum concentration

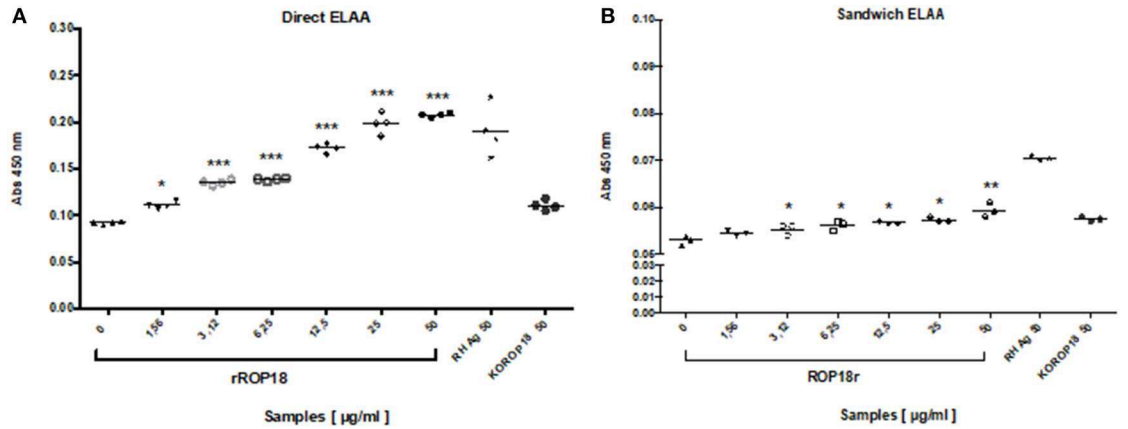

FIGURE 5 | Evaluation of the detection limit of rROP18 protein in serum through direct **(A)** and sandwich **(B)** ELAA. Protein concentrations from 50 to 1.56 µg/mL diluted in serum from a seronegative individual for *T. gondii* were included. Total Ag of the RH strain (RH Ag at 50 µg / ml) was included as a positive control, and total antigen of the KOROP18 strain (KOROP18 at 50 µg / ml) was included as a negative control. The data are represented with the average of each sample evaluated in quadruplicate. Welch *t* test. $^{*}p < 0.05$, $^{**}p < 0.01$, $^{***}p < 0.001$ vs. the negative control KOROP18 (serum without antigen).

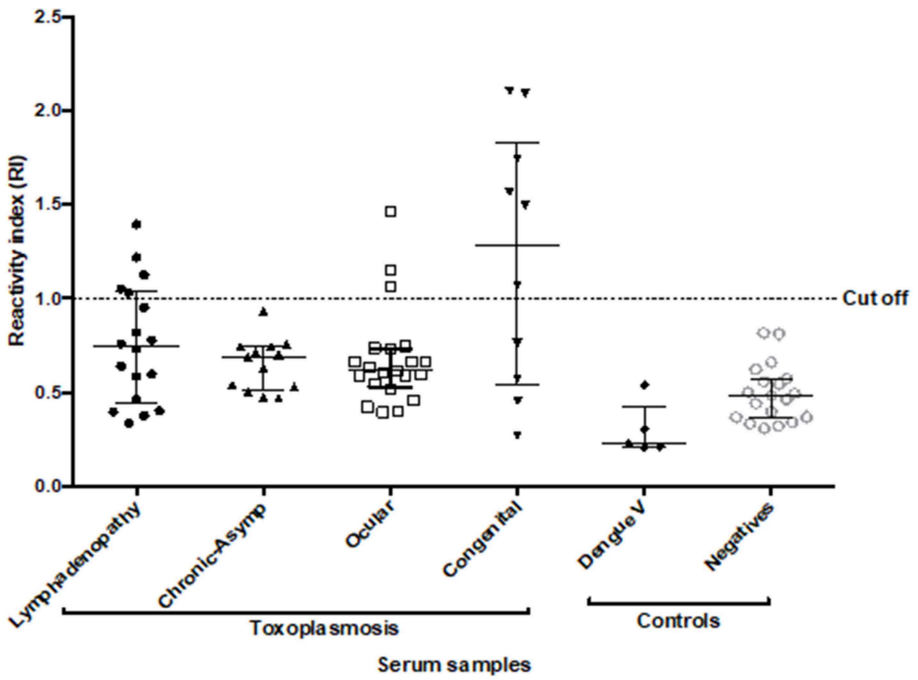

FIGURE 6 | Reactivity Index values obtained with ROP18-ELAA for the human serum samples. Serum samples with different clinical forms were included: toxoplasmic lymphadenitis ($n = 18$), chronic-asymptomatic toxoplasmosis ($n = 13$), ocular toxoplasmosis ($n = 21$), and congenital toxoplasmosis ($n = 10$). Additionally, samples with Dengue virus ($n = 5$) and individuals seronegative for *Toxoplasma* ($n = 20$) were included as negative controls. Two tests were performed for each sample. The data are represented with the median and the interquartile range. Serum samples with IR > 1 are considered positive.

of rROP18 protein (**Figure 5B**); while in the direct ELAA the absorbance values in the same concentration of the protein were 0.111 ± 0.001 and 0.207 ± 0.001, respectively (**Figure 5A**). Therefore, we concluded that direct ELAA was a more suitable configuration to be applied in the serum samples of individuals with toxoplasmosis.

ROP18-ELAA Tests in Human Serum Samples From Individuals With Toxoplasmosis

To validate the suitability of the ROP18-ELAA platform on serum samples from individuals with toxoplasmosis, the direct ELAA with AP001 aptamer was applied. A total of

62 serum samples from individuals with different clinical manifestations of toxoplasmosis and 20 samples from seronegative individuals were included. The Reactivity Index (RI) was calculated for each sample. Due to the samples were processed in duplicate and two tests were performed per sample, the respective variation coefficients (VC) were calculated.

All the samples presented values lower than 10% for the intra-assay VC and <20% for the inter-assay VC. Due to the complexity of the human serum samples, ELAA test was positive for 22.6% (14/62) (IC95 = 13.8–34.5%) of the total samples with toxoplasmosis. We also found a positivity of 27.7% (5/18) (IC95 = 12.2–51.2%) in the group with toxoplasmic lymphadenitis, no positive samples (0/13) (IC95 = 0–26.5%) for the group with chronic-asymptomatic toxoplasmosis; 14.3% (3/21) (IC95 = 4.14–35.4%) in the group with ocular toxoplasmosis and finally 60% of positivity (6/10) (IC95 = 31.2–83.3%) for the group with congenital toxoplasmosis. Additionally, five serum samples from individuals with dengue virus were included, in which no reactivity was found for the test (**Figure 6**).

The comparison of RI between the group of individuals with toxoplasmic lymphadenitis and chronic-asymptomatic toxoplasmosis indicated that there were no statistically significant differences ($p = 0.412$). In the same way, although the percentage of positivity was higher in the group with lymphadenitis, no significant association was found between ELAA positivity and the acute or chronic stage of the infection ($p = 0.058$). Similarly, when comparing the RI between the groups with different clinical manifestations of toxoplasmosis, no statistically significant differences were found between them ($p = 0.162$) (**Figure 6**).

We found that the group with congenital toxoplasmosis had the highest RI values (Me: 1.285 Range: 0.270–2.104) and the highest positivity percentage in the test. So, the statistical analysis showed a significant association between this clinical form and the positivity for the ELAA test ($p = 0.006$). Additionally, after a stratified analysis according the clinical characteristics inside this group, we found that the positivity of the ELAA test was associated with higher severity of the disease, in other words the test was significantly positive for children with severe clinical manifestations such as presence of ocular and/or neurological symptoms than in children with congenital asymptomatic infection ($p = 0.033$, **Table 1**).

For the group of ocular toxoplasmosis, no statistical association was found between this clinical manifestation and ELAA positivity ($p = 0.342$). In the same way, other variables analyzed inside this group didn't show significant associations with the RI values obtained in the ELAA test; except for the total number of chorioretinal scars where we found a negative correlation ($r = -0.74$, $p = 0.003$) with the RI values (**Supplementary Table S1**).

Finally, some other characteristics in the total population, like age, gender, total IgM and IgG levels, as well as avidity percentage were related with the positivity of the ELAA test or the RI values; however, we didn't find any significant association between these variables (**Supplementary Table S2**).

TABLE 1 | Clinical characteristics of the relationship between population with congenital toxoplasmosis and the ELAA positivity or RI value.

Statistical test	Variable (*n*)	*p*-value	*r*
Fisher's exact test (ELAA % positivity)	IgM positive ($n = 10$)	0.400	
	Sex ($n = 10$)	0.523	
	Symptoms (ocular and/or neurologic vs. asymptomatic) ($n = 10$)	**0.033***	
	Neurologic symptoms ($n = 10$)	0.200	
Spearman correlation test (RI values)	Age ($n = 10$)	0.624	−0.170
	Total IgM (UI/ml) ($n = 10$)	0.441	−0.222
	Total IgG (UI/ml) ($n = 10$)	0.664	0.161

Bold values indicates statistical significant values p< 0.05.

DISCUSSION

Previous studies have reported that *T. gondii* produces some virulence factors that can modulate the host immune response and could explain the severe manifestations of toxoplasmosis, especially in South America (Bradley and Sibley, 2007; Etheridge et al., 2014; Petersen et al., 2017). The ROP18 protein has been described as one of the major virulence factors of *T. gondii*, involved in the regulation of the host innate immune response, promoting the survival and replication of the parasite (Saeij et al., 2006; Taylor et al., 2006). IgM and IgG antibodies have been identified against the ROP18 (Gatkowska et al., 2015) or against peptides derived from it (Sánchez et al., 2014), which indicates that the immune system recognizes the protein. However, until now, the presence of the protein in serum from individuals with toxoplasmosis has not been reported and it is unknown if its presence could be related to the clinical manifestation of the disease.

Although antibodies to detect ROP18 protein are available, are difficult to obtain in developing countries and there are no other tools to readily and routinely assess *T. gondii* protein in serum. Aptamers are nucleic acids that are capable of selective binding to targets of interest. In addition to the easiest and cheaper production, the use of aptamers as biorecognition tools have several advantages in terms of storage compared to antibodies. Therefore, development and testing of aptamers-based technology for *T. gondii* protein opens a window for low-cost and rapid diagnostics that could in part support the great demand for point-of-care diagnostics in developing countries.

In this study, we developed DNA aptamers against ROP18 from *T. gondii* by the SELEX method. By utilizing those newly enriched aptamers, we developed a novel aptamer based biosensing platform for serum samples from people with toxoplasmosis. A direct ELAA was initially evaluated using recombinant protein ROP18 (rROP18) and total antigen from *T. gondii* RH strain. The optimal conditions, including time and temperature of incubation, as well as the buffer composition and aptamer concentration were achieved, allowing a best detection performance. Additionally, we found that AP001 was the aptamer with the higher affinity against the antigen.

The detection limit of the direct ELAA with aptamer AP001 was evaluated with rROP18 diluted in human serum samples. Similarly, we developed a sandwich ELAA configuration in order to compare which configurations allowing a greater sensitivity. The results indicated that direct ELAA was more sensible, allowing the detection of the protein in serum since a concentration of 1.56 μg/mL, while the sandwich configuration showed a detection limit of 3.12 μg/mL. Considering those results, we used the direct ELAA to analyze the serum samples from individuals with different clinical manifestations of toxoplasmosis. Our results indicated that the presence of the ROP18 protein was found significantly in higher proportion in serum from people with congenital toxoplasmosis group, but also, they had the highest RI values compared with the other groups. These data suggested that the group of congenital individuals may present a higher parasitic load and therefore a possible secretion of ROP18 proteins at higher levels. Also, it could be explained because the immune response generated in these individuals is not as efficient to control the infection caused by the pathogen as occurs in other clinical forms. It has been described that clinical manifestations in congenital infection are related to a host genetic susceptibility that lead to an insufficient control of the parasite compared to children also congenitally infected but without symptoms (Jamieson et al., 2010).

Additionally, we found interesting association between the presence of ocular and/or cerebral symptoms in the group with congenital toxoplasmosis and the positivity of ELAA test; therefore, the presence of ROP18 could be suggested as a biomarker related to a greater severity in this clinical form. On the other hand, although no statistically significant association was found between the acute or chronic stage of toxoplasmosis and the positivity of the ELAA test, we observed a tendency of higher percentage of positivity and elevated RI values in the group of individuals with toxoplasmic lymphadenitis. This result could suggest that individuals with the acute stage of the infection and the presence of *T. gondii* tachyzoites in blood (Halonen and Weiss, 2013) have more probability to be secreting the ROP18 protein. In support of this assumption, we found a negative correlation with the number of chorioretinal scars, that could be explained because increased number of scar indicates longer time from acquisition that it is related to the number of recurrences in one individual (De-la-Torre et al., 2009). Likewise, in chronic-asymptomatic individuals (negative for the ELAA assay) the absence of the ROP18 protein could be explained by the chronic stage of the infection, in which the parasite is found in a dormant stage called bradyzoite, which is slow growing and it is controlled by the host's immune system (Blader and Saeij, 2009).

Importantly, we didn't find positivity in the ELAA test with serum samples from individuals with dengue virus, which indicated that the test was specific and did not detect antigens from another pathogenic agent. However, it is important to evaluate more serum samples with other parasitic diseases such as malaria and leishmaniosis, as well as with other viral and bacterial infections.

A relevant fact of the present study is the explanation of how the ROP18 protein of *T. gondii* reaches the serum of individuals with toxoplasmosis. Previous studies indicate that ROP18 is secreted by the rhoptry organelles inside the host cell during the process of parasite invasion and later it is located in the membrane of the parasitophorous vacuole (Saeij et al., 2006; Hunter and Sibley, 2012). However, it is possible to suggest that the parasite secretes a certain amount of the ROP18 protein before entering to the host cell and it also could explain the presence of IgM and IgG antibodies in mouse and human serum that recognize specifically the ROP18 protein (Gatkowska et al., 2015; Grzybowski et al., 2015). Additionally, it could be assumed that the ROP18 protein is secreted once the parasite has been established within the host cell. A recent study shows that the secretion of proteins by the microneme organelles is directed by *in vitro* exposure to serum albumin, a host protein (Brown et al., 2016). A similar event could occur with the rhoptry organelles, being stimulated by any host protein to secrets some ROP kinases. Furthermore, we can propose that the ROP18 protein is released after the disruption of the host cell, caused by the uncontrolled replication of the parasite. This cellular breakdown has been reported mainly by infection with type I virulent strains in mice, which are not effectively controlled by the immune system of this murine host (Melo et al., 2011).

In conclusion, two ROP18-aptamers were selected by a SELEX method and were used to standardize an ELAA test. Results showed that AP001 aptamer had a higher affinity for rROP18 and RH *T. gondii* antigen, and therefore it was used to detect ROP18 in serum samples from people with different clinical forms of toxoplasmosis. The ELAA test with AP001 was positive in 60% of people with congenital infection and in 22.6% of the cases with toxoplasmosis. These results suggest that ROP18-ELAA could be used as a potential test to identify severity of the congenital toxoplasmosis. One limitation of this study is that were analyzed only one sample per patient, and it would be important to have a longitudinal follow up in order to identify how is the variation in levels of ROP18 according evolution of symptoms and the effect of treatment. This should be analyzed in a future study. Present findings open new research avenues to understand the role of virulence factors of *T. gondi* on the pathogenesis of toxoplasmosis in humans.

DATA AVAILABILITY STATEMENT

The datasets generated for this study are available on request to the corresponding author.

ETHICS STATEMENT

The studies involving human participants were reviewed and approved by the Institutional Review Board from Universidad Tecnológica de Pereira. Written informed consent to participate in this study was provided by the participants' legal guardian/next of kin.

AUTHOR CONTRIBUTIONS

MV-M: conceptualization, methodology, validation, formal analysis, investigation, and writing-original draft. NC: conceptualization, methodology and formal analysis, and

writing-original draft. DAM: methodology, analysis and formal analysis. DMM: conceptualization, methodology, and formal analysis. YZ: conceptualization, methodology, and writing-review and editing. JG-M: conceptualization, writing-reviewing and editing, supervision.

FUNDING

The project financially supported by the Natural Science Foundation of Shenzhen City (Project number JCYJ20170307150444573 and JCYJ20180306172131515). It was also financed by a Young researcher grant awarded by Colciencias, Colombia.

SUPPLEMENTARY MATERIAL

The Supplementary Material for this article can be found online at: https://www.frontiersin.org/articles/10.3389/fcimb.2019.00386/full#supplementary-material

REFERENCES

Ajzenberg, D. (2012). Editorial commentary: high burden of congenital toxoplasmosis in the United States: the strain hypothesis? *Clin. Infect. Dis.* 54, 1606–1607. doi: 10.1093/cid/cis264

Alegria-Schaffer, A., Lodge, A., and Vattem, K. (2009). Chapter 33 performing and optimizing western blots with an emphasis on chemiluminescent detection. *Methods Enzymol.* 463, 573–599. doi: 10.1016/S0076-6879(09)63033-0

Balogh, Z., Lautner, G., Bardóczy, V., Komorowska, B., Gyurcsányi, R. E., and Mészáros, T. (2010). Selection and versatile application of virus-specific aptamers. *FASEB J.* 24, 4187–4195. doi: 10.1096/fj.09-144246

Behnke, M. S., Khan, A., Lauron, E. J., Jimah, J. R., Wang, Q., Tolia, N. H., et al. (2015). Rhoptry proteins ROP5 and ROP18 are major murine virulence factors in genetically divergent south american strains of *Toxoplasma gondii*. *PLoS Genet.* 11:e1005434. doi: 10.1371/journal.pgen.1005434

Blader, I. J., and Saeij, J. P. (2009). Communication between *Toxoplasma gondii* and its host: impact on parasite growth, development, immune evasion, and virulence. *APMIS* 117, 458–476. doi: 10.1111/j.1600-0463.2009.02453.x

Bradley, P. J., and Sibley, L. D. (2007). Rhoptries: an arsenal of secreted virulence factors. *Curr. Opin. Microbiol.* 10, 582–587. doi: 10.1016/j.mib.2007.09.013

Brown, K. M., Lourido, S., and Sibley, L. D. (2016). Serum albumin stimulates protein kinase G-dependent microneme secretion in *Toxoplasma gondii*. *J. Biol. Chem.* 291, 9554–9565. doi: 10.1074/jbc.M115.700518

Caballero-Ortega, H., Castillo-Cruz, R., Murieta, S., Ortíz-Alegría, L. B., Calderón-Segura, E., Conde-Glez, C. J., et al. (2014). Diagnostic-test evaluation of immunoassays for anti-*Toxoplasma gondii* IgG antibodies in a random sample of Mexican population. *J. Infect. Dev. Ctries.* 8, 642–7. doi: 10.3855/jidc.3858

Cardona, N., Basto, N., Parra, B., Zea, A. F., Pardo, C. A., Bonelo, A., et al. (2011). Detection of toxoplasma DNA in the peripheral blood of HIV-positive patients with neuro-opportunistic infections by a real-time PCR assay. *J. Neuroparasitology* 2, 1–6. doi: 10.4303/jnp/N110402

De La Torre, A., López-Castillo, C. A, and Gómez-Marín, J. E. (2009). Incidence and clinical characteristics in a Colombian cohort of ocular toxoplasmosis. *Eye* 23, 1090–1093. doi: 10.1038/eye.2008.219

de-la- Torre, A., Sauer, A., Pfaff, A. W., Bourcier, T., Brunet, J., Speeg-Schatz, C., et al. (2013). Severe south american ocular toxoplasmosis is associated with decreased Ifn-γ/Il-17a and increased Il-6/Il-13 intraocular levels. *PLoS Negl. Trop. Dis.* 7:e2541. doi: 10.1371/journal.pntd.0002541

de-la-Torre, A., González, G., Díaz-Ramirez, J., and Gómez-Marín, J. E. (2007). Screening by ophthalmoscopy for toxoplasma retinochoroiditis in Colombia. *Am. J. Ophthalmol.* 143, 354–356. doi: 10.1016/j.ajo.2006.09.048

De-la-Torre, A., Rios-Cadavid, A. C., Cardozo-García, C. M., and Gomez-Marín, J. E. (2009). Frequency and factors associated with recurrences of ocular toxoplasmosis in a referral centre in Colombia. *Br. J. Ophthalmol.* 93, 1001–1004. doi: 10.1136/bjo.2008.155861

Drolet, D. W., Moon-McDermott, L., and Romig, T. S. (1996). An enzyme-linked oligonucleotide assay. *Nat. Biotechnol.* 14, 1021–1025. doi: 10.1038/nbt0896-1021

Ellington, A. D., and Szostak, J. W. (1990). *In vitro* selection of RNA molecules that bind specific ligands. *Nature* 346, 818–822. doi: 10.1038/346818a0

Etheridge, R. D., Alaganan, A., Tang, K., Lou, H. J., Turk, B. E., and Sibley, L. D. (2014). The Toxoplasma pseudokinase ROP5 forms complexes with ROP18 and ROP17 kinases that synergize to control acute virulence in mice. *Cell Host Microbe* 15, 537–550. doi: 10.1016/j.chom.2014.04.002

Franco-Hernandez, E. N., Acosta, A., Cortés-Vecino, J., and Gómez-Marín, J. E. (2016). Survey for *Toxoplasma gondii* by PCR detection in meat for human consumption in Colombia. *Parasitol. Res.* 115, 691–695. doi: 10.1007/s00436-015-4790-7

García-Recio, E. M., Pinto-Díez, C., Pérez-Morgado, M. I., García-Hernández, M., Fernández, G., Martín, M. E., et al. (2016). Characterization of MNK1b DNA aptamers that inhibit proliferation in MDA-MB231 breast cancer cells. *Mol. Ther. Acids* 5:e275. doi: 10.1038/mtna.2015.50

Gatkowska, J. M., Grzybowski, M. M., Dziadek, B., Dzitko, K., and Długonska, H. (2015). Human toxoplasmosis: a comparative evaluation of the diagnostic potential of recombinant *Toxoplasma gondii* ROP5 and ROP18 antigens. *J. Med. Microbiol.* 64, 1201–1207. doi: 10.1099/jmm.0.000148

Gilbert, R. E., Freeman, K., Lago, E. G., Bahia-Oliveira, L. M. G., Tan, H. K., Wallon, M., et al. (2008). Ocular sequelae of congenital toxoplasmosis in Brazil compared with Europe. *PLoS Negl. Trop. Dis.* 2:e277. doi: 10.1371/journal.pntd.0000277

Gold, L., Ayers, D., Bertino, J., Bock, C., Bock, A., Brody, E. N., et al. (2010). Aptamer-based multiplexed proteomic technology for biomarker discovery. *PLoS ONE* 5:e15004. doi: 10.1371/journal.pone.0015004

Grigg, M. E., Ganatra, J., Boothroyd, J. C., and Margolis, T. P. (2001). Unusual abundance of atypical strains associated with human ocular toxoplasmosis. *J. Infect. Dis.* 184, 633–639. doi: 10.1086/322800

Grzybowski, M. M., Dziadek, B., Gatkowska, J. M., Dzitko, K., and Długonska, H. (2015). Towards vaccine against toxoplasmosis: evaluation of the immunogenic and protective activity of recombinant ROP5 and ROP18 *Toxoplasma gondii* proteins. *Parasitol. Res.* 114, 4553–4563. doi: 10.1007/s00436-015-4701-y

Hakimi, M.-A., Olias, P., and Sibley, L. D. (2017). Toxoplasma effectors targeting host signaling and transcription. *Clin. Microbiol. Rev.* 30, 615–645. doi: 10.1128/CMR.00005-17

Halonen, S. K., and Weiss, L. M. (2013). Toxoplasmosis. *Handb. Clin. Neurol.* 114, 125–145. doi: 10.1016/B978-0-444-53490-3.00008-X

Hunter, C. A., and Sibley, L. D. (2012). Modulation of innate immunity by *Toxoplasma gondii* virulence effectors. *Nat. Rev. Microbiol.* 10, 766–778. doi: 10.1038/nrmicro2858

Jamieson, S. E., Peixoto-Rangel, A. L., Hargrave, A. C., Roubaix, L. A. D., Mui, E. J., Boulter, N. R., et al. (2010). Evidence for associations between the purinergic receptor P2X 7 (P2RX7) and toxoplasmosis. *Genes Immun.* 11, 374–383. doi: 10.1038/gene.2010.31

Jones, J. L., and Dubey, J. P. (2012). Foodborne toxoplasmosis. *Clin. Infect. Dis.* 55, 845–851. doi: 10.1093/cid/cis508

Lebech, M., Joynson, D. H. M., Seitz, H. M., Thulliez, P., Gilbert, R. E., Dutton, G. N., et al. (1996). Classification system and case definitions of *Toxoplasma gondii* infection in immunocompetent pregnant women and their congenitally infected offspring. *Eur. J. Clin. Microbiol. Infect. Dis.* 15, 799–805. doi: 10.1007/BF01701522

Lora-Suárez, F. M., Aricapa, H., Perez, J. E., Arias, L., Idarraga, S., Mier, D., et al. (2007). Detección de *Toxoplasma gondii* en carnes de consumo humano por la

técnica de reacción en cadena de la polimerasa en tres ciudades del eje cafetero. *Infectio* 11, 117–123. Available online at: http://revistainfectio.org/index.php/infectio/article/view/150/185

Luo, Y., Liu, X., Jiang, T., Liao, P., and Fu, W. (2013). Dual-aptamer-based biosensing of toxoplasma antibody. *Anal. Chem.* 85, 8354–8360. doi: 10.1021/ac401755s

Martin, M. E., Garcia-Hernandez, M., Garcia-Recio, E. M., Gomez-Chacon, G. F., Sanchez-Lopez, M., and Gonzalez, V. M. (2013). DNA aptamers selectively target leishmania infantum H2A protein. *PLoS ONE* 8:e78886. doi: 10.1371/journal.pone.0078886

McLeod, R., Boyer, K. M., Lee, D., Mui, E., Wroblewski, K., Karrison, T., et al. (2012). Prematurity and severity are associated with *toxoplasma gondii* alleles (NCCCTS, 1981–2009). *Clin. Infect. Dis.* 54, 1595–1605. doi: 10.1093/cid/cis258

Melo, M. B., Jensen, K. D. C., and Saeij, J. P. J. (2011). *Toxoplasma gondii* effectors are master regulators of the inflammatory response. *Trends Parasitol.* 27, 487–495. doi: 10.1016/j.pt.2011.08.001

Murphy, M. B., Fuller, S. T., Richardson, P. M., and Doyle, S. A (2003). An improved method for the *in vitro* evolution of aptamers and applications in protein detection and purification. *Nucleic Acids Res.* 31:e110. doi: 10.1093/nar/gng110

Ospina-Villa, J. D., López-Camarillo, C., Castañón-Sánchez, C. A., Soto-Sánchez, J., Ramírez-Moreno, E., and Marchat, L. A. (2018). Advances on aptamers against protozoan parasites. *Genes.* 9:E584. doi: 10.3390/genes9120584

Pappas, G., Roussos, N., and Falagas, M. E. (2009). Toxoplasmosis snapshots: global status of *Toxoplasma gondii* seroprevalence and implications for pregnancy and congenital toxoplasmosis. *Int. J. Parasitol.* 39, 1385–1394. doi: 10.1016/j.ijpara.2009.04.003

Petersen, E., Ajzenberg, D., Mandelbrot, L., and Gomez-Marin, J. E. (2017). "Protozoan diseases: toxoplasmosis," in *International Encyclopedia of Public Health*, ed S. R. Quah (Amsterdam: Elsevier), 114–132. doi: 10.1016/B978-0-12-803678-5.00361-1

Pfaff, A. W., de-la-Torre, A., Rochet, E., Brunet, J., Sabou, M., Sauer, A., et al. (2014). New clinical and experimental insights into Old World and neotropical ocular toxoplasmosis. *Int. J. Parasitol.* 44, 99–107. doi: 10.1016/j.ijpara.2013.09.007

Ramos, E., Piñeiro, D., Soto, M., Abanades, D. R., Martín, M. E., Salinas, M., et al. (2007). A DNA aptamer population specifically detects Leishmania infantum H2A antigen. *Lab. Invest.* 87, 409–416. doi: 10.1038/labinvest.3700535

Reese, M. L., Zeiner, G. M., Saeij, J. P. J., Boothroyd, J. C., and Boyle, J. P. (2011). Polymorphic family of injected pseudokinases is paramount in Toxoplasma virulence. *Proc. Natl. Acad. Sci. U.S.A.* 108, 9625–9630. doi: 10.1073/pnas.1015980108

Robertson, L. J., van der Giessen, J. W. B., Batz, M. B., Kojima, M., and Cahill, S. (2013). Have foodborne parasites finally become a global concern? *Trends Parasitol.* 29, 101–103. doi: 10.1016/j.pt.2012.12.004

Rotherham, L. S., Maserumule, C., Dheda, K., Theron, J., and Khati, M. (2012). Selection and application of ssDNA aptamers to detect active TB from sputum samples. *PLoS ONE* 7:e46862. doi: 10.1371/journal.pone.0046862

Saeij, J. P. J., Boyle, J. P., Coller, S., Taylor, S., Sibley, L. D., Brooke-Powell, E. T., et al. (2006). Polymorphic secreted kinases are key virulence factors in toxoplasmosis. *Science* 314, 1780–1783. doi: 10.1126/science.1133690

Sánchez, V., De-la-Torre, A., and Gómez-Marín, J. E. (2014). Characterization of ROP18 alleles in human toxoplasmosis. *Parasitol. Int.* 63, 463–469. doi: 10.1016/j.parint.2013.10.012

Stoltenburg, R., Krafčiková, P., Víglaský, V., and Strehlitz, B. (2016). G-quadruplex aptamer targeting Protein A and its capability to detect Staphylococcus aureus demonstrated by ELONA. *Sci. Rep.* 6:33812. doi: 10.1038/srep33812

Talevich, E., and Kannan, N. (2013). Structural and evolutionary adaptation of rhoptry kinases and pseudokinases, a family of coccidian virulence factors. *BMC Evol. Biol.* 13:117. doi: 10.1186/1471-2148-13-117

Taylor, S., Barragan, A., Su, C., Fux, B., Fentress, S. J., Tang, K., et al. (2006). A secreted serine-threonine kinase determines virulence in the eukaryotic pathogen *Toxoplasma gondii*. *Science* 314, 1776–1780. doi: 10.1126/science.1133643

Toh, S. Y., Citartan, M., Gopinath, S. C. B., and Tang, T.-H. (2015). Aptamers as a replacement for antibodies in enzyme-linked immunosorbent assay. *Biosens. Bioelectron.* 64, 392–403. doi: 10.1016/j.bios.2014.09.026

Torgerson, P. R., and Mastroiacovo, P. (2013). The global burden of congenital toxoplasmosis: a systematic review. *Bull. World Health Organ.* 91, 501–508. doi: 10.2471/BLT.12.111732

Torres-Morales, E., Taborda, L., Cardona, N., De-la-Torre, A., Sepulveda-Arias, J. C. J. C., Patarroyo, M. A. M. A., et al. (2014). Th1 and Th2 immune response to P30 and ROP18 peptides in human toxoplasmosis. *Med. Microbiol. Immunol.* 203, 315–322. doi: 10.1007/s00430-014-0339-0

Triviño-Valencia, J., Lora, F., Zuluaga, J. D., and Gomez-Marin, J. E. (2016). Detection by PCR of pathogenic protozoa in raw and drinkable water samples in Colombia. *Parasitol. Res.* 115, 1789–1797. doi: 10.1007/s00436-016-4917-5

Tuerk, C., and Gold, L. (1990). Systematic evolution of ligands by exponential enrichment: RNA ligands to bacteriophage T4 DNA polymerase. *Science* 249, 505–510. doi: 10.1126/science.2200121

Vivekananda, J., and Kiel, J. L. (2006). Anti-Francisella tularensis DNA aptamers detect tularemia antigen from different subspecies by Aptamer-Linked Immobilized Sorbent Assay. *Lab. Invest.* 86, 610–618. doi: 10.1038/labinvest.3700417

Zhang, Y., Lai, B., and Juhas, M. (2019). Recent advances in aptamer discovery and applications. *Molecules* 24:941. doi: 10.3390/molecules24050941

Zhou, J., and Rossi, J. (2017). Aptamers as targeted therapeutics: current potential and challenges. *Nat. Rev. Drug Discov.* 16:440. doi: 10.1038/nrd.2017.86

Conflict of Interest: The authors declare that the research was conducted in the absence of any commercial or financial relationships that could be construed as a potential conflict of interest.

frontiers in Cellular and Infection Microbiology

ORIGINAL RESEARCH
published: 27 November 2019
doi: 10.3389/fcimb.2019.00395

Toxoplasma gondii Impairs Myogenesis *in vitro*, With Changes in Myogenic Regulatory Factors, Altered Host Cell Proliferation and Secretory Profile

*Paloma de Carvalho Vieira[1], Mariana Caldas Waghabi[2], Daniela Gois Beghini[3], Danilo Predes[4], Jose Garcia Abreu[4], Vincent Mouly[5], Gillian Butler-Browne[5], Helene Santos Barbosa[1] and Daniel Adesse[1]**

[1] Laboratório de Biologia Estrutural, Instituto Oswaldo Cruz, Fiocruz, Rio de Janeiro, Brazil, [2] Laboratório de Genômica Funcional e Bioinformática, Instituto Oswaldo Cruz, Fiocruz, Rio de Janeiro, Brazil, [3] Laboratório de Inovação em Terapias, Ensino e Bioprodutos, Instituto Oswaldo Cruz, Fiocruz, Rio de Janeiro, Brazil, [4] Laboratório de Embriologia de Vertebrados, Instituto de Ciências Biomédicas, Universidade Federal do Rio de Janeiro, Rio de Janeiro, Brazil, [5] Sorbonne Université, INSERM, Institut de Myologie, Myology Research Center UMRS974, Paris, France

OPEN ACCESS

Edited by:
Jeroen P. J. Saeij,
University of California, Davis,
United States

Reviewed by:
Carsten Lüder,
Institut für Medizinische Mikrobiologie,
Universitätsmedizin
Göttingen, Germany
Sarah Ewald,
University of Virginia, United States

***Correspondence:**
Daniel Adesse
adesse@ioc.fiocruz.br

Specialty section:
This article was submitted to
Parasite and Host,
a section of the journal
Frontiers in Cellular and Infection
Microbiology

Received: 21 June 2019
Accepted: 04 November 2019
Published: 27 November 2019

Citation:
Vieira PC, Waghabi MC, Beghini DG, Predes D, Abreu JG, Mouly V, Butler-Browne G, Barbosa HS and Adesse D (2019) Toxoplasma gondii Impairs Myogenesis in vitro, With Changes in Myogenic Regulatory Factors, Altered Host Cell Proliferation and Secretory Profile. Front. Cell. Infect. Microbiol. 9:395. doi: 10.3389/fcimb.2019.00395

Toxoplasma gondii is the causative agent of toxoplasmosis, a parasitic disease with a wide global prevalence. The parasite forms cysts in skeletal muscle cells and neurons, although no evident association with inflammatory infiltrates has been typically found. We studied the impact of *T. gondii* infection on the myogenic program of mouse skeletal muscle cells (SkMC). The C2C12 murine myoblast cell line was infected with *T. gondii* tachyzoites (ME49 strain) for 24 h followed by myogenic differentiation induction. *T. gondii* infection caused a general decrease in myotube differentiation, fusion and maturation, along with decreased expression of *myosin heavy chain*. The expression of Myogenic Regulatory Factors Myf5, MyoD, Mrf4 and myogenin was modulated by the infection. Infected cultures presented increased proliferation rates, as assessed by Ki67 immunostaining, whereas neither host cell lysis nor apoptosis were significantly augmented in infected dishes. Cytokine Bead Array indicated that IL-6 and MCP-1 were highly increased in the medium from infected cultures, whereas TGF-β1 was consistently decreased. Inhibition of the IL-6 receptor or supplementation with recombinant TGF-β failed to reverse the deleterious effects caused by the infection. However, conditioned medium from infected cultures inhibited myogenesis in C2C12 cells. Activation of the Wnt/β-catenin pathway was impaired in *T. gondii*-infected cultures. Our data indicate that *T. gondii* leads SkMCs to a pro-inflammatory phenotype, leaving cells unresponsive to β-catenin activation, and inhibition of the myogenic differentiation program. Such deregulation may suggest muscle atrophy and molecular mechanisms similar to those involved in myositis observed in human patients.

Keywords: *Toxoplasma gondii*, myogenesis, C2C12 cells, myotube, myogenic regulatory factor, congenital toxoplasmosis

INTRODUCTION

Toxoplasma gondii is an obligate intracellular protozoan parasite that can cause a devastating disease in immune-compromised patients and fetuses (Montoya and Liesenfeld, 2004; Dubey, 2008). Transmission occurs by ingestion of tissue cysts, present in undercooked meat, or by ingestion/inhalation of sporulated oocysts that are shed along with the feces of infected felids (Dubey and Frenkel, 1972). The cysts rupture inside the host's digestive system and release the parasites, which rapidly infect host cells and, in a few days, spread throughout the entire organism. The ability for the parasite to cause disease is directly linked to its replication inside a parasitophorous vacuole in the cytoplasm of host cells. From this vacuole, parasites scavenge nutrients from the host cell while causing reorganization of host organelles and cytoskeletal elements, preventing host cell apoptosis and altering host gene expression to its own benefit (Saeij et al., 2007; Wu et al., 2016; Acquarone et al., 2017).

Upon the host's immunological response, intracellular tachyzoites differentiate into slow-dividing bradyzoite forms, which, in turn modify the parasitophorous vacuole membrane, transforming it into the newly formed cyst wall. *T. gondii* displays an interesting interaction with post-mitotic cells, and cysts can be found in the neurons and skeletal muscle fibers of chronically infected individuals (Dubey, 1998). Intense myositis, altered electromyograms and reduced grip strength have also been reported in immunocompetent infected humans (Montoya et al., 1997; Hassene et al., 2008; Cuomo et al., 2013), suggesting that infection impairs skeletal muscle function.

In order to better characterize the interplay between *T. gondii* and skeletal muscle cells (SkMC), our group used a primary mouse SkMC culture that promotes high rates of spontaneous tachyzoite-bradyzoite conversion (Guimarães et al., 2008; Ferreira-da-Silva Mda et al., 2009) and leads to the production of inflammatory intermediates, such as prostaglandins, IFN-γ and interleukin-12 (Gomes et al., 2014). We have also described a decrease in M-cadherin content in primary SkMC cultures infected by *T. gondii* and a reduction in the number of myotubes when muscle cells were infected with the highly virulent RH strain (Gomes et al., 2011).

Myogenesis is a precisely coordinated differentiation program, starting from the first weeks of embryonic development, when somitic cells generate muscle cell progenitors, called myoblasts (Berendse et al., 2003). These elongated mononucleated cells progressively fuse to form long, multinucleated fibers called myotubes that express the differentiated gene pattern of mature muscle cells (Dedieu et al., 2002). Muscle cell early determination and differentiation are controlled by a set of transcription factors (McKarney et al., 1997), known as Myogenic Regulatory Factors (MRFs), which are active at precise developmental stages and functionally correlated to each other (De Angelis et al., 1999). Myf5 and MyoD control paraxial muscle differentiation, and both activate myogenin, known to be associated with final muscle maturation. Mrf4 plays a role in determining the fiber phenotype in postnatal life (Zhang et al., 1995), although a potential role during early development has also been suggested (Kassar-Duchossoy et al., 2004). The expression of muscle-specific proteins (such as α-actin, myosin heavy and light chain, tropomyosin, among others) is closely MRF-dependent. Myogenesis is also crucial for SkMC repair in adult life, through the activation and differentiation of adult muscle stem cells, also named satellite cells.

We investigated which mechanisms underlie myogenesis defects during *T. gondii* infection, using the C2C12 mouse myoblast cell line, since they allow for myogenic differentiation process synchronization. Using this model, we describe how *T. gondii* affects MRFs expression and other mechanisms, such as proliferation, apoptosis and cytokines/chemokines secretion and we identified defects in the Wnt/β-catenin pathway activation, which is also involved in myogenesis.

METHODS

Cell Culture

The mouse skeletal myoblast C2C12 cell line was purchased from ATCC and maintained in a proliferation medium [PM, DMEM high glucose (Sigma Aldrich) with 10% fetal bovine serum (Cultilab, São Paulo, Brazil) and 1% antibiotic solution (Thermo Fisher)]. Before reaching confluency, cells were dissociated with Trypsin/EDTA solution in PBS and plated for experiments. For myogenesis induction, cells were cultivated in PM until reaching 70% confluency, when the medium was changed to a differentiation medium (DM, DMEM with 2% horse serum and 1% antibiotics solution).

T. gondii Infection

Parasites from the ME49 strain were obtained from the brains of C57Bl/6 mice infected 45 days before isolation. Cysts were ruptured with an acid pepsin solution and free parasites were added to Vero cell (ATCC) monolayers. After 2 weeks of culture re-infections, tachyzoites released from the supernatant were collected and centrifuged prior to use. For the experiments, 60,000 C2C12 cells were plated onto 13-mm diameter glass round coverslips in 500 μl of PM per well for 24 h. Subsequently, cultures were infected with tachyzoites at a MOI of 3:1 parasite:host cell for 2 h. Cells were then washed in Ringer solution, fresh PM was added, and cells were then maintained at 37°C for an additional 22 h. After this period (total of 24 h of infection), half of the cultures were switched to DM while the other half was maintained in PM. The cultures were analyzed at 24 and 120 h after differentiation induction, corresponding to 48 and 144 h of infection, respectively.

Immunofluorescence

Cells were plated onto 13-mm glass round coverslips in 24-well plates. At desired times, the conditioned medium was collected for cytokine analyses, as described below. Cultures were washed in PBS and fixed with 4% paraformaldehyde for 5 min at 20°C, permeabilized with a 0.5% Triton x-100 (Sigma Aldrich) solution in PBS, blocked with 4% bovine serum albumin solution for 30 min and incubated overnight with primary antibodies at 4°C. The primary antibodies used in this study

and their references are listed in **Table 1**. Secondary antibodies goat anti-mouse conjugated to AlexaFluor 594 and donkey anti-rabbit conjugated to AlexaFluor 488 (Thermo Fisher) were incubated for 1 h at 37°C. For necrosis assessments, live cells were incubated with 40 μg/ml propidium iodide solution diluted in PBS for 10 min. As a positive control, 0.25% Triton x-100 was incubated on a separate coverslip for 5 min at 37 °C. Nuclei were visualized by incubating the cells with DAPI (4',6-diamidino-2-phenylindole dihydrochloride) at 0.2 μg/ml for 5 min at 20°C and slides were mounted in a DABCO solution containing 50% glycerol.

Real Time qPCR

A total of 6.6×10^5 cells were cultured in 60 mm plastic petri dishes (Corning) and total RNA was extracted using the RNeasy kit (Qiagen). Contamination with genomic DNA was avoided by treating the samples with DNase I (Qiagen) following the manufacturer's instructions. Concentrations were measured using a NanoDrop equipment (Thermo Fisher) and RNA samples were validated for the experiments when the 260/230 ratio was above 1.9. A total of 1 μg of total RNA was reversely transcribed into cDNA with Superscript III kit (Invitrogen). Real time PCR analyses were performed with 0.5 μL of cDNA and Power SYBR Green Master Mix (Thermo Fisher) and 0.05 μmol/L of endogenous control (PPIA) or 0.027 μmol/L of muscle-specifics primers. Cycling conditions were 94°C for 10 min, followed by 40 cycles of 94°C for 30 s and 60°C for 30 s, with a fluorescence reading at the end of each cycle. Target gene expression data were plotted as normalized by endogenous control (PPIA) and relative to uninfected cells maintained in PM for each time point, using $2^{-\Delta\Delta ct}$. The primer sequences used herein are listed in **Table 2**.

TGF-β1 Measurements

Conditioned medium was obtained from C2C12 cultures at the different experimental conditions analyzed, as described above. To obtain conditioned medium for cytokine assays, each well of 24-well plates was incubated with 300 μl of either PM or DM for 1 day. The medium was collected in 1.5 ml centrifuge tubes and kept on ice, centrifuged at 14,000 rpm for 5 min. Supernatants were then transferred to new tubes and the conditioned medium was kept at −80°C until use. Total TGF-β1 levels present in the conditioned medium derived from C2C12 cultures were measured using the Mouse TGF-β1 ELISA DuoSet Kit (R&D Systems) following the manufacturer's instructions. Proliferation and differentiation media not exposed to cells were also measured to determine basal TGF-β1 levels. The results of final secretion from the C2C12 supernatants was calculated by subtracting the basal values of either PM or DM from each sample.

Cytokine Bead Array (CBA)

Cytokine levels were evaluated by flow cytometry in culture supernatants of infected or uninfected C2C12 cells, in PM or DM at 24 and 120 h of induction. IL-6, IL-10, IL-12p70, TNF, IFN-γ, and MCP-1 were detected using a Cytometric Bead Array (CBA) Mouse Inflammation kit (BD), according to the manufacturer's instructions. Data were acquired using a FACScalibur flow cytometer (BD), and the data analysis was performed by a CBA analysis using the FCAP software (BD).

Treatments With Conditioned Medium

Conditioned medium (CM) obtained from C2C12 cells, as described in Section TGF-β1 Measurements, was used to treat fresh C2C12 cells. Cells were plated on coverslips in PM. After

TABLE 1 | List of primary antibodies used for the immunofluorescence assays.

Antibody	Host species	Company name	Reference number	Dilution
Myogenin	Mouse	DSHB	F5D-s	1:100
MyHC type II (fast twitch)	Mouse	Sigma Aldrich	M4276	1:400
MyHC type I	Mouse	DSHB	MF20	1:25
MyoD	Mouse	DSHB	D7F2-s	1:100
Desmin	Rabbit	Sigma Aldrich	D8281	1:100
Ki67	Rabbit	ABCAM	ab15580	1:80
SAG1 (P30)	Mouse	Santa Cruz Biotechnologies	Sc-52255	1:100
Cleaved Caspase-3	Rabbit	Cell signaling	9661	1:400

TABLE 2 | List of primers used for RT-qPCR.

Gene name	Sense sequence	Anti-sense sequence	References
MyHC beta (slow twitch)	CGCAATGCAGAGTCAGTGAA	TTGCGGAACTTGGACAGGTT	Nishida et al., 2015
myogenin	CTACAGGCCTTGCTCAGCTC	ACGATGGACGTAAGGGAGTG	Hildyard and Wells, 2014
MyoD	TACAGTGGCGACTCAGATGC	GAGATGCGCTCCACTATGCT	Hildyard and Wells, 2014
Myf5	CTGTCTGGTCCCGAAAGAAC	AGCTGGACACGGAGCTTTTA	Hildyard and Wells, 2014
Mrf4	GGCTGGATCAGCAAGAGAAG	CCTGGAATGATCCGAAACAC	Hunt et al., 2013
PPIA (*Peptidyl-prolyl cis-trans isomerase*)	GGCCGATGACGAGCCC	TGTCTTTGGAACTTTGTCTGCAA	Hunt et al., 2013

24 h of plating, cultures were treated with CM diluted 1:1 in fresh medium (either PM or DM). The medium was replaced daily for 5 days and cells were fixed for immunofluorescence. Untreated controls were maintained either in PM or DM.

Dual Luciferase Reporter Assay

6×10^4 C2C12 cells/well were cultured on 24-well plates in DMEM containing 10% fetal bovine serum (Gibco) without antibiotics. Twenty-four hours later, cells were transfected with 200 ng TOPFLASH plasmid and 100 ng Tk-Renilla plasmid using FuGENE HD (Promega) at 4:1 ratio. 18 h after transfection, cells were infected with 3.6×10^5 tachyzoite *T. gondii* forms (ME49 strain). After 2 h, cells were washed with simple medium and fresh proliferation medium was added. After 22 h, the medium of half of the cells was switched to DM and/or were treated with 2 μM BIO (CAS Number 667463-62-9, Sigma) for 20 h in order to activate the Wnt/β-catenin signaling pathway. Cells were then lysed using Passive Lysis Buffer (Promega) and Firefly and Renilla luciferase activities were detected according to the manufacturer's protocol (Dual Luciferase Reporter Assay System, Promega).

Morphometric and Statistical Analyses

At least six microscopic fields were obtained from each experimental condition in three independent experiments, corresponding to a 0.09 mm^2 area each. The relative differentiation rate was calculated by counting the number of nuclei inside MyHC-positive cells divided by the number of total DAPI positive cells per microscopy field. The relative fusion index was determined as the number of MyHC-positive cells with more than two nuclei and divided by the total number of cells (DAPI-positive) per microscopic field (Joulia et al., 2003). The number of mature myotubes was estimated by the number of MyHC-positive cells that contained at least five myonuclei divided by the number of MyHC-positive cells per field, multiplied by 100. Morphometric analyses of the myotube areas were performed with the Zen Software (Zeiss) using images acquired with a confocal Zeiss microscope (Plataforma de Microscopia Óptica de Luz Gustavo de Oliveira Castro, PLAMOL, UFRJ). The percentage of positive myogenin and MyoD positive nuclei were obtained by dividing the number of positive nuclei by the total number of DAPI positive nuclei per microscopic field and multiplied by 100. Data were analyzed using the GraphPad Prism software version 5.0 for Windows, GraphPad Software, La Jolla California USA, www.graphpad.com. A two-way ANOVA test was used applying Bonferroni's post-test, and changes were considered statistically significant when $p < 0.05$. An unpaired Student's *T*-test was applied to the morphometric analyses, also considering statistically significant changes when $p < 0.05$.

RESULTS

T. gondii Impairs C2C12 Differentiation and Fusion

C2C12 cells were infected by *T. gondii* as described in the section Method. The establishment of *T. gondii* infection was assessed by light microscopy, in Giemsa-stained cells (**Figures S1**, **S2**), and by immunofluorescence to SAG1, a marker for the tachyzoite forms of the parasite (**Figure 1**). Twenty-four hours post-infection, cells were either maintained in proliferation conditions or switched to differentiation by changing their medium for DM. 24 h later, corresponding to 48 h post infection (hpi), cultures maintained with PM or DM displayed a total of 4.5 ± 3.3 and 6.5 ± 2% of cells bearing parasites, respectively (**Figure 1**). One hundred and forty-four hours post infection, cultures maintained in PM exhibited 29 ± 9.8% cells containing intracellular parasites, whereas cells in DM displayed 13 ± 7.2% parasitism ($p < 0.01$).

The impact of *T. gondii* on the capacity of C2C12 cells to differentiate and fuse was evaluated as indicated by Giemsa staining (**Figures S1**, **S2**) and MyHC immunostaining (**Figure 2**),

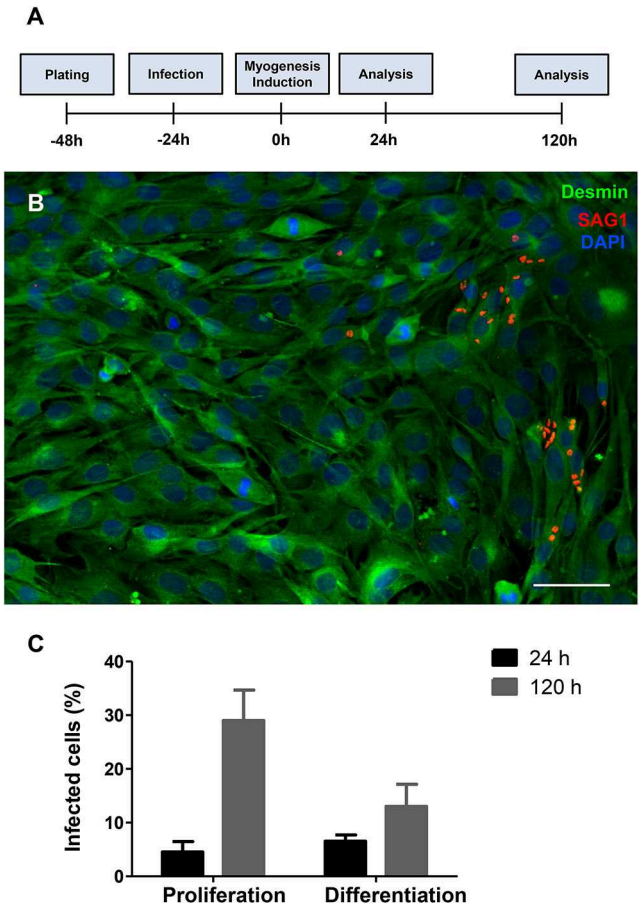

FIGURE 1 | *T. gondii* infection profile in C2C12 cells. The experimental design is shown in **(A)** Cells are plated and infected with tachyzoites after 24 h of plating. Then, half of the cultures have their medium changed to DM. Analyses were carried out 24 and 120 h after myogenesis stimulus with DM. Enrichment in muscle cells was confirmed by desmin staining (**B**, in green) and the presence of tachyzoite forms of *T. gondii* was detected with anti-SAG1 staining (red) as shown in this representative micrograph of infected cells treated with DM for 24 h. Cells were stained with Giemsa stain and the percentage of infected cells was determined by light microscopy. Graphs in **(C)** show the average and standard error of three independent experiments. Scale bar = 50 μm.

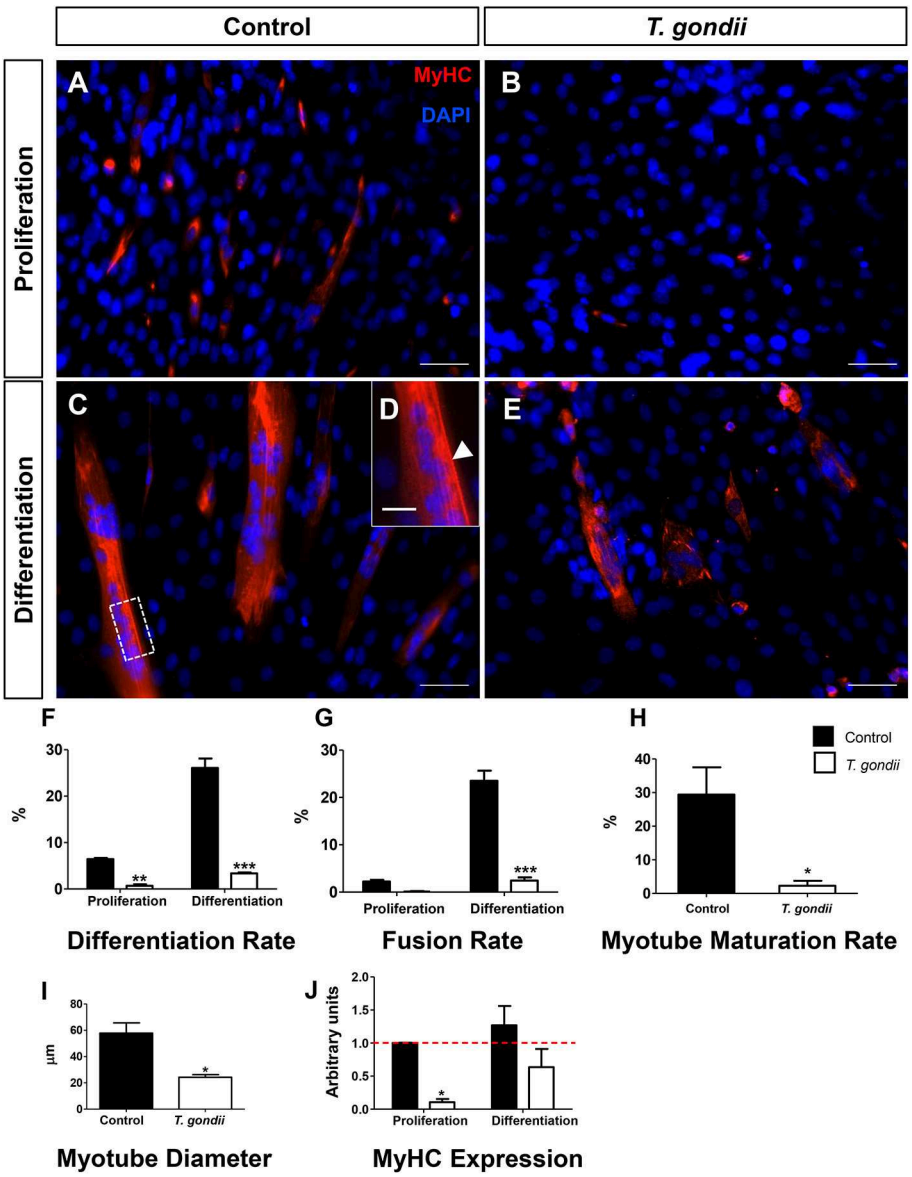

FIGURE 2 | *T. gondii* impairs myogenesis and myotube maturation. C2C12 cells were stained for MyHC, a terminal marker of SkMC differentiation and analyzed by confocal microscopy **(A–E)**. Differentiation was considered in positively MyHC-stained cells **(F)**. Treatment with DM for 5 days greatly increased the number of stained cells from 6 to 26% in uninfected cultures **(F)**. *T. gondii* infection reduced the differentiation rate. Decreases in fusion rates were also observed in *T. gondii*-infected cultures **(G)**, as determined by the number of nuclei within MyHC-positive cells with at least two nuclei. Myotube formation was also impaired by infection in DM treated cultures **(H)**. The deleterious effect of the infection was also reflected in the size of the myotubes **(I)**. Changes in myogenesis induced by the parasite were also observed at the transcriptional level, since MyHC mRNA levels were reduced in infected cultures **(J)**. Results of at least three independent experiments. $^{*}p < 0.05$, $^{**}p < 0.01$; $^{***}p < 0.0001$, Two-Way ANOVA with Bonferroni post-test. Red dotted line represents the value of control uninfected cultures maintained in Proliferation Medium. Scale bars in **(A–C,E)** = 50 µm, **(D)**= 20 µm.

after 120 h. Cells maintained in PM exhibited low levels of differentiation (cells with positive MyHC staining with at least one nucleus), as indicated by <6.4 ± 0.4% MyHC positivity, whereas uninfected dishes maintained in DM reached 26 ± 0.3% of MyHC-stained cells, either mononuclear or multinuclear cells (**Figures 2A,C,D**). Notably, *T. gondii* infection was highly disruptive to C2C12 differentiation, since infected cultures kept either in PM and DM exhibited only 0.6 and 3.3% MyHC positive stained cells, respectively (**Figures 2B,E,F**). While uninfected cells in PM exhibited a low basal fusion (2.2%), uninfected DM-treated cultures reached 23%. Infected cultures maintained in DM presented a drastic reduction in the number of fused cells (2.44%, $p < 0.0001$) when compared to uninfected cells maintained in DM (**Figure 2G**). This reduction in fusion rates led to a proportional decrease in the number of mature myotubes in infected cultures (2.2 vs. 29.4% in uninfected controls, $p <$

0.05, Unpaired Student's t test, **Figure 2H**). Myotubes found in infected cultures also displayed decreased diameter (57.8 vs. 24.2 μm, $p < 0.05$, Unpaired Student's *t*-test, **Figure 2I**). To confirm that *T. gondii* infection impairs myocyte differentiation, RT-qPCR for *myosin heavy chain* was performed. Five days after myogenesis induction, DM-treated cultures exhibited a slight, yet not statistically significant, increase in *MyHC* expression when compared to PM (1.3-fold, $p > 0.05$). *T. gondii*-infected dishes showed a drastic down-regulation of *MyHC* expression, both in PM (90%, $p < 0.05$) and DM (63%, $p > 0.05$) (**Figure 2J**).

Infection Alters MRFs Expression/Immunoreactivity

The influence of *T. gondii* infection on the expression and immunolocalization of myogenic regulatory transcription factors (MRFs) MyoD, myogenin, Myf5, and Mrf4 (Myf6) was assessed on C2C12 cells.

Myf5, expressed in committed satellite cells and myoblasts showed no change after 24 h of culture in DM (**Figure 3A**). However, after 120 h, non-infected cultures maintained in DM exhibited an 83% decrease in Myf5 expression, as indicated by RT-qPCR (**Figure 3B**). Interestingly, at this time point *T. gondii*-infected cultures displayed higher Myf5 levels when compared to their respective controls (1.85-fold in PM and 3.58-fold in DM, $p < 0.0001$ and $p < 0.01$, respectively, Two-Way ANOVA with Bonferroni post-test), confirming their immaturity regarding myogenesis.

Next, the presence of MyoD, an activated myoblast and myocyte marker, was investigated. No changes in MyoD immunostaining were detected in infected dishes after 24 h of differentiation (48 hpi) when compared to non-infected cultures (**Figures 3C,G,E**). However, at 120 h, the number of

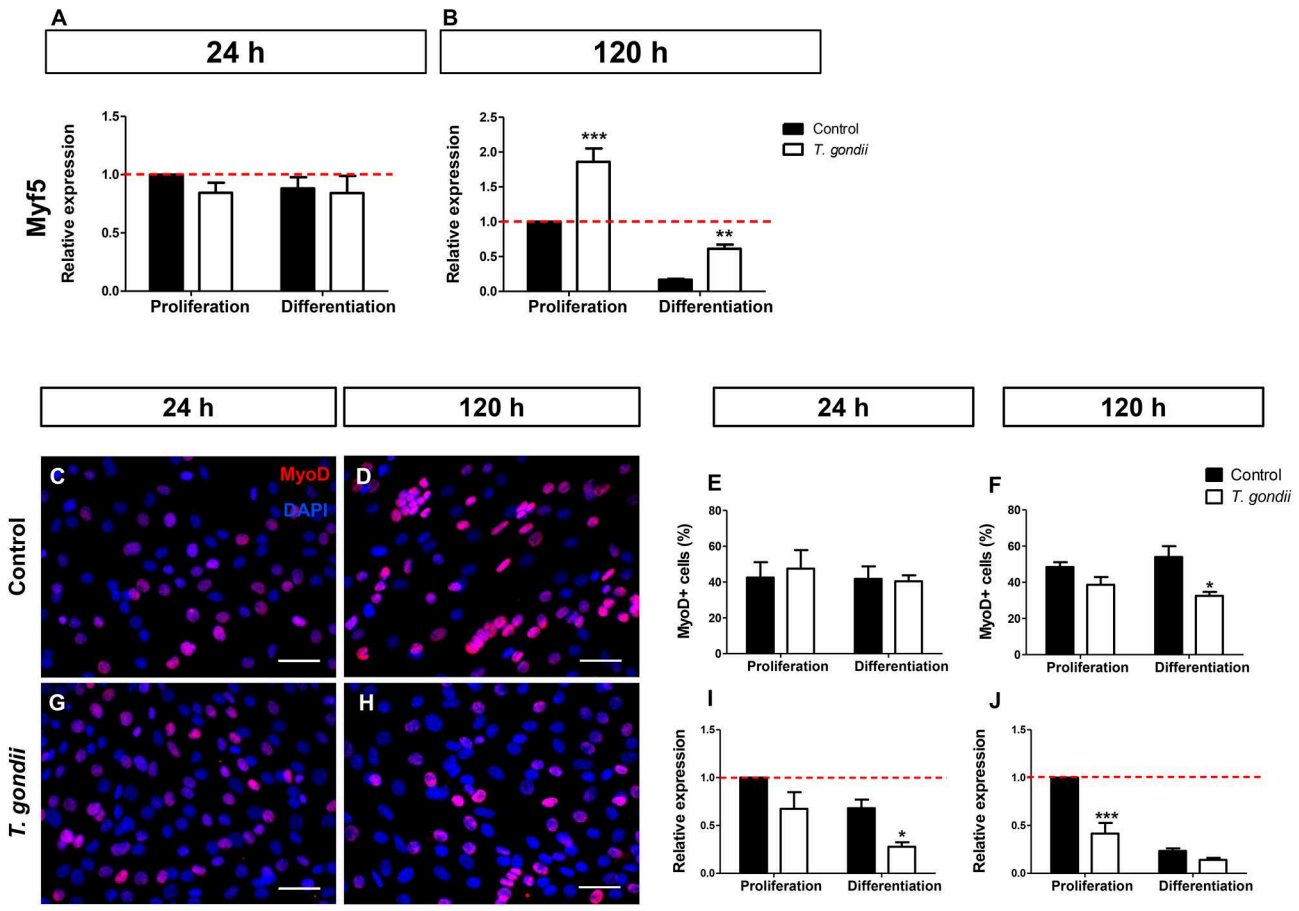

FIGURE 3 | Infection affects early myogenic gene expression. Relative expression of Myf5 was analyzed by RT-qPCR. Myf5 levels were determined at the initial time of myogenesis (24 h, **A**) and at the latest time point (120 h, **B**). Uninfected and infected cells in PM or DM were immunostained for MyoD (red) and DAPI (blue) at 24 **(C,G)** and 120 h of induction **(D,H)**. Quantification of MyoD-positive cells at 24 h indicate that infection led to no significant changes in the number of MyoD cells **(E)**. After 120 h of myogenic stimulation, infected-DM cultures displayed 32% of MyoD-positive cells, whereas in uninfected DM dishes a 54% rate was observed **(F)**. RT-qPCR revealed that at 24 h of induction, MyoD transcript was significantly less abundant in infected-DM dishes, when compared to the controls **(I)**. During late stage myogenesis (120 h), *T. gondii*-infected cells in PM presented a 59% decrease in MyoD expression when compared to controls **(J)**. Results of at least three independent experiments $^{*}p < 0.05$, $^{**}p < 0.01$; $^{***}p < 0.0001$, Two-Way ANOVA with Bonferroni post-test. The red dotted line represents the value of control uninfected cultures maintained in the Proliferation Medium. Scale bar = 50 μm.

MyoD-positive cells were decreased by 21% ($p > 0.05$) and 40% ($p < 0.05$, Two-way ANOVA, with Bonferroni post-test) in infected cultures maintained in PM and DM, respectively, when compared to uninfected ones (**Figures 3D,H,F**). The RT-qPCR analysis confirmed altered MyoD expression after *T. gondii* infection. After 24 h of differentiation in DM, uninfected cultures showed no significant alteration in MyoD expression when compared to PM, although a decreasing trend was observed (**Figure 3I**). At this time point, *T. gondii* infection induced a decrease in MyoD expression in cultures maintained in PM (33%, $p > 0.05$) and in DM (60%, $p < 0.05$, Two-way ANOVA, with Bonferroni post-test) when compared to uninfected cultures at 24 h (**Figure 3I**). The same effect was observed at 120 h of myogenesis induction. *T. gondii*-infected cultures displayed a 59% ($p < 0.0001$) and 40% ($p > 0.05$) decrease when compared to their respective uninfected cultures in PM and DM, respectively (**Figure 3J**).

Mrf4, expressed only in later stages of the myogenic process, was analyzed by RT-qPCR. The levels of *Mrf4* transcripts in our cultures were low, with CT values near 35. No significant changes in *Mrf4* relative expression were verified in our cultures (**Figures 4A,B**).

Finally, the expression and immunoreactivity of *myogenin* in C2C12 cells was evaluated. At 24 h of differentiation in DM, 5% of the uninfected cells were *myogenin*+ while *T. gondii*-infected cultures showed only 2% of positivity ($p < 0.05$, Two-Way ANOVA, with Bonferroni post-test, **Figures 4C,G,E**). At 120 h of differentiation, this number increased to 28.35% when compared to cells in PM (14.3%) (**Figures 4D,H,F**). *T. gondii* infection induced a strong inhibition of *myogenin* immunoreactivity at 120 h of differentiation (144 hpi). Infected cultures in PM displayed 2.96% of *myogenin*-positive nuclei and those kept in DM showed only 12.34% positivity. This observation was confirmed by RT-qPCR, indicating that uninfected cells in DM exhibited a 5.7-fold increase in *myogenin* expression

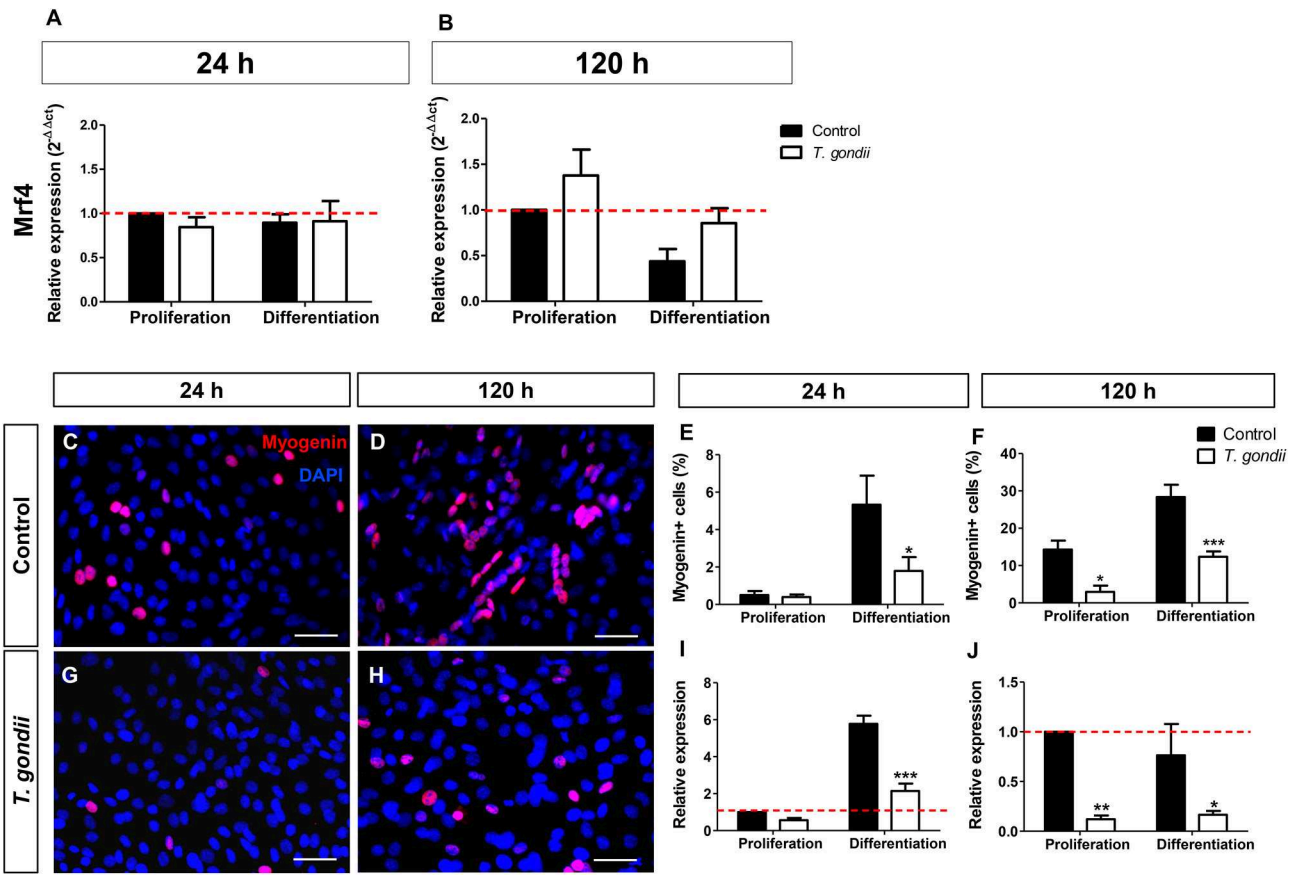

FIGURE 4 | Analysis of late myogenic genes expression in *T. gondii*-infected C2C12 cultures. After 24 h **(A)** and at 120 h **(B)** of myogenic stimulation Mrf4 expression was assessed by RT-qPCR and no significant changes were observed. Uninfected and infected cells in PM or DM were immunostained for myogenin (red) at 24 **(C,G)** and 120 h in DM **(D,H)**. The cell nucleus was stained with DAPI (blue). At 24 h of induction, uninfected cultures treated with DM showed significant increase in the number of myogenin-positive cells **(E)**, accompanied by a 6-fold increase in myogenin gene expression **(I)**. Infected cultures failed to show myogenin immunoreactivity at 24 h **(G,E)**, as well as mRNA expression **(I)**. 120 h after the initiation of the myogenic stimulus, *T. gondii* significantly reduced number of myogenin-positive cells **(F)** and expression **(J)**. Results of at least three independent experiments. $^*p < 0.05$, $^{**}p < 0.01$; $^{***}p < 0.0001$, Two-Way ANOVA with Bonferroni post-test. Red dotted line represents the value of control uninfected cultures maintained in Proliferation Medium. Scale bar = 50 μm.

at 24 h induction (**Figure 4I**), while infected C2C12 cultures presented decreased *myogenin* expression when compared to their correspondent controls (44%, $p > 0.05$ in PM and 63%, $p < 0.0001$ in DM, Two-Way ANOVA, with Bonferroni post-test, **Figure 4I**). At 120 h, *T. gondii* infection greatly reduced the level of myogenin transcript in both conditions (88% in PM, $p < 0.01$ and 78% in DM, $p < 0.05$, Two-Way ANOVA with Bonferroni post-test, **Figure 4J**).

T. gondii Infection Leads to a Proliferative, Undifferentiated State of C2C12 Cells

Following the observations that infected cultures exhibited altered MRF expression patterns and, consequently, decreased myotube formation, we investigated whether the infection also altered C2C12 cell proliferation using the proliferation marker Ki67. Cells maintained in PM for 24 h exhibited an average of 84.6 ± 9% Ki67-positive cells. At 24 h of induction with DM a slight, yet non-significant, decrease in the proportion of Ki67-positive cells (69.3 ± 12%) was detected (**Figure 5**), and infected cultures displayed comparable proliferation rates (82.4 ± 11 in PM and 63 ± 20% in DM). At 120 h, non-infected cultures in both PM and DM presented less Ki67 staining than non-infected cultures at 24 h, reaching 26 ± 9 and 11.7 ± 3% of the total cellular population, respectively. As expected, fully differentiated myotubes did not show positive staining for Ki67 (**Figure 5A**). Infected dishes kept in PM for 120 h exhibited 28.5 ± 9% of proliferative cells (**Figure 5E**), very similar to what was observed in the non-infected controls at this same time point. However,

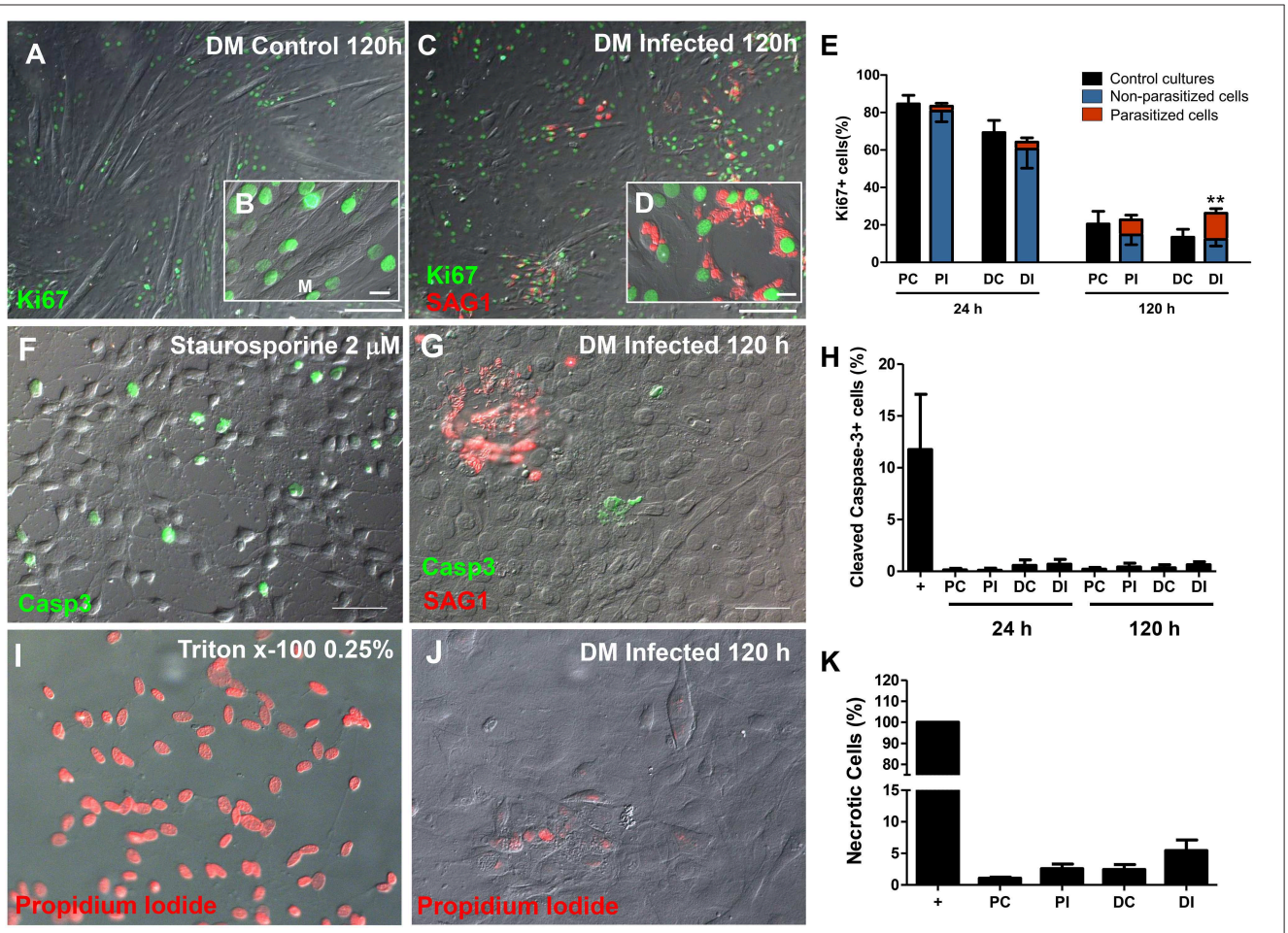

FIGURE 5 | The C2C12 proliferation rate was altered by infection. Ki67 immunostaining was used as parameter to determine the number of mitotic cells. Micrographs depict Ki67 staining of cultures in DM after 120 h of induction in uninfected **(A,B)** and *T. gondii*-infected dishes **(C,D)**. 24 h after treatment with DM no changes were detected **(E)**. *T. gondii* increased the proliferation of DM-treated cultures, when compared to uninfected dishes **(E)**. No Ki67 staining was observed in myotubes (M, in **B**), whereas cells harboring tachyzoites (shown in more detail in **D**) displayed intense nuclear immunolabeling. Cell death was assessed by staining for cleaved caspase-3 for apoptosis **(F–H)** and by propidium iodide uptake experiments for necrosis **(I–K)**. *T. gondii* infection did not induce apoptotic cell death, since caspase-3 stained cells ranged from 0.1 to 0.7% in all experimental conditions **(H)**. Treatment with Staurosporine 2 μM in DMEM high glucose with no serum for 2 h was used as a positive control **(F)**. Tachyzoites were detected with anti-SAG1 antibody and displayed no correlation to the presence of caspase-3-stained cells **(G,H)**. Necrosis was calculated by the percentage of PI-stained nuclei. Triton x-100 0.25% was used as positive control **(I)** and led to 100% of stained cells **(K)**. Infected C2C12 cells at 120 h of myogenesis induction **(J)** displayed no significant difference when compared to uninfected cultures, both in PM or DM. $N = 4$, $^{**}p < 0.01$, Two-Way ANOVA with Bonferroni post-test. Scale bars: 100 μm in **(B,D)**, 20 μm in **(C,E)**.

Ki67 positivity reached 29.8 ± 14% ($p < 0.01$, Two-Way ANOVA, with Bonferroni post-test) in infected cultures kept in DM when compared to uninfected dishes in DM, indicating a ∼2.5-fold increase in the number of proliferative cells (**Figure 5E**). A differential quantification of Ki67-positive staining in infected dishes was performed in order to determine whether cells harboring parasites would be preferentially proliferating, or if a bystander effect would be involved in increased proliferation. In infected C2C12 cultures maintained in DM for 120 h, 46% of Ki67-stained cells corresponded to parasitized cells (14.4% out of 29.8%, **Figure 5E**, red bars).

In order to exclude the possibility that increased proliferation could be due to a compensatory mechanism in response to parasite-induced cell death, the cultures were stained for cleaved caspase-3, a classic effector apoptosis marker (Nicholson et al., 1995). Staurosporine at 2 μM was used as a positive control for 2 h in uninfected cultures and presented an average of 11.75% of caspase-3 staining. The different C2C12 treatments (differentiation and infection) did not lead to changes in apoptosis levels (**Figures 5F,H**). Host cell necrosis was assessed by permeability to propidium iodide, which indicates loss of membrane integrity. Triton x-100 0.25% was used as the positive control for 5 min and led to positive staining in 100% of cells (**Figures 5I,K**). Uninfected cultures in PM presented 1.07% cells with positive PI staining, whereas this number reached 2.44% in uninfected DM-treated cultures ($p > 0.05$, One Way ANOVA with Bonferroni post-test). Infected cultures displayed a slight, albeit non-statistically significant, increase in the number of PI positive cells (**Figures 5I,K**).

T. gondii-Infected C2C12 Cells Display an Altered Secretory Pattern

T. gondii infection is known to modulate host cell responses and induce an inflammatory milieu that can generate paracrine effects in the cell culture. CBA was used to determine which cytokines and chemokines were released during the infection and which may, therefore, influence the myogenic process. Among the tested factors (IL-6, IL-10, IL-12p70, IFN-γ, TNF, and MCP-1), only IL-6 and MCP-1 were detected as secreted.

At 48 hpi, infected cells maintained in PM exhibited a 20-fold increase in IL-6 ($p > 0.05$, **Figure 6A**) and a 4-fold increase in MCP-1 ($p < 0.05$, Two-Way ANOVA, with Bonferroni post-test) secretion when compared to uninfected cultures in PM (**Figure 6C**). Infected C2C12 cells maintained in DM for 24 h also displayed increased levels of secreted IL-6 compared to non-infected cells (7-fold, $p > 0.05$, **Figure 6A**) and MCP-1 levels were increased by 6.8-fold ($p > 0.05$) (**Figure 6C**). IL-6 was greatly increased in infected cells in PM at 144 hpi (28,89-fold, $p < 0.01$, Two-Way ANOVA, with Bonferroni post-test) but not in DM (**Figure 6B**). MCP-1 levels in infected cultures at 120 h remained comparable to uninfected cultures (**Figure 6D**).

TGF-β1 is an anti-inflammatory cytokine known to greatly inhibit myogenesis in C2C12 cells (Massagué et al., 1986; Olson et al., 1986). We hypothesized that TGF-β1 secretion could be the mechanism through which *T. gondii* impaired myogenesis. However, we observed that this cytokine was greatly reduced in the supernatant of infected cultures, at all assessed times (**Figures 6E,F**). Regardless of the culture medium, infected dishes presented TGF-β1 secretion ranging from 71 to 114 pg/ml, while TGF-β1 concentrations ranged between 242 and 288 pg/ml in uninfected cultures.

In order to determine whether increased IL-6 or decreased TGF-β secretion plays a role in myogenesis impairment in C2C12 cells, treatments with 10 μg/ml Tocilizumabe (TCZ), a neutralizing antibody that inhibits the IL-6 receptor and with recombinant TGF-β1 (rTGF, 0.5 ng) were performed (**Figure 7A**). TCZ had no impact on myogenesis rates and myotube formation in uninfected cultures (**Figure 7B**). Treatment with TCZ of *T. gondii*-infected cultures led to no significant alteration in the number of MyHC-positive cells and myotubes (**Figure 7B**). rTGF addition caused no alteration in the number of MyHC-positive cells in PM-treated cultures (**Figure 7C**), although a negative effect on myogenesis in both uninfected and infected DM-treated cultures was observed, with reduced numbers of MyHC-positive cells (**Figure 7C**).

Since neither IL-6 nor TGF-β seem to be directly involved in defective myogenesis in infected cultures, conditioned medium transfer experiments were carried out. Uninfected C2C12 cells were treated for 5 days with a 1:1 mixture of conditioned medium with fresh medium (either PM or DM, **Figure 7D**). Cells treated with CM from uninfected or infected cultures maintained in PM for 24 h (PM-Cont and PM-Inf) presented 0.96 and 0.76% of MyHC-positive cells, respectively (**Figure 7E**). Cultures treated with DM-Cont 24h displayed differentiation rates similar to that observed in cultures maintained with DM alone (19.2%), whereas treatment with CM from DM-Inf 24h indicated 6.2% MyHC-positive cells ($p < 0.0001$, One-Way ANOVA with Bonferroni post-test). The same effect was observed in cultures treated with CM from DM-Cont 120 h, which displayed 5.6% of MyHC cells, vs. 1.25% found in DM-Inf 120h-treated dishes ($p < 0.01$, One-Way ANOVA, with Bonferroni post-test, **Figure 7E**).

Wnt/β-Catenin Pathway Activation Is Impaired by *T. gondii*

Since *T. gondii* infection altered MRFs expression and cytokine secretion at times as early as 24 h of induction (corresponding to 48 hpi), we investigated an upstream myogenesis regulating pathway, the Wnt/β-catenin pathway (**Figure 8A**). The effect of the infection on the activation of the Wnt/β-catenin pathway was confirmed by dual luciferase reporter assays for the TCF/LEF reporter. Infected cultures maintained in PM presented a 33% reduction in luciferase activity when compared to controls (**Figure 8B**, $p < 0.05$, unpaired Student's *T*-test). In addition, a significant decrease was observed in infected DM-treated cultures, when compared to uninfected DM-treated controls (**Figure 8C,** $p < 0.05$, unpaired Student's *T*-test). BIO, a selective pharmacological GSK3 inhibitor and, therefore a Wnt/β-catenin pathway activator, was used to confirm these findings. Indeed, luciferase activity increased ∼25-fold in uninfected cultures treated with PM and DM (**Figures 8D,E**, $p < 0.001$ unpaired Student's T test). This effect was impaired in *T. gondii*-infected cultures by 46 and 34% in PM and DM-treated cultures,

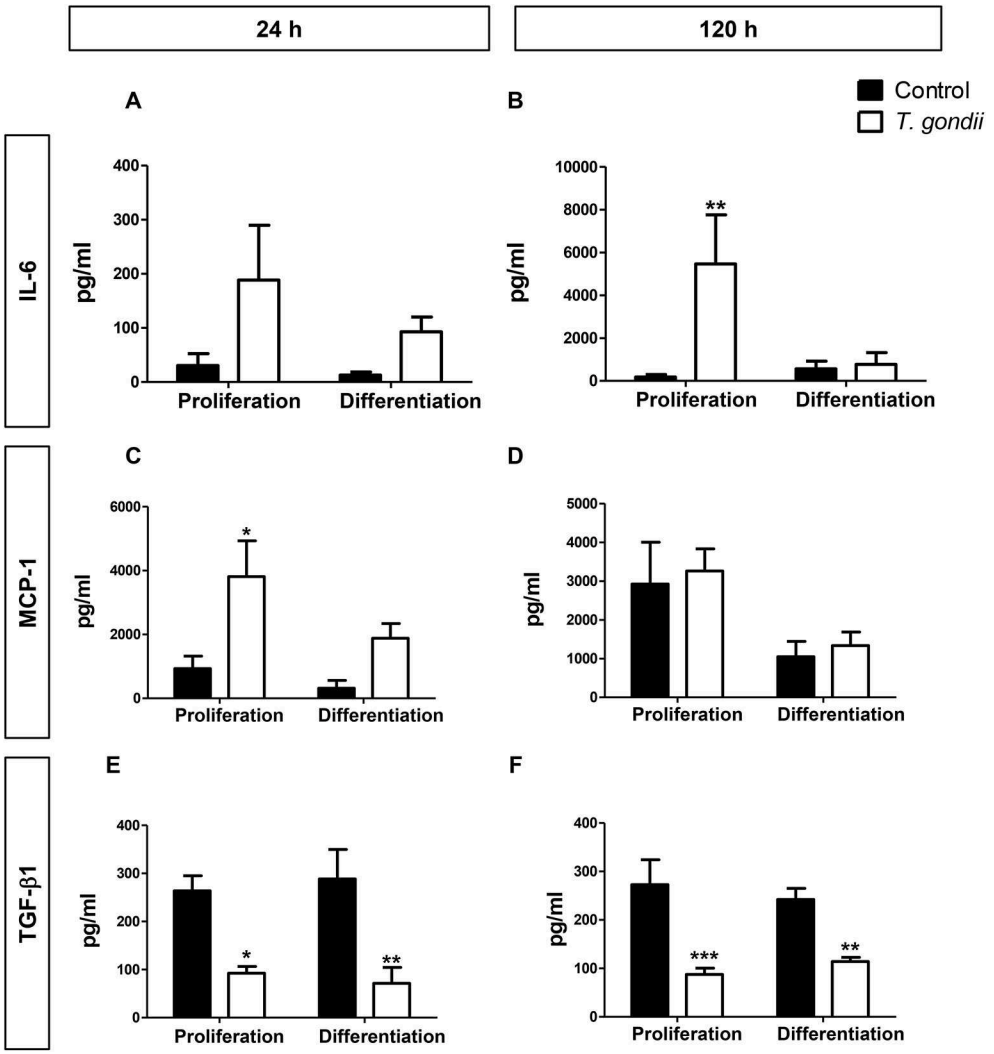

FIGURE 6 | Secretory profile during *T. gondii* infection. Conditioned medium from C2C12 cells was assayed for INF-γ, TNF-α, IL-10, IL-12p70, IL-6, and MCP-1 with CBA assay. The experimental design in shown in **(A)**. IL-6 **(B)** and MCP-1 **(C)** were greatly increased with *T. gondii* infection, whereas a decrease of TGF- β1 secretion was observed at both evaluated times, as assesses by ELISA **(E,F)**. MCP-1 remained unaltered at 120 h of myogenesis **(D)**. Results of at least three independent experiments. $^{*}p < 0.05$, $^{**}p < 0.01$; $^{***}p < 0.0001$, Two-Way ANOVA with Bonferroni post-test.

respectively (**Figures 8D,E**, $p < 0.0001$ and <0.01, respectively). However, the overall content of β-catenin remained unaltered in *T. gondii*-infected cultures (data not shown).

DISCUSSION

T. gondii displays an interesting interaction with the skeletal muscle system, in which tissue cysts are formed (Dubey, 1998). Such tropism is important for the transmission cycle of the parasite, since predation of infected prey by felids may favor the sexual cycle (Dubey and Frenkel, 1972). However, the acquired infection can cause damages to the skeletal muscle in intermediate hosts, and clinical reports have demonstrated that *T. gondii* infection may cause intense myositis, electromyographic abnormalities and muscle pain (Montoya et al., 1997; Hassene et al., 2008; Cuomo et al., 2013). We used the mouse myoblast cell line C2C12 to investigate the mechanism by which *T. gondii* infection may impact skeletal muscle physiology. Previous data from our laboratory using primary skeletal muscle cell cultures have demonstrated that infection with the highly virulent RH strain of the parasite reduced the number of multinucleated cells (Gomes et al., 2011). We chose the type II strain ME49 that exhibits reduced virulence compared to the laboratory-adapted RH strain, thus avoiding the confounding factor of high levels of host cell lysis by the latter (Kirkman et al., 2001). Moreover, previous observations from our group showed that vertical transmission of *T. gondii* induces alterations in the fetal myogenesis (Gomes and Barbosa, 2016). Low levels of parasitism were detected when C2C12 cells were infected with ME49 tachyzoites (5% at 48 hpi and 10-30% at 144 hpi). However,

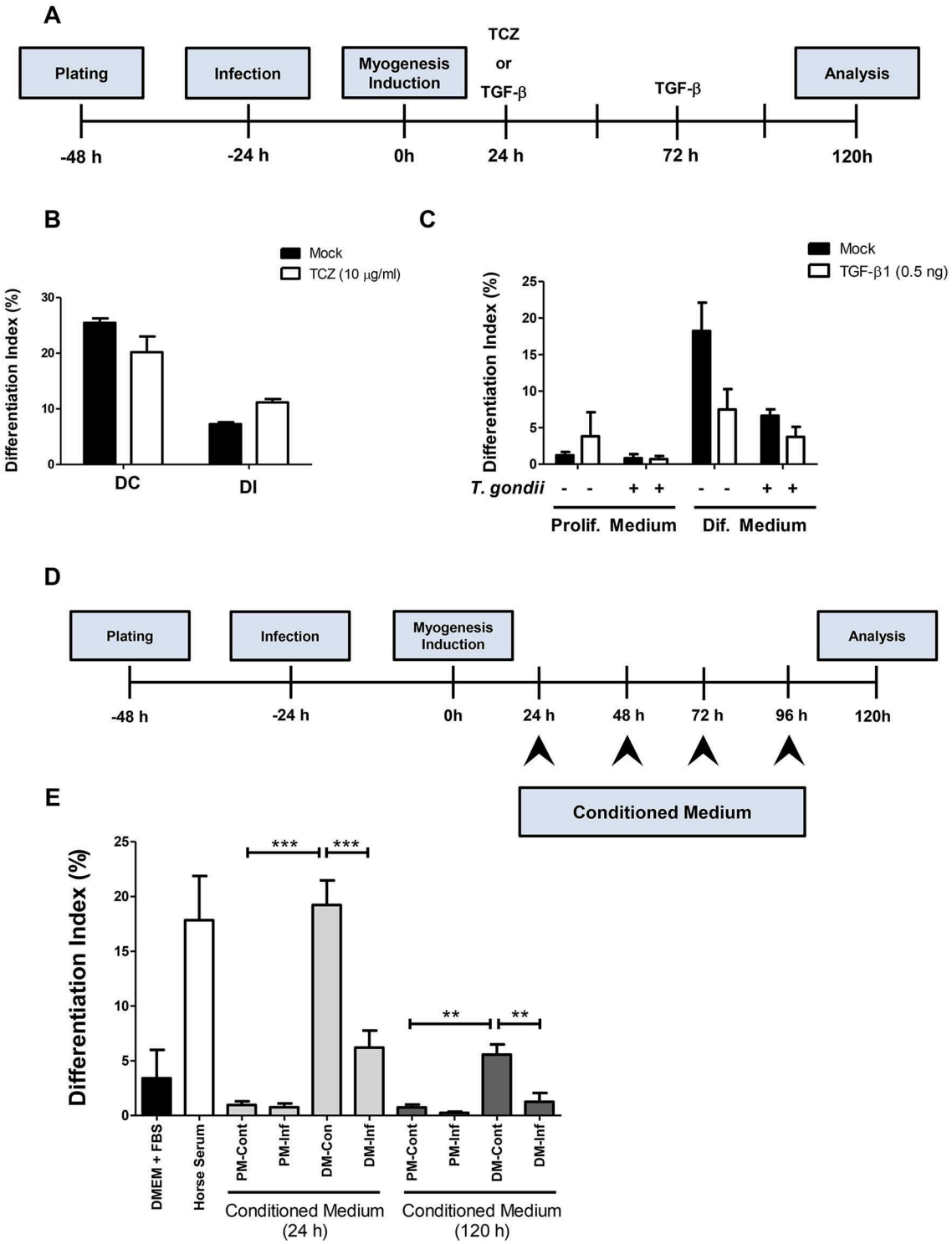

FIGURE 7 | Soluble factors released from infected cultures have an impact on myogenesis. In order to test whether increased IL-6 or decreased TGF-β1 played a role on impairment of myogenesis, C2C12 were infected and treated with Tocilizumabe **(B)** or recombinant TGF-β1 **(C)**. The experimental designs are shown in **(A,D)**. TCZ had no significant impact on differentiation rate in cultures maintained in DM **(B)**. TGF-β decreased the differentiation rate, as shown by the number of MyHC-positive cells per field in both PM and DM **(C)**. Conditioned medium (CM) from infected C2C12 cells was used to treat fresh myoblasts. CM from DM-treated cultures (DM-Cont) 24 and 120 h increased the differentiation rate **(E)**, whereas DM-Inf 24 and 120 h had an opposite effect, reducing myogenesis. Results of at least three independent experiments. $^{**}p < 0.01$; $^{***}p < 0.0001$, One-Way ANOVA with Bonferroni post-test.

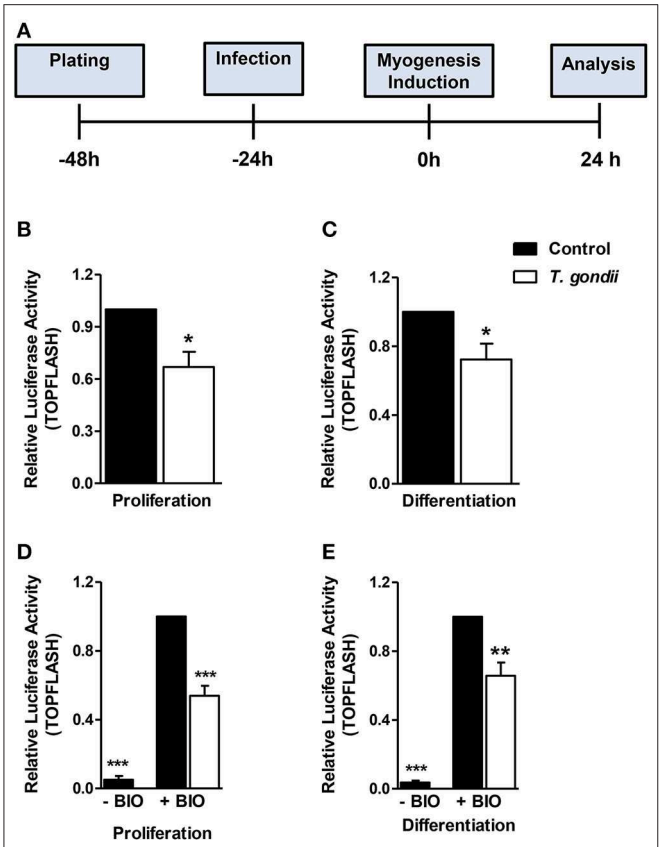

FIGURE 8 | Wnt/β-catenin pathway is decreased in *T. gondii*-infected cultures. The experimental design in shown in **(A)**. Luciferase assay for TCF/LEF promoter activation by β-catenin showed that *T. gondii*-infected cultures at 24 h of induction displayed significantly lower luciferase signal when compared to controls **(B,C)**. BIO treatment significantly increased luciferase activity in uninfected controls **(D,E)**. However, *T. gondii* infection impaired such effect. $*p < 0.05$, $**p < 0.01$, $***p < 0.001$, unpaired Student's T test. Scale bars: 20 μm.

the number of MyHC+ cells and myotubes were drastically reduced, thus confirming that this infection displays a more general deleterious effect on the differentiation of the C2C12 cell population, despite the low infectivity rate. This deleterious effect on myogenesis was also observed in proliferating cells, which display a basal spontaneous myogenic induction, due to high cellular density (Tanaka K. et al., 2011).

Myogenesis, characterized by myocyte differentiation and fusion (Dedieu et al., 2002; Berendse et al., 2003) is essential in muscle development, after birth for breathing and for muscle growth, and also in adults for muscle regeneration, following injury (Le Grand and Rudnicki, 2007). In order to gain insights into the molecular mechanisms through which *T. gondii* impairs myotube formation, we investigated the expression levels of the main MRFs: Myf5, MyoD, Mrf4 and myogenin. Myf5 is a transcription factor that, along with MyoD, is activated and expressed in early myogenic program steps (Rudnicki et al., 1993). We found Myf5 transcripts to be decreased in uninfected cultures maintained in DM for 120 h when compared to cells kept in PM, in accordance with known Myf5 decreased expression after commitment to differentiation (Zammit et al., 2006). *T. gondii*-infected cultures presented higher levels of Myf5 when compared to their respective controls, suggesting a delay in the myogenic program of these cells.

It is known that MyoD expression is capable of initiating the myogenic program, even in non-muscle cells (Davis et al., 1987; Weintraub et al., 1989). MyoD targets are related to differentiation, such as myogenin, but also to the cell cycle, such as Ankrd2, Cdkn1c, and calcyclin (Bean et al., 2005), which suggested that proliferation or differentiation pathways are mutually exclusive during myogenesis, and one depends on inhibition of the other. We demonstrated that higher amounts of proliferating cells are found in infected cultures, but it is unclear if the cell cycle itself is affected by *T. gondii* infection. MyoD reduction at the protein level could affect cell proliferation by decreasing myogenin expression, one of its known targets (Buckingham and Rigby, 2014). However, increased Myf5 expression together with decreased MyoD expression suggests that myoblasts in infected cultures are kept in a proliferating myogenic precursor state.

TGF is part of a family of pluripotent growth factors involved in diverse physiological processes, including myogenesis (Liu et al., 2001). During the maturation of C2C12 myotubes, bone morphogenetic proteins (BMPs) are gradually down-regulated, whereas TGF-β (1, 2, and 3) are up-regulated (Furutani et al., 2011). TGF-β1 presents a deleterious effect on myogenesis (Olson et al., 1986), and it has been demonstrated that *T. gondii* infection induce TGF-β secretion in macrophages (Bermudez et al., 1993). However, our data indicate that infected C2C12 cells display reduced TGF-β1 secretion. This behavior was also observed by our group after *T. gondii* infection of neural progenitors (Adesse et al., 2018). Regarding muscle cells, Swierzy et al. (2014) previously demonstrated *T. gondii* infection effects on the TGF-β mRNA expression of myoblasts and myotubes. In that study *T. gondii* infection with the NTE strain (also type II) did not alter TGF-β gene expression. Infected cultures were treated with rTGF, which did not rescue the myogenesis defect. This finding indicates that TGF-β1 found in the supernatant of uninfected cultures may be a marker of differentiated myocytes/myotubes and its decreased secretion in infected cultures may be only the indication that cells remained undifferentiated.

IL-6 is a myokine (Pedersen et al., 2003) and its secretion is increased in muscle cells following exercise acting in physiological processes, not only in skeletal muscle but also systemically (Forcina et al., 2018). However, excessive IL-6 levels can lead to an acute inflammatory response. In this scenario, muscular atrophy and satellite cell exhaustion may occur, leading to tissue inflammation and increased ROS production, along with insulin resistance and possible chronic inflammation (Visser et al., 2002; Haddad et al., 2005; Carson and Baltgalvis, 2010). Pelosi et al. (2014) demonstrated that treatment with IL-6 impaired C2C12 myogenesis, with myogenin and MyHC downregulation, whereas MyoD and Pax7 levels remained unaltered. Treatment with Tocilizumabe, a neutralizing antibody for IL-6R, had no effect on myogenesis rescue in infected cultures. This suggests that IL-6 may not be the major soluble component involved in myogenesis defects induced by *T. gondii*. Another explanation would be that IL-6-mediated defect could

act via other receptors that are not blocked by TCZ. Other cytokines and chemokines known to be up-regulated by *T. gondii* infection not included in the CBA kit may also play an important role in controlling the myogenic process in infected cultures. This idea was reinforced by the fact that conditioned medium from infected C2C12 cultures also impaired myogenesis. Indeed, extracellular vesicles released by *T. gondii* or by *T. gondii*-infected cells led to increased proliferation of rat myoblasts (Kim et al., 2016; Li et al., 2018).

T. gondii possesses effector proteins that act on host cells, which are capable of inducing the activation of the STAT3, STAT6, and NF-κB pathways (Hakimi et al., 2017), thus leading to the production of many cytokines and immunomodulatory molecules that may interfere in infection latency. It has been demonstrated that the *T. gondii* type II strain could induce the NF-κB pathway through release of the GRA15 protein (Rosowski et al., 2011). As IL-6 and MCP-1 are known NF-κB targets (Libermann and Baltimore, 1990; Shoelson et al., 2006) this effect could be the trigger that leads to the myogenic defects observed in the present model. Since a pro-inflammatory profile can favor myoblast proliferation (Arnold et al., 2007), the environment induced by *T. gondii* infection may promote proliferation, leaving

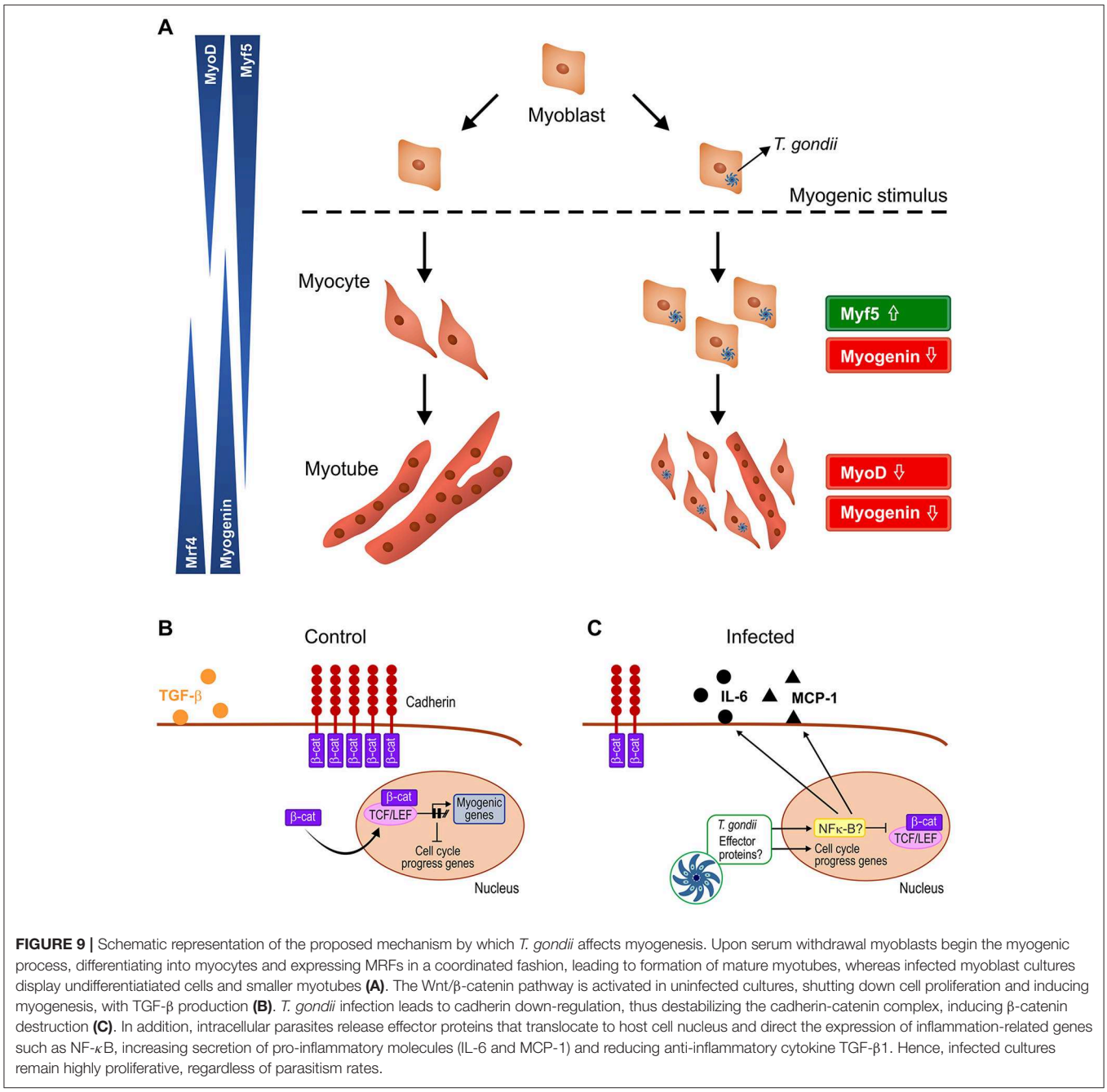

FIGURE 9 | Schematic representation of the proposed mechanism by which *T. gondii* affects myogenesis. Upon serum withdrawal myoblasts begin the myogenic process, differentiating into myocytes and expressing MRFs in a coordinated fashion, leading to formation of mature myotubes, whereas infected myoblast cultures display undifferentiatiated cells and smaller myotubes **(A)**. The Wnt/β-catenin pathway is activated in uninfected cultures, shutting down cell proliferation and inducing myogenesis, with TGF-β production **(B)**. *T. gondii* infection leads to cadherin down-regulation, thus destabilizing the cadherin-catenin complex, inducing β-catenin destruction **(C)**. In addition, intracellular parasites release effector proteins that translocate to host cell nucleus and direct the expression of inflammation-related genes such as NF-κB, increasing secretion of pro-inflammatory molecules (IL-6 and MCP-1) and reducing anti-inflammatory cytokine TGF-β1. Hence, infected cultures remain highly proliferative, regardless of parasitism rates.

myoblasts unresponsive to myogenic stimulus. Moreover, *T. gondii* effector proteins were also shown to affect c-Myc (Franco et al., 2014) and p21 (Chang et al., 2015) expression, two proteins that regulate host cell proliferation and might explain the increase in Ki67-positive cells found in our system.

The Wnt/β-catenin pathway is one of the regulators of the myogenic program acting on the switch from proliferation to differentiation in SkMCs (Tanaka S. et al., 2011; von Maltzahn et al., 2012). The results presented herein indicate that infected cultures presented reduced β-catenin activation despite the maintenance of global β-catenin contents, as shown by luciferase assays, thus indicating that infection impairs endogenous β-catenin activation, followed by its correct translocation to the myonucleus. β-catenin directly binds cadherins, linking this junctional complex to the actin cytoskeleton. Interestingly, M-cadherin transcripts and protein levels have been shown to be down-regulated on *T. gondii* infection of muscle cells as early as 3 and 24 h post infection, respectively (Gomes et al., 2011). Indeed, M-cadherin down-regulation is capable of reducing myogenesis through reduction in active β-catenin, thus resulting in decreased myogenesis (Wang et al., 2013). Since myogenesis induction began at 24 hpi, it is suggested that the cadherin-catenin complex is already dismantled and, therefore, cells cannot respond to Wnt activation. The observation that *T. gondii* infection inhibits BIO-induced activation of β-catenin pathway indicates that this effect occurs downstream of the β-catenin destruction complex (MacDonald et al., 2009).

In summary, our results point to a disruptive effect of *T. gondii* on C2C12 myogenesis, creating a pro-inflammatory milieu that spreads to neighboring cells and impairs their response to myogenic stimuli (**Figure 9**). These findings are relevant in the context of congenital and acquired infection and may shed light on the impact of this parasite on muscle physiology.

DATA AVAILABILITY STATEMENT

The datasets generated for this study are available on request to the corresponding author.

AUTHOR CONTRIBUTIONS

DA and HB conceptualization, supervision, and funding acquisition. DA and PV methodology, data curation, and writing—original draft. DA, HB, VM, and PV validation. DA, PV, MW, DB, and DP formal analysis. PV, MW, DB, DP, and JA investigation. DA, HB, MW, VM, GB-B, and JA resources. HB, MW, and VM writing—review & editing. DA visualization and project administration.

FUNDING

This work was supported by Conselho Nacional de Pesquisa e Desenvolvimento Tecnológico (CNPq, grant Numbers: 401772/2015-2 and 444478/2014-0 for DA and 304917/2016-8 e 407490/2012-4 for HB), FAPERJ and Fundação Oswaldo Cruz (Fiocruz), through the INOVA Fiocruz program, grant number 3231984391. VM and GB-B are supported by the French association against muscular dystrophy AFM.

ACKNOWLEDGMENTS

The authors would like to thank Ms. Sandra Maria Oliveira da Silva (LBE, IOC, Fiocruz) for the excellent technical support and Profs. Ingo Riederer (IOC, Fiocruz) and Prof. Claudia Mermelstein (ICB, UFRJ) for critical discussions about the experimental design of this manuscript; Mrs. Heloisa Diniz from the Department of Image Production and Processing (Serviço de Produção e Tratamento de Imagem – IOC) at the Oswaldo Cruz Institute for help in generating the schematic images presented in **Figure 9**.

SUPPLEMENTARY MATERIAL

The Supplementary Material for this article can be found online at: https://www.frontiersin.org/articles/10.3389/fcimb.2019.00395/full#supplementary-material

Figure S1 | Culture evaluation with Giemsa stain after 24 h of myogenesis induction. **(A,B)** PM-treated cells, **(C,D)** DM-treated cells. Infected cultures are on the right panels. Parasites are indicated by white arrows. Scale bars: 200 μm. Insets in **(C,D)** 20 μm.

Figure S2 | Culture evaluation with Giemsa stain after 120 h of induction of myogenesis. **(A,B)** PM-treated cells, **(C,D)** DM-treated cells. Infected cultures are on the right panels. Parasites within parasitophorous vacuoles are indicated by arrows and cyst-like structures are indicated by asterisks (*). Scale bars: 200 μm. Insets: 20 μm.

REFERENCES

Acquarone, M., Ferreira-da-Silva, M. F., Guimarães, E. V., and Barbosa, H. S. (eds.). (2017). "*Toxoplasma gondii* tissue cyst: cyst wall incorporation activity and matrix cytoskeleton proteins paving the way to nutrient acquisition," in *Toxoplasmosis, 1st Edn* (IntechOpen), 3–19. doi: 10.5772/intechopen.68202

Adesse, D., Marcos, A. C., Siqueira, M., Cascabulho, C. M., Waghabi, M. C., Barbosa, H. S., et al. (2018). Radial Glia cell infection by *Toxoplasma gondii* disrupts brain microvascular endothelial cell integrity. *bioRxiv* 378588. doi: 10.1101/378588

Arnold, L., Henry, A., Poron, F., Baba-Amer, Y., van Rooijen, N., Plonquet, A., et al. (2007). Inflammatory monocytes recruited after skeletal muscle injury switch into antiinflammatory macrophages to support myogenesis. *J. Exp. Med.* 204, 1057–1069. doi: 10.1084/jem.20070075

Bean, C., Salamon, M., Raffaello, A., Campanaro, S., Pallavicini, A., and Lanfranchi, G. (2005). The Ankrd2, Cdkn1c and calcyclin genes are under the control of MyoD during myogenic differentiation. *J. Mol. Biol.* 349, 349–366. doi: 10.1016/j.jmb.2005.03.063

Berendse, M., Grounds, M. D., and Lloyd, C. M. (2003). Myoblast structure affects subsequent skeletal myotube morphology and sarcomere assembly. *Exp. Cell Res.* 291, 435–450. doi: 10.1016/j.yexcr.2003.07.004

Bermudez, L. E., Covaro, G., and Remington, J. (1993). Infection of murine macrophages with *Toxoplasma gondii* is associated with release of transforming growth factor beta and downregulation of expression of tumor necrosis factor receptors. *Infect. Immun.* 61, 4126–4130.

Buckingham, M., and Rigby, P. W. (2014). Gene regulatory networks and transcriptional mechanisms that control myogenesis. *Dev. Cell*. 28, 225–238. doi: 10.1016/j.devcel.2013.12.020

Carson, J. A., and Baltgalvis, K. A. (2010). Interleukin 6 as a key regulator of muscle mass during cachexia. *Exerc Sport Sci. Rev*. 38, 168–176. doi: 10.1097/JES.0b013e3181f44f11

Chang, S., Shan, X., Li, X., Fan, W., Zhang, S. Q., Zhang, J., et al. (2015). *Toxoplasma gondii* rhoptry protein ROP16 mediates partially SH-SY5Y cells apoptosis and cell cycle arrest by directing Ser15/37 phosphorylation of p53. *Int. J. Biol. Sci*. 11, 1215–1225. doi: 10.7150/ijbs.10516

Cuomo, G., D'Abrosca, V., Rizzo, V., Nardiello, S., La Montagna, G., Gaeta, G. B., et al. (2013). Severe polymyositis due to *Toxoplasma gondii* in an adult immunocompetent patient: a case report and review of the literature. *Infection* 41, 859–862. doi: 10.1007/s15010-013-0427-x

Davis, R. L., Weintraub, H., and Lassar, A. B. (1987). Expression of a single transfected cDNA converts fibroblasts to myoblasts. *Cell* 51, 987–1000. doi: 10.1016/0092-8674(87)90585-X

De Angelis, L., Berghella, L., Coletta, M., Lattanti, L., Zanchi, M., Cusella-De Angelis, M. G., et al. (1999). Skeletal myogenic progenitors originating from embryonic dorsal aorta coexpress endothelial and myogenic markers and contribute to postnatal muscle growth and regeneration. *J. Cell Biol*. 147, 869–878. doi: 10.1083/jcb.147.4.869

Dedieu, S., Mazères, G., Cottin, P., and Brustis, J. J. (2002). Involvement of myogenic regulator factors during fusion in the cell line C2C12. *Int. J. Dev. Biol*. 46, 235–241. Available online at: http://www.ijdb.ehu.es/web/paper.php?doi=11934152

Dubey, J. P. (1998). Advances in the life cycle of *Toxoplasma gondii*. *Int. J. Parasitol*. 28, 1019–1024. doi: 10.1016/S0020-7519(98)00023-X

Dubey, J. P. (2008). The history of *Toxoplasma gondii*–the first 100 years. *J. Eukaryot. Microbiol*. 55, 467–475. doi: 10.1111/j.1550-7408.2008.00345.x

Dubey, J. P., and Frenkel, J. K. (1972). Cyst-induced toxoplasmosis in cats. *J. Protozool*. 19, 155–177. doi: 10.1111/j.1550-7408.1972.tb03431.x

Ferreira-da-Silva Mda, F., Takács, A. C., Barbosa, H. S., Gross, U., and Lüder, C. G. (2009). Primary skeletal muscle cells trigger spontaneous *Toxoplasma gondii* tachyzoite-to-bradyzoite conversion at higher rates than fibroblasts. *Int. J. Med. Microbiol*. 299, 381–388. doi: 10.1016/j.ijmm.2008.10.002.

Forcina, L., Miano, C., and Musar,ò, A. (2018). The physiopathologic interplay between stem cells and tissue niche in muscle regeneration and the role of IL-6 on muscle homeostasis and diseases. *Cytokine Growth Factor Rev*. 41, 1–9. doi: 10.1016/j.cytogfr.2018.05.001

Franco, M., Shastri, A. J., and Boothroyd, J. C. (2014). Infection by *Toxoplasma gondii* specifically induces host c-Myc and the genes this pivotal transcription factor regulates. *Eukaryot Cell*. 13, 483–493. doi: 10.1128/EC.00316-13

Furutani, Y., Umemoto, T., Murakami, M., Matsui, T., and Funaba, M. (2011). Role of endogenous TGF-β family in myogenic differentiation of C2C12 cells. *J. Cell Biochem*. 112, 614–624. doi: 10.1002/jcb.22953

Gomes, A. F., and Barbosa, H. S. (2016). "Congenital toxoplasmosis: *In vivo* impact of *Toxoplasma gondii* infection on myogenesis and neurogenesis," *Toxoplasmosis, 1st Edn*. Ed I. Akyar (Rijeka: Intech), 55–68. doi: 10.5772/intechopen.68619

Gomes, A. F., Guimarães, E. V., Carvalho, L., Correa, J. R., Mendonça-Lima, L., and Barbosa, H. S. (2011). *Toxoplasma gondii* down modulates cadherin expression in skeletal muscle cells inhibiting myogenesis. *BMC Microbiol*. 11:110. doi: 10.1186/1471-2180-11-110

Gomes, A. F., Magalhães, K. G., Rodrigues, R. M., de Carvalho, L., Molinaro, R., Bozza, P. T., et al. (2014). *Toxoplasma gondii*-skeletal muscle cells interaction increases lipid droplet biogenesis and positively modulates the production of IL-12, IFN-g and PGE2. *Parasit. Vectors*. 7:47. doi: 10.1186/1756-3305-7-47

Guimarães, E. V., de Carvalho, L., and Barbosa, H. S. (2008). Primary culture of skeletal muscle cells as a model for studies of *Toxoplasma gondii* cystogenesis. *J. Parasitol*. 94, 72–83. doi: 10.1645/GE-1273.1

Haddad, F., Zaldivar, F., Cooper, D. M., and Adams, G. R. (2005). IL-6-induced skeletal muscle atrophy. *J. Appl. Physiol*. 98, 911–917. doi: 10.1152/japplphysiol.01026.2004

Hakimi, M. A., Olias, P., and Sibley, L. D. (2017). Toxoplasma effectors targeting host signaling and transcription. *Clin. Microbiol. Rev*. 30, 615–645. doi: 10.1128/CMR.00005-17

Hassene, A., Vital, A., Anghel, A., Guez, S., and Series, C. (2008). Acute acquired toxoplasmosis presenting as polymyositis and chorioretinitis in immunocompetent patient. *Joint Bone Spine* 75, 603–605. doi: 10.1016/j.jbspin.2007.08.009

Hildyard, J. C., and Wells, D. J. (2014). Identification and validation of quantitative PCR reference genes suitable for normalizing expression in normal and dystrophic cell culture models of myogenesis. *PLoS Curr muscu. dystrophy*. 6. doi: 10.1371/currents.md.faafdde4bea8df4aa7d06cd5553119a6

Hunt, L. C., Gorman, C., Kintakas, C., McCulloch, D. R., Mackie, E. J., and White, J. D. (2013). Hyaluronan synthesis and myogenesis: a requirement for hyaluronan synthesis during myogenic differentiation independent of pericellular matrix formation. *J Biol Chem*. 288, 13006–13021. doi: 10.1074/jbc.M113.453209

Joulia, D., Bernardi, H., Garandel, V., Rabenoelina, F., Vernus, B., and Cabello, G. (2003). Mechanisms involved in the inhibition of myoblast proliferation and differentiation by myostatin. *Exp. Cell Res*. 286, 263–275. doi: 10.1016/S0014-4827(03)00074-0

Kassar-Duchossoy, L., Gayraud-Morel, B., Gomès, D., Rocancourt, D., Buckingham, M., Shinin, V., et al. (2004). Mrf4 determines skeletal muscle identity in Myf5: Myod double-mutant mice. *Nature* 431, 466–471. doi: 10.1038/nature02876

Kim, M. J., Jung, B. K., Cho, J., Song, H., Pyo, K. H., Lee, J. M., et al. (2016). Exosomes Secreted by *Toxoplasma gondii*-Infected L6 Cells: their effects on host cell proliferation and cell cycle changes. *Korean J. Parasitol*. 54, 147–154. doi: 10.3347/kjp.2016.54.2.147

Kirkman, L. A., Weiss, L. M., and Kim, K. (2001). Cyclic nucleotide signaling in *Toxoplasma gondii* bradyzoite differentiation. *Infect. Immun*. 69, 148–153. doi: 10.1128/IAI.69.1.148-153.2001

Le Grand, F., and Rudnicki, M. A. (2007). Skeletal muscle satellite cells and adult myogenesis. *Curr. Opin. Cell Biol*. 19, 628–633. doi: 10.1016/j.ceb.2007.09.012

Li, Y., Xiu, F., Mou, Z., Xue, Z., Du, H., Zhou, C., et al. (2018). Exosomes derived from *Toxoplasma gondii* stimulate an inflammatory response through JNK signaling pathway. *Nanomedicine* 13, 1157–1168. doi: 10.2217/nnm-2018-0035

Libermann, T. A., and Baltimore, D. (1990). Activation of interleukin-6 gene expression through the NF-kappa B transcription factor. *Mol. Cell Biol*. 10, 2327–2334. doi: 10.1128/MCB.10.5.2327

Liu, D., Black, B. L., and Derynck, R. (2001). TGF-beta inhibits muscle differentiation through functional repression of myogenic transcription factors by Smad3. *Genes Dev*. 15, 2950–2966. doi: 10.1101/gad.925901

MacDonald, B. T., Tamai, K., and He, X. (2009). Wnt/beta-catenin signaling: components, mechanisms, and diseases. *Dev Cell*. 17, 9–26. doi: 10.1016/j.devcel.2009.06.016

Massagué, J., Cheifetz, S., Endo, T., and Nadal-Ginard, B. (1986). Type beta transforming growth factor is an inhibitor of myogenic differentiation. *Proc. Natl. Acad. Sci. U.S.A*. 83, 8206–8210. doi: 10.1073/pnas.83.21.8206

McKarney, L. A., Overall, M. L., and Dziadek, M. (1997). Myogenesis in cultures of uniparental mouse embryonic stem cells: differing patterns of expression of myogenic regulatory factors. *Int J Dev Biol*. 41, 485–490.

Montoya, J. G., Jordan, R., Lingamneni, S., Berry, G. J., and Remington, J. S. (1997). Toxoplasmic myocarditis and polymyositis in patients with acute acquired toxoplasmosis diagnosed during life. *Clin Infect Dis*., 24, 676–683. doi: 10.1093/clind/24.4.676

Montoya, J. G., and Liesenfeld, O. (2004). Toxoplasmosis, *Lancet* 363, 1965–1976. doi: 10.1016/S0140-6736(04)16412-X

Nicholson, D. W., Ali, A., Thornberry, N. A., Vaillancourt, J. P., Ding, C. K., Gallant, M., et al. (1995). Identification and inhibition of the ICE/CED-3 protease necessary for mammalian apoptosis. *Nature* 376, 37–43. doi: 10.1038/376037a0

Nishida, T., Kubota, S., Aoyama, E., Janune, D., Lyons, K. M., and Takigawa, M. (2015). CCN family protein 2 (CCN2) promotes the early differentiation, but inhibits the terminal differentiation of skeletal myoblasts. *J. Biochem*. 157, 91–100. doi: 10.1093/jb/mvu056

Olson, E. N., Sternberg, E., Hu, J. S., Spizz, G., and Wilcox, C. (1986). Regulation of myogenic differentiation by type beta transforming growth factor. *J. Cell Biol*. 103, 1799–1805. doi: 10.1083/jcb.103.5.1799

Pedersen, B. K., Steensberg, A., Fischer, C., Keller, C., Keller, P., Plomgaard, P., et al. (2003). Searching for the exercise factor: is IL-6 a candidate? *J. Muscle Res. Cell Motil*. 24, 113–119. doi: 10.1023/A:1026070911202

Pelosi, M., De Rossi, M., Barberi, L., and Musarò, A. (2014). IL-6 impairs myogenic differentiation by downmodulation of p90RSK/eEF2 and mTOR/p70S6K axes, without affecting AKT activity. *Biomed. Res. Int*. 2014:206026. doi: 10.1155/2014/206026

Rosowski, E. E., Lu, D., Julien, L., Rodda, L., Gaiser, R. A., Jensen, K. D., et al. (2011). Strain-specific activation of the NF-kappaB pathway by GRA15, a novel *Toxoplasma gondii* dense granule protein. *J. Exp. Med*. 208, 195–212. doi: 10.1084/jem.20100717

Rudnicki, M. A., Schnegelsberg, P. N., Stead, R. H., Braun, T., Arnold, H. H., and Jaenisch, R. (1993). MyoD or Myf-5 is required for the formation of skeletal muscle. *Cell* 75, 1351–1359. doi: 10.1016/0092-8674(93)90621-V

Saeij, J. P., Coller, S., Boyle, J. P., Jerome, M. E., White, M. W., and Boothroyd, J. C. (2007). *Toxoplasma* co-opts host gene expression by injection of a polymorphic kinase homologue. *Nature*. 445, 324–327. doi: 10.1038/nature05395

Shoelson, S. E., Lee, J., and Goldfine, A. B. (2006). Inflammation and insulin resistance. *J. Clin. Invest*. 116, 1793–1801. doi: 10.1172/JCI29069

Swierzy, I. J., Muhammad, M., Kroll, J., Abelmann, A., Tenter, A. M., and Lüder, C. G. (2014). *Toxoplasma gondii* within skeletal muscle cells: a critical interplay for food-borne parasite transmission. *Int. J Parasitol*. 44, 91–98. doi: 10.1016/j.ijpara.2013.10.001

Tanaka, K., Sato, K., Yoshida, T., Fukuda, T., Hanamura, K., Kojima, N., et al. (2011). Evidence for cell density affecting C2C12 myogenesis: possible regulation of myogenesis by cell-cell communication. *Muscle Nerve*. 44, 968–977. doi: 10.1002/mus.22224

Tanaka, S., Terada, K., and Nohno, T. (2011). Canonical Wnt signaling is involved in switching from cell proliferation to myogenic differentiation of mouse myoblast cells. *J. Mol. Signal*. 6:12. doi: 10.1186/1750-2187-6-12

Visser, M., Pahor, M., Taaffe, D. R., Goodpaster, B. H., Simonsick, E. M., Newman, A. B., et al. (2002). Relationship of interleukin-6 and tumor necrosis factor-alpha with muscle mass and muscle strength in elderly men and women: the Health ABC Study. *J Gerontol A Biol. Sci. Med. Sci*. 57, M326–M332. doi: 10.1093/gerona/57.5.M326

von Maltzahn, J., Chang, N. C., Bentzinger, C. F., and Rudnicki, M. A. (2012). Wnt signaling in myogenesis. *Trends Cell Biol*. 22, 602–609. doi: 10.1016/j.tcb.2012.07.008

Wang, Y., Mohamed, J. S., and Alway, S. E. (2013). M-cadherin-inhibited phosphorylation of ß-catenin augments differentiation of mouse myoblasts. *Cell Tissue Res*. 351, 183–200. doi: 10.1007/s00441-012-1515-4

Weintraub, H., Tapscott, S. J., Davis, R. L., Thayer, M. J., Adam, M. A., Lassar, A. B., et al. (1989). Activation of muscle-specific genes in pigment, nerve, fat, liver, and fibroblast cell lines by forced expression of MyoD. *Proc. Natl. Acad. Sci. U.S.A*. 86, 5434–5438. doi: 10.1073/pnas.86.14.5434

Wu, L., Wang, X., Li, Y., Liu, Y., Su, D., Fu, T., et al. (2016). *Toxoplasma gondii* ROP18: potential to manipulate host cell mitochondrial apoptosis. *Parasitol. Res*. 115, 2415–2422. doi: 10.1007/s00436-016-4993-6

Zammit, P. S., Partridge, T. A., and Yablonka-Reuveni, Z. (2006). The skeletal muscle satellite cell: the stem cell that came in from the cold. *J. Histochem. Cytochem*. 54, 1177–1191. doi: 10.1369/jhc.6R6995.2006

Zhang, W., Behringer, R. R., and Olson, E. N. (1995). Inactivation of the myogenic bHLH gene MRF4 results in up-regulation of myogenin and rib anomalies. *Genes Dev*. 9, 1388–1399. doi: 10.1101/gad.9.11.1388

Conflict of Interest: The authors declare that the research was conducted in the absence of any commercial or financial relationships that could be construed as a potential conflict of interest.

frontiers in Cellular and Infection Microbiology

ORIGINAL RESEARCH
published: 04 December 2019
doi: 10.3389/fcimb.2019.00413

Influence of Two Major *Toxoplasma gondii* Virulence Factors (ROP16 and ROP18) on the Immune Response of Peripheral Blood Mononuclear Cells to Human Toxoplasmosis Infection

Alejandro Hernández-de-los-Ríos[1], *Mateo Murillo-Leon*[1], *Luz Eliana Mantilla-Muriel*[2], *Ailan Farid Arenas*[1], *Mónica Vargas-Montes*[1], *Néstor Cardona*[1,2,3], *Alejandra de-la-Torre*[4], *Juan Carlos Sepúlveda-Arias*[2] *and Jorge Enrique Gómez-Marín*[1]*

[1] *Grupo de Estudio en Parasitología Molecular (GEPAMOL), Facultad de Ciencias de la Salud, Centro de Investigaciones Biomédicas, Universidad del Quindío, Armenia, Colombia,* [2] *Grupo Infección e Inmunidad, Facultad de Ciencias de la Salud, Universidad Tecnológica de Pereira, Pereira, Colombia,* [3] *Universidad Antonio Nariño, Armenia, Colombia,* [4] *Grupo NeURos, Unidad de Inmunología, Escuela de Medicina y Ciencias de la Salud, Universidad del Rosario, Bogota, Colombia*

OPEN ACCESS

Edited by:
Tiago W. P. Mineo, Federal University of Uberlandia, Brazil

Reviewed by:
Carsten Lüder, Universitätsmedizin Göttingen, Germany
Dong-Hui Zhou, Fujian Agriculture and Forestry University, China

***Correspondence:**
Jorge Enrique Gómez-Marín
gepamol2@uniquindio.edu.co

In Memoriam:
This paper is dedicated to the memory of Prof. Ermanno Candolfi (1957–2019)

Specialty section:
This article was submitted to Parasite and Host, a section of the journal Frontiers in Cellular and Infection Microbiology

Received: *06 September 2019*
Accepted: *20 November 2019*
Published: *04 December 2019*

Citation:
Hernández-de-los-Ríos A, Murillo-Leon M, Mantilla-Muriel LE, Arenas AF, Vargas-Montes M, Cardona N, de-la-Torre A, Sepúlveda-Arias JC and Gómez-Marín JE (2019) Influence of Two Major Toxoplasma gondii Virulence Factors (ROP16 and ROP18) on the Immune Response of Peripheral Blood Mononuclear Cells to Human Toxoplasmosis Infection. Front. Cell. Infect. Microbiol. 9:413. doi: 10.3389/fcimb.2019.00413

Toxoplasma gondii ROP16 and ROP18 proteins have been identified as important virulence factors for this parasite. Here, we describe the effect of ROP16 and ROP18 proteins on peripheral blood mononuclear cells (PBMCs) from individuals with different clinical status of infection. We evaluated IFN-γ, IL-10, and IL-1β levels in supernatants from PBMCs cultures infected with tachyzoites of the *T. gondii* wild-type RH strain or with knock-out mutants of the *rop16* and *rop18* encoding genes (RHΔ*rop16* and RHΔ*rop18*). Cytokine secretion was compared between PBMCs obtained from seronegative individuals ($n = 10$), with those with chronic asymptomatic ($n = 8$), or ocular infection ($n = 12$). We also evaluated if polymorphisms in the genes encoding for *IFN-γ*, *IL-10*, *IL-1β*, Toll-like receptor 9 (*TLR9),* and purinoreceptor *P2RX7* influenced the production of the encoded proteins after *ex vivo* stimulation. In individuals with chronic asymptomatic infection, only a moderate effect on IL-10 levels was observed when PBMCs were infected with RHΔ*rop16*, whereas a significant difference in the levels of inflammatory cytokines IFN-γ and IL-1β was observed in seronegative individuals, but this was also dependent on the host's cytokine gene polymorphisms. Infection with ROP16-deficient parasites had a significant effect on IFN-γ production in previously non-infected individuals, suggesting that ROP16 which is considered as a virulence factor plays a role during the primary infection in humans, but not in the secondary immune response.

Keywords: peripheral blood mononuclear cells, *Toxoplasma,* ROP16 protein, ROP18 protein, ocular toxoplasmosis, cytokines, polymorphisms

INTRODUCTION

Toxoplasma gondii is an obligate intracellular parasite that infects a broad range of vertebrate hosts. In humans, the most important clinical manifestations are as follows: (*i*) retinochoroiditis, being the most important cause of posterior uveitis and an important cause of blindness in certain countries (De-la-Torre et al., 2009), (*ii*) congenital toxoplasmosis, a public health problem

responsible for early childhood morbidity and mortality (Gómez-Marin et al., 2011), and (*iii*) cerebral toxoplasmosis, the most important cause of neurological symptoms in HIV-infected patients (Cardona et al., 2011). There are host and parasite factors that contribute to the clinical outcome of the infection. One of the most extensively studied are ROP proteins, produced by a set of specialized secretory organelles in the parasite called the rhoptries.

In murine models, quantitative trait locus analysis has allowed the identification of genes that contribute to differences between virulent and non-virulent strains of the parasite (Saeij et al., 2006; Taylor et al., 2006). These genes, which encode the polymorphic serine/threonine (S/T) protein kinases secreted by the rhoptries, are also called ROP kinases proteins (Peixoto et al., 2010). Two of the most extensively studied are ROP16 (TGME49_062730) and ROP18 (TGME49_005250) kinases. ROP16 phosphorylates STAT3 (Ong et al., 2010) and STAT6 (Yamamoto et al., 2009) transcription factors, thereby leading to altered cytokine profiles and the repression of IL-12 signaling (Saeij et al., 2007) required for the generation of IFN-γ by CD4+ and CD8+ T lymphocytes. Both, IL-12 and IFN-γ production are essential for the host to survive infection with *T. gondii* (Scharton-Kersten et al., 1996), and the control of these proinflammatory mediators is achieved by the induction of anti-inflammatory cytokines such as IL-10 (Denkers et al., 2012). On the other hand, in mice, ROP18 interferes with the function of host immunity related GTPases by phosphorylating these proteins thus, avoiding their interaction with the parasitophorous vacuole membrane (Steinfeldt et al., 2010). Although the discovery of these virulence factors in mice prompted an explosion of work to reveal the mechanisms underlying parasite virulence, there are only a few reports on the possible roles of these genes in the human immune response against the parasite (Niedelman et al., 2012; Portillo et al., 2017). Therefore, the aim of this study was to evaluate the secretion of IFN-γ, IL-10, and IL-1β in PBMCs from individuals with different clinical status of infection (ocular, chronic asymptomatic, and non-infected) when stimulated with the virulent wild-type (WT) *T. gondii* RH strain, and with knock-out (KO) *T. gondii rop16* and *rop18* mutants.

MATERIALS AND METHODS

Ethical Considerations

This study was conducted according to the tenets of the Declaration of Helsinki, and strictly adhered to the Guide for Good Laboratory Procedures. It was approved by the Ethics Committee of the Universidad del Quindío, Colombia. All patients agreed to participate in the study and signed the informed consent according to the *Minsalud 8430-resolution*. The results of pertinent clinical laboratory analysis were given to the patient and the attending physician.

Sample Population

Peripheral blood samples were collected from 12 patients with ocular toxoplasmosis (OT), 8 with chronic asymptomatic infection (Asym), and 10 individuals seronegative for IgG and IgM anti-*Toxoplasma* antibodies (Neg) who agreed to participated in this study. Patients with OT were recruited during ophthalmological consultation at the Universidad del Quindío. The clinical diagnosis of OT was based on criteria previously described (De-la-Torre et al., 2009). Briefly, active OT was defined by the presence of an active creamy-white focal retinal lesion, which eventually resulted in hyperpigmented retinochoroidal scars in either eye. Central lesions were defined as lesions located within the large vascular arcades. Lesion sizes were measured in disk diameters, and the inflammation intensity in the anterior segment was measured by counting the number of cells in the anterior chamber using biomicroscopy, and in the posterior pole also by visualizing the vitreous haze using fundoscopy. The inflammation grade was registered according to the standardization of uveitis nomenclature for the reporting of clinical data (Jabs et al., 2005). When the lesions were inactive, the results of the last inflammatory period were recorded from the clinical charts. Asymptomatic patients that agreed to participate had a serological status of chronic infection (IgG anti-*Toxoplasma* positive and IgM anti-*Toxoplasma* negative) and a fundoscopic eye examination negative for ocular lesions.

Parasites

The WT *T. gondii* strain RH or ROP16 and ROP18 null mutants (RHΔ*rop16* and RHΔ*rop18*) tachyzoites were maintained by serial passes in confluent monolayers of human foreskin fibroblast (HFF, ATCC® SCRC-1041™) cultured in DMEM medium (Gibco, Grand Island, NY, USA) supplemented with 2% fetal bovine serum (Gibco), 100 μg/mL streptomycin, and 100 U/mL penicillin. After lysing the cells, the culture supernatant was collected and centrifuged at 500 *g* for 5 min. The cellular debris-free tachyzoites were centrifuged at 1,800 *g* for 15 min and the pellet was resuspended in RPMI 1640 medium (Gibco, Thermo Fisher Scientific, Waltham, MA, United States of America) without supplementation.

Isolation of PBMCs and Cytokine Quantification

About 15 mL of peripheral blood, which was collected from 30 individuals as described above, was centrifuged as separate samples in a Histopaque 1,077 g/mL (Sigma-Aldricth Produtcs, Merck KGaA, Darmstadt, Germany) gradient. The fraction of mononuclear cells was adjusted to 1×10^6 cells/well, after which the cells were plated in 24-well plates and cultured in RPMI 1640 medium (Gibco) without supplementation at 37°C with 5% CO_2. The PBMCs were incubated with concanavalin A (10 μg/mL) or infected with *T. gondii* RH, RHΔ*rop16* or RHΔ*rop18* live tachyzoites with a multiplicity of infection (MOI) of 1:3 over a 24 h period. RPMI was used as control. Supernatants were collected and IFN-γ, IL-10, and IL-1β levels were determined using a commercial enzyme-linked immunosorbent assay (Biolegend, San Diego, CA, USA), results were expressed as pg/mL.

Immune-Related Host Genes Polymorphisms

Single Nucleotide Polymorphisms (SNPs) in the genes encoding the following proteins were evaluated: IL-1β (rs1143634,

rs16944, rs1143627); IL-10 (rs1800871), and IFN-γ (rs2430561). Polymorphisms in the purinoreceptor *P2RX7* (rs1718119, rs1621388, rs2230912) and in the Toll-like receptor gene, *TLR-9* (rs352140), were included. Amplification products were analyzed by capillary electrophoresis. The mini-sequencing technique or "ddNTP primer extension" was used as previously reported (Naranjo-Galvis et al., 2018). Briefly, after genomic DNA was isolated from blood cells using the QIAGEN DNA mini kit (QIAGEN), the SNP-containing regions of interest were PCR-amplified using initiation primers. PCRs, which were carried out in 10 μL volumes, contained 1 to 10 ng of genomic DNA, 1X QIAGEN Multiplex PCR Master Mix (QIAGEN N.V., Venlo, The Netherlands), 1X Q-solution and 0.2–0.6 μM of each specific primer. PCR-amplification of the fragments was performed in a Veriti Thermal Cycler (Applied Biosystems, USA). Using this pre-amplification product as template, multiplex reactions for the detection of SNPs were carried out using the mini-sequencing method (SBE, single base extension). The data were analyzed according the color of the peaks and fragment sizes, using the GeneMapper v3.2 software (Applied Biosystems, USA).

Western Blot Analysis

PBMCs were cultured for 24 h with RH, RHΔ*rop16* or RHΔ*rop18* strains. Then, cells were lysed in RIPA buffer (Amresco, USA) containing a protease inhibitor cocktail (Amresco) and phosphatase inhibitor (Sigma-Aldrich, Darmstadt, Germany). Equivalent amounts of protein were electrophoresed on 10% SDS polyacrylamide gels and then electroblotted onto 0.45 μm nitrocellulose membranes (10600007, GE healthcare). After blocking with 3% milk protein for 30 min at room temperature, the membranes were incubated with the following primary antibodies: anti-phopho-STAT3 (Tyr 705) (Abcam, UK), anti-phopho-STAT6 (Tyr 641) (Abcam), and anti-IL1β (Santa Cruz Biotechnology, USA). The membranes were then washed three times with PBS containing Tween 20 and incubated with polyclonal goat anti-rabbit IgG conjugated with alkaline phosphatase (Sigma-Aldrich, Darmstadt, Germany) for 1 h at room temperature. Positive reactions were detected using Novex® AP Chromogenic Substrate BCIP/NBT (Thermo Fisher, USA). Densitometry analysis was conducted using ImageJ (Schneider et al., 2012), and the signal value from each band was normalized using β-actin (Ambion, USA) as the normalization protein. PBMCs from 3 individuals were randomly selected from each group and the normalized protein expression levels were plotted in a histogram.

Statistical Analysis

The concentration of each cytokine was expressed in pg/mL. The normality of the data was determined using the Kolmogorov-Smirnov test. The non-parametric Mann–Whitney test was

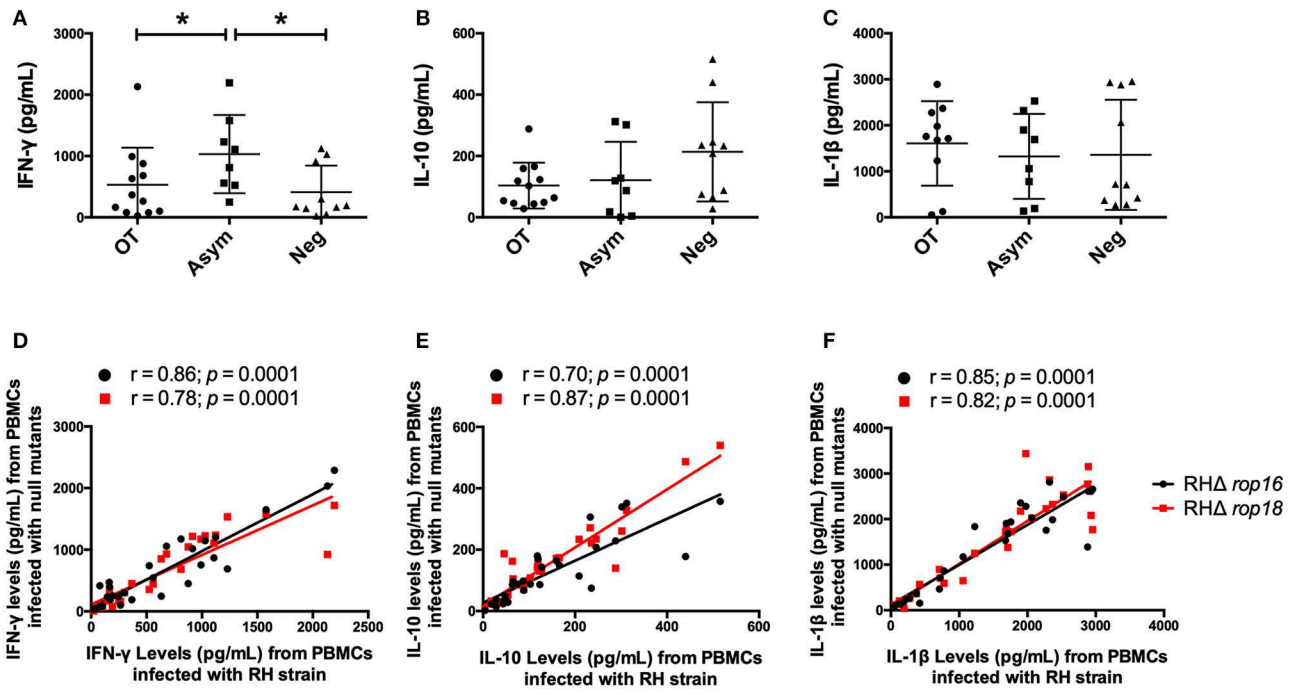

FIGURE 1 | Cytokine secretion by PBMCs infected with the RH strain of *T. gondii*. The concentration of IFN-γ **(A)**, IL-10 **(B)**, and IL-1β **(C)** were determined by ELISA in supernatants at 24 h post-infection (h.p.i.). A correlation analysis on RH, RHΔ*rop*16 and RHΔ*rop*18 strains for each cytokine was performed. The x axis indicates the concentration of IFN-γ **(D)**, IL-10 **(E)**, and IL-1β **(F)** for RH infections. The y axis indicates the same cytokine as in x axes for RHΔ*rop*16 (black circles) or RHΔ*rop*18 (red squares) *T. gondii* infected cells. Each point represents the concentration of cytokines of a single patient. Results **(A–C)** are represented as mean ± SD; $^*p < 0.05$, Mann-Whitney *U* test and the correlations were determined by Spearman's correlation tests. OT, Ocular toxoplasmosis; Asym, Chronic asymptomatic infection; Neg, *T. gondii* seronegative individuals.

used for comparing the cytokine levels between the different groups (OT, Asym, and Neg). To compare differences in cytokine production under the different stimuli (RH, RHΔ*rop16,* and RHΔ*rop18*) within the groups, non-parametric data were analyzed using Wilcoxon signed-rank test. Bar error represent the mean and standard deviation of each group. Correlation analyses were based on the Spearman coefficient. Statistical significance was defined as $p < 0.05$. All data were analyzed using Prism 6.01 software (GraphPad Software version 6.01, San Diego California).

RESULTS

Clinical Characteristics of the Study Subjects

Twenty IgG positive individuals for *T. gondii* (12 OT and 8 Asym), and 10 Neg individuals participated in this study, having a mean age of 32.8 years (range: 23–61 years) and 58% female overall. There were no significant differences in gender or age distribution between groups.

Lower IFN-γ Production Occurred in the Ocular Toxoplasmosis Group Compared With the Chronic Asymptomatic Group Independently of ROP16 and ROP18

We first investigated the cytokines secreted by the PBMCs obtained from individuals with toxoplasmosis (OT and Asym groups) and Neg individuals upon stimulation with WT *T. gondii* RH tachyzoites. IFN-γ production after parasite infection was higher in PBMCs from the Asymp group than in the OT group ($P = 0.0287$) or the Neg group ($P = 0.0205$), indicating that this cytokine tended to be higher in individuals whose infections were resolved and did not have ocular lesions (**Figure 1A**). In contrast, no significant differences were observed for IL-10 and IL-1β secretion among groups (**Figures 1B,C**).

We next investigated whether differences observed in cytokine secretion among groups was related to the *T. gondii* ROP16 and ROP18 virulence factors. First, we confirmed that the mutant parasites indeed lacked the ROP18 protein (**Figure S1**) or the *rop16* gene (**Figure S2**). Then, we evaluated the cytokine

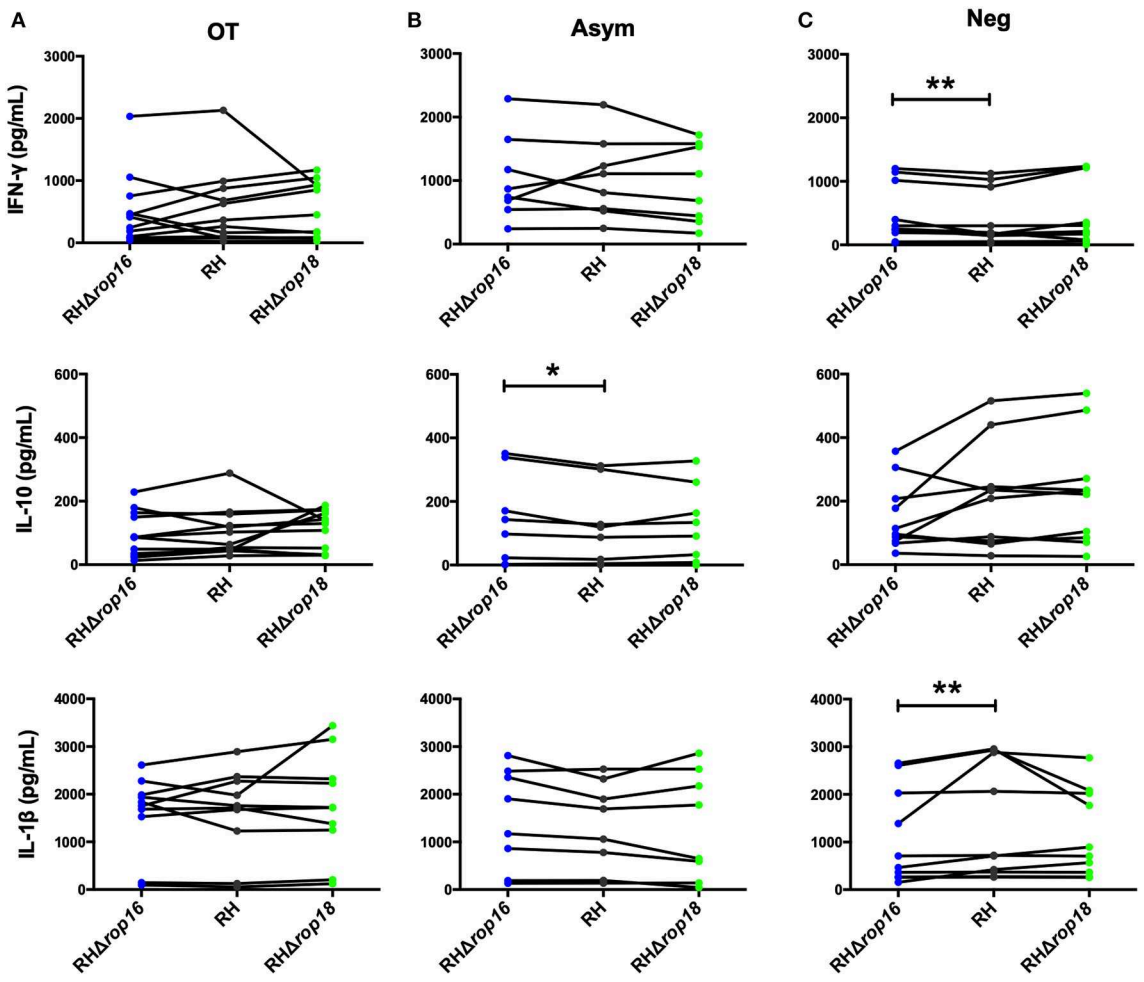

FIGURE 2 | Comparison of cytokine production by PBMCs infected with *T. gondii* RH, RHΔ*rop*16, and RHΔ*rop*18 in culture supernatants at 24 h. OT **(A)**, Asym **(B)**, and Neg **(C)**. *$p < 0.05$, **$p < 0.01$; Wilcoxon signed-rank test. Lines are representative of each individual. OT, Ocular toxoplasmosis; Asym, Chronic asymptomatic infection; Neg, *T. gondii* seronegative individuals.

secretion levels of PBMCs obtained from Asymp, OT, or Neg individuals after infection with live RHΔ*rop16* and RHΔ*rop18* parasite strains. In the group OT, a difference in cytokine production was not observed after *ex-vivo* infection with *rop16* or *rop18* knock-out and WT strains (**Figure 2A**). However, it is important to note that PBMCs from some individuals clearly responded differently to the KO strains when compared with the WT strain, but this was not related with the status of the infection. Only chronic-asymptomatic individuals (Asym) showed a moderately significant increase in IL-10 production when stimulated with RHΔ*rop16* compared to WT (**Figure 2B**). In seronegative (Neg) individuals, infection with RHΔ*rop16* strain induced higher levels of IFN-γ compared with WT strain infection. Conversely, the IL-1β concentration was lower when infected with RHΔ*rop16* strain (**Figure 2C**), showing an opposite relationship between IFN-γ and IL-1β, which are markers for Th1 response. Thus, individuals with OT produced lower levels of IFN-γ than chronic asymptomatic individuals, but this difference seems not to be dependent of the ROP16 and ROP18 *T. gondii* proteins.

We also performed a linear regression analysis with RH, RHΔ*rop16* and RHΔ*rop18,* in order to evaluate the production of each cytokine (**Figures 1D–F**). The tendency in the levels of each cytokine produced by the PBMCs was similar when infected with each strain. However, a slight correlation was observed between IFN-γ and IL-10 (**Figure S3**) and no correlation was observed between IL-1β and IL-10 **(Figure S4)**, which indicates that the increase in these inflammatory cytokines was not followed by the regulatory effect of IL-10 in any group of the individuals we evaluated.

Polymorphisms in the Host's Immune-Related Genes Influence the Cytokine Profile

As knocking out of *T. gondii rop16* or *rop18* genes did not explain most of the differences observed in the cytokine production between individuals or groups, we decided to evaluate polymorphisms in the aforementioned cytokines and other genes from the host that are immune response related. Therefore, to determine the influence of polymorphisms on the cytokine profile, we evaluated SNPs in encoding genes for *IFN-γ*, *IL-10,* and *IL-1β* in a subgroup of 9 individuals with OT, 4 Asym, and 5 Neg. We also included polymorphisms in encoding genes for the purinoreceptor *P2RX7* and *TLR-9,* these two genes were of interests since polymorphisms in them are related with toxoplasmic retinochoroiditis (Ferrari et al., 1997; Peixoto-Rangel et al., 2009). As no statistical differences among clinical groups were found we decided to perform an analysis assuming all samples in one single group regardless of clinical condition or

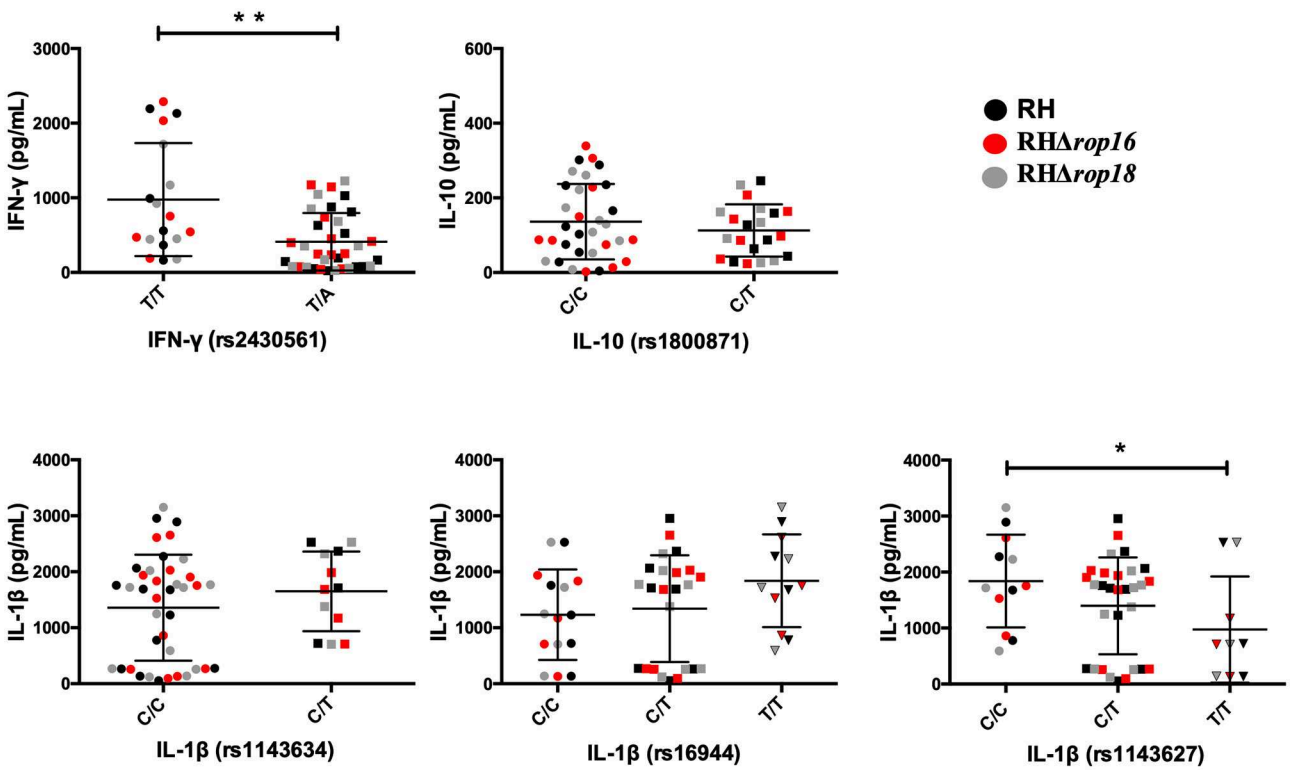

FIGURE 3 | Cytokine production by PBMCs at 24 h post-infection with *T. gondii* RH (Black), RHΔ*rop16* (red), and RHΔ*rop18* (gray) was stratified by genotype of the following SNPs: IFN-γ (rs2430561), IL-10 (rs1800871), and IL-1β (rs1143634, rs16944, rs1143627). The cytokines levels were measured by ELISA. Results are represented by circles or square for individual data and bars are the mean ± SD; $*p < 0.05$, $**p < 0.005$. Mann-Whitney *U* test was performed.

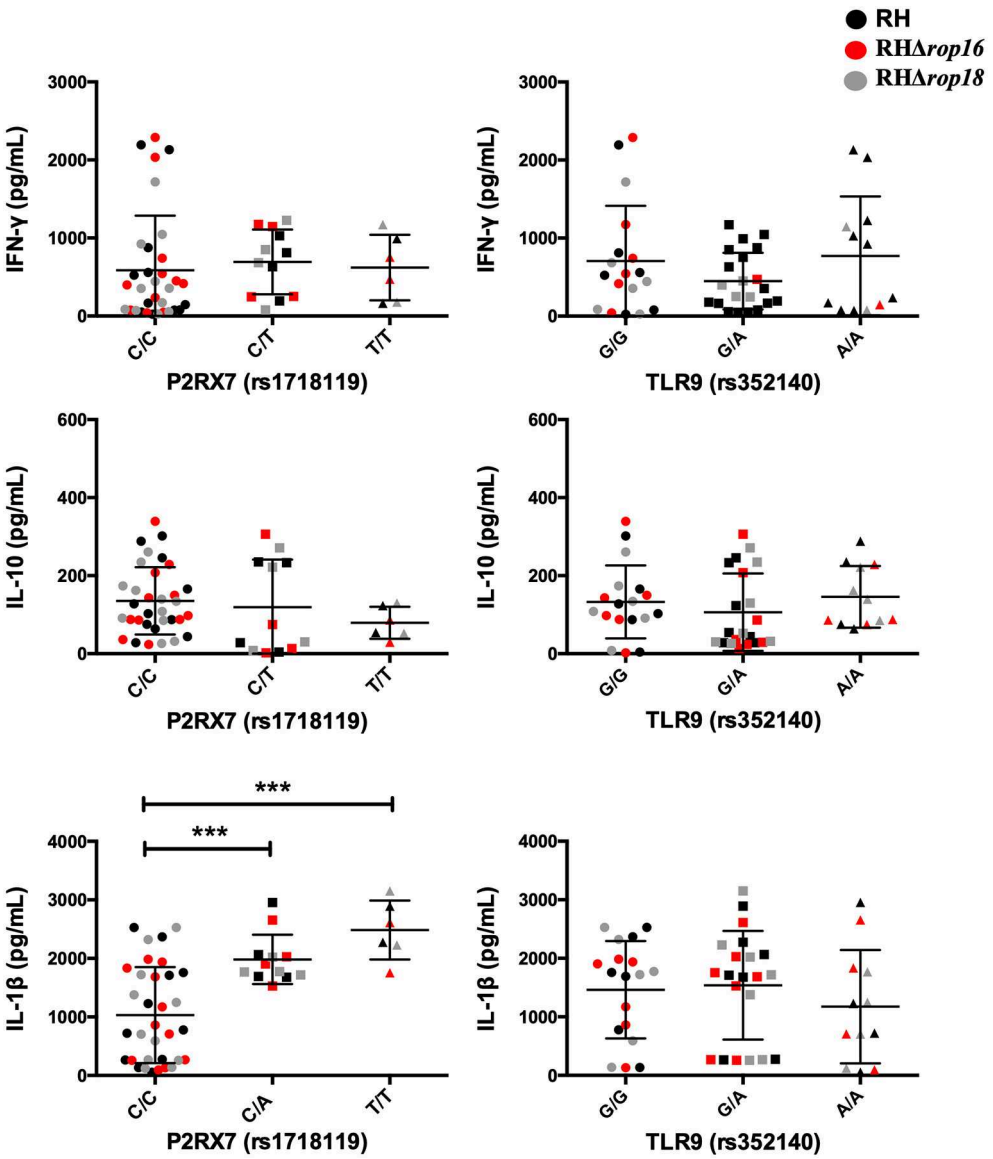

FIGURE 4 | Cytokine production by PBMCs at 24 h post-infection with *T. gondii* RH (Black), RHΔ*rop16* (red), and RHΔ*rop18* (gray) was stratified by genotype of the following SNPs: P2RX7 (rs1718119) and TLR9 (rs352140). The levels of cytokines were measured by ELISA. Results are represented by circles or square for individual data and bars are the mean ± SD; ***$p < 0.001$. Mann-Whitney *U* test was performed.

infecting strain. The IFN-γ, IL-10, and IL-1β levels stratified by the reference SNP (rs) and genotype are shown in **Figure 3**.

The levels of IFN-γ were higher in individuals with T/T genotype when compared with the T/A genotype (656.2 vs. 248 pg/mL, $P = 0.002$). In the same way, a significant difference was observed in IL-1β polymorphism (rs 1143627), where C/C genotype is related to higher production of this cytokine compared with T/T genotype ($P = 0.033$). In contrast, no statistical differences were found for IL-10 levels and polymorphisms. On the other hand, when we evaluated the influence of the genotype of the P2RX7 (rs1718119) membrane receptor on the cytokine profile, we found that the T/T ($P = 0.0004$) and C/A genotype ($P = 0.0009$) are related to IL-1β higher levels than the C/C genotype (**Figure 4**). Finally, no statistical differences were found between TLR-9 polymorphisms (rs352140; C/C $n = 2$; C/T $n = 4$, T/T $n = 3$) and the cytokines levels we evaluated (IFN-γ mean levels: C/C 715 pg/ml vs. C/T 1402 vs. T/T 1688 pg/ml, $P = 0.86$; IL1-β mean levels: C/C 65 vs. C/T 331 pg/ml vs. T/T 445 pg/ml, $P = 0.54$; IL10 mean levels: C/C 367 pg/ml vs. C/T 692 pg/ml vs. T/T 668 pg/ml, $P = 0.54$).

STAT3 and STAT6 Phosphorylation Is Not Dependent on the *T. gondii* ROP16 Protein in Human PBMCs

The kinase activity of ROP16 has been shown to be essential for downregulating the IL-12 mediated response by phosphorylating

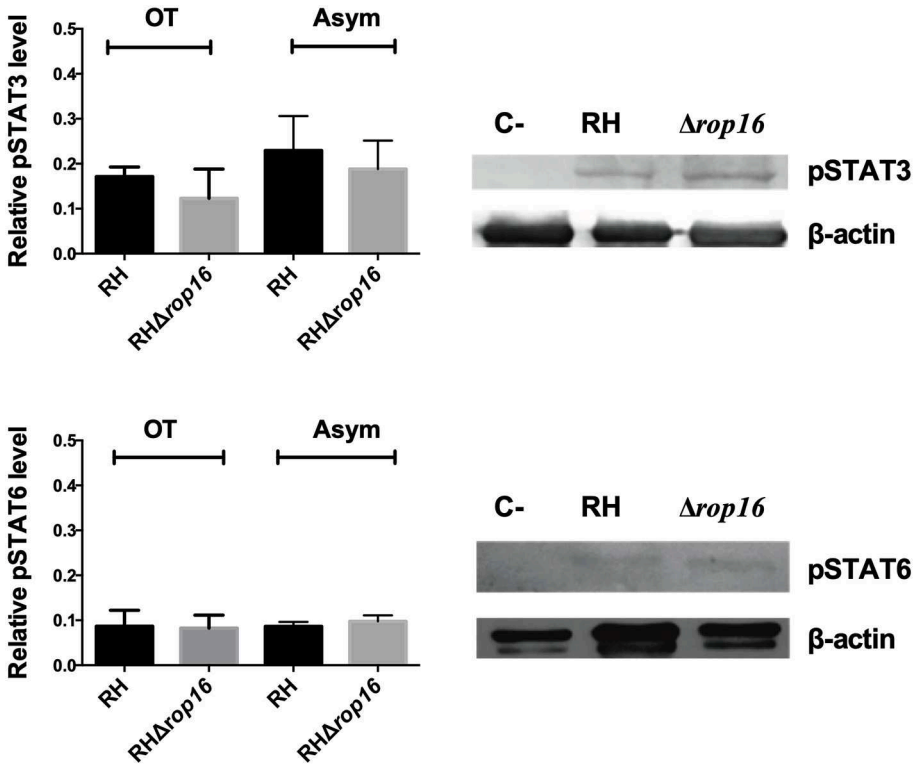

FIGURE 5 | Phosphorylation of STAT3 and STAT6 by ROP16 protein. PBMCs were infected with *T. gondii* RH or RHΔ*rop16* strains for 24 h. STAT phosphorylation was evaluated by Western blot of PBMCs lysates from OT and Asym individuals. The western blot results were quantified by densitometry and Mann-Whitney *U* test was performed with no statistically significant differences ($p > 0.05$) between the stimulus in either of the clinical cases evaluated (TO and Asym). Histogram represent mean of relative levels of protein ± SEM of three independent experiments. One representative western blot result for OT and Asym group is shown. C(-), Uninfected PBMCs were used as a negative control; OT, Ocular toxoplasmosis; Asym, Chronic asymptomatic infection.

STAT3 and STAT6 transcription factors (Saeij et al., 2006, 2007). However, we did not find a significant difference in proinflammatory cytokine levels (IFN-γ and IL-1β) in the OT and Asym groups. To evaluate whether the kinase activity of ROP16 might affect the STAT3 (Tyr 705) and STAT6 (Tyr 641) transcription factors, we infected human PBMCs with live RH or RHΔ*rop16* strains over a 24 h period. The resultant cells were lysed, and their intracellular extracts were analyzed by western blot. In the absence of *rop16* (RHΔ*rop16*), the amount of phosphorylated STAT3 and STAT6 when separately infected with each parasite strain was not significantly different ($P > 0.05$) (**Figure 5**).

Immature Pro-IL-1β Levels in Human PBMCs Were Higher in RHΔrop18 Infections

It has been reported that the ROP18 virulence factor phosphorylates the dimerization domain of the p65 NF-κB subunit, leading to its downregulation and further reduction of TNF-α, IL-6, and IL-12 secretion in murine and human macrophages cell lines (Du et al., 2014). Because transcription of the IL-1β gene is under NF-κB control, we evaluated the levels of pro-IL-1β in cell lysates of PBMCs infected with either RH or RHΔ*rop18* tachyzoites. We found higher levels of pro-IL-1β in cells infected with RHΔ*rop18* than in cells infected with RH tachyzoites in all groups (OT, Asym, Neg) (**Figure 6**). Intriguingly, as we showed before in this work, there were no significant difference in the secretion of IL-1β when PBMCs are infected with RH or RHΔ*rop18* strains (**Figures 1C**, **2**), suggesting the existence of a second mechanism influencing the observed differences between the groups in the production of this cytokine.

DISCUSSION

Cytokines have been shown to play an important role in the pathogenesis of toxoplasmosis (Sullivan and Jeffers, 2012). Following the multiplication phase, where the parasites disseminate throughout the body, the host's immune system takes control and eliminates most of the parasites, mainly by cellular responses such as IFN-γ production driven by Th1 type responses (Pifer and Yarovinsky, 2011). Here we found that individuals with ocular toxoplasmosis produce low levels of IFN-γ compared with the chronic asymptomatic individuals, suggesting that the development of this clinical manifestation (OT) is associated with a defect to produce adequate levels of

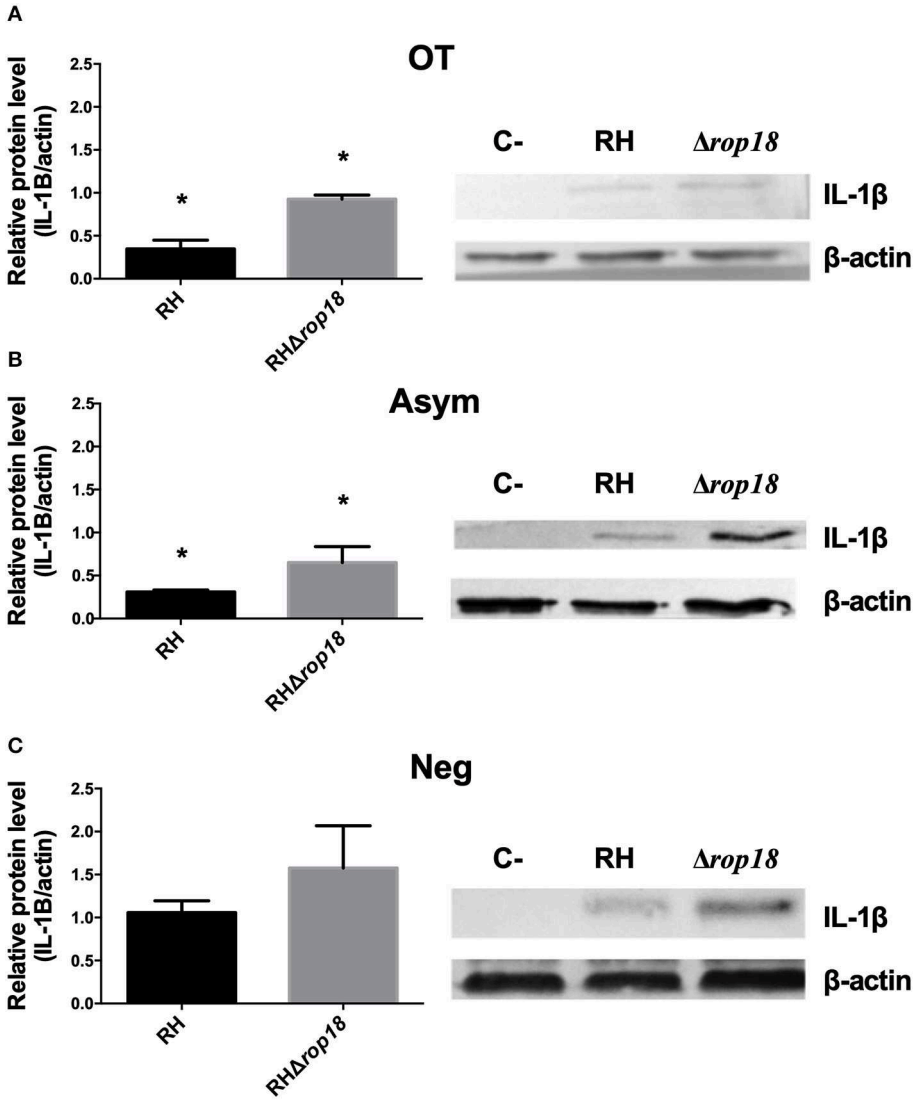

FIGURE 6 | Immature IL-1β in lysates from PBMCs stimulated with *T. gondii* RH and RHΔ*rop*18. The presence of immature pro-IL-1β was evaluated using a western blot and quantified by densitometry. Histogram represent the mean of relative levels of protein ± SEM of three independent experiments. The OT **(A)**, Asym **(B)**, and Neg **(C)** clinical groups are shown. *$p < 0.05$, Mann-Whitney *U* test. One representative western blot for each clinical group is shown.

IFN-γ. This finding is similar to that reported previously, where IFN-γ levels were higher in asymptomatic individuals than in patients with cerebral (Meira et al., 2014) or ocular (De-la-Torre et al., 2013) toxoplasmosis. We also found that the IFN-γ levels were higher in the asymptomatic infected group than in the seronegative group. This finding could be related to the release of high levels of IFN-γ during a chronic infection, by the parasite-specific T lymphocytes, that are required to prevent cyst reactivation (Sarciron and Gherardi, 2000).

A concomitantly produced cytokine that normally acts as a negative feedback mechanism of IFN-γ is IL-10 (Damsker et al., 2010). IL-10 is an immunomodulatory cytokine produced by several cell types (Garra et al., 2004), and in OT Colombian patients it seems to be central in the induction of the permissive state seen in the eye (De-la-Torre et al., 2014; Torres-Morales et al., 2014). However, we did not find any difference in the secretion of this cytokine between groups. One possible explanation lies in the fact that in our previous studies we used total lysate antigen to stimulate PBMCs, but because *T. gondii* release proteins that are involved in the parasite's immune evasion mechanisms in a highly regulated manner (Tosh et al., 2016), the use of live parasites is recommended for this type of immunological experiments (Acosta Davila and Hernandez De Los Rios, 2019).

Our research group has previously suggested that severe ocular infections in South America are caused by highly

variable *T. gondii* strains and are characterized by a completely different local immune response pattern and much higher ocular parasite loads (De-la-Torre et al., 2013; Pfaff et al., 2014), where the lower Th1 response in Colombian patients with OT, as compared with European patients, can be explained by a specific modulation of the immune response by South American strains (De-la-Torre et al., 2014). To determine whether this immune response modulation is related to the ROP16 or ROP18 virulence factors, we stimulated the PBMCs obtained from the chronic asymptomatic individuals, patients with OT and *T. gondii* seronegative controls with the knock-out (RHΔ*rop16* and RHΔ*rop18*) parasite strains, separately. Our findings show that ROP16 have a modulatory effect on the production of IFN γ only in seronegative individuals, suggesting that secondary response can overcome the immunoregulatory effect of this virulent protein.

Furthermore, it has been reported that the ROP16 protein phosphorylates host STAT3 and STAT6 transcription factors, which limits the protective Th1 cytokine response (Butcher et al., 2011) and rop16-deficient type I parasites fail to active STAT3/6 (Denkers et al., 2012). In our study, phosphorylation of STAT3 and STAT6 transcription factors after infection with *T. gondii* RH or RHΔ*rop16* was not different between the OT and Asym groups. It is possible that an alternative phosphorylation pathway or pathways are activated during the invasion process, as occurs in other mammalian cells where *T. gondii* activated-signaling mediates ROP16-independent STAT3 activation (Portillo et al., 2017). It is also possible that chronic inflammation can set up altered microenvironments that are encountered by circulating PBMCs, and that abnormal cytokines profiles within these microenvironments could alter the host's signaling pathways (Montag and Lotze, 2006).

The next question we addressed was whether polymorphisms in the host's immune system-related genes were associated with differences in cytokine secretion from the PBMCs infected with *T. gondii*. We investigated this because during toxoplasmosis infection, polymorphisms in both IFN-γ (rs2430561) and IL-10 (rs1800871) and the "GAG" haplotype in the IL-1β gene's promoter (SNPs at rs1143634, rs1143627, rs16944) are associated with the development of OT in the Colombian population (Naranjo-Galvis et al., 2018). Regarding the IFN-γ promoter (SNP rs2430561) polymorphism, we found that individuals with the T/T genotype produced higher levels of IFN-γ than those with T/A alleles. This results are in agreement with the findings from previous studies (De Albuquerque et al., 2009; Neves et al., 2013; Naranjo-Galvis et al., 2018) where the A-allele was found to enhance susceptibility to OT, and also shown the importance of host genetics in terms of IFN-γ secretion in the anti-parasite response. The T/T genotype has previously been reported to be associated with protection against the retinochoroiditis caused by toxoplasmosis (De Albuquerque et al., 2009). In the present study, the T/T genotype and IFN-γ showed no relationship with the clinical condition, but this may have been related to the lower statistical power that came into play with our study.

Finally, it is known that ATP-binding to the purinergic P2X7 (encoded by P2RX7) receptor, stimulates pro-inflammatory cytokines and can lead to killing of intracellular pathogens. Activation of P2X7 stimulates inflammasome activation and secretion of IL-1β (Ferrari et al., 1997). Here, we found that individuals carrying the T-allele in *P2RX7* gene (SNP rs1718119) produced higher levels of IL-1β, which may represent a protective factor against *T. gondii*. This result is in agreement with previous work where the ancestral T-allele (SNP rs1718119) was strongly protective against toxoplasmic retinochroiditis (Jamieson et al., 2010).

In summary, our data show that in PBMCs from individuals with chronic infection (OT and Asym), the production of proinflammatory cytokines such as IFN-γ and IL-1β does not seem to be influenced by ROP16 or ROP18 proteins from *T. gondii*, but by the host's polymorphisms in the cytokine genes. These results indicate that the immune response to the parasite in humans does no only depend on the presence of virulence factors like ROP16 and ROP18 in the parasite, but on the genetic susceptibility of the host to the parasitic infection also.

DATA AVAILABILITY STATEMENT

The raw data supporting the conclusions of this manuscript will be made available by the authors, without undue reservation, to any qualified researcher.

ETHICS STATEMENT

The studies involving human participants were reviewed and approved by Comité de Bioética, Universidad del Quindío. The patients/participants provided their written informed consent to participate in this study.

AUTHOR CONTRIBUTIONS

AH designed and performed the experiments and wrote the paper. MM-L, LM-M, AA, MV-M, and NC performed experiments. AT recruited and examined the OT patients. JS-A designed experiments. JG-M designed experiments and analyzed the data.

FUNDING

This work was funded by COLCIENCIAS (Projects 1113-744-55483 and 1110-569-34589), Universidad del Quindío and Universidad Tecnológica de Pereira (Projects 5-14-1 and 5-11-13).

ACKNOWLEDGMENTS

We thank David Sibley (Washington University School of Medicine) for providing RHΔ*rop18* strain and to Professor Ermanno Candolfi (University of Strasbourg, France) for providing us with the ROP Δ*rop16* strain.

SUPPLEMENTARY MATERIAL

The Supplementary Material for this article can be found online at: https://www.frontiersin.org/articles/10.3389/fcimb.2019.00413/full#supplementary-material

Figure S1 | Verification of the absence of ROP18 protein in the total antigen extracts by western blot. (1) Molecular weight markers. (2) *T. gondii* RH strain. (3) *T. gondii* KO-*rop18* strain.

Figure S2 | Verification of absence of *rop16* gene after specific PCR in a KO strain. (1) Molecular marker. (2) *T. gondii* RH strain. (3) *T. gondii* KO-*rop16* strain.

Figure S3 | Linear regression analysis on RH, RHΔ*rop*16 and RHΔ*rop*18 strains between IFN-γ and IL-10, showing no correlation between these cytokines.

Figure S4 | Linear regression analysis on RH, RHΔ*rop*16 and RHΔ*rop*18 strains between IL-1β and IL-10, showing no correlation between these cytokines.

REFERENCES

Acosta Davila, J. A., and Hernandez De Los Rios, A. (2019). An overview of peripheral blood mononuclear cells as a model for immunological research of *Toxoplasma gondii* and other apicomplexan aarasites. *Front. Cell. Infec. Microbiol.* 9, 1–10. doi: 10.3389/fcimb.2019.00024

Butcher, B. A., Fox, B. A., Rommereim, L. M., Kim, S. G., Maurer, K. J., and Yarovinsky, F. (2011). Toxoplasma gondii Rhoptry Kinase rop16 activates stat3 and stat6 resulting in cytokine inhibition and arginase-1-dependent growth control. *PLoS Pathog.* 7:e1002236. doi: 10.1371/journal.ppat.1002236

Cardona, N., Basto, N., Parra, B., Zea, A. F., Pardo, C. A., and Bonelo, A. (2011). Detection of toxoplasma DNA in the peripheral blood of HIV-positive patients with neuro-opportunistic infections by a Real-Time PCR assay. *J. Neuroparasitol.* 2, 1–6. doi: 10.4303/jnp/N110402

Damsker, J. M., Hansen, A. M., and Caspi, R. R. (2010). Th1 and Th17 cells. *An. N. Y. Acad. Sci.* 1183, 211–221. doi: 10.1111/j.1749-6632.2009.05133.x

De Albuquerque, M. C., do Couto Aleixo, A. L. Q., Benchimol, E. I., Leandro, A. C. C. S., das Neves, L. B., and Vicente, R. T. (2009). The IFN-γ+874T/A gene polymorphism is associated with retinochoroiditis toxoplasmosis susceptibility. *Mem. Inst. Oswaldo Cruz* 104, 451–455. doi: 10.1590/S0074-02762009000300009

De-la-Torre, A., López-Castillo, C. A., Rueda, J. C., Mantilla, R. D., Gómez-Marín, J. E., and Anaya, J. M. (2009). Clinical patterns of uveitis in two ophthalmology centres in Bogota, Colombia. *Clin. Exp. Ophthal.* 37, 458–466. doi: 10.1111/j.1442-9071.2009.02082.x

De-la-Torre, A., Pfaff, A. W., Grigg, M. E., Villard, O., Candolfi, E., and Gomez-Marin, J. E. (2014). Ocular cytokinome is linked to clinical characteristics in ocular toxoplasmosis. *Cytokine.* 68, 23–31. doi: 10.1016/j.cyto.2014.03.005

De-la-Torre, A., Sauer, A., Pfaff, A. W., Bourcier, T., Brunet, J., and Speeg-Schatz, C. (2013). severe South American ocular toxoplasmosis is associated with decreased Ifn-γ/Il-17a and increased Il-6/Il-13 intraocular levels. *PLoS Negl. Trop. Dis.* 7:e2541. doi: 10.1371/journal.pntd.0002541

Denkers, E. Y., Bzik, D. J., Fox, B. A., and Butcher, B. A. (2012). An inside job: hacking into janus kinase/signal transducer and activator of transcription signaling cascades by the intracellular protozoan *Toxoplasma gondii*. *Infect. Imm.* 80, 476–482. doi: 10.1128/IAI.05974-11

Du, J., An, R., Chen, L., Shen, Y., Chen, Y., Cheng, L., et al. (2014). *Toxoplasma gondii* virulence factor rop18 inhibits the host nf-kb pathway by promoting p65 degradation. *J. Biol. Chem.* 289, 12578–12592. doi: 10.1074/jbc.M113.544718

Ferrari, D., Chiozzi, P., Falzoni, S., Dal Susino, M., Melchiorri, L., and Baricordi, O. R. (1997). Extracellular ATP triggers IL-1 beta release by activating the purinergic P2Z receptor of human macrophages. *J. Immunol.* 159, 1451–1458.

Garra, A. O., Vieira, P. L., Vieira, P., and Goldfeld, A. E. (2004). Review series IL-10 – producing and naturally occurring CD4 + Tregs : limiting collateral damage. *J. Clin. Invest.* 114, 1–7. doi: 10.1172/JCI23215

Gómez-Marin, J. E., de-la-Torre, A., Angel-Muller, E., Rubio, J., Arenas, J., and Osorio, E. (2011). First colombian multicentric newborn screening for congenital toxoplasmosis. *PLoS Negl. Trop. Dis.* 5:e1195. doi: 10.1371/journal.pntd.0001195

Jabs, D. A., Nussenblatt, R. B., Rosenbaum, J. T., Atmaca, L. S., Becker, M. D., and Brezin, A. P. (2005). Standardization of uveitis nomenclature for reporting clinical data. results of the first international workshop. *Am. J. Ophthalmol.* 140, 509–516. doi: 10.1016/j.ajo.2005.03.057

Jamieson, S. E., Hargrave, A. C., De Roubaix, L., Mui, E. J., Boulter, N. R., and Miller, E. N. (2010). Evidence for associations between the purinergic receptor. *Genes Immun.* 11, 374–383. doi: 10.1038/gene.2010.31

Meira, C. S., Pereira-Chioccola, V. L., Vidal, J. E., de Mattos, C. C. B., Motoie, G., and Costa-Silva, T. A. (2014). Cerebral and ocular toxoplasmosis related with IFN-γ, TNF-α, and IL-10 levels. *Front. Microbiol.* 5, 1–7. doi: 10.3389/fmicb.2014.00492

Montag, D. T., and Lotze, M. T. (2006). Rapid flow cytometric measurement of cytokine-induced phosphorylation pathways [CIPP] in human peripheral blood leukocytes. *Clin. Immunol.* 121, 215–226. doi: 10.1016/j.clim.2006.06.013

Naranjo-Galvis, C. A., de-la-Torre, A., Mantilla-Muriel, L. E., Beltrán-Angarita, L., Elcoroaristizabal-Martín, X., McLeod, R., et al. (2018). Genetic polymorphisms in cytokine genes in colombian patients with ocular toxoplasmosis. *Infect. Immun.* 86:e00597. doi: 10.1128/IAI.00597-17

Neves, E., de, S., Curi, A. L. L., de Albuquerque, M. C., Palhano-Silva, C. S., Silva, L. B., and da, Bueno, W. F. (2013). Genetic polymorphism for IFNγ +874T/A in patients with acute toxoplasmosis. *Rev. Soc. Bras. Med. Trop.* 45, 757–760. doi: 10.1590/S0037-86822012000600020

Niedelman, W., Gold, D. A., Rosowski, E. E., Sprokholt, J. K., Lim, D., and Arenas, A. F. (2012). The rhoptry proteins ROP18 and ROP5 mediate *Toxoplasma gondii* evasion of the murine, but not the human, interferon-gamma response. *PLoS Pathog.* 8:e1002784. doi: 10.1371/journal.ppat.1002784

Ong, Y. C., Reese, M. L., and Boothroyd, J. C. (2010). Toxoplasma rhoptry protein 16 (ROP16) subverts host function by direct tyrosine phosphorylation of STAT6. *J. Biol. Chem.* 285, 28731–28740. doi: 10.1074/jbc.M110.112359

Peixoto, L., Chen, F., Harb, O. S., Davis, P. H., Beiting, D. P., and Brownback, C. S. (2010). Integrative genomic approaches highlight a family of parasite-specific kinases that regulate host responses. *Cell Host Microbe* 8, 208–218. doi: 10.1016/j.chom.2010.07.004

Peixoto-Rangel, A. L., Miller, E. N., Castellucci, L., Jamieson, S. E., Peixe, R. G., Elias Lde, S., et al. (2009). Candidate gene analysis of ocular toxoplasmosis in Brazil: evidence for a role for toll-like receptor 9 (TLR9). *Mem. Inst. Oswaldo Cruz* 104, 1187–1190. doi: 10.1590/S0074-02762009000800019

Pfaff, A. W., de-la-Torre, A., Rochet, E., Brunet, J., Sabou, M., and Sauer, A. (2014). New clinical and experimental insights into Old World and neotropical ocular toxoplasmosis. *Int. J. Parasitol.* 44, 99–107. doi: 10.1016/j.ijpara.2013.09.007

Pifer, R., and Yarovinsky, F. (2011). Innate responses to *Toxoplasma gondii* in mice and humans. *Trends Parasitol.* 27, 388–393. doi: 10.1016/j.pt.2011.03.009

Portillo, J. A. C., Muniz-Feliciano, L., Lopez Corcino, Y., Lee, S. J., Van Grol, J., and Parsons, S. J. (2017). *Toxoplasma gondii* induces FAK-Src-STAT3 signaling during infection of host cells that prevents parasite targeting by autophagy. *PLoS Pathog.* 13, 1–23. doi: 10.1371/journal.ppat.1006671

Saeij, J. P. J., Boyle, J. P., Coller, S., Taylor, S., Sibley, L. D., and Brooke-Powell, E. T. (2006). Polymorphic secreted kinases are key virulence factors in toxoplasmosis. *Science* 314, 1780–1783. doi: 10.1126/science.1133690

Saeij, J. P. J., Coller, S., Boyle, J. P., Jerome, M. E., White, M. W., and Boothroyd, J. C. (2007). Toxoplasma co-opts host gene expression by injection of a polymorphic kinase homologue. *Nature* 445, 324–327. doi: 10.1038/nature05395

Sarciron, M. E., and Gherardi, A. (2000). Cytokines involved in toxoplasmic encephalitis. *Scand. J. Immunol.* 52, 534–543. doi: 10.1046/j.1365-3083.2000.00817.x

Scharton-Kersten, T. M., Wynn, T. A., Denkers, E. Y., Bala, S., Grunvald, E., and Hieny, S. (1996). In the absence of endogenous IFN-gamma, mice develop unimpaired IL-12 responses to *Toxoplasma gondii* while failing to control acute infection. *J. Immunol.* 157, 4045–4054.

Schneider, C. A., Rasband, W. S., and Eliceiri, K. W. (2012). NIH image to imagej: 25 years of image analysis. *Nat. Met.* 9, 671–675. doi: 10.1038/nmeth.2089

Steinfeldt, T., Könen-Waisman, S., Tong, L., Pawlowski, N., Lamkemeyer, T., and Sibley, L. D. (2010). Phosphorylation of mouse immunity-related gtpase (IRG) resistance proteins is an evasion strategy for virulent *Toxoplasma gondii*. *PLoS Biol.* 8:e1000576. doi: 10.1371/journal.pbio.1000576

Sullivan, W. J., and Jeffers, V. (2012). Mechanisms of *Toxoplasma gondii* persistence and latency. *FEMS Microbiol. Rev.* 36, 717–733. doi: 10.1111/j.1574-6976.2011.00305.x

Taylor, S., Barragan, A., Su, C., Fux, B., Fentress, S. J., and Tang, K. (2006). A secreted serine-threonine kinase determines virulence in the eukaryotic pathogen *Toxoplasma gondii*. *Science* 314, 1776–1780. doi: 10.1126/science.1133643

Torres-Morales, E., Taborda, L., Cardona, N., De-la-Torre, A., Sepulveda-Arias, J. C., Patarroyo, M. A., et al. (2014). Th1 and Th2 immune response to P30 and ROP18 peptides in human toxoplasmosis. *Med. Microbiol. Immunol.* 203, 315–322. doi: 10.1007/s00430-014-0339-0

Tosh, K. W., Mittereder, L., Bonne-Annee, S., Hieny, S., Nutman, T. B., and Singer, S. M. (2016). The IL-12 response of primary human dendritic cells and monocytes to *Toxoplasma gondii* is stimulated by phagocytosis of live parasites rather than host cell invasion. *J. Immunol.* 196, 345–356. doi: 10.4049/jimmunol.1501558

Yamamoto, M., Standley, D. M., Takashima, S., Saiga, H., Okuyama, M., and Kayama, H. (2009). A single polymorphic amino acid on *Toxoplasma gondii* kinase ROP16 determines the direct and strain-specific activation of Stat3. *J. Exp. Med.* 206, 2747–2760. doi: 10.1084/jem.20091703

Conflict of Interest: The authors declare that the research was conducted in the absence of any commercial or financial relationships that could be construed as a potential conflict of interest.

frontiers in Cellular and Infection Microbiology

METHODS
published: 14 January 2020
doi: 10.3389/fcimb.2019.00461

Serum IgG Anti-*Toxoplasma gondii* Antibody Concentrations Do Not Correlate Nested PCR Results in Blood Donors

*Fabiana Nakashima[1], Valquíria Sousa Pardo[1], Marcos Paulo Miola[1,2], Fernando Henrique Antunes Murata[3], Natalia Paduan[1], Stefani Miqueline Longo[1], Cinara Cássia Brandão de Mattos[1,3], Vera Lucia Pereira-Chioccola[4], Octávio Ricci Jr.[2] and Luiz Carlos de Mattos[1,3]**

[1] Immunogenetics Laboratory, Molecular Biology Department, Faculdade de Medicina de São José do Rio Preto, São Paulo, Brazil, [2] Blood Bank São José do Rio Preto, Fundação Faculdade Regional de Medicina, São Paulo, Brazil, [3] FAMERP Toxoplasma Research Group, São Paulo, Brazil, [4] Parasite Molecular Biology Laboratory, Instituto Adolfo Lutz, São Paulo, Brazil

OPEN ACCESS

Edited by:
Jorge Enrique Gómez Marín, University of Quindío, Colombia

Reviewed by:
Elisa Azuara-Liceaga, Universidad Autónoma de la Ciudad de México, Mexico
Travis Bourret, Creighton University, United States

***Correspondence:**
Luiz Carlos de Mattos
luiz.demattos@famerp.br;
luiz.demattos@outlook.com

Specialty section:
This article was submitted to Parasite and Host, a section of the journal Frontiers in Cellular and Infection Microbiology

Received: 09 September 2019
Accepted: 16 December 2019
Published: 14 January 2020

Citation:
Nakashima F, Pardo VS, Miola MP, Murata FHA, Paduan N, Longo SM, Brandão de Mattos CC, Pereira-Chioccola VL, Ricci O Jr and de Mattos LC (2020) Serum IgG Anti-Toxoplasma gondii Antibody Concentrations Do Not Correlate Nested PCR Results in Blood Donors. Front. Cell. Infect. Microbiol. 9:461. doi: 10.3389/fcimb.2019.00461

Background: *Toxoplasma gondii* infects millions of individuals worldwide. This protozoan is food and water-borne transmitted but blood transfusion and organ transplantation constitute alternative forms for transmission. However, the influence of IgG anti-*T. gondii* antibodies in molecular analysis carried out in peripheral blood still remain unclear. This study aimed to investigate the serum IgG anti-*T. gondii* antibody concentrations correlate Nested PCR results in blood donors.

Methods: 750 blood donors were enrolled. IgM and IgG anti-*T. gondii* antibodies were assessed by ELISA (DiaSorin, Italy). Nested PCR was performed with primers JW62/JW63 (288 bp) and B22/B23 (115 bp) of the *T. gondii B1* gene. The mean values of IgG concentration were compared for PCR positive and PCR Negative blood donors using the *t*-test or Mann-Whitney according to the normal distribution (p-value ≤ 0.05).

Results: 361 (48.1%) blood donors presented positive serology as follow: IgM^+/IgG^-: 5 (0.6%); IgM^+/IgG^+: 21 (2.8%); IgM^-/IgG^+: 335 (44.7%) and 389 (51.9%), negative serology. From 353 blood donors with positive serology tested, the Nested PCR was positive in 38 (10.8%) and negative in 315 (89.2%). There were no differences statistically significant between the mean values of serum IgG anti-*T. gondii* antibody concentrations and the Nested PCR results.

Conclusions: In conclusion, our data show that variations in the serum IgG anti-*T. gondii* antibody concentrations do not correlate *T. gondii* parasitemia detected by Nested PCR in chronically infected healthy blood donors.

Keywords: *Toxoplasma gondii*, serology, molecular diagnosis, Nested PCR, serology assay, transfusion, blood donation and transfusion, blood donnors

BACKGROUND

The infection by *Toxoplasma gondii* is frequent around the world and its prevalence range from <30% to more than 60% (Pappas et al., 2009; Dubey et al., 2012; Wallon and Peyron, 2018; Greigert et al., 2019). Different clinical forms of toxoplasmosis resulting from the infection by this Apicomplexan parasite arises and drawn attention especially for pregnant women, newborns and other immunosuppressed patients (Robert-Gangneux and Dardé, 2012; Neu et al., 2015; Rostami et al., 2019; Vidal, 2019).

T. gondii infection is a subject of social, epidemiological, clinical and scientific interest in Brazil. The rates of seroprevalence and the great genomic diversity of this parasite are high around the country (Dubey et al., 2012). Among the different ways to transmit *T. gondii* infection, the transfusion of blood products has been less explored. Two studies carried out in the past reported transmission of *T. gondii* by transfusion of leucocytes and platelets but the authors reached their conclusions after exclude other potential ways by which this parasite could be transmitted (Siegel et al., 1971; Nelson et al., 1989). Even so, this matter still represents a challenge for contemporaneous transfusion medicine (Foroutan et al., 2018; La Hoz et al., 2019).

The diagnosis of infection by *T. gondii* is essentially serological but there are number of published papers demonstrating that the high sensitivity of molecular methods can offer more accurate results on the investigation of infection by this parasite (Mattos et al., 2011; Brenier-Pinchart et al., 2015; Robert-Gangneux et al., 2015; Camilo et al., 2017; Murata et al., 2017; Roux et al., 2018; Greigert et al., 2019; Lévêque et al., 2019; Pleyer et al., 2019). The combination of serology and molecular methods has been used to improve the diagnosis of infection by *T. gondii*. One of them reported that IgG anti-*T. gondii* antibody low avidity correlates positive PCR in pregnant women (Yamada et al., 2011; Murata et al., 2016, 2017; Olariu et al., 2019). The other one also showed that IgG anti-*T. gondii* antibody low avidity correlate positive PCR among patients with ocular toxoplasmosis (Costa-Silva et al., 2008; Mattos et al., 2011; Tsirouki et al., 2018; Cortés et al., 2019; Greigert et al., 2019; Rahimi Esboei et al., 2019). However, correlations between serum anti-*T. gondii* antibody concentrations and molecular diagnosis of *T. gondii* infection among blood donors are scarce in the literature.

Evaluation of the serum IgG anti-*T. gondii* antibody concentrations could contribute to the understanding of the importance of these antibodies as risk biomarkers for transfusional purposes in respect to *T. gondii* transfusional transmission. The aim of this study is to test the hypothesis that low serum concentrations of IgG anti-*T. gondii* antibodies correlate *T. gondii* parasitemia.

METHODS

Ethics Considerations

This study was approved by Research Ethics Committee from Faculdade de Medicina de São José do Rio Preto (case 006/2011). All blood donors received information about the objectives of the study and gave their informed consent.

Selection of Blood Donors

We selected a total of 750 blood donors from both genders able to donate at Regional Blood Center from São José do Rio Preto. All of them were seronegative for other infectious diseases as required by Brazilian policy for blood donation—B and C hepatitis, HIV, Chagas, syphilis, HTLV I/II (Ministério da Saúde, 2011).

Blood Sampling

Two blood samples were obtained from each blood donor by venipuncture from peripheral blood. One of them was collected with EDTA as anticoagulant and used to DNA extraction. The other one was collected without anticoagulant and stored at −20°C until used for detection of IgM and IgG anti-*T. gondii* antibodies.

Serology Assays for IgM and IgG Anti-*T. gondii* Antibodies

Serological tests for specific IgM and IgG antibodies anti-*T. gondii* were carried out by a commercial immunoenzymatic assay kit (DiaSorin, Italy). IgG anti-*T. gondii* antibody concentrations were defined according to the calibrators representing the cut-off values. All the manufacturer's instructions were precisely followed.

DNA Extraction

Genomic DNA of buffy coat from 5 mL of blood samples collected with EDTA was extracted using PureLink Genomic DNA Kits (Invitrogen, Carlsbad, CA), as previously described (Mattos et al., 2011).

PCR Nested Molecular Analysis

Nested PCR was performed using the *B1* gene (accession numbers: *B1* gene *T. gondii* = GenBank: KR559682.1) of *T. gondii* genomic DNA was carried out according to the protocol published by Okay and colleagues (Okay et al., 2009).

The first PCR reaction used the set of primers JW62 (Anti-sense: 5′-TTCTCGCCTCATTTCTGGGTCTAC-3′) and JW63 (Sense: 5′-GCACCTTTCGGACCTCAACAACCG-3′) to amplify a fragment of 288 base pairs. The composition of the mix for each reaction with 25 μL of final volume was: 0.2 μL of each primer, 100 ng of genomic DNA and 1× of Go Taq Green Master Mix (Promega, USA). The conditions of amplification were: 1× initial denaturation at 95°C: 5 min, 40× (denaturation at 95°C: 45 s, annealing at 55°C: 45 s, extension at 72°C: 45 s), 1× final extension at 72°C: 5 min, final at 4°C: 30 min. The amplified fragments were electrophoresed in 2% agarose gel stained with ethidium bromide under UV light.

The second PCR reaction used the set of primers B22 (Sense: 5′-AACGGGCGAGTAGCACCTGAGGAGA-3′) and B23 (Anti-sense: 5′-TGGGTCTACGTCGATGGCATGACAACT-3′) to amplify a fragment of 115 base pairs. The composition of the mix for each reaction with 25 μL of final volume was: 1.2 μM of each primer, 0.5 μL of pre-amplified DNA and 1× of Go Taq Green Master Mix (Promega, USA). The conditions of amplification were: 1× initial denaturation at 95°C: 5 min, 45× (denaturation at 95°C: 45 s, annealing at 55°C: 45 s, extension at 72°C: 45 s), 1×

TABLE 1 | Serology results and the interpretation of the serological profiles and Nested PCR for blood donors.

Serology			Interpretation*	Male		Female		OR	CI 95%	*p***
	n	%		*n*	%	*n*	%			
IgM^+/IgG^-	5	0.6	Recent infection	3	0.6	2	0.8	0.721	0.119–4.349	0.662
IgM^+/IgG^+	21	2.8	Recent infection	19	3.7	2	0.8	4.721	1.090–20.440	0.030
IgM^-/IgG^+	335	44.7	Chronic infection	233	46.0	102	41.8	1.188	0.872–1.618	0.308
IgM^-/IgG^-	389	51.9	Non-immunized	251	49.7	138	56.6	0.756	0.556–1.028	0.086
Total	750	100.0		506		244				

**According to Montoya (2002).*
***Calculated by exact Fisher's test.*

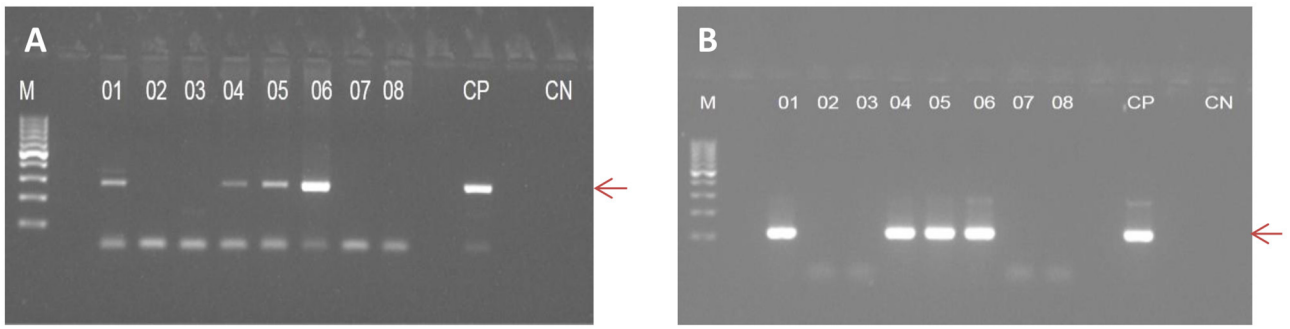

FIGURE 1 | Electrophoretic profile of fragments of *B1* gene from *T. gondii* genomic DNA extracted from peripheral blood of blood donors, amplified by Nested PCR. In **(A)**, the first amplification is showing a fragment of 288 base pairs; in **(B)**, the second amplification is showing a fragment of 115 base pairs. M, molecular marker; PC, Positive Control; CN, Negative Control.

final extension at 72°C: 5 min, final at 4°C: 30 min. The amplified fragments were electrophoresed in 2% agarose gel stained with ethidium bromide under UV light.

Statistical Analysis

The mean values of IgG concentration were compared for blood donors with positive and negative PCR using the *t*-test or Mann-Whitney according to the normal distribution. The level of significance was set at 5% (p-value $\leq$ 0.05). The GraphPad Instat® (GraphPad Software Inc., USA) computer program version 3.06 was used for all analyses.

RESULTS

The serology results and their interpretation are shown in **Table 1**. From the overall blood donors able to donate ($n = 750$), 244 were female (mean age: 32.7 ± 10.7 years), and 506 were male (mean age: 34.7 ± 11.6) ($p = 0.097$). The IgM^+/IgG^+ serology was more frequent in males than in females ($p = 0.0308$). We performed the Nested PCR in 353 blood donors carrying serum IgG antibodies (IgM^+/IgG^+ and IgM^-/IgG^+). **Figure 1** shows the amplified fragment from the genomic DNA of *T. gondii* extracted from peripheral blood carrying 288 and 115 bp, respectively.

There were no differences statistically significant between the mean serum IgG anti-*T. gondii* antibody concentrations and positive or negative Nested PCR results even when the comparisons were made by gender. **Table 2** shows the data from male and female blood donors with positive and negative Nested PCR and serum IgG anti-*T. gondii* antibody concentrations.

DISCUSSION

The aim of this study was to test the hypothesis that serum concentrations of IgG anti-*T. gondii* antibodies correlate *T. gondii* parasitemia in healthy blood donors. As the screening for anti-*T. gondii* antibodies is not compulsory for blood donors in Brazil (Ministério da Saúde, 2011) we performed serological tests to detect IgM and IgG anti-*T. gondii* antibodies as well as Nested PCR targeting *B1* gene from *T. gondii* to detect parasitemia.

Serum IgM and IgG anti-*T. gondii* antibodies have been investigated in blood donors aiming to determine the prevalence of infection in different countries as reviewed by Foroutan-Rad and colleagues (Foroutan-Rad et al., 2016; Foroutan et al., 2018) as well as to estimate the risk of transfusional transmission of this parasite (Siransy et al., 2016; Ferreira et al., 2017; Botein et al., 2019; El-Tantawy et al., 2019). However, correlations between serum IgG anti-*T. gondii* antibody concentrations and the parasitemia determined by molecular methods have not been explored in healthy blood donors. A correlation between high serum IgG anti-*T. gondii* concentrations and negative PCR could be explored as an indicator for low risk of transfusional transmission of this parasite by blood products.

TABLE 2 | Mean age, median, range, normal distribution, IgG anti-*T. gondii* antibodies concentrations according to Nested PCR Positive and Negative in male and female healthy blood donors.

Values	Nested PCR (*N* = 353)			
	Positive (*n* = 38)		Negative (*n* = 315)	
	Male (*n* = 31)	Female (*n* = 7)	Male (*n* = 221)	Female (*n* = 94)
Mean age ± SD	37.7 ± 11.2	38.7 ± 11.9	37.9 ± 10.9	35.0 ± 10.5
Median	38	33	37	34
Range	19–60	23–52	18–65	18–59
25th Percentile (range)	28 (19–37)	23 (23–32)	28 (18–36)	27 (18–33)
75th Percentile (range)	47 (39–60)	51 (50–52)	46 (38–65)	43 (34–59)
Normal distribution	Yes	Yes	Yes	No
IgG^+				
IgG ± SD (UI/mL)	196.0 ± 35.2	165.6 ± 62.7	204.0 ± 33.2	196.6 ± 39.5
Median	205.6	186.8	208.3	205.9
Range	66.1–232.1	36.1–222.8	21.4–257.3	55.2–244.7
25th Percentile (range)	171.9 (66.1–202.1)	145.1 (36.1–168.9)	180.1 (21.4–208.2)	169.6 (55.2–205.8)
75th Percentile (range)	219.5 (206.0–232.1)	212.5 (186.9–222.8)	227.9 (208.4–257.3)	223.6 (205.9–244.7)
Normal distribution	No	Yes	No	No

OBS: Male-PCR+ vs. Male-PCR–: p = 0.2252 (Mann–Whitney U′ = 3,887.0); Female-PCR+ vs. Female-PCR–: p = 0.0960 (Mann–Whitney U′ = 454.00); Male-PCR+ vs. Female-PCR+: p = 0.1065 (Mann–Whitney U′ = 152.00); Male-PCR– vs. Female-PCR–: p = 0.2486 (Mann–Whitney U′ = 11,241.00).

In this study, we observed that none of the IgM^+/IgG^- blood donors were positive for Nested PCR. Only one of the IgM^+/IgG^+ presented positive Nested PCR. Moreover, male and female blood donors with positive Nested PCR presented the mean values of serum IgG anti-*T. gondii* antibody concentrations lower in comparison to their counterpart with negative Nested PCR. However, the differences were not statistically significant. Therefore, low or high serum IgG anti-*T. gondii* antibody concentrations do not correlate the result of molecular analysis by Nested PCR aiming to detect genomic DNA from *T. gondii* in peripheral blood from healthy blood donors.

Molecular methods, such as conventional PCR, Nested PCR, and real-time PCR have been used either in isolation or in association, to detect *T. gondii* parasitemia in acute and chronically infected individuals since they show high sensitivity (Brenier-Pinchart et al., 2015; Dard et al., 2016; Camilo et al., 2017; Roux et al., 2018; Botein et al., 2019; Greigert et al., 2019). In this study, we used the Nested PCR to target the *B1* gene which is one of the most used tests in the literature for detecting *T. gondii* parasitemia (Okay et al., 2009; Mattos et al., 2011; Teixeira et al., 2013; Roux et al., 2018). Moreover, it has been demonstrated that the *B1* gene might be targeted for molecular detection of *T. gondii* parasitemia in Brazilian samples, especially when the investigation is limited to one gene (Okay et al., 2009; Teixeira et al., 2013).

It would be desirable to obtain *T. gondii* isolates from the blood donor or the donate samples (blood bags). However, due to the short length of parasitemia, which is apparently restricted to the acute phase of infection, is difficult to obtain viable parasites from blood samples. Maybe, an alternative would be to isolate parasite's mRNA from the donated blood but this procedure could interfere in the routine process in blood banks and contaminate the blood bags. Due to these difficulties, the studies that explored molecular approaches to detect the infection by this parasite among blood donors carry some limitations. Molecular methods aiming to detect *T. gondii* genomic DNA in the peripheral blood, such as conventional and Nested PCR are unable to distinguish live or dead parasites as well as residual DNA. They can only give a measure of the risk of transmission as well as overestimate the presence of the parasite in the peripheral blood (Rousseau et al., 2018).

The data presented here are supported by other reports. Three Iranian studies detected *T. gondii* infection only in blood donors carrying IgM anti-*T. gondii* antibodies by real-time PCR (Mahmoudvand et al., 2015) and Nested PCR (Sadooghian et al., 2017; Saki et al., 2019). In fact, there is a strong correlation between the IgM anti-*T. gondii* antibodies and parasitemia. However, parasitemia cannot be discharged in immunocompetent individuals (potential blood donors) carrying circulating IgG anti-*T. gondii* antibodies (Mattos et al., 2011; Park, 2012), especially when these antibodies present low avidity (Mattos et al., 2011; Yamada et al., 2011; Saki et al., 2019). All these studies did not correlate the serum concentration of anti-*T. gondii* antibodies to the PCR results.

The role of the host's immune response is crucial to protect chronically infected individuals (Coombes and Hunter, 2015). On the one hand, the cellular immune response led by macrophages, T CD8 lymphocytes, Natural Killer cells and cytokines as Interferon gama (IFN-ɤ) protects against the intracellular forms of the parasite. On the other hand, humoral immune response, which is thought to play a minor role in the immune protection of the host, seems to be effective against *T. gondii* extracellular forms, such as tachyzoites (Cohen and Denkers, 2015). The anamnestic immune response against *T. gondii* is characterized by the expression of IgG antibodies with high avidity and this class of immunoglobulins is effective at least in three immune events: opsonization and phagocytosis, Complement activation and Antibody-Dependent Cytotoxicity (ADCC) by Natural Killer cells and other white blood cells (Pleass and Woof, 2001; Filisetti and Candolfi, 2004; Ortiz-Alegría et al., 2010).

Erbe et al. (1991) demonstrated that human myeloid and lymphoid cells to kill *T. gondii* tachyzoites. These authors concluded that opsonization allows the binding of Fc IgG portion to Fc receptors (FcɤR) on phagocytic cells and significantly enhances the killing of tachyzoites coated by IgG anti-*T. gondii* antibodies. Additionally, Costa-Silva et al. (2012) reported that high levels of IgG from chronically infected mice decreases *T. gondii* RH strain parasitemia in comparison to those from naive mice. Exploring an experimental model, Seeber (2000) demonstrated the lytic activity mediated by Complement against *T. gondii* tachyzoites (Seeber, 2000). Other experimental study demonstrated the ability of IgG anti-excreted-secreted antigens from *T. gondii* to agglutinate tachyzoites and kill them by Complement lysis in a mouse model (Costa-Silva et al., 2008).

Pleass and Woof (2001) reported that NK cells activated by IFN-γ display Fc receptor for Fc IgG portion which binds IgG anti-*T. gondii* antibodies and kills tachyzoites through ADCC (Pleass and Woof, 2001). All these observations suggest that IgG anti-*T. gondii* antibodies are effective and promote the clearance of parasitemia in chronically infected healthy blood donors.

Despite the limitations of this study which evaluated only the *B1* gene and did not determine the IgG avidity, our data confirm the potential parasitemia in blood donors with circulating IgG anti-*T. gondii* antibodies, and demonstrate that the mean values of serum concentration of these antibodies do not correlate the results of Nested PCR. Also, it supports the view that blood products collected from chronically infected blood donors constitute a risk for transfusional transmission of *T. gondii*. In conclusion, our data show that variations in the serum IgG anti-*T. gondii* antibody concentrations do not correlate *T. gondii* parasitemia detected by Nested PCR in chronically infected healthy blood donors. Therefore, the use of serum IgG anti-*T. gondii* antibody concentrations to estimate the risk of transfusional transmission of this parasite does not constitute a potential biomarker for transfusional purposes.

DATA AVAILABILITY STATEMENT

All datasets generated for this study are included in the article/supplementary material.

ETHICS STATEMENT

The studies involving human participants were reviewed and approved by Research Ethics Committee from Faculdade de Medicina de São José do Rio Preto (case 006/2011). All blood donors received information about the objectives of the study and gave their informed consent. The patients/participants provided their written informed consent to participate in this study.

AUTHOR CONTRIBUTIONS

FN, CB, VP-C, and LM designed the study and wrote the manuscript. FN and FM performed the molecular tests. OR selected the blood donors. VP, NP, MM, and SL collected the blood samples from blood donors and performed the serology tests.

FUNDING

This work was supported by Fundação de Amparo à Pesquisa do Estado de São Paulo/São Paulo Research Foundation (FAPESP 2011/13939-8 to VP-C; 2012/07716-9 to LM; 2012/07750-2 to FN; 2013/15879-8 to FM; 2014/00900-4 to VP). The opinions, assumptions, and conclusions or recommendations expressed in this material are the responsibility of the authors and do not necessarily reflect the views of the FAPESP.

REFERENCES

Botein, E. F., Darwish, A., El-Tantawy, N. L., EL-baz, R., Eid, M. I., Shaltot, A. M., et al. (2019). Serological and molecular screening of umbilical cord blood for *Toxoplasma gondii* infection. *Transpl. Infect. Dis.* 21:e13117. doi: 10.1111/tid.13117

Brenier-Pinchart, M. P., Capderou, E., Bertini, R. L., Bailly, S., Fricker-Hidalgo, H., Varlet-Marie, E., et al. (2015). Molecular diagnosis of toxoplasmosis: value of the buffy coat for the detection of circulating *Toxoplasma gondii*. *Diagn. Microbiol. Infect. Dis.* 82, 289–291. doi: 10.1016/j.diagmicrobio.2015.04.004

Camilo, L. M., Pereira-Chioccola, V. L., Gava, R., Meira-Strejevitch, C. D. S., Vidal, J. E., Brandão de Mattos, C. C., et al. (2017). Molecular diagnosis of symptomatic toxoplasmosis: a 9-year retrospective and prospective study in a referral laboratory in São Paulo, Brazil. *Braz. J. Infect. Dis.* 21, 638–647. doi: 10.1016/j.bjid.2017.07.003

Cohen, S. B., and Denkers, E. Y. (2015). The gut mucosal immune response to *Toxoplasma gondii*. *Parasite Immunol.* 37, 108–117. doi: 10.1111/pim.12164

Coombes, J. L., and Hunter, C. A. (2015). Immunity to *Toxoplasma gondii*–into the 21st century. *Parasite Immunol.* 37, 105–107. doi: 10.1111/pim.12177

Cortés, J. A., Roncancio, Á., Uribe, L. G., Cortés-Luna, C. F., and Montoya, J. G. (2019). Approach to ocular toxoplasmosis including pregnant women. *Curr. Opin. Infect. Dis.* 32, 426–434. doi: 10.1097/QCO.0000000000000577

Costa-Silva, T. A., Borges, M. M., Galhardo, C. S., and Pereira-Chioccola, V. L. (2012). Immunization with excreted/secreted proteins in AS/n mice activating cellular and humoral response against *Toxoplasma gondii* infection. *Acta Trop.* 124, 203–209. doi: 10.1016/j.actatropica.2012.08.013

Costa-Silva, T. A., Meira, C. S., Ferreira, I. M., Hiramoto, R. M., and Pereira-Chioccola, V. L. (2008). Evaluation of immunization with tachyzoite excreted–secreted proteins in a novel susceptible mouse model (A/Sn) for *Toxoplasma gondii*. *Exp. Parasitol.* 120, 227–234. doi: 10.1016/j.exppara.2008.07.015

Dard, C., Fricker-Hidalgo, H., Brenier-Pinchart, M. P., and Pelloux, H. (2016). Relevance of and new developments in serology for toxoplasmosis. *Trends Parasitol.* 32, 492–506. doi: 10.1016/j.pt.2016.04.001

Dubey, J. P., Lago, E. G., Gennari, S. M., Su, C., and Jones, J. L. (2012). Toxoplasmosis in humans and animals in Brazil: high prevalence, high burden of disease, and epidemiology. *Parasitology* 139, 1375–1424. doi: 10.1017/S0031182012000765

El-Tantawy, N., Darwish, A., and Eissa, E. (2019). Seroprevalence of *Toxoplasma gondii* infection among B-thalassemia major pediatric population: implications for transfusion transmissible toxoplasmosis. *Pediatr. Infect. Dis. J.* 38, 236–240. doi: 10.1097/INF.0000000000002111

Erbe, D. V., Pfefferkorn, E. R., and Fanger, M. W. (1991). Functions of the various IgG Fc receptors in mediating killing of *Toxoplasma gondii*. *J. Immunol.* 146, 3145–3151.

Ferreira, M. N., Bonini-Domingos, C. R., Fonseca Estevão, I., De Castro Lobo, C. L., Souza Carrocini, G. C., Silveira-Carvalho, A. P., et al. (2017). Anti-*Toxoplasma gondii* antibodies in patients with beta-hemoglobinopathies: the first report in the Americas. *BMC Res. Notes* 1:211. doi: 10.1186/s13104-017-2535-7

Filisetti, D., and Candolfi, E. (2004). Immune response to *Toxoplasma gondii*. *Ann. Ist. Super Sanita.* 40, 71–80.

Foroutan, M., Rostami, A., Majidiani, H., Riahi, S. M., Khazaei, S., Badri, M., et al. (2018). A systematic review and meta-analysis of the prevalence of toxoplasmosis in hemodialysis patients in Iran. *Epidemiol. Health* 40:e2018016. doi: 10.4178/epih.e2018016

Foroutan-Rad, M., Majidiani, H., Dalvand, S., Daryani, A., Kooti, W., Saki, J., et al. (2016). Toxoplasmosis in blood donors: a systematic review and meta-analysis. *Transfus. Med. Rev.* 30, 116–122. doi: 10.1016/j.tmrv.2016.03.002

Greigert, V., Di Foggia, E., Filisetti, D., Villard, O., Pfaff, A. W., Sauer, A., et al. (2019). When biology supports clinical diagnosis: review of techniques to diagnose ocular toxoplasmosis. *Br. J. Ophthalmol.* 103, 1008–1012. doi: 10.1136/bjophthalmol-2019-313884

La Hoz, R. M., Morris, M. I., and Infectious Diseases Community of Practice of the American Society of Transplantation (2019). Tissue and blood protozoa including toxoplasmosis, chagas disease, leishmaniasis, babesia, acanthamoeba, balamuthia, and naegleria in solid organ transplant recipients—guidelines

from the American Society of Transplantation. *Clin. Transplant.* 33:e13546. doi: 10.1111/ctr.13546

Lévêque, M. F., Chiffré, D., Galtier, C., Albaba, S., Ravel, C., Lachaud, L., et al. (2019). Molecular diagnosis of toxoplasmosis at the onset of symptomatic primary infection: a straightforward alternative to serological examinations. *Int. J. Infect. Dis.* 79, 131–133. doi: 10.1016/j.ijid.2018.11.368

Mahmoudvand, H., Saedi Dezaki, E., Soleimani, S., Baneshi, M. R. R., Kheirandish, F., Ezatpour, B., et al. (2015). Seroprevalence and risk factors of *Toxoplasma gondii* infection among healthy blood donors in south-east of Iran. *Parasite Immunol.* 37, 362–367. doi: 10.1111/pim.12198

Mattos, C. C., Meira, C. S., Ferreira, A. I., Frederico, F. B., Hiramoto, R. M., Almeida, G. D. Jr., et al. (2011). Contribution of laboratory methods in diagnosing clinically suspected ocular toxoplasmosis in Brazilian patients. *Diagn. Microbiol. Infect. Dis.* 70, 362–366. doi: 10.1016/j.diagmicrobio.2011.02.002

Ministério da Saúde (2011). *Portaria no 1353, de 13 de Junho de 2011*. Ministério da Saúde.

Montoya, J. G. (2002). Laboratory diagnosis of *Toxoplasma gondii* infection and toxoplasmosis. *J. Infect. Dis.* 185, S73–S82. doi: 10.1086/338827

Murata, F. H., Ferreira, M. N., Camargo, N. S., Santos, G. S., Spegiorin, L. C., Silveira-Carvalho, A. P., et al. (2016). Frequency of anti-*Toxoplasma gondii* IgA, IgM, and IgG antibodies in high-risk pregnancies, in Brazil. *Rev. Soc. Bras. Med. Trop.* 49, 512–514. doi: 10.1590/0037-8682-0046-2016

Murata, F. H. A., Ferreira, M. N., Pereira-Chioccola, V. L., Spegiorin, L. C. J. F., Meira-Strejevitch, C. D. S., Gava, R., et al. (2017). Evaluation of serological and molecular tests used to identify *Toxoplasma gondii* infection in pregnant women attended in a public health service in São Paulo state, Brazil. *Diagn. Microbiol. Infect. Dis.* 89, 13–19. doi: 10.1016/j.diagmicrobio.2017.06.004

Nelson, J. C., Kauffmann, D. J., Ciavarella, D., and Senisi, W. J. (1989). Acquired toxoplasmic retinochoroiditis after platelet transfusions. *Ann. Ophthalmol.* 21, 253–254.

Neu, N., Duchon, J., and Zachariah, P. (2015). TORCH infections. *Clin. Perinatol.* 42, 77–103. doi: 10.1016/j.clp.2014.11.001

Okay, T. S., Yamamoto, L., Oliveira, L. C., Manuli, E. R., Andrade Junior, H. F., Del Negro, G. M., et al. (2009). Significant performance variation among PCR systems in diagnosing congenital toxoplasmosis in São Paulo, Brazil: analysis of 467 amniotic fluid samples. *Clinics* 64, 171–176. doi: 10.1590/S1807-59322009000300004

Olariu, T. R., Blackburn, B. G., Press, C., Talucod, J., Remington, J. S., and Montoya, J. G. (2019). Role of toxoplasma IgA as part of a reference panel for the diagnosis of acute toxoplasmosis during pregnancy. *J. Clin. Microbiol.* 57, e01357–e01318. doi: 10.1128/JCM.01357-18

Ortiz-Alegría, L. B., Caballero-Ortega, H., Cañedo-Solares, I., Rico-Torres, C. P., Sahagún-Ruiz, A., Medina-Escutia, M. E., et al. (2010). Congenital toxoplasmosis: candidate host immune genes relevant for vertical transmission and pathogenesis. *Genes Immun.* 11, 363–373. doi: 10.1038/gene.2010.21

Pappas, G., Roussos, N., and Falagas, M. E. (2009). Toxoplasmosis snapshots: global status of *Toxoplasma gondii* seroprevalence and implications for pregnancy and congenital toxoplasmosis. *Int. J. Parasitol.* 39, 1385–1394. doi: 10.1016/j.ijpara.2009.04.003

Park, Y. H. (2012). *Toxoplasma gondii* in the peripheral blood of patients with ocular toxoplasmosis. *Br. J. Ophthalmol.* 96:766. doi: 10.1136/bjophthalmol-2011-301068

Pleass, R. J., and Woof, J. M. (2001). Fc receptors and immunity to parasites. *Trends Parasitol.* 17, 545–551. doi: 10.1016/S1471-4922(01)02086-4

Pleyer, U., Gross, U., Schlüter, D., Wilking, H. H., Seeber, F., Groß, U., et al. (2019). Toxoplasmosis in Germany. *Dtsch. Arztebl. Int.* 116, 435–444. doi: 10.3238/arztebl.2019.0435

Rahimi Esboei, B., Kazemi, B., Zarei, M., Mohebali, M., Keshavarz Valian, H., Shojaee, S., et al. (2019). Evaluation of RE and B1 genes as targets for detection of *Toxoplasma gondii* by Nested PCR in blood samples of patients with ocular toxoplasmosis. *Acta Parasitol.* 64, 384–389. doi: 10.2478/s11686-019-0056-6

Robert-Gangneux, F., and Dardé, M. L. (2012). Epidemiology of and diagnostic strategies for toxoplasmosis. *Clin. Microbiol. Rev.* 25, 264–296. doi: 10.1128/CMR.05013-11

Robert-Gangneux, F., Sterkers, Y., Yera, H., Accoceberry, I., Menotti, J., Cassaing, S., et al. (2015). Molecular diagnosis of toxoplasmosis in immunocompromised patients: a 3-year multicenter retrospective study. *J. Clin. Microbiol.* 53, 1677–1684. doi: 10.1128/JCM.03282-14

Rostami, A., Riahi, S. M., Contopoulos-Ioannidis, D. G., Gamble, H. R., Fakhri, Y., Shiadeh, M. N., et al. (2019). Acute Toxoplasma infection in pregnant women worldwide: a systematic review and meta-analysis. *PLoS Negl. Trop. Dis.* 13:e0007807. doi: 10.1371/journal.pntd.0007807

Rousseau, A., La Carbona, S., Dumètre, A., Robertson, L. J., Gargala, G., Escotte-Binet, S., et al. (2018). Assessing viability and infectivity of foodborne and waterborne stages (cysts/oocysts) of Giardia duodenalis, *Cryptosporidium* spp., and *Toxoplasma gondii*: a review of methods. *Parasite* 25:14. doi: 10.1051/parasite/2018009

Roux, G., Varlet-Marie, E., Bastien, P., and Sterkers, Y. (2018). Evolution of Toxoplasma-PCR methods and practices: a French national survey and proposal for technical guidelines. *Int. J. Parasitol.* 48, 701–707. doi: 10.1016/j.ijpara.2018.03.011

Sadooghian, S., Mahmoudvand, H., Mohammadi, M. A., Nazari Sarcheshmeh, N., Tavakoli Kareshk, A., Kamiabi, H., et al. (2017). Prevalence of *Toxoplasma gondii* Infection among healthy blood donors in Northeast of Iran. *Iran. J. Parasitol.* 12, 554–562.

Saki, J., Foroutan, M., Khodkar, I., Khodadadi, A., and Nazari, L. (2019). Seroprevalence and molecular detection of *Toxoplasma gondii* in healthy blood donors in southwest Iran. *Transfus. Apher. Sci.* 58, 79–82. doi: 10.1016/j.transci.2018.12.003

Seeber, F. (2000). An enzyme-release assay for the assessment of the lytic activities of complement or antimicrobial peptides on extracellular *Toxoplasma gondii*. *J. Microbiol. Methods* 39, 189–196. doi: 10.1016/S0167-7012(99)00117-7

Siegel, S. E., Lunde, M. N., Gelderman, A. H., Halterman, R. H., Brown, J. A., Levine, A. S., et al. (1971). Transmission of toxoplasmosis by leukocyte transfusion. *Blood* 37, 388–394. doi: 10.1182/blood.V37.4.388.388

Siransy, L., Dasse, S. R., Dou Gonat, S. P., Legbedji, A., N'guessan, K., Kouacou, P. A., et al. (2016). Immunity status of blood donors regarding *Toxoplasma gondii* infection in a low-income district of Abidjan, côte d'ivoire, West Africa. *J. Immunol. Res.* 2016, 1–7. doi: 10.1155/2016/6830895

Teixeira, L. E., Kanunfre, K. A., Shimokawa, P. T., Targa, L. S., Rodrigues, J. C., Domingues, W., et al. (2013). The performance of four molecular methods for the laboratory diagnosis of congenital toxoplasmosis in amniotic fluid samples. *Rev. Soc. Bras. Med. Trop.* 46, 584–588. doi: 10.1590/0037-8682-0095-2013

Tsirouki, T., Dastiridou, A., Symeonidis, C., Tounakaki, O., Brazitikou, I., Kalogeropoulos, C., et al. (2018). A focus on the epidemiology of uveitis. *Ocul. Immunol. Inflamm.* 26, 2–16. doi: 10.1080/09273948.2016.1196713

Vidal, J. E. (2019). HIV-related cerebral toxoplasmosis revisited: current concepts and controversies of an old disease. *J. Int. Assoc. Provid. AIDS Care* 18:232595821986731. doi: 10.1177/2325958219867315

Wallon, M., and Peyron, F. (2018). Congenital toxoplasmosis: a plea for a neglected disease. *Pathogens* 7:25. doi: 10.3390/pathogens7010025

Yamada, H., Nishikawa, A., Yamamoto, T., Mizue, Y., Yamada, T., Morizane, M., et al. (2011). Prospective study of congenital toxoplasmosis screening with use of IgG avidity and multiplex Nested PCR methods. *J. Clin. Microbiol.* 49, 2552–2556. doi: 10.1128/JCM.02092-10

Conflict of Interest: The authors declare that the research was conducted in the absence of any commercial or financial relationships that could be construed as a potential conflict of interest.

frontiers in Cellular and Infection Microbiology

ORIGINAL RESEARCH
published: 07 February 2020
doi: 10.3389/fcimb.2019.00472

Evaluation of Serological and Molecular Tests Used for the Identification of *Toxoplasma gondii* Infection in Patients Treated in an Ophthalmology Clinic of a Public Health Service in São Paulo State, Brazil

Fernando Henrique Antunes Murata[1,2†], Mariana Previato[1,2], Fábio Batista Frederico[2,3], Amanda Pires Barbosa[3], Fabiana Nakashima[1†], Geraldo Magela de Faria Jr.[1,2], Aparecida Perpétuo Silveira Carvalho[1,2], Cristina da Silva Meira Strejevitch[4], Vera Lucia Pereira-Chioccola[4], Lilian Castiglioni[1], Luiz Carlos de Mattos[1,2], Rubens Camargo Siqueira[1,2] and Cinara Cássia Brandão de Mattos[1,2]*

[1] Faculdade de Medicina de São José Do Rio Preto, São José Do Rio Preto, Brazil, [2] FAMERP Toxoplasma Research Group, São José Do Rio Preto, Brazil, [3] Ambulatório de Oftalmologia Do Hospital de Base, Fundação Faculdade Regional de Medicina de São José Do Rio Preto, São José Do Rio Preto, Brazil, [4] Laboratório de Biologia Molecular de Parasitas e Fungos Do Centro de Parasitologia e Micologia, Instituto Adolfo Lutz, São Paulo, Brazil

Ocular toxoplasmosis is one of the most common complications caused by the infection with the parasite *Toxoplasma gondii*. The risk of developing eye lesions and impaired vision is considered higher in Brazil than other countries. The clinical diagnosis is difficult and the use of sensitive and specific laboratorial methods can aid to the correct diagnosis of this infection. We compared serological methods ELISA and ELFA, and molecular cPCR, Nested PCR and qPCR for the diagnosis of *T. gondii* infection in groups of patients clinically evaluated with ocular diseases non-toxoplasma related (G1 = 185) and with lesions caused by toxoplasmosis (G2 = 164) in an Ophthalmology clinic in Brazil. Results were compared by the Kappa index, and sensitivity (S), specificity (E), positive predictive value (PPV), and negative (NPV) were calculated. Serologic methods were in agreement with ELISA more sensitive and ELFA more specific to characterize the acute and chronic infections while molecular methods were discrepant where qPCR presented higher sensitivity, however, lower specificity when compared to cPCR and Nested PCR.

Keywords: ocular toxoplasmosis, toxoplasma antibodies, *Toxoplasama gondii*, retinochoroiditis, polimerase chain reaction (PCR), qPCR, uveites

OPEN ACCESS

Edited by:
Jeroen P. J. Saeij, University of California, Davis, United States

Reviewed by:
Fred David Mast, Seattle Children's Research Institute, United States
Bellisa Freitas Barbosa, Federal University of Uberlandia, Brazil

***Correspondence:**
Cinara Cássia Brandão de Mattos
cinara.brandao@famerp.br

†Present address:
Fernando Henrique Antunes Murata, Animal Parasitic Diseases Laboratory, Beltsville Agricultural Research Center, Agricultural Research Service, United States Department of Agriculture, Beltsville, MD, United States
Fabiana Nakashima, Universidade Federal de Roraima, Boa Vista, Brazil

Specialty section:
This article was submitted to Parasite and Host, a section of the journal Frontiers in Cellular and Infection Microbiology

Received: *21 August 2019*
Accepted: *23 December 2019*
Published: *07 February 2020*

Citation:
Murata FHA, Previato M, Frederico FB, Barbosa AP, Nakashima F, Faria GM Jr, Silveira Carvalho AP, Meira Strejevitch CS, Pereira-Chioccola VL, Castiglioni L, de Mattos LC, Siqueira RC and Brandão de Mattos CC (2020) Evaluation of Serological and Molecular Tests Used for the Identification of Toxoplasma gondii Infection in Patients Treated in an Ophthalmology Clinic of a Public Health Service in São Paulo State, Brazil. Front. Cell. Infect. Microbiol. 9:472. doi: 10.3389/fcimb.2019.00472

INTRODUCTION

Toxoplasmosis is a disease caused by the obligate intracellular parasite *Toxoplasma gondii*. In immunocompetent individuals the disease is usually asymptomatic, and its infection is commonly detected by serological tests (Saadatnia and Golkar, 2012). When symptomatic, ocular toxoplasmosis (OT) is the most common clinical manifestation (Garweg and Peyron, 2008;

Tsirouki et al., 2018) which can be due to congenital or acquired infection (Montoya, 2002; Oréfice et al., 2010; Maenz et al., 2014).

The clinical manifestations result from tachyzoite invasion into host cells from an acute infection and also in chronic infection by the reactivation of tissue-cysts contained in the retina which release bradyzoites, leading to an intense inflammatory response and tissue destruction (Garweg and Peyron, 2008; Maenz et al., 2014; Tsirouki et al., 2018).

The prevalence of ocular toxoplasmosis in Brazil is high, and the severity and risk of ocular involvement are notably higher compared to the United States and Europe (Glasner et al., 1992; Garcia et al., 1999; Aleixo et al., 2009; Furtado et al., 2013; Grigg et al., 2015). Studies in the northwestern region of São Paulo showed that seroprevalence was 74.5%, of these, 27.3% had ocular disease (Ferreira et al., 2014).

The high rates of ocular disease caused by *T. gondii* infection in Brazil is still unknown, and it is still not clear why these strains can cause more ocular involvement than in the rest of the world. Genetic diversity of these strains and host immune response are important factors that have been related to the severity of this disease in Brazil (Grigg et al., 2001, 2015; Silveira et al., 2015; Greigert et al., 2019).

Clinical diagnosis is challenging and serological and molecular tests are mostly used to confirm the disease. However, there is still no consensus regarding which method would be the best to identify *T. gondii* infection (Garweg and Peyron, 2008; Maenz et al., 2014; Greigert et al., 2019).

Since there is no standard test for diagnosis of *T. gondii* infection in Brazil, the use of methods with higher sensitivity and specificity are essential to lead to the correct diagnosis of this disease. The aim of this study was to evaluate the serological and molecular methods for diagnosis of toxoplasmosis in patients with and without ocular lesions, suggestive of toxoplasmosis treated at the ambulatory of Ophthalmology at the Hospital de Base in the city of São José do Rio Preto, São Paulo, Brazil.

MATERIALS AND METHODS

Ethics Statement

This study was approved by the Ethics Committee of the Medicine School in São José do Rio Preto (FAMERP-CAAE 32259714.8.0000.5415).

Patients and Clinical Samples

This is a retrospective study that evaluated 349 blood samples from patients of both genders treated and clinically evaluated at the ambulatory of Ophthalmology of the Fundação Faculdade Regional de Medicina, Hospital de Base (FUNFARME), São José do Rio Preto, São Paulo, Brazil, from 2009 to 2014. All patients were invited to participate in the project, and signed the free and informed consent form after receiving all the information about the objectives and the procedures to be performed in this research. All selected patients were immunocompetent and were divided into two groups: Group 1 (G1): Patients with ocular injury caused by diseases such as glaucoma, diabetic retinopathy type I, retinal detachment, macular degeneration related to age, uveitis of unknown cause, corneal transplantation, cataract, macular changes, post-operative injury, among other eye diseases not related to toxoplasma infection ($N = 185$), and Group 2 (G2): Patients with uveitis characteristics of toxoplasmosis ($N = 164$). The criteria for inclusion in this group was the presence of lesions in the retina characteristics of toxoplasmosis and, retinochoroiditis with active lesions. Ocular clinical evaluation of all patients was performed by fundus examination, and photo documentation using fundus photography, angiography and OCT (Optical Coherence Tomography).

Peripheral blood samples were collected from all subjects in a dry tube for serological analysis and in a tube containing ethylenediaminetetraacetic acid (EDTA) for DNA extraction and molecular tests. Serological and molecular analyses were performed in the Immunogenetics Laboratory, Molecular Biology Department, FAMERP, São José do Rio Preto, São Paulo, Brazil.

Serological Diagnosis

The presence of anti-*T. gondii* was confirmed using the semi-automated test by Enzyme Linked Immunosorbent assay (ELISA, DiaSorin, Italy) using the ETI-TOXOK-M reverse plus kit for IgM and ETI-TOXOK-G plus for IgG, and an automated test by enzyme linked fluorescent assay (ELFA, Biomerieux, France) using the Vidas®Toxo IgM kits (TXM) for IgM, Vidas®Toxo IgG II (TXG) to IgG and Vidas®Toxo IgG avidity (TXGA) for IgG avidity. The detection of IgM antibodies was performed by capture ELISA. The ELFA was performed in automated equipment (Mini Vidas, Biomerieux, France). Samples were considered positive for IgG antibodies by ELISA when the concentration was >15 IU/ml and negative when the IgG concentration was ≤15 IU/ml. For the IgM ELISA test, the absorbance values of the samples were compared with the average cut-off point, samples were considered positive when the absorbance values were higher than or equal to the cut-off limit point (>10% of the average cut-off) with the remaining samples being considered negative. Samples results with absorbance value between ±10% of the average cut-off were re-tested to confirm the result. By ELFA, samples were considered positive for IgG antibodies when >8 IU/mL, indeterminate from ≥4 to ≤8 IU/mL and negative when <4 IU/mL. For IgM antibodies, ELFA results were positive when the reagent index was ≥0.65 IU/mL, indeterminate from <0.65 to ≥0.55 IU/mL and negative <0.55 IU/mL. The IgG avidity was considered low when result was <0.200; intermediate avidity between ≤0.200 and <0.300; and high avidity when result was ≥0.300. The performance of the tests and results interpretation were made according to each manufacturer's instructions.

Molecular Diagnosis

Genomic DNA Extraction

The genomic DNA was extracted from 5 ml of peripheral blood collected in EDTA tube using a commercial kit (Qiamp DNA blood mini kit, Qiagen, Germany) according to the protocol described by Mattos et al. (2011). The extracted DNA was stored at −20°C until the polymerase chain reaction (PCR) was performed.

Identification of *Toxoplasma gondii B1* Gene

Conventional polymerase chain reaction (cPCR)

Conventional PCR (cPCR) was performed to identify *T. gondii* DNA in blood samples. Two cPCR reactions were performed, one using the JW62/63 primer pair and the other using the B22/23 primer pair. The B22 (sense: 5′-AACGGGCGAGTAGC ACCTGAGGAGA-3′) and B23 primers (anti-sense: 5′-TGGG TCTACGTCGATGGCATGACAACT-3′) amplify a 115 base-pair sequence of a specific repetitive region of the *B1* gene (accession numbers: *B1* gene *T. gondii* = GenBank: AF146527.1) (Burg et al., 1989; Colombo et al., 2005). The PCR mixture consisted of 8.5 μL of nuclease-free water (Promega, USA); 12.5 μL of GoTaq Green Master Mix (Promega, USA) and 1.0 μL of each B22 and B23 primers (25 pmol each—IDT, USA). DNA from patients and controls (5 μL in [100 ng/μL]) were added to the PCR mixture in a final volume of 25 μL. The PCR cycling conditions consisted of an initial denaturation step at 95°C for 5 min, 35 amplification cycles of 45 s at 95°C, 45 s at 62°C, and 45 s at 72°C with a final extension of 5 min at 72°C in a thermocycler (Verity, Applied Biosystems, USA). The PCR products were electrophoresed in 1.5% agarose gel using SYBR Safe stain (Invitrogen, USA).

Nested PCR

Conventional PCR was performed using the JW62 (antisense: 5′-TTCTCGCCTCATTTCTGGGTCTAC-3′) and JW63 primer pair (Sense: 5′-GCACCTTTCGGACCTCAACAACCG-3′), which amplifies a fragment of 288 base pairs of the *T. gondii B1* gene. The PCR mixture was prepared using 6.5 μL nuclease-free water (Promega, USA), 12.5 μL of GoTaq Green Master Mix (Promega, USA) and 0.5 μL of each of the JW62 and JW63 primers (10 μM each primer—IDT, USA). DNA from patients and controls (5 μL in [100 ng/μL]) were added to the PCR mixture in a final volume of 25 μL. The PCR cycling conditions consisted of an initial denaturation step at 95°C for 5 min, 40 amplification cycles of 45 s at 95°C, 45 s at 55°C, and 45 s at 72°C with a final extension of 5 min at 72°C in a thermocycler (Verity, Applied Biosystems, USA). The PCR products were electrophoresed in 1.5% agarose gel using SYBR Safe stain (Invitrogen, USA). The amplified product was subjected to a second PCR (Nested PCR) using the B22/23 primer pair following the protocol published by Okay et al. (2009) with modifications. The PCR mixture was prepared for the second reaction using 6.5 μL nuclease-free water (Promega, USA), 12.5 μL of GoTaq Green Master Mix (Promega, USA) and 0.5 μL of each of the B22 and B23 primers (25 pmol of each primer—IDT, USA). Five microliters from the first amplification reaction using the JW62/63 primer pair were added. The PCR cycling conditions consisted of an initial denaturation step at 95°C for 5 min, 25 amplification cycles of 45 s at 95°C, 45 s at 62°C, and 45 s at 72°C with a final extension of 5 min at 72°C in a thermocycler (Verity, Applied Biosystems, USA). The PCR products were electrophoresed in 1.5% agarose gel using SYBR Safe stain (Invitrogen, USA).

Real-time PCR (qPCR)

Genomic DNA was also subjected to real-time PCR (qPCR) using primers to amplify 16S rRNA gene. The primers used in the real-time PCR reactions were forward (5′-TGCATCCAACGAGTTTATAA-3′), reverse (5′-GGCATTCC TCGTTGAAGATT-3′), and TaqMan (FAM-ATTGCAATAATC TATCCCCATCACGATGCATAC-BBQ). Real-time PCR was performed in a Step One Plus system (Applied Biosystems, USA) using the following mixture: 4.5 μL nuclease-free water, 10.0 μL 2× QuantiTect Probe PCR Master Mix, 0.5 μL of PrimeTime kit (500 nM of each primer and 250 nM of probe) (Qiagen, Germany). DNA from patients and controls (5 μL in [100 ng/μL]) were added to the PCR mixture in a final volume of 25 μL. The PCR cycling conditions used for qPCR consisted of an initial denaturation step at 50°C for 2 min, once at 95°C for 15 min, 40 amplification cycles of 15 s at 94°C and 1 min at 60°C with a final extension of 30 s at 50°C. The primers and probe used in this analysis have been described by Gunel et al. (2012). Ultrapure water and DNA extracted from *T. gondii* (RH strain) were included as negative and positive controls, respectively in all PCR reactions (cPCR, Nested PCR and qPCR). To control the course of DNA extraction and check for PCR inhibitors, all samples were assayed using the HGH primer (Accession number: HGH = GenBank: U55206.1—sense: 5′-GCCTTCCC AACCATTCCCT-3′ and antisense: 5′-TCACGGATTTCTGTTG TGTTTC-3′), which amplifies a 400-base-pair fragment of the human growth hormone gene.

Statistical Analysis

IBM SPSS software v.23 was used to determine the Kappa index (KI) and GraphPad Stat Software v. 3.06 to determine the sensitivity, specificity, positive predictive value and negative value. Sensitivities and specificities were calculated as: (i) percent of sensitivity = ratio of true positives/true positives + false negatives × 100; and (ii) percent of specificity = ratio of true negatives/true negatives +false positives × 100. $P \leq 0.05$ was considered statistically significant. The strength of the agreement between two serological tests was calculated using the KI. The results are interpreted considering the ranges published by Landis and Koch (1977) where the agreement is considered poor, slight, fair, moderate, substantial and almost perfect when the KI is 0, 0–0.19, 0.2–0.39, 0.4–0.59, 0.6–0.79, and 0.8–1.0, respectively.

RESULTS

Group 1 (G1) was composed of 185 patients, 97 (52.4%) males and 88 (47.6%) females, with an average age of 51.6 years [range: 17–85; standard deviation (SD): 19.3]. G2 was composed of 164 patients, 95 (57.9%) males and 69 (42.1%) females, with an average age of 45.7 years (range: 10–90; *SD*: 19.6). The mean ages between G1 and G2 showed a statistically significant difference ($P = 0.0054$; student t-test = 2.799; $df = 347$; 95% confidence interval: 1,734–9,936).

In G1, serological tests detected 6 (IgM) and 121 (IgG) positive samples by ELISA, while 2 (IgM) and 119 (IgG) were positive by ELFA. For G2, 10 (IgM) and 158 (IgG) samples were positive by ELISA, while 6 (IgM) and 156 (IgG) samples were positive by ELFA. Compared results of serological tests are shown in **Table 1**.

TABLE 1 | Comparison of serological and molecular tests of group without ocular toxoplasmosis (G1) with group with ocular toxoplasmosis (G2).

Groups	Serological tests ELISA/ELFA positive		Molecular tests cPCR (JW62/63)/cPCR (B22/23)/Nested PCR/qPCR positive
	IgM	IgG	
G1 (185 samples)	6 (3.2%)/2 (1.1%)	121 (65.4%)/119 (64.3%)	1 (0.5%)/1 (0.5%)/3 (1.6%)/3 (1.6%)
G2 (164 samples)	10 (6.1%)/6 (3.7%)	158 (96.3%)/156 (95.1%)	3 (1.8%)/10 (6.1%)/4 (2.4%)/14 (8.5%)

Statistical analysis of IgG in G1. ELISA vs. ELFA: P-value = 0.913; 95% CI (0.875–1.181); IgM—ELISA vs. ELFA: P-value = 0.283; 95% CI (0.613–14.677); cPCR (JW62/63) vs. Nested PCR vs. cPCR (B22/23) vs. qPCR: P = 0.567; GL = 3; $\chi^2 = 2.022$. Statistical analysis of IgG in G2. ELISA vs. ELFA: P-value = 0.785; 95% CI (0.967–1.06); IgM—ELISA vs. ELFA: P-value = 0.443; 95% CI (0.619–4.481); cPCR (JW62/63) vs. Nested PCR vs. cPCR (B22/23) vs. qPCR: P = 0.012; GL = 3; $\chi^2 = 10.936$.
Statistical analysis of G1: cPCR (JW62/63) vs. Nested PCR vs. cPCR (B22/23) vs. qPCR: P = 0.567; GL = 3; $\chi^2 = 2.022$. Statistical analysis of G2: cPCR (JW62/63) vs. Nested PCR vs. cPCR (B22/23) vs. qPCR: P = 0.012; GL = 3; $\chi^2 = 10.936$.

The KIs for the detection of anti-*T. gondii* IgG antibodies in G1 was 0.97 (almost perfect agreement between the two techniques, ELISA × ELFA), and 0.49 for IgM antibodies (moderate agreement between the two techniques, ELISA × ELFA). The KIs for anti-*T. gondii* antibodies of G2 was 0.85 (almost perfect agreement, ELISA × ELFA), and for IgM antibodies was 0.74 (substantial agreement between the two techniques, ELISA × ELFA).

Regarding molecular tests on G1, one sample was positive by one round-PCR using primer JW62/63 and by one round-PCR using B22/23. Nested-PCR using the primer B22/23 amplified three samples and qPCR using the 16S rRNA gene amplified three samples. On G2, one round-PCR using primer JW62/63 amplified three samples, and 10 by one round-PCR using B22/23. Nested-PCR using the primer B22/23 detected four samples and qPCR 16S rRNA gene amplified 14 samples. Results are shown in **Table 1**.

The sensitivity (S), specificity (E), positive predictive value (PPV), and negative (NPV) was calculated for each serological and molecular test separately. Results are presented in **Table 2**.

TABLE 2 | Results for sensitivity (S), specificity (E), positive predictive value (PPV), and negative predictive value (NPV) between the serological tests in G1 and G2, performed by ELISA (DiaSorin) and ELFA (Biomerieux) and between the molecular tests performed by cPCR (JW62/63), Nested PCR, cPCR (B22/23), and qPCR.

	S (%)	E (%)	PPV (%)	NPV (%)
ELISA IgG	96.3	34.6	56.6	91.4
ELISA IgM	6.1	96.8	62.5	53.7
ELFA IgG	95.1	35.7	56.7	89.2
ELFA IgM	3.7	98.9	75.0	53.7
cPCR (JW62/63)	1.8	99.5	75.0	53.3
Nested PCR	2.4	99.5	80.0	53.5
cPCR (B22/23)	6.1	98.4	76.7	54.2
qPCR	8.5	98.4	82.3	54.8

DISCUSSION

This study evaluated serological and molecular methods used to identify *T. gondii* infection in patients treated at the Ophthalmology Clinic in the city of São José do Rio Preto, northwestern region of São Paulo state.

Most common enzyme immunoassays, ELISA and ELFA were evaluated in this study. ELISA detected more positive cases in both groups but for acute and chronic disease ELFA was more specific.

High sensitivity and specificity of serological test is essential, since a misdiagnosis would lead to wrong or late treatment of these patients, which could increase the changes of eye damage and loss of vision (Dhakal et al., 2015).

In this study, ELISA and ELFA had almost perfect agreement when compared by the Kappa index for the identification of IgG in both groups, indicating that these tests are very useful for the diagnosis of chronic infection. However, for IgM, Kappa index was moderate for G1 and with substantial agreement for G2 with higher detection by ELISA than ELFA.

All the samples tested positive for ELISA and negative for ELFA were also negative in the molecular tests, one sample was negative for IgG and high avidity of IgG for all samples. These findings may suggest that those IgM results detected by ELISA could be a result of persistence of Toxoplasma IgM in chronic infection. False positive results might be troublesome specially during prenatal care, as it could lead to undesirable consequences and unnecessary treatment and interventions, therefore, assays which do not detect these residual IgM antibodies would be ideal (Dhakal et al., 2015; Villard et al., 2016). Unfortunately, we just had access to one sample of these patients and consequently no follow-up was performed. In any case, confirming the IgM test is not easy since there is no reference method for its detection (Dhakal et al., 2015). The use of a test that could eliminate the risks of detecting residual IgM would be paramount, since a follow-up study to confirm the infection is expensive and time-consuming (Gras et al., 2004).

Automated method as ELFA have shown high sensitivity and specificity when compared to other methods with advantages of eliminating interferences that may occur during manual testing (Del Bono et al., 1989; Murat et al., 2013). The evaluation of IgM antibodies in the acute infection has been discussed since it still can be detected in chronic infection and there is a risk of false-positive results by cross-reactivity with antibodies, rheumatoid factor and other viral and bacterial diseases (Naot et al., 1981; Montoya, 2002; Bichara et al., 2012; Villard et al., 2012). In a study conducted by Dao et al. (2003) comparing the reaction of IgM antibodies by ELISA and ISAGA in patients without clinical suspicion of infection by *T. gondii*, it was

observed that 5 samples were positive in ELISA but none in ISAGA. The authors concluded that the different antigen compositions in solid phase reactions may have led to false-positive results by ELISA (Dao et al., 2003). The difference in the composition of the antigens of ELFA and ELISA kits may also have contributed to the difference finding in our study.

The low specificity of the IgG in this study could be related to high rates of seroprevalence in the region, and the permanence of these antibodies for the whole life of the host, even without the clinical signs of the disease. Melamed describes the difficulty of serologic diagnosis in patients with eye injuries, as these antibodies are present in patients with or without clinical signs of the disease, making the proper identification of the etiologic agent difficult (Melamed, 2009).

Since there is no standardization to detect *T. gondii* by PCR, different protocols have been used (Roux et al., 2018; Greigert et al., 2019). Selection of primer, applied technology and a more suitable sample are some reasons for this challenge (Saadatnia and Golkar, 2012). Several studies analyzing different targets and samples were done and there is still no consensus of the best test (Homan et al., 2000; Jones et al., 2000; Calderaro et al., 2006; Okay et al., 2009; Menotti et al., 2010).

In a study conducted by Jones et al. (2000) comparing three *T. gondii* genes (*B1*, P30, and 16S rRNA gene) in aqueous humor, *B1* was more sensitive than P30 and 16S rRNA gene, when it was submitted to a nested-PCR. In our study, 16S rRNA gene was more sensitive than *B1* and less specific when compared to one-round PCR with JW62/63 and nested-PCR, and same specificity compared with one-round on *B1* conventional PCR. Some factors may have contributed for these results.

First, 16S rRNA gene is the most highly repeated region of the gene studied (110 copies in the *T. gondii* genome) compared to 35 copies of *B1* gene, increasing the chances for amplification (Jones et al., 2000; Calderaro et al., 2006; Ivovic et al., 2012).

Second, the kind of specimen analyzed, as it seems that results of molecular tests can vary according to the kind of sampling, as shown by Calderaro et al. (2006) who found same sensitivity between nested-PCR using *B1* gene and real time PCR using 16S rRNA gene when analyzing blood samples and less sensitivity of 16S rRNA gene when analyzing cerebrospinal fluid samples.

The sensitivity of B1 gene was higher when samples were submitted just to one-round PCR using B22/23 primer than compared to one-round PCR using JW62/63 and nested-PCR. Primer B22/23 amplifies a 115-base pair sequence of *B1* gene and has been reported as highly sensitive and specific primer used to detect *T. gondii* DNA in blood, cerebrospinal fluid, and amniotic fluid (Vidal et al., 2004; Okay et al., 2009; Mattos et al., 2011; Camilo et al., 2017; Murata et al., 2017). In a study conducted by Camilo et al. (2017) evaluating two real time-PCR for *B1* gene and REP-529 with a conventional PCR using the B22/23 primer, the authors found that REP-529 had better performance compared with the *B1* gene. However, the primer B22/23 had the same rate of detection as REP-529 (Camilo et al., 2017).

The lowest detection of *T. gondii* DNA was observed when samples were submitted to a cPCR using primers JW62/63 and nested-PCR. Contrary to our results, Okay et al. (2009) found more positive results when analyzed amniotic fluid samples using the JW62/63 (120/467) than using the 16S rRNA gene (0/467). The authors also submitted 50 samples from negative result on JW62/63 to a nested-PCR using primer B22/23, which detected more nine positive samples (Okay et al., 2009). In our study, all samples analyzed with JW62/63 were also submitted to a nested-PCR using the primer B22/23 irrespectively to the first one-round result. All the samples positive on the JW62/63 were also positive for the nested-PCR, which detected three more positive samples, suggesting that nested-PCR can be more sensitive than conventional PCR (Jones et al., 2000; Okay et al., 2009).

This study shows that the most common used serological tests ELISA and ELFA are good tests for the detection of *T. gondii* antibodies in the groups of patients analyzed with higher sensitivity for ELISA but better specificity for ELFA. For molecular tests, real time PCR using the 16S rRNA gene was the most sensitive, however, less specific than JW62/63 and nested-PCR using the primer B22/23.

Despite the limitation of this study related to the lack of follow up of these patients, our results show that even with no consensus of the best protocol to use, the combinate use of these tests with clinical evaluation and follow up could be a great tool for the correct diagnosis of *T. gondii* infection.

DATA AVAILABILITY STATEMENT

All datasets generated for this study are included in the article/supplementary material.

ETHICS STATEMENT

The studies involving human participants were reviewed and approved by the Ethics Committee of the Medicine School in São José do Rio Preto (FAMERP-CAAE 32259714.8.0000.5415). The patients/participants provided their written informed consent to participate in this study.

AUTHOR CONTRIBUTIONS

CB and FM coordinated the experiments and designed the study. CB, FM, LM, and VP-C wrote the manuscript. MP, FF, RS, and AB performed the selection of clinical samples and clinical evaluation. FM, MP, FN, AS, GF, CM, and VP-C performed the serological and molecular diagnosis for toxoplasmosis. FM and LC performed the statistical analyses. All authors contributed substantially to the interpretation of the data and to the manuscript. In addition, all authors revised the manuscript, approved the final version submitted, published, and agreed to be accountable for all aspects of the work in ensuring that questions related to the accuracy or integrity of any part of the work are appropriately investigated and resolved.

FUNDING

This study was supported by research grants from Fundação de Amparo à Pesquisa do Estado de São Paulo (FAPESP

#2012/07716-9 to LM; #2012/07750-2 to FN; #2013/15879-8 to FM; #2013/10050-5 to MP; #2018/04709-8 to VP-C; #2014/05302-8 to LC; 2018/09448-8 to GF); by CAPES scholarship (to GF); by Fundação de Apoio à Pesquisa e Extensão de São José do Rio Preto (FAPERP to FM #175/2015). The opinions, assumptions, and conclusions or recommendations expressed in this material are strictly those of the authors and do not necessarily reflect the views of FAPESP.

REFERENCES

Aleixo, A. L., Benchimol, E. I., Neves, E. S., Silva, C. S., Coura, L. C., and Amendoeira, M. R. (2009). Frequency of lesions suggestive of ocular toxoplasmosis among a rural population in the State of Rio de Janeiro. *Rev. Soc. Bras. Med. Trop*. 42, 165–169. doi: 10.1590/S0037-86822009000200014

Bichara, C. N., Canto, G. A., Tostes, C. L., Freitas, J. J., Carmo, E. L., Póvoa, M. M., et al. (2012). Incidence of congenital toxoplasmosis in the City of Belém, State of Pará, Northern Brazil, determined by a neonatal screening program: preliminary results. *Rev. Soc. Bras. Med. Trop*. 45, 122–124. doi: 10.1590/S0037-86822012000100024

Burg, J. L., Grove, C. M., Pouletty, P. J., and Boothroyd, J. C. (1989). Directed and sensitive detection of a pathogenic protozoan, *Toxoplasma gondii*, by polymerase chain reaction. *J. Clin. Microbiol.* 27, 1787–1792.

Calderaro, A., Piccolo, G., Gorrini, C., Peruzzi, S., Zerbini, L., Bommezzadri, S., et al. (2006). Comparison between two real-time PCR assays and a nested-PCR for the detection of *Toxoplasma gondii*. *Acta Biomed*. 77, 75–80. Available online at: https://mattioli1885journals.com/index.php/actabiomedica/article/view/1989

Camilo, L. M., Pereira-Chioccola, V. L., Gava, R., Meira-Strejevitch, C. D. S., Vidal, J. E., Brandão de Mattos, C. C., et al. (2017). Molecular diagnosis of symptomatic toxoplasmosis: a 9-year retrospective and prospective study in a referral laboratory in São Paulo, Brazil. *Braz. J. Infect. Dis*. 21, 638–647. doi: 10.1016/j.bjid.2017.07.003

Colombo, F. A., Vidal, J. E., Penalva de Oliveira, A. C., Hernández, A. V., Bonasser-Filho, F., Nogueira, R. S., et al. (2005). Diagnosis of cerebral toxoplasmosis in AIDS patients in Brazil: importance of molecular and immunological methods using peripheral blood samples. *J. Clin. Microbiol*. 43, 5044–5047. doi: 10.1128/JCM.43.10.5044-5047.2005

Dao, A., Azzouz, N., Eloundou, N. G. A. C., Dubremetz, J. F., Schwarz, R. T., and Fortier, B. (2003). Unspecific reactivity of IgM directed against the low-molecular-weight antigen of *Toxoplasma gondii*. *Eur. J. Clin. Microbiol. Infect. Dis*. 22, 418–421. doi: 10.1007/s10096-003-0948-9

Del Bono, V., Canessa, A., Bruzzi, P., Fiorelli, M. A., and Terragna, A. (1989). Significance of specific immunoglobulin M in the chronological diagnosis of 38 cases of toxoplasmic lymphadenopathy. J. Clin. *Microbiol*. 27, 2133–2135.

Dhakal, R., Gajurel, K., Pomares, C., Talucod, J., Press, C. J., and Montoya, J. G. (2015). Significance of a positive toxoplasma immunoglobulin M test result in the United States. *J. Clin. Microbiol*. 53, 3601–3605. doi: 10.1128/JCM.01663-15

Ferreira, A. I., de Mattos, C. C., Frederico, F. B., Meira, C. S., Almeida, G. C. Jr., Nakashima, F., et al. (2014). Risk factors for ocular toxoplasmosis in Brazil. *Epidemiol. Infect*. 142, 142–148. doi: 10.1017/S0950268813000526

Furtado, J. M., Winthrop, K. L., Butler, N. J., and Smith, J. R. (2013). Ocular toxoplasmosis I: parasitology, epidemiology and public health. *Clin. Exp. Ophthalmol*. 41, 82–94. doi: 10.1111/j.1442-9071.2012.02821.x

Garcia, J. L., Navarro, I. T., Ogawa, L., de Oliveira, R. C., and Kobilka, E. (1999). Seroprevalence, epidemiology and ocular evaluation of human toxoplasmosis in the rural zone Jauguapitã (Paraná) Brazil. *Ver. Panam. Salud. Publ*. 6, 157–163. doi: 10.1590/S1020-49891999000800002

Garweg, J. G., and Peyron, F. (2008). Clinical and laboratory diagnosis of ocular toxoplasmosis. *Expert. Rev. Ophthalmol*. 3, 333–346. doi: 10.1586/17469899.3.3.333

Glasner, P. D., Silveira, C., Kruszon-Moran, D., Martins, M. C., Burnier Júnior, M., Silveira, S., et al. (1992). An unusually high prevalence of ocular toxoplasmosis in southern Brazil. *Am. J. Ophthalmol*. 114, 136–144. doi: 10.1016/S0002-9394(14)73976-5

Gras, L., Gilbert, R. E., Wallon, M., Peyron, F., and Cortina-Borja, M. (2004). Duration of the IgM response in women acquiring *Toxoplasma gondii* during pregnancy: implications for clinical practice and cross-sectional incidence studies. *Epidemiol. Infect*. 132, 541–548. doi: 10.1017/S0950268803001948

Greigert, V., Di Foggia, E., Filisetti, D., Villard, O., Pfaff, A. W., Sauer, A., et al. (2019). When biology supports clinical diagnosis: review of techniques to diagnose ocular toxoplasmosis. *Br. J. Ophthalmol*. 103, 1008–1012. doi: 10.1136/bjophthalmol-2019-313884

Grigg, M. E., Dubey, J. P., and Nussenblatt, R. B. (2015). Ocular toxoplasmosis: lessons from Brazil. *Am. J. Ophthalmol*. 159, 999–1001. doi: 10.1016/j.ajo.2015.04.005

Grigg, M. E., Ganatra, J., Boothroyd, J. C., and Margolis, T. P. (2001). Unusual abundance of atypical strains associated with human ocular toxoplasmosis. *J. Infect. Dis*. 184, 633–639. doi: 10.1086/322800

Gunel, T., Kalelioglu, I., Ermis, H., Has, R., and Aydinli, K. (2012). Large scale pre-diagnosis of *Toxoplasma gondii* DNA genotyping by real-time PCR on amniotic fluid. *Biotechnol. Biotechnol. Equip*. 26, 2913–2915. doi: 10.5504/BBEQ.2011.0106

Homan, W. L., Vercammen, M., De Braekeleer, J., and Verschueren, H. (2000). Identification of a 200 to 300-fold repetitive 529 bp DNA fragment in *Toxoplasma gondii*, and its use for diagnostic and quantitative PCR. *Int. J. Parasitol*. 30, 69–75. doi: 10.1016/S0020-7519(99)00170-8

Ivovic, V., Vujanic, M., Zivkovic, T., Klun, I., and Djurkovic-Djakovic, O. (2012). "Molecular detection and genotyping of Toxoplasma gondii from clinical samples," in *Toxoplasmosis-Recent Advances Subject* (Rijek: InTech), 103–120. doi: 10.5772/2845

Jones, C. D., Okhravi, N., Adamson, P., Tasker, S., and Lightman, S. (2000). Comparison of PCR detection methods for B1, P30, and 18S rDNA genes of *T. gondii* in aqueous humor. *Invest. Ophthalmol. Vis. Sci.* 41, 634–644.

Landis, J. R., and Koch, G. G. (1977). The measurement of observer agreement for categorical data. *Biometrics* 33, 159–174. doi: 10.2307/2529310

Maenz, M., Schlüter, D., Liesenfeld, O., Schares, G., Gross, U., and Pleyer, U. (2014). Ocular toxoplasmosis past, present and new aspects of an old disease. *Prog. Retin. Eye Res*. 39, 77–106. doi: 10.1016/j.preteyeres.2013.12.005

Mattos, C. C., Meira, C. S., Ferreira, A. I., Frederico, F. B., Hiramoto, R. M., Almeida, G. D. Jr., et al. (2011). Contribution of laboratory methods in diagnosing clinically suspected ocular toxoplasmosis in Brazilian patients. *Diagn. Microbiol. Infect. Dis*. 70, 362–366. doi: 10.1016/j.diagmicrobio.2011.02.002

Melamed, J. (2009). Contributions to the history of ocular toxoplasmosis in Southern Brazil. *Mem. Inst. Oswaldo Cruz*. 104, 358–363. doi: 10.1590/S0074-02762009000200032

Menotti, J., Garin, Y. J., Thulliez, P., Sérugue, M. C., Stanislawiak, J., Ribaud, P., et al. (2010). Evaluation of a new 5′-nuclease real-time PCR assay targeting the *Toxoplasma gondii* AF146527 genomic repeat. *Clin. Microbiol. Infect*. 16, 363–368. doi: 10.1111/j.1469-0691.2009.02809.x

Montoya, J. G. (2002). Laboratory diagnosis of *Toxoplasma gondii* infection and toxoplasmosis. *J. Infect. Dis*. 185, 73–82. doi: 10.1086/338827

Murat, J. B., Hidalgo, H. F., Brenier-Pinchart, M. P., and Pelloux, H. (2013). Human toxoplasmosis: which biological diagnostic tests are best suited to which clinical situations? *Expert. Rev. Anti. Infect. Ther*. 11, 943–956. doi: 10.1586/14787210.2013.825441

Murata, F. H. A., Ferreira, M. N., Pereira-Chioccola, V. L., Spegiorin, L. C. J. F., Meira-Strejevitch, C. D. S., Gava, R., et al. (2017). Evaluation of serological and molecular tests used to identify *Toxoplasma gondii* infection in pregnant women attended in a public health service in São Paulo state, Brazil. *Diagn. Microbiol. Infect. Dis*. 89, 13–19. doi: 10.1016/j.diagmicrobio.2017.06.004

Naot, Y., Barnett, E. V., and Remington, J. S. (1981). Method for avoiding false-positive results occurring in immunoglobulin M enzyme-linked immunosorbent assays due to presence of both rheumatoid factor and antinuclear antibodies. *J. Clin. Microbiol.* 14, 73–78.

Okay, T. S., Yamamoto, L., Oliveira, L. C., Manuli, E. R., Andrade Junior, H. F., and Del Negro, G. M. (2009). Significant performance variation

among PCR systems in diagnosing congenital toxoplasmosis in São Paulo, Brazil: analysis of 467 amniotic fluid samples. *Clinics* 64, 171–176. doi: 10.1590/S1807-59322009000300004

Oréfice, F., Filho, R. C., Barboza, A. L., Oréfice, J. L., and Calucci, D. (2010). Toxoplasmose ocular adquirida. Toxoplasmose ocular pós-natal. *Rev. Bras. Oftalmol*. 69, 184–207. doi: 10.1590/S0034-72802010000300009

Roux, G., Varlet-Marie, E., Bastien, P., Sterkers, Y., and French National Reference Center for Toxoplasmosis Network (2018). Evolution of toxoplasma-PCR methods and practices: a French national survey and proposal for technical guidelines. *Int. J. Parasitol*. 48, 701–707. doi: 10.1016/j.ijpara.2018.03.011

Saadatnia, G., and Golkar, M. (2012). A review on human toxoplasmosis. *Scand. J. Infect. Dis*. 44, 805–814. doi: 10.3109/00365548.2012.693197

Silveira, C., Muccioli, C., Holland, G. N., Jones, J. L., Yu, F., de Paulo, A., et al. (2015). Ocular involvement following an epidemic of *Toxoplasma gondii* infection in Santa Isabel do Ivaí, Brazil. *Am. J. Ophthalmol*. 159, 1013–1021. doi: 10.1016/j.ajo.2015.02.017

Tsirouki, T., Dastiridou, A., Symeonidis, C., Tounakaki, O., Brazitikou, I., Kalogeropoulos, C., et al. (2018). A focus on the epidemiology of uveitis. *Ocul. Immunol. Inflamm*. 26, 2–16. doi: 10.1080/09273948.2016.1196713

Vidal, J. E., Colombo, F. A., de Oliveira, A. C., Focaccia, R., and Pereira-Chioccola, V. L. (2004). PCR assay using cerebrospinal fluid for diagnosis of cerebral toxoplasmosis in Brazilian AIDS patients. *J. Clin. Microbiol*. 42, 4765–4768. doi: 10.1128/JCM.42.10.4765-4768.2004

Villard, O., Cimon, B., Franck, J., Fricker-Hidalgo, H., Godineau, N., Houze, S., et al. (2012). Network from the French national reference center for toxoplasmosis. Evaluation of the usefulness of six commercial agglutination assays for serologic diagnosis of toxoplasmosis. *Diagn. Microbiol. Infect. Dis*. 73, 231–235. doi: 10.1016/j.diagmicrobio.2012.03.014

Villard, O., Cimon, B., L'Ollivier, C., Fricker-Hidalgo, H., Godineau, N., Houze, S., et al. (2016). Help in the Choice of Automated or Semiautomated Immunoassays for Serological Diagnosis of Toxoplasmosis: Evaluation of Nine Immunoassays by the French National Reference Center for Toxoplasmosis. *J. Clin. Microbiol*. 54, 3034–3042. doi: 10.1128/JCM.01193-16

Conflict of Interest: The authors declare that the research was conducted in the absence of any commercial or financial relationships that could be construed as a potential conflict of interest.

frontiers in Cellular and Infection Microbiology

ORIGINAL RESEARCH
published: 16 April 2020
doi: 10.3389/fcimb.2020.00161

Early Kinetics of Intestinal Infection and Immune Responses to Two *Toxoplasma gondii* Strains in Pigs

*Mizanur Rahman[1], Bert Devriendt[1], Malgorzata Jennes[1], Ignacio Gisbert Algaba[2], Pierre Dorny[3,4], Katelijne Dierick[2], Stéphane De Craeye[2] and Eric Cox[1]**

[1] Laboratory of Immunology, Department of Virology, Parasitology and Immunology, Faculty of Veterinary Medicine, Ghent University, Merelbeke, Belgium, [2] Sciensano, National Reference Center for Toxoplasmosis, Infectious Diseases in Humans, Brussels, Belgium, [3] Department of Biomedical Sciences, Institute for Tropical Medicine, Antwerp, Belgium, [4] Laboratory of Parasitology, Department of Virology, Parasitology and Immunology, Faculty of Veterinary Medicine, Ghent University, Merelbeke, Belgium

OPEN ACCESS

Edited by:
Jeroen P. J. Saeij,
University of California, Davis,
United States

Reviewed by:
Tiago W. P. Mineo,
Federal University of Uberlandia, Brazil
David Smith,
Moredun Research Institute,
United Kingdom
Julio Benavides,
Consejo Superior de Investigaciones Científicas (CSIC), Spain

***Correspondence:**
Eric Cox
eric.cox@ugent.be

Specialty section:
This article was submitted to Parasite and Host, a section of the journal Frontiers in Cellular and Infection Microbiology

Received: 09 January 2020
Accepted: 26 March 2020
Published: 16 April 2020

Citation:
Rahman M, Devriendt B, Jennes M, Gisbert Algaba I, Dorny P, Dierick K, De Craeye S and Cox E (2020) Early Kinetics of Intestinal Infection and Immune Responses to Two Toxoplasma gondii Strains in Pigs. Front. Cell. Infect. Microbiol. 10:161. doi: 10.3389/fcimb.2020.00161

Toxoplasma gondii is an obligate intracellular parasite, able to infect all homeothermic animals mostly through ingestion of (oo)cysts contaminated food or water. Recently, we observed a *T. gondii* strain-specific clearance from tissues upon infection in pigs: while the swine-adapted LR strain persisted in porcine tissues, a subsequent infection with the human-isolated Gangji strain cleared parasites from several tissues. We hypothesized that intestinal immune responses shortly after infection might play a role in this strain-specific clearance. To assess this possibility, the parasite load in small intestinal lymph node cells and blood immune cells as well as the IFNγ secretion by these cells were evaluated at 2, 4, 8, 14, and 28 days post oral inoculation of pigs with tissue cysts of both strains. Interestingly, at day 4 post inoculation with the LR strain the parasite was detected by qPCR only in the duodenal lymph node cells, while in the jejunal and ileal lymph node cells and PBMCs the parasite was detected from day 8 post inoculation onwards. Although we observed a similar profile upon inoculation with the Gangji strain, the parasite load in the examined cells was much lower. This was reflected in a significantly higher *T. gondii*-specific serum IgG response in LR compared to Gangji infected pigs at day 28 post inoculation. Unexpectedly, this was not reflected in the IFNγ secretion upon re-stimulation of the cells where almost equal IFNγ secretion was observed in both groups. In conclusion, our results show that *T. gondii* first enters the host at the duodenum and then probably disseminates from this site to the other tissues. How the early immune response influences the clearance of parasite from tissues needs further study.

Keywords: *Toxoplasma gondii*, pigs, magnetic capture-qPCR, intestine, IFNγ

INTRODUCTION

The obligate intracellular protozoan parasite *Toxoplasma gondii* causes toxoplasmosis in all homeothermic animals which is life-long and often asymptomatic. In immunocompromised patients, toxoplasmosis can be fatal, while in pregnant women congenital toxoplasmosis might result in fetal and neonatal mortality, neurologic abnormalities, chorioretinitis, and other

symptoms reviewed by Torgerson and Mastroiacovo (2013). In 2013, the global annual incidence of congenital toxoplasmosis was calculated to be equivalent to a disease burden of 1.20 million disability-adjusted life years (Torgerson and Mastroiacovo, 2013).

T. gondii is an important foodborne pathogen and natural human infection commonly results from the ingestion of raw or undercooked meat containing tissue cysts or food/drinks contaminated with sporulated oocysts. After ingestion, the cyst wall protects the parasites from the gastric pH and ensures passage to the small intestine where they excyst upon contact with bile salts and trypsin (Dubey, 1997; Dubey et al., 1998). Upon excystation, initial bradyzoite invasion and replication takes place at the tips of the villi and subsequently results in the release of tachyzoites into the lumen to colonize neighboring villi and in the lamina propria to disseminate in the host (Dubey, 1997; Dubey et al., 1998; Coombes et al., 2013; Verhelst et al., 2014). In mice, the proximal jejunum seems to be the preferred replication site (Gregg et al., 2013). Transmigration through the intestinal epithelial cells possibly involves an unusual form of gliding motility, paracellular transmigration, penetration of the apical cell membrane, and use of immune cells in a Trojan horse-like mechanism (Barragan et al., 2005; Courret et al., 2006; Gregg et al., 2013; Jones et al., 2017). In response to the infection, neutrophils are rapidly recruited to the infected sites and are subsequently invaded by progeny *T. gondii* egressing from the infected epithelial cells (Coombes et al., 2013). Part of the parasite invaded neutrophils migrate to the lumen and facilitate re-infection of neighboring villi, while the rest spreads to the draining lymph nodes and enters the blood circulation to disseminate to other organs. In addition, many other cell types can be invaded by *T gondii* including dendritic cells (DCs), mononuclear phagocytes, NK cells, and lymphocytes (Courret et al., 2006; Lambert et al., 2006; Coombes et al., 2013). Interestingly, *T. gondii* within immune cells can sense the arrival of these cells at the target organs via adhesion to certain surface molecules on capillary endothelial cells, e.g., CD162 on lung endothelial cells, and immediately egress the immune cells to infect target organs (Baba et al., 2017).

However, most of these mouse data are inapposite for humans and warrant further investigation in relevant large animal models. For example, upon *T. gondii* infection, murine DCs undergo maturation in response to the parasite antigen profilin via TLR11 and TLR12. However, in humans and pigs TLR11 and TLR12 are non-functional pseudogenes (Tosh et al., 2016). Therefore, to elicit an immune response they rely on phagocytosis of tachyzoites and subsequent recognition of *T. gondii* RNA and DNA via TLR7,−8, and−9 (Forsbach et al., 2008; Ishii et al., 2008; Andrade et al., 2013; Weidner et al., 2013; Betancourt et al., 2019).

In humans there is still a major knowledge gap between the early infection of the small intestinal epithelium and the dissemination of the parasite to other organs to establish tissue cysts as well as the associated immune responses. To address this gap pigs may be a particularly interesting model. Indeed, the immune system as well as the gut physiology of pigs closely resembles that of humans (Meurens et al., 2012). In addition, pigs are susceptible to *T. gondii* infection. However, also in pigs thorough knowledge is lacking on the initial events during infection of the small intestine, the subsequent dissemination and the associated small intestinal immune responses.

T. gondii virulence not only differs between animals, but also among *T. gondii* strains, which in Europe belong to three major genotypes (e.g., type I, II, and III) based on the DNA sequence of multilocus analysis. Genotype II is the most prevalent genotype in livestock species and humans (Howe and Sibley, 1995; Dubey, 2010). Our previous results showed that different genotypes trigger variable immune responses in pigs (Jennes et al., 2017). A genotype II strain (IBP LR) elicited stronger IFNγ^+ T cell responses as compared to a hybrid genotype I/II strain (IBP Gangji). These LR strain-specific immune responses seemed to play a role in the clearance of tissue cysts upon infection of pigs with the Gangji strain (Jennes et al., 2017). However, our understanding on how different genotypes impact the early infection stages of *T. gondii* is incomplete. In this study, we aimed to investigate the early infection kinetics, antibody and IFNγ response for both strains. The latter since IFNγ seems to play a crucial role in clearance of the parasite from infected hosts (Jennes et al., 2017).

MATERIALS AND METHODS

Animals and Ethics Statement

Thirty-six four-week-old piglets (Belgian Landrace x large white) were obtained from a high health-status farm in Belgium and transported to the Faculty of Veterinary Medicine, Ghent University, where the piglets were housed in isolation units and were given *ad libitum* access to feed and water. The animal procedures were approved by the Ethical Committee (EC) of the Faculty of Veterinary Medicine and the Faculty of Bioscience Engineering, Ghent University (EC 2009/149) and by the EC of Sciensano, Belgium (176 20140704-01).

T. gondii Strains

The *T. gondii* IPB LR and Gangji strains were used to inoculate pigs. The LR strain was originally isolated from pigs and belongs to genotype II, which is commonly present in the European pig population. It is less virulent in mice than the hybrid genotype I/II Gangji strain, which is highly virulent in mice (Dubey et al., 2012; Jennes et al., 2017). The latter strain was isolated from the placenta of a pregnant woman having a congenitally infected baby (Ajzenberg et al., 2010). Both strains were isolated and maintained at the National Reference Laboratory for Toxoplasmosis, Sciensano, Brussels, Belgium by passage in Swiss Webster female mice (EC: 176 20140704-01).

Abbreviations: ELISA, Enzyme-Linked ImmunoSorbent Assay; IFA, Indirect Immunofluorescence Assay; MAT, Modified Agglutination Test; MC-qPCR, Magnetic Capture Quantitative Polymerase Chain Reaction; Cp, Crossing point (also known as Ct or Cq); PBS, Phosphate-buffered saline; ng/ml, Nanogram/milliliter; TLA, Total Lysate Antigen; FACS, Fluorescence-activated cell sorting; IFN-γ, Interferon gamma; PBMCs, Peripheral blood mononuclear cells; LOD, Limit of detection; SD, Standard deviation; CD, Cluster of differentiation; NK cells, Natural killer cells; IL, Interleukin; APCs, Antigen presenting cells; CTLs, Cytotoxic T lymphocytes; Th cells, T helper cells.

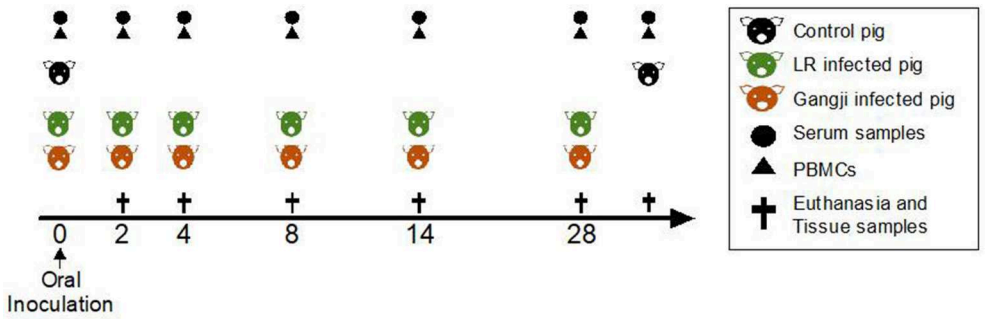

FIGURE 1 | Scheme of the study. Experiment day is indicated as numbers (0–35). TLA-ELISA: *T. gondii* lysate antigen-specific enzyme-linked immunosorbent assay. PBMCs, peripheral blood mononuclear cells. MCqPCR, magnetic capture real time quantitative polymerase chain reaction.

For oral inoculation, tissue cysts of both strains were harvested from infected mouse brain tissue, counted by phase-contrast microscopy and suspended in sterile phosphate buffered saline (PBS) at a concentration of 1,000 tissue cysts/ml (Jennes et al., 2017).

Antigen Preparation

T. gondii lysate antigen (TLA) was prepared from tachyzoites of the RH-strain as previously described (Jongert et al., 2007). The TLA antigens were concentrated and dialyzed with Amicon® filter units (cut-off = 10 kDa) and finally diluted in PBS. The bicinchoninic acid (BCA) reaction (Thermo Scientific Pierce BCA protein Assay Kit, Erembodegem, Belgium) was used to determine the protein concentration and upon filter sterilization with low protein binding filters (0.22 μm, Millex-GV) TLA was stored at −20°C until further use.

Experimental Set-Up

Upon arrival, 36 four-week-old piglets (Belgian Landrace x large white) were confirmed to be *T. gondii* seronegative by the modified agglutination test (ToxoScreen DA, Biomérieux, Capronne, France) and an immunofluorescence test (Toxo-Spot IF, Biomérieux) as described previously (Verhelst et al., 2015). The piglets were randomly selected with taking into account their gender and divided into three groups: control ($n = 6$), LR group ($n = 15$), and Gangji group ($n = 15$).

At day zero (D0) the piglets were inoculated with 6,000 tissue cysts of the *T. gondii* IPB LR strain or Gangji strain, respectively (**Figure 1**). Blood was sampled at the indicated time points to evaluate serum antibody responses by ELISA and the presence of antigen-specific immune cells in an *in vitro* recall assay. At 2, 4, 8, 14, and 28 days post infection, 3 LR strain infected and 3 Gangji strain infected piglets, and at day 0 and day 35, 3 control animals, were euthanized by injecting sodium pentobarbital (20%, 0.125 ml/kg bodyweight; Nembutal; Sanofi) and following exsanguination lymph nodes and tissue samples were collected to assess the parasite load.

In vitro Antigen Recall Assay

Peripheral blood MCs (PBMCs) were isolated from heparinized blood samples with density gradient centrifugation as described (Verhelst et al., 2014). Mononuclear cells (MCs) from the duodenum, jejunum, ileum and mediastinal lymph nodes were harvested in RPMI (1640; Gibco, Merelbeke, Belgium) supplemented with 100 U/ml penicillin and 100 μg/ml streptomycin (P/S; Gibco) as described (Verhelst et al., 2011). The cell suspension was cleared with a 70 μm cell strainer (Corning, USA) and erythrocytes were lysed in lysis buffer (9:1 of 0.83% w/v NH_4Cl and 2.06% w/v Tris ($C_4H_{11}NO_3$), pH 7.2). After washing in PBS + 1 mM EDTA and centrifugation at 380 g for 10 min at 18°C, the pelleted cells were resuspended in complete leukocyte medium [RPMI 1640 supplemented with 10% fetal calf serum (FCS, Greiner Bio-One, Belgium), 292 μg/ml L-glutamin (Gibco), 100 IU/ml penicillin and 100 μg/ml streptomycin (P/S; Gibco), 100 mM non-essential amino acids (Gibco) and 100 μg/ml kanamycin (Gibco)] at a final concentration of 1×10^7 cells/ml.

The MCs were seeded in sterile 96-well flat bottom cell culture plates (Greiner Bio-One) at 1×10^6 cells/well in complete leukocyte medium. After an initial incubation of 1 h, the plates were incubated with 20 μg/ml TLA or medium for 72 h at 37°C in a humidified atmosphere with 5% CO_2. After incubation, the cell-free supernatant was collected and stored at −20°C until analysis of the IFNγ concentration by ELISA.

DNA Extraction and qPCR

DNA was extracted from the isolated mononuclear cells (1.1×10^7 cells) using the QIAamp® DNA Mini kit (Qiagen GmbH, Hilden, Germany) according to the manufacturer's instructions.

The *T. gondii* DNA was quantified by a duplex real-time TaqMan quantitative PCR analysis as described (Gisbert Algaba et al., 2017). Briefly, 10 μl of the DNA extract was tested in a final reaction volume of 25 μl containing 12.5 μl of ExTaq 2 × probe mix (Takara, Saint-Germain-en-Laye, France), 400 nM of primers T2 and T3, 200 nM of primers VF1 and VR1, 66 nM of *Toxoplasma* probe and 40 nM of r18S probe. Each DNA sample was tested twice in each PCR run: one to check the presence of *T. gondii* DNA and cellular r18S and the other one with only the primers and probes to amplify the *T. gondii* target. The real-time PCR was performed with the following cycling program: 3 min at 95°C, followed by 41 cycles of 15 s at 95°C and 20 s at 60°C on a BioRad CFX 96 thermocycler (Hercules, California, USA). In

each run, non-template controls were included. The qPCR results were analyzed to obtain the quantification cycle (Cq) values using the BioRad CFX manager software. For the quantification of *T. gondii* parasite DNA, a standard curve was generated from the Cq values of a 10 fold diluted known number of tachyzoites, i.e., *T. gondii* RH strain (Gisbert Algaba et al., 2017).

TLA ELISA

Blood samples were collected in vacuum tubes (Vacutest KIMA, Italy) from the vena jugularis and were allowed to clot at room temperature for 30 min. Subsequently, serum samples were collected upon centrifugation at 15,000 g for 10 min, aliquoted and stored at −20°C until further use. TLA-specific serum IgG responses were evaluated by ELISA as described (Verhelst et al., 2015). Briefly, 96-well microliter plates were coated with TLA (5 μg/ml, Microbix Biosystems, Canada), serial diluted serum samples were added and detected with HRP-conjugated anti-porcine IgG (Bethyl Laboratories Inc., Montgomery, Texas, USA) and ABTS, i.e., 2,2′-azino-bis (3-ethylbenzothiazoline-6-sulphonic acid) as a substrate. On each plate previously collected sera from positive and negative control animals, as established by IgM and IgG immunofluorescence assay (IFA), were included. After 45 min incubation with substrate at 37°C, the absorbance at 405 nm was measured with a microplate reader (TECAN Spectra Fluor, Tecan Group Ltd., Männedorf, Switzerland) and the obtained data were analyzed in GraphPad Prism 6 software. Serum samples from infected animals were considered positive when exceeding the cut-off value (= mean OD_{405} negative controls + 3× the standard deviation). Antibody titers were calculated as the inverse of that dilution with a signal above the cut-off value.

IFNγ ELISA

IFNγ secretion was determined in the supernatant (1/10, 1/20, and/or 1/50 dilution) of MCs cultured in medium or stimulated with antigens as described above with a sandwich ELISA using the swine-specific IFNγ antibody pair kit (ThermoFisher). The IFNγ concentration in the supernatants was calculated from a regression line (4-parameter curve fit) of serially diluted standard using the DeltaSoft JV 2.1.2 software. The limit of detection of this ELISA was 12.3 pg/ml.

Magnetic Capture qPCR

To assess the *T. gondii* load in lungs and heart, these tissues were collected upon euthanasia and the parasite load was determined via an ISO 17025 validated magnetic capture qPCR (MCqPCR) as described (Gisbert Algaba et al., 2017). This technique combines the magnetic isolation of *T. gondii*-specific DNA from large tissue samples (>100 g) with the sensitivity of qPCR. It has an improved sensitivity of 94.12% as compared to another MCqPCR method (Opsteegh et al., 2010).

The samples with a quantification cycle (Cq) crossing the threshold were considered positive for *T. gondii*, while samples with no Cq for the *T. gondii* target, but Cq of the not competitive internal amplification control were considered negative. The detection limit of this method is 65.4 parasites per 100 g of tissue sample. For each round of samples, a positive control with a known number of parasites was included to correct for possible deviations due to manipulation errors. The number of parasites (n° p) was calculated according to the following formula:

$$\log_{10}(\text{n}^\circ\text{p}) = \frac{\text{Cq}_{\text{value}} - 44.75}{-3.0788}$$

The formula resulted from a standard curve established with known concentrations of parasites ranging from 100 to 10^5 spiked in 100 g of muscle tissue samples or in 50 g of brain tissue (Gisbert Algaba et al., 2017). $\text{Log}_{10}(\text{n}^\circ\text{ p})$ represents the log10-transformed parasitic load, while the Cq_{value} represents the point on the exponential amplification curve crossing the threshold.

Data Analysis

The antibody responses, IFNγ response and *T. gondii* parasite load in tissue samples of the different groups are presented as mean ± SD. Data were analyzed in GraphPad Prism 6 software with the Friedman test and a *post hoc* analysis via Dunn's test. In all analyses $p<0.05$ was considered statistically significant.

RESULTS

The Parasite Load in Gut Lymph Node Cells Indicates That *T. gondii* Initially Enters the Host via the Duodenum

Since *T. gondii* migrate to the mesenteric lymph nodes for rapid dissemination to the target organs via the blood circulation, we assessed the parasite load in immune cells isolated from small intestinal mesenteric lymph nodes (LNs) to trace the initial entry site of the parasite. In the LR group, the parasite load reached its maximum at D8 in all mesenteric lymph nodes as compared to PBMCs in which the parasite load peaked at D14. However, the parasite load in duodenal, jejunal and ileal LNs differed considerably (**Figure 2**) (**Table 1**). *T. gondii* DNA in mononucleated cells (MCs) of duodenal LNs was first detected at day 4 post inoculation, which further increased to reach its maximum at D8 ($P = 0.0196$) and then steadily dropped. In contrast, in jejunal and ileal LNs *T. gondii* DNA was only first detected at day 8 post inoculation, and subsequently decreased following a similar pattern as the duodenal LNs. On the other hand, in the Gangji group, the *T. gondii* DNA load in the MCs of duodenal, jejunal and ileal LNs reached its peak at D8 ($P = 0.045$) and dropped below the detection limit at D28 (**Figure 2**). Interestingly, in duodenal mesenteric LN of this group, the parasite load was below the detection limit at D4.

The parasite dissemination from mesenteric LNs to blood was confirmed by assessing the kinetics of the parasite DNA load in PBMCs. In the LR group, the parasite load in PBMCs continued to increase from D4 until its peak at D14. In contrast, in the Gangji infected pigs, parasite DNA was only detected at D8 and D14 post inoculation (**Figure 2**).

Because *T. gondii* infected immune cells adhesion to lung capillary endothelial cells has been described to trigger parasite egression to immediately coincide in lung tissue and because *T. gondii* cysts preferentially develop in heart tissues during the chronic infection stage (Baba et al., 2017), we also examined the

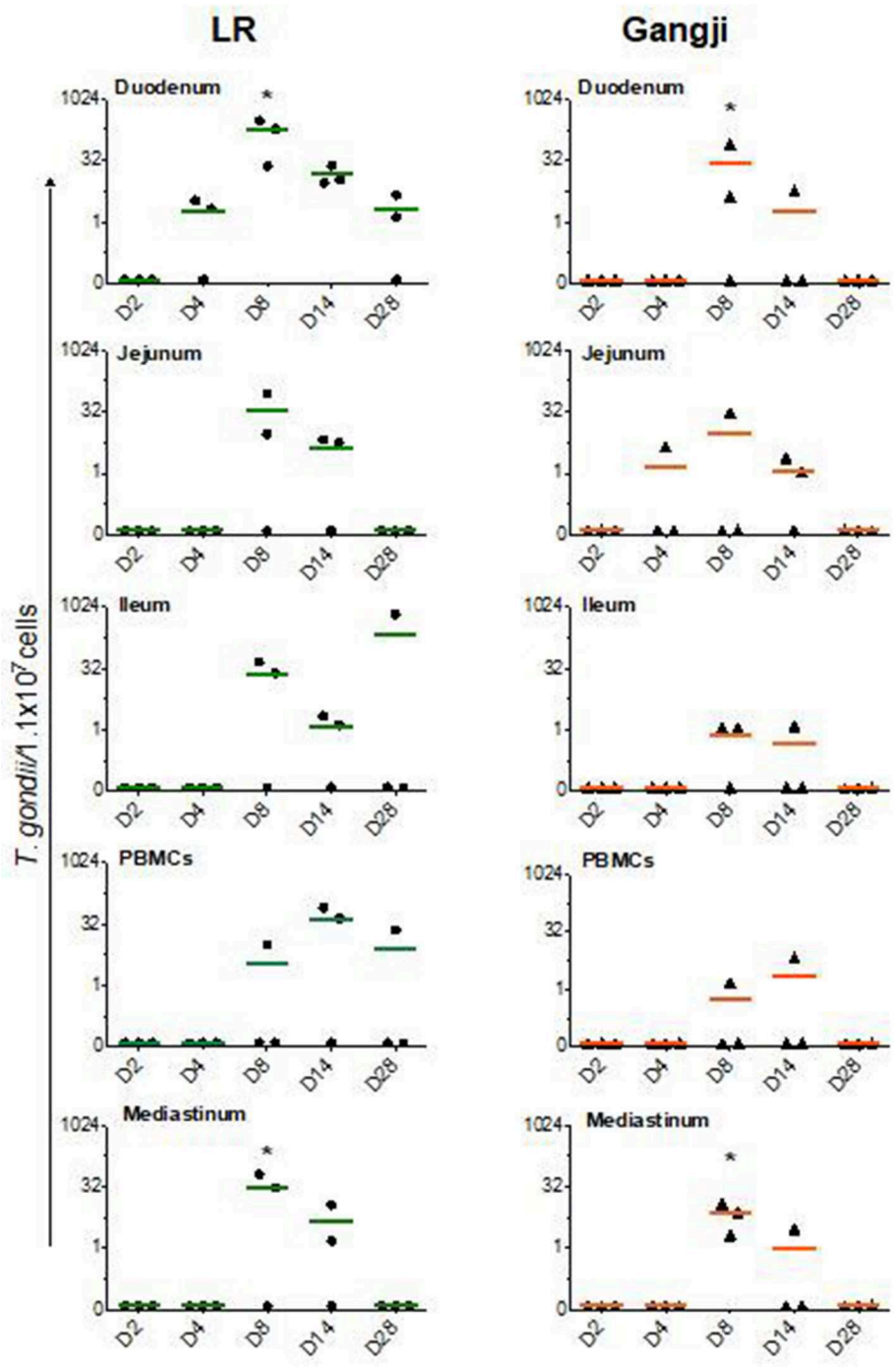

FIGURE 2 | *T. gondii* DNA load in immune cells isolated from lymph nodes and blood. The data are presented as the number of *T. gondii* parasites/1.1 × 10^7 cells. LN, Lymph node. The horizontal line represents the mean, *significantly different than D2, *$P < 0.05$.

parasite load in heart tissue and highly vascularized lung tissue to confirm the presence of *T. gondii* parasites at this early stage of infection.

As shown in **Figure 3**, in lungs, *T. gondii* was already detected in very low amounts at D2, even before being detected in the duodenal lymph nodes, and reached its maximum at D8 in LR ($P = 0.016$). At day 14 the parasite load decreased to remain less or more stable at D28 in both LR and Gangji groups. In heart, the parasite was detected at D4 in both groups which then steadily increased until reaching its maximum at D14 and D28 in LR ($P = 0.032$) and Gangji ($P = 0.095$) groups, respectively (**Figure 3**). The lymph nodes draining these

TABLE 1 | Parasite load in mononuclear immune cells isolated from lymph nodes and blood as determined by qPCR.

Group	Experiment Day	Animals	*T. gondii* load				
			LN duodenum	LN jejunum	LN ileum	PBMCs	LN mediastinum
LR		1	0	0	0	0	0
	D2	2	0	0	0	0	0
		3	0	0	0	0	0
		Average	**0**	**0**	**0**	**0**	**0**
		4	0	0	0	0	0
	D4	5	2.09	0	0	0	0
		6	3.35	0	0	0	0
		Average	**1.81**	**0**	**0**	**0**	**0**
		7	299.91	88.66	24.59	0	64.50
	D8	8	187.86	0	46.12	0	0
		9	23.17	9.10	1	10.16	30.26
		Average	**170.31**	**32.59**	**23.90**	**3.39**	**31.58**
		10	23.81	5.70	2.21	79.90	11.43
	D14	11	10.75	0	0	43.69	0
		12	8.98	6.61	1.33	0	1.51
		Average	**14.51**	**4.10**	**1.18**	**41.20**	**4.31**
		13	0	0	0	0	0
	D28	14	1.33	0	496.5	0	0
		15	4.54	0	0	22.41	0
		Average	**1.95**	**0**	**165.50**	**7.47**	**0**
Gangji		16	0	0	0	0	0
	D2	17	0	0	0	0	0
		18	0	0	0	0	0
		Average	**0**	**0**	**0**	**0**	**0**
		19	0	0	0	0	0
	D4	20	0	4.44	0	0	0
		21	0	0	0	0	0
		Average	**0**	**1.48**	**0**	**0**	**0**
		22	4.33	0	1.10	1	7.67
	D8	23	81.10	29.70	1.14	1.51	12.05
		24	0	0	0	0	2.13
		Average	**28.48**	**9.90**	**0.75**	**0.83**	**7.28**
		25	5.72	2.31	0	1	2.96
	D14	26	0	1.09	1.27	0	0
		27	0	0	0	6.88	0
		Average	**1.91**	**1.13**	**0.42**	**2.29**	**0.99**
		28	0	0	0	0	0
	D28	29	1	0	0	0	0
		30	0	0	5.38	8.12	0
		Average	**0.33**	**0**	**1.79**	**2.71**	**0**

LN, Lymph node. Cut-off T. gondii DNA load: <1 parasite DNA per 1.1 × 10^7 cells considered as negative (0). D, day post inoculation.
Data are presented as the mean number of T. gondii parasite per 1.1 × 10^7 cells.
Average number of parasites is indicated in bold.

organs are connected with the thoracic duct in the mediastinum (Riquet et al., 2000). Therefore, the parasite load in immune cells isolated from mediastinal lymph nodes (LNs) might reflect the parasite load in both organs. However, the parasite load in MCs of mediastinal LN slowly increased from D4 to reach its maximum at D8 in both LR ($P = 0.045$) and Gangji ($P = 0.0196$) groups and subsequently decreased in a similar manner as observed for the mesenteric LNs of LR infected pigs (**Figure 2**).

T. gondii Strains Trigger Different Kinetics of Serum IgG Responses

As the LR strain showed earlier and higher loads in lymphoid tissues, we looked if this resulted in a more pronounced TLA-specific IgG response. This was not the case the first week after infection. For both strains low TLA-specific IgG responses could already be detected at D4 after infection, which further increased up until D8, but subsequently started to differ with approximately 50 folds high titer in LR infected pigs at D28,

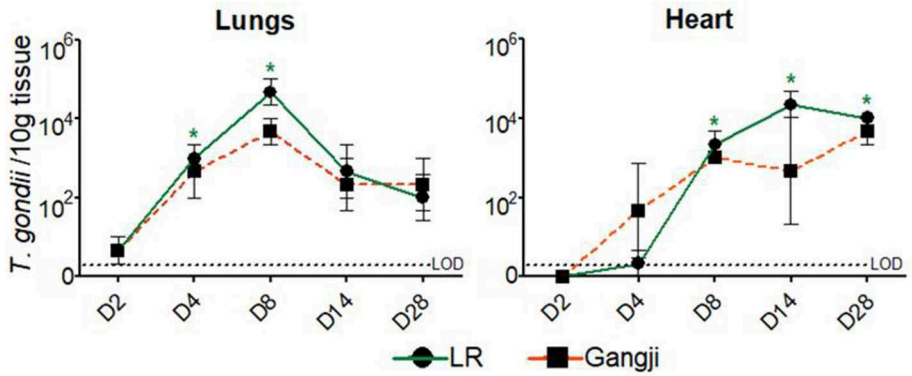

FIGURE 3 | Presence of *T. gondii* DNA in the examined tissues by MCqPCR. The data are presented as the mean ± SD of the number of *T. gondii* parasites/10 g tissue, *significantly different than pre-inoculation, $*P < 0.05$.

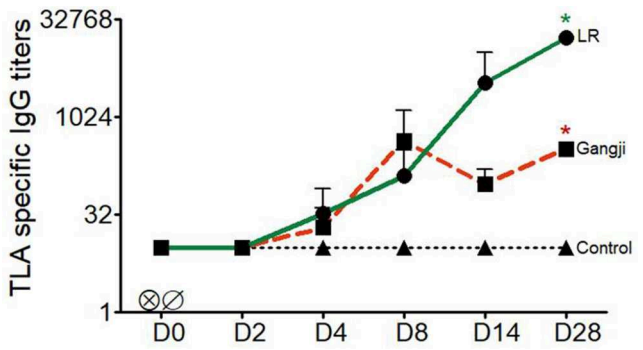

FIGURE 4 | Kinetics of *T. gondii* specific serum IgG titers of LR, Gangji and control groups. Piglets were inoculated orally with tissue cysts of the *T. gondii* IPB LR and Gangji strain on day 0. TLA, *T. gondii* lysate antigens; D, experiment day. The lines are presented as the mean for LR, Gangji and control groups, *LR vs. control, *Gangji vs. control, * or $*P < 0.05$.

whereas no further increase occurred in the Gangji strain infected pigs (**Figure 4**) (**Supplementary Table 1**). Nevertheless, the TLA-specific IgG titers significantly differed at D28 from the pre-infection timepoint in the LR ($P = 0.015$) and Gangji ($P = 0.025$) groups.

T. gondii Infection Elicits IFNγ Secreting Immune Cells in Blood and Lymph Nodes

To be able to correlate the parasite load in the different samples with activation of the cellular immunity, we also assessed the presence of *T. gondii* antigen experienced immune cells in the small intestinal and mediastinal LNs and PBMCs by evaluating their production of IFNγ in an antigen recall assay. As shown in **Figure 5**, TLA stimulation triggered IFNγ secretion by PBMCs and mediastinal LN cells from D8 onwards for LR and Gangji-infected pigs (**Figure 5**). IFNγ secretion by mesenteric LN cells was negligible. Unexpectedly, the IFNγ secretion kinetics in both groups was almost equal, which does not correspond with the parasite burden of immune cells and the serum IgG responses.

DISCUSSION

Oral inoculation of mice with *T. gondii* leads to a primary infection in gut epithelial cells. The *T. gondii* progeny egressing the epithelial cells then infects immune cells in the lamina propria, which subsequently migrate to the adjacent lymph nodes for dissemination in the host (Buzoni-Gatel et al., 2001; Luangsay et al., 2003; Courret et al., 2006; Norose et al., 2008; Baba et al., 2017). Here, we used pigs as an animal model to study infection dynamics and associated immune responses due to the similarity of their gastrointestinal tract with that of humans in terms of physiology, anatomy, immunology and dimensions. We quantified the parasite DNA load in immune cells isolated from duodenal, jejunal, and ileal lymph nodes to be able to assess in which part of the small intestine *T. gondii* first establishes infection. In addition, we included PBMCs to assess the kinetics of systemic spread and cells from mediastinal lymph nodes, as the latter drain the heart, one of the most parasitized tissues after brain during *T. gondii* infection (Gisbert Algaba et al., 2017).

The LR strain showed a more pronounced replication in pigs than the Gangji strain, as evidenced by an earlier detection in duodenal mesenteric LNs, a longer persistence in the mesenteric LNs and blood and a higher antibody response upon infection. The reason might be that the LR strain was isolated from pigs and therefore is more adapted to infect pigs, whereas the human isolated Gangji strain is not and might need to adapt to efficiently infect pigs. A similar phenomenon was for instance observed for influenza as human species/strains need to adapt to pigs to establish efficient infection (Rajao et al., 2019). That *T. gondii* DNA in mononucleated cells (MCs) of duodenal LNs was first detected at day 4 post inoculation, indicates that upon excystation the *T. gondii* LR strain might first infect the duodenum. On the other hand, in the Gangji group, the parasite load in PBMCs and MLNs was below the detection limit until D8. Moreover, as *T. gondii* DNA was detected in blood and lymph node immune cells, this seems to indicate that the dissemination from the intestine to the lymph nodes and other organs in pigs is at least in part immune cell mediated and might occur via a "Trojan horse" mechanism, as

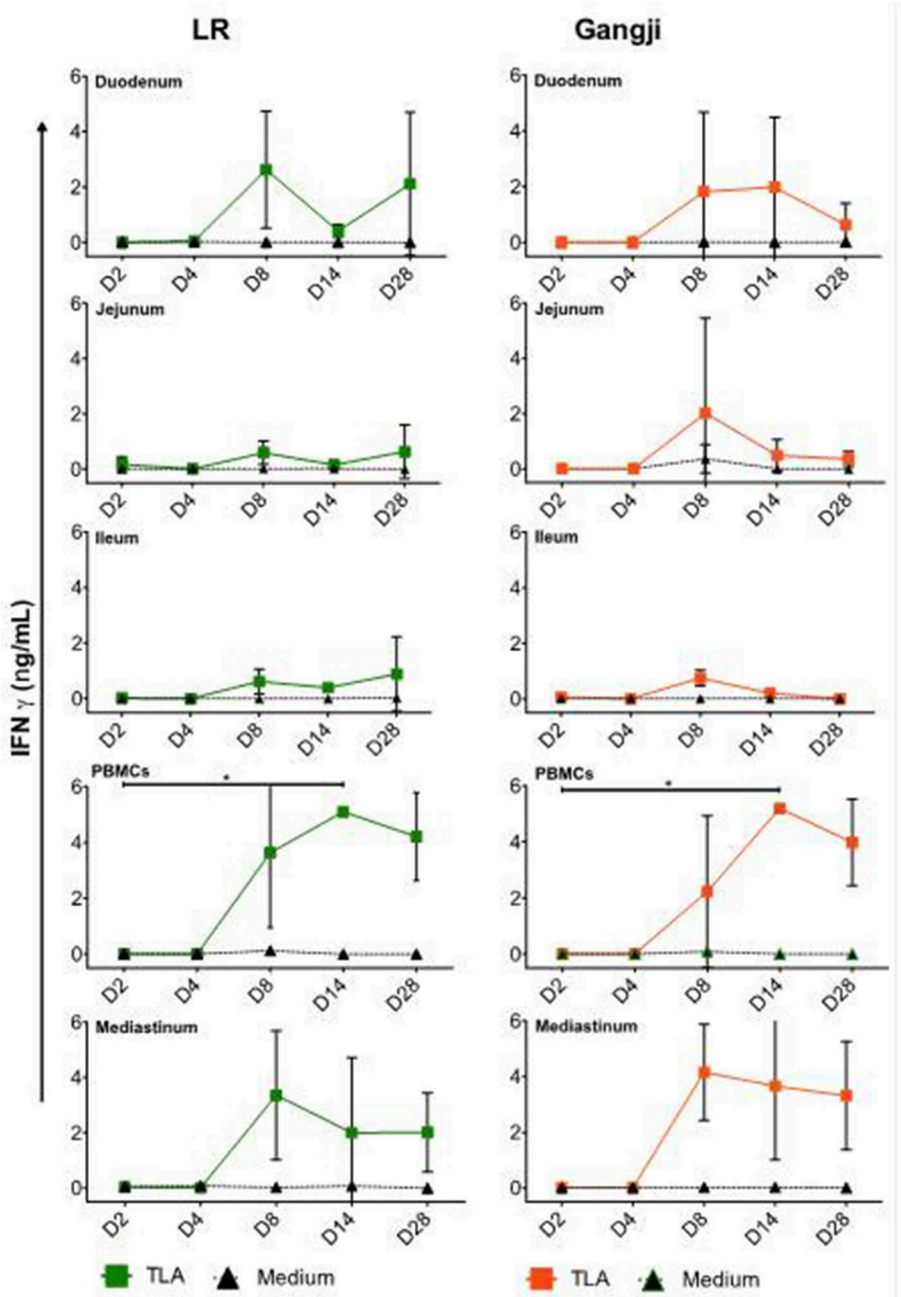

FIGURE 5 | Kinetics of IFNγ secretion by MCs upon oral infection. The data are presented as the mean ± SD, The IFNγ concentration of the control group was below the detection limit and thus was not included. *TLA vs. medium, $^{*}P < 0.05$.

described for *T. gondii* dissemination in mice (Courret et al., 2006; Sanecka and Frickel, 2012). However, this finding requires further investigation as the presence of viable parasites in immune cells was not assessed.

In addition to lymph node and blood immune cells, we also assessed the parasite load in lungs and heart. Surprisingly, the parasite load in lung tissue of the LR and Gangji strain-infected groups was almost equal despite the more pronounced replication of LR in mesenteric LN and blood. Interestingly, *T. gondii* was detected at day 2 post inoculation in lungs, even before we could detect it in duodenal LNs, indicating that the parasite quickly disseminates from its initial point of entry in the gut to the lungs. A potential route might be via the pancreatic LNs, which drain both pancreas and cranial duodenum or directly via the inferior pancreaticoduodenal veins. Alternatively, since we orally inoculated the pigs, we cannot exclude a mis-direction of some inoculant into the respiratory tract.

In mice, *T. gondii* is able to infect vascular endothelial cells and use these cells as a replication niche for dissemination to other organs (Gregg et al., 2013; Konradt et al., 2016). Our results seem to indicate that porcine lung cells support *T. gondii* replication. This could be explained the oxygen levels in the tissue. In most tissues, *T. gondii* requires activation of hypoxia-inducible factor 1 (HIF1) for replication at physiologically relevant oxygen levels (3%). In lung tissue, HIF1 activation is not required as oxygen levels range between 4 and 14% (Spear et al., 2006). However, further studies are needed to confirm *T. gondii* stage conversion from rapidly multiplying tachyzoites to the slow replicating bradyzoites and to investigate if the replication in the lungs might result in the formation of tissue cysts during later stages of infection, as *T. gondii* DNA did not increase beyond day 8 post inoculation. The parasite load in heart tissue on the other hand continuously increased from day 4 onward and remained high until the end of the experiment in both groups. These results agree with the fact that the heart is indeed the most parasitized organ in early *T. gondii* infection stage irrespective of the strain (Jennes et al., 2017). Based on the profile in heart tissue, we assume that we should have detected consistent *T. gondii* DNA in the mediastinal LN after D8; however, we did not. This seems to indicate that there is drainage to other lymph nodes, such as peritracheobronchial lymph nodes (Riquet et al., 2000).

In addition to the quantification of the parasite load in immune cells and tissues, antibody and cellular immune responses were evaluated in LR and Gangji infected groups over time as well. A robust serum IgG response was detected in both LR and Gangji groups. However, the serum IgG response in the LR group was stronger than in the Gangji group, which corresponds to our previous study (Jennes et al., 2017). We also assessed IFNγ secretion by blood and lymph node immune cells of both groups. As expected from our previous research, IFNγ secretion was detected in PBMCs at D14 in both LR and Gangji groups, indicating the presence of peripheral antigen experienced T cells in both groups (Jennes et al., 2017; Rahman et al., 2019). For the lymph nodes, immune cells from mediastinal and duodenal lymph nodes secreted IFNγ, while jejunal and ileal lymph node immune cells did not secrete IFNγ upon TLA re-stimulation. This result further supports that *T. gondii* first infects duodenal epithelial cells. Unexpectedly, a similar IFNγ secretion profile was observed for immune cells isolated from Gangji infected pigs, although the LR strain consistently showed a higher parasite DNA load in these tissues and a higher antibody response than the Gangji strain. A better host adaptation of the LR strain to pigs might explain this. In mice, tachyzoite proliferation of a *T. gondii* strain has been related to IFNγ-inducible cytoplasmic effector proteins, the 47 kDa immunity-related GTPases (IRG proteins). These proteins can inhibit proliferation. Some *T. gondii* strains secrete kinases and pseudokinases that can inactivate IRG proteins resulting in increased replication. Adaptation of the *T. gondii* strain might have resulted in sufficient overriding of the IRG control mechanism to allow more replication (Lilue et al., 2013). A more thorough genetic comparison of both strains might confirm this. Whether this is due to genotype differences between both strains, warrants further investigation. It would be interesting to study the efficiency of both strains at invading intestinal epithelial cells and undergoing replication via an *in vitro* plaque assay (Di Cristina et al., 2017). This would provide some information as to whether the higher parasite load of the LR strain is due to the host response or immune escape mechanisms of the LR strain.

Taking these results into account we assume that the parasite burden in the small intestine is related to the serum antibody responses. In the LR group, high parasite loads in the gut correspond to high serum IgG responses, while in the Gangji group low intestinal parasite loads correspond to low serum IgG responses. Although this seems to contradict the parasite load in the tissues, we speculate that the significant antibody responses in the LR group restrict dissemination to the target organs, while in the Gangji group dissemination is less restricted. This might explain the almost equal parasite load in heart and lungs and the similar T cell responses in both groups.

In conclusion, pigs serve as an interesting model to study initial *T. gondii* infection kinetics in the gut, the associated immune responses and the subsequent dissemination to organs. Our data indicate that upon ingestion *T. gondii* first enters the host at the duodenum and then disseminates to other tissues. This is associated with the activation of IFNγ secreting immune cells. However, it does not yet explain why a re-infection with the Gangji strain in LR strain infected pigs cleared the *T. gondii* DNA from tissue. Nevertheless, these findings lay a foundation to further study the early stages of *T. gondii* intestinal infection and might inform on strategies to prevent initial invasion of the host by this parasite.

DATA AVAILABILITY STATEMENT

All datasets generated for this study are included in the article/**Supplementary Material**.

ETHICS STATEMENT

The animal procedures were approved by the Ethical Committee (EC) of the Faculty of Veterinary Medicine and the Faculty of Bioscience Engineering, Ghent University (EC 2009/149) and by the EC of Sciensano, Belgium (176 20140704-01).

AUTHOR CONTRIBUTIONS

MR, MJ, and EC designed the study. MR and MJ performed the experiments. MR acquired and analyzed the data and drafted the manuscript. BD analyzed the data and wrote the manuscript. IG performed MCqPCR and revised the manuscript. PD and KD helped to design the study, gave valuable input, and revised the manuscript. SD revised the manuscript. EC analyzed the data and reviewed the manuscript.

FUNDING

This study was granted by the Belgian Federal Public Service for Health, Food Chain Safety and Environment (grant RF 09/6213).

BD was supported by a postdoctoral grant of the Research Foundation Flanders (F.W.O.-Vlaanderen).

ACKNOWLEDGMENTS

We wish to thank R. Cooman for the animal management. In addition, a special thanks goes to Raquel Sanz García, Hans Van Der Weken, Michael Pelst, Haixiu Wang, Simon Brabant, and Charlotte Helsmoortel for their help to collect and process tissue samples.

SUPPLEMENTARY MATERIAL

The Supplementary Material for this article can be found online at: https://www.frontiersin.org/articles/10.3389/fcimb.2020.00161/full#supplementary-material

REFERENCES

Ajzenberg, D., Collinet, F., Mercier, A., Vignoles, P., and Dardé, M.-L. (2010). Genotyping of *Toxoplasma gondii* isolates with 15 microsatellite markers in a single multiplex PCR assay. *J. Clin. Microbiol.* 48, 4641–4645. doi: 10.1128/JCM.01152-10

Andrade, W. A., Souza, M. C., Ramos-Martinez, E., Nagpal, K., Dutra, M. S., Melo, M. B., et al. (2013). Combined action of nucleic acid-sensing Toll-like receptors and TLR11/TLR12 heterodimers imparts resistance to *Toxoplasma gondii* in mice. *Cell Host Microbe* 13, 42–53. doi: 10.1016/j.chom.2012.12.003

Baba, M., Batanova, T., Kitoh, K., and Takashima, Y. (2017). Adhesion of *Toxoplasma gondii* tachyzoite-infected vehicle leukocytes to capillary endothelial cells triggers timely parasite egression. *Sci. Rep*. 7:5675. doi: 10.1038/s41598-017-05956-z

Barragan, A., Brossier, F., and Sibley, L. D. (2005). Transepithelial migration of *Toxoplasma gondii* involves an interaction of intercellular adhesion molecule 1 (ICAM-1) with the parasite adhesin MIC2. *Cell. Microbiol.* 7, 561–568. doi: 10.1111/j.1462-5822.2005.00486.x

Betancourt, E. D., Hamid, B., Fabian, B. T., Klotz, C., Hartmann, S., Seeber, F., et al. (2019). From entry to early dissemination—*Toxoplasma gondii*'s initial encounter with its host. *Front. Cell. Infect. Microbiol.* 9:46. doi: 10.3389/fcimb.2019.00046

Buzoni-Gatel, D., Debbabi, H., Mennechet, F. J., Martin, V., Lepage, A. C., Schwartzman, J. D., et al. (2001). Murine ileitis after intracellular parasite infection is controlled by TGF-beta-producing intraepithelial lymphocytes. *Gastroenterology* 120, 914–924. doi: 10.1053/gast.2001.22432a

Coombes, J. L., Charsar, B. A., Han, S.-J., Halkias, J., Chan, S. W., Koshy, A. A., et al. (2013). Motile invaded neutrophils in the small intestine of *Toxoplasma gondii*-infected mice reveal a potential mechanism for parasite spread. *Proc. Natl. Acad. Sci. U.S.A.* 110, E1913–E1922. doi: 10.1073/pnas.1220272110

Courret, N., Darche, S., Sonigo, P., Milon, G., Buzoni-Gâtel, D., Tardieux, I., et al. (2006). CD11c- and CD11b-expressing mouse leukocytes transport single *Toxoplasma gondii* tachyzoites to the brain. *Blood* 107, 309 LP—316. doi: 10.1182/blood-2005-02-0666

Di Cristina, M., Dou, Z., Lunghi, M., Kannan, G., Huynh, M. H., McGovern, O. L., et al. (2017). Toxoplasma depends on lysosomal consumption of autophagosomes for persistent infection. *Nat. Microbiol.* 2:17096. doi: 10.1038/nmicrobiol.2017.96

Dubey, J. P. (1997). Bradyzoite-induced murine toxoplasmosis: stage conversion, pathogenesis, and tissue cyst formation in mice fed bradvzoites of - different strains of *Toxoplasma gondii*. *J. Eukaryot. Microbiol.* 44, 592–602. doi: 10.1111/j.1550-7408.1997.tb05965.x

Dubey, J. P. (2010). *Toxoplasmosis of Animals and Humans*. Florida, FL: CRC Press. Taylor & Francis Group. doi: 10.1201/9781420092370

Dubey, J. P., Hill, D. E., Rozeboom, D. W., Rajendran, C., and Choudhary, S. (2012). High prevalence and genotypes of Toxoplasma gondii isolated from organic pigs in northern USA. *Vet. Parasitol.* 188, 14–18. doi: 10.1016/j.vetpar.2012.03.008

Dubey, J. P., Lindsay, D. S., and Speer, C. A. (1998). Structures of *Toxoplasma gondii* tachyzoites, bradyzoites, and sporozoites and biology and development of tissue cysts. *Clin. Microbiol. Rev.* 11, 267–299. doi: 10.1128/CMR.11.2.267

Forsbach, A., Nemorin, J.-G., Montino, C., Muller, C., Samulowitz, U., Vicari, A. P., et al. (2008). Identification of RNA sequence motifs stimulating sequence-specific TLR8-dependent immune responses. *J. Immunol.* 180, 3729–3738. doi: 10.4049/jimmunol.180.6.3729

Gisbert Algaba, I., Geerts, M., Jennes, M., Coucke, W., Opsteegh, M., Cox, E., et al. (2017). A more sensitive, efficient and ISO 17025 validated Magnetic Capture real time PCR method for the detection of archetypal *Toxoplasma gondii* strains in meat. *Int. J. Parasitol.* 47, 875–884. doi: 10.1016/j.ijpara.2017.05.005

Gregg, B., Taylor, B. C., John, B., Tait-Wojno, E. D., Girgis, N. M., Miller, N., et al. (2013). Replication and distribution of *Toxoplasma gondii* in the small intestine after oral infection with tissue cysts. *Infect. Immun.* 81, 1635 LP—1643. doi: 10.1128/IAI.01126-12

Howe, D. K., and Sibley, L. D. (1995). *Toxoplasma gondii* comprises three clonal lineages: correlation of parasite genotype with human disease. *J. Infect. Dis.* 172, 1561–1566. doi: 10.1093/infdis/172.6.1561

Ishii, K. J., Koyama, S., Nakagawa, A., Coban, C., and Akira, S. (2008). Host innate immune receptors and beyond: making sense of microbial infections. *Cell Host Microbe*. 3, 352–363. doi: 10.1016/j.chom.2008.05.003

Jennes, M., De Craeye, S., Devriendt, B., Dierick, K., Dorny, P., Cox, E., et al. (2017). Strain- and dose-dependent reduction of *Toxoplasma gondii* burden in pigs is associated with interferon-gamma production by $CD8^+$ lymphocytes in a heterologous challenge model. *Front. Cell. Infect. Microbiol.* 7, 1–20. doi: 10.3389/fcimb.2017.00232

Jones, E. J., Korcsmaros, T., and Carding, S. R. (2017). Mechanisms and pathways of *Toxoplasma gondii* transepithelial migration. *Tissue Barriers*. 5:e1273865. doi: 10.1080/21688370.2016.1273865

Jongert, E., De Craeye, S., Dewit, J., and Huygen, K. (2007). GRA7 provides protective immunity in cocktail DNA vaccines against *Toxoplasma gondii*. *Parasite Immunol.* 29, 445–453. doi: 10.1111/j.1365-3024.2007.00961.x

Konradt, C., Ueno, N., Christian, D. A., Delong, J. H., Pritchard, G. H., Herz, J., et al. (2016). Endothelial cells are a replicative niche for entry of *Toxoplasma gondii* to the central nervous system. *Nat. Microbiol.* 1:16001. doi: 10.1038/nmicrobiol.2016.1

Lambert, H., Hitziger, N., Dellacasa, I., Svensson, M., and Barragan, A. (2006). Induction of dendritic cell migration upon *Toxoplasma gondii* infection potentiates parasite dissemination. *Cell. Microbiol.* 8, 1611–1623. doi: 10.1111/j.1462-5822.2006.00735.x

Lilue, J., Müller, U. B., Steinfeldt, T., and Howard, J. C. (2013). Reciprocal virulence and resistance polymorphism in the relationship between *Toxoplasma gondii* and the house mouse. *eLife* 2:e01298. doi: 10.7554/eLife.01298

Luangsay, S., Kasper, L. H., Rachinel, N., Minns, L. A., Mennechet, F. J. D., Vandewalle, A., et al. (2003). CCR5 mediates specific migration of *Toxoplasma gondii*-primed CD8 lymphocytes to inflammatory intestinal epithelial cells. *Gastroenterology* 125, 491–500. doi: 10.1016/S0016-5085(03)00903-X

Meurens, F., Summerfield, A., Nauwynck, H., Saif, L., and Gerdts, V. (2012). The pig: a model for human infectious diseases. *Trends Microbiol.* 20, 50–57. doi: 10.1016/j.tim.2011.11.002

Norose, K., Naoi, K., Fang, H., and Yano, A. (2008). *In vivo* study of toxoplasmic parasitemia using interferon-gamma-deficient mice: absolute cell number of leukocytes, parasite load and cell susceptibility. *Parasitol. Int.* 57, 447–453. doi: 10.1016/j.parint.2008.05.007

Opsteegh, M., Langelaar, M., Sprong, H., den Hartog, L., De Craeye, S., Bokken, G., et al. (2010). Direct detection and genotyping of Toxoplasma gondii in meat samples using magnetic capture and PCR. *Int. J. Food Microbiol.* 139, 193–201. doi: 10.1016/j.ijfoodmicro.2010.02.027

Rahman, M., Devriendt, B., Gisbert Algaba, I., Verhaegen, B., Dorny, P., Dierick, K., et al. (2019). QuilA-adjuvanted *T. gondii* lysate antigens trigger robust antibody and IFNγ+ T cell responses in pigs leading to reduction in

parasite DNA in tissues upon challenge infection. *Front. Immunol.* 10:2223. doi: 10.3389/fimmu.2019.02223

Rajao, D. S., Vincent, A. L., and Perez, D. R. (2019). Adaptation of human influenza viruses to swine. *Front. Vet. Sci.* 5:347. doi: 10.3389/fvets.2018.00347

Riquet, M., Souilamas, R., Hubsch, J. P., Briere, J., Colomer, S., Hidden, G., et al. (2000). Lymphatic drainage of heart and lungs: comparison between pig and man. *Surg. Radiol. Anat.* 22, 47–50. doi: 10.1007/s00276-000-0047-x

Sanecka, A., and Frickel, E.-M. (2012). Use and abuse of dendritic cells by *Toxoplasma gondii*. *Virulence* 3, 678–689. doi: 10.4161/viru.22833

Spear, W., Chan, D., Coppens, I., Johnson, R. S., Giaccia, A., Blader, I. J., et al. (2006). The host cell transcription factor hypoxia-inducible factor 1 is required for *Toxoplasma gondii* growth and survival at physiological oxygen levels. *Cell. Microbiol.* 8, 339–352. doi: 10.1111/j.1462-5822.2005.00628.x

Torgerson, P. R., and Mastroiacovo, P. (2013). The global burden of congenital toxoplasmosis: a systematic review. *Bull. World Health Organ.* 91, 501–508. doi: 10.2471/BLT.12.111732

Tosh, K. W., Mittereder, L., Bonne-Annee, S., Hieny, S., Nutman, T. B., Singer, S. M., et al. (2016). The IL-12 response of primary human dendritic cells and monocytes to toxoplasma gondii is stimulated by phagocytosis of live parasites rather than host cell invasion. *J. Immunol.* 196, 345–356. doi: 10.4049/jimmunol.1501558

Verhelst, D., De Craeye, S., Dorny, P., Melkebeek, V., Goddeeris, B., Cox, E. et al. (2011). IFN-γ expression and infectivity of Toxoplasma infected tissues are associated with an antibody response against GRA7 in experimentally infected pigs. *Vet. Parasitol.* 179, 14–21. doi: 10.1016/j.vetpar.2011.02.015

Verhelst, D., De Craeye, S., Entrican, G., Dorny, P., and Cox, E. (2014). Parasite distribution and associated immune response during the acute phase of *Toxoplasma gondii* infection in sheep. *BMC Vet. Res.* 10:293. doi: 10.1186/s12917-014-0293-5

Verhelst, D., De Craeye, S., Jennes, M., Dorny, P., Goddeeris, B., Cox, E. et al. (2015). Interferon-gamma expression and infectivity of Toxoplasma infected tissues in experimentally infected sheep in comparison with pigs. *Vet. Parasitol.* 207, 7–16. doi: 10.1016/j.vetpar.2014.11.014

Weidner, J. M., Kanatani, S., Hernandez-Castaneda, M. A., Fuks, J. M., Rethi, B., Wallin, R. P. A., et al. (2013). Rapid cytoskeleton remodelling in dendritic cells following invasion by *Toxoplasma gondii* coincides with the onset of a hypermigratory phenotype. *Cell. Microbiol.* 15, 1735–1752. doi: 10.1111/cmi.12145

Conflict of Interest: The authors declare that the research was conducted in the absence of any commercial or financial relationships that could be construed as a potential conflict of interest.

frontiers in Cellular and Infection Microbiology

ORIGINAL RESEARCH
published: 09 June 2020
doi: 10.3389/fcimb.2020.00203

Potent Tetrahydroquinolone Eliminates Apicomplexan Parasites

Martin J. McPhillie[1†], Ying Zhou[2†], Mark R. Hickman[3†‡], James A. Gordon[1†‡], Christopher R. Weber[4†], Qigui Li[3], Patty J. Lee[3], Kangsa Amporndanai[5], Rachel M. Johnson[6‡], Heather Darby[1], Stuart Woods[7], Zhu-hong Li[8], Richard S. Priestley[9], Kurt D. Ristroph[10], Scott B. Biering[4‡], Kamal El Bissati[2], Seungmin Hwang[4‡], Farida Esaa Hakim[2], Sarah M. Dovgin[2‡], Joseph D. Lykins[2‡], Lucy Roberts[7], Kerrie Hargrave[7‡], Hua Cong[1‡], Anthony P. Sinai[11], Stephen P. Muench[6], Jitender P. Dubey[12], Robert K. Prud'homme[10], Hernan A. Lorenzi[13†], Giancarlo A. Biagini[9], Silvia N. Moreno[8], Craig W. Roberts[7], Svetlana V. Antonyuk[5*], Colin W. G. Fishwick[1*] and Rima McLeod[2,14*]*

[1] School of Chemistry, The University of Leeds, Leeds, United Kingdom, [2] Department of Ophthalmology and Visual Sciences, The University of Chicago, Chicago, IL, United States, [3] Experimental Therapeutics Branch, Walter Reed Army Institute of Research, Silver Spring, MD, United States, [4] Department of Pathology, The University of Chicago, Chicago, IL, United States, [5] Department of Biochemistry and Systems Biology, Faculty of Health and Life Sciences, Institute of Systems, Molecular and Integrative Biology, The University of Liverpool, Liverpool, United Kingdom, [6] School of Biomedical Sciences, Faculty of Biological Sciences, and Astbury Centre for Structural Molecular Biology, The University of Leeds, Leeds, United Kingdom, [7] Strathclyde Institute of Pharmacy and Biomedical Sciences, The University of Strathclyde, Glasgow, United Kingdom, [8] Department of Cellular Biology, Center for Tropical and Emerging Global Diseases, University of Georgia, Athens, GA, United States, [9] Department of Tropical Disease Biology, Research Center for Drugs and Diagnostics, The Liverpool School of Tropical Medicine, Liverpool, United Kingdom, [10] Department of Chemical and Biological Engineering, Princeton University, Princeton, NJ, United States, [11] Microbiology, Immunology and Molecular Genetics, The University of Kentucky College of Medicine, Lexington, KY, United States, [12] Animal Parasitic Diseases Laboratory (APDL), USDA-ARS, Beltsville, MD, United States, [13] Department of Infectious Diseases, J Craig Venter Institute, Rockville, MD, United States, [14] Department of Pediatrics (Infectious Diseases), Institute of Genomics, Genetics, and Systems Biology, Global Health Center, Toxoplasmosis Center, CHeSS, The College, University of Chicago, Chicago, IL, United States

Apicomplexan infections cause substantial morbidity and mortality, worldwide. New, improved therapies are needed. Herein, we create a next generation anti-apicomplexan lead compound, JAG21, a tetrahydroquinolone, with increased sp3-character to improve parasite selectivity. Relative to other cytochrome *b* inhibitors, JAG21 has improved solubility and ADMET properties, without need for pro-drug. JAG21 significantly reduces *Toxoplasma gondii* tachyzoites and encysted bradyzoites *in vitro,* and in primary and established chronic murine infections. Moreover, JAG21 treatment leads to 100% survival. Further, JAG21 is efficacious against drug-resistant *Plasmodium falciparum in vitro*. Causal prophylaxis and radical cure are achieved after *P. berghei* sporozoite infection with oral administration of a single dose (2.5 mg/kg) or 3 days treatment at reduced dose (0.625 mg/kg/day), eliminating parasitemia, and leading to 100% survival. Enzymatic, binding, and co-crystallography/pharmacophore studies demonstrate selectivity for apicomplexan relative to mammalian enzymes. JAG21 has significant promise as a pre-clinical candidate for prevention, treatment, and cure of toxoplasmosis and malaria.

Keywords: *Toxoplasma gondii*, *Plasmodium falciparum*, cytochrome bc1, tetrahydroquinolone, nanoformulation, structure-guided design, transcriptomics, RPS13Δ

OPEN ACCESS

Edited by:
Jeroen P. J. Saeij, University of California, Davis, United States

Reviewed by:
Louis Weiss, Albert Einstein College of Medicine, United States
Renato Augusto DaMatta, State University of the North Fluminense Darcy Ribeiro, Brazil

***Correspondence:**
Silvia N. Moreno
smoreno@uga.edu
Svetlana V. Antonyuk
S.Antonyuk@liverpool.ac.uk
Colin W. G. Fishwick
C.W.G.Fishwick@leeds.ac.uk
Rima McLeod
rmcleod@bsd.uchicago.edu

[†] *These authors have contributed equally to this work*

[‡] ***Present address:***
Mark R. Hickman, Fort Detrick, Frederick, MD, United States
James A. Gordon, Charles River, Cambridge, United Kingdom
Rachel M. Johnson, Monash University, Melbourne, VIC, Australia
Scott B. Biering, University of California at Berkeley, Berkeley, CA, United States
Seungmin Hwang, VIR Biotechnology, San Francisco, CA, United States
Sarah M. Dovgin, Case Western Reserve University, Cleveland, OH, United States
Joseph D. Lykins, Virginia Commonwealth University Health System, Richmond, VA, United States
Kerrie Hargrave, University of Glasgow, Glasgow, United Kingdom
Hua Cong, Shandong University, Shandong, China

Specialty section:
This article was submitted to Parasite and Host, a section of the journal Frontiers in Cellular and Infection Microbiology

INTRODUCTION

Malaria results in the death of ∼0.5 million children a year, with drug resistance impacting the usefulness of successive generations of new medicines (www.who.int/malaria/publications/world-malaria-report-2017/en/). The related apicomplexan parasite, *Toxoplasma gondii,* is the most frequent parasitic infection of humans in the world. It plays a significant role in food-borne associated death in the USA, destruction of the human retina (Phan et al., 2008), and death and illness from recrudescent disease in the immune compromised or immunologically immature (McLeod et al., 2006; McLeod and Boyer, 2019). It has been estimated that there are 1.9 million new cases of this congenital *T. gondii* infection globally over a 10 year period, causing 12 million disability adjusted life years (Torgerson and Mastroiacovo, 2013) from damage to the fetal brain and eye. Toxoplasmosis is an often neglected, untreated, or mistreated disease. There are ∼2 billion people throughout the world who have this parasite in their brain lifelong, some with known, severe, adverse consequences (Delair et al., 2011; Wallon et al., 2013; Lykins et al., 2016). There are possible additional, harmful effects for a substantial number of chronically infected people as this parasite modulates signature pathways of neurodegeneration, motor diseases, epilepsy, and malignancies (Ngô et al., 2017). No medicine eliminates this chronic, encysted form of the parasite. New and improved medicines are greatly needed to cure *Toxoplasma* and Plasmodia infections (McLeod et al., 2006). These parasites often share the same molecular targets for medicines due to a relatively close, apicomplexan, phylogenetic relationship (McPhillie et al., 2016). Thus, medicine development for each of these parasites can inform development of medicines that benefit treating the other (Muench et al., 2007; Fomovska et al., 2012a).

One such shared molecular target is the mitochondrial cytochrome *bc1* complex that is important for the survival of apicomplexan parasites such as Plasmodia and *T. gondii*. Cytochrome *b* is a subunit of the cytochrome bc_1 complex, an inner mitochondrial membrane protein that is part of the electron transport chain. Activity of this complex is integral to oxidative phosphorylation and generation of ATP (Vercesi et al., 1998). Cytochrome *b* activity appears to be necessary for the replication and persistence of the parasite (McPhillie et al., 2016), and is the site of action of atovaquone (McPhillie et al., 2016). Cytochrome *b* is the target for quinolone-based compounds, but, significant problems with solubility, and toxicity have been noted with earlier cytochrome *b* inhibitors. In an attempt to design novel quinolone-like inhibitors with improved solubility, and lower toxicity, compared to known compounds in the literature, we synthesized a series of tetrahydroquinolinones (THQs). Our preliminary efforts were described in McPhillie et al. (2016). We reasoned that the increased "sp3" character of the THQs (i.e., moving from rod-like to sphere-like 3D space) could provide the required improvement in solubility that would allow for optimal pharmacokinetic properties. Molecules with an increased percentage of "sp3 character" tend to be more three-dimensional, than their planar ("sp2-rich") counterparts. The terms "sp2" and "sp3" refer to the shape of their hybridized atomic orbitals, which have trigonal planar and tetrahedral geometries, respectively. Flat aromatic rings ("sp2-rich") are ubiquitous in drug discovery campaigns, but molecules with more "sp3 character" are often more specific for their protein target and can have better physicochemical properties. Further, we reasoned that the larger binding pocket in the parasite enzymes (McPhillie et al., 2016), compared to their mammalian counterparts, would provide room for bulkier substituents to minimize effect on the human enzyme. Within this new series of compounds, we aimed to identify a mature lead compound with both anti-*Plasmodium* and anti-*T. gondii* activity.

Our work developed as follows: We recently found markedly increased expression of cytochrome *b* in the currently untreatable *T. gondii* bradyzoite life-cycle stage (McPhillie et al., 2016). Thus, we set out to develop a compound that would inhibit tachyzoites, bradyzoites, and three life cycle stages of even drug-resistant Plasmodia. We sought to do this without a need for a pro-drug as has been needed in other attempts to target apicomplexan cytochrome *b* (Frueh et al., 2017). Our aim was to improve upon the physicochemical properties of napthoquinones and endochin-like quinolones (ELQs) targeting cytochrome *b*, including poor aqueous solubility and toxicity (Khan et al., 1998; Doggett et al., 2012; Capper et al., 2015; Miley et al., 2015; McPhillie et al., 2016). The intent was further to provide potential solutions for limitations of other compounds active against apicomplexan parasites (Waxman and Herbert, 1969; Caumes et al., 1995). Our concurrent crystallographic studies also enable better understanding of the interactions between ligand and the binding pocket of the Q_i site (McPhillie et al., 2016).

Herein, we have identified a preclinical lead candidate based on potent and selective inhibition of *Plasmodium falciparum, Plasmodium berghei,* and *T. gondii* cytochrome *bc1* for the treatment of malaria and toxoplasmosis. The candidate compound demonstrates high efficacy in relevant *in vitro* and *in vivo* models of the diseases, and has considerable potential for broad-spectrum use (i.e., against *T. gondii* tachyzoites and encysted bradyzoites, and drug resistant Plasmodia). The data which follow present the creation and characterization of this novel, broad-spectrum, anti-apicomplexan lead compound which has promise for definitive treatment of these infections.

MATERIALS AND METHODS

Syntheses of Compounds

Synthesis of Tetrahydroquinolones (THQs) Compounds

The THQ compounds were synthesized at the University of Leeds as described below. Ten millimolars stock solutions were made with 100% Dimethyl Sulfoxide (DMSO) [Sigma Aldrich] and working concentrations were made with IMDM-C (1x, [+] glutamine, [+] 25 mM HEPES, [–] Phenol red, 10% FBS)[Gibco, Denmark]). Compounds are shown in **Figure 1A**. Compound name with "0" or no "0" between letters and number, e.g., JAG21 or JAG021, refer to the same compound. This is throughout the manuscript. Final compounds had >95% purity determined

by high performance liquid chromatography (HPLC), high resolution mass spectrometry, and NMR spectrometry. Liquid chromatography-mass spectrometry (LC-MS) and NMR spectrometry were used to determine the integrity and purity of all intermediates. THQ compounds were synthesized as described in **Schemes 1**, **2**, which describe compounds MJM170 and JAG21 as exemplars. Building blocks 1, 8, 9, and 14 were varied to create the complete series (**Figure 1A**).

Synthesis of 2-Methyl-5,6,7,8-Tetrahydroquinolin-4-one (2)

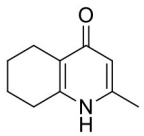

Platinum oxide (0.100 g, 10 mol %) was added to a solution of 4-hydroxy-2-methylquinoline (**1**, 1.00 g, 6.28 mmol, 1.00 eq) in glacial acetic acid (10.0 mL). The heterogeneous mixture was catalytically hydrogenated under a balloon of hydrogen. After 22 h, TLC (10% MeOH–DCM) confirmed complete reaction. The mixture was filtered through celite under vacuum, washing thoroughly with EtOAc (50 mL). The filtrate was concentrated and the resulting residue purified by column chromatography (10% MeOH–DCM) to give the desired product as a pale yellow oil (0.917 g, 5.65 mmol, 89%); R_f 0.14 (10% MeOH–DCM); δ_H **(300 MHz, $CDCl_3$)** 1.74–1.76 (4H, m, CH_2), 2.29 (3H, s, Me), 2.49–2.52 (2H, m, CH_2), 2.67–2.70 (2H, m, CH_2), 6.16 (1H, s, Ar-H); δ_C **(125 MHz, $CDCl_3$)** 19.0 (Me), 21.8 (CH_2), 22.1 (CH_2), 27.1 (CH_2), 112.5 (CH), 122.4 (Cq), 146.4 (Cq), 147.0 (Cq), 178.3 (Cq); Spectroscopic data consistent with literature values (Bradbury et al., 1993).

Synthesis of 2-Methyl-3-iodo-5,6,7,8-Tetrahydroquinolin-4-One (3)

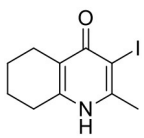

^{n}Butylamine (6.20 mL, 62.8 mmol, 10.0 eq) was added to a suspension of 2-methyl-5,6,7,8-tetrahydroquinolin-4-one (**2**, 1.02 g, 6.28 mmol, 1.00 eq) in DMF (10.0 mL). To this heterogeneous mixture was added I_2 (1.60 g, 6.28 mmol, 1.00 eq) in a saturated solution of KI (6.00 mL). After 20 h stirring at R.T., a precipitate formed in the orange solution, excess iodine was quenched with 0.1 M sodium thiosulfate solution (10.0 mL). The precipitate was filtered by vacuum filtration, washed with distilled H_2O and dried (Na_2SO_4) to give the desired product as a colorless solid (1.76 g, 6.09 mmol, quantative yield); δ_H **(300 MHz, DMSO-d_6)** 1.61–1.70 (4H, m, CH_2), 2.29 (2H, t, *J* 6.0, CH_2), 2.43 (2H, s, CH_2), CH_3 under DMSO peak.

Synthesis of 2-Methyl-3-Iodo-4-Ethoxy-5,6,7,8-Tetrahydroquinoline (4)

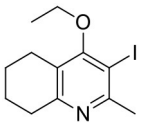

Potassium carbonate (1.53 g, 11.1 mmol, 2.00 eq) was added to a heterogeneous mixture of 2-methyl-3-iodo-5,6,7,8-tetrahydroquinolin-4-one (**3**, 1.60 g, 5.56 mmol, 1.00 eq) in DMF (15.0 mL), and the reaction heated to 50°C for 30 min. The R.B. flask was removed from the heating mantle and ethyl iodide (0.67 mL, 8.33 mmol, 1.50 eq) was added dropwise. The reaction was then heated at 50°C for 18 h. The reaction was cooled to R.T., quenched with water (40 mL). The resulting emulsion formed which was extracted with EtOAc (50 mL). EtOAc layer were washed with water (3 × 30 mL), brine (3 × 30 mL), dried (Na_2SO_4) and concentrated to give a pale yellow oil (1.09 g, 3.44 mmol, 61%); R_f 0.88 (1:1 Pet–EtOAc); **HPLC** (RT = 1.67 min); **LCMS** (Method A), (RT = 1.6 min, *m/z* (ES) Found MH^+ 318.0); δ_H **(500 MHz, $CDCl_3$)** 1.49 (3H, t, *J* 7.0, ethoxy CH_3), 1.73–1.78 (2H, m, CH_2) 1.84–1.88 (2H, m, CH_2), 2.78–2.69 (5H, m, CH_2 & CH_3), 2.84 (2H, t, *J* 6.5, CH_2), 3.97 (2H, q, *J* 7.0, OCH_2); δ_C **(125 MHz, $CDCl_3$)** 15.6 (CH_3), 22.3 (CH_2), 22.8 (CH_2), 23.6 (CH_2), 29.3 (CH_3), 32.0 (CH_2), 68.4 (OCH_2), 90.9 (Cq), 124.5 (Cq), 158.3 (Cq), 158.9 (Cq), 163.9 (Cq).

Synthesis of 2-Methyl-3-(4-Phenoxyphenyl)-4-Ethoxy-5,6,7,8-Tetrahydroquinoline (6)

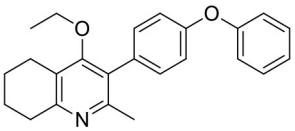

2-Methyl-3-iodo-4-ethoxy-5,6,7,8-tetrahydroquinoline (**4**, 0.266 g, 0.839 mmol, 1.00 eq), $Pd(PPh_3)_4$ (0.048 g, 0.0419 mmol, 5 mol%) and 4-phenoxyphenylboronic acid (**5**, 0.270 g, 1.26 mmol, 1.50 eq) were charged to a R.B. flask under N_2(g). Degassed DMF (10.0 mL) was added to the flask followed by 2M K_2CO_3 (1.60 mL). The flask was heated to 85°C under N_2(g). After 15 min, TLC (4:1 Pet–EtOAc) confirmed reaction was complete. The reaction was cooled and diluted with EtOAc (15 mL), filtered through celite and partitioned between EtOAc (10 mL) and H_2O (25 mL). Combined organics were washed with H_2O (3 × 30 mL), then brine (3 × 30 mL), dried (Na_2SO_4) and concentrated to give a red oil which was purified by column chromatography (3:1 Pet–EtOAc), to give the desired product as a pale yellow oil (0.235 g, 0.655 mmol, 78%); R_f 0.31 (3:1 Pet–EtOAc); **HPLC** (RT = 3.08 min); δ_H **(300 MHz, $CDCl_3$)** 1.04 (3H, t, *J* 7.0, ethoxy CH_3), 1.76–1.93 (4H, m, 2xCH_2), 2.32 (3H, s, CH_3) 2.72 (2H, t, *J* 6.0, CH_2), 2.91 (2H, t, *J* 6.5, CH_2), 3.50 (2H, q, *J* 7.0, OCH_2), 7.05–7.16 (5H, m, Ar-H), 7.20–7.29 (2H, m, Ar-H), 7.31–7.43 (2H, m, Ar-H); δ_C **(125 MHz, $CDCl_3$)** 15.7 (CH_3), 22.5 (CH_2), 23.0 (CH_3), 23.3 (CH_2), 23.4 (CH_2), 32.7 (CH_2), 68.2 (OCH_2), 118.6 (CH), 118.9 (CH), 123.4 (CH), 126.8 (Cq), 129.8 (CH), 131.5 (CH), 154.9 (Cq), 156.5 (Cq), 157.1

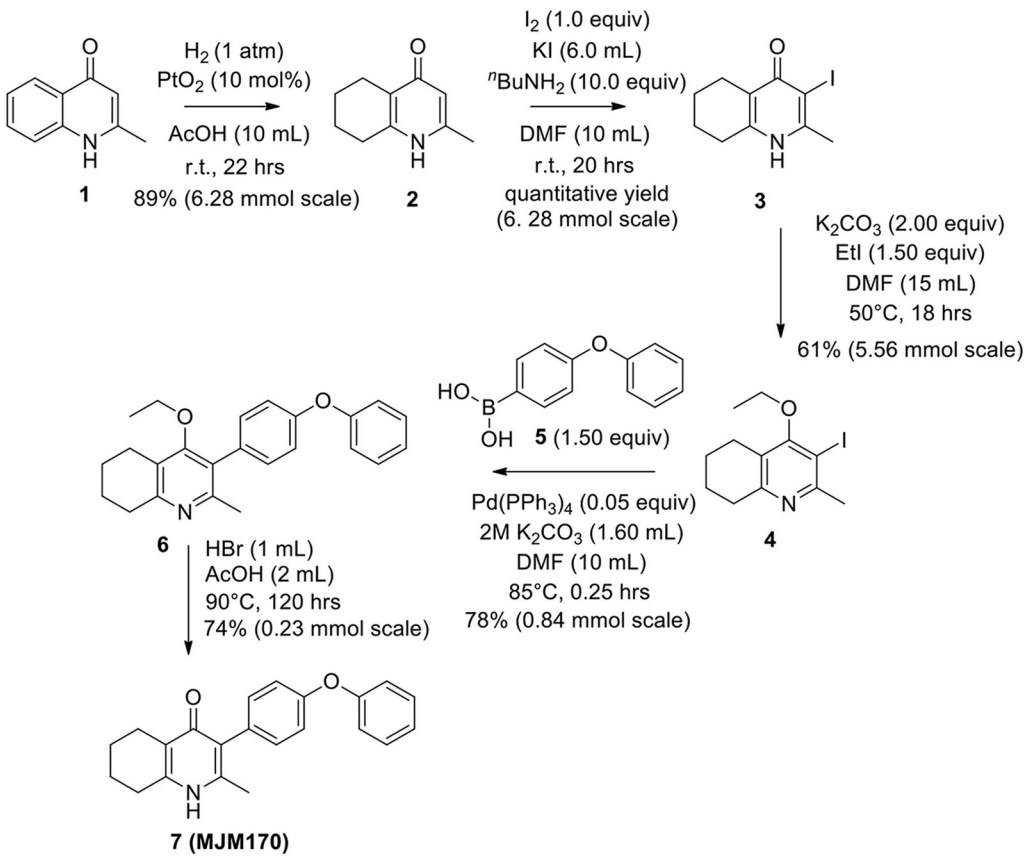

SCHEME 1 | Synthesis of hit compound 7, also known as MJM170 (McPhillie et al., 2016). Synthetic scheme inspired by the route to endochin-like quinolones (ELQs) reported by Doggett et al. (2012).

(Cq), 157.3 (Cq); ***m/z* (*ES*)** (Found: MH^+, 360.1973. $C_{24}H_{26}NO_2$ requires *MH*, 360.1964).

Synthesis of 2-Methyl-3-(4-Phenoxyphenyl)-4-Ethoxy-5,6,7,8-Tetrahydroquinoline (7, MJM170)

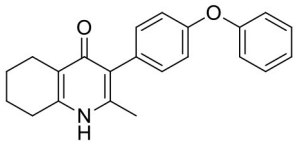

Aqueous hydrobromic acid (>48%) (1.00 mL) was added to a solution of 2-methyl-3-(4-phenoxyphenyl)-4-ethoxy-5,6,7,8-tetrahydroquinoline (**6**, 0.226 g, 0.630 mmol, 1.00 eq) in glacial acetic acid (2 mL). The reaction was stirred at 90°C for 5 days, monitoring by LMCS. The reaction was cooled to R.T. and the pH adjusted to pH 5 with 2M NaOH. The precipitate was collected by vacuum filtration and recrystallized from MeOH:H_2O to give the desired product as an off-white solid (0.155 g, 0.467 mmol, 74%); **HPLC** (RT = 2.56 min); δ_H **(500 MHz, DMSO-d_6)** 1.66–1.72 (4H, m, 2xCH_2), 2.08 (3H, s, CH_3) 2.31 (2H, t, *J* 6.0, CH_2), 2.56 (2H, t, *J* 6.0, CH_2), 6.99 (2H, d, *J* 8.5, Ar-H), 7.06 (2H, d, *J* 7.5, Ar-H), 7.14–7.18 (3H, m, Ar-H), 7.40–7.43 (2H, m, Ar-H), 11.0 (1H, s, NH); δ_C **(125 MHz, DMSO-d_6)** 17.7 (CH_3), 21.5 (CH_2), 21.8 (CH_2), 21.9 (CH_2), 26.2 (CH_2), 117.8 (CH), 118.6 (CH), 121.2 (Cq), 123.3 (CH), 123.7 (Cq), 130.0 (CH), 131.4 (Cq), 132.3 (CH), 142.3 (Cq), 143.2 (Cq), 155.0 (Cq), 156.8 (Cq), 175.4 (Cq); ***m/z* (*ES*)** (Found: MH^+, 332.1654. $C_{22}H_{22}NO_2$ requires *MH*, 332.1645).

Synthesis of 1-(4-Bromophenyl)-4-(Trifluoromethoxy)Benzene (10)

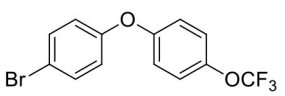

Copper (II) acetate (0.435 g, 2.39 mmol, 1.00 eq) was added to a suspension of 4-bromophenol (**8**, 0.414 g, 2.39 mmol, 1.00 eq), 4-trifluoromethoxybenzeneboronic acid (**9**, 0.983 g, 4.79 mmol, 2.00 eq) and 4 Å molecular sieves (0.566 g) in DCM (12 mL) at R.T. A solution of triethylamine (1.7 mL, 11.9 mmol, 5.00 eq) and pyridine (1 mL, 11.9 mmol, 5.00 eq) was added and the reaction was stirred for 16 h, open to the atmosphere. After 18 h, the reaction was quenched with 0.5 M HCl (20 mL) and the organic layer washed with water (20 mL), brine (20 mL), dried (Na_2SO_4), and concentrated to give a red oil which was purified by column chromatography (hexane) to give the desired product as a colorless oil (0.582 g, 1.75 mmol, 73%); R_f 0.58 (hexane).

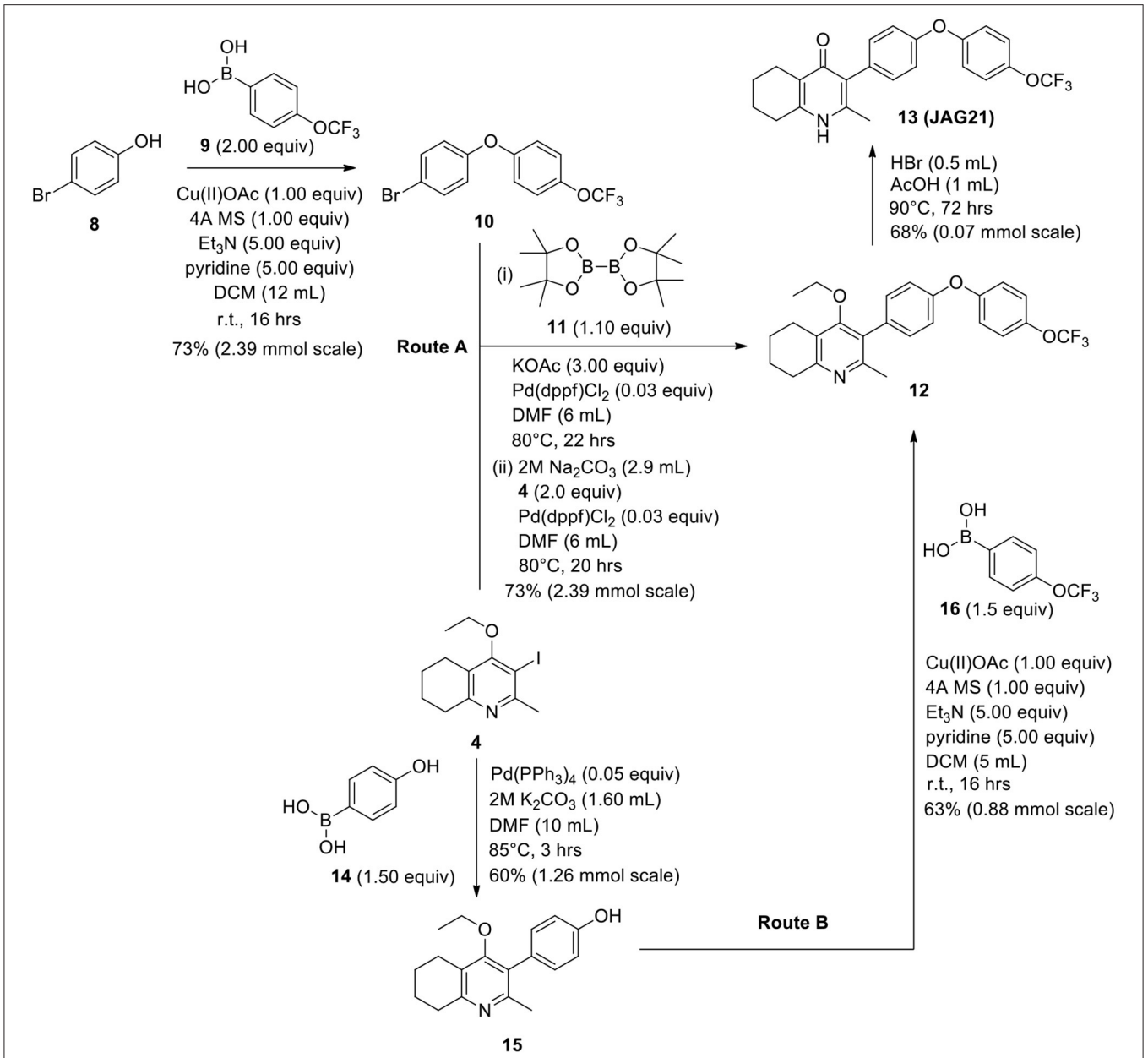

SCHEME 2 | Synthetic route to analogs of 7 (MJM170) via route A or route B. Route A is the original route to analogs but is linear and involves a tricky Suzuki step to intermediate 12 from intermediates 4 and 10. Route B allows quicker access to analogs since intermediate 15 can be made in larger quantities and derivatives can be synthesized via the Chan-Lam reaction to give final intermediate 12 by varying the boronic acid 16.

Synthesis of 2-Methyl-3-(4-Hydroxyphenyl)-4-Ethoxy-5,6,7,8-Tetrahydroquinolin-4-One (15)

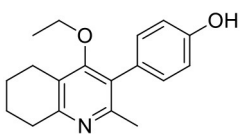

2-Methyl-3-iodo-4-ethoxy-5,6,7,8-tetrahydroquinoline (**4**, 0.400 g, 1.26 mmol, 1.00 eq), $Pd(PPh_3)_4$ (0.073 g, 0.06 mmol, 5 mol%) and 4-hydroxylphenylboronic acid (**14**, 0.260 g, 1.89 mmol, 1.50 eq) were charged to a R.B. flask under N_2(g). Degassed DMF (10.0 mL) was added to the flask followed by 2M K_2CO_3 (3.00 mL). The flask was heated to 85°C under N_2(g). After 3 h, TLC (EtOAc) confirmed reaction was complete. The reaction was cooled to 50°C, diluted with EtOAc (15 mL) and activated charcoal was added. After stirring for 30 min, the mixture was filtered through celite and partitioned between EtOAc (10 mL) and H_2O (25 mL). Combined organics were washed with H_2O (3 × 30 mL), then brine (3 x 30 mL), dried (Na_2SO_4) and concentrated to give a brown solid which was triturated with diethyl ether to give the desired product as a

A

Code	Structure	PBS Sol /Toxicity* pH7.4 μM	$T_{1/2}$ (H)	$T_{1/2}$ (M)	Tachy/ Brady IC_{50} μM
JAG021	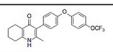	7.07/*	>7 days	101.09	0.12/2
JAG022	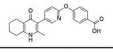	ND/5	ND	ND	7.6/ ND
JAG046	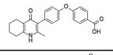	ND/5	ND	ND	>10/ND
JAG047	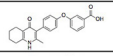	ND/5	ND	ND	>10/ND
JAG050	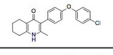	16.41/*	99.04	68.55	0.085/2
JAG062	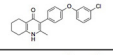	0.33/*	135.3	12.42	0.016/1
JAG069	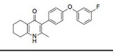	0.5/*	201.98	17.38	0.03/1
JAG084	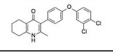	0.68/*	ND	63.1	0.055/1
JAG204	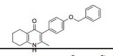	ND/5	ND	ND	0.02/1
JAG208	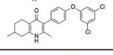	ND/5	ND	ND	0.02/1
JAG058	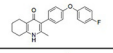	2.38/*	263.1	39.17	0.04/1
JAG063	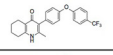	0.45/*	536.6	126.96	0.2/ND
JAG023	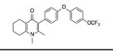	ND/5	ND	ND	0.8/ND
JAG077	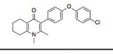	ND/5	ND	ND	0.4/ND
AS006**	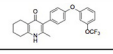	0.55/*	ND	25.88	0.06/1
AS012**	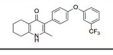	2.19/*	ND	30.05	0.26/ND
AS021	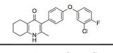	2/*	ND	41.09	0.065/1
AS034	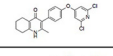	5.05/*	ND	24.93	0.28/ND
AS022	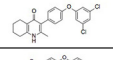	6.25/*	ND	28.62	0.03/1
JAG091	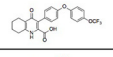	ND/5	ND	ND	>10/ND
JAG092	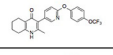	ND/5	ND	ND	1/ ND
JAG095	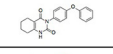	ND/5	ND	ND	>10/ND
JAG099	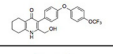	4.05/*	ND	ND	0.38/ND
AS032**	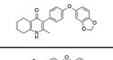	ND/5	ND	ND	0.2/ND
AS033	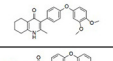	ND/5	ND	ND	ND
JAG100**	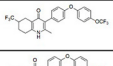	ND/5	ND	ND	>10/ND
JAG106	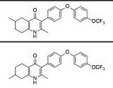	ND/5	ND	ND	2.5/ND
JAG107	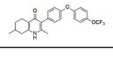	0.03	ND	111.93	0.05/ND

Code	Structure	PBS Sol /Toxicity* pH7.4 μM	$T_{1/2}$ (H)	$T_{1/2}$ (M)	Tachy/Brady IC_{50} μM
JAG121"**	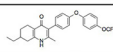	0.16	ND	63.28	0.055/ND
JAG162**	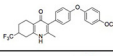	0.02	ND	144.43	0.3/ND
JAG094	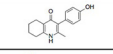	ND/5	ND	ND	1/ND
JAG171	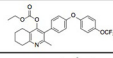	ND/5	ND	ND	0.1/ND
JAG174	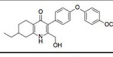	ND/5	ND	ND	0.38/ND
JAG187**	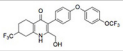	ND/5	ND	ND	2/ND
JAG193	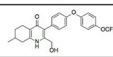	ND/5	ND	ND	0.05/ND
NP032	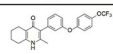	ND/5	ND	ND	0.2/ND
NP034	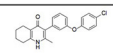	ND/5	ND	ND	0.08/ND
NP035	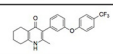	ND/5	ND	ND	0.65/ND
JAG199	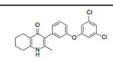	ND/5	ND	ND	0.2/ND
JAG200	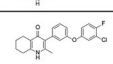	ND/5	ND	ND	0.06/ND
MJM170		1.97/*	146.33	20.97	0.03/4
ELQ271		0.15/*	171.93	448.13	0.03/5
JAG039		ND/5	ND	ND	7.6/ND
JAG129		5.12	N.D.	∞	0.085/ND
JAG006		ND/5	ND	ND	5/>10
JAG013		ND/5	ND	ND	10/ND
JAG014		ND/5	ND	ND	>10/ ND
JAG015		ND/5	ND	ND	10/ND
MJM129		ND/5	ND	ND	0.05/>10
MJM136		ND/5	ND	ND	3.1/ >10
MJM141		0.94/*	278.33	ND	8.2/10

B

FIGURE 1 | Characteristics and effects of compounds on inhibition of *Toxoplasma gondii* replication and enzyme activity, and Structure Activity Relationship analysis. **(A)** Cytochrome b/c inhibitor code, Chem Draw structure, solubility in PBS 7.4, toxicity against HFF, predicted half-life, and inhibitory effect of compounds on RH strain tachyzoites and EGS strain bradyzoites *in vitro* and saffarine O assay enzyme activity. PBS Sol/Toxicity pH7.4 refers to solubility of the compound in Phosphate Bufferred Saline (PBS) at pH 7.4. Toxicity refers to the highest concentration tested that does not show toxicity to Human Foreskin Fibroblast (HFF) in tissue culture in WST assay; T1/2 (H) refers to the predicted half-life in human liver microsomes; T1/2 (M) refers to the predicted half-life in mouse liver microsomes. Tachy/Brady IC50

(Continued)

FIGURE 1 | was determined in studies in which cultures of parasites in HFF were treated with varying concentrations of the compound and there was 50% inhibition of the replication (number) of parasites. Parasites were RH-YFP expressing tachyzoites (Tachy) and EGS (Brady) strains. Studies of effects of inhibitors on HFF or on *T. gondii* tachyzoites were performed with triplicate wells in at least 2 biological replicate experiments. Studies of effects on bradyzoites were performed at least twice in at least 2 biological replicate experiments. Compounds with much less inhibition of mammalian than *T. gondii* cytochrome *bc*, relative to JAG21 effect on parasite enzyme, in the saffarine enzyme assay (indicated by **) provide potential to further develop compounds, if unanticipated toxicity occurs from JAG21. **(B)** Structure Activity Relationship analysis (SAR). The effects of changing R1 as 7-Et, 7-Me, 6-CF_3, or 6-Me on activity against *T. gondii* RH strain tachyzoites, solubility, and stability were compared in the SAR. Color Key in **(B)** *Activity*: Green <50 nM, Red > 1 μM; *Solubility* in 100 mM Phosphate Buffer (pH 7.4): Amber>10 μM, Red <10 μM; *Metabolic Stability*: Green >120 min, Amber 60–120 min, red < 60 min. SAR panel displays only representative structures and trends within the JAG compound series. JAG21 (blue font) is highly active, has the longest predicted half-life for humans of initial compounds tested (green), combined with improved solubility, no hERG liability, and predicted capacity to cross the blood brain barrier (BBB). Definitions of ADMET terminology are in the Materials and Methods. In summary, in the SAR overall, nitrogen atoms were not tolerated in aryl ring marked by green c, and the 4-position was optimal for phenol substituent. Compound name with "0" or no "0" between letters and number, e.g., JAG21 or JAG021, refer to the same compound. This is throughout the manuscript.

pale red crystalline solid (0.220 g, 0.777 mmol, 60%); R_f 0.22 (EtOAc); **m.p.** 225–226°C (EtOAc); δ_H **(500 MHz, MeOD-d_4)** 7.07 (d, J = 8.6 Hz, 2H, H-3 & 5), 6.86 (d, J = 8.6 Hz, 2H, H-2 & 6), 3.51 (q, J = 7.0 Hz, 2H, CH_3CH_2O), 2.83 (t, J = 6.3 Hz, 2H, H-8'), 2.72 (t, J = 6.1 Hz, 2H, H-5'), 2.23 (s, 3H, Me), 1.95–1.72 (m, 4H, H-6' & 7'), 1.00 (t, J = 7.0 Hz, 3H, CH_3CH_2O); δ_C **(125 MHz, MeOD-d_4)** 164.0 (Cq), 158.1 (C-1), 157.4 (C_q), 156.1 (C_q), 132.2 (C-3 & 5), 129.1 (Cq), 127.9 (Cq), 124.9 (Cq), 116.2 (CH), 69.1 (OCH_2), 32.7 (CH_2), 23.9 (CH_2), 23.4 (CH_3), 22.9 (CH_2), 22.3 (CH_2), 15.7 (CH_3); ***m/z* (*ES*)** (Found MH^+, 284.1664, $C_{18}H_{21}NO_2$ requires *MH*, 284.1651).

Synthesis of 2-Methyl-3-(4-Hydroxyphenyl)-4-Ethoxy-5,6,7,8-Tetrahydroquinolin-4-One (12)

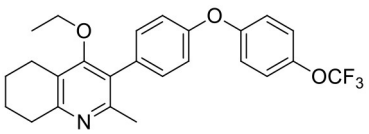

1-(4-bromophenyl)-4-(trifluoromethoxy)benzene (**10**, 0.100 g, 0.30 mmol, 1.00 eq), bis(pinacolato) diboron (1.10 eq), potassium acetate (3.00 eq) and $Pd(dppf)Cl_2$ (0.03 eq) were added to a oven-dried flask under inert (N_2) atmosphere. Anhydrous DMF (6 mL) was added and the reaction heated to 80°C under N_2 (g). After 22 h, the reaction was cooled to R.T., fresh $Pd(dppf)Cl_2$ (0.03 eq) added, followed by 2-methyl-3-iodo-4-ethoxy-5,6,7,8-tetrahydroquinoline (**4**, 0.400 g, 1.26 mmol, 2.00 eq) and 2M Na_2CO_3 (2.9 mL). The reaction was heated to 80°C for 20 h, cooled, diluted with EtOAc (20 mL), filtered through celite and partitioned between EtOAc (20 mL) and H_2O (20 mL). Combined organics were washed with brine (3 × 20 mL), dried (Na_2SO_4) and concentrated to give a brown solid which was purified by column chromatography (3:1 Pet–EtOAc) to give the desired product as a colorless oil (30 mg, 0.07 mmol, 23%); **HPLC** (RT = 2.41 min); δ_H **(500 MHz, acetone)** 7.28 (d, J = 8.7 Hz, 2H, H-2′ & 6′), 7.26 (d, J = 9.1 Hz, 2H, H-2″ & 6″), 7.09 (d, J = 9.1 Hz, 2H, H-3″ & 5″), 7.07 (d, J = 8.7, 2H, H-3′ & 5′), 3.52 (q, J = 7.0 Hz, 2H, CH_3CH_2O), 2.85 (t, J = 6.5 Hz, 2H, H-8), 2.78 (t, J = 6.2 Hz, 2H, H-5), 2.26 (s, 3H, Me), 1.89–1.81(m, 2H, H-7), 1.81–1.72 (m, 2H, H-6), 0.93 (t, J = 7.0 Hz, 3H, C H_3CH_2O); δ_C **(125 MHz, acetone)** δ 161.9 (Cq), 157.1 (Cq), 156.5 (Cq), 156.0 (Cq), 154.5 (Cq), 145.3 (Cq), 132.5 (Cq), 132.0 (CH), 126.7 (Cq), 123.0 (CH), 119.8 (CH), 119.0 (CH), 68.0 (OCH_2), 32.5 (CH_2), 23.0 (CH_2), 22.9 (CH_3), 22.7 (CH_2), 22.5 (CH_2), 15.05 (CH_3); ***m/z* (*ES*)** (Found: MH^+, 444.1792. $C_{25}H_{24}F_3NO_3$ requires *MH*, 444.1781).

Synthesis of 2-Methyl-3-(4-(4-(Trifluoromethoxy)Phenoxy)Phenyl)-5,6,7,8-Tetrahydroquinolin-4-One (13, JAG21)

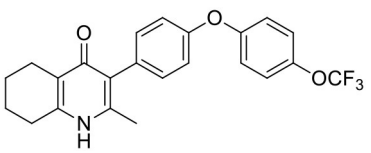

Aqueous hydrobromic acid (>48%) (1.00 mL) was added to a solution of 2-methyl-3-(4-phenoxyphenyl)-4-ethoxy-5,6,7,8-tetrahydroquinoline (**12**, 30.0 mg, 0.07 mmol, 1.00 eq) in glacial acetic acid (2 mL). The reaction was stirred at 90°C for 3 days, monitoring by LMCS. The reaction was cooled to R.T. and the pH adjusted to pH 5 with 2M NaOH. The precipitate was collected by vacuum filtration and recrystallized from MeOH:H_2O to give the desired product as a colorless solid (25.0 mg, 0.06 mmol, 68%); **m.p.** >250°C; **HPLC** (RT = 2.78 min); δ_H **(500 MHz, DMSO-d_6)** 11.07 (s, 1H, NH), 7.40 (d, J = 8.5 Hz, 2H, H-2′ & 6′), 7.19 (d, J = 8.6 Hz, 2H, H-3″ & 5″), 7.13 (d, J = 9.0 Hz, 2H, H-3′ & 5′), 7.02 (d, J = 8.5 Hz, 2H, H-2″ & 6″), 2.54 (t, J = 6.0 Hz, 2H, H-8), 2.28 (t, J = 5.9 Hz, 2H, H-5), 2.07 (s, 3H, Me), 1.71 (m, 2H, H-7), 1.65 (m, 2H, H-6); δ_C **(125 MHz, DMSO-d_6)** 175.7 (Cq), 155.9 (Cq), 154.5 (Cq), 143.5 (Cq), 143.2 (Cq), 142.2 (Cq), 132.5 (CH), 132.2 (Cq), 123.6 (Cq), 123.0 (CH), 121.3 (Cq), 119.6 (CH), 118.2 (CH), 26.2 (CH_2), 21.9 (CH_2) 21.8 (CH_2), 21.5 (CH_2), 17.7 (CH_3); ***m/z* (*ES*)** (Found: MH^+, 416.1492. $C_{23}H_{20}F_3NO_3$ requires *MH*, 416.1473).

Toxoplasma gondii

Parasite Strains (Isolates)

RH-YFP tachyzoites (Gubbels et al., 2003; Fomovska et al., 2012a; McPhillie et al., 2016), EGS strain (Vidigal et al., 2002; Paredes-Santos et al., 2013, 2018; McPhillie et al., 2016), Pru-luciferase, Me49, and RPS13Δ on the RH strain background (Hutson et al., 2010) were prepared and passaged in human foreskin fibroblasts [HFF] as described.

T. gondii in vitro

In vitro Challenge Assay for T. gondii

RH strain YFP Tachyzoites. Protocol was adapted from Fomovska et al. (2012a,b) for HFF. HFF were cultured on a flat, clear-bottomed, black 96-well plate to 90–100% confluence. IMDM (1x, [+] glutamine, [+] 25 mM HEPES, [+] Phenol red, 10% FBS [Gibco, Denmark]) was removed and replaced with IMDM-C(1x, [+] glutamine, [+] 25 mM HEPES, [−] Phenol red, 10% FBS)[Gibco, Denmark]). RH-YFP, lysed from host cells by passing twice through a 27-gauge needle, were counted, then diluted to 32,000/mL in IMDM-C. HFF were infected with 3200 RH-YFP, then returned to 37°C, CO_2 (5%) incubator for 1–2 h for infection. Various concentrations of the compounds in 20 μL IMDM-C were added to each well. There were triplicates for each condition. Controls were pyrimethamine/sulfadiazine (standard treatment), 0.1% DMSO only, HFF only, and untreated cultures of HFF infected with 2-fold dilutions of YFP expressing parasites (called "YFP gradient" to establish amount of color from known numbers of YFP expressing parasites). Cells were incubated at 37°C for 72 h. Plates were read using a fluorimeter (Synergy H4 Hybrid Reader, BioTek) to ascertain amount of relative fluorescence units (RFU) YFP, to measure parasite burden after treatment. Data were collected using Gen5 software with IC_{50} calculated by graphical analysis in Excel.

An initial screening assay of 10 μM, 1 μM, 100 nM, and 10 nM of the compounds was performed. Compounds were not considered effective or pursued for further analysis if there was no inhibition of tachyzoites at 1 μM. If compounds were effective at 1 μM, another experiment was performed to assess effect at 1 μM, 500, 250, 125, 62.5, and 31.25 nM.

Cytotoxicity Assays in Parallel With RH Strain *T. gondii in vitro* Studies

Toxicity assays used WST-1 cell proliferation reagent (Roche) as in Fomovska et al. (2012a). HFF were grown on a flat, clear-bottomed, black 96-well plate. Confluent HFF were treated with inhibitory compounds at concentrations of 10 and 50 μM. Compounds were diluted in IMDM-C, and 20 μL were added to each designated well, with triplicates for each condition. A gradient with 2-folddecreasing concentrations of DMSO from 10 to 0% in colorless, translucent IMDM-C was used as a control. The plate was incubated for 72 h at 37°C. Ten microlitre WST-1 reagent (Roche) were added to each well. Cells were incubated for 30–60 min. Absorbance was read using a fluorimeter at 420 nm. A higher degree of color change (and absorbance) indicated mitochondrial activity and cell viability.

In vitro Challenge Assay for EGS Strain Bradyzoites

HFF cells were grown in IMDM on removable, sterile glass cover slips in the bottom of a clear, flat-bottomed 24-well plate. Cultures were infected with 3×10^4 EGS strain parasites per well, in 0.5 mL media. The plate was returned to incubator at 37°C overnight. The following day, the media was removed. Colorless IMDM and compounds were added to make various concentrations of the drug. Total volume was 0.5 mL. Two wells had media only, as a control. Plates were returned to the 37°C incubator for 72 h, checked once each 24 h. If tachyzoites were visible in the control before 72 h, cells were fixed and stained.

Cells were fixed using 4% paraformaldehyde and stained with Fluorescein-labeled Dolichos Biflorus Agglutinin, DAPI, and antibody to BAG1. Disks were removed, mounted on glass slides, and visualized using microscopy (Nikon Tl7). Slides were scanned using a CRi Panoramic Scan Whole Slide Scanner and viewed using Panoramic Viewer Software. Effects of compounds were quantitated by counting cysts in controls and treated cultures. Dolichos staining delimited structures and single organisms that remained were counted in a representative field of view. This was then multiplied by a factor determined by the total area of the cover slip in order to estimate the number of cysts and organisms in each condition. When the following forms were observed: "true cysts" with a dolichos-staining wall, "pseudocysts" or tight clusters of parasites, and small organisms, if there were fewer than four parasites visible in a cluster, organisms were counted individually (as "small organisms"). The entire scanned coverslip with all fields was also reviewed by 3 observers to confirm consistency.

Synergy Studies With RH Strain YFP Tachyzoites

Atovaquone and pyrimethamine were used to test whether they are synergistic with JAG21. Serial dilutions of the combination of JAG21 and either atovaquone or pyrimethamine were used in an *in vitro* challenge assay as described above. The EC50 of each compound and the combination of two compounds were determined. The effect of the combination of drugs was calculated with the following formula:C= [A]c/[A]a+[B]c/[B]a. If C is lower than 1, the two compounds tested have synergistic effect; if C is >1, the two compounds tested have antagonist effect and if C is 1 they are additive.

T. gondii and HFF Mitochondrial Membrane Potential Measurements

The mitochondrial membrane potential was measured by the safranine method according to Vercesi et al. (1998). Freshly egressed *T. gondii* tachyzoites were filtered and washed twice with intracellular buffer (125 mM sucrose, 65 mM KCl, 10 mM HEPES-KOH buffer, pH 7.2, 1 mM $MgCl_2$, and 2.5 mM potassium phosphate). After washing, the parasites were resuspended in the same buffer at 10^9/mL. An aliquot of 50 μL of this suspension was added to a cuvette containing Safranin O, 2.5 μM and Succinate 1 mM in final volume of 2 mL of the intracellular buffer. The fluorescence was measured with a Hitachi 7000 spectrofluorometer with settings Ex. 495/Em. 586. Once the baseline fluorescence was stable, 30 μM digitonin was added to permeabilize the parasites. Eighty five seconds after permeabilization, the THQ derivatives, dissolved in DMSO, were added. Five micromolars of FCCP (Carbonyl cyanide-4-(trifluoromethoxy) phenylhydrazone) was used as an uncoupler reference for calculations and its effect was considered 100%. We used similar conditions for measuring the mitochondrial membrane potential of mammalian cells with the following changes: the mammalian cells were resuspended at 10^8/mL. We also used 50 μL of this suspension for each experiment in a total volume of 2 mL. The substrate used for mammalian cells was

5 mM glutamate and 5 mM malate. A higher concentration of digitonin (50 μM) was used to permeabilize the mammalian cells. The compounds were added at ∼400 s after permeabilization. Each experiment was repeated at least three times in duplicates. Statistical analysis, unpaired student *t*-test, was performed using GraphPad Prism 8.0 (GraphPad Software, Inc., San Diego, CA).

Structure Activity Relationship (SAR) and Comparison of Effect on Toxoplasma gondii and HFF Enzyme Activity

The effects of changing R1 as 7-Et, 7-Me, 6-CF_3, or 6-Me on activity against RH strain tachyzoites, kinetic solubility, and metabolic stability were compared. Kinetic solubility and metabolic stability in human or murine liver microsomes were measured. The hERG (human Ether-à-go-go-Related) liability was also determined. The hERG gene (KCNH2) encodes a protein K_v11.1, the alpha subunit of a potassium ion channel. This channel conducts the rapid component of the delayed rectifier potassium current, IKr, which is critical for repolarization of cardiac action potentials. A reduction in hERG currents from adverse drug effects can lead to long QT interval syndromes. These syndromes are characterized by action potential prolongation, lengthening of the QT interval on surface EKG, and an increased risk for "torsade de pointes" arrhythmias and sudden death. The MDCK-MDR1 Permeability Assay was also performed. MDCK-MDR1 refers to the ability of a compound to permeate across membranes of MDCK-MDR1 (Madin Darby canine kidney [MDCK] cells with the *MDR1* gene [ABCB1], the gene encoding for the efflux protein, P-glycoprotein (*P-gp*)) *in vitro*. Assessing transport in both directions (apical to basolateral and basolateral to apical) across the cell monolayers enables an efflux ratio to be determined. This provides an indication as to whether a compound undergoes active efflux (mediated by P-*gp*). This provides a prediction of blood brain barrier (BBB) penetration potential/permeability and efflux ratio. Effect in CACO-2 (Colon Adenocarcinoma cells) as a permeability assay and on cytochrome P450 (CYP 450) were also determined. CYP enzymes catalyze oxidative biotransformation (phase 1 metabolism) of most drugs. CYP enzymes, bind to membranes in a cell (cyto) and contain a heme pigment (chrome and P) that absorbs light at a wavelength of 450 nm when exposed to carbon monoxide. Metabolism of a drug by CYP enzymes is a major source of variability in drug effect. These were measured by Chem Partners. The relative effect on HFF and parasite enzymes also were compared.

RPS13Δ Tachyzoites in Human Primary Brain Neuronal Stem Cells *in vitro* for Transcriptomics and Transcriptomics Analyses

Culture of Human Primary Brain Neuronal Stem Cells (NSC) was as described (McPhillie et al., 2016; Ngô et al., 2017); *T. gondii* RPS13Δ on RH strain background (Hutson et al., 2010) was used to infect the NSC as described (McPhillie et al., 2016; Ngô et al., 2017). RNA was isolated and prepared and used for transcriptomic experiments as described (McPhillie et al., 2016; Ngô et al., 2017). Briefly, NSC, initially isolated from a temporal lobe biopsy (Walton et al., 2006) were infected with either wild-type or RPS13Δ RH tachyzoites using biological duplicates at a multiplicity of infection of 2:1 and incubated as previously described Ngô et al. (2017). Eighteen hours post-infection, extracellular parasites were washed out with cold PBS before total RNA extraction. Further isolation of the mRNA fraction was carried out with miRNeasy Mini Kit columns (Qiagen) following manufacturer instructions and Illumina barcoded mRNA sequencing libraries were constructed with TruSeq RNA Sample Preparation Kits v2 (Illumina). Libraries were sequenced as 100 bp single reads with Illumina HiSeq 2000 apparatus at a sequencing depth of ∼3 Gbp per sample. Sequencing reads were mapped to the human (release GRCh38) and *T. gondii* ME49 strain (ToxoDB release 13.0) reference genome assemblies with hisat2 (Kim et al., 2015) and raw read counts were per gene were estimated with HTSeq (Anders et al., 2015). Identification of parasite genes that were differentially expressed between wild-type and RPS13Δ parasites was performed with the R package DESeq2 (Love et al., 2014) using a generalized linear model likelihood ratio test. Identification of orthologous genes between *T. gondii* and *P. cynomolgi* was carried out by best-reciprocal matches between *T. gondii* and *P. cynomolgi* proteomes using Blastp and a e-value cutoff of 1×10^{-3}. The list of Genes that are differentially expressed between *P. cynomolgi* hypnozoites and the liver-schizont stage was extracted from a previously published study by Cubi et al. (2017). Gene set enrichment analysis was carried out with the GSEA tool (Subramanian et al., 2005) using *T. gondii* Gene Ontology and cell cycle gene sets developed by Croken et al. (2014) and visualized with the Enrichment Map application in Cytoscape (Su et al., 2014).

Toxoplasma gondii in vivo

Type II Parasites *in vivo*

IVIS

Balb/C mice were infected intraperitoneally (IP) with 20×10^3 *T. gondii* (Prugneaud strain expressing luciferase) tachyzoites. Treatment began 2 h later with JAG21 (5 mg/kg) which was dissolved in DMSO, administered IP in a total volume of 0.05 mL. Mice were imaged every second day starting on day 4 post infection using an IVIS Spectrum (Caliper Life Sciences) for minute exposures, with medium binning, 20 min post injection with 150 mg/kg of D-luciferin potassium salt solution.

Brain cysts

Brain cysts were searched for in paraffin imbedded tissue of the surviving Prugneaud strain infected treated Balb/C mice in the IVIS study, 30 days after infection which was 16 days after treatment had been discontinued. All treated mice had survived. There were no surviving untreated mice in those experiments.

In separate experiments, Balb/C mice were infected IP with 20×10^3 *T. gondii* Me49 strain tachyzoites. In these separate studies of mice with established chronic infection, after 30 days, IP treatment with JAG21 was begun each day for 14 days. JAG21 was dissolved in DMSO and administered IP in a total volume of 0.05 mL. In experiments when tafenoquine was administered alone or with JAG21 in some groups 3 mg/kg tafenoquine was administered once on day−1 from when JAG21 treatment

was initiated. Cysts in brain were quantitated on day 30, 16 days after discontinuing JAG21. Immunoperoxidase staining was performed. Parasite burden was quantitated in two ways. The first was using a positive pixel count algorithm of Aperio ImageScope software. Positive pixels were normalized to tissue area (mm^2). Briefly, automated quantitation was done by counting positive pixels per square area. The entire brain in one section was scanned for each mouse. The Cyst burden was quantitated as units of positive pixels per mm^2. The average ± S.E.M. numbers of mm^2 per slide quantitated was 30.2±1.6 square mm per mouse for this quantification. Each highpower field of view shown in **Figure 5C** is ∼0.02 mm^2 per field of view. Cysts on each slide for each condition in two biological replicate experiments were also quantitated by 2 separate observers independently and results compared with automated counting, separately.

RPS13 Δ *in vivo*

This G1 arrested parasite persists in tissue culture for prolonged times in the absence of tetracycline (Hutson et al., 2010), but in immune competent mice it cannot be rescued with teteracycline, or LNAME (L-N^G-Nitro arginine methyl ester, an analog of arginine) used as an antagonist of nitric oxide synthase (NOS) that inhibits NO production, or both together (Hutson et al., 2010).

In pilot studies, herein, interferon γ receptor knockout mice that were not treated were observed following infection. At 7 and at 14 days following infection, spleen, and liver were removed and immune peroxidase stained. At 14 days a group of mice were treated with anhydrotetracycline and when a subset of these mice died, their spleen and liver were removed and immune peroxidase stained.

As in the pilot studies, this RPS13 Δ parasite also was used to infect interferon γ receptor knockout mice in a treatment study. The design of this experiment with these immune compromised mice is shown in **Figure 6**. In this separate study, groups of mice were infected with RPS13 Δ. They were treated with tafenoquine on day−1, or JAG21 for 14 days 2 h after infection, or the two together with tafenoquine on day−1 and JAG21 for the first 14 days, or with diluent only for 14 days, as described above. For the initial 14 days, no tetracycline was administered. After that time tetracycline was administered. Mice were observed each day. At the time they appeared to have substantial illness or at the termination of the experiment they were euthanized, tissues fixed in formalin and stained with hematoxylin and eosin or immunoperoxidase stained and parasite burden was assessed.

RH Challenge in a Study of Oral Administration of a Novel Nano Formulation of JAG21

Nanoformulation of JAG21 for oral administration in T. gondii studies

JAG21 was prepared using hydroxyethyl cellulose (HEC) and Tween 80. Briefly, this dispersant solution containing 5 mg/mL HEC and 2 mg/mL Tween 80 in water was prepared. Solid JAG21 was added to 20 mg/mL, and the dispersion was sonicated for 60 s using a Sonics vc50 probe-tip sonicator set to 20 kHz to homogenize. Sonication was performed at room temperature. Aliquots of the homogeneous dispersion were frozen and lyophilized using a VirTis AdVantage freeze drier. These aliquots were stored at room temperature for 5–6 months. Prior to dosing, aliquots were reconstituted using water. Controls containing no JAG21 were also prepared. Following reconstitution with water, the dispersion was imaged using a Nikon ECLIPSE E200 optical microscope set to 40x magnification. The average particle size of the JAG21 dispersion in HEC/Tween 80 was determined using an in-house image analysis program. This novel method to stably formulate JAG21 was discovered after all other studies were completed and this was the last experiment in this manuscript performed as a consequence.

RH YFP challenge

For studies of the nano formulated JAG 21, this was administered for 1 or 3 days by gavage in the doses shown in the results section. These C57BL6 background mice received 2000 RH tachyzoites IP. on day the first day of the experiment and peritoneal fluid was collected 5 days later to quantitate fluorescence and numbers of parasites.

Malaria Assays

Enzyme Assays

Methods for enzyme assays: Materials

P. falciparum 3D7 strain were obtained from the Liverpool School of Tropical Medicine. Protease cocktail inhibitor was obtained from Roche. Bradford protein assay dye reagent was obtained from Bio-Rad. All other reagents were obtained from Sigma-Aldrich. Decylubiquinol was produced as per Fisher et al. (2009). In brief, 25 mg of decylubiquinone were dissolved in 400 μL of nitrogen-saturated hexane. An equal volume of aqueous 1 M sodium dithionite was added, and the mixture vortexed until colorless. The organic phase containing the decylubiquinol was collected, the solvent was evaporated under N_2 and the decylubiquinol finally dissolved in 100 μL of 96% ethanol (acidified with 10 mM HCl). Concentrations of decylubiquinol was determined spectrophotometrically on a Cary 300 Bio UV/visible spectrophotometer (Varian, UK) from absolute spectra, using $\varepsilon_{288--320} = 8.1\ mM^{-1}.cm^{-1}$. Decylubiquinol was stored at −80°C and used within 2 weeks.

P. falciparum culture and extract preparation

P. falciparum strain 3D7 blood-stage cultures were maintained by the method of Trager and Jensen (1976). Cultures contained a 2% suspension of O+ human erythrocytes in RPMI 1640 medium containing L-glutamine and sodium carbonate, and supplemented with 10% pooled human AB+ serum, 25 mM HEPES (pH 7.4) and 20 μM gentamicin sulfate. Cultures were grown under a gaseous headspace of 4% O_2 and 3% CO_2 in N_2 at 37°C. Cultures were grown to a parasitemia of 5% before use.

The protocol for the preparation of parasite extract was adapted from Fisher et al. (2009). Free parasites were prepared from infected erythrocytes pooled from five T75 flasks, by adding 5 volumes of 0.15% (w/v) saponin in phosphate-buffered saline (137 mM NaCl, 2.7 mM KCl, 1.76 mM K_2HPO_4, 8.0 mM Na_2HPO_4, 5.5 mM D-glucose, pH 7.4) for 5 min, followed by

three washes by centrifugation in RPMI containing HEPES (25 mM), and a final resuspension in potassium phosphate buffer (50 mM K_2HPO_4, 50 mM KH_2PO_4, 2 mM EDTA, pH7.4) containing a protease inhibitor cocktail (Complete Mini; Roche). Parasite extract was then prepared by disruption with a sonicating probe for 5 s, followed by a 1 min rest period on ice to prevent the sample overheating. This process was performed three times. The parasite extract was used immediately. The protein concentration of the parasite extract was determined by Bradford protein assay (Bio-Rad).

Pfbc$_1$ native assay

P. falciparum bc_1 complex cytochrome c reductase (*Pfbc$_1$*) activity was measured by monitoring cytochrome c reduction at 550 vs. 542 nm using a Cary 300 Bio UV-Visible Spectrophotometer (Varian, UK), using a protocol adapted from Fisher et al. (2009).The assay was performed in potassium phosphate buffer in a quartz cuvette and in a final volume of 700 μL. Potassium cyanide (10 μM), oxidized cytochrome c (30 μM), parasite extract (100 μg protein), and compound/DMSO were added sequentially to the cuvette, with mixing between each addition. Test compounds were added to a final concentration of 1 μM. DMSO (0.1% v/v) and atovaquone (1 μM), a known malarial cytochrome bc_1 complex inhibitor, were used as negative and positive controls, respectively. The reaction was initiated by the addition of 50 μM decylubiquinol and allowed to proceed for 3 min.

Malaria Parasite *in vitro* Studies

Malaria potency testing *in vitro* was performed using 4 different *P. falciparum* strains, D6, TM91-C235, W2, and C2B. The D6 strain is a drug sensitive strain from Sierra Leone, the TM91-C235 strain is a multi-drug resistant strain from Thailand, the W2 strain is a chloroquine resistant strain from Thailand, and the C2B strain is a multi-drug resistant strain with resistance against atovaquone. These assays were performed as described below.

Compound Activity against Plasmodium falciparum

Compound activity against *P. falciparum*, was tested using the Malaria SYBR Green I–Based Fluorescence (MSF) Assay. The complete method for performing this microtiter assay is described in previous work published by Plouffe et al. (2008) and Johnson et al. (2007). In brief, this assay uses the binding of the fluorescent dye SYBR Green I to malaria DNA to measure parasite growth in the presence of 2-fold diluted experimental or control. The relative fluorescence of the intercalated SYBR Green I proportional to parasite growth, and inhibitory compounds will result in lower observed fluorescence compared to untreated parasites.

Cytotoxicity assays in parallel with P.falcipaum assays in vitro

Toxicity studies also were performed with HepG2 cells (human liver cancer immortal cell line derived from the liver tissue of a 15-year-old African American, ATCC ^{R} HB-8065^{TM}) in parallel with the studies of *P. falciparum,* with inhibitors *in vitro*, as described in McPhillie et al. (2016).

P. berghei Causal Prophylaxis *in vivo* Model

P. berghei sporozoites were obtained from laboratory-reared female *Anopheles stephensi* mosquitoes which were maintained at 18 degrees C for 17–22 days after feeding on a luciferase expressing *P. berghei* infected Swiss CD1ICR. Using a dissecting microscope, the salivary glands were extracted from malaria-infected mosquitoes and sporozoites were obtained. Briefly, mosquitoes were separated into head/thorax and abdomen. Thoraxes and heads were triturated with a mortar and pestle and suspended in medium RPMI 1640 containing 1% C57BL/6 mouse serum (Rockland Co, Gilbertsville, PA, USA). 50–80 heads with salivary glands were placed into a 0.5 mL Osaki tube on top of glass wool with enough dissection media to cover the heads. Until all mosquitoes had been dissected, the Osaki tube was kept on ice. Sporozoites that were isolated from the same batch of mosquitoes were inoculated into C57BL/6, 2D knock-out, and 2D knock-out/2D6 knock-in C57BL/6 mice on the same day to control for biological variability in sporozoite preparations. On day 0, each mouse was inoculated intravenously in the tail vein with ∼10,000 sporozoites suspended in 0.1 mL volume. They were stained with a vital dye containing fluorescein diacetate (50 mg/mL in acetone) and ethidium bromide (20 μg/mL in phosphate buffered saline; Sigma Chemical Co, St. Louis, MO, USA) and counted in a hemocytometer to ensure that inoculated sporozoites were viable following the isolation procedure. Viability of the sporozoites ranged from 90 to 100%.

Animals

The mice used in these experiments were albino C57BL/6 female mice which were housed in accordance with the current Guide for the Care and Use of Laboratory Animals (1996) under an IACUC approved protocol. All animals were quarantined for 7 days upon arrival, and the animals were fed standard rodent maintenance food throughout the study.

Test compounds, homogenization of JAG21 creating a nanoformulation, and administration

Animals were dosed with experimental compounds based on body weight. The suspension solution of orally administered drugs were conducted in 0.5% (w/v) hydroxyethyl cellulose and 0.2% Tween 80 in distilled water. To insure the size of the compounds in the dosing solution were under 50 μM (measured they were 4–6 μM), the suspension was homogenized using a homogenizer (PRO Scientific Inc, Monroe, CT, USA) with a 10 mm open-slotted generator running at 20,000–22,000 rpm for 5 min in an ice bath. The compounds were made fresh each day and used immediately (always in <1/2 h). Stability beyond that time was not determined. It was not anticipated that they would be stable beyond that time.

Compounds were administered on 3 consecutive days (−1, 0, +1) relative to sporozoite infection or a single dose on day 0. Drug suspensions were administered to mice by oral gavage using an 18 gauge intragastric feeder. For the 3 day dosing regimen, compounds were administered at 0.625 mg/kg and for the single dose regimen administered on day 0, compounds were administered at 2.5 mg/kg.

In vivo imaging

All of the *in vivo* bioluminescent imaging methods utilized have been described previously. Briefly, JAG21 was administered orally on days −1, 0, and 1 with respect to sporozoite inoculation. All inoculated mice were imaged using the Xenogen IVIS-200 Spectrum (Caliper Life Sciences, Hopkinton, MA, USA) IVIS instrument at 24, 48, and 72 h post-sporozoite infection. The bioluminescent imaging experiments were conducted by IP injection of the luciferase substrate, D-Luciferin potassium salt (Xenogen, California and Goldbio, St Louis, MO, USA), into mice at a concentration of 200 mg/kg 15 min before bioluminescent images were obtained. Three minutes after luciferin administration the mice were anesthetized using isoflurane, and the mice were positioned ventral side up on a 37°C platform with continual anesthesia provided through nose cone delivery of isoflurane. All bioluminescent images were obtained using 5 min exposures with f-stop = 1 and large binning setting. Photon emission from specific regions was quantified using Living Image® 3.0 software (Perkin Elmer).

Additionally, blood stage parasitemia was assessed 3 days after imaging was completed by treating small quantities of blood obtained from tail bleeds with the fluorescent dye Yoyo-1 measured by using a flow cytometry system (FC500 MPL, Beckman Coulter, Miami, FL, USA) (Pybus et al., 2013; Marcsisin et al., 2014).

Methods for Co-crystallization and Binding Studies

Bovine Cytochrome bc_1 Activity Assays

Bovine cytochrome bc_1 inhibition assay was carried out in 50 mM KPi pH 7.5, 2 mM EDTA, 10 mM KCN, 30 μM equine heart cytochrome *c* (Sigma Aldrich), and 2.5 nM bovine cytochrome bc_1 at room temperature. 20 mM inhibitors dissolved in DMSO were added to the assay at a desired concentration without prior incubation. The working concentration of DMSO in the assay did not exceed 0.3% v/v. The reaction was initiated by the addition of 50 μM decylubiquinol (Abcam). The reduced cytochrome *c* was monitored by the different absorption between 550 and 542 nm using extinction coefficient of 18.1 mM^{-1} cm^{-1} in a SPECTRAmax Plus 384 UV-visible Spectrometer. The initial kinetic rate is determined as a zero-order reaction and used as the specific activity of cytochrome bc_1.

Bovine Cytochrome bc1 Purification Protocol

Preparation of crude mitochondria

Whole fresh bovine heart was collected after slaughter and transported in ice. All work was carried out at 4°C. Lean heart muscle was cut into small cubes and homogenized in the buffer composed from 250 mM sucrose; 20 mM K_2HPO_4; 2 mM succinic acid; 0.5 mM EDTA. Buffer was added at a ratio of 2.5 L per 1 kg of muscle tissue. Ph of resulting homogenate was adjusted to 7.8 using 2 M Tris and PMSF protease inhibitor was added to 0.1 mM concentration. The homogenate was then centrifuged in a Sorvall GS-3 rotor at 5,000 g for 20 min. The resulting supernatant was then transferred to a Sorvall GSA rotor and centrifuged at 20,000 g for 20 min. Obtained mitochondrial pellet was washed in 50 mM KPi (pH 7.5); 0.1 mM PMSF buffer before second centrifugation under the same condition. The pellet was collected and sored at −80°C for further use.

Solubilization of Membrane Proteins

The frozen mitochondria were thawed and re-suspended in 50 mM KPi (pH 7.5); 250 mM NaCl; 0.5 mM EDTA; 0.1 mM PMSF buffer; a small sample was taken for quantification of total mitochondrial proteins by BCA assay. The remaining sample was centrifuged at 180,000 g in Beckman Ti70 rotor for 60 min. The pellet was re-suspended in the same wash buffer with the addition 1 mg DDM per 1 mg of protein and then centrifuged under the same conditions for 60 min. The pellet was discarded and the supernatant was collected for ion exchange chromatography.

Purification of Cytochrome bc1

During purification the presence of protein was detected using 280 nm absorbance and the presence of heme was detected using 415 nm Soret band peak and 562 nm absorbance. The solubilized protein solution was applied on DEAE-Sepharose CL-6B column (ca. 50 mL, GE Healthcare) pre-equilibrated with buffer A [50 mM KPi (pH 7.5); 250 mM NaCl; 0.01% w/v DDM; 0.5 mM EDTA] and washed with 3 CV of buffer A. The protein was eluted by linear gradient with buffer B [50 mM KPi (pH 7.5); 500 mM NaCl; 0.01%w/v DDM; 0.5 mM EDTA]. Fractions containing cytochrome bc_1 were pooled and concentrated to 0.5 mL using an Amicon Ultra-15 (Amicon, MWCO 100,000) concentrator. Concentrated sample was applied to a Sephacryl-S300 gel filtration column (ca. 120 mL) pre-equilibrated in buffer C [20 mM KMOPS (pH 7.2); 100 mM NaCl; 0.01%w/v DDM; 0.5 mM EDTA] and eluted at a flow rate of 0.5 mL/min. Purified cytochrome bc_1 fractions were collected and concentrated to 40 mg/m. PEG fractionation with increasing concentration of PEG4000 was used to precipitate cytochrome bc_1. Precipitating solution (100 mM KMES pH 6.4; 10% PEG4000; 0.5 mM EDTA) was mixed with the protein to a desired PEG concentration. The precipitated protein pellet was re-solubilised in buffer D (25 mM KPi pH 7.5, 100 mM NaCl, 0.5 mM EDTA, 0.015% DDM) and dialysed in the same buffer in a centrifugal ultrafilter to remove residual PEG. Five micromolars cytochrome bc_1 was incubated at 4°C for 12 h with 50 μM JAC21 (10-fold molar excess) diluted from 20 mM solution stock in DMSO.

Crystallization, Data Collection, and Refinement of Cytochrome bc1–JAG21 Complex

The inhibitor-bound cytochrome bc_1 was mixed with 1.6% HECAMEG to the final protein concentration of 40 mg/mL. Hanging drop method was used for crystallization. Two microliter of final protein solution with 2 μL of reservoir solution (50 mM KPi pH 6.8, 100 mM NaCl, 3 mM NaN_3, 10–12% PEG4000) was equilibrated over reservoir solution at 4°C. The crystals were grown to 100 μm within 4 days. The single crystal was transferred in reservoir solution containing increasing to 50% concentrations of ethylene glycol prior to cryo-cooling in liquid nitrogen. X-ray data were collected from single crystal PROXIMA2 beamline, SOLEIL light source, France using DECTRIS EIGER X 9M detector at 0.9801Å wavelength

up to 3.45Å resolution. Data were indexed and integrated using iMosflm (Battye et al., 2011), and scaled using Aimless (Evans, 2011). The starting model for refinement was 5OKD. All ligands except co-factors were removed from the model prior to refinement. Jelly-body refinement was carried out with Refmac5 (Murshudov et al., 2011). The inhibitor model was generated by Jligand (Lebedev et al., 2012). The model was manually edited in COOT (between cycle refinements. Data collection and refinement statistics are shown in **Supplemental Table 1A**).

Cryo Electron Microscopy

Electron Microscopy and Image Processing

Cryo-EM was carried out as described in Amporndanai et al. (2018). Briefly, 3 μL of sample at 5 mg/mL concentration were applied to Quantifoil Cu R1.2/1.3, 300 mesh holey carbon grids and plunge frozen using an FEI Vitribot (blot time 6 s, blot force 6). Data were collected on an FEI Titan Krios with a Falcon III direct electron detector operated in integrating mode at 300 kV. Automated data collection was carried out using EPU software with a defocus range of −1 to −3.5 μm, and a magnification of 75,000 × which yielded a pixel size of 1.065 Å. Data were collected for 72 h resulting in 5,356 micrographs. The total dose was 66.4 e^{-}/Å over a 1.5 s exposure which was split into 59 frames. All of the processing was performed in RELION 2.1 unless otherwise stated. The initial drift and CTF correction was carried out using MOTIONCORR2 (Zheng et al., 2017) and Gctf (Zhang et al., 2016), respectively. The micrographs were examined and those with crystalline ice were initially removed resulting in 2,960 micrographs. A subset of ∼2,000 particles were manually picked to generate 2D references to facilitate auto-picking resulting in 439,009 particles. These particles underwent an initial round of 2D classification with those classes that displayed clear secondary structure detail being taken forward to 3D classification and split into three classes. Two of the three classes generated a high-quality cytochrome bc_1 reconstruction with secondary structure information clearly visible. The particles from these two classes were recombined to form the final datasets consisting of 211,916 particles in the final reconstruction. The particles were 3D refined using C2 symmetry to produce a map with resolution 3.8 Å. The particles also underwent movie refinement and particle polishing which further improved the resolution of the map to 3.7 Å. A previously refined EM structure for SCR0911 (pdb 6FO6) was fit into the map using UCSF chimera and subsequently refined using phenix with the correct ligand. The maps were then inspected manually in COOT (Emsley and Cowtan, 2004) and the model corrected for any errors in refinement and the placement of residues.

Statistical Analysis

A Pearson test was used to confirm a correlation between increasing dose and increasing inhibition. An ANOVA and subsequent pairwise comparison with Dunnett correction was used to determine whether or not inhibition or toxicity at a given concentration was statistically significant. Stata/SE 12.1 was used for this analysis.

RESULTS

THQ Compounds Are Potent *in vitro*

Initially, a small library of seven compounds (**Figure 1** [blue and green font, **Figure 1A**] and **Figure 2**) were tested, and each compound was tested at least twice against *T. gondii* tachyzoites. JAG21 and JAG50 demonstrated effect below 1 μM, and were tested at lower concentrations. JAG50 and JAG21 were identified as lead compounds given the IC_{50} values obtained were 33 and 55 nM, respectively. Correlation between concentration of compound and inhibition of parasite replication (as measured by fluorescence) was observed for all compounds except JAG46. The relative effect on HFF and parasite enzymes were also compared, with those marked ** in **Figure 1A** having the most effect on the parasite enzyme activity relative to host HFF enzyme activity as shown below in **Figure 3**.

A representative graph of these *in vitro* data is shown in **Figure 2A.** Subsequently, a larger library of 54 compounds was synthesized to ascertain structure-activity relationships (SAR) (**Figure 1B**). Our primary aims were to block putative metabolism of the terminal phenol ring of MJM170 and improve the solubility across the compound series. Substituents were generally tolerated at the meta and para positions on the phenol ring (R_1), similar to the trends observed in the ELQ series (Vidigal et al., 2002; Doggett et al., 2012; McPhillie et al., 2016). The incorporation of heteroatoms into the aryl rings of the biphenyl moiety did not lead to improvements in solubility and biological activity. Small substituents were tolerated at the 7-position of the THQ bicyclic ring (**Figure 1B**; R_1), improving selectivity (see below, SAR) but not at the 6-position unlike the ELQ series. In summary, overall, nitrogen atoms were not tolerated in aryl ring (C) and the 4-position was optimal for phenol substituent. Ultimately, no other compound had all the advantages of JAG21, although some of these were identified as potential back up compounds (marked with **), with greater selectivity for the parasite relative to the mammalian enzyme activity. Compound JAG21 displayed synergy against RH strain tachyzoites with atovaquone (**Figure 2C**) but not with pyrimethamine, although no antagonism was observed (data not shown).

Cytotoxicity assays performed in parallel using HFF, WST-1 (Fomovska et al., 2012a,b), and HEP G2 cells demonstrated a lack of toxicity at concentrations substantially in excess of the concentrations effective against tachyzoites. Because *T. gondii* grows inside cells, if a compound were toxic to host HFF then it would make the compound appear to be spuriously effective (Fomovska et al., 2012a,b), when in actuality only toxicity for the host cell would be measured. Cytotoxicity to HFF was therefore assessed for all compounds at 10 μM. Results of this experiment are in **Figure 1A**, toxicity column. A two-way ANOVA and subsequent pairwise comparison found none of the differences in absorbance, compared to the media-DMSO vehicle controls, to be statistically significant ($p > 0.05$). Most of these compounds are not toxic at 10 μM (the limit of solubility) and that cytotoxicity to cells can be attributed to DMSO in the solution, not the compound. Dose response testing (IC50) was performed with HEP G2 cells as described and the observed

A

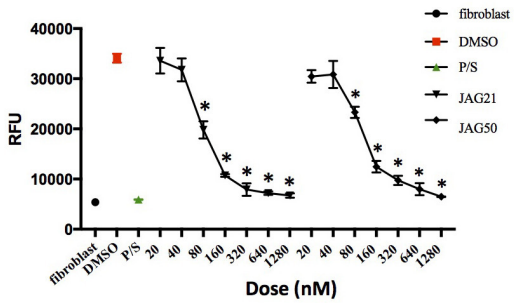

B

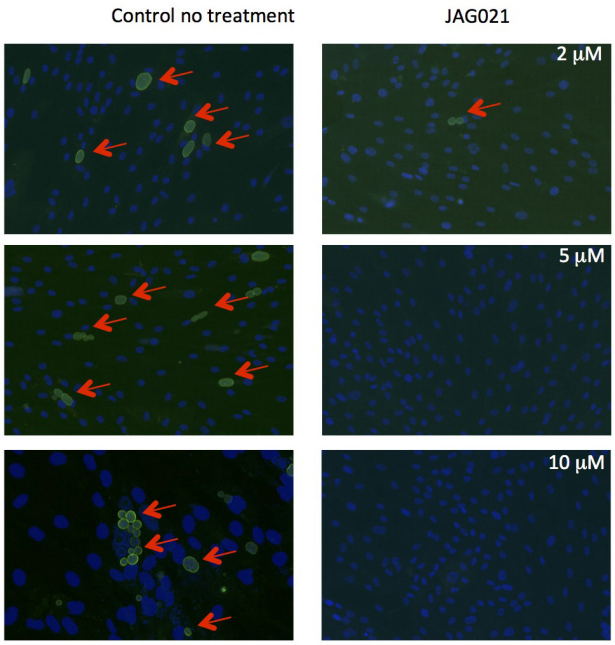

C

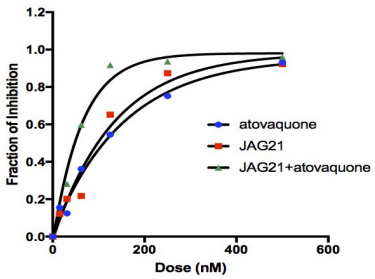

D

Compound ID	SYBR Green D6 IC50 (µM)	SYBR D6 R^2	SYBR Green C235 IC50 (µM)	SYBR TM91C235 R^2	SYBR Green W2 IC50 (µM)	SYBR W2 R^2	SYBR Green C2B IC50 (µM)	SYBR C2B R^2
JAG021	0.01435	0.9572	0.06164	0.9706	0.05518	0.9727	0.04042	0.9847
JAG050	0.04664	0.9138	0.06913	0.9562	0.03136	0.9693	0.03635	0.9427
JAG047	3.746	0.9738	12.56	0.9218	9.072	0.9358	7.781	0.9575
JAG039	9.595	0.9532	>20	N/A	>20	N/A	>20	N/A
JAG046	6.716	0.9844	>20	N/A	>20	N/A	>20	N/A
JAG006	0.29	0.90	0.88	0.92	2.46	0.92	1.66	0.94
RG38	2.884	0.8936	13.66	0.8338	9.245	0.7954	>20	N/A

E

Compound ID	Solubility (pH 7.4) (µM)	Human liver microsomes (min)	Mouse liver microsomes (min)
MJM170	1.97	146.33	20.97
JAG021	7.07	∞	101.09
JAG050	16.41	99.04	68.55

F

JAG21 **CYP450 inhibition**: IC_{50} >10 µM 4/5 isoforms (2C9 = 4.0 µM); **Caco-2 permeability**: P_{app}A-B >10x10^{-6} cm/s; **hERG** IC_{50} = 22 µM; **PPB** (human) = 99.9%; **MDCK-MDR1 BBB permeability:** P_{app}A-B >10x10^{-6} cm/s & **P-gp efflux ratio**: <1.5

FIGURE 2 | JAG21 is potent *in vitro* against *Toxoplasma gondii*, tachyzoites and bradyzoites, and multiple drug resistant strains of *P. falciparum*. **(A) JAG21** is effective against RH-YFP tachyzoites, and does not harm human cells. Potent effect of JAG50 is also shown. A representative experiment is shown. *N* = triplicate wells in at least 2 biological replicate experiments. Relative fluorescence units are shown on the vertical axis, where decrease in fluorescence compared to diluent DMSO in media control indicates parasite inhibition (*$p < 0.05$). Horizontal axis indicates different treatment conditions: This shows results of testing of fibroblasts in media (HFF), DMS0 control, positive control pyrimethamine and sulfadiazine(P/S), and concentrations of JAG21 and JAG50 utilized. Differences were not statistically

(Continued)

FIGURE 2 | significant in the cytotoxicity assay (data not shown). **(B)** JAG21 is effective against EGS bradyzoites. Effect of JAG21 in reducing bradyzoites in HFF by parasite strain EGS. HFF were infected by EGS and treated with JAG21 at concentrations indicated. Slides were stained with Dolichos Biflorus Agglutinin conjugated with FITC (which stains the cyst wall) and DAPI, and observed with fluorescence microscopy. The red arrows point to the Dolichos enclosed organisms formed in tissue culture. These were eliminated with treatment with JAG21. This experiment was performed >4 times. These experiments were performed with 3 different observers reviewing slides at the microscope quantitating fields for each condition. Slides were also scanned and the scans of the slides were reviewed so all fields in the entire slide were noted to be consistent. **(C)** Synergy of JAG21 and atovaquone against Rh-YFP tachyzoites *in vitro*. Isobologram comparing JAG21, atovoquone, and JAG21 plus atovaquone demonstrates synergy. **(D)** THQs effective against drug resistant *P. falciparum*. Dose-response phenotypes of a panel of *P. falciparum* parasite lines. IC50 values were calculated using whole-cell SYBR Green assay and listed as mean ± standard deviation of three biological replicates, each with triplicate measurements. The D6 strain is a drug sensitive strain from Sierra Leone, the TM91-C235 strain is a multi-drug resistant strain from Thailand, the W2 strain is a chloroquine resistant strain from Thailand, and the C2B strain is a multi-drug resistant strain with resistance against atovaquone. **(E)** Solubility and Stability in human and mouse liver microsomes comparing MJM 170, JAG21, and JAG50. Performed by Chem Partners. **(F)** JAG21 CYP450 Inhibition, CACO-2, hERG, PPB, BBB (MDCK-MDK1) efflux analyses. These were performed by Chem Partners and are as defined in the section Materials and Methods. RG38 is a structurally related inactive THQ analog.

toxicity was: HEP G2 IC50 17.70 μM ($r^2 = 0.97$) for JAG21; 7.1 μM ($r^2 = 0.98$) for JAG50.

Lead compounds JAG50, JAG21, and others were tested against EGS strain (Vidigal et al., 2002; Paredes-Santos et al., 2013, 2018; McPhillie et al., 2016) tachyzoites and encysted bradyzoites using methods described earlier (McPhillie et al., 2016). We found a number of these compounds including JAG21 were highly effective against tachyzoites (RH-YFP; Fomovska et al., 2012a) (**Figures 1A, 2A,C**) and bradyzoites of EGS (Vidigal et al., 2002; Paredes-Santos et al., 2013, 2018; McPhillie et al., 2016) (**Figure 2B**). For example, in a separate experiment (data not shown) using immunofluorescence microscopy, the following forms were observed: "true cysts" with a dolichos-staining wall, "pseudocysts" or tight clusters of parasites, and small organisms. If there were fewer than four parasites visible in a cluster, organisms were counted individually (as "small organisms"). A statistically significant reduction in the number of true cysts and small organisms was observed at 1 and 10 μM for both compounds ($p < 0.05, p < 0.005$). Five hundred nanomolars JAG21 treatment results in cultures where we do not see EGS bradyzoites (e.g., **Figure 2B**).

Results against *P. falciparum* using methodology described earlier (Trager and Jensen, 2005; Johnson et al., 2007; Plouffe et al., 2008; McPhillie et al., 2016) also are shown in **Figure 2D**. JAG 21 is potent against *P. falciparum* with IC50 values ranging from 14 to 61 nM against a variety of drug sensitive and resistant strains (McPhillie et al., 2016) including D6, TM91-C235, W2, and C2B. The D6 strain is a drug sensitive strain from Sierra Leone, the TM91-C235 strain is a multi-drug resistant strain from Thailand, the W2 strain is a chloroquine resistant strain from Thailand, and the C2B strain is a multi-drug resistant strain resistant to atovaquone. Effects of other comparison compounds are also shown in this table and range from 31 to 20,000 nM (**Figure 2D**).

ADMET Superiority of JAG21

In vitro absorption, distribution, metabolism, excretion, and toxicity (ADMET) analyses of the THQ compounds were outsourced to ChemPartner Shanghai Ltd. ELQ-271 (synthesized in-house) was tested as a comparison. THQs which were potent inhibitors of *T. gondii* tachyzoites were assessed for their kinetic solubility, metabolic stability in human, and mouse liver microsomes (**Figure 2E**), hERG, and their ability to permeate across MDCK-MDR1 cell membranes (*in vitro* measure of blood-brain barrier (BBB) penetration potential/permeability). Solubility, half-life, HERG, and BBB permeability/efflux results are shown in **Figure 2F**. The aqueous solubility (PBS, pH 7.4) of amorphous compounds JAG21 and JAG50 was 7 and 16 μM, respectively, which is improved over MJM170 (2 μM) and ELQ-271 (0.2 μM). We also tested solubility of the microcrystalline form of JAG21 and found that the solubility was 3.5 μM. JAG21 was the most metabolically stable compound in human liver microsomes (>99% remaining after 45 min) compared with other THQs and ELQ-271, although it displayed a much shorter half-life of 101 min in mouse liver microsomes. All THQs tested in the MDCK-MDR1 system for blood brain barrier (BBB) permeability (including MJM170, JAG21, and JAG50), exhibited high permeability ($P_{app} > 10 \times 10^6$ cm/s) and low efflux (efflux ratio <1.5).

THQs Potently Inhibit Parasite Cytochrome bc1 (Cytbc1) Enzyme Activity

JAG21 is the most active of the initially tested THQs against *T. gondii* Cytbc1, which also showed selectivity for the parasite over the mammalian mitochondrial membrane potential (**Figure 3**). Following the full SAR testing *in vitro* against tachyzoites, the full set of compounds was tested against HFF; then the initial compounds also were tested against the *T. gondii* and HFF enzyme benchmarked against atovaquone, and ultimately the full set of compounds was compared for effect against the *T. gondii* and HFF enzymes.

Mitochondrial membrane potential measurements were performed with permeabilized *T. gondii* tachyzoites in suspension using safranin O, which loads into polarized membranes [see section Materials and Methods in the **Supplemental Materials** (Vercesi et al., 1998)]. *T. gondii* tachyzoites were permeabilized with digitonin to allow the mitochondrial substrate succinate to cross the membrane and energize the mitochondrion. The fluorescence of safranin O, which loads into energized mitochondria was used to measure the membrane potential. The energized state of the mitochondrion is observed by a decrease in fluorescence (**Figures 3A,C,E**). Trifluoromethoxy carbonylcyanide phenylhydrazone (FCCP) was used to depolarize the membrane, which is observed as an increase in fluorescence (**Figures 3A,B**). JAG21 depolarized the membrane potential even at concentrations as low as 2 nM

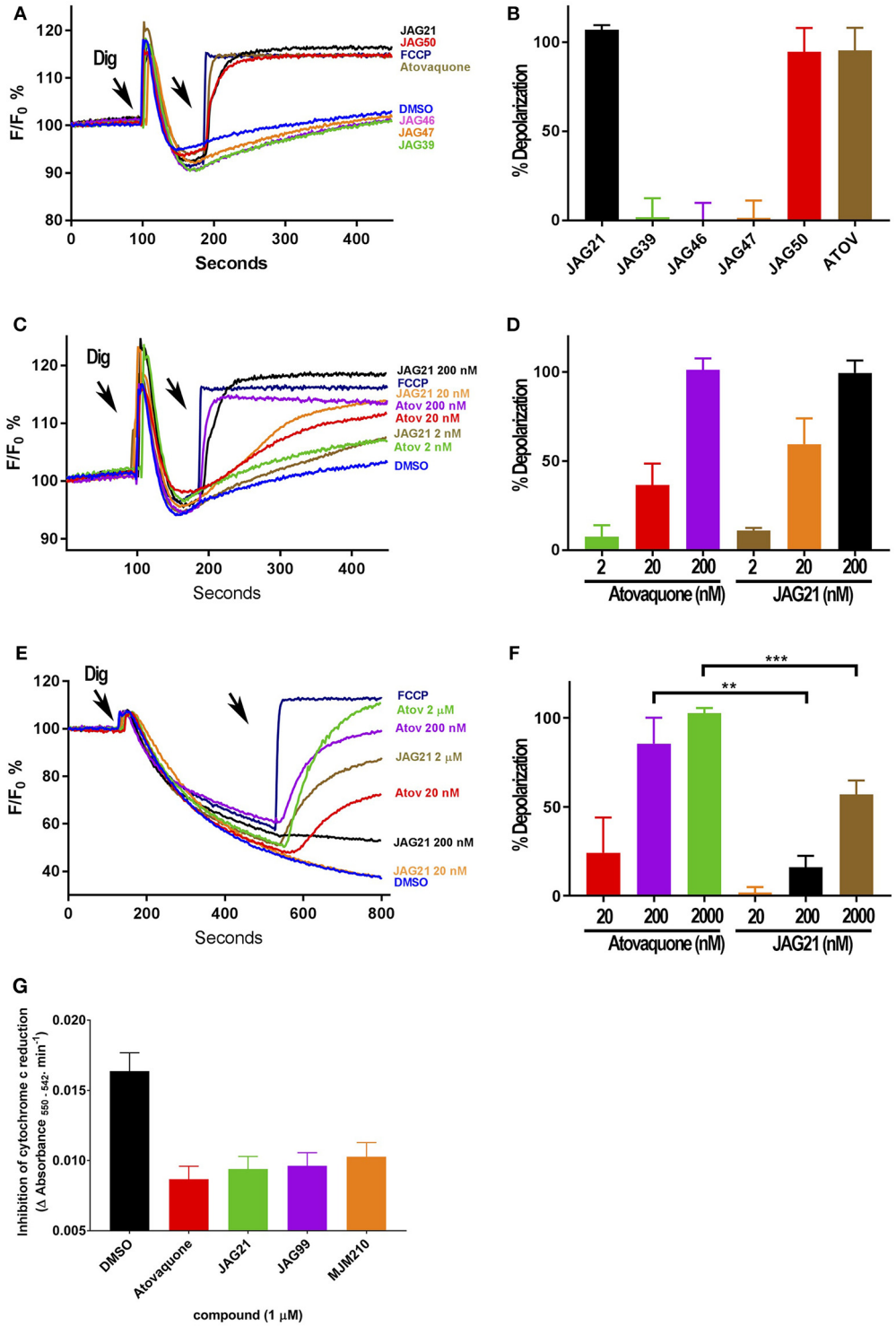

FIGURE 3 | Effect of JAG21, and other THQ compounds on mitochondrial functions of *Toxoplasma gondii*, *Plasmodium falciparum* and HFF-hTE RT **(A)**. Maximum mitochondrial membrane depolarization of JAG21, JAG39, JAG46, JAG47, JAG50, and Atovaquone (4 μM) and FCCP (5 μM). Digitonin was added where indicated by the arrow to permeabilize cells and permit a necessary mitochondrial substrate (Succinate) to reach intracellular organelles. The addition of the indicated compounds is shown by the second arrow. **(B)** Quantification of the depolarization shown in **(A)**. The relative depolarization of each compound was normalized to the depolarization by FCCP which was considered 100% depolarization. **(C)** Effect of various concentrations of JAG21 and Atovaquone on the mitochondrial membrane

(Continued)

FIGURE 3 | potential measured as in **(A)**. The first arrow indicates digitonin addition and the second arrow indicates the addition of compounds at the specified concentration. **(D)** Quantification of the depolarization measured in **(C)**. The relative depolarization of each compound was normalized to the depolarization by FCCP (100%). **(E)** Mitochondrial membrane depolarization of HFF-hTERT in suspension by JAG21 and atovaquone. The first arrow indicates the addition of digitonin, and the second arrow indicates addition of the indicated compounds at the indicated concentration. **(F)** Quantification of the depolarization measured in **(E)**. The relative depolarization of each compound was normalized with the depolarization by FCCP, which was considered 100%. **(B,D,E)** X ± S.D., $N = 3$ independent experiments. Statistical analysis (unpaired student *t*-test) was performed using GraphPad Prism 8.0 (GraphPad Software, Inc., San Diego, CA). $^{**}P < 0.01$. $^{***}P < 0.001$. **(G)** JAG21, JAG99, and MJM210 (1 μM) inhibited *P. falciparum* cytochrome c reduction. Vehicle (DMSO)/atovaquone (1 μM) were negative/positive controls, 1,290 respectively. X ± S.D., $N = 4$ independent experiments.

(**Figures 3C,D**). JAG21 and Atovaquone had similar effects on the mitochondrial membrane potential (**Figure 3D**). Other compounds like JAG46 and 47 showed almost no effect at doses as high as 4 μM (**Figures 3A,B**). JAG50 showed depolarizing activity at doses of 200 nM and higher. The effect of these THQ compounds against the *T. gondii* mitochondrial membrane potential was greater than the effect on the human foreskin fibroblast mitochondrial membrane potential (**Figures 3E,F**). This is consistent with the observation that JAG21 is less toxic against human Telomerase reverse transcriptase immortalized (hTERT) HFF cells than atovaquone. We had newly created THQ compounds, not yet characterized fully, that show even less toxicity to the human fibroblast cytochrome b/c complex marked with ** in **Figure 1A**. These could be developed in a second phase of our program, were reductions in toxicity needed. However, as data presented herein demonstrates, there are significant advantages in the ADMET properties of JAG21, and its dramatic efficacy *in vivo,* without toxicity. There may be no need to further develop any of those potential additional leads.

Enzyme reduction of cytochrome *c* by *P. falciparum* parasite extract (Fisher et al., 2004, 2009) is mediated by *P. falciparum* bc_1 complex cytochrome *c* reductase (*Pfbc*$_1$) enzyme. All three compounds tested (1 μM) significantly inhibited the reduction of cytochrome *c* by the *P. falciparum* parasite extract (JAG21 = 86.4 ± 3.2; JAG99 = 81.3 ± 6.0; MJM170 = 69.7 ± 11.3% of the atovaquone response, **Figure 3G**. Additional data demonstrated selective effect on *P. falciparum* enzyme compared with bovine enzyme (data not shown).

Binding, Co-crystallography, Pharmacophore, and Cryo-electron Microscopy Studies Demonstrate Selectivity

In binding assays and in co-crystallography (Emsley and Cowtan, 2004; Emsley et al., 2010; Battye et al., 2011; Laskowski and Swindells, 2011; Murshudov et al., 2011; Lebedev et al., 2012; Capper et al., 2015; McPhillie et al., 2016; Zhang et al., 2016; Zheng et al., 2017; Amporndanai et al., 2018), JAG21 has lower binding affinity to bovine cytochrome *bc* in comparison with previous compounds that we have tested. JAG21 "inhibits" Cyt*bc1* but not fully, indicating that it will be less toxic for mammalian (bovine/human) cyt *bc1* than the apicomplexan enzymes (**Figure 4A**). The electron density map in the Qi site of bovine cytochrome bc_1complex with JAG21 (**Supplemental Table 1,** Data Collection Statistics) reveals an additional electron density, which allowed unambiguous positioning of the inhibitor (**Figure 4B**). No additional electron density was found within the Q_o site. After the refinement, $2F_o$-F_c electron around JAG21 becomes clearer (**Figure 4C**). The second aromatic ring in the tail group of the compound is less defined due to high flexibility introduced by the oxygen linker. The quinolone head of JAG21 is held between Asp228 and His201 and adapted the same conformation as 4(1H)-pyridone (GSK932121) (Capper et al., 2015) (**Figure 4D**) and tetrahydro-4(1H)-quinolone (MJM170) (McPhillie et al., 2016) (**Figure 4E**) by directing the NH group to His201 and the carbonyl group to Asp228. The carbonyl of the quinolone head and OG1 atom of Ser35 are within 3.0 Å distance that allows hydrogen bonding and enhances the binding affinity to the bovine enzyme. The 3-diarylether tail extends along a hydrophobic channel defined by Gly38, Ile39, and Ile42. The trifluoromethoxy group at the phenoxy ring points toward Met190 and Met194 (**Figure 4F**). CryoEM studies of the complex also demonstrate reasons for selectivity. In **Figure 4F**, the density suggests that the inhibitor can adopt two different binding poses as observed previously in the cryo-EM structure of GSK932121 (Capper et al., 2015). The binding pose shown in yellow, which has the strongest density, agrees with the crystal structure and has the trifluoromethoxy group pointing toward Met194. However, there is additional density which could result from a second binding pose (green) in which the trifluoromethoxy group points toward Asp228 (McPhillie et al., 2016). **Figure 4F** shows GSK932121 pyridone (PDB:4D6U) (**Figure 4G**) MJM170 quinolone (PDB:5NMI). The EM map has been deposited at the EMDB (EMDB-11002).

JAG21 Is Potent *in vivo*

In vivo studies of JAG21 against *T. gondii* demonstrated high efficacy in a variety of settings. JAG21 at 5 mg/kg/day administered IP improves well-being and eliminates illness and *T. gondii* Type II Prugneaud luciferase tachyzoites completely in luminescence studies (**Figure 5A**). Further, treatment beginning on day one after infection results in no cysts being found in brains of these mice treated for 14 days with 5 mg/kg/day of JAG21, when brains were evaluated 30 days after stopping JAG21 treatment in two replicate experiments. Treatment beginning on day 30 after initiation of infection with Type II Me49 parasites results in marked, statistically significant reduction in normal appearing cysts, free organisms, and immunoperoxidase stained cysts detected by automated imaging of scanned slides (**Figures 5B,C**, $p < 0.03$ experiment 1: $p < 0.01$ experiments 1 and 2 together, **Supplemental Figure 1**). The automated analysis confirmed results from the blinded microscopic visual quantitation of cysts and free organisms in slides by two

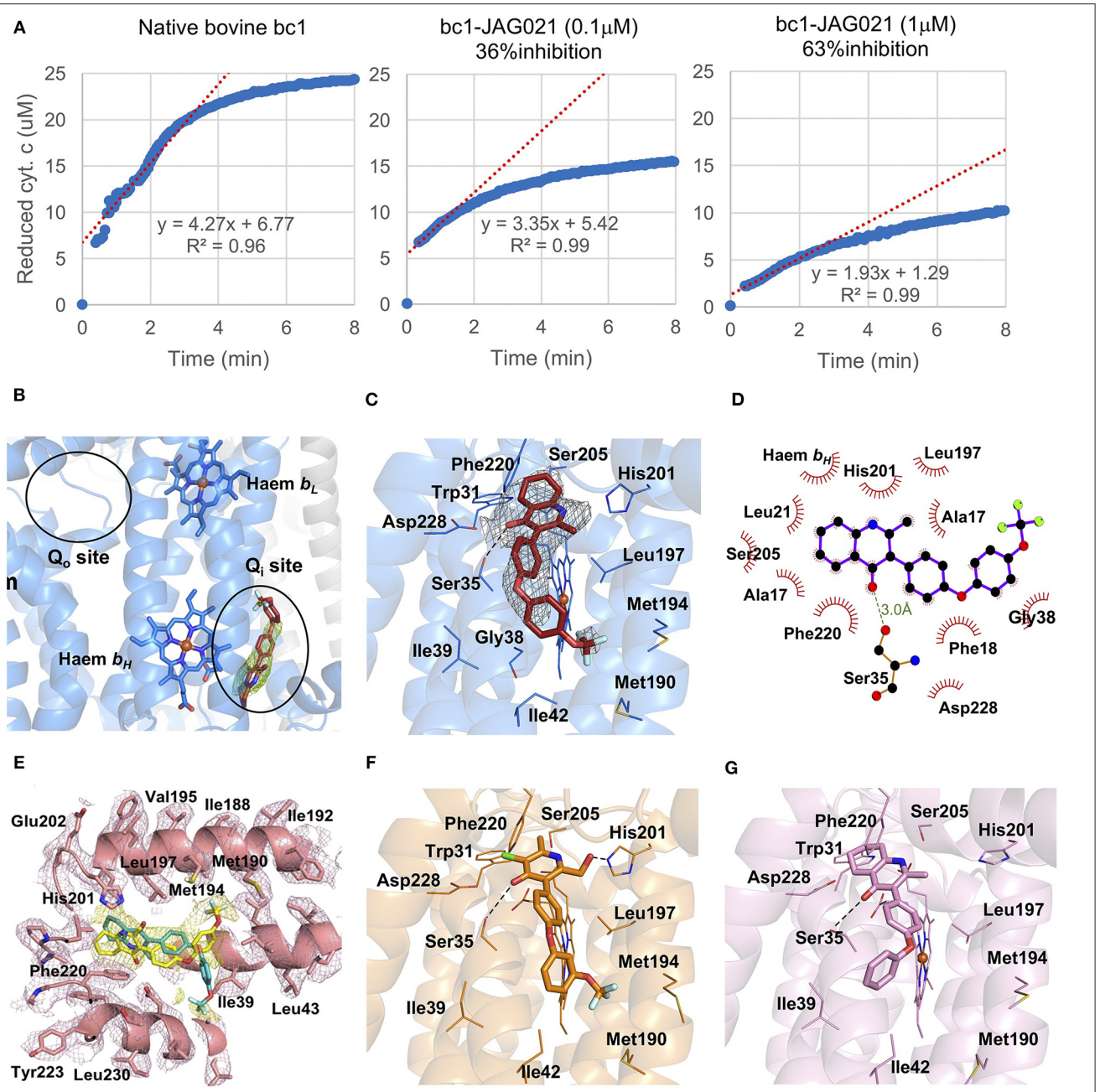

FIGURE 4 | Binding studies of JAG21 to bovine bc1. **(A)** Bovine Cytbc1 activity assays showing 36 and 63% inhibition at 0.1 and 1 μM concentration of JAG21, respectively. *N* = at least 2 biological replicate experiments with similar results. **(B)** The Cytbc1 structure presented in cartoon style with clear omit (Fo-Fc) electron density map for the bound JAG21 compound only in the Q_i site showing selectivity within the binding pocket. Qi and Qo sites are marked by black ellipsoids. **(C)** The bound JAG21 compound (orange) within the Qi site with corresponding (2Fo-Fc) electron density map contoured at 1 σ level as gray mesh. The residues which make close interactions with the bound inhibitor are shown in stick format and labeled. **(D)** 2D pharmacophore analysis of JAG21 binding pocket produced using Ligplot+ LS-2011. Hydrophobic interactions are shown as red spikes, hydrogen bond with Ser35 is shown by green dashes. **(E)** Cryo-EM derived structure of the Cytbc1 bound JAG021 structure with corresponding density map contoured at 3 σ level suggesting two different positions for the head group represented by two regions of density shown as yellow mesh. The Cytbc1 structure bound to the pyridone GSK932121 (PDB:4D6U) **(F)** and quinolone MJM170 (PDB:5NMI) **(G)** in the Q_i site. Haem and compounds are shown as colored sticks, Fe ion as orange sphere and hydrogen bonding as black lines. Hydrogen bonding with Ser35 is shown as black dashes. Terms JAG021 and JAG21 used interchangeably for this same compound.

observers. Adding tafenoquine or primaquine to treatments of active plus dormant malarias (St Jean et al., 2016; Lacerda et al., 2019; Llanos-Cuentas et al., 2019) is partially effective against both active and dormant phase plasmodia, when neither treatment of active nor dormant disease alone is effective for either *in vivo*. We developed experiments based on these

observations where experiments with tafenoquine alone or with JAG21 alone was used in the experiments with established cysts with immune competent mice. This was to determine whether tafenoquine might add to efficacy of JAG21. The efficacy of treatment with JAG21 alone was so robust (**Figure 5B**), that no additive effect was seen, or could have been detected, by adding Tafenoquine to JAG21. Efficacy was shown when data were analyzed as separate groups, i.e., control vs. JAG21 alone ($p < 0.03$) or control vs. JAG21 plus tafenoquine, or grouping the JAG21 and JAG21 plus tafenoquine results as "untreated" vs. "treated" ($p < 0.01$). Analysis shown combining both treatment groups from two replicate experiments showed similar results ($p < 0.01$, **Figure 5B**), and when results from replicate experiments were grouped (**Supplemental Figure 1**). In **Figure 5C** the control mice had cysts with usual morphology (Top two panels), whereas treated mice had very few morphologically recognizable usual cysts that were immunostained (bottom panels).

A nano formulation homogenized (<6 μM) was used effectively orally for the *P. bergheii* experiments, further, importantly, was effective in the single oral dose causal prophylaxis in 5 C57BL/6 albino mice at 2.5 mg/kg dosed on day 0, 1 h after intravenous administration of 10,000 *P. berghei* sporozoites was completely protective. In addition, 3 dose causal prophylaxis treatment in 5 C57BL/6 albino mice at 0.625 mg/kg dosed on days −1, 0, and +1 also was completely protective. A representative experiment at a higher dose (5 mg/kg) is shown, but all experiments with the oral dosing regimen with the nanoformulation specified above showed 100% survival 30 days post infection with *P. berghei*, where all liver and blood stage parasites were eliminated (**Figures 5D,E**) demonstrates not only efficacy of JAG21 against the three life cycle stages of *P. berghei*, but also demonstrates the efficacy of oral administration of the nanoformulation when used immediately, at a low dose.

G1 Arrest, Persisters, Companion Compounds

In mice that were treated with JAG21 early after infection (**Figure 5A**) we could find no residual immunostaining for *T. gondii* in brain tissue of any mice. This suggests that very early treatment could prevent established, chronic infection, for example in epidemics such as those that occurred in Victoria, Canada, the U.S.A., and Brazil. In mice with established cysts, following treatment with JAG21, we occasionally saw a small number of cysts (**Figure 5B**) and amorphous immunostained structures (**Figure 5C,** bottom panels). This was reminiscent of persistence in some malaria infections (Cubi et al., 2017) and abnormal immunostained structures we previously identified with a conditional, tetracycline-on regulatable, mutant *T. gondii* (Hutson et al., 2010 and **Supplemental Figure 2**). In this ΔRPS*13* tachyzoite, small ribosomal protein 13 can be regulated, depending on whether anhydrotetracycline (ATc) is absent or present, leading the ATc responsive repressor to be on or off response elements engineered into the promoter (Hutson et al., 2010). ΔRPS*13* replicates with ATc present and is arrested in G1 when ATc is absent in HFF cultures (Hutson et al., 2010). The dormant parasite could persist for extended periods (Hutson et al., 2010). The parasite could be rescued from its dormant—ATc state by adding ATc, months after removing tetracycline from infected HFF cultures, although it could not be rescued in immunocompetent mice with LNAME and ATc when tested 1 week after infection (Hutson et al., 2010). We wondered if this type of dormant organism could form *in vivo*, whether it could contribute in a biologically relevant way to dormancy and recrudescence, similar to the malaria hypnozoite (Cubi et al., 2017; Muller et al., 2019), and whether JAG21 might be able to eliminate it, or whether a companion compound effective against this form might be needed or work in conjunction with JAG21 if needed. To begin to address these questions and to investigate how close the *T. gondii* ΔRPS*13* -ATc phenotype might be to the malaria hypnozoite, we compared the transcriptome of *T. gondii* ΔRPS*13* in human, primary, brain, neuronal stem cells +/− ATc to the recently published *P. cynomolgi* hypnozoite transcriptome, established with single cell RNA sequencing in laser captured organisms (Cubi et al., 2017). This analysis identified 28 orthologous genes with similar expression pattern in both *T. gondii* ΔRPS*13* -ATc and *P. cynomolgi* hypnozoites, including the downregulation of rps*13* and upregulation of the eukaryotic initiation factor-2α kinase IF2K-B, a protein involved in translational control in response to stress (Cubi et al., 2017) (**Figure 6A**). Further. assessment of the *T. gondii* ΔRPS*13* transcriptome in the absence or presence of ATc showed upregulation of additional IF2K members, 25 Apetela (AP) 2 transcription factors and a number of genes that participate as protein ubiquitin ligases, and in trafficking as well as in RNA binding, and GCN1 (**Supplemental Table 2**). None of them, except for AP2VIIa-7, have been shown to be upregulated nor downregulated during differentiation to bradyzoites. Gene set enrichment analysis showed that in the absence of ATc, the *T. gondii* ΔRPS*13* transcriptome is enriched in genes typically expressed during G1, confirming previous results indicating that downregulation of *rps13* arrests the parasite at this stage of the cell cycle (**Figure 6B**) (Hutson et al., 2010). Moreover, a number of biological processes are downregulated without ATc, including protein synthesis and degradation as well as energy metabolism (**Figure 6B**). Noteworthy, some gene ontology (GO) terms enriched in *T. gondii* ΔRPS*13* -Tc are also overrepresented in the *P. cynomolgi* hypnozoite (stars in **Figure 6D**). Further, without ATc the transcriptome of *T. gondii* ΔRPS*13* is compatible with a parasite transitioning from an active replicating form to a dormant stage, reflected by the downregulation of genes typical of the S and M stages of the cell cycle, and of genes that participate in energy metabolism and virulence (**Figures 6B,D**, **Supplemental Table 2**, **Supplemental Figure 2**). It has been reported that with treatment of active forms of malaria, hypnozoites still persist, and recrudesce later (Hutson et al., 2010; St Jean et al., 2016; Cubi et al., 2017; Lacerda et al., 2019; Llanos-Cuentas et al., 2019). Also, compounds that target cytochrome b/c were not effective against malaria hypnozoites. If primaquine or tafenoquine, which do not treat the active *Plasmodium vivax* parasites, were added *in vivo,* hypnozoites have been shown not to recrudesce, or do so less often (St Jean et al., 2016; Lacerda et al., 2019; Llanos-Cuentas et al., 2019). Testing with primaquine or tafenoquine could

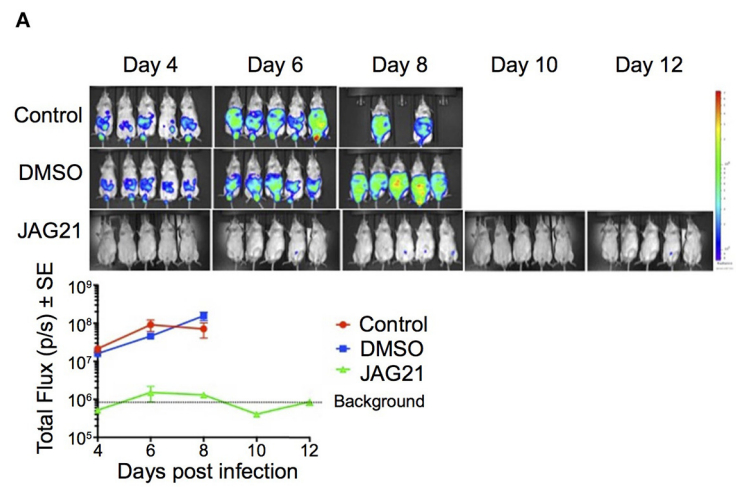

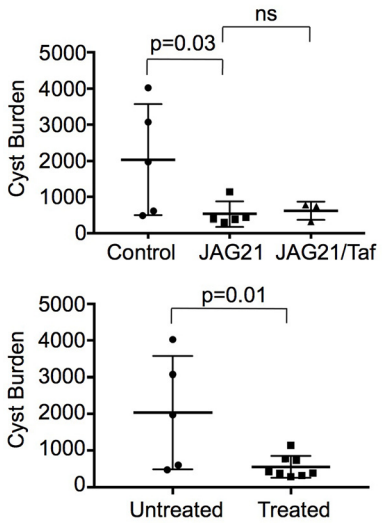

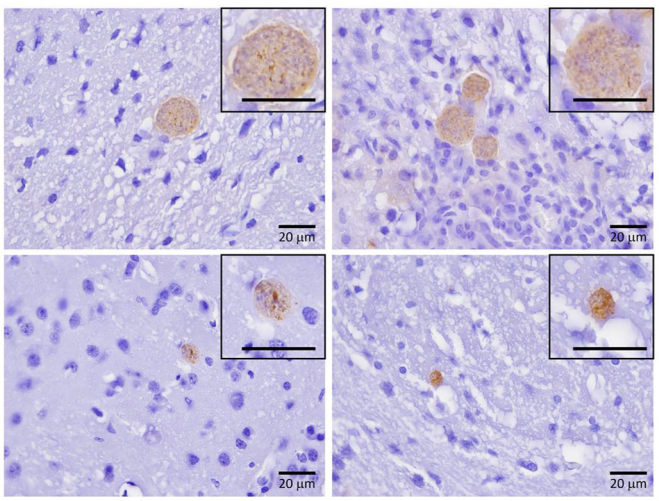

D

In vivo efficacy P.berghei model	JAG21			
P.O. (3 doses) -D1, D0, D1	10 mg/kg	5 mg/kg	2.5 mg/kg	0.625 mg/kg
IVIS @ 72h	0	0	0	0
Mean Survival Days	30	30	30	30
	ED90 < 1.25 mg/kg for 3 daily doses			

In vivo efficacy P.berghei model	JAG21			
P.O. (single dose)	1.25 mg/kg -D1	2.5 mg/kg -D1	1.25 mg/kg D0	2.5 mg/kg D0
IVIS @ 72 h	> $10x10^6$	> $10x10^6$	0	0
Mean Survival Days	8	15	>17	30
	ED90 < 2.5 mg/kg single dose			

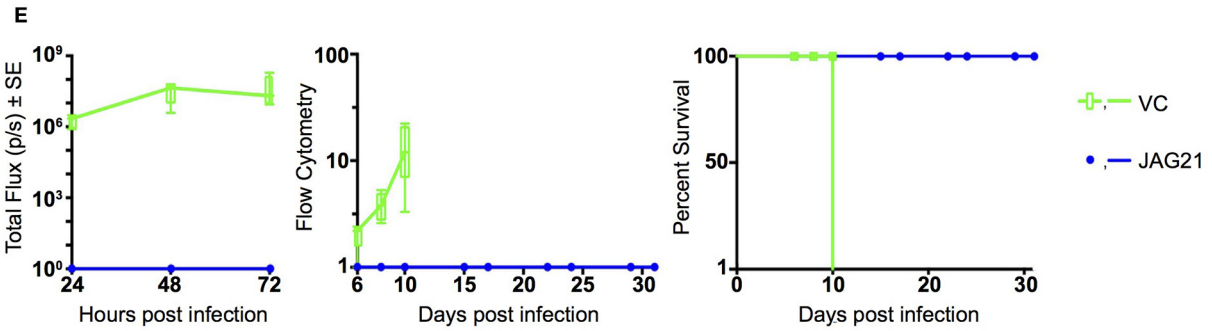

FIGURE 5 | JAG21 is a mature lead that protects against *Toxoplasma gondii* and *Plasmodium berghei in vivo*. **(A)** JAG21 treatment for 14 days protects against *T. gondii* tachyzoites *in vivo*. Tachyzoite challenge with Prugneaud luciferase parasites imaged with leuciferin using IVIS demonstrates that treatment with JAG21 eliminates leuciferase expressing parasites and leads to 100% survival of JAG21 treated infected mice. No cysts were found in brains of mice at 30 days after infection when they have been treated with JAG21 for the first 14 days after infection. There were 2 biological replicate experiments with 5 mice per group with similar results. **(B)** JAG21 and JAG21 plus tafenoquine markedly reduce Me49 strain brain cyst numbers *in vivo* in Balb/C mice at 30 days after infection. Parasites were quantitated by scanning the entire immunoperoxidase stained slide in an automated manner and by two observers blinded to the experimental treatment using microscopic evaluation. In each of two experiments, the numbers of mice per group were as follows: Experiment 1 had 4 diluent controls, 5 JAG21, 4 JAG21/Tafenoquine treated mice; and Experiment 2 had 5 diluent controls, 5 JAG21, 3 JAG21/Tafenoquine treated mice. Immunoperoxidase staining was performed. Parasite burden was quantitated using a positive pixel count algorithm of Aperio ImageScope software. Positive pixels were normalized to tissue area (mm^2). Quantification was by counting positive pixels per square area. The entire brain in one section was scanned for each mouse. The parasite burden was quantitated as units of positive pixels per mm^2. The average ± S.E.M. numbers of mm^2 per slide quantitated was 30.2±1.6 mm^2 per mouse for this quantification. Each high power field of view shown in

(Continued)

FIGURE 5 | C is ∼0.02 mm^2 per field of view. A representative single experiment is presented and the data from the two experiments analyzed together also demonstrated significant differences between the untreated and treated groups ($p < 0.01$; **Supplemental Figure 1**). **(C)** Microscopic evaluation of the slides reveal effect of JAG21 and JAG21 plus tafenoquine having the same pattern as the automated quantitation of immunoperoxidase stained material. There are usual appearing cysts in the DMSO control untreated mice as shown in the top panels, and rare cysts in the treated mice with most of the brown material appearing amorphous (bottom panels). **(D)** JAG21 nanoformulation dosages administered to *P. berghei* infected C57Bl6/albino mice compared with vehicle control. Design of single dose and 3 day dose experiments. **(E)** JAG21 nanoformulation cures *P. berghei* sporozoites (left panel), blood (middle panel), and liver stages, leading to 100% survival (right panel). This is with oral administration of a single dose of 2.5 mg/kg or 3 doses at 0.625 mg/kg. Single dose causal prophylaxis in 5 C57BL/6 albino mice at 2.5 mpk dosed on day 0, 1 h after intravenous administration of 10,000 *P. berghei* sporozoites. Shown is 3 dose causal prophylaxis treatment in 5 C57BL/6 albino mice at 0.625 mpk dosed on days −1, 0, and +1. Representative figure showing survival (right panel), luminescence (left panel), and parasitemia quantitated by flow cytometry (middle panel) for 5 mg/kg.

only be performed *in vivo,* as activity against the hypnozoite requires hepatic metabolism of primaquine or tafenoquine (St Jean et al., 2016; Lacerda et al., 2019; Llanos-Cuentas et al., 2019). Tafenoquine is not active in tissue culture which is consistent with the findings that these compounds require hepatic metabolism. To establish a parallel *in vivo* system, we studied immune compromised mice (Interferon ϒ receptor knockout mice with the knockout in the germline) infected with ΔRPS*13* herein. Although in immune competent mice ΔRPS*13* does not recrudesce with ATc treatment initially, beyond 3 days after infection, we found that when ATc was added after treatment of the immune compromised mice with JAG21 dosed intraperitoneally for 14 days, the dormant ΔRPS*13* parasite could still recrudesce after JAG21 treatment was discontinued and tetracycline added (**Figure 6C** and **Supplemental Figure 2**). Consistent with adding tafenoquine to treatment of *P.vivax* malaria with chloroquine where both medicines together were partially effective against the active and hypnozoite forms, the combination of JAG21 and tafenoquine had a modest effect together on transiently improving survival time when ATc was added when compared with JAG21 or tafenoquine alone (**Figure 6C** and **Supplemental Figure 2**). The trend in the result seems similar to the malaria infections where hypnozoites form, although protection was not as robust, as in the malaria model, and we did not achieve complete, durable protection against ΔRPS*13*. These results in **Figure 6C** and **Supplemental Figure 2** suggest: (a) In G1 arrested organisms that begin as tachyzoites, they can persist *in vivo* even if their morphology as parasites is difficult to discern; (b) Treatment with JAG21+Tafenoquine can prolong time to death more robustly than other treatments; (c) But, in these immune compromised mice at this dosage regimen this treatment did not robustly, durably protect these mice from death later; (d) In these immune compromised mice, whether this lack of complete protection was because of immune compromise, or less than optimal duration of treatment, or suboptimal dose or timing of treatments, or that this G1 arrested organism is harder to treat, remains to be determined in future studies. The modest efficacy of the two compounds, administered together, suggests that treating both tachyzoites and the G1 arrested organisms is important. This seems similar to *P. cynomogli* and *P. vivax* treatment with tafenoquine and chloroquine studies, which also showed efficacy but was not completely successful in preventing relapse. At the time this study was performed, formulation and dosing (including duration and timing) had not yet been optimized formally for the *T. gondii* model. *P. vivax* treatment requires chloroquine to treat blood schizonts and tafenoquine to treat hypnozoites. Treatment in man, per the FDA approved label, consists of a single dose of 300 mg on day 1 co-administered with chloroquine treatment on days 1 or 2. Both medicines have long half-lives in humans. This treatment was relatively effective in humans, with about a 30% recurrence rate.

Sinai et al. have demonstrated heterogeneity in the phenotypes of organisms within established cysts. Their work found bradyzoites within cysts are not uniform with regard to their replication potential (Watts et al., 2015), mitochondrial activity (Sinai, unpublished), and levels of the glucose storage polymer amylopectin (Sinai, unpublished). These properties of bradyzoites (Watts et al., 2015), and properties of tissue cysts that vary during the course of infection, demonstrated that there are unappreciated levels of complexity in the progression of chronic toxoplasmosis (Watts et al., 2015). The analysis (**Figure 6D**) of the ΔRPS*13* infected NSC suggests molecular targets that are modified in this G1 arrested ΔRPS*13* parasite as shown in **Figure 6D** and **Supplemental Table 2**. In the future, with formulation and pharmacokinetics of JAG21 optimized, it will be of interest to determine whether JAG21 can eliminate these organisms and any residual structures as in **Figure 6C**, or whether adding synergistic compounds such as atovaquone (**Figure 4B**) or antisense effective against these upregulated molecular targets, such as kinases, ATPases, AP2s (**Figure 6D** and **Supplemental Table 2**), or a newly recognized bradyzoite master regulator of differentiation might be effective alone or might be synergistic with JAG21 against this ΔRPS*13*, as well as the conventional recognized tachyzoite and bradyzoite life cycle stages. Chen et al. reported in the transcriptomes of established bradyzoite *in vivo* cysts that EIF2kinase of stressed parasites is present (Chen et al., 2018), but we have not found other overlap of Chen's transciptome with *P cynomogli* or ΔRPS*13* transcriptomes. Others have described EIF2kinase and stress granules only in transitioning or extracellular parasites (Watts et al., 2015). Bradyzoites within tissue cysts are not monolithic. Thus, in future studies, single cell RNA sequencing of bradyzoites obtained by laser capture of bradyzoites *in vivo*, defined on the basis of their physiological state, may be needed to determine whether a transcriptome signature similar to ΔRPS*13* is sometimes present. This could be linked to morphologic/immunostaining features that might functionally distinguish them to define the character of a hypnozoite-like state in *T. gondii*. We noted heterogeneity of parasite phenotype, even in the same vacuoles, in our earlier IFA and electron microscopic characterization of G1 arrested ΔRPS*13* in HFF (Hutson et al., 2010). Heterogeneity also was found very recently

A

Description	*P. cynomolgi* Gene_ID	*P. cynomolgi*	*T. gondii*	*T. gondii* Gene_ID	Description
erythrocyte binding protein	PCYB_083210			TGME49_310170	hypothetical protein
hypothetical protein	PCYB_061360			TGME49_261960	hypothetical protein
hypothetical protein	PCYB_073220			TGME49_268240	hypothetical protein
hypothetical protein	PCYB_091490			TGME49_234410	small conductance mechanosensitive ion channel
serine/threonine protein kinase	PCYB_021650			TGME49_311510	eIF2 kinase IF2K-B
hypothetical protein	PCYB_073210			TGME49_292330	hypothetical protein
protein kinase domain containing protein	PCYB_032180			TGME49_268010	hypothetical protein
hypothetical protein	PCYB_145980			TGME49_276180	histone acetyltransferase TAF1/250
TBC domain containing protein	PCYB_071500			TGME49_203910	TBC domain-containing protein
hypothetical protein	PCYB_127100			TGME49_206550	hypothetical protein
hypothetical protein	PCYB_093980			TGME49_273860	hypothetical protein
hypothetical protein	PCYB_111820			TGME49_293820	calpain family cysteine protease, putative
eukaryotic initiation factor	PCYB_091430			TGME49_269180	MIF4G domain-containing protein
hypothetical protein	PCYB_141480			TGME49_231480	GCN1, putative
Sec20-like protein	PCYB_142610			TGME49_217780	Sec20 protein
hypothetical protein	PCYB_052770			TGME49_249870	hypothetical protein
DEAD/DEAH box helicase	PCYB_071120			TGME49_294350	DEAD/DEAH box helicase, putaitve
hypothetical protein	PCYB_091600			TGME49_277080	microneme protein MIC5
origin recognition subunit	PCYB_011270			TGME49_245570	origin recognition complex subunit 2 protein
hypothetical protein	PCYB_113090			TGME49_261230	ankyrin repeat-containing protein
hypothetical protein	PCYB_073640			TGME49_309170	TAF7-like RNA polymerase II TAF7L
hypothetical protein	PCYB_063170			TGME49_258820	hypothetical protein
hypothetical protein	PCYB_143620			TGME49_229740	hypothetical protein
40S ribosomal protein S13	PCYB_112180			TGME49_270380	ribosomal protein RPS13
20S proteasome subunit alpha type 2	PCYB_114800			TGME49_287210	proteasome subunit alpha2, putative
hypothetical protein	PCYB_143610			TGME49_242890	hypothetical protein
pre-mRNA splicing factor	PCYB_031320			TGME49_231970	pre-mRNA processing splicing factor PRP8
4-methyl-5(B-hydroxyethyl)-thiazol monophosph. biosynth.	PCYB_113050			TGME49_214290	DJ-1 family protein
5'-3' exonuclease N-terminal resolvase-like domain	PCYB_042630			TGME49_284010	5'-3' exonuclease, N-terminal resolvase family
multidrug resistance protein 2	PCYB_126720			TGME49_249820	ATP-binding cassette sub-family B member 5
2-oxoglutarate dehydrogenase E1 comp. mitoch. prec.	PCYB_052050			TGME49_244200	2-oxoglutarate dehydrogenase E1 component
protein disulfide isomerase	PCYB_051340			TGME49_211680	protein disulfide isomerase
pyruvate dehydrogenase E1 component alpha subunit	PCYB_093050			TGME49_245670	pyruvate dehydrogenase complex subunit PDH-E1∝
hypothetical protein	PCYB_133950			TGME49_291140	CCR4-Not complex component, Not1 protein
hypothetical protein	PCYB_113850			TGME49_313590	hypothetical protein
hypothetical protein	PCYB_146850			TGME49_240910	hypothetical protein
elongation factor 1 alpha	PCYB_112350			TGME49_286420	elongation factor 1-alpha (EF-1-ALPHA), putative
cytochrome c oxidase subunit	PCYB_073540			TGME49_209260	cytochrome c oxidase subunit, putative
ubiquinol-cytochrome c reductase	PCYB_082210			TGME49_288750	ubiquinol-cytochrome c reductase
proteasome beta-subunit type 4	PCYB_012310			TGME49_280710	20S proteasome subunit beta 7, putative
DNA polymerase alpha	PCYB_031930			TGME49_217910	DNA polymerase (pol2) superfamily protein
hypothetical protein	PCYB_082250			TGME49_228330	NLI interacting factor family phosphatase
ubiquitin-like protease 1 homolog Ulp1 homolog	PCYB_012530			TGME49_251510	Ulp1 protease family, catalytic domain
hypothetical protein	PCYB_095140			TGME49_224590	DNA-directed RNA polymerase III POLR3C
vacuolar ATP synthetase	PCYB_102260			TGME49_212310	vacuolar ATP synthetase

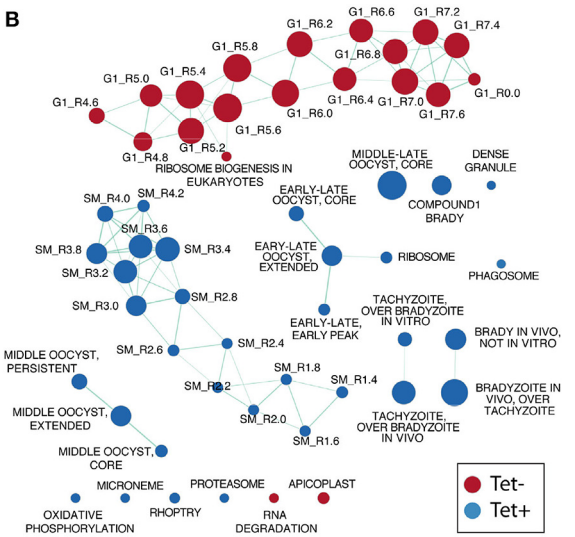

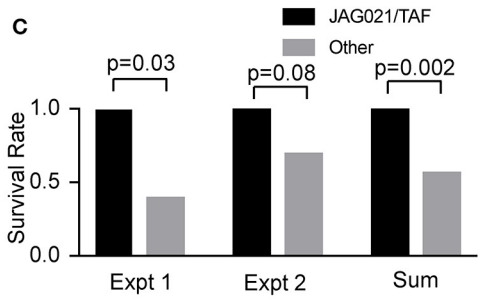

RhRPS13 infection mortality prior to initial JAG21+TAF mortality					
Rx	Single Rx			Sum of Single Rx	Combined Rx
	DMSO	TAF	JAG21	DMSO or TAF or JAG21	JAG21 + TAF
Expt 1	2/5	4/5	3/5	9/15	0/6
Expt 2	3/10	2/5	1/5	6/20	0/9
Total	**5/15**	**6/10**	**4/10**	**15/35**	**0/15**

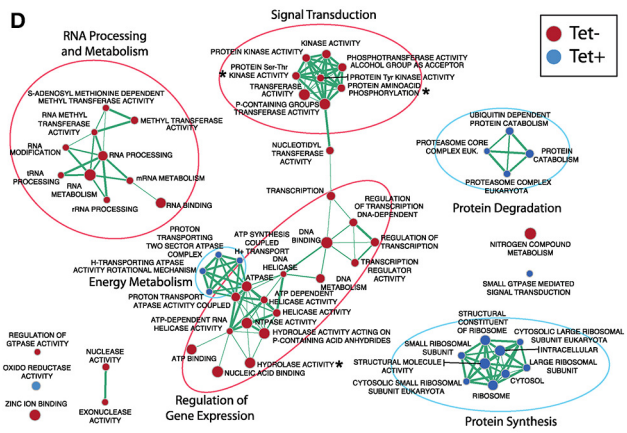

FIGURE 6 | *Toxoplasma gondii* ΔRPS13 transcriptome during Primary Human Brain Neuronal Stem Cell (NSC) infection and *in-vivo* susceptibility to JAG21 and TAF treatment are reminiscent of literature findings with malaria hypnozoites. **(A)** *P. cynomolgi-T. gondii* best reciprocal match genes significantly upregulated (red) or downregulated (blue) in *P. cynomolgi* hypnozoites compared to liver-schizont stage and in ΔRPS13 after downregulation of *rps13* gene expression ($p \leq 0.05$, FDR $\leq$ 0.2). **(B)** Gene-set enrichment analysis of ΔRPS13 +/– Tc. Blue and red nodes denote gene-sets enriched in presence or absence of Tc, respectively. Node diameters are proportional to number of genes belonging to corresponding gene-sets. Edge thickness is proportional to number of genes shared between connected nodes. **(C)** Survival rate of mice infected with 100,000 ΔRPS13 followed by treatment with diluent, JAG21, tafenoquine (TAF) or the two together (JAG21/TAF). Then tetracycline was added at 14 days. The combination of the two compounds resulted in improved time of survival ($p < 0.03$, Experiment 1; $p = 0.08$ Experiment 2, $p = 0.002$ Experiment 1+2). The full data are presented in the box below the image in **(C). (C)** Rx refers to treatment of mice with diluent (DMSO), Tafenoquine (TAF), or JAG21, or JAG21 and TAF. ΔRPS13 is referred to as RhRPS13Δ in the title of the box in **(C)**. In **Supplemental Figure 2**, histological preparations that are immunoperoxidase stained for *T. gondii* antigens from a pilot study were prepared (**Supplemental Figure 2**). These are images, in **Supplemental Figure 2** of liver and spleen from IFN γ receptor knock out mice without treatment on days 7 and 14 after infection. In those mice without any treatment there was amorphous brown immunoperoxidase stained material in **Supplemental Figure 2A**. When tetracycline (aTet) was administered on day 14 after infection in drinking water, with tissues obtained and immunostained for *T. gondii* antigens from mice that died or became very ill, organisms that were clearly recognizable could be seen (**Supplemental Figures 2B–E**). Design of the treatment experiment with control DMSO diluent, JAG21 alone, Tafenoquine alone (TAF) or the two together (JAG/TAF) with full data for each of the groups and with the composite analysis from replicate experiments, including numbers of mice, are shown in **Supplemental Figures 2C,D. Supplemental Figures 2C,D** shows prolongation of survival time, but there is not durable protection against ΔRPS13 in these immune compromised mice treated with JAG21/TAF as described. This is summarized in **C** to demonstrate early prolongation of survival time with the detailed data in **Supplemental Figure 2. (D)** Gene ontology enrichment analysis of ΔRPS13 +/–Tc. Node and edge conventions are the same as in **(B)**. There were at least 2 biologic replicates of each experiment.

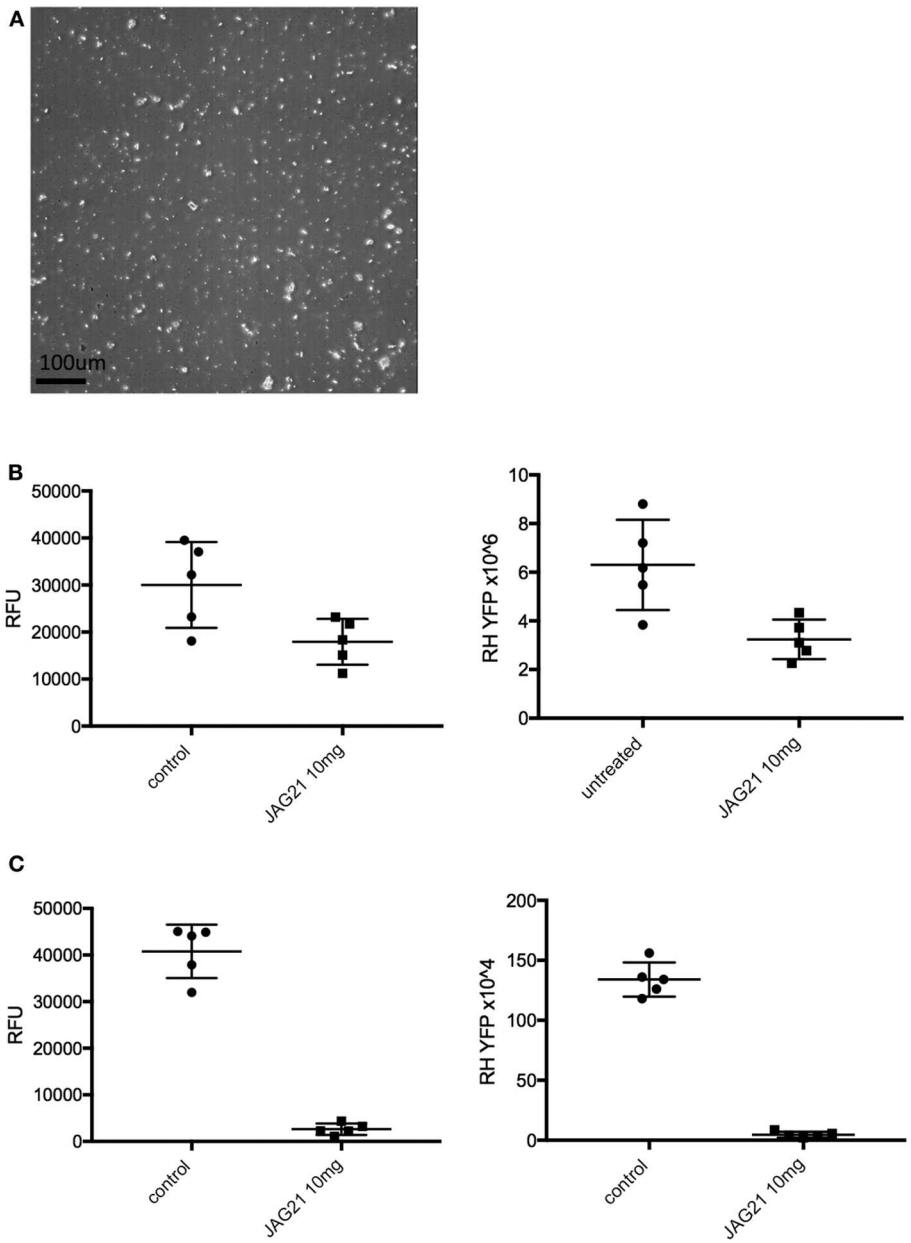

FIGURE 7 | Oral nanoformulation of JAG21 potently protects against 2000 highly virulent RH strain tachyzoites given intraperitoneally. **(A)** Following sonication produces nanoparticles of ∼2.86 μM. **(B)** Single oral dose of 10 mg/kg reduced intraperitoneal tachyzoites measured by RH YFP expression and counting with hematocytometer ($p < 0.03$). **(C)** Three daily 10 mg/kg doses markedly and significantly reduces intraperitoneal parasite burden measured as fluorescence and by hematocytometer on the fifth day ($p < 0.001$). No compound was administered after the third day. *N* = at least 2 biological replicate experiments with 5 mice per group with similar results.

in tachyzoites and bradyzoites created by alkaline conditions in culture across the cell cycle *in vitro* in HFF, using single cell RNA sequencing (Xue et al. Biorx, 6/3/2019 in press). These authors also noted that what had been interpreted as "noise" earlier was found actually to be signal in a more complex environment. These authors suggest that such heterogeneity might make developing curative treatments more complex. Our analysis of JAG21 effects and the ΔRPS*13*-ATet knockdown herein begin to help address this question: We noted that consistent with heterogeneity in our IFAs, in our comparison with the Xue et al.'s heterogeneous P1-6 clusters analysis, we found that most of the up- or down-regulated genes are within P3-P5 tachyzoite clusters. Also, consistent with the heterogeneity we observed in our G1 arrested ΔRPS*13* -ATet comparison, ΔRPS*13* has a drop in SAG1 and elevated SRS44 that is consistent with a brady-like phenotype. BAG1 expression was too low overall to draw any

conclusion about BAG1. It is also noteworthy that in our -ATet relative to +Atet conditions in primary, human, brain, neuronal stem cells, the master regulator of bradyzoite differentiation is slightly overexpressed (Log_2 Fold Change=0.7, adjusted $p = 0.043$). Although JAG21 is highly potent against tachyzoites and bradyzoites, it did not eliminate every long-established encysted bradyzoite or -ATet ΔRPS*13* completely either *in vitro* or in IFNγ knock-out mice *in vivo*. Consistent with heterogeneity, herein JAG21 treatment of ΔRPS*13* and transcriptomics analyses define a metabolically quiescent, persister, "stasis" state that is reversible even after substantial periods of dormancy. These observations contribute to conceptual and functional understanding of both Plasmodia species and *T. gondii* infections and molecular mechanisms whereby "persisters" might be eliminated.

An Oral Nanoformulation Is Potent Against Virulent RH

To further develop JAG21 for practical, clinical use, our next step was to make a formulation that is stable at room temperature, and would be effective when administered orally: Following a number of unsuccessful alternative methods (data not shown), a dispersion of JAG21 was prepared using hydroxyethyl cellulose (HEC) and Tween 80. This new formulation method is described in the Materials and Methods. When this dispersion was imaged using a Nikon ECLIPSE E200 optical microscope set to 40x magnification, the average particle size of the JAG21 dispersion in HEC/Tween 80 was determined using an in-house image analysis program and was found to be 2.85 μm (**Figure 7A**). Material was re-sonciated the same way just prior to administration after being stored for 6 months and retained the same properties (**Figure 7A**) when imaged. Following administration of 2,000 highly virulent RH Strain tachyzoites intraperitoneally, the oral nanoformulation was administered by gavage using a 21 gauge needle. This was given either (1) as a single dose of 5, 10, or 20 mg/kg, or (2) three daily doses of 10 mg/kg given for the first 3 days after infection. After 5 days the RH strain tachyzoites in peritoneal fluid of each mouse were quantitated by measurement of YFP they expressed using a fluorimeter and by quantitating parasites present in peritoneal fluid using a hemocytometer. Parasite burden was reduced by ∼60% 5 days later following the single doses of 10 and 20 mg/kg (representative experiment with 10 mg/kg shown in **Figure 7B**; $p < 0.03$) and markedly reduced with three doses of 10 mg/kg administered on each of the first 3 days after intraperitoneal injection of the virulent RH strain tachyzoites (**Figure 7C**, representative experiment, $p < 0.001$). This is the proof of principle that will facilitate media milling, dispersant, and a self disintegrating tablet in the future. JAG21 has real promise as a mature lead compound to treat both *T. gondii* and Plasmodium species infections.

DISCUSSION

T. gondii infections are highly prevalent and the impact of this disease can be devastatingly severe. Current treatments have toxicity or hypersensitivity side effects. New compounds that are without toxicity or hypersensitivity, and that are highly active against tachyzoites would be of considerable clinical usefulness. Further, no medicines are active against the encysted stage or definitively curative. In addition, malaria is lethal for 1 child every 11 s and a threat to travelers going to endemic areas. Development of drug resistance also increases the need for new anti-malarial compounds. Our goal in this work herein was to identify compounds highly effective against *T. gondii* and *P. falciparum*, and we believe we have achieved our goal by developing lead compounds with dual activity.

To further develop the THQ series, 54 compounds were synthesized to improve kinetic solubility, solubility in physiologically-relevant media (FaSSIF, FeSSIF), and metabolic stability (microsomes and hepatocytes), and other ADMET properties. Compounds JAG50 and JAG21 were identified as lead compounds, demonstrating potent inhibition on both tachyzoites and bradyzoites life stages and were not toxic to human cells in our *in vitro* model (HFF). In addition, both compounds displayed low nanomolar efficacy against multiple drug resistant strains of *P. falciparum in vitro*. JAG50 and JAG21 demonstrate promising ADMET properties, with JAG21 slightly superior due to the compound's longer metabolic stability in human and mouse microsomes.

A striking result with JAG21 in our *in vivo* parasite studies is the compound's high efficacy against *T. gondii* tachyzoites and bradyzoites. In our *P. berghei in viv*o model for malaria, we observed that a single dose causal prophylaxis in 5 C57BL/6 albino mice at 2.5 mpk dosed on day 0, 1 h after intravenous administration of 10,000 *P. berghei* sporozoites was achieved. Causal prophylaxis was also observed after a 3-dose treatment in 5 C57BL/6 albino mice at 0.6 mpk dosed on days −1, 0, and +1. A representative figure at a higher dose (5 mg/kg) is shown, and all experiments with the amounts mentioned above demonstrated identical high efficacy in luminescence, parasitemia, and survival results. This demonstrates that JAG21 functions better in this *in vivo* model than the ELQ 300 series where prodrug formulation is required to achieve solubility and efficacy, in contrast to the efficacy of JAG21 at 2.5 mg/kg in a single oral dose model resulting in cure without a prodrug. ELQ 300 (not the prodrug) was not effective at doses between 1 and 20 mg/kg although the prodrug was more effective (Doggett et al., 2012; Frueh et al., 2017).

JAG50 and JAG21 are lead compounds, with JAG21 being a superior compound due to its favorable predicted ADMET properties, potency, efficacy, and lack of toxicity. JAG21 demonstrates increased solubility and potential for advanced formulation. There also is potential for improving solubility and reducing toxicity further because of the larger binding pocket in the apicomplexan Cytbc1 enzyme compared with the mammalian Cytbc1 enzyme. This was determined by modeling occupancy of the structure, enzyme assays and empirically. We have created and tested additional compounds that take advantage of these properties, although none at present, have the proven ADMET and marked *in vivo* efficacy we found to be advantageous in our proof of principle studies of JAG21. At present, however, our mature lead compound has sufficient drug like properties to move to advanced formulations, suggesting increased bulk will not be needed to reduce toxicity. It has

selectivity as demonstrated by our enzymatic, binding, and structure studies, although there are additional compounds that show even greater selectivity. It is highly effective in an oral nano preparation against *P. berghei's* three life cycle stages, and with early treatment appears to be capable of curing toxoplasmosis in immunocompetent mice. This work demonstrates the promising nature of this novel tetrahydroquinolone scaffold and mature lead compound. JAG21 has the potential to become an orally administered medicine or with partners, part of a medicine combination that is curative for toxoplasmosis and is a single dose cure for malaria. It is suitable for partnering with other compounds to obviate problems with selection of resistant mutants. We have demonstrated earlier that the parent compound with this new scaffold is synergistic with atovaquone and additive with cycloguanil (in proguanil) against *P. falciparum* (McPhillie et al., 2016). Herein, we also found synergy between JAG21 and atovaquone against *T. gondii* tachyzoites *in vitro*. This compound is a mature lead compound to treat both *T. gondii* and Plasmodium species infections. If utility and safety retained, and no toxicity appears in next stage studies, this compound may become suitable for treatment of *T. gondii* and *P. falciparum* infections.

CONCLUSION

JAG21 has real promise as a mature lead compound to treat both *T. gondii* and Plasmodium species infections, demonstrated *in vitro* and *in vivo*. It has high efficacy against *T. gondii* tachyzoites and bradyzoites, and established encysted organisms. Treatment with a single low oral dose is effective for causal prophylaxis and radical cure *of P. berghei* infections. JAG 21 has complete efficacy against three life cycle stages of *P. berghei*. In terms of companion inhibitors, JAG21, a Q_i inhibitor, synergizes against tachyzoites with atovaquone (a Q_o inhibitor) *in vitro*. It appears able to contribute modestly to protection of immune compromised mice in conjunction with tafenoquine against an initially replicating, then G1 arrested, *T. gondii* parasite that shares key transcriptomic components with *P. cynomolgi* hypnozoites. Our mature lead compound has sufficient selectivity and drug-like properties to support ongoing efforts to further develop this compound through preparation of advanced formulations and testing in additional studies of pharmacokinetics, efficacy, and safety.

DATA AVAILABILITY STATEMENT

The EM map has been deposited at the EMDB (EMDB-11002). Structure coordinates are deposited and available from Protein Data Bank under the accession code: 6XVF.

ETHICS STATEMENT

This animal study was reviewed by, approved by, and carried out in accordance with regulations of the University of Chicago IACUC and IBC and of The Home Office of the UK Government under the Animals [Scientific Procedures] Act 1986. All work in the UK with mice was covered by License PPL60/4568, Treatment and Prevention of Toxoplasmosis with approval by the University of Strathclyde ethical review board.

AUTHOR CONTRIBUTIONS

MM, RM, MH, HL, SNM, CF, CR, SPM, GB, SA, KR, RKP, and YZ conceptualized and designed the overall study. MM, RM, MH, and HL wrote manuscript. All authors wrote subparts of manuscript, performed experiments, and/or analyzed data. All authors reviewed and edited manuscript in final form.

FUNDING

This work was supported by NIAID NIH DMID U01 AI082180 (RM) and the National Institute of Diabetes and Digestive and Kidney Diseases (NIDDK) Grant #5T35DK062719-28 to FH. This was also supported by National Institutes of Health (NIH) contract number HHNS272200900007C, NIH. National Institute of Allergy and Infectious Diseases of the National Institutes of Health (NIAID) award numbers R01AI071319(NIAID) and R01AI027530 (NIAID) (RM); NIAID contract Number HHNS272200900007C; NIAID award number U19AI110819 (HL): NIAID award number U01 AI077887(NIAID) and Defense Threat Reduction Agency award number 13-C-0055, and Department of Defense award numbers W911NF-09-D0001 and W911SR-07-C0101(MH). This work was also supported by R01 AI128356 to SNM. The work also was supported by the Bill and Melinda Gates Foundation (BMGF, OPP1150755) (RKP). This material is based upon work supported by the National Science Foundation Graduate Research Fellowship under Grant No. #DGE-1656466 awarded to KR. RJ was funded by a Ph.D scholarship by the Wellcome Trust (109158/B/15/Z).

ACKNOWLEDGMENTS

We thank and gratefully also acknowledge the support of the Cornwell Mann family, the Rodriguez, Musillami, Quinn, Rosenthal, Greenberg, Morel, Rooney and Engel families, Taking out Toxo, and The Toxoplasmosis Research Institute. We would like to thank beamline scientists at Proxima2, Synchrotron Soeil, France, Proposal 20161037 and iNEXT (Proposal 1728) for Financial support for synchrotron access. We thank Abigail Spedding and Nisha Pokar for their assistance in helping JG at Leeds University with compound synthesis, and Ryan Gonciarz ('RG') for his compound RG38. We also acknowledge the assistance of Leon Wang, Ph.D of Princeton University with size determination for the final step of nanoformulation for this proof of principle study. Dennis Steindler kindly provided the primary human brain neuronal stem cells used in this study.

SUPPLEMENTARY MATERIAL

The Supplementary Material for this article can be found online at: https://www.frontiersin.org/articles/10.3389/fcimb.2020.00203/full#supplementary-material

REFERENCES

Amporndanai, K., Johnson, R. M., O'Neill, P. M., Fishwick, C. W. G., Jamson, A. H., Rawson, S., et al. (2018). X-ray and cryo-EM structures of inhibitor-bound cytochrome bc 1 complexes for structure-based drug discovery. *IUCrJ* 5, 200–210. doi: 10.1107/S2052252518001616

Anders, S., Pyl, P. T., and Huber, W. (2015). HTSeq–a Python framework to work with high-throughput sequencing data. *Bioinformatics* 31, 166–169. doi: 10.1093/bioinformatics/btu638

Battye, T. G., Kontogiannis, L., Johnson, O., Powell, H. R., and Leslie, A. G. (2011). iMOSFLM: a new graphical interface for diffraction-image processing with MOSFLM. *Acta Crystallogr. Sect. D* 67, 271–281. doi: 10.1107/S0907444910048675

Bradbury, R. H., Allot, C. P., Dennis, M., Girdwood, J. A., Kenny, P. W., Major, J. S., et al. (1993). New nonpeptide angiotensin II receptor antagonists. 3. Synthesis, biological properties, and structure-activity relationships of 2-alkyl-4-(biphenylylmethoxy)pyridine derivatives. *J. Med. Chem.* 36, 1245–1254.

Capper, M. J., O'Neill, P. M., Fisher, N., Strange, R. W., Moss, D., Ward, S. A., et al. (2015). Antimalarial 4(1H)-pyridones bind to the Qi site of cytochrome bc1. *Proc. Natl. Acad. Sci. U.S.A.* 112, 755–760. doi: 10.1073/pnas.1416611112

Caumes, E., Bocquet, H., Guermonprez, G., Rogeaux, O., Bricaire, F., Katlama, C., et al. (1995). Adverse cutaneous reactions to pyrimethamine/sulfadiazine and pyrimethamine/clindamycin in patients with AIDS and toxoplasmic encephalitis. *Clin. Infect. Dis.* 21, 656–658. doi: 10.1093/clinids/21.3.656

Chen, L. F., Han, X. L., Li, F. X., Yao, Y. Y., Fang, J. P., and Liu, X. J., et al. (2018). Comparative studies of *Toxoplasma gondii* transcriptomes: insights into stage conversion based on gene expression profiling and alternative splicing. *Parasites Vect.* 11:402. doi: 10.1186/s13071-018-2983-5

Croken, M. M., Qiu, W., White, M. W., and Kim, K. (2014). Gene set enrichment analysis (GSEA) of *Toxoplasma gondii* expression datasets links cell cycle progression and the bradyzoite developmental program. *BMC Genomics* 15:515. doi: 10.1186/1471-2164-15-515

Cubi, R., Vembar, S. S., Biton, A., Franetich, J. F., Bordessoulles, M., and Sossau, D. (2017). Laser capture microdissection enables transcriptomic analysis of dividing and quiescent liver stages of Plasmodium relapsing species. *P cynomogli. Cell. Microbiol.* 19. doi: 10.1111/cmi.12735

Delair, E., Latkany, P., Noble, A. G., Rabiah, P., McLeod, R., and Brézin, A. (2011). Clinical manifestations of ocular toxoplasmosis. *Ocul. Immunol. Inflamm.* 19, 91–102. doi: 10.3109/09273948.2011.564068

Doggett, J. S., Nilsen, A., Forquer, I., Wegmann, K. W., Jones-Brando, L., Yolken, R. H., et al. (2012). Endochin-like quinolones are highly efficacious against acute and latent experimental toxoplasmosis. *Proc. Natl. Acad. Sci. U.S.A.* 109, 15936–15941. doi: 10.1073/pnas.1208069109

Emsley, P., and Cowtan, K. (2004). Coot: model building tools for molcular graphics. *Acta Cryst. D*60, 2126–2132. doi: 10.1107/S0907444904019158

Emsley, P., Lohkamp,B., Scott, W. G., and Cowtan, K. (2010). Features and development of coot. *Acta Crystallogr. D* 66, 486–501. doi: 10.1107/S0907444910007493

Evans, P. R. (2011). An introduction to data reduction: space-group determination, scaling and intensity statistics. *Acta Crystallogr. Sect. D* 67, 282–292. doi: 10.1107/S090744491003982X

Fisher, N., Castleden, C. K., Bourges, I., Brasseur, G., Dujardin, G., and Meunier, B. (2004). Human disease-related mutations in cytochrome b studied in yeast. *J. Biol. Chem.* 279, 12951–12958. doi: 10.1074/jbc.M313866200

Fisher, N., Warman, A., Ward, S. A., and Biagini, G. A. (2009). "Chapter 17 Type II NADH: quinone oxidoreductases of *Plasmodium falciparum* and *Mycobacterium tuberculosis*: kinetic and high-throughput assays. *Methods Enzymol.* 456, 303–320. doi: 10.1016/S0076-6879(08)04417-0

Fomovska, A., Huang, Q., El Bissati, K., Mui, E. J., Witola, W. H., Cheng, G., et al. (2012b). Novel N-Benzoyl-2-hydroxybenzamide disrupts unique parasite secretory pathway. *Antimicrob. Agents Chemother.* 56, 2666–2682. doi: 10.1128/AAC.06450-11

Fomovska, A., Wood, R. D., Mui, E., Dubey, J. P., Ferreira, L. R., Hickman, M. R., et al. (2012a). Salicylanilide inhibitors of *Toxoplasma gondii*. *J. Med. Chem.* 55, 8375–8391 doi: 10.1021/jm3007596

Frueh, L., Li, Y., Mather, M., Li, Q., Pou, S., and Nilsen, A. (2017). Alkoxycarbonate ester prodrugs of preclinical drug candidate ELQ-300 for prophylaxis and treatment of malaria. *ACS Infect. Dis.* 10, 728–735. doi: 10.1021/acsinfecdis.7b00062

Gubbels, M.-J., Li, C., and Striepen, B. (2003). High-throughput growth assay for *Toxoplasma gondii* using yellow fluorescent protein. *Antimicrob. Agents Chemother.* 47, 309–316. doi: 10.1128/AAC.47.1.309-316.2003

Hutson, S. L., Mui, E., Kinsley, K., Witola, W. H., Behnke, M. S., and El Bissati, K., et al. (2010). *T. gondii* RP promoters and knockdown reveal molecular pathways associated with proliferation and cell-cycle arrest. *PLoS ONE* 5:e14057. doi: 10.1371/journal.pone.0014057

Johnson, J. D., Dennull, R. A., Gerena, L., Lopez-Sanchez, M., Roncal, N. E., and Waters, N. C. (2007). Assessment and continued validation of the malaria SYBR green I-based fluorescence assay for use in malaria drug screening. *Antimicrob. Agents Chemother.* 51, 1926–1933. doi: 10.1128/AAC.01607-06

Khan, A. A., Nasr, M., and Araujo, F. G. (1998). Two 2-hydroxy-3-alkyl-1,4-naphthoquinones with *in vitro* and *in vivo* activities against *Toxoplasma gondii*. *Antimicrob. Agents Chemother*. 42, 2284–2289. doi: 10.1128/AAC.42.9.2284

Kim, D., Langmead, B., and Salzberg, S. L. (2015). HISAT: a fast spliced aligner with low memory requirements. *Nat. Methods* 12, 357–360. doi: 10.1038/nmeth.3317

Lacerda, M. V. G., Llanos-Cuentas, A., Krudsood, S., Lon, C., Saunders, D. L., Mohammed, R., et al. (2019). Single-dose Tafenoquine to prevent relapse of *Plasmodium vivax* Malaria. *N. Engl. J. Med.* 380, 215–228. doi: 10.1056/NEJMoa1710775

Laskowski, R. A., and Swindells, M. B. (2011). LigPlot +: multiple ligand à protein interaction diagrams for drug discovery. *J. Chem. Inform. Model.* 51, 2778–2786. doi: 10.1021/ci200227u

Lebedev, A. A., Young, P., Isupov, M. N., Moroz, O. V., Vagin, A. A., Murshudov, G. N. (2012). JLigand: a graphical tool for the CCP4 template-restraint library. *Acta Crystallogr. Sect. D* 68, 431–440. doi: 10.1107/S090744491200251X

Llanos-Cuentas, A., Lacerda, M. V. G., Hien, T. T., Vélez, I. D., Namaik-Larp, C., Chu, C. S., et al. (2019). *Tafenoquine versus* primaquine to prevent relapse of *Plasmodium vivax* malaria. *N. Engl. J. Med.* 380, 229–241. doi: 10.1056/NEJMoa1802537

Love, M. I., Huber, W., and Anders, S. (2014). Moderated estimation of fold change and dispersion for RNA-seq data with DESeq2. *Genome Biol.* 15:550. doi: 10.1186/s13059-014-0550-8

Lykins, J., Wang, K., Wheeler, K., Clouser, F., Dixon, A., and El Bissati, K., et al. (2016). Understanding Toxoplasmosis in the United States through "Large Data" analyses. *Clin. Infect. Dis.* 63, 468–475. doi: 10.1093/cid/ciw356

Marcsisin, S. R., Sousa, J. C., Reichard, G. A., Caridha, D., Zeng, Q., and Roncal, N. (2014). Tafenoquine and NPC-1161B require CYP 2D metabolism for anti-malarial activity: implications for the 8-aminoquinoline class of anti-malarial compounds. *Malar. J.* 13:2. doi: 10.1186/1475-2875-13-2

McLeod, R., and Boyer, K. (2019). "Toxoplasmosis (*Toxoplasma gondii*)," in *Nelson Textbook of Pediatrics, 21st Edn* (Philadelphia, NY; Oxford: Elsevier), 528–540.

McLeod, R., Khan, A. R., Noble, G. A., Latkany, P., Jalbrzikowski, J., and Boyer, K. (2006). Severe sulfadiazine hypersensitivity in a child with reactivated congential toxoplasmic chorioretinitis. *Pediatr. Infect. Dis. J.* 25, 270–272. doi: 10.1097/01.inf.0000202070.59190.9a

McPhillie, M., Zhou, Y., El Bissati, K., Dubey, J., Lorenzi, H., and Capper, M., et al. (2016). New paradigms for understanding and step changes in treating active and chronic, persistent apicomplexan infections. *Sci. Rep.* 6:29179. doi: 10.1038/srep29179

Miley, G. P., Pou, S., Winter, R., Nilsen, A., Li, Y., and Kelly, J. X., et al. (2015). ELQ-300 prodrugs for enhanced delivery and single-dose cure of Malaria. *AAC* 59, 5555–5556. doi: 10.1128/AAC.01183-15

Muench, S. P., Prigge, S. T., McLeod, R., Rafferty, J. B., Kirisits, M. J., and Roberts, C. W. (2007). Studies of *Toxoplasma gondii* and *Plasmodium falciparum* enoyl acyl carrier protein reductase and implications for the development of antiparasitic agents. *Acta Crystallogr. D Biol. Crystallogr.* 63(Pt 3), 328–338. doi: 10.1107/S0907444906053625

Muller, I., Jex, A. R., Kappe, S. H. I., Mikolajczak, S. A., Sattabongkot, J., Patrapuvich, R., et al. (2019). Transcriptome and histone 1 epigenome of *Plasmodium vivax* salivary-gland sporozoites point to tight regulatory control and potential mechanisms for liver-stage differentiation. *Int. J. Parasitol.* 49, 501–513. doi: 10.1016/j.ijpara.2019.02.007

Murshudov, G. N., Skubák, P., Lebedev, A. A., Pannu, N. S., Steiner, R. A., Nicholls, R. A., et al. (2011). REFMAC5 for the refinement of macromolecular crystal structures. *Acta Crystallogr. Sect. D* 67, 355–367. doi: 10.1107/S0907444911001314

Ngô, H. M., Zhou, Y., Lorenzi, H., Wang, K., Kim, T. K., and Zhou, Y., et al. (2017). Toxoplasma modulates signature pathways of human epilepsy, neurodegeneration and cancer. *Sci. Rep*. 7:11496. doi: 10.1038/s41598-017-10675-6

Paredes-Santos, T. C., Martins-Duarte, E. S., de Souza, W., Attias, M., and Vommaro, R. C. (2018). *Toxoplasma gondii* reorganizes the host cell architecture during spontaneous cyst formation *in vitro*. *Parasitology* 145, 1027–1038. doi: 10.1017/S0031182017002050

Paredes-Santos, T. C., Martins-Duarte, E. S., Vitor, R. W., de Souza, W., Attias, M., and Vommaro, R. C. (2013). Spontaneous cystogenesis *in vitro* of a Brazilian strain of *Toxoplasma gondii*. *Parasitol. Int*. 62, 181–188. doi: 10.1016/j.parint.2012.12.003

Phan, L., Kasza, K., Jalbrzikowski, J., Noble, A. G., Latkany, P., Kuo, A., et al. (2008). Longitudinal study of new eye lesions in children with toxoplasmosis who were not treated during the first year of life. *Am. J. Ophthalmol*. 146, 375–384. doi: 10.1016/j.ajo.2008.04.033

Plouffe, D., Brinker, A., McNamara, C., Henson, K., Kato, N., Kuhen, K., et al. (2008). *In silico* activity profiling reveals the mechanism of action of antimalarials discovered in a high-throughput screen. *Proc. Natl. Acad. Sci. U.S.A*. 105, 9059–9064. doi: 10.1073/pnas.0802982105

Pybus, B. S., Marcsisin, S. R., Jin, X., Deye, G., Sousa, J. C., and Li, Q. (2013). The metabolism of primaquine to its active metabolite is dependent on CYP 2D6. *Malar. J*. 12:212. doi: 10.1186/1475-2875-12-212

St Jean, P. L., Xue, Z., Carter, N., Koh, G. C., Duparc, S., and Taylor, M. (2016). Tafenoquine treatment of *Plasmodium vivax* malaria: suggestive evidence that CYP2D6 reduced metabolism is not associated with relapse in the Phase 2b DETECTIVE trial. *Malar. J*. 15:97. doi: 10.1186/s12936-016-1145-5

Su, G., Morris, J. H., Demchak, B., and Bader, G. D. (2014). Biological network exploration with Cytoscape 3. *Curr. Protoc. Bioinform.* 13, 1–24. doi: 10.1002/0471250953.bi0813s47

Subramanian, A., Tamayo, P., Mootha, V. K., Mukherjee, S., Ebert, B. L., Gillette, M. A., et al. (2005). Gene set enrichment analysis: a knowledge-based approach for interpreting genome-wide expression profiles. *Proc. Natl. Acad. Sci. U.S.A*. 102, 15545–15550. doi: 10.1073/pnas.0506580102

Torgerson, P. R., and Mastroiacovo, P. (2013). The global burden of congenital toxoplasmosis: a systematic review. *Bull. World Health Organ*. 91, 501–508. doi: 10.2471/BLT.12.111732

Trager, W., and Jensen, J. B. (1976). Human malaria parasites in continuous culture. *Science* 193, 673–675.

Trager, W., and Jensen, J. B. (2005). Human malaria parasites in continuous culture. 1976. *J. Parasitol.* 91, 484–486. doi: 10.1645/0022-3395(2005)091[0484:HMPICC]2.0.CO;2

Vercesi, A. E., Rodrigues, C. O., Uyemura, S. A., Zhong, L., and Moreno, S. N. J. (1998). Respiration and oxidative phosphorylation in the apicomplexan parasite *Toxoplasma gondii*. *J. Biol. Chem*. 273:31040. doi: 10.1074/jbc.273.47.31040

Vidigal, P. V. T., Santos, D. V. V., Castro, F. C., de Couto, J. C. F., de Vitor, R. W. A., and Brasileiro Filho, G. (2002). Prenatal toxoplasmosis diagnosis from amniotic fluid by PCR. *Rev. Soc. Bras. Med. Trop*. 35, 1–6. doi: 10.1590/S0037-86822002000100001

Wallon, M., Peyron, F., Cornu, C., Vinault, S., Abrahamowicz, M., and Kopp, C. B. (2013). Congenital toxoplasma infection: monthly prenatal screening decreases transmission rate and improves clinical outcome at age 3 years. *Clin. Infect. Dis*. 56, 1223–1231. doi: 10.1093/cid/cit032

Walton, N. M., Sutter, B. M., Chen, H. X., Chang, L. J., Roper, S. N., Scheffler, B., et al. (2006). Derivation and large-scale expansion of multipotent astroglial neural progenitors from adult human brain. *Development* 133, 3671–3681. doi: 10.1242/dev.02541

Watts, E., Zhao, Y., Dhara, A., Eller, B., Patwardhan, A., and Sinai, A. P. (2015). *Toxoplasma gondii* bradyzoites within tissue cysts are dynamic and replicating entities *in vivo*. Novel approaches reveal that *Toxoplasma gondii* bradyzoites within tissue cysts are dynamic and replicating entities *in vivo*. *MBio* 6:e01155–e01115. doi: 10.1128/mBio.01155-15

Waxman, S., and Herbert, V. (1969). Mechanism of pyrimethamine-induced megaloblastosis in human bone marrow. *N. Engl. J. Med*. 280, 1316–1319. doi: 10.1056/NEJM196906122802402

Zhang, J., Tan, P., Guo, L., Gong, J., Ma, J., Li, J., et al. (2016). p53-dependent autophagic. Cryo-EM of cellular machineries. *Proc. Natl. Acad. Sci. U.S.A*. 113, 11519–11524. doi: 10.1073/pnas.1609482113

Zheng, S. Q., Palovcak, E., Armache, J. P., Verba, K. A., Cheng, Y., and Agard, D. A. (2017). MotionCor2 - anisotropic correction of beam-induced motion for improved cryo-electron microscopy. *Nat. Methods* 14, 331–332. doi: 10.1038/nmeth.4193

Conflict of Interest: RM, MM, CF, CR, KE, MH, QL, and HL are inventors on an International patent application PCT/US2016/067795 pertinent to the work in this study. RM has completed an unrelated literature review for Sanofi-Pasteur.

The remaining authors declare that the research was conducted in the absence of any commercial or financial relationships that could be construed as a potential conflict of interest.

Received: 20 February 2020; Accepted: 16 April 2020; Published: 09 June 2020

Citation: McPhillie MJ, Zhou Y, Hickman MR, Gordon JA, Weber CR, Li Q, Lee PJ, Amporndanai K, Johnson RM, Darby H, Woods S, Li Z, Priestley RS, Ristroph KD, Biering SB, El Bissati K, Hwang S, Hakim FE, Dovgin SM, Lykins JD, Roberts L, Hargrave K, Cong H, Sinai AP, Muench SP, Dubey JP, Prud'homme RK, Lorenzi HA, Biagini GA, Moreno SN, Roberts CW, Antonyuk SV, Fishwick CWG and McLeod R (2020) Potent Tetrahydroquinolone Eliminates Apicomplexan Parasites. Front. Cell. Infect. Microbiol. 10:203. doi: 10.3389/fcimb.2020.00203

frontiers in Cellular and Infection Microbiology

BRIEF RESEARCH REPORT
published: 02 July 2020
doi: 10.3389/fcimb.2020.00295

A Homolog of Structural Maintenance of Chromosome 1 Is a Persistent Centromeric Protein Which Associates With Nuclear Pore Components in *Toxoplasma gondii*

Maria E. Francia[1†], Sheila Bhavsar[1], Li-Min Ting[2], Matthew M. Croken[3], Kami Kim[2], Jean-Francois Dubremetz[4] and Boris Striepen[1,5*†]*

[1] Department of Cellular Biology, University of Georgia, Athens, GA, United States, [2] Morsani College of Medicine, University of South Florida Health, Tampa, FL, United States, [3] Pathology, Molecular and Cell Based Medicine, Mount Sinai Medical Center, New York, NY, United States, [4] UMR 5235 CNRS, Université de Montpellier 2, Montpellier, France, [5] Center for Tropical and Emerging Global Diseases, University of Georgia, Athens, GA, United States

Apicomplexa are obligate intracellular parasites which cause various animal and human diseases including malaria, toxoplasmosis, and cryptosporidiosis. They proliferate by a unique mechanism that combines physically separated semi-closed mitosis of the nucleus and assembly of daughter cells by internal budding. Mitosis occurs in the presence of a nuclear envelope and with little appreciable chromatin condensation. A long standing question in the field has been how parasites keep track of their uncondensed chromatin chromosomes throughout their development, and hence secure proper chromosome segregation during division. Past work demonstrated that the centromeres, the region of kinetochore assembly at chromosomes, of *Toxoplasma gondii* remain clustered at a defined region of the nuclear periphery proximal to the main microtubule organizing center of the cell, the centrosome. We have proposed that this mechanism is likely involved in the process. Here we set out to identify underlying molecular players involved in centromere clustering. Through pharmacological treatment and structural analysis we show that centromere clustering is not mediated by persistent microtubules of the mitotic spindle. We identify the chromatin binding factor a homolog of structural maintenance of chromosomes 1 (SMC1). Additionally, we show that both TgSMC1, and a centromeric histone, interact with TgExportin1, a predicted soluble component of the nuclear pore complex. Our results suggest that the nuclear envelope, and in particular the nuclear pore complex may play a role in positioning centromeres in *T. gondii*.

Keywords: centromere, cohesin, nuclear pore, centrosome, cell division, microtubues, toxoplasma, toxoplasmosis

OPEN ACCESS

Edited by:
Tiago W. P. Mineo, Federal University of Uberlandia, Brazil

Reviewed by:
Raj Gaji, University of Michigan, United States
Andréa Rodrigues Ávila, Instituto Carlos Chagas (ICC), Brazil

***Correspondence:**
Maria E. Francia
mfrancia@pasteur.edu.uy
Boris Striepen
striepen@vet.upenn.edu

†Present address:
Maria E. Francia, Laboratory of Apicomplexan Biology, Institut Pasteur de Montevideo, Montevideo, Uruguay; Departamento de Parasitología y Micología, Facultad de Medicina, Universidad de la Republica, Montevideo, Uruguay
Boris Striepen, Department of Pathobiology, School of Veterinary Medicine, University of Pennsylvania, Philadelphia, PA, United States

Specialty section:
This article was submitted to Parasite and Host, a section of the journal Frontiers in Cellular and Infection Microbiology

Received: *11 March 2020*
Accepted: *19 May 2020*
Published: *02 July 2020*

Citation:
Francia ME, Bhavsar S, Ting L-M, Croken MM, Kim K, Dubremetz J-F and Striepen B (2020) A Homolog of Structural Maintenance of Chromosome 1 Is a Persistent Centromeric Protein Which Associates With Nuclear Pore Components in Toxoplasma gondii. Front. Cell. Infect. Microbiol. 10:295. doi: 10.3389/fcimb.2020.00295

INTRODUCTION

Apicomplexa are obligate intracellular parasites that cause various animal and human diseases including malaria, toxoplasmosis, and cryptosporidiosis. Apicomplexan parasites invade and replicate within the cells of their hosts. Following intracellular replication, parasites lyse their host cell and invade a neighboring healthy cell thus perpetuating

the infection. Apicomplexan parasites replicate by modes of division that differ from those used by their hosts (Francia and Striepen, 2014). Mammalian cells divide their nucleus by open mitosis in which the nuclear envelope breaks down, giving way to the mitotic spindle, and is immediately followed by cytokinesis (with few exceptions). Apicomplexa, however, combine semi-closed mitosis, in which the nuclear envelope remains practically intact, with the generation of multiple daughter cells by budding (Gubbels et al., 2008; Francia and Striepen, 2014; White and Suvorova, 2018) (schematically represented in **Figure 1A**). In apicomplexan cell division, daughter cells do not derive from fission but instead are formed *de novo* in the mother cell cytosol. The fundamental differences between these modes suggest that cell division could be a rich source of druggable targets to treat apicomplexan-caused diseases. However, many structural and regulatory aspects of apicomplexan cell division are not well-understood (White and Suvorova, 2018).

Direct visualization of chromosomes is impaired by the apparent lack of chromatin condensation throughout the cell cycle in the parasites' nuclei. Centromeres are typically a single location on a chromosome where kinetochore components, the point of attachment for microtubules of the mitotic spindle, assemble during mitosis. Centromeres are marked by the presence of a variant histone H3, known as CenH3 or CenPA. In the past, a *T. gondii* strain bearing an epitope tag in its CenH3 homolog, allowed visualization of the centromere-associated nucleosomes, allowing the mapping of the chromosomal position of the centromeres in *T. gondii*, and visualization of chromosomal dynamics during mitosis (Brooks et al., 2011). All stages observed in canonical eukaryotic mitosis (i.e., metaphase, anaphase, and telophase) are present in the *T. gondii* mitosis. However, all centromeres of *T. gondii* cluster into a single location at the periphery of the nucleus, not only during division but also outside of mitosis (Brooks et al., 2011). Moreover, the site of centromere clustering is intimately related to the position of the centrosome, the main microtubule organizing center (MTOC) of the cell, which nucleates microtubules of the mitotic spindle during division. Centromeres of *Plasmodium falciparum* were also shown to cluster in the proximity of its centrosome equivalent outside of mitosis (Hoeijmakers et al., 2012). Interestingly, while *T. gondii*, divides by endodyogeny, assembling two daughter cells every round of division, *P. falciparum*'s schizogony can yield hundreds of daughters per division. Thus, centromere clustering appears to be a widespread phenomenon among apicomplexans using different modes of division (Bunnik et al., 2019).

The molecular mechanisms mediating chromatin sequestration to defined nuclear territories and specialized sub-compartments are unknown in Apicomplexa. Here, we set out to identify novel molecular players involved in centromere positioning in *Toxoplasma gondii*.

METHODS

Chromatin Immunoprecipitation

ChIP was performed as described in Wells and Farnham (2002), Gissot et al. (2007), and Brooks et al. (2011). Briefly, chromatin from SMC1-HA transgenic tachyzoites was cross-linked for 10 min with 1% formaldehyde at room temperature and purified after sonication yielding fragments of 500–1,000 bp. Chromatin was immunoprecipitated at 4°C overnight using a HA polyclonal antibody (Abcam ab9110) and washed extensively. The DNA was treated with proteinase K for 2 h and subsequently purified using the Qiagen PCR purification kit. Hundred nanogram of precipitated DNA was amplified using the DNA Genomeplex whole genome amplification kit (Sigma) and subsequently labeled using random primers coupled to a fluorochrome. Probes were hybridized to a tiled oligonucleotide array representing the complete *T. gondii* genome according to NimbleGen Systems procedures. The array was fabricated by NimbleGen Systems and contained 740,000 oligonucleotides representing version 4 of the ME49 genome with an approximate spacing of 80 bp between each oligonucleotide.

Co-immunoprecipitation (Co-IP) and Mass Spectrometry Analysis

Approximately 1×10^9 SMC1_YFP, RHΔKu80 or the HA-tagged lines generated in this study (TgImportin1-HA, TgExportin1-HA, TgSUN-HA), were collected by centrifugation, and washed once with PBS. Parasites were lysed by resuspension in hypotonic buffer (20 mM Hepes, 10 mM KCl, 400 mM Mannitol, 2 nM EDTA) supplemented with EDTA free protease inhibitor (Roche) to $\sim 5 \times 10^8$ parasites/ml, followed by 4 cycles of freeze/thaw with liquid nitrogen. Efficient lysis was assessed by light microscopy. Debris and intact parasites were pelleted by centrifugation at 10,000 g for 10 min at 4°C. Soluble fractions were incubated overnight at 4°C with 20 µl of the antibody of interest. The next day, 100 µl of Sepharose bound Protein A or Protein G (Santa Cruz) for rabbit or mouse antibody, respectively, were added and incubated at room temperature for 2 h. Complexes were washed six times with Co-IP wash buffer (50 mM Tris pH 8, 200 mM NaCl, 2 mM EDTA, 1% NP-40) supplemented with protease inhibitor, then resuspended in 200 µl of SDS-PAGE loading buffer and boiled for 5 min. Elution fractions were used either for mass spectrometry or western blotting. Negative controls were performed using the pre-immune serum for each antibody or ProteinA/G Sepharose alone. Four independently obtained samples were analyzed. Sample 1 consisted of proteins obtained from a wild type parasite strain using rabbit serum raised against TgSMC1. Sample 2 was obtained using the same a-TgSMC1 antibody but subjected to affinity purification prior to the experiment. Sample 3 consisted of proteins obtained from the TgSMC1-YFP strain using a-GFP and Sample 4 was obtained from a wild type strain using a-GFP, and served as a negative control. **Figure 4A** shows sample 3 as a representative example of the immunoprecipitation scheme.

Construction of Tagged Reporter Parasites

Toxoplasma gondii RH strain parasites were maintained by serial passage in human foreskin fibroblast (HFF) cells and genetically manipulated as previously described (Jacot et al., 2013). To tag the genomic locus of TgSMC1, TgExportin1, TgImportin1, and TgSUN1 with a 3xHA or a YFP tag, ∼1,500 bp of the open reading frame ending before the stop codon were amplified from *T. gondii* genomic DNA. All primer sequences used are

shown in **Table S2**. These amplicons were cloned via ligation independent cloning (LIC) (Aslanidis and de Jong, 1990) into the pLIC-HA-CAT or pLIC-YFP-DHFR vector, respectively, to create in-frame fusions (Huynh and Carruthers, 2009). Transgenic clones were established by transfection of ΔKu80-TaTi parasites and chloramphenicol or pyrimethamine selection, respectively. Integration was confirmed by PCR and western blot in all cases.

Protein Expression and Antibody Production

Sequences encoding for the last 400 C-terminal amino-acids of TgSMC1 were amplified from *T. gondii* cDNA and inserted into plasmid pAVA-421 6xHis (Alexandrov et al., 2004). Recombinant fusion protein was purified on Ni^2-NTA resin (Qiagen, Hilden, Germany). Rabbits were immunized with 1 mg of purified protein, and serum was collected after 10 weeks (Cocalico Biologicals, Reamstown, PA, USA). Mice were immunized with 0.4 mg of purified protein, and serum was collected after 3 weeks.

Fluorescence Microscopy

For immunofluorescence assays, host cells (HFF) were inoculated onto coverslips and infected with parasites. Coverslips were fixed 24 h after infection and processed as previously described (Francia et al., 2011). Primary antibodies used were mouse anti-alpha tubulin at a dilution of 1:1,000 (12G10, a gift of Jacek Gaertig, University of Georgia), rabbit anti-Centrin1 at 1:1,000 (gift of Iain Cheeseman, MIT), mouse anti-GFP at 1:1,000–1:400 (Torry Pines Biolabs), rat anti-HA at 1:1,000 (clone 3F10, Roche), mouse anti-IMC1 mAb 45.15 at 1:1,000 (gift of Gary Ward, University of Vermont), mouse anti-TgChromo1 at 1:1,000 (Gissot et al., 2012), mouse anti-CenH3 (Francia et al., 2012) at 1:20, rabbit anti-MORN1 (Gubbels et al., 2006) at 1:250, and rabbit and mouse anti-SMC1 at 1:1,000 (this study). The secondary antibodies used were AlexaFluor 350, AlexaFluor 488, and AlexaFluor 546 (Invitrogen), at a dilution of 1:2,000. Images were collected on an Applied Precision Delta Vision inverted epifluorescence microscope using a UPlans APO 100×/1.40 oil lens. Images were subjected to deconvolution and contrast adjustment using Applied Precision software (Softworx). For quantitative image analysis (as described in the results section) a minimum of 50 vacuoles were scored in at least three independent experiments. Super-Resolution images were acquired using the Zeiss ELYRA S1 (SR-SIM) microscope. Images were collected and processed using Zeiss Zen software. Means and standard deviations were calculated and plotted using Graph Pad Prism Version 5.0c (La Jolla, California, USA).

Transmission Electron Microscopy

Infected cells were fixed in 2% glutaraldehyde in sodium phosphate buffer 0.1 M, pH 7.4, followed by post-fixation with 1% osmium tetroxide in sodium phosphate buffer, alcohol dehydration, and Epon resin embedding. Serial sections were obtained with a Leica UCT cryo-ultramicrotome, collected in carbon coated single hole grids and observed in a JEOL 1200 EX transmission electron microscope.

Western Blotting

Western blotting was performed as previously described (Brooks et al., 2011). We used anti-HA (Roche) antibodies at a dilution of 1:1,000, anti-tubulin at 1:1,000, anti-GFP at 1:500, anti-CenH3 at 1:500 and anti-SMC1 antibodies at a dilution of 1:1,000. Pre-immune sera for anti-SMC1 antibodies were used at a comparable dilution. Horseradish peroxidase (HRP)-conjugated anti-rat, anti-mouse, or anti-rabbit antibody (Pierce) were used at a dilution of 1:20,000

RESULTS

To investigate the mechanism mediating centromere clustering in *T. gondii* we propose to test two alternative hypotheses. First, we envision that a persistent microtubules spindle could constitutively interact with centromeres, thus maintaining their position, and ascribing the centrosome (MTOC) direct involvement in the process (**Figure 1B**). Alternatively, proteins present at the centromere mediate the interaction between it and the nuclear envelope (**Figure 1B**).

We first set out to investigate whether microtubules mediate centromere clustering. To test this, we subjected parasites to treatment with oryzalin, a tubulin-binding drug which prevents tubulin polymerization in Apicomplexa (Stokkermans et al., 1996; Morrissette et al., 2004). At concentrations of 2.5 mM oryzalin prevents polymerization of microtubules into daughter cells as well as the mitotic spindle (Stokkermans et al., 1996). Parasites expressing TgCenH3-HA (Brooks et al., 2011), a marker for centromeres, were subjected to treatment with 2.5 mM oryzalin for 24 h, fixed and observed by immunofluorescence assay (IFA) staining for a-HA and a-IMC1. IMC1 (Inner membrane complex protein 1) marks of the outline of dividing and non-dividing parasites. In dividing parasites, IMC1 labels the emerging daughter cell structures (**Figure 1C**). Upon drug treatment, parasites continue to grow and replicate their DNA but fail to assemble daughter cells (**Figure 1C**). Interphase as well as dividing parasites treated with oryzalin exhibit continued clustered localization for TgCenH3 (**Figures 1B,C**). These results suggested that the mitotic spindle is likely not responsible for centromere clustering during interphase. However, consistent with previous reports that oryzalin disrupts nuclear division (Morrissette and Sibley, 2002b), we note that oryzalin-treated parasites frequently fail to segregate their genome properly (**Figure 1C**). However, we cannot rule out incomplete spindle disruption upon drug treatment.

To independently examine interphase nuclei in *T. gondii*, we serially sectioned fixed parasites and observed them by transmission electron microscopy (**Figures 1D,E**). In all cases, the entire nucleus was sectioned and in most sets sections spanned the entire parasite. Parasites were assigned to interphase by the presence of a single, unduplicated centrosome, and the absence of budding daughters. Upon three dimensional reconstruction, we observed that while spindle microtubules are readily observed in dividing parasites (duplicated centrosomes) (**Figure 1E**) they cannot be detected in interphase parasites (**Figure 1D**). Overall, we could detect intranuclear microtubules

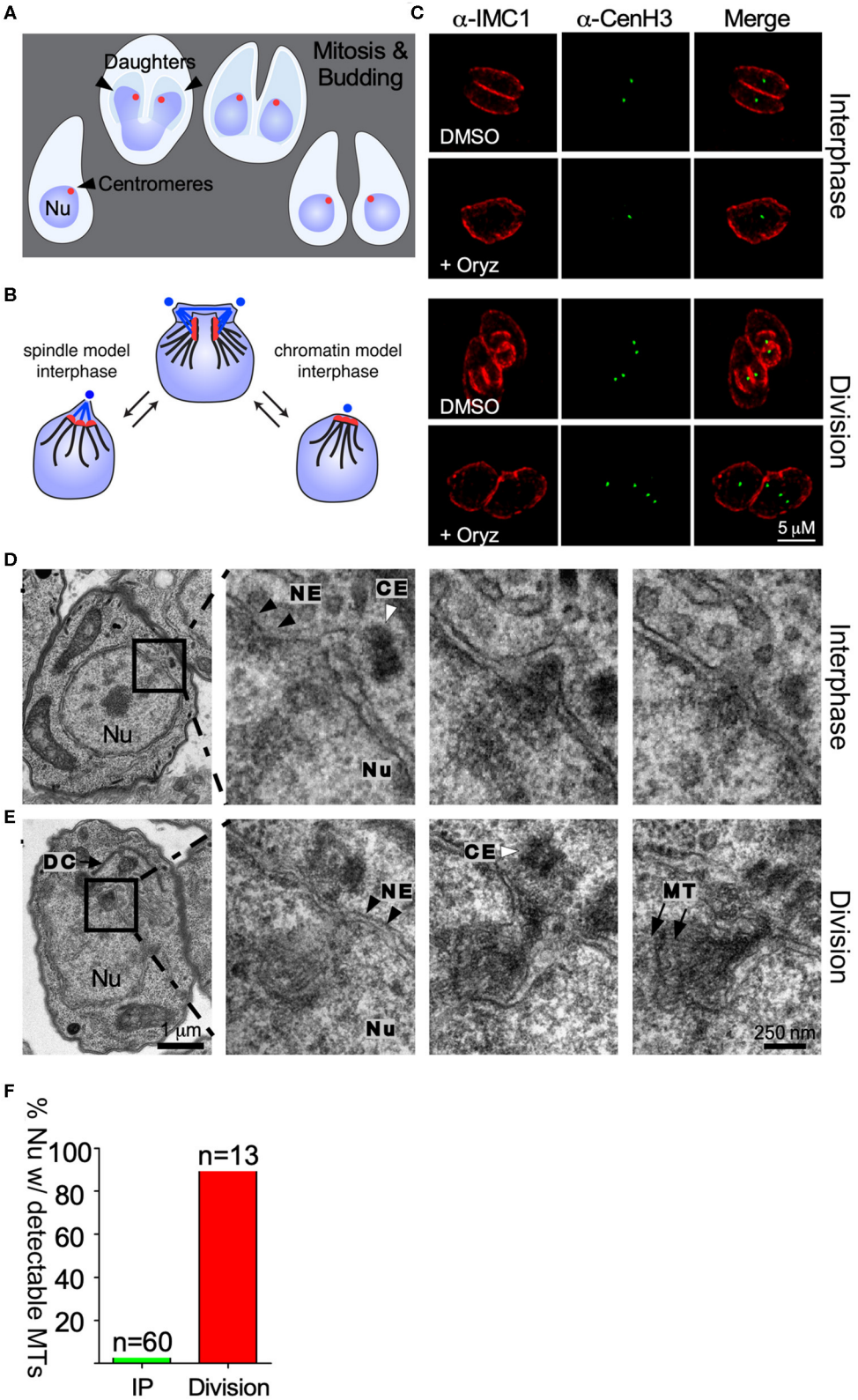

FIGURE 1 | Centromere clustering is not mediated by spindle microtubules. **(A)** Apicomplexan parasite division schematic. Apicomplexa divide by closed mitosis and internal daughter cell assembly. Centromeres (represented as a red dot) remain clustered at the periphery of the nucleus throughout the cell cycle. **(B)** Alternative

(Continued)

FIGURE 1 | models proposed to explain centromere clustering. Blue dots represent the centrosome. Blue lines represent the mitotic spindle microtubules. Red dots represent the chromosomes' centromeres. **(C)** Parasites were treated with DMSO (control) or 2.5 mM Oryzalin, fixed and stained with anti-IMC1 and anti-CenH3. Both in DMSO and Oryzalin treated samples, interphase parasites display a single TgCenH3 dot corresponding to clustered centromeres. Both Oryzalin treated and untreated dividing parasites display duplicated TgCenH3 foci. In Oryzalin treated parasites daughter cell assembly and proper chromosome segregation is impaired as evidenced by the presence of multiple (>2) TgCenH3 foci within a single parasite. **(D)** TEM series through a parasite in interphase containing a single centrosome (CE, white arrowhead). Zoomed-in panels show consecutive series. Microtubules (MT) are not seen proximal to the centrosome (CE, white arrowheads) or the nuclear envelope (NE, black arrowheads) at the site of centromere sequestration. **(E)** TEM series through a dividing nucleus. A forming daughter cell (DC) is detectable proximal to the nucleus (Nu). The mitotic spindle organizes within the nuclear envelope (NE, black arrowheads). Zoomed-in panels show consecutive series. Microtubules (MT, black arrows) of the mitotic spindle are clearly visible in the proximity of the centrosome (CE, white arrowhead). Note that all serial sections were obtained from the same block, and thus were subject to identical fixation and post-fixation treatments. The scale for **(D,E)** is the same. **(F)** Parasites present in TEM serial sections were classified as "interphase" (IP) or "dividing", depending on the presence of a single or a duplicated centrosome respectively, and scored for the presence of visible spindle microtubules.

in 98% of the dividing parasites ($n = 13$), while microtubules were seen only in 4% of nuclei considered to be in interphase by our morphological criteria ($n = 60$) (**Figure 1F**). The latter may represent parasites just emerged from mitosis.

Local actin polymerization was reported to affect telomere positioning in the *P. falciparum* nucleus (Zhang et al., 2011). To assess a potential role of actin in centromere clustering, parasites were treated with Cytochalasin D, an actin de-polymerizing agent. Treated parasites did not exhibit centromere dispersion (**Figure S1B**). Similarly, *a T. gondii* temperature sensitive mutant of the nuclear actin ARP4 exhibits normal centromere clustering at the restrictive temperature (**Figure S1D**) (Suvorova et al., 2012). Taken together, our pharmacological, ultra-structural and genetic analysis, strongly suggest that neither microtubules nor actin filaments are responsible for persistent centromere clustering in interphase.

We next set out to identify chromatin-binding factors which could potentially mediate centromere clustering by *in silico* identification of known centromeric proteins. Structural Maintenance of Chromosome proteins (SMCs) are a family of ATPases with multiple roles in chromatin organization during mitosis and meiosis (Jeppsson et al., 2014; Uhlmann, 2016). Homologs of Structural Maintenance of Chromosomes 1 (SMC1) have been implicated in the control of gene expression, DNA repair and recombination, cross linking of mitotic spindle microtubules and membrane anchoring of heterochromatin (Nasmyth and Haering, 2009; Wong, 2010). Importantly, the yeast and *Drosophila* SMC1s have been shown to directly associate with the centromeric histone H3 (Nasmyth and Haering, 2009; Wong, 2010). Searching for homologs of the *Saccharomyces cerevisiae* SMCs we identified four candidate genes for SMC proteins in the *T. gondii* genome (**Figure S2A**). Maximum likelihood phylogenetic tree of the full length protein coding sequences showed that each of *T. gondii*'s predicted SMC protein coding genes clustered with a given SMCs sub-class.TgME49_288700 clusters with SMC1-like SMCs; TgME49_297800 is more closely related to SMC2 from yeast and plants, while TgME49_106310 and TgME49_231170 are homologous to SMC3 and SMC4, respectively (**Figure S2A**).

To further investigate the SMC1 homolog in *T. gondii* we generated strains with an insertion of a triple HA tag or a yellow fluorescent protein (YFP) cassette at the 3′ end of TgME49_288700 (from here on referred to as TgSMC1, **Figure S2B**). In addition, we raised mouse and rabbit anti-sera against a recombinant C-terminal fragment of TgSMC1 consisting of the 400 C-termini amino-acids of the protein. These anti-sera recognize a single protein of a size consistent with the predicted molecular mass of 183 kD (or 211 for the YFP fusion protein, respectively, **Figure S2C**). Using these reagents we investigated the localization of TgSMC1 by IFA. When co-stained with a monoclonal antibody raised against TgCenH3 (Brooks et al., 2011) we observed that TgSMC1 nuclear punctae coincide with TgCENH3 both in interphase and in dividing parasites (**Figures 2A,B**). Interestingly, when observed by structured Illumination super resolution microscopy (SIM-SR), the localization of TgSMC1 is better defined as a semi-circle arranged around the spot filled by the centromeres marked by TgCenH3 (**Figures 2C,D**).

To unequivocally determine whether TgSMC1 is a centromeric protein, we immunoprecipitated TgSMC1-associated chromatin, and probed a microarray chip covering most of the *T. gondii* genome with the precipitated DNA (ChIP-CHIP). Significant hybridization was obtained for 10 chromosomes. The hybridization peaks for chromosomes II, III, V, VI, and VIII-XI coincide with the position of the centromere on these chromosomes as mapped by ChIP-CHIP of TgCenH3 (**Figure 2E**). Moreover, TgSMC1 ChIP-CHIP hybridization signal shows almost perfect overlap with the chromatin regions bound by TgCENH3 (**Figure 2F**). Taken together, TgSMC1 localization appears intimately linked to the centromere.

Lastly, we determined potential interactors of TgSMC1 by co-immunoprecipitation (**Figures 3A,B**). Proteins co-immunoprecipitated with TgSMC1 were identified by LC-MS. TgSMC1's elution fraction contains a significant amount of TgCenH3, suggesting that not only do they co-localize at the centromere but they also interact physically (**Figure 3C**). In contrast, TgChromo1 (Gissot et al., 2012) which binds chromatin immediately adjacent to the centromeres, does not co-precipitate with TgSMC1 (**Figure 3C**).

The ten most abundant proteins recovered in all four purifications are shown in **Figure 3D**. A complete list of LC-MS results can be found in **Table S1** ordered by ascending order of accession number in the *T. gondii* genome database (Kissinger et al., 2003). Four protein-coding genes, one being TgSMC1, showed the highest number of unique peptides in all three positive samples, and a 10-fold enrichment in number

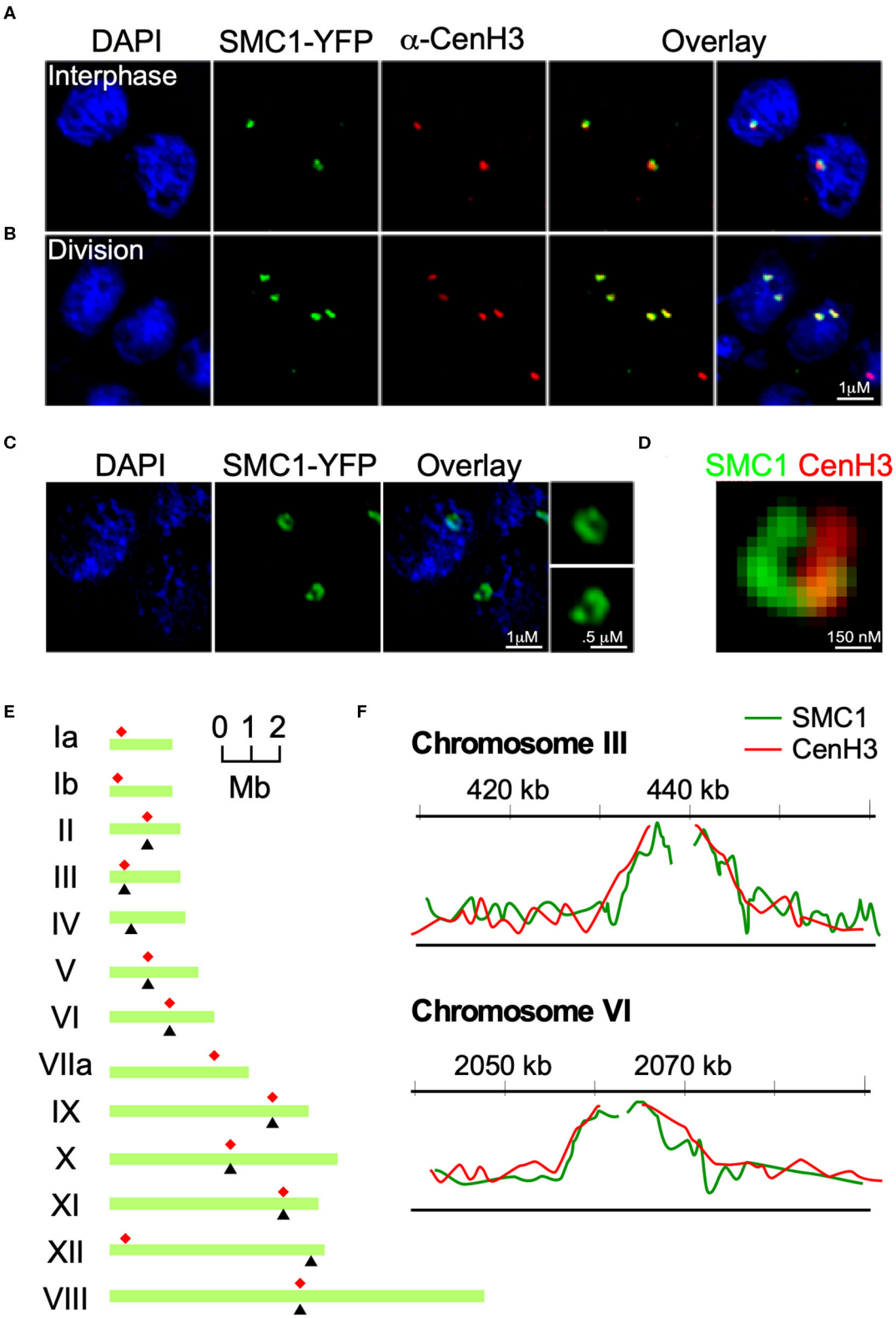

FIGURE 2 | TgSMC1 is a persistent centromeric protein. **(A,B)** Immunofluorescence assay. TgSMC1-YFP (green) was co-stained with anti-TgCenH3 antibodies (green). The signals for TgSMC1 and the marker for the *T. gondii* centromeres show tight co-localization both in interphase **(A)** and dividing **(B)** parasites. TgSMC1

(Continued)

FIGURE 2 | persists at the centromere both during all stages of mitosis and interphase. **(C)** Super Resolution (SR-SIM) image of TgSMC1-YFP stained with anti-GFP. TgSMC1 localization appears to be in the shape of a hollow oval **(D)** Zoom of the SR-SIM image of TgSMC1-YFP, co-stained with anti-GFP and anti-TgCenH3. TgSMC1 (green) appears to surround the centromeres marked by TgCenH3 (red). **(E)** Schematic representation of *T. gondii's* chromosomes. Red asterisks indicate the position of the centromeres, mapped previously, for each chromosome. Black arrowheads correspond to the hybridization peaks obtained from the TgSMC1-HA cell line ChIP-CHIP experiments for each chromosome. **(F)** Hybridization peaks on a microarray CHIP covering the genome of *T. gondii*, of immunoprecipitated chromatin from the TgSMC1-HA cell line (green line). Chromosomes III and VI are shown as representative examples. Our previous ChIP-CHIP results using the TgCenH3-HA cell line (red line) are shown, overlaid, as reference.

of unique peptides as compared to the negative control. The remaining three are TgME49_222380, TgME49_253730, and TgME49_249530. The first two are annotated as proteins belonging to the Importinb family, while the third is annotated as Exportin 1. To further study TgSMC1's interactors, we generated reporter strains by introducing a 3-HA tag at the C-terminus of the proteins encoded by TgME49_253730 and TgME49_249530, which we named TgImportin1 (TgImp1) and TgExportin1 (TgExp1), respectively (**Figure S3A**). To validate these interactions, we performed reciprocal co-immunoprecipitation assays. As an internal control, we also generated a reporter strain for TgME49_288530 (TgSUN1) which presented 2 peptides in "sample 2" but was absent from all others. We were able to reproduce the co-precipitation of TgSMC1 with TgImp1 or TgExp1, but we did not detect interactions with TgSUN1 (**Figure 3E**). Interestingly, we found TgCenH3 to co-precipitate with TgExp1 (**Figure 3E**).

Importins and exportins are nuclear proteins which interact peripherally with transmembrane components of the nuclear pore complex (NPC). As expected, we determined that both TgExp1 and TgImp1 localize to the nucleus (**Figure 4A**). Super resolution microscopy revealed that TgExp1 localizes to discrete or clustered foci on the nucleus, consistent with its predicted NPC localization (**Figure 4F**). However, neither TgImp1 nor TgExp1 exclusively localize to the centromeric foci, consistent with their predicted peripheral localization to the NPC. We reasoned that if components of the NPC are involved in centromere clustering, this should be observable in sections of interphase nuclei in the vicinity of where centromeres cluster (i.e., the centrosome). Nuclear pores are readily observed by TEM in the *T. gondii* nucleus as interruptions in the nuclear envelope or as an oval with octagonal symmetry (**Figures 4B,C**). Indeed, when we observed the region of the nuclear envelope adjacent to the centrosome in interphase parasites sectioned perpendicularly, we could observe a pore in 84% of the nuclei ($n = 60$, **Figures 4D,E**). Co-labeling of either TgImp1 or TgExp1 and TgSMC1 revealed that these proteins co-localize (**Figure 4F**). Importantly, TgCenH3's localization coincides or is flanked by individual foci or clusters of TgExp1 (**Figure 4G**).

DISCUSSION

A long standing question in the field has been "how do apicomplexans keep track of the position of their chromosomes, without condensing their chromatin during division?" Chromosomes move, organize, and cluster by interacting with the mitotic spindle through kinetochore components that assemble at the centromere during mitosis. Electron microscopy studies in *T.gondii, Eimeria* spp., and *Sarcocystis neurona* demonstrated the presence of an intranuclear spindle (Dubremetz, 1973; Morrissette and Sibley, 2002a; Francia and Striepen, 2014). These studies identified spindle microtubules that link the centrosomes to what appear to be the kinetochores of the chromosomes (Dubremetz, 1973). More recently, *bona fide* residents of the mitotic spindle, such as the MT-binding protein TgEB1, have been identified suggesting a canonical mitotic spindle is assembled by Apicomplexa (Chen et al., 2015). Consistently, parasites treated with microtubule-disrupting agents fail to segregate their chromosomes properly (Morrissette and Sibley, 2002b), and knock-down of kinetochore proteins uncouple mitosis from cytokinesis (Farrell and Gubbels, 2014).

Our first set of experiments investigated whether cytoskeletal elements mediated centromere clustering. We demonstrated that neither microtubules of the mitotic spindle nor actin mediate this process. We propose that, instead, chromatin binding factors at the centromeres mediate the maintenance of their localization at the periphery of the nucleus. We identified and characterized the localization of a homolog of SMC1 in *Toxoplasma gondii*. SMCs are a family of proteins containing two ATPase globular domains at their C and N-terminals, and a hinge domain which establishes interactions with chromatin and other SMC and non-SMC proteins. SMCs have multiple roles in higher order chromatin organization and dynamics, powered by the hydrolysis of ATP (Losada and Hirano, 2005; Hirano, 2006). We determined that TgSMC1 is a centromere-associated protein which interacts with the centromeric histone variant H3, TgCenH3, and centromeric chromatin. SMC1 interactions with CenH3 homologs have been previously reported in yeast and *Drosophila* (Tanaka et al., 1999; Losada and Hirano, 2000).

SMC1 homologs have a role in chromosome segregation during mitosis as part of the cohesin complex, which ensures the maintenance of sister chromatid cohesion until chromosomes separate in anaphase (Onn et al., 2008). Typically, SMC1 localizes to sister chromatids, in the proximities of or at the centromeres, during mitosis and up until late metaphase/early anaphase, but it is absent from centromeric regions outside of mitosis (Gruber et al., 2003; Huang et al., 2005; Peters et al., 2008). During interphase, SMC1 homologs normally localize to the cytosol or associate with non-centromeric chromatin (Losada et al., 1998; Losada and Hirano, 2000). In *Toxoplasma gondii*, however, we observed that TgSMC1 persists at the centromeres throughout the cell cycle. It is possible that it remains inactive at the centromeres outside of mitosis, and that its activity depends on interacting partners or specific activation during mitosis. Alternatively, TgSMC1 could play additional roles in chromatin organization in *T. gondii*. Cohesin

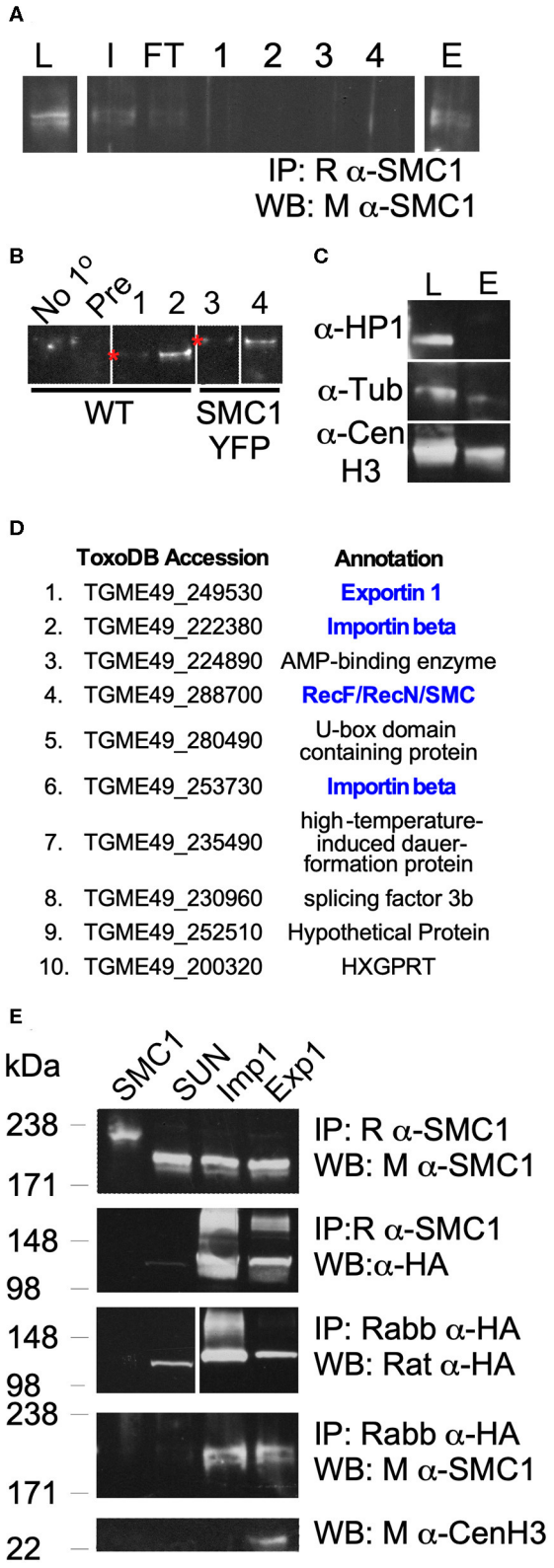

FIGURE 3 | TgSMC1 Co-precipitates with Peripheral Components of the Nuclear Pore Complex. **(A)** Representative western blot of an immuno-precipitation experiment from parasite lysate using an anti-TgSMC1 antibody (L, lysate; I, input; FT, flow through; 1–4, washes; E, elution). **(B)** Western Blot. Elutions fractions E of immunoprecipitations using no primary antibody (No-1°), pre-immune sera (Pre) or the following antibodies: 1- Rabbit anti-SMC1, 2- Affinity Purified Rabbit anti-SMC1, 3, and 4- anti-GFP, and probed with mouse anti-SMC1. The strains used to generate parasite lysates (input) are specified below. **(C)** Western blot. Parasite lysate or the elution fraction of an immuno-precipitation using rabbit anti-SMC1 were probed with the indicated antibodies. Mouse anti-HP1 recognizes TgChromo1, a chromodomain protein which binds peri-centromeric DNA, and was used as a control for the specificity of our pull downs (L, total lysate; E, elution fraction). **(D)** The 10 most abundant co-precipitants of TgSMC1 are listed. Complete results of the Mass spectrometry analysis of all elution fractions of multiple immuno-precipitation experiments can be found in **Table S1**. Proteins highlighted in blue were followed up. **(E)** TgExp1 and TgImp1 (TgME49_249530 and TgME49_253730 respectively), which co-immunoprecipitated with TgSMC1, were endogenously tagged with a C-terminal 3xHA. TgSUN1 (TgME49_288530) is annotated as a hypothetical protein containing a Sun domain. This protein was represented by 2 peptides in the Mass spectrometry analysis of SMC1-YFP anti-GFP Co-IP, but was not found in other samples, and was used as a negative control (**Table S1**). TgSMC1 was pulled down using Rabbit anti-SMC1 antibodies in TgSMC1-YFP, TgImp1-HA, TgExp1-HA, and TgSUN-HA cells lines, and probed with mouse anti-SMC1 or anti-HA. Conversely, TgImp1, TgExp1, and TgSUN were pulled down using anti-HA antibodies, and the elution fractions were probed with anti-TgSMC1. These results recapitulate our LC-MS results. In addition to co-precipitating with TgSMC1, TgExp1 also co-precipitates with TgCENH3.

has been shown to contribute to gene regulation, DNA damage repair, transcriptional control, and maintenance of higher order chromatin structure in other systems (Peters et al., 2008). In human cells, SMC1 has been shown to mediate transcriptional insulation by binding chromatin boundaries in post-mitotic cells (Parelho et al., 2008; Peric-Hupkes and van Steensel, 2008; Wendt et al., 2008). Interestingly, in the closely related Apicomplexa *Eimeria tenella*, SMC1 is part of a plaque formed at the nuclear envelope to which telomeres attach during meiotic division (del Cacho et al., 2010). Our results suggest that TgSMC1 could fulfill a similar role in mediating the attachment of centromeres to the nuclear envelope.

The latter is supported by our identification of TgSMC1 interactors. In particular, we determined that TgSMC1 co-precipitated with soluble proteins predicted to function at nuclear pores; TgExportin7, TgExportin1, and TgImportin1. Nuclear pores are basket-like structure of octagonal shape and consist of a central scaffold which spans the nuclear envelope (Hoelz et al., 2011; Kahms et al., 2011). Proteins of the nuclear pore are collectively known as nucleoporins (NUPs) are anchored by transmembrane domains, and form a molecular sieve by the presence of FG repeats in a central channel, preventing diffusion of molecules larger than 40 KDa or 5 nm. For larger molecules to travel through the pore, they must reversibly associate with FG nucleoporins (Wente and Rout, 2010; Hoelz et al., 2011). Translocation of large molecules depends on nuclear transport receptors (NTRs), i.e., importins, exportins, and transportins (Görlich and Kutay, 1999).

The TgSMC1 interactors identified, TgExp1 and TgImp1, localize to discrete foci in the nucleus, and co-localize or flank the location of centromeres in the nuclear periphery. By TEM

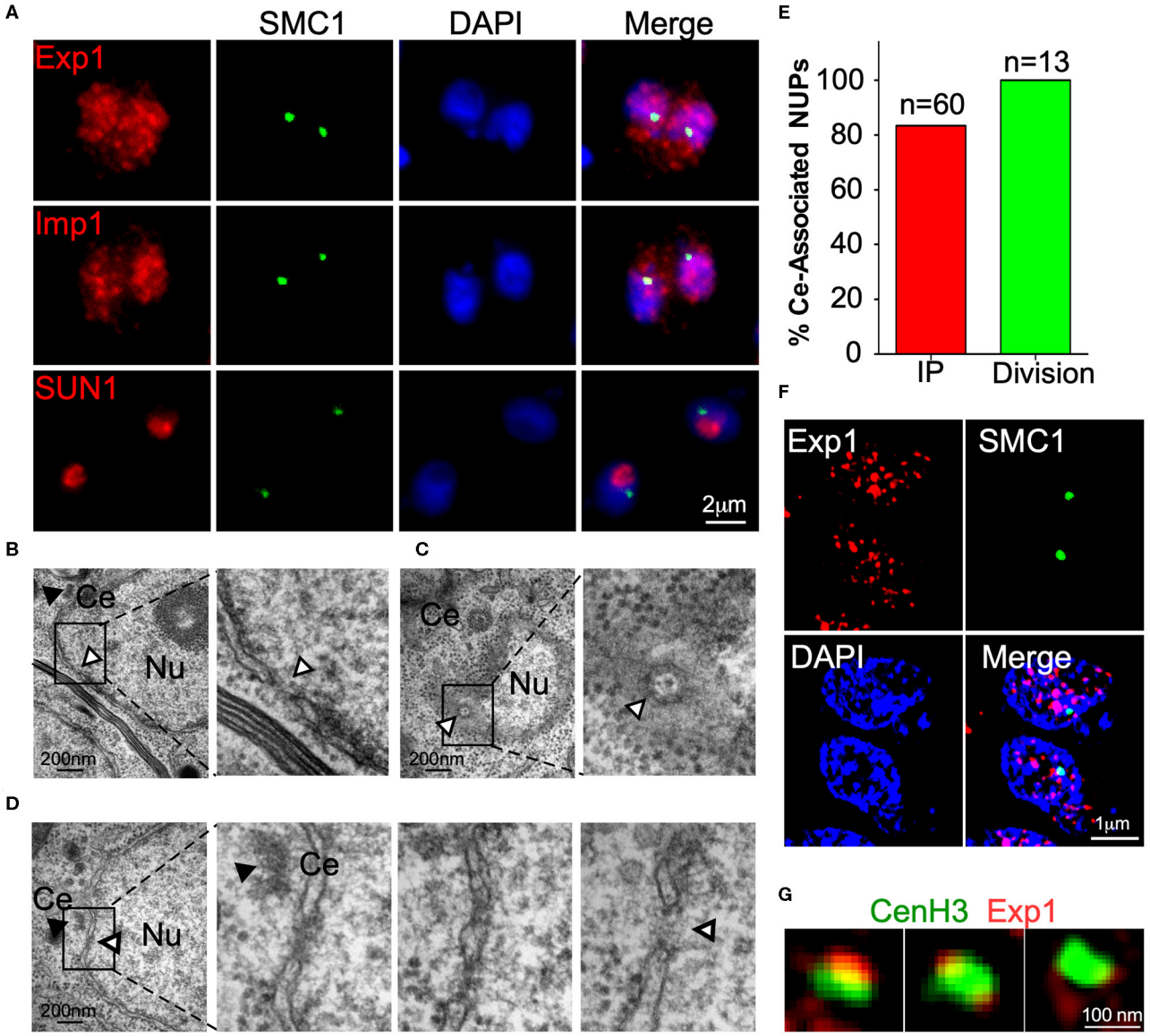

FIGURE 4 | A nuclear pore is found in the proximity of the centrosome. **(A)** IFA of TgExp1-HA, TgImp –HA and TgSUN-HA using anti-HA antibodies reveal that these proteins localize to the nucleus. TgSUN1 is restricted to a discrete region of the nucleus, and does not co-localize with TgSMC1. **(B)** TEM section perpendicular to a nucleus (Nu). A nuclear pore (white arrowhead) is seen as a discontinuation in the nuclear envelope. **(C)** TEM section parallel to a nucleus (Nu). A nuclear pore (white arrowhead) is seen as a basket-like octagonal structure on the nuclear, distant from the centrosome (Ce, black arrowhead). **(D)** TEM Serial sections through an interphase nucleus reveal the presence of a nuclear pore (white arrowhead) visible as an interruption in the nuclear envelope adjacent to the centrosome (Ce, black arrowhead). Detailed panels are zoomed in at 200% **(E)**. The appearance of nuclear pores proximal to the centrosome (% Ce-associated NUPs) was quantified in serial sections of both dividing (green) and non-dividing (red) parasites. Note that the mitotic spindle penetrates and interrupts the nuclear envelope during division. Hence an interruption of the nuclear envelope, proximal to the centrosome, is observable in the vast majority of the dividing nuclei and is indistinguishable, by microscopy, from a canonical nuclear pore. **(F)** SR-SIM of TgExp1-HA reveals that TgExp1 localizes to heterogenous discrete foci in the nucleus. **(G)** TgExp1-HA foci co-localize with, flank or surround the localization of TgCenH3 marked by anti-TgCenH3 staining.

we established that an opening in the nuclear envelope can be observed adjacent to the centrosome in interphase nuclei, implying that centromeres arrange in the vicinity of an NPC.

Proteins associated peripherally with the NPC, such as NTRs, have been shown to fulfill roles independent from their transport function. Several transportins have been shown to exert strong boundary activity by mediating the association of chromatin with core components of the nuclear pore. Intriguingly, like TgExp1 and TgImp1, they all belong to the Importin-β superfamily of NTRs. In particular Nup2, a peripheral NUP associated with the nuclear pore basket, is essential for boundary activity of transportins in yeast (Ishii et al., 2002; Shinkura and

Forrester, 2002). *Schizosaccharomyces pombe*, a fission yeast which divides by closed mitosis and clusters centromeres, presents a TgExportin1 homolog, named CRM1, first identified in a cold-sensitive mutant screen (Adachi and Yanagida, 1989). Conspicuously, CRM1 has been shown to be essential for maintenance of centromere clustering during interphase (Adachi and Yanagida, 1989; Funabiki et al., 1993). Interestingly, characterization of the effect of temperature sensitive mutations identified that a point mutation caused CRM1 to mis-localize to the cytosol (Adachi and Yanagida, 1989), an effect that can be mimicked on wild type CRM1 by Leptomycin B treatment (Nishi et al., 1994; Kudo et al., 1999). At the restrictive temperature or upon Leptomycin B treatment, centromeres of *S. pombe* come apart and disperse in the nucleus.

Core nucleoporins (NUPs) have also been shown to directly interact with chromatin, and to regulate chromatin organization in other systems. Particularly relevant to this study; Nup98 co-precipitates with SMC1 in *Drosophila* (Wong and Blobel, 2008). ChIP-CHIP of Nup93 demonstrated direct chromatin association with the nuclear pore complex in human cells (Brown et al., 2008). Dynamic changes in the distribution of nuclear pores on the nuclear envelope were observed by elegant microscopy techniques during the intracellular development of the apicomplexan *Plasmodium falciparum* (Weiner et al., 2011). Late schizonts exhibit 2–6 nuclear pores per nucleus, which cluster together and invariably are surrounded by heterochromatin suggesting that nuclear pores associate with specific states of chromatin condensation (Weiner et al., 2011). Noteworthy, heterochromatin flanks the centromeres of *T. gondii* (Brooks et al., 2011; Gissot et al., 2012). A recent study which characterized the *T. gondii* Nup98 homolog (TgNUP302) revealed that this protein interacted with facilitates chromatin transcription complex (FACT) components, suggesting the existence of an NPC-chromatin interaction in *T. gondii* (Courjol et al., 2017). Therefore, centromere clustering could be part of a more general organizational scheme of nuclear elements in apicomplexan parasites, dependent on interactions with components of the nuclear envelope, and in particular with the NPC.

While we have started to unravel the mechanism by which centromeres are held in position at the nuclear envelope, we do not yet understand how centromeres are recruited to a specific site on the nuclear periphery, adjacent to the centrosome. Intriguingly, TgNUP302 was shown to physically associate to TGGT1_246190, a coiled-coiled protein (named TgCEP530) shown to localize at the centrosome, thereby identifying a physical connection between the nuclear pore complex and the centrosome (Courjol and Gissot, 2018). Together, the connection between nuclear pore components and the centrosome, and peripheral components of the nuclear pore-chromatin, described herein, could be the basis of the centromere-centrosome connection. Further study of centrosome-associated factors could shed light on the identity of components with roles in targeting or maintaining the position of centrosome-associated nuclear components.

DATA AVAILABILITY STATEMENT

The raw data supporting the conclusions of this article will be made available by the authors, without undue reservation, to any qualified researcher.

ETHICS STATEMENT

The animal study was reviewed and approved by the University of Georgia Institutional Animal Care and Use Committee or IACUC.

AUTHOR CONTRIBUTIONS

MF designed and performed experiments and wrote the manuscript. L-MT, MC, and J-FD performed experiments. KK supervised L-MT and MC. BS secured funding, designed experiments, and wrote the manuscript. All authors contributed to the article and approved the submitted version.

FUNDING

Work in our laboratory was funded by grants from the National Institutes of Health to BS, and MF was supported by an EMBO short-term fellowship.

ACKNOWLEDGMENTS

We thank Michael White, Lena Suvorova, Marc-Jan Gubbels and Mathieu Gissot for discussion and for sharing reagents.

SUPPLEMENTARY MATERIAL

The Supplementary Material for this article can be found online at: https://www.frontiersin.org/articles/10.3389/fcimb.2020.00295/full#supplementary-material

REFERENCES

Adachi, Y., and Yanagida, M. (1989). Higher order chromosome structure is affected by cold-sensitive mutations in a Schizosaccharomyces pombe gene crm1+ which encodes a 115-kD protein preferentially localized in the nucleus and its periphery. *J. Cell Biol.* 108, 1195–1207. doi: 10.1083/jcb.108.4.1195

Alexandrov, A., Vignali, M., LaCount, D. J., Quartley, E., de Vries, C., De Rosa, D., et al. (2004). A facile method for high-throughput co-expression of protein pairs. *Mol. Cell. Proteomics* 3, 934–938. doi: 10.1074/mcp.T400008-MCP200

Aslanidis, C., and de Jong, P. J. (1990). Ligation-independent cloning of PCR products (LIC-PCR). *Nucleic Acids Res.* 18, 6069–6074. doi: 10.1093/nar/18.20.6069

Brooks, C. F., Francia, M. E., Gissot, M., Croken, M. M., Kim, K., and Striepen, B. (2011). *Toxoplasma gondii* sequesters centromeres to a specific nuclear region throughout the cell cycle. *Proc. Natl.*

Acad. Sci. U. S. A. 108, 3767–3772. doi: 10.1073/pnas.1006741108

Brown, C. R., Kennedy, C. J., Delmar, V. A., Forbes, D. J., and Silver, P. A. (2008). Global histone acetylation induces functional genomic reorganization at mammalian nuclear pore complexes. *Genes Dev.* 22, 627–639. doi: 10.1101/gad.1632708

Bunnik, E. M., Venkat, A., Shao, J., McGovern, K. E., Batugedara, G., Worth, D., et al. (2019). Comparative 3D genome organization in apicomplexan parasites. *Proc. Natl. Acad. Sci. U.S.A.* 116, 3183–3192. doi: 10.1073/pnas.1810815116

Chen, C. T., Kelly, M., De Leon, J., Nwagbara, B., Ebbert, P., Ferguson, D. J. P., et al. (2015). Compartmentalized Toxoplasma EB1 bundles spindle microtubules to secure accurate chromosome segregation. *Mol. Biol. Cell* 26, 4562–4576. doi: 10.1091/mbc.E15-06-0437

Courjol, F., and Gissot, M. (2018). A coiled-coil protein is required for coordination of karyokinesis and cytokinesis in *Toxoplasma gondii*. *Cell. Microbiol.* 20:e12832. doi: 10.1111/cmi.12832

Courjol, F., Mouveaux, T., Lesage, K., Saliou, J. M., Werkmeister, E., Bonabaud, M., et al. (2017). Characterization of a nuclear pore protein sheds light on the roles and composition of the *Toxoplasma gondii* nuclear pore complex. *Cell. Mol. Life Sci.* 74, 2107–2125. doi: 10.1007/s00018-017-2459-3

del Cacho, E., Pagés, M., Gallego, M., Barbero, J. L., Monteagudo, L., and Sánchez-Acedo, C. (2010). Meiotic chromosome pairing and bouquet formation during Eimeria tenella sporulation. *Int. J. Parasitol.* 40, 453–462. doi: 10.1016/j.ijpara.2009.09.008

Dubremetz, J. F. (1973). Etude ultrastructurale de la mitose schizogonique chez la coccidie Eimeria necatrix (Johnson 1930). *J. Ultrastruct. Res.* 42, 354–376. doi: 10.1016/S0022-5320(73)90063-4

Farrell, M., and Gubbels, M. J. (2014). The Toxoplasma gondii kinetochore is required for centrosome association with the centrocone (spindle pole). *Cell. Microbiol.* 16, 78–94. doi: 10.1111/cmi.12185

Francia, M. E., Jordan, C. N., Patel, J. D., Sheiner, L., Demerly, J. L., Fellows, J. D., et al. (2012). Cell division in apicomplexan parasites is organized by a homolog of the striated rootlet fiber of algal flagella. *PLoS Biol.* 10:e1001444. doi: 10.1371/journal.pbio.1001444

Francia, M. E., and Striepen, B. (2014). Cell division in apicomplexan parasites. *Nat. Rev. Microbiol.* 12, 125–136. doi: 10.1038/nrmicro3184

Francia, M. E., Wicher, S., Pace, D. A., Sullivan, J., Moreno, S. N. J., and Arrizabalaga, G. (2011). A Toxoplasma gondii protein with homology to intracellular type Na+/H+ exchangers is important for osmoregulation and invasion. *Exp. Cell Res.* 317, 1382–1396. doi: 10.1016/j.yexcr.2011.03.020

Funabiki, H., Hagan, I., Uzawa, S., and Yanagida, M. (1993). Cell cycle-dependent specific positioning and clustering of centromeres and telomeres in fission yeast. *J. Cell Biol.* 121, 961–976. doi: 10.1083/jcb.121.5.961

Gissot, M., Kelly, K. A., Ajioka, J. W., Greally, J. M., and Kim, K. (2007). Epigenomic modifications predict active promoters and gene structure in *Toxoplasma gondii*. *PLoS Pathog.* 3:e77. doi: 10.1371/journal.ppat.0030077

Gissot, M., Walker, R., Delhaye, S., Huot, L., Hot, D., and Tomavo, S. (2012). Toxoplasma gondii chromodomain protein 1 binds to heterochromatin and colocalises with centromeres and telomeres at the nuclear periphery. *PLoS ONE* 7:e32671. doi: 10.1371/journal.pone.0032671

Görlich, D., and Kutay, U. (1999). Transport between the cell nucleus and the cytoplasm. *Annu. Rev. Cell Dev. Biol.* 15, 607–660. doi: 10.1146/annurev.cellbio.15.1.607

Gruber, S., Haering, C. H., and Nasmyth, K. (2003). Chromosomal cohesin forms a ring. *Cell* 112, 765–777. doi: 10.1016/S0092-8674(03)00162-4

Gubbels, M. J., Vaishnava, S., Boot, N., Dubremetz, J. F., and Striepen, B. (2006). A MORN-repeat protein is a dynamic component of the Toxoplasma gondii cell division apparatus. *J. Cell Sci.* 119, 2236–2245. doi: 10.1242/jcs.02949

Gubbels, M. J., White, M., and Szatanek, T. (2008). The cell cycle and *Toxoplasma gondii* cell division: Tightly knit or loosely stitched? *Int. J. Parasitol.* 38, 1343–1358. doi: 10.1016/j.ijpara.2008.06.004

Hirano, T. (2006). At the heart of the chromosome: SMC proteins in action. *Nat. Rev. Mol. Cell Biol.* 7, 311–322. doi: 10.1038/nrm1909

Hoeijmakers, W. A. M., Flueck, C., Françoijs, K. J., Smits, A. H., Wetzel, J., Volz, J. C., et al. (2012). *Plasmodium falciparum* centromeres display a unique epigenetic makeup and cluster prior to and during schizogony. *Cell. Microbiol.* 14, 1391–1401. doi: 10.1111/j.1462-5822.2012.01803.x

Hoelz, A., Debler, E. W., and Blobel, G. (2011). The structure of the nuclear pore complex. *Annu. Rev. Biochem.* 80, 613–643. doi: 10.1146/annurev-biochem-060109-151030

Huang, C. E., Milutinovich, M., and Koshland, D. (2005). Rings, bracelet or snaps: Fashionable alternatives for Smc complexes. *Philos. Trans. R. Soc. B Biol. Sci.* 360, 537–542. doi: 10.1098/rstb.2004.1609

Huynh, M.-H., and Carruthers, V. B. (2009). Tagging of endogenous genes in a *Toxoplasma gondii* strain lacking Ku80. *Eukaryot. Cell* 8, 530–539. doi: 10.1128/EC.00358-08

Ishii, K., Arib, G., Lin, C., Van Houwe, G., and Laemmli, U. K. (2002). Chromatin boundaries in budding yeast: the nuclear pore connection. *Cell* 109, 551–562. doi: 10.1016/S0092-8674(02)00756-0

Jacot, D., Meissner, M., Sheiner, L., Soldati-Favre, D., and Striepen, B. (2013). "Genetic manipulation of *Toxoplasma gondii*," in *Toxoplasma Gondii: The Model Apicomplexan - Perspectives and Methods: Second Edition*, eds L. M. Weiss and K. Kim (Burlington, VT: Elsevier Academic Press), 577–611.

Jeppsson, K., Kanno, T., Shirahige, K., and Sjögren, C. (2014). The maintenance of chromosome structure: positioning and functioning of SMC complexes. *Nat. Rev. Mol. Cell Biol.* 15, 601–614. doi: 10.1038/nrm3857

Kahms, M., Hüve, J., Wesselmann, R., Farr, J. C., Baumgärtel, V., and Peters, R. (2011). Lighting up the nuclear pore complex. *Eur. J. Cell Biol.* 90, 751–758. doi: 10.1016/j.ejcb.2011.04.004

Kissinger, J. C., Gajria, B., Li, L., Paulsen, I. T., and Roos, D. S. (2003). ToxoDB: accessing the *Toxoplasma gondii* genome. *Nucleic Acids Res.* 31, 234–236. doi: 10.1093/nar/gkg072

Kudo, N., Matsumori, N., Taoka, H., Fujiwara, D., Schreiner, E. P., Wolff, B., et al. (1999). Leptomycin B inactivates CRM1/exportin 1 by covalent modification at a cysteine residue in the central conserved region. *Proc. Natl. Acad. Sci. U.S.A.* 96, 9112–9117. doi: 10.1073/pnas.96.16.9112

Losada, A., Hirano, M., and Hirano, T. (1998). Identification of Xenopus SMC protein complexes required for sister chromatid cohesion. *Genes Dev.* 12, 1986–1997. doi: 10.1101/gad.12.13.1986

Losada, A., and Hirano, T. (2000). New light on sticky sisters. *Curr. Biol.* 10:R615. doi: 10.1016/S0960-9822(00)00670-9

Losada, A., and Hirano, T. (2005). Dynamic molecular linkers of the genome: the first decade of SMC proteins. *Genes Dev.* 19, 1269–1287. doi: 10.1101/gad.1320505

Morrissette, N. S., Mitra, A., Sept, D., and Sibley, L. D. (2004). Dinitroanilines bind α-tubulin to disrupt microtubules. *Mol. Biol. Cell* 15, 1960–1968. doi: 10.1091/mbc.e03-07-0530

Morrissette, N. S., and Sibley, L. D. (2002a). Cytoskeleton of apicomplexan parasites. *Microbiol. Mol. Biol. Rev.* 66, 21–38. doi: 10.1128/MMBR.66.1.21-38.2002

Morrissette, N. S., and Sibley, L. D. (2002b). Disruption of microtubules uncouples budding and nuclear division in *Toxoplasma gondii*. *J. Cell Sci.* 115, 1017–1025.

Nasmyth, K., and Haering, C. H. (2009). Cohesin: its roles and mechanisms. *Annu. Rev. Genet.* 43, 525–558. doi: 10.1146/annurev-genet-102108-134233

Nishi, K., Yoshida, M., Fujiwara, D., Nishikawa, M., Horinouchi, S., and Beppu, T. (1994). Leptomycin B targets a regulatory cascade of crm1, a fission yeast nuclear protein, involved in control of higher order chromosome structure and gene expression. *J. Biol. Chem.* 269, 6320–6324.

Onn, I., Heidinger-Pauli, J. M., Guacci, V., Ünal, E., and Koshland, D. E. (2008). Sister chromatid cohesion: a simple concept with a complex reality. *Annu. Rev. Cell Dev. Biol.* 24, 105–129. doi: 10.1146/annurev.cellbio.24.110707.175350

Parelho, V., Hadjur, S., Spivakov, M., Leleu, M., Sauer, S., Gregson, H. C., et al. (2008). Cohesins functionally associate with CTCF on mammalian chromosome arms. *Cell* 132, 422–433. doi: 10.1016/j.cell.2008.01.011

Peric-Hupkes, D., and van Steensel, B. (2008). Linking cohesin to gene regulation. *Cell* 132, 925–928. doi: 10.1016/j.cell.2008.03.001

Peters, J. M., Tedeschi, A., and Schmitz, J. (2008). The cohesin complex and its roles in chromosome biology. *Genes Dev.* 22, 3089–3114. doi: 10.1101/gad.1724308

Shinkura, N., and Forrester, W. C. (2002). Pushing the envelope: chromatin boundaries at the nuclear pore. *Mol. Cell* 9, 1156–1158. doi: 10.1016/S1097-2765(02)00556-7

Stokkermans, T. J. W., Schwartzman, J. D., Keenan, K., Morrissette, N. S., Tilney, L. G., and Roos, D. S. (1996). Inhibition of *Toxoplasma*

gondii replication by dinitroaniline herbicides. *Exp. Parasitol.* 84, 355–370. doi: 10.1006/expr.1996.0124

Suvorova, E. S., Lehmann, M. M., Kratzer, S., and White, M. W. (2012). Nuclear actin-related protein is required for chromosome segregation in *Toxoplasma gondii*. *Mol. Biochem. Parasitol.* 181, 7–16. doi: 10.1016/j.molbiopara.2011.09.006

Tanaka, T., Cosma, M. P., Wirth, K., and Nasmyth, K. (1999). Identification of cohesin association sites at centromeres and along chromosome arms. *Cell* 98, 847–858. doi: 10.1016/S0092-86740081518-4

Uhlmann, F. (2016). SMC complexes: from DNA to chromosomes. *Nat. Rev. Mol. Cell Biol.* 17, 399–412. doi: 10.1038/nrm.2016.30

Weiner, A., Dahan-Pasternak, N., Shimoni, E., Shinder, V., von Huth, P., Elbaum, M., et al. (2011). 3D nuclear architecture reveals coupled cell cycle dynamics of chromatin and nuclear pores in the malaria parasite *Plasmodium falciparum*. *Cell. Microbiol.* 13, 967–977. doi: 10.1111/j.1462-5822.2011.01592.x

Wells, J., and Farnham, P. J. (2002). Characterizing transcription factor binding sites using formaldehyde crosslinking and immunoprecipitation. *Methods* 26, 48–56. doi: 10.1016/S1046-20230200007-5

Wendt, K. S., Yoshida, K., Itoh, T., Bando, M., Koch, B., Schirghuber, E., et al. (2008). Cohesin mediates transcriptional insulation by CCCTC-binding factor. *Nature* 451, 796–801. doi: 10.1038/nature06634

Wente, S. R., and Rout, M. P. (2010). The nuclear pore complex and nuclear transport. *Cold Spring Harb. Perspect. Biol.* 2, a000562. doi: 10.1101/cshperspect.a000562

White, M. W., and Suvorova, E. S. (2018). Apicomplexa cell cycles: something old, borrowed, lost, and new. *Trends Parasitol.* 34, 759–771. doi: 10.1016/j.pt.2018.07.006

Wong, R. W. (2010). An update on cohesin function as a "molecular glue" on chromosomes and spindles. *Cell Cycle* 9, 1754–1758. doi: 10.4161/cc.9.9.11806

Wong, R. W., and Blobel, G. (2008). Cohesin subunit SMC1 associates with mitotic microtubules at the spindle pole. *Proc. Natl. Acad. Sci. U.S.A.* 105, 15441–15445. doi: 10.1073/pnas.0807660105

Zhang, Q., Huang, Y., Zhang, Y., Fang, X., Claes, A., Duchateau, M., et al. (2011). A critical role of perinuclear filamentous Actin in spatial repositioning and mutually exclusive expression of virulence genes in malaria parasites. *Cell Host Microbe* 10, 451–463. doi: 10.1016/j.chom.2011.09.013

Conflict of Interest: The authors declare that the research was conducted in the absence of any commercial or financial relationships that could be construed as a potential conflict of interest.

frontiers in Cellular and Infection Microbiology

ORIGINAL RESEARCH
published: 11 September 2020
doi: 10.3389/fcimb.2020.00401

Outbreak of Amazonian Toxoplasmosis: A One Health Investigation in a Remote Amerindian Community

Romain Blaizot[1,2†], Cécile Nabet[3†], Laure Laghoe[2], Benjamin Faivre[4], Sandie Escotte-Binet[5,6], Felix Djossou[7], Emilie Mosnier[8,9], Fanny Henaff[4,8], Denis Blanchet[1,2], Aurélien Mercier[10,11], Marie-Laure Dardé[10,11], Isabelle Villena[5,6] and Magalie Demar[1,2]*

[1] Department of Parasitology-Mycology, Hôpital Andrée Rosemon, Cayenne, French Guiana, [2] EA 3593, Ecosystèmes Amazoniens et Pathologies Tropicales, Université de Guyane, Cayenne, French Guiana, [3] Sorbonne Université, INSERM, Institut Pierre-Louis d'Epidémiologie et de Santé Publique, AP-HP, Groupe Hospitalier Pitié-Salpêtrière, Service de Parasitologie-Mycologie, Paris, France, [4] Department of Pediatrics, Hôpital Andrée Rosemon, Cayenne, French Guiana, [5] EA 7510 ESCAPE, Université de Reims Champagne-Ardenne, SFR Cap Santé, Reims, France, [6] Centre National de Référence (CNR) Toxoplasmose/Toxoplasma Biological Resource Center (BRC), Centre Hospitalier-Universitaire de Reims, Reims, France, [7] Department of Infectious Diseases, Hôpital Andrée Rosemon, Cayenne, French Guiana, [8] Centres Délocalisés de Prévention et de Soins, Hôpital Andrée Rosemon, Cayenne, French Guiana, [9] INSERM, IRD, SESSTIM, Sciences Economiques & Sociales de La Santé & Traitement de l'Information Médicale, Aix Marseille University, Marseille, France, [10] Centre National de Référence (CNR) Toxoplasmose/Toxoplasma Biological Resource Center (BRC), Centre Hospitalier-Universitaire Dupuytren, Limoges, France, [11] INSERM, Univ. Limoges, CHU Limoges, UMR 1094, Institut d'Epidémiologie et de Neurologie Tropicale, GEIST, Limoges, France

OPEN ACCESS

Edited by:
Jorge Enrique Gómez Marín,
University of Quindío, Colombia

Reviewed by:
Olgica Djurkovic-Djakovic,
University of Belgrade, Serbia
Pikka Jokelainen,
Statens Serum Institut (SSI), Denmark

***Correspondence:**
Romain Blaizot
blaizot.romain@gmail.com

[†] These authors have contributed equally to this work

Specialty section:
This article was submitted to Parasite and Host, a section of the journal Frontiers in Cellular and Infection Microbiology

Received: 23 February 2020
Accepted: 30 June 2020
Published: 11 September 2020

Citation:
Blaizot R, Nabet C, Laghoe L, Faivre B, Escotte-Binet S, Djossou F, Mosnier E, Henaff F, Blanchet D, Mercier A, Dardé M-L, Villena I and Demar M (2020) Outbreak of Amazonian Toxoplasmosis: A One Health Investigation in a Remote Amerindian Community. Front. Cell. Infect. Microbiol. 10:401. doi: 10.3389/fcimb.2020.00401

Background: *Toxoplasma gondii* is a parasite of worldwide importance but its burden in indigenous communities remains unclear. In French Guiana, atypical strains of *T. gondii* originating from a complex rainforest cycle involving wild felids have been linked to severe infections in humans. These cases of Amazonian toxoplasmosis are sporadic and outbreaks are rarely described. We report on the investigation of an outbreak of acute toxoplasmosis in a remote Amerindian village. We discuss the causes and consequences of this emergence.

Methods: In May 2017, during the rainy season and following an episode of flooding, four simultaneous cases of acute toxoplasmosis were serologically confirmed in two families living the village. Other non-diagnosed cases were then actively screened by a medical team along with epidemiological investigations. Inhabitants from nine households were tested for *T. gondii* antibodies and parasite DNA by PCR when appropriate. Samples of water, cat feces and cat rectal swabs, soil, and meat were tested for *T. gondii* DNA by PCR. Positive PCR samples with sufficient DNA amounts were genotyped using 15 microsatellite markers.

Results: Between early May and early July 2017, out of 54 tested inhabitants, 20 cases were serologically confirmed. A fetus infected at gestational week 10 died but other cases were mild. Four patients tested positive for parasite DNA and two identical strains belonging to an atypical genotype could be isolated from unrelated patients. While domestic cats had recently appeared in the vicinity, most families drank water from unsafe

sources. Parasite DNA was recovered from one water sample and nine soil samples. Three meat samples tested positive, including wild and industrial meat.

Conclusions: The emergence of toxoplasmosis in such a community living in close contact with the Amazon rainforest is probably multifactorial. Sedentary settlements have been built in the last few decades without providing safe water sources, increasing the risk of parasite circulation in cases of dangerous new habits such as cat domestication. Public health actions should be implemented in these communities such as safe water supply, health recommendations, and epidemiological surveillance of acute toxoplasmosis. A "One Health" strategy of research involving medical anthropology, veterinary medicine, and public health needs to be pursued for a better understanding of the transmission routes and the emergence of this zoonosis.

Keywords: indigenous, toxoplasmosis, outbreak, rainforest (Amazon forest), parasitology

INTRODUCTION

Toxoplasma gondii is a ubiquitous parasite that may be transmitted by the consumption of uncooked meat containing viable tissue cysts, or food and water contaminated with oocysts from the feces of infected felids (Hill and Dubey, 2002; Jones and Dubey, 2010). Outbreaks of *T. gondii* have been linked to water contamination (Benenson et al., 1982; Bowie et al., 1997; Isaac-Renton et al., 1998; Aramini et al., 1999; de Moura et al., 2006; Heukelbach et al., 2007; Meireles et al., 2015), exposure to domestic cats (Dubey et al., 2004), consumption of meat from infected animals (Choi et al., 1997), or contaminated vegetables (Ekman et al., 2012). This infection is of special concern in pregnant women and immunosuppressed patients (Hill and Dubey, 2002). In the Amazon, the transmission cycle is complex, involving wild animals, humans living close to the rainforest, and atypical strains. These strains do not belong to the main lineages of *T. gondii* and are responsible for severe symptoms, including in immunocompetent patients. These atypical cases have led to the recent description of the entity called "Amazonian toxoplasmosis" (Dardé et al., 1998; Carme et al., 2002, 2009; Demar et al., 2007, 2012). Autochthonous communities such as Amerindians and Maroon people are particularly at risk, due to their low income, lack of health care access, and the importance of hunting and traditional agriculture. Though severe acute toxoplasmosis has been reported in French Guiana, a few cases have been described in Peru and Brazil (Leal et al., 2007; Nunura et al., 2010; Neves Ede et al., 2011). This infection is likely to be under-diagnosed in many rainforest areas of South America (Carme and Demar-Pierre, 2006).

In French Guiana, only one major *T. gondii* outbreak has been described, in the Maroon community in 2003 (Demar et al., 2007). A unique atypical strain was isolated in five of the 11 patients and was responsible for three deaths (one adult and two congenitally infected fetus or neonate). The high lethality of some atypical strains implies that the emergence of *T. gondii* would represent a special concern. Nevertheless, the burden of *T. gondii* is still poorly documented in these remote areas. Indeed, investigating *T. gondii* outbreaks in remote tropical settings is challenging due to unspecific symptoms, shipping delays, and difficulties in processing analyses. In addition, epidemiological investigations may be complicated by difficulties in interviewing patients about food and cultural habits (Robert-Gangneux and Dardé, 2012), or in logistics. Here we describe the first outbreak of severe acute toxoplasmosis in an Amerindian village of French Guiana and investigate the possible routes for infection, via a One Health approach, testing patients, soil, water, and cats. We discuss the challenges posed by *T. gondii* in traditional communities of tropical areas.

METHODS

In May 2017, during the rainy season and following an episode of flooding (Meteo France, 2017), two adult men were seen in outpatient consultation in the health center of Camopi. One presented diarrhea and vomiting, and was accompanied by his 14-year-old daughter who presented similar symptoms. The other adult presented lymphadenopathy, as did his 12-year-old son. All patients had fever for more than 2 weeks. Given the persistence of symptoms after symptomatic treatment, a suspicion of Amazonian toxoplasmosis was raised and a serology was performed, which confirmed these four cases (positive IgM and IgG).

Camopi is an Amerindian village along the Oyapock River, surrounded by tropical rainforest (**Figure 1**). This remote village of 1,800 inhabitants can be reached from the coastal road after 1 day of canoe. Hunting and fishing are the main productive activities. A demographic transition is under way in this village, as habitations are increasingly sedentary. This transition provides some benefits and new habits such as electrification, drinking water for a few households, and domestication of cats. Teko and Wayampi are the two ethnic groups represented in the village.

After this first epidemiological signal, advice was then given to local physicians to spread information about this possible outbreak throughout the village and encourage villagers with compatible symptoms to get tested. A medical team was dispatched to the village to perform an epidemiological investigation and look for non-diagnosed cases. The investigation team reached the village 1 week after the identification of

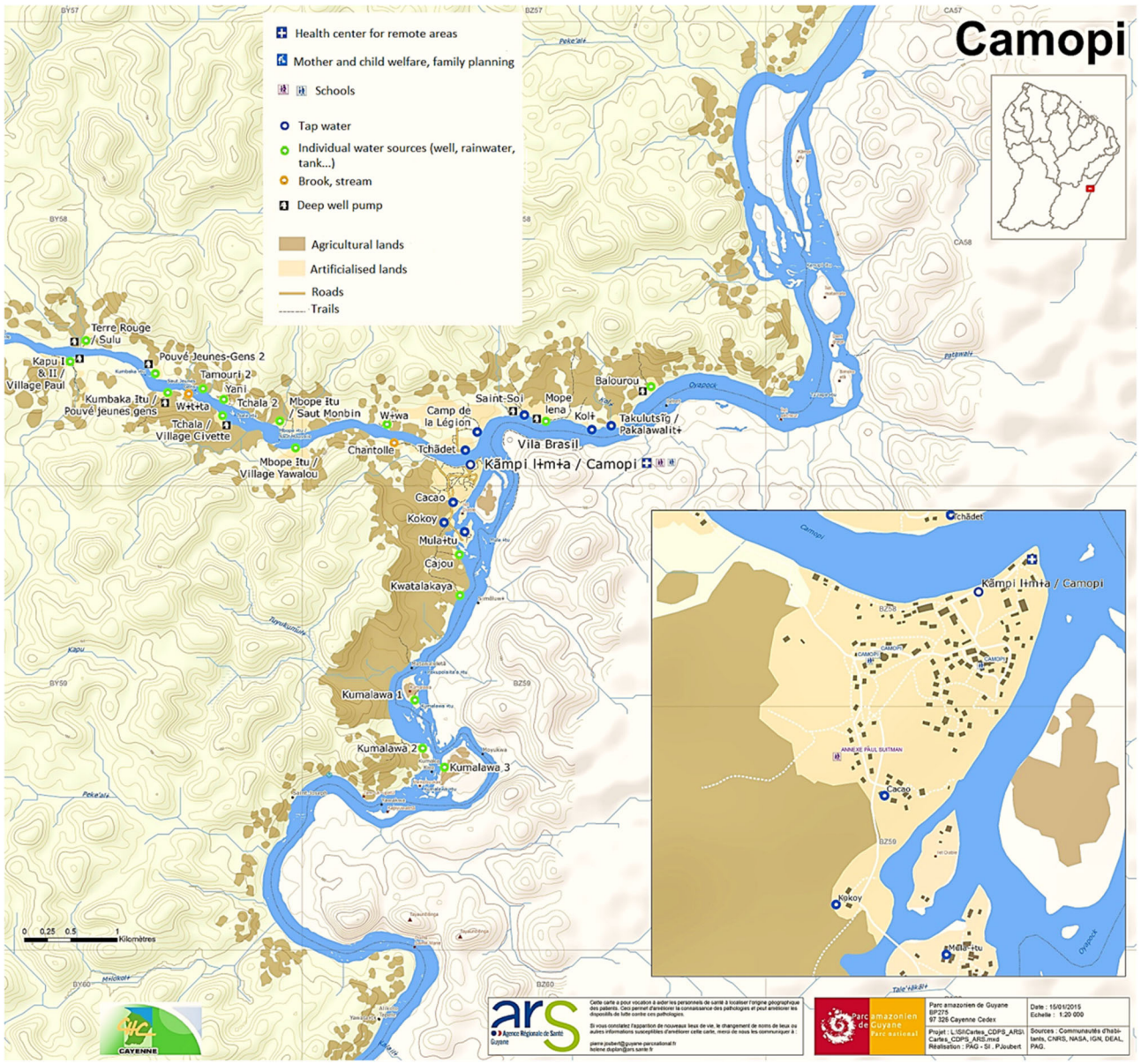

FIGURE 1 | Map of the village of Camopi, provided by the Guiana Amazonian Park (Parc Amazonien de Guyane).

the first cases. By this time, four new cases had requested a consultation and were serologically confirmed. During the on-field investigation, five other patients spontaneously consulted at the health center and were confirmed by serology.

For each confirmed case, all members of the household were considered contact cases and investigated to look for asymptomatic or mildly symptomatic patients who had not asked for consultation. In case of compatible symptoms and positive serology (positive IgM and positive IgG or IgG seroconversion on two successive blood tests), these contact cases were requalified as confirmed cases (Demar et al., 2007). In each household, individuals were questioned about compatible symptoms and serology was performed for all of them. Individuals were questioned about food practices or other risk factors using questionnaires evaluated during previous investigations (Demar et al., 2007). If present, cat feces were collected and rectal cotton swabs were used to look for carriage of *T. gondii* in cats. Water samples were collected in rainwater cisterns, little streams, and brooks. Meat samples were acquired from the inhabitants and from stores of the Brazilian bank. Soil samples were collected around all houses, gardens, and water sources of infected families. Random soil samples were also collected around the village. Soil sampling was done by electing places in the village where cats had been spotted; sandy or muddy areas close to human habitations;

entrances to gardens and orchards; banks of brooks and streams; and surface runoff pathways.

All serum samples were analyzed using the EIA for Toxoplasma-specific immunoglobulin, IgG, and IgM (Abbot Diagnostics). Seropositivity could define either acute toxoplasmosis (IgG+, IgM+) or chronic infection (IgG+, IgM–) and seronegativity meant an absence of infection (IgG–, IgM–), as in previous studies (Demar et al., 2007). When acute toxoplasmosis was serologically confirmed, blood samples and fetal tissues were sent to the National Reference Center (Limoges, France) for *T. gondii* real-time PCR, targeting the AF 487550 gene, strain isolation in mice (two mice for each PCR positive samples), and genotyping with 15 microsatellite markers and strain isolation in mice (Ajzenberg et al., 2010). To analyze the position of the isolated strains, a neighbor-joining tree was reconstructed from the genetic distances Dc (Cavalli-Sforza and Edwards, 1967) using a selection of nine reference strains (Type I, Type II, and Type III) and 42 strains previously isolated from different areas in French Guiana (1000 bootstrap replicates). Unrooted trees were obtained with MEGA version 6 software (Tamura et al., 2013).

Water samples were collected using Envirocheck capsules (Pall Life Sciences, Port Washington, NY, USA). Elution was performed according to previous studies (Lélu et al., 2011; Gotteland et al., 2014). Soil samples went through the first step of treatment with Tween 80 (0.1%) and sucrose 1.20, before a series of centrifugations. Meat samples were homogenized with trypsin and gentamycin before incubation, filtration, and centrifugation according to previous protocols (Mercier et al., 2011). Rectal swabs from cats were incubated overnight at 37°C in PBS-Tween 80 (0.1%). DNA extraction was then performed with a QIAmp®DNA Mini Kit (Qiagen, Courtaboeuf, France) for water, meat samples (from a 200 µl aliquot of the final suspension), and cat rectal swabs and using a FastDNA SPIN kit (MP Biomedical) for soil samples. Amplification of *T. gondii* DNA was assessed targeting the AF 487550 gene (Ajzenberg et al., 2010). Each DNA sample was tested in duplicates. Samples were deemed positive when both wells were positive and undetermined in the case of only one positive well.

PCR analyses were performed between 1 month and 1 year after sample collection, in the Parasitology Laboratories of Cayenne (cats feces and rectal swabs, meat) Limoges (blood samples), and Reims (water and soils).

Ethics Statement

Methods of this urgent investigation were approved by the relevant Ethics and Public Health authorities (*Agence Régionale de Santé de Guyane, Santé Publique France, Collectivité Territoriale de Guyane, Parc Amazonien de Guyane*). Animal care and use protocol as well as human investigations were approved by the Presidency of the *Collectivité Territoriale de Guyane* (Territorial Collectivity of French Guiana) on behalf of the *Comité Accès et Partages des Avantages* (Committee for Accessing Biodiversity and Sharing Benefits) under the emergency procedure "APA-973-24" (Document N° 340542/2017/PATDDT/DDDT//FB) according to national (article L.331-15-56, Code de l'Environnement; decree 2013-968 approving the charter for the Guiana Amazonian Park) and European (rule 511/2014 of the European Parliament) guidelines. Animal experimentation conducted in Limoges respecting the 3R aspects was approved and accepted by the Ethics Committee for Animal Experimentation n°33 validated by the French Ministry of National Education, Higher Education and Research (Registration numbers: APAFIS#13914-2018030516473189 v2). All adult patients provided a written consent for themselves and their underage children.

RESULTS

During May and June 2017, 60 people were reached, six refused sampling. Twenty cases out of 54 tested inhabitants (37%) (among a population of roughly 1,800) presented a serology compatible with acute toxoplasmosis (positivity of both IgG and IgM anti-*T. gondii*). These 54 people all belonged to households where at least one of the initial patients was diagnosed (**Table 1**). Some of these contact cases turned out to be confirmed cases after medical examination and blood tests. Confirmed cases were observed in six adults and 14 children belonging to nine different households. All confirmed cases, including asymptomatic ones, presented very high levels of *T. gondii* IgM and IgG, a typical feature of Amazonian toxoplasmosis which favors acute infection rather than chronic infection with residual IgM (**Table 2**). Other tested inhabitants presented a chronic infection (18.5%) or absence of infection (44.5%). Among the 10 patients with chronic infection, three were more than 50 years old, three were <20 years old, four were aged between 20 and 50. Sex ratio among these patients was 1:1. An epidemiological curve and a chart of the investigation timeline are presented in **Figure 2**.

Concerning confirmed cases, mean time to diagnosis was 30 days (median 38 [7–51]), median age of the cohort was 14.5 years old, sex ratio was 3:2. Clinical and biological features of these cases are presented in **Table 2**. The most frequent clinical symptoms were fever (15 patients, 75%) and cough (eight patients, 40%). The most frequent biological disorders were hyponatremia and hepatic cytolysis (six patients, 30%). Four patients were asymptomatic and diagnosed in the systematic screening of people in contact with cases. Four patients (two adults and two children) were hospitalized due to the risk of clinical worsening, but none of them evolved toward severe pneumonia. Intensive care was never required. A pregnant woman was infected at week 10 of pregnancy and a treatment with spiramycin (rovamycin) 3 g/d was started. At week 19 of pregnancy, fetal cardiac pulsations could no longer be heard and intrauterine death was confirmed by echography. One clonal strain was isolated by PCR in the fetus (liver, brain and cardiac biopsies, and peritoneal fluid) (GUY070-KEL, ID of the Toxoplasma Biological Resource Centre: TgH 18070) and by PCR and mouse bioassay from the blood of a 2-year-old boy with no family relation (GUY066-MON, TgH 18066). These strains clearly belong to the Amazonian genetic group as shown in the divergence tree (**Figure 3**).

TABLE 1 | Epidemiological investigation of the 9 infected households, Camopi, French Guiana.

	No. people living in household	Date of first symptoms	IgM+ IgG+ confirmed cases	IgM– IgG+[d] contact cases, chronic infection	IgM– IgG–[d] contact cases, absence of infection	PCR +[d] confirmed cases with parasitemia
Household 1	5	05/05/2017	5 ($n = 2$ adults and $n = 3$ children)	0/5	0/5	0/5
Household 2	6	05/24/2017	2 ($n = 1$ adult and $n = 1$ child)	0/6	4/6	1 (girl, age 14)
Household 3	6	05/17/2017	1 (child)	1/6	4/6	0
Household 4	6[a]	05/31/2017	4 ($n = 1$ adult and $n = 3$ children)	1/5	0/5	2 (pregnant woman and fetus[c])
Household 5	5[a]	05/29/2017	1 (adult)	0/6	3/6	0
Household 6	6	05/08/2017	2 (children)	1/6	3/6	0
Household 7	6[b]	05/19/2017	3 ($n = 1$ adult and $n = 2$ children)	0/6	1/6	1[c](boy, age 2)
Household 8	7	06/20/2017	1 (child)	3/7	3/7	0
Household 9	8[b]	06/20/2017	1 (child)	2/6	4/6	0

[a] *One person refused sampling.*
[b] *Two persons refused sampling.*
[c] *Genotyped strain.*
[d] *IgG+, positive T. gondii IgG antibodies; IgG–, negative T. gondii IgG antibodies; IgM+, positive T. gondii IgM antibodies; IgM–, negative T. gondii IgM antibodies; PCR+, positive T. gondii DNA detection by PCR.*

All households shared risk factors for *T. gondii* linked to their traditional way of life: most heads of families were hunters, and children used to eat both game meat and Brazilian chicken. In addition, all families produced and drank homemade caichiri (traditional cassava alcohol) and often shared it with neighbors and relatives. Water was boiled by only one household. Households 7 and 8 used water from deep pumps but could have been infected when drinking caichiri prepared by other families. Other risk factors reflected a new exposure to the parasite due to changes in habits such as domestication of cats and consumption of industrialized meat from stores of Vila Brazil, a small trading post located just on the other side of the river, on the Brazilian bank (**Table 3**, **Figure 1**). Epidemiological features of each household are detailed in **Table 3**. These households are numbered according to their date of diagnosis. Households 1 and 2 harbored the four first cases.

Toxoplasma gondii was detected by PCR in one water sample out of six from a brook used by a household (**Table 4**). Parasites were also detected in two out of three pieces of meat, corresponding to frozen chicken from a Brazilian store and a piece of game meat (peccary). Cats rectal swabs were all negative, as were 12 samples of cat feces collected across four households. Two soil samples collected during the investigation were clearly positive, including one collected in front of Household 4 and one random sample from the riverfront of the health center. Seven soil samples were undetermined, five of them around infected households (on the soil of the brook used by Households 5 and 2, and close to homes of Households 4, 5, and 9) and two random samples across the village. MS genotyping was not possible for the PCR positive environmental and meat samples due to an insufficient amount of DNA. Detailed results of environmental samples and meats are presented in **Table 4**.

DISCUSSION

This is the largest outbreak of acute toxoplasmosis ever reported in French Guiana, and the first one in an Amerindian community. This epidemiological investigation provided evidence for the spread of *T. gondii* in this remote area, which until now had only reported sporadic cases. We observed several changes in human habits in this community that may have reinforced the exposure to *T. gondii*. The outbreak occurred following an abnormal climatic event with an important episode of flooding and warming. The conjunction of all these factors may have paved the way for an increased parasitic circulation of this zoonotic disease.

Though 16 patients were symptomatic, clinical presentations lacked the respiratory severity that was often reported in Amazonian toxoplasmosis (Carme et al., 2002; Demar et al., 2012). As in previous studies, the involvement of an atypical strain does not seem to be necessarily associated with a poor outcome (Demar et al., 2007; Carme et al., 2009; Blaizot et al., 2018). Indeed, atypical strains are characterized by a high genotypic diversity, especially in the Amazon region, which may correspond to diverse pathogenicity in humans and mice. Moreover, host factors probably play an important role in the severity of Amazonian toxoplasmosis, and genetic susceptibility might be different in this Amerindian population. Indeed, no respiratory involvement was reported in a *T. gondii* outbreak of US military occurring in the Panama jungle (Benenson et al., 1982) nor during the Santa Isabel outbreak in Brazil, which was linked to an atypical strain (de Moura et al., 2006; Vaudaux et al., 2010). Another feature of the Camopi outbreak is the absence of eye involvement, in contrast to what occurs frequently in Amazonian cases of *T. gondii* infection (Carme et al., 2009; Blaizot et al., 2018).

TABLE 2 | Clinical and laboratory features of the 20 cases of acute toxoplasmosis, Camopi, French Guiana.

Clinical and laboratory features	No. cases (%)
Clinical signs[a]	
Asymptomatic	4/20 (20)
Fever	15/20 (75)
Cough/Pneumonia	8/20 (40)
Lymphadenopathy	6/20 (30)
Headache	6/20 (30)
Digestive signs	5/20 (25)
Myalgia	1/20 (5)
Conjunctivitis	1/20 (5)
Skin rash	1/20 (5)
Hepatomegaly	1/20 (5)
Inpatient care	5/20 (25)
Adults[b]	3/6 (50)
Children	2/14 (14.3)
Laboratory disorders	
Positive *T. gondii* IgG and IgM[c]	20/20 (100)
Mean levels in IU/mL (min, max):	780 (25.2–1814.4)
IgG	19.25 (4.1–31.0)
IgM	
Hyponatremia	6/20 (30)
Hepatic cytolysis	6/20 (30)
Lymphocytosis	3/20 (15)
Elevated creatine kinase	3/20 (15)
High lactate dehydrogenase	3/20 (15)
High C-reactive protein	2/20 (10)
Eosinophilia	2/20 (10)
Outcome[d],	
Complete response[e]	20/20 (100)
Death	0/20 (0)
Normal Fundoscopy at 6 months	20/20 (100)

[a] *Splenomegaly was not detected, but proper examination with an examination table was not possible in traditional houses.*
[b] *One adult was hospitalized in the Dermatology Department (important skin rash), one in the Infectious Diseases Department, and a pregnant woman was treated in the Obstetrics Department.*
[c] *Detection threshold: 3IU/mL (IgG) and 0.6 IU/mL (IgM).*
[d] *All confirmed cases were treated with sulfamethoxazole (1,600 mg/d) and trimethoprim (320 mg/d) for 21 days. A fetus died at week 19 of pregnancy but was not included in this table of born patients.*
[e] *Clearance of all symptoms after 21 days of treatment.*

A traditional way of life based on hunting, fishing, gathering, and agriculture seems to be associated with accidental exposures to wild strains of *T. gondii*. Indeed, seroprevalence of *T. gondii* was as low as 18.5% (95% CI [8.1–28.9]) of sampled people during this outbreak. Seroprevalence was even lower (8.3%) amongst the tested population during the Patam outbreak (Demar et al., 2007). In contrast, in a study of three indigenous populations in Brazil, including Wayampi from the Brazilian bank who are ethnically related to their French Guiana counterparts, the authors reported a seroprevalence varying between 50 and 80% (Sobral et al., 2005). An even higher prevalence of specific IgG antibodies was reported in Amerindians of the Venezuelan Amazon (88%) (de la Rosa et al., 1999). These findings show that the level of exposure to *T. gondii* can be very diverse between indigenous populations of Amazonia. In addition, the very low level of exposure in Amerindians leaves them vulnerable to sudden outbreaks, such as the one hereby reported. Even if our sample size is small, it should be noted that we did not report any significant increase of the IgG prevalence with age, in contrast with Brazilian findings (Sobral et al., 2005). We did, however, found an equal sex ratio between male and women with chronic infection, as in the findings of Sobral et al. Men and women are engaged in activities which are frequently at risk of contact with *T. gondii* (hunting for men, cooking for women, agriculture for both genders).

Wild and domestic felids possibly played an important role in spreading oocysts throughout the village. Though seven of the soil samples brought undetermined results, they still bear some significance, due to the poor sensitivity of PCR and the small amount of DNA in soil samples (Lélu et al., 2011; Gotteland et al., 2014). Several families reported a recent domestication of cats in the last 6 months, with multiple births of kittens which were traded or offered as gifts. This recent breeding could have amplified the wild cycle in the direct proximity of dwellings as these felids can mix with their wild counterparts or can hunt infected mammals (Carme et al., 2009; Mercier et al., 2011). Though PCR was negative on all cat feces samples and rectal swabs, these results do not rule out the involvement of domestic or wild felids in this outbreak, due to the low rate of detection for both techniques and the inconstant shedding of oocysts in felids feces (Jones and Dubey, 2010). Though examined cats may not have been shedding cysts at the time of the investigation, they might have shed in the environment several weeks before and contaminated water sources.

A hypothesis of waterborne outbreak can be supported by the detection of *T. gondii* DNA in a water sample from an infected household, consumption of unfiltered water by most inhabitants, sharing of caichiri, and dispersion of cases throughout the village. The 2017 rain season was one of the wettest and hottest ever recorded in French Guiana (Meteo France, 2017), particularly in May, when rainfalls were 32% above normal. As the outbreak happened following this episode of rainfall, oocysts may have contaminated rivers used as water sources. Indeed, it has been shown that oocysts can persist in the soil and can be washed into bodies of water via rain and river flowing (Jones and Dubey, 2010; Lélu et al., 2011). Previous reports in Vancouver and Santa Isabel have highlighted the role of cougars or cats directly infecting water supplies with their feces (Aramini et al., 1999; Vaudaux et al., 2010). This scenario could also have happened in Camopi as most brooks, including the positive one, were not protected by a cap. Consumption of contaminated water has been incriminated in several outbreaks of *T. gondii* in the Americas (Benenson et al., 1982; Pino et al., 2009). Several oocysts-borne outbreaks have been described in Brazil after consumption of contaminated water (Ferreira et al., 2018). Socio-economic and logistical factors such as low access to healthcare, poverty, and lack of water infrastructure have been shown to contribute to oocysts transmission (Ferreira et al., 2018). In peri-urban regions of

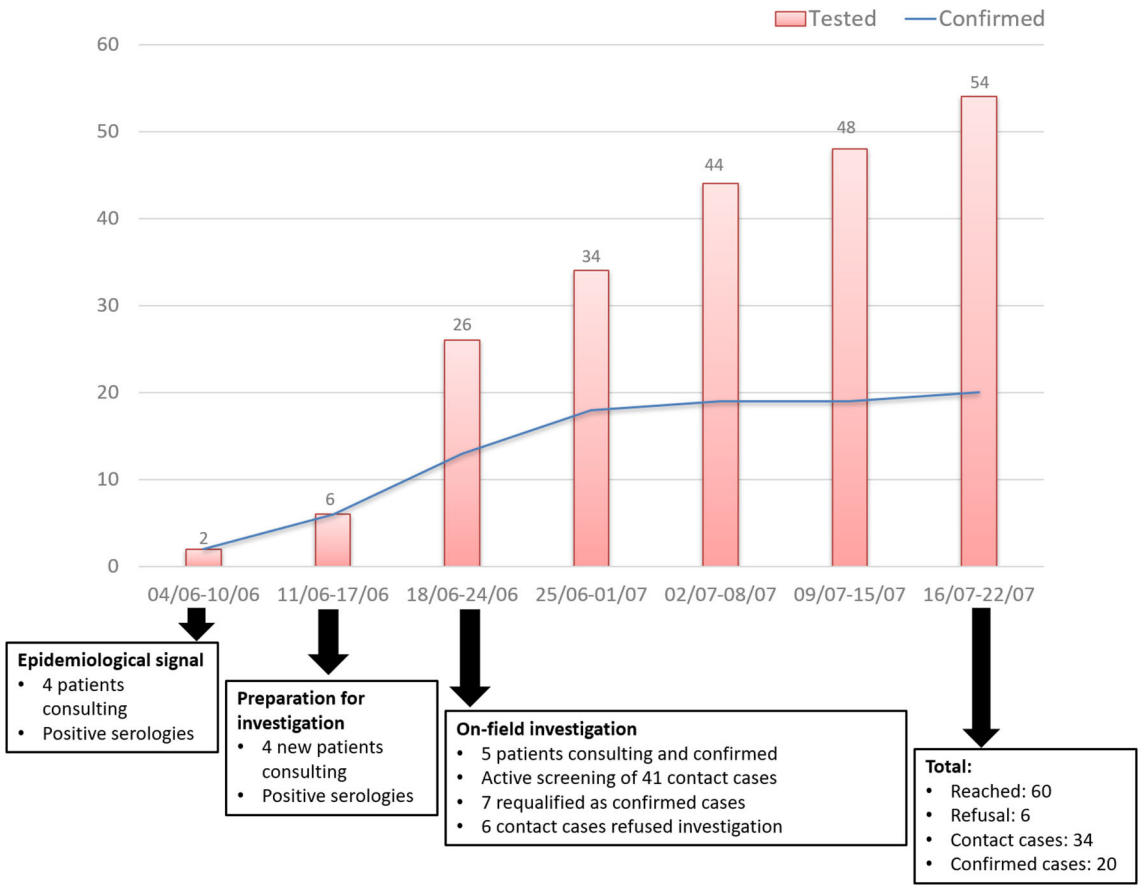

FIGURE 2 | Timeline of the investigation and epidemiological curve of tested and confirmed cases, Camopi toxoplasmosis outbreak, 2017.

Brazil, high levels of environmental contamination with oocysts, the presence of a *T. gondii* genetic diversity of strains, a rich wild feline biodiversity in peri-urban, rural, and forested areas, and the proliferation of stray and domestic cats were described as specific factors contributing to a high prevalence of *T. gondii* infections (Shapiro et al., 2019). These features are likely to be found in many endemic areas and were observed in Camopi. A non-archetypal strain of *T. gondii*, isolated from a water supply, was identified as the causative agent of an outbreak in Brazil (Vaudaux et al., 2010). Waterborne infections in previous reports frequently involved hundreds of cases in urban settings due to the contamination of big water reservoirs (Bowie et al., 1997; de Moura et al., 2006) and cases spread over several weeks (Meireles et al., 2015). Similarly, we observed a temporal dispersion of cases from early May to late June. However, the rural environment of the village and the small population along with the absence of a common reservoir for the whole village might explain the relatively small number of cases. Positivity of one water sample out of six was not surprising due to a delay of water collection after the beginning of the outbreak and the small volume used for filtration (10L) to avoid membrane saturation due to the high turbidity. The importance of improving the quality of drinking and irrigation water has been emphasized by a recent review of *T. gondii* outbreaks which highlighted a shift in the epidemiology over the last 20 years, oocysts-mediated outbreaks becoming more frequent in the 2000s (Pinto-Ferreira et al., 2019).

Toxoplasmosis has long been characterized as a food-borne disease and consumption of uncooked game meat has historically been described as a typical cause of Amazonian toxoplasmosis (Carme et al., 2002; Demar et al., 2012). Implication of food in this outbreak was supported by a positive PCR in both game meat and industrial chicken samples. Villagers have changed their habits and now tend to trust frozen meat from Brazilian stores. A broken cold chain could have happened in groceries as we have noticed that this area is not continuously supplied with electricity and power outages are frequent due to the lack of a backup generator. There is no sanitary control in this remote settlement completely isolated from the rest of Brazil. As for cooking, either for industrial or game meat, heating at 60°C for 10 min is necessary to kill all cysts in muscles (El-Nawawi et al., 2008). However, interrogated Amerindians cooked the meat by boiling or buccan. Buccan is a native South American name for a wooden framework on which meat is smoked over a fire. Several men complained of eating meat undercooked by their wives. Fresh vegetables cultivated in rural areas are a possible source of *T. gondii*

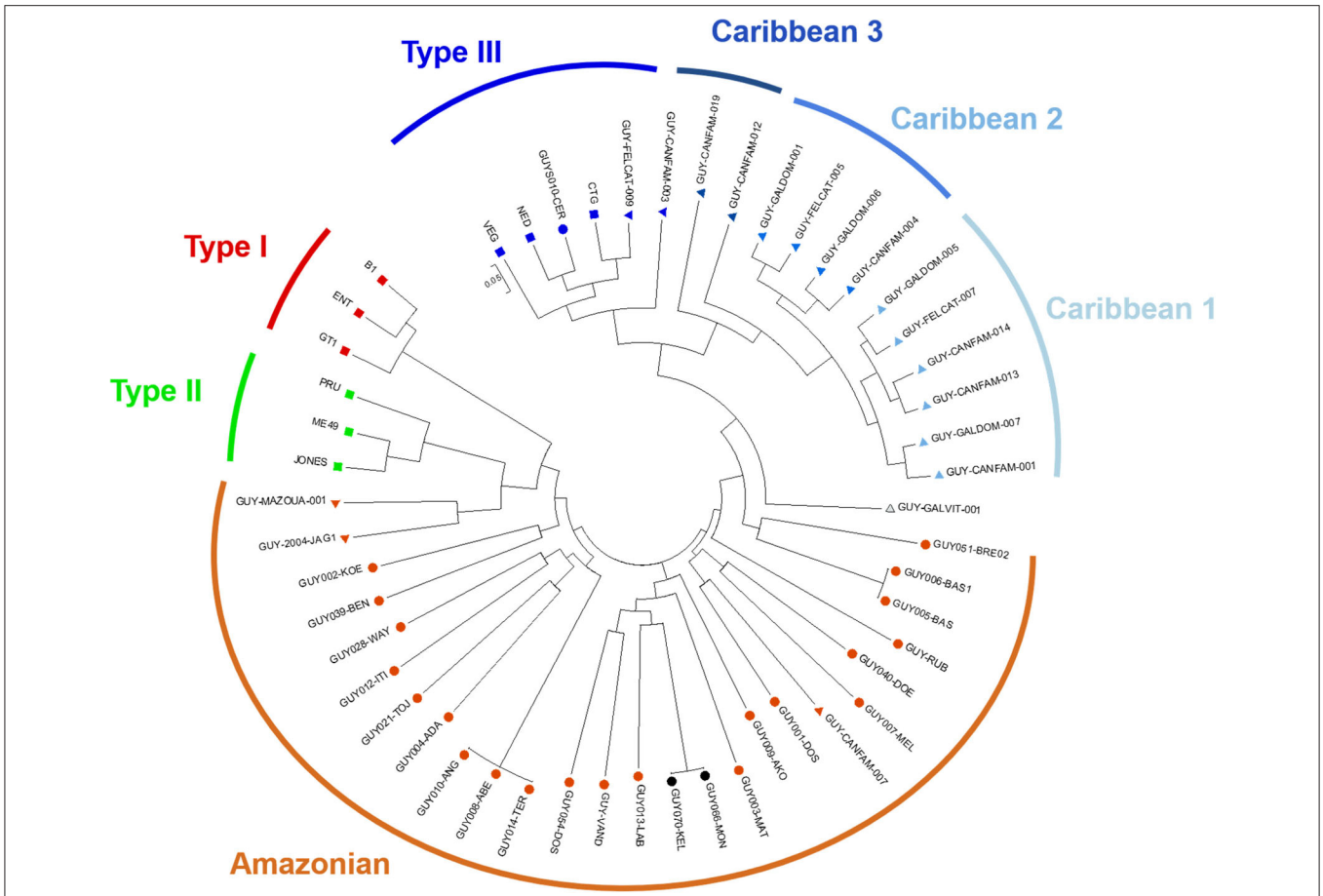

FIGURE 3 | Neighbor-joining clustering of *T. gondii* strains from French Guiana, based on 15 microsatellite markers: circles and triangles correspond, respectively to strains of human and animal origin; black circles correspond to the 2 strains isolated during the Camopi outbreak with 15/15 markers amplified; red, green, and dark blue squares are reference strains of Type I, Type II, and Type III genotype, respectively.

contamination (Hohweyer et al., 2016) and the ingestion of green vegetables has been associated with an outbreak in Saõ Paulo (Ekman et al., 2012). All households also practiced traditional agriculture in small gardens exposed to felids feces but only two cassava samples could be tested and found negative in PCR.

Amerindian populations of French Guiana have always been exposed to toxoplasmosis due to their practice of hunting and traditional agriculture. However, the recent domestication of cats, which until now were very rare in the village of Camopi, along with the shift from nomadic life to fixed habitations, constitute new risk factors for this disease. The brutal introduction of new life habits in a population not prepared for Western civilization is called an acculturation process. This phenomenon has been previously analyzed as a factor of increased circulation of *T. gondii*, particularly in communities of South America where the presence of domestic cats is coupled with the absence of modern water supply (Chacin-Bonilla et al., 2001; Sobral et al., 2005; Bóia et al., 2008). However, the threat posed by acculturation on the health of Amerindians has never been analyzed to such an extent. Moreover, one should also bear in mind that these findings apply not only to Native Amerindians of South America but also to non-indigenous populations of low economic level and marginal communities in South America (Diaz-Suárez and Estevez, 2009) and many indigenous populations worldwide (Fan et al., 2003; Hotez, 2010; Ngui et al., 2011). Indeed, we report among the Teko and Wayampi people several risk factors such as close contact with cats and dogs, consumption of undercooked game meat, drinking un-boiled and unsafe water, children playing in the dirt, or houses with floors made of mixed soil and sand. Interestingly, many of these epidemiological features have been described in indigenous populations who are over-exposed to toxoplasmosis, such as the Orang Asli of Malaysia (Ngui et al., 2011), or aboriginal populations of Northern Thailand (Fan et al., 2003), and the mountainous areas of Taiwan (Fan et al., 1998). In the same way, in Inuit communities of the Arctic, toxoplasmosis has been associated with consumption of caribou and seal meat, or contaminated water (Hotez, 2010).

Although a clonal atypical strain of *T. gondii* was identified in two unrelated patients in this study and confirmed

TABLE 3 | Risk factors of toxoplasmosis of the 9 infected households, Camopi, French Guiana.

	Felids around the house	Cooking method	Water boiling	Water sources	Homemade products	Ethnicity
Household 1	Domestic cats ($n = 2$)	Boiling buccan	No	Deep well pump Brook	Caichiri Wasai juice	Wayampi
Household 2	No	Boiling buccan stew	No	Rainwater tank Brook	Caichiri Wasai juice Sugar cane juice	Teko
Household 3	Domestic kitten ($n = 1$)	Boiling stewing	Yes	Rainwater tank Brook	Caichiri	Teko
Household 4	Domestic cats (n =1 adult and $n = 1$ kitten)	Boiling	Caichiri only	Brook	Caichiri Sugar cane juice	Teko
Household 5	Wild cat ($n = 1$) Domestic cats ($n = 1$ adult and $n = 1$ kitten)	Boiling buccan stew	Cramanioc only	Rainwater tank, brook	Caichiri	Wayampi
Household 6	Puma Jaguarondi Domestic kitten ($n = 1$)	Boiling buccan	Yes	Deep well pump Brook	Caichiri	Wayampi
Household 7	Puma	Boiling	No	Deep well pump	Caichiri	Teko
Household 8	No	Boiling buccan	No	Deep well pump	Caichiri	Wayampi
Household 9	No	Boiling buccan	No	Brook	Caichiri	Teko

the epidemic transmission, it did not support a specific transmission route. Thus, the main limitation of our study was the difficulty to isolate and compare the strains from positive human and environmental samples. Isolation of strains is challenging due to the transient presence of the parasite and the difficulty in obtaining a complete genotype due to a low amount of DNA. Another limitation derives from the difficulties of medical interrogation in Amerindian villages despite the presence of a translator. Hunters were often reluctant to give away information on their hunting practices and women who are responsible for cooking were unwilling to answer questions. Finally, the absence of a negative control group did not allow us to perform a real case-control study in order to determine a specific way of contamination.

Our findings suggest that numerous actions should be undertaken to improve the management of toxoplasmosis in remote tropical areas. Eradication of cats in islands has been linked to important benefits in terms of public health (de Wit et al., 2019) and should be contemplated in Amerindian communities where intermingling with wild felids is particularly dangerous, as it can enhance human contact with the wild cycle of *T. gondii*. As recently suggested by Pinto-Ferreira et al. (2019), a greater attention should be paid to the quality of drinking and irrigation water, and to the adoption of recommendations for tracking outbreaks with the aim of eliminating transmission routes, avoiding exposure, or inactivating the parasite before consumption. Another improvement in public health policies would be the development of accurate point-of-care tests for *T. gondii* in isolated areas (Begeman et al., 2017). Indeed, the median time between the first symptoms and diagnosis for each patient was very long in our report (38 days) due to a lack of awareness in local clinicians and due to logistical issues in analyzing blood samples. Point-of-care tests should be improved to detect both IgG and IgM, in order to allow biological confirmation of acute toxoplasmosis, and should be tested with atypical genotypes which do not belong to the main lineages. The burden of acute toxoplasmosis in pregnant women has benefited from some attention, showing that the prevalence during pregnancy can be high in low-income, tropical countries (Rostami et al., 2019). However, one should not forget the possible occurrence of acute toxoplasmosis among men and non-pregnant, immunocompetent women, such as in this outbreak in the village of Camopi. Additionally, one must keep in mind that severe toxoplasmosis might occur in other parts of the world and remain under-diagnosed, even though numerous reports of severe acute toxoplasmosis in South America have led to the description of the "Amazonian toxoplasmosis" entity. Indeed, five cases of severe toxoplasmosis in French travelers returning from West and Central Africa have recently been reported in France (Leroy et al., 2019).

In conclusion, the investigation of this toxoplasmosis outbreak highlighted new life habits among this Amerindian community. Fixed habitations have been built in the last few decades but without providing safe water sources. These sedentary settlements increase the risk of grouped cases, particularly if domestic or wild felids are allowed to come in close contact with habitations. Public health policies should target these indigenous communities, providing safe water supply, health recommendations, and epidemiological surveillance of acute toxoplasmosis. Toxoplasmosis was not listed among a recent review of Neglected Tropical Diseases in the Americas (Hotez et al., 2008). There is consequently no roadmap for its control in remote areas and traditional communities. Future studies should look for possible outbreaks or emerging circulation of *T. gondii* in subtropical areas, including outside South America, in order to assess the exact burden of the disease.

TABLE 4 | Results of *Toxoplasma gondii* PCR on environmental and meat samples collected during the outbreak investigation, Camopi village, French Guiana.

	Cat rectal swabs	Cat feces	Vegetables	Meat	Water	Soil
Household 1	Negative[a] (4/4)	Negative (3/3)	–	–	Negative (1 brook)	Negative (3/3)
Household 2	–	–	–	–	Negative (1 brook)	Undetermined (1/1) (Ct 37.8)
Household 3	Negative (2/2)	Negative (2/2)	–	–	–	Negative (3/3)
Household 4	–	Negative (3/3)	Negative (1 fresh cassava)	**Positive (1 peccari, Ct[c] 36.1)**	–	**Positive (1/5) (Ct 29 and 33.9)** Undetermined (2/5) (Ct 39 35.5) Negative (2/5)
Household 5	Negative (1 kitten, 1 adult)	Negative (4/4)	Negative (1 fried cassava)	–	–	Undetermined (1/1) (Ct 39.4)
Household 6	–[b]	–	–	–	Negative (1 brook)	Negative (2/2)
Household 7	–	–	–	–	–	Negative (2/2)
Household 8	–	–	–	–	Negative (1 deep, 1 well pump)	Negative (2/2)
Household 9	–	–	–	–	**Positive (1 brook, Ct 36.6)**	Undetermined (1/1) (Ct 38.2)
Random soil samples	–	–	–	–	–	**Positive (1/33) (Ct 34.8 and 35.5)** Undetermined (2/33) (Ct 39.3 and 38.9) Negative (30/33)
Brazilian stores	–	–	–	**Positive (2 frozen chicken, Ct 38.1 and 36.8)**	–	–

[a] *"Positive", "negative" and "undetermined" corresponds to T. gondii PCR results. Number of tested samples and type of samples are indicated into brackets. Undetermined samples correspond to positivity of only one well over two duplicates.*
[b] *Not assessed.*
[c] *Cycle threshold.*
Bold values correspond to positive PCR.

DATA AVAILABILITY STATEMENT

All datasets generated for this study are included in the article.

ETHICS STATEMENT

The studies involving human participants were reviewed and approved by Collectivité Territoriale de Guyane (Territorial Collectivity of French Guiana) on behalf of the Comité Accès et Partages des Avantages (Committee for Accessing Biodiversity and Sharing Benefits) under the emergency procedure APA-973-24 (Document N° 340542/2017/PATDDT/DDDT//FB). Written informed consent to participate in this study was provided by the participants' legal guardian/next of kin. This animal study was reviewed and approved by Collectivité Territoriale de Guyane (Territorial Collectivity of French Guiana) on behalf of the Comité Accès et Partages des Avantages (Committee for Accessing Biodiversity and Sharing Benefits).

AUTHOR CONTRIBUTIONS

RB, FD, EM, and FH: clinical data. LL, SE-B, DB, AM, M-LD, and IV: laboratory analysis. RB, CN, LL, BF, and MD: field investigation. RB and CN: drafting. AM, M-LD, IV, and MD: revising. MD: supervision. All authors contributed to the article and approved the submitted version.

FUNDING

This work did not receive any external funding. Internal funding from the National Reference Center for Toxoplasmosis was used for laboratory analysis.

ACKNOWLEDGMENTS

The authors are grateful to the Guiana Amazonian Park (Parc Amazonien de Guyane) and to the French Armed Forces in Guiana (Forces armées en Guyane) for their logistical support. The authors want to thank Elsa Thery-Casari and Coralie Hardy for their help in the collection of samples; Emma Cuadro, Mélanie Gaillet, and Sophie Tondeur-Ortega for some clinical data; Paul Brousse for logistical support; Isabelle Vallée for help with samples of meat; Karine Passebosc-Faure for her contribution on genotyping.

REFERENCES

Ajzenberg, D., Collinet, F., Mercier, A., Vignoles, P., and Dardé, M. L. (2010). Genotyping of *Toxoplasma gondii* isolates with 15 microsatellite markers in a single multiplex PCR assay. *J. Clin. Microbiol.* 48, 4641–4645. doi: 10.1128/JCM.01152-10

Aramini, J. J., Stephen, C., Dubey, J. P., Engelstoft, C., Schwantje, H., and Ribble, C. S. (1999). Potential contamination of drinking water with *Toxoplasma gondii* oocysts. *Epidemiol. Infect.* 122, 305–315. doi: 10.1017/S0950268899002113

Begeman, I. J., Lykins, J., Zhou, Y., Lai, B. S., Levigne, P., El Bissati, K., et al. (2017). Point-of-care testing for *Toxoplasma gondii* IgG/IgM using Toxoplasma ICT IgG-IgM test with sera from the United States and implications for developing countries. *PLoS Negl. Trop. Dis.* 11:e0005670. doi: 10.1371/journal.pntd.0005670

Benenson, M. W., Takafuji, E. T., Lemon, S. M., Greenup, R. L., and Sulzer, A. J. (1982). Oocyst-transmitted toxoplasmosis associated with ingestion of contaminated water. *N. Engl. J. Med.* 307, 666–669. doi: 10.1056/NEJM198209093071107

Blaizot, R., Nabet, C., Blanchet, D., Martin, E., Mercier, A., Dardé, M. L., et al. (2018). Pediatric Amazonian toxoplasmosis caused by atypical strains in French Guiana, 2002-2017. *Pediatr. Infect. Dis. J.* 73, 330–331. doi: 10.1016/j.ijid.2018.04.4164

Bóia, M. N., Carvalho-Costa, F. A., Sodré, F. C., Pinto, G. M., and Amendoeira, M. R. (2008). Seroprevalence of *Toxoplasma gondii* infection among indian people living in Iauareté, São Gabriel da Cachoeira, Amazonas, Brazil. *Rev. Inst. Med. Trop. Saõ Paulo*. 50, 17–20. doi: 10.1590/S0036-46652008000100004

Bowie, W. R., King, A. S., Werker, D. H., Isaac-Renton, J. L., Bell, A., Eng, S. B., et al. (1997). Outbreak of toxoplasmosis associated with municipal drinking water. The BC Toxoplasma Investigation Team. *Lancet* 350, 173–177. doi: 10.1016/S0140-6736(96)11105-3

Carme, B., Bissuel, F., Ajzenberg, D., Bouyne, R., Aznar, C., Demar, M., et al. (2002). Severe acquired toxoplasmosis in immunocompetent adult patients in French Guiana. *J. Clin. Microbiol.* 40, 4037–4044. doi: 10.1128/JCM.40.11.4037-4044.2002

Carme, B., Demar, M., Ajzenberg, D., and Dardé, M. L. (2009). Severe acquired toxoplasmosis caused by wild cycle of *Toxoplasma gondii*, French Guiana. *Emerging Infect. Dis.* 15, 656–658. doi: 10.3201/eid1504.081306

Carme, B., and Demar-Pierre, M. (2006). [Toxoplasmosis in French Guiana. Atypical (neo-)tropical features of a cosmopolitan parasitosis]. *Med. Trop.* 66, 495–503.

Cavalli-Sforza, L. L., and Edwards, A. W. F. (1967). Phylogenetic analysis: models and estimation procedures. *Evolution.* 21, 550–570. doi: 10.1111/j.1558-5646.1967.tb03411.x

Chacin-Bonilla, L., Sanchez-Chavez, Y., Monsalve, F., and Estevez, J. (2001). Seroepidemiology of toxoplasmosis in amerindians from western Venezuela. *Am. J. Trop. Med. Hyg.* 65, 131–135. doi: 10.4269/ajtmh.2001.65.131

Choi, W. Y., Nam, H. W., Kwak, N. H., Huh, W., Kim, Y. R., Kang, M. W., et al. (1997). Foodborne outbreaks of human toxoplasmosis. *J. Infect. Dis.* 175, 1280–1282. doi: 10.1086/593702

Dardé, M. L., Villena, I., Pinon, J. M., and Beguinot, I. (1998). Severe toxoplasmosis caused by a *Toxoplasma gondii* strain with a new isoenzyme type acquired in French Guyana. *J. Clin. Microbiol.* 36:324. doi: 10.1128/JCM.36.1.324-324.1998

de la Rosa, M., Bolívar, J., and Pérez, H. A. (1999). [*Toxoplasma gondii* infection in Amerindians of Venezuela Amazon]. *Medicina* 59, 759–762.

de Moura, L., Bahia-Oliveira, L. M. G., Wada, M. Y., Jones, J. L., Tuboi, S. H., Carmo, E. H., et al. (2006). Waterborne toxoplasmosis, Brazil, from field to gene. *Emerging Infect. Dis.* 12, 326–329. doi: 10.3201/eid1202.041115

de Wit, L. A., Croll, D. A., Tershy, B., Correa, D., Luna-Pasten, H., Quadri, P., et al. (2019). Potential public health benefits from cat eradications on islands. *PLoS Negl. Trop. Dis.* 13:e0007040. doi: 10.1371/journal.pntd.0007040

Demar, M., Ajzenberg, D., Maubon, D., Djossou, F., Panchoe, D., Punwasi, W., et al. (2007). Fatal outbreak of human toxoplasmosis along the Maroni River: epidemiological, clinical, and parasitological aspects. *Clin. Infect. Dis.* 45:e88–e95. doi: 10.1086/521246

Demar, M., Hommel, D., Djossou, F., Peneau, C., Boukhari, R., Louvel, D., et al. (2012). Acute toxoplasmoses in immunocompetent patients hospitalized in an intensive care unit in French Guiana. *Clin. Microbiol. Infect.* 18:E221–E231. doi: 10.1111/j.1469-0691.2011.03648.x

Diaz-Suárez, O., and Estevez, J. (2009). Seroepidemiology of toxoplasmosis in women of childbearing age from a marginal community of Maracaibo, Venezuela. *Rev. Inst. Med. Trop. Saõ Paulo.* 51, 13–17. doi: 10.1590/S0036-46652009000100003

Dubey, J. P., Navarro, I. T., Sreekumar, C., Dahl, E., Freire, R. L., Kawabata, H. H., et al. (2004). *Toxoplasma gondii* infections in cats from Paraná, Brazil: seroprevalence, tissue distribution, and biologic and genetic characterization of isolates. *J. Parasitol.* 90, 721–726. doi: 10.1645/GE-382R

Ekman, C. C. J., Chiossi MF do, V, Meireles, L. R., Andrade Júnior, H. F., de Figueiredo, W. M., Marciano, M. A. M., et al. (2012). Case-control study of an outbreak of acute toxoplasmosis in an industrial plant in the state of São Paulo, Brazil. *Rev. Inst. Med. Trop. Saõ Paulo.* 54, 239–244. doi: 10.1590/S0036-46652012000500001

El-Nawawi, F. A., Tawfik, M. A., and Shaapan, R. M. (2008). Methods for inactivation of *Toxoplasma gondii* cysts in meat and tissues of experimentally infected sheep. *Foodborne Pathog. Dis.* 5, 687–690. doi: 10.1089/fpd.2007.0060

Fan, C. K., Liao, C. W., Wu, M. S., Su, K. E., and Han, B. C. (2003). Seroepidemiology of *Toxoplasma gondii* infection among Chinese aboriginal and Han people residing in mountainous areas of northern Thailand. *J. Parasitol.* 89, 1239–1242. doi: 10.1645/GE-3215RN

Fan, C. K., Su, K. E., Chung, W. C., Tsai, Y. J., Chiou, H. Y., Lin, C. F., et al. (1998). Seroprevalence of *Toxoplasma gondii* antibodies among Atayal aboriginal people and their hunting dogs in northeastern Taiwan. *Jpn. J. Med. Sci. Biol.* 51, 35–42. doi: 10.7883/yoken1952.51.35

Ferreira, F. P., Caldart, E. T., Freire, R. L., Mitsuka-Breganó, R., Freitas, F. M., Miura, A. C., et al. (2018). The effect of water source and soil supplementation on parasite contamination in organic vegetable gardens. *Rev. Bras. Parasitol. Vet.* 27, 327–337. doi: 10.1590/s1984-296120180050

Gotteland, C., Gilot-Fromont, E., Aubert, D., Poulle, M.-L., Dupuis, E., Dardé, M.-L., et al. (2014). Spatial distribution of *Toxoplasma gondii* oocysts in soil in a rural area: Influence of cats and land use. *Vet. Parasitol.* 205, 629–637. doi: 10.1016/j.vetpar.2014.08.003

Heukelbach, J., Meyer-Cirkel, V., Moura, R. C. S., Gomide, M., Queiroz, J. A. N., Saweljew, P., et al. (2007). Waterborne toxoplasmosis, northeastern Brazil. *Emerging Infect. Dis.* 13, 287–289. doi: 10.3201/eid1302.060686

Hill, D., and Dubey, J. P. (2002). *Toxoplasma gondii*: transmission, diagnosis and prevention. *Clin. Microbiol. Infect.* 8, 634–640. doi: 10.1046/j.1469-0691.2002.00485.x

Hohweyer, J., Cazeaux, C., Travaillé, E., Languet, E., Dumètre, A., Aubert, D., et al. (2016). Simultaneous detection of the protozoan parasites Toxoplasma, Cryptosporidium and Giardia in food matrices and their persistence on basil leaves. *Food Microbiol.* 57, 36–44. doi: 10.1016/j.fm.2016.01.002

Hotez, P. J. (2010). Neglected infections of poverty among the indigenous peoples of the arctic. *PLoS Negl. Trop. Dis.* 4:e606. doi: 10.1371/journal.pntd.0000606

Hotez, P. J., Bottazzi, M. E., Franco-Paredes, C., Ault, S. K., and Periago, M. R. (2008). The neglected tropical diseases of Latin America and the Caribbean: a review of disease burden and distribution and a roadmap for control and elimination. *PLoS Negl. Trop. Dis.* 2:e300. doi: 10.1371/journal.pntd.0000300

Isaac-Renton, J., Bowie, W. R., King, A., Irwin, G. S., Ong, C. S., Fung, C. P., et al. (1998). Detection of *Toxoplasma gondii* oocysts in drinking water. *Appl. Environ. Microbiol.* 64, 2278–2280. doi: 10.1128/AEM.64.6.2278-2280.1998

Jones, J. L., and Dubey, J. P. (2010). Waterborne toxoplasmosis–recent developments. *Exp. Parasitol.* 124, 10–25. doi: 10.1016/j.exppara.2009.03.013

Leal, F. E., Cavazzana, C. L., de Andrade, H. F., Jr., Galisteo, A. Jr., de Mendonça, J. S., and Kallas, E. G. (2007). *Toxoplasma gondii* pneumonia in immunocompetent subjects: case report and review. *Clin. Infect. Dis.* 44:e62–e66. doi: 10.1086/511871

Lélu, M., Gilot-Fromont, E., Aubert, D., Richaume, A., Afonso, E., Dupuis, E., et al. (2011). Development of a sensitive method for *Toxoplasma gondii* oocyst extraction in soil. *Vet. Parasitol.* 183, 59–67. doi: 10.1016/j.vetpar.2011.06.018

Leroy, J., Delhaes, L., Houzé, S., Loubet, P., Yéra, H., Rossi, B., et al. (2019). La toxoplasmose aiguë rare mais grave chez le voyageur de retour d'Afrique tropicale. *Médecine et Maladies Infectieuses* 49, S118–S128. doi: 10.1016/j.medmal.2019.04.291

Meireles, L. R., Ekman, C. C. J., Andrade, H. F., and de, Luna, E. J. A. (2015). Human toxoplasmosis outbreaks and the agent infecting form. Findings from a systematic review. *Rev. Inst. Med. Trop. Saõ Paulo.* 57, 369–376. doi: 10.1590/S0036-46652015000500001

Mercier, A., Ajzenberg, D., Devillard, S., Demar, M. P., de Thoisy, B., Bonnabau, H., et al. (2011). Human impact on genetic diversity of *Toxoplasma gondii*: example of the anthropized environment from French Guiana. *Infect Genet. Evol.* 11, 1378–87. doi: 10.1016/j.meegid.2011.05.003

Meteo France (2017). *Bulletin Climatique Annuel*. Matoury: Meteo France, Climatologie Guyane.

Neves Ede, S., Kropf, A., Bueno, W. F., Bonna, I. C., Curi, A. L., Amendoeira, M. R., et al. (2011). Disseminated toxoplasmosis: an atypical presentation in an immunocompetent patient. *Trop. Doct*. 41, 59–60. doi: 10.1258/td.2010.100228

Ngui, R., Lim, Y. A., Amir, N. F., Nissapatorn, V., and Mahmud, R. (2011). Seroprevalence and sources of toxoplasmosis among Orang Asli (indigenous) communities in Peninsular Malaysia. *Am. J. Trop. Med. Hyg*. 85, 660–666. doi: 10.4269/ajtmh.2011.11-0058

Nunura, J., Vásquez, T., Endo, S., Salazar, D., Rodriguez, A., Pereyra, S., et al. (2010). Disseminated toxoplasmosis in an immunocompetent patient from Peruvian Amazon. *Rev. Inst. Med. Trop. Saõ Paulo*. 52, 107–110. doi: 10.1590/S0036-46652010000200008

Pino, L. E., Salinas, J. E., and López, M. C. (2009). Description of an epidemic outbreak of acute toxoplasmosis in immunocompetent patients from Colombian Armed Forces during jungle operations. *Infectio* 13, 83–91. doi: 10.1016/S0123-9392(09)70729-5

Pinto-Ferreira, F., Caldart, E. T., Pasquali, A. K. S., Mitsuka-Breganó, R., Freire, R. L., and Navarro, I. T. (2019). Patterns of transmission and sources of infection in outbreaks of human toxoplasmosis. *Emerging Infect. Dis*. 25, 2177–2182. doi: 10.3201/eid2512.181565

Robert-Gangneux, F., and Dardé, M. L. (2012). Epidemiology of and diagnostic strategies for toxoplasmosis. *Clin. Microbiol. Rev*. 25, 264–296. doi: 10.1128/CMR.05013-11

Rostami, A., Riahi, S. M., Contopoulos-Ioannidis, D. G., Gamble, H. R., Fakhri, Y., Shiadeh, M. N., et al. (2019). Acute Toxoplasma infection in pregnant women worldwide: a systematic review and meta-analysis. *PLoS Negl. Trop. Dis*. 13:e0007807. doi: 10.1371/journal.pntd.0007807

Shapiro, K., Bahia-Oliveira, L., Dixon, B., Dumètre, A., de Wit, L. A., VanWormer, E., et al. (2019). Environmental transmission of *Toxoplasma gondii*: oocysts in water, soil and food. *Food Waterborne Parasitol*. 15:e00049. doi: 10.1016/j.fawpar.2019.e00049

Sobral, C. A., Amendoeira, M. R., Teva, A., Patel, B. N., and Klein, C. H. (2005). Seroprevalence of infection with *Toxoplasma gondii* in indigenous Brazilian populations. *Am. J. Trop. Med. Hyg*. 72, 37–41. doi: 10.4269/ajtmh.2005.72.37

Tamura, K., Stecher, G., Peterson, D., Filipski, A., and Kumar, S. (2013). MEGA6: molecular evolutionary GeneticsAnalysis version 6.0. *Mol. Biol. Evol*. 30, 2725–2729. doi: 10.1093/molbev/mst197

Vaudaux, J. D., Muccioli, C., James, E. R., Silveira, C., Magargal, S. L., Jung, C., et al. (2010). Identification of an atypical strain of *Toxoplasma gondii* as the cause of a waterborne outbreak of toxoplasmosis in Santa Isabel do Ivai, Brazil. *J. Infect. Dis*. 202, 1226–1233 doi: 10.1086/656397

Conflict of Interest: The authors declare that the research was conducted in the absence of any commercial or financial relationships that could be construed as a potential conflict of interest.

frontiers in Cellular and Infection Microbiology

REVIEW
published: 26 October 2020
doi: 10.3389/fcimb.2020.585727

Implications of TORCH Diseases in Retinal Development—Special Focus on Congenital Toxoplasmosis

Viviane Souza de Campos[1,2], *Karin C. Calaza*[1] *and Daniel Adesse*[2]*

[1] *Laboratório de Neurobiologia da Retina, Instituto de Biologia, Universidade Federal Fluminense, Niteroi, Brazil,* [2] *Laboratório de Biologia Estrutural, Instituto Oswaldo Cruz, Fiocruz, Rio de Janeiro, Brazil*

There are certain critical periods during pregnancy when the fetus is at high risk for exposure to teratogens. Some microorganisms, including *Toxoplasma gondii*, are known to exhibit teratogenic effects, interfering with fetal development and causing irreversible disturbances. *T. gondii* is an obligate intracellular parasite and the etiological agent of Toxoplasmosis, a zoonosis that affects one third of the world's population. Although congenital infection can cause severe fetal damage, the injury extension depends on the gestational period of infection, among other factors, like parasite genotype and host immunity. This parasite invades the Central Nervous System (CNS), forming tissue cysts, and can interfere with neurodevelopment, leading to frequent neurological abnormalities associated with *T. gondii* infection. Therefore, *T. gondii* is included in the **TORCH** complex of infectious diseases that may lead to neurological malformations (**T**oxoplasmosis, **O**thers, **R**ubella, **C**ytomegalovirus, and **H**erpes). The retina is part of CNS, as it is derived from the diencephalon. Except for astrocytes and microglia, retinal cells originate from multipotent neural progenitors. After cell cycle exit, cells migrate to specific layers, undergo morphological and neurochemical differentiation, form synapses and establish their circuits. The retina is organized in nuclear layers intercalated by plexus, responsible for translating and preprocessing light stimuli and for sending this information to the brain visual nuclei for image perception. Ocular toxoplasmosis (OT) is a very debilitating condition and may present high severity in areas in which virulent strains are found. However, little is known about the effect of congenital infection on the biology of retinal progenitors/ immature cells and how this infection may affect the development of this tissue. In this context, this study reviews the effects that congenital infections may cause to the developing retina and the cellular and molecular aspects of these diseases, with special focus on congenital OT.

Keywords: congenital toxoplasmosis, TORCH, retinal development, *Toxoplasma gondii*, congenital infections, teratogenesis

OPEN ACCESS

Edited by:
Jeroen P. J. Saeij,
University of California, Davis,
United States

Reviewed by:
Carlos Subauste,
Case Western Reserve University,
United States
Lucy H. Young,
Massachusetts Eye & Ear Infirmary
and Harvard Medical School,
United States

***Correspondence:**
Daniel Adesse
adesse@ioc.fiocruz.br

Specialty section:
This article was submitted to Parasite and Host, a section of the journal Frontiers in Cellular and Infection Microbiology

Received: *21 July 2020*
Accepted: *09 September 2020*
Published: *26 October 2020*

Citation:
Campos VS, Calaza KC and Adesse D (2020) Implications of TORCH Diseases in Retinal Development—Special Focus on Congenital Toxoplasmosis. Front. Cell. Infect. Microbiol. 10:585727. doi: 10.3389/fcimb.2020.585727

THE RETINA AND VISION

For many vertebrates, especially humans, the main environmental perception mechanism is the sense of vision. Vision determines physiological behaviors such as feeding, predation, and in the case of humans, complex social behaviors, such as bonding and the ability to recognize people's emotions by observing their faces. This fundamental skill is permitted by the presence of the

visual system. Visual impairment can limit people's ability to perform everyday tasks, and impaired interaction with the surrounding world affects quality of life. People with visual impairment are three times more likely to suffer from depression and anxiety disorders and to be unemployed. Therefore, it is particularly important to prevent and/or to treat visual impairment and research therapeutic alternatives to vision pathologies. The tissue responsible for the transduction of light stimulus and pre-processing of visual information is the retina, a highly organized network of nerve cells located in the back of the eye.

The vertebrate retina presents a well-conserved laminar organization with three layers of cell bodies, intercalated by two layers of synaptic contacts (**Figure 1**). The outer nuclear layer (ONL) lies in the outer portion of the retina, close to the choroid, and contains the photoreceptor cell bodies (cones and rods). The inner nuclear layer (INL), in turn, contains the cell bodies of horizontal, bipolar, amacrine and Müller glia, and a small number of interplexiform cells and displaced ganglion cells. Finally, in the inner portion of the retina, closer to the vitreous chamber of the eye, lies the ganglion cell layer (GCL), which comprises the cell bodies of retinal ganglion cells (RGCs) and displaced amacrine cells. All these neuronal cell types communicate through synapses, forming the outer (OPL) and inner (IPL) plexiform layers. In the innermost portion of the retina, axons from the RGCs form the nerve fiber layer (NFL). These axons transmit the preprocessed information from the retina to the brain visual nuclei through the optic nerve (ON). It is important to note that, contiguous to the photoreceptors, located in the outermost part of the retina, lies the retinal pigmented epithelium (RPE), an important player for appropriate retinal development and for the physiology of the mature retina (for review, Strauss, 2005).

Photoreceptors contain photosensitive molecules (visual pigments) that enable the transduction of the light stimulus. These visual pigments are located in the outer portion of photoreceptors, named the outer segment. Rods and cones possess a specific visual pigment and, due to morphological and neurochemical specializations, work under different light conditions. As rods are highly sensitive to light, they mediate vision in dim light (scotopic) conditions, such as during the night. Although cones are less sensitive to light, mediating vision in daylight conditions (photopic), the cone circuitry is responsible for the high resolution (temporal and spatial) capacity of the retina and for color vision (Kolb, 2003).

Bipolar cells receive information from photoreceptors through synapses in the OPL, transferring it to ganglion cells, in IPL synapses, forming the radial pathway of the retina. Horizontal and amacrine cells modulate this signal through the horizontal/lateral pathway, enriching retina performance (visual acuity, contrast, among others).

Regarding the glial cells present in the mature retina, the main cell types are Müller glia, astrocytes and microglia. Müller glia is the only type of glia originated from retinal precursors (Turner and Cepko, 1987) and the predominant retinal glia in all species. Its cell body is located in the middle of the INL, with processes extending throughout the entire radial thickness of the retina, which arborize to form the outer (OLM) and inner (ILM) limiting membranes (**Figure 1**) (Bringmann and Reichenbach, 2001; Newman, 2004). Astrocytes, non-retinal originated cells, migrate to the retina through the optic nerve (ON) during development (Stone and Dreher, 1987; Chan-Ling, 1994), and assume a location in the NFL (**Figure 1**) where they establish a close relationship with blood capillaries. The microglia, a mesodermal originated cell, also migrates to the retina during development (Chan-Ling, 1994) forming a resident population located mainly in the OPL, IPL and NFL (**Figure 1**).

The blood supply of the mammalian retina comes from two sources, the central retinal artery (CRA) and from choroidal vascularization (**Figure 1**). In humans, the CRA is derived from the ophthalmic artery, a branch of the internal carotid artery. It enters the eye through the optic disc and branches into the retina, forming peripapillary and intraretinal (inner and outer) beds, which supply blood to the innermost layers of the retina. The peripapillary bed is located in the innermost portion of the NFL, while the inner intraretinal bed is located in the GCL, and the outer intraretinal bed occupies the IPL and INL to the OPL. Mouse retina follows the same vascular organization as the human retina but, interestingly, in the rat retina, the peripapillary bed is absent. The outermost layers of the retina, especially the ONL, depend on the choroidal vascularization supply (Zhang, 1994).

Abbreviations: ALCAM, activated leukocyte cell adhesion molecule; ARPE-19, human retinal pigmented epithelial cells; CCL21, C-C Motif Chemokine Ligand 21; CTB, Cytotrophoblast; CMV, Cytomegalovirus; CNS, Central Nervous System; CRA, Central Retinal Artery; CT, Congenital Toxoplasmosis; CXCL10, C-X-C motif chemokine 10; E, Embryonic day; GCL, Ganglion Cell Layer; GFAP, glial fibrillary acidic protein; GW, Gestational Week; HIV, Human Immunodeficiency Virus; HSV, Herpes simplex virus; HVEM, Herpesvirus entry mediator; ICAM-1, Intercellular Adhesion Molecule 1; IFN-γ, Interferon Gamma; ILM, Inner Limiting Membrane; INL, Inner Nuclear Layer; IPL, Inner Plexiform Layer; iPS, induced pluripotent stem cell; NFL, Nerve Fiber Layer; OLM, Outer Limiting Membrane; ON, Optic Nerve; ONL, Outer Nuclear Layer; OPL, Outer Plexiform Layer; OT, Ocular Toxoplasmosis; P, Postnatal day; PCD, Programmed Cell Death; RGC, Retinal Ganglion Cells; RPC, Retinal Progenitor Cells; RPE, Retinal Pigmented Epithelium; RV, Rubella Virus; TEER, Transepithelial (/endothelial) Electrical Resistance; TNF-α, Tumor Necrosis Factor alpha; TORCH, Toxoplasmosis, Others, Rubella, Cytomegalovirus and Herpes; V-CAM, Vascular cell adhesion protein; ZikV, Zika virus.

RETINAL DEVELOPMENT

The retina is a highly organized tissue with a complex array of synapses resulting in efficient light information transduction, pre-processing, and transmission. Therefore, retinal development must produce the right number of different retinal cell types, as well as the functional circuitries. According to this, this phenomenon is highly regulated by both intrinsic and extrinsic factors.

The retina originates from the posterior part of the forebrain, the diencephalon (Hamburger and Hamilton, 1951; Ambroise-Thomas and Petersen, 2000), being a part of the central nervous system. Optical vesicles generated from the diencephalon undergo invaginations to form the optic cup (Smirnov and

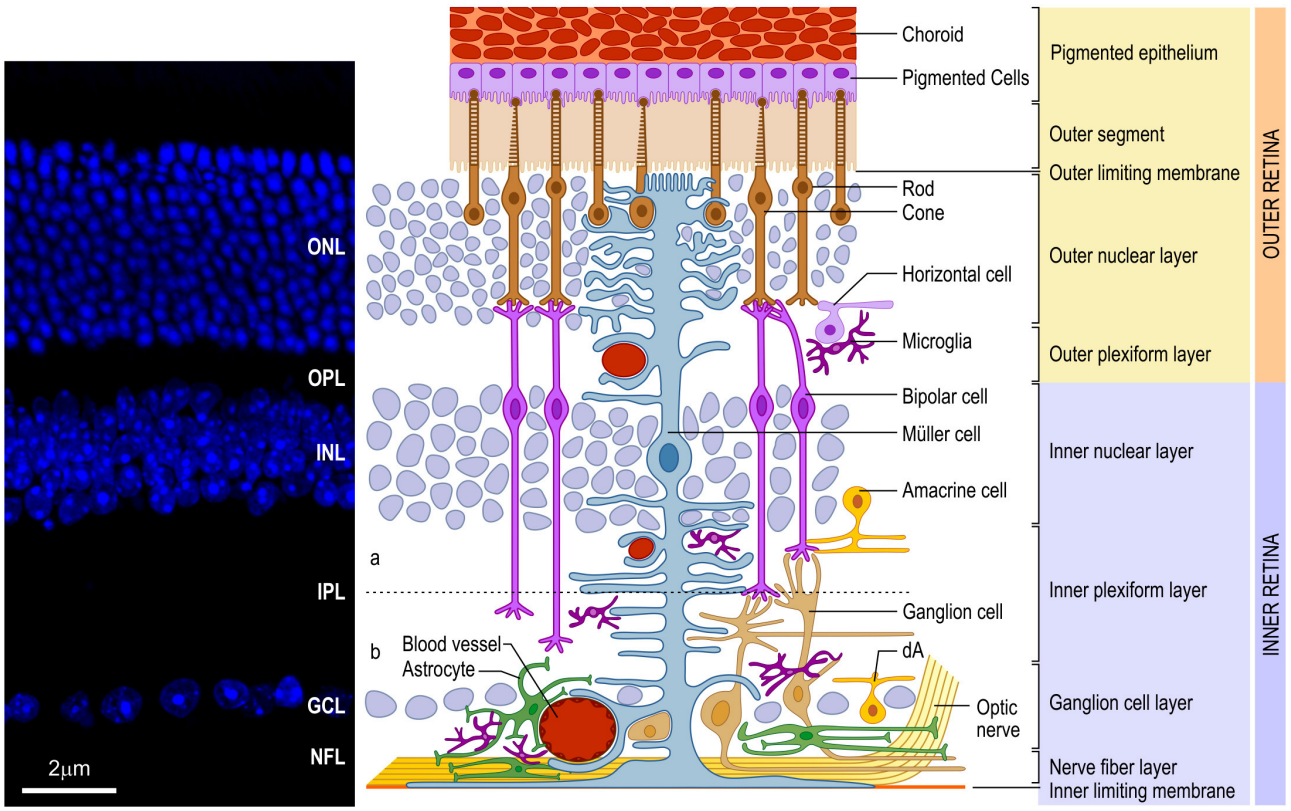

FIGURE 1 | Schematic organization of the vertebrate retina. **(Left)** Vertical section of mouse retina labeled with nuclear marker DAPI revealing the organization of the retina in layers of cell bodies and process named as follows: ganglion cell layer (GCL), inner plexiform layer (IPL), inner nuclear layer (INL), outer plexiform layer (OPL), outer nuclear layer (ONL), and inner/outer segment of photoreceptors (IS/OS). **(Right)** The retina consists of different cell types located in specific layers. Cell bodies of rod and cone photoreceptors (brown) are located in the ONL. Both photoreceptors perform synapses in the OPL with bipolar (purple) and horizontal (lilac) cells, which, in turn, show the cell bodies in the outer portion of INL, as well as amacrine (yellow) cells and Müller (blue) cells. Bipolar and amacrine cells arborize in the IPL, contacting ganglion cell dendrites. Rod bipolar cells arborizes in the inner portion of IPL. Cone bipolar cells (right pair of purple cells) are subdivided in ON and OFF bipolar cell contacting the same cone in the OPL and synapsing, respectively, in the ON (b) or OFF portion of the IPL [dashed line shows the functional division of the IPL in OFF (a) and ON (b) circuitries. Ganglion (orange), as well as displaced amacrine (dA) cell bodies are situated in the GCL. Axons of ganglion cells form the nerve fiber layer (NFL), leave the retina through the optic head nerve taking the information to visual brain nuclei by optic nerve (ON). The three types of glial cells (Müller, astrocytes, and microglia) are found in different retinal layers. Astrocytes (green) are restricted to the inner portion of the retina, in the NFL and GCL, and have a close relation to blood vessels. Microglia (dark purple) appear preferentially in the plexiform layers (IPL and OPL). Finally, Müller cells, the predominant glia in the retina, extend their processes radially throughout the retina forming the inner limiting membrane (ILM) and the outer limiting membrane (OLM). Muller glia processes interacts with almost all retinal cell types, including blood vessels, displaying a crucial role in the physiology of this tissue. In mice and humans, the inner retina is vascularized by three capillary branches of central retinal artery. The outer retina, with the avascular photoreceptor region, relies on the choriocapillaris (Ch) lying beneath the retinal pigment epithelium (RPE)]. Scale bar: 20 μm.

Puchkov, 2004; Heavner and Pevny, 2012). The inner wall of this structure forms the retina, while the outer wall forms the pigmented epithelium (Ambroise-Thomas and Petersen, 2000; Smirnov and Puchkov, 2004; Fan et al., 2016).

Early vertebrate retinogenesis is characterized by two aspects: the multipotency of retinal progenitor cells (RPC) and the well-conserved birth order of retinal cell subtypes (Dyer and Cepko, 2001; Marquardt and Gruss, 2002). In particular, retinal progenitor subpopulations have the ability to originate all neurons found in the retina, demonstrating the multipotent nature of these cells (Wetts and Fraser, 1988). Concerning the conserved order of retinal cell birth, ganglion cells are the first cells to be generated while bipolar cells are typically the last (Carter-Dawson and Lavail, 1979; Dräger, 1985; Young, 1985; Prada et al., 1991, **Figure 2**). However, the generation period of a given cell type usually overlaps and correlates with that of another cell type during the embryonic and/or postnatal period, depending on the species (Young, 1985; Prada et al., 1991; Cepko et al., 1996; Georges et al., 1999; Yang, 2004; Voinescu et al., 2009). It is noteworthy that all retinal development phenomena (cell generation, programmed cell death and synaptogenesis, among others) occur in a central-periphery gradient, with central regions (fovea in the human retina) maturing first, followed by the periphery.

In order to generate all retinal cell types, RPCs first undergo repeated cell divisions to increase the proliferating cell pool before chronologically leaving the cell cycle. Thus, some RPCs leave the cell cycle earlier to originate early cell types (ganglion and horizontal cells), while others stay in the cell cycle to generate late cell types (bipolar cells and Müller's glia) (Martins and

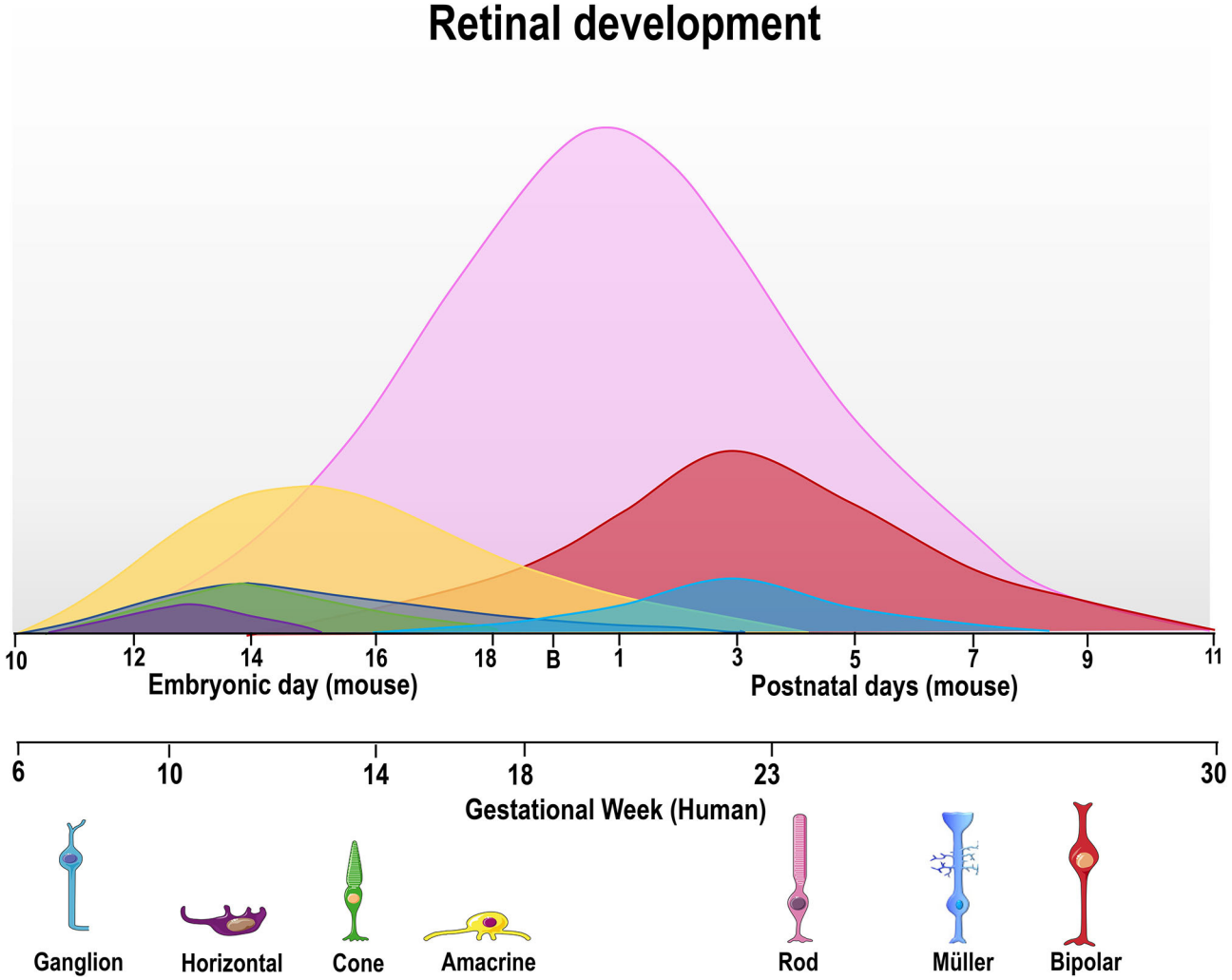

FIGURE 2 | Time course of retinal neurogenesis in human and mice. There are two main waves of retinal cell birth from early and late progenitors. The first wave begins around embryonic day (E) 10–18 in mice and gestational week (GW) 6–18 in humans, with ganglion (dark blue) cells being the first cell type to exit the cell cycle, followed by horizontal (purple), cone photoreceptors (green), and amacrine cells (yellow line). Late progenitors generate rod photoreceptors (magenta line) from E12/GW6, bipolar cells (red line) from E16/GW14 and Müller glial cells (light blue) from E18/GW18 until P7/GW30.

Pearson, 2008). As mentioned previously, the cell generation sequence is well-conserved in vertebrate species but the specific day that each cell type exits the cell cycle will differ (**Table 1**, **Figure 2**). For ganglion cells, the generation period occurs from E11 to E19 in mouse (Dräger, 1985), and from gestational week (GW) 6 to GW14 in the human fovea (finishing at GW30 in the whole retina).

After the cell cycle exit, immature neuron/glial cells will migrate to a portion of the tissue, forming the retinal layers. According to the fact that ganglion cells are the first cell type to exit the cell cycle, the ganglion cell layer is the first to appear. These cells begin to differentiate soon after their generation and begin neurite growth, forming the inner plexiform layer (IPL). RPCs maintain the generation of new cells which migrate and form other retinal layers in a chronologically maintained sequence of INL, ONL, OPL. In humans, Smirnov and Puchkov (2004) described the migration of RPCs, forming INL and ONL from GW7, which maintains a proliferative state at these layers. The generated cells began to differentiate and generate synapses. The first synapses in the IPL and OPL were visualized at GW12 in the future fovea of human retina (Hollenberg and Spira, 1973), whereas synaptophysin, a good marker for synaptogenesis, only appeared in the OPL at GW16 (Nag and Wadhwa, 2001). In mouse retina, a small but already detectable number of conventional synapses in the IPL first appear at P5 (Fisher, 1979) and the first few ribbon synapses in the IPL, from P10-P12 (Olney, 1968; Fisher, 1979). In the OPL, ribbons in photoreceptors could be seen from P2, whereas synaptic terminals with synaptic vesicles making synaptic contact with other cells are only visualized from P7 (Olney, 1968).

Retinal development, as well as in the brain, involves programmed cell death (PCD) which plays a very important

TABLE 1 | Comparison of the temporal course of retinal development in mice and in humans.

Developmental milestone	Mouse	Human
Formation of the optic cup	E9–9.5 (Heavner and Pevny, 2012)	GW5 (Smirnov and Puchkov, 2004)
Pigmented epithelium layer separated from the visual layer	From E13 (Fan et al., 2016)	From GW6 (Smirnov and Puchkov, 2004)
Ganglion cells generation period	E11–E19 (HRP retrograde labeled cells and ^{3}H-Thy; Dräger, 1985) E8–E16 (peak E12) (Brn3a labeled cells and BrdU; Voinescu et al., 2009)	GW6 to GW14 in the fovea (finishing at GW30 in the whole retina)
IPL appearance	E17 (Fan et al., 2016)	GW8-9 in the fovea; GW15 temporal and GW18 far periphery (Hendrickson, 2016)
OPL formation	P4–P5 (Olney, 1968)	GW11 (fovea); GW30 (far periphery) (Hendrickson, 2016; Hendrickson and Zhang, 2017)
Ganglion cell PCD	Peak P2–P4 (Young, 1984) and P15 (Péquignot et al., 2003)	Peak GW15–20 (Georges et al., 1999)
PCD in the INL	Inner INL P0–P11 (peak P4–P6) Outer INL P5–P18 (peak P8–P10) (Young, 1984)	From GW15–35 (peak GW20) mainly in the bipolar location
PCD in the ONL	Inner rods P5–P11 (peak P7–8) Outer rods P5–P21/24 (peak P15, Young, 1984; Péquignot et al., 2003)	Significantly lower than other layers (GW15-GW35)
Synapses in the IPL	Conventional synapses P5 (Fisher, 1979) Ribbon synapses P10–P12 (Olney, 1968; Fisher, 1979)	GW12 (future fovea) (Hollenberg and Spira, 1973)
Synapses in the OPL	P7 (Olney, 1968)	GW12 in the future fovea (Hollenberg and Spira, 1973)
Invasion of vascular cells from optic disc	From P2 (Young, 84)	From GW14-15 (Hughes et al., 2000)

E, Embryonic day; P, Post-natal day; PCD, Programmed Cell Death; GW, Gestational week.

role in tissue refinement, regulating the number of specific cell types leading to a mature tissue. PCD follows a central-peripheral gradient, similarly to the other retinal development events (Chavarría et al., 2013). Four PCD phases are recognized in mouse retinal development: (1) morphogenic cell death associated to cell death of the optic cup invagination and closure of the optic fissure; (2) early neural cell death targeting proliferating neuroepithelial cells and recently born neurons and glia; (3) neurotrophic cell death affecting differentiated neurons competing for neurotrophic supply and regulated by activity-dependent processes, associated with intra- and extra-retinal synaptogenesis; and (4) a late phase, with a peak at P15, probably related with intraretinal synaptogenesis (Laemle et al., 1999; Péquignot et al., 2003; Vecino et al., 2004; Valenciano et al., 2009; Chavarría et al., 2013; Braunger et al., 2014; Francisco-Morcillo et al., 2014; Vecino and Acera, 2015).

Morphogenic PCD is higher at E10.5, with most of apoptotic cells located in the middle of the retina, decreasing progressively from E11.5 to E13.5 (Péquignot et al., 2003; Valenciano et al., 2009), when fissure closure in mice ends, by E13 (Strongin and Guillery, 1981). Early PCD was described from E15.5-E17.5 (Péquignot et al., 2003) but recently it has been reported that the elimination of RGCs also occurs from E12.5 to E16.5, through microglia phagocytosis (see below; Anderson et al., 2019). Neurotrophic PCD consists of two waves, the first initiating at E18.5, when cell death begins to increase in the inner neuroblastic layer and peaks at P2-P4, and the second peaking at P9 (Young, 1984; Péquignot et al., 2003). At P0, neurotropic PCD occurs at a higher rate in the GCL, with a peak at P2-P4 (Young, 1984). Georges et al. (1999) evaluated PCD in human retinas from GW15 to GW35 and found apoptotic cells in all layers during this period. However, the highest rate of cell death at GW15 was found in the GCL, which was greatly decreased by GW23-24 (Georges et al., 1999). The cell death of ganglion cell population leads to a substantial loss of axons in the NFL (∼70%) from GW15 to GW30 (Provis et al., 1985). In the INL, the incidence of apoptotic cells was two to eight times that observed in the GCL, peaking at GW20 (Georges et al., 1999). Interestingly, 85–90% of the apoptotic cells in the INL occupied the middle and outer third location, suggesting that most INL cells undergoing PCD were bipolar cells. Young (1984) observed the same phenomenon in the INL of mouse retina, with significantly higher incidence of pyknotic cells in the bipolar/Müller cell position. The window of cell death in the inner/outer INL was also slightly different, with inner INL undergoing PCD from P0 to P11 (peak P4–P6) and the outer INL from P5 to P18 (peak P8–P10) (Young, 1984). PCD of cells in the ONL remain low throughout retinal development, and occurs later on from P5 to P11 (peak P7–P8) for the inner rods (differentiating rods found in the inner part of the ONL) and, at a significantly lower rate, for outer rods in the ONL from P5 to P21/24 (Young, 1984). Péquignot et al. (2003) reported a peak at P15 in ONL as well as a second peak in the GCL. PCD in the ONL of the human retina also occurs at a significantly lower rate than other layers with few pyknotic nuclei found from GW15 to GW35 (peak at GW23–GW24) (Georges et al., 1999).

The mechanisms of these PCD phases in the mouse retina can be distinctly regulated. Morphogenic PCD related to optic fissure closure involves BMP, FasL and Msx2 (Péquignot et al., 2003; Wu et al., 2003; Francisco-Morcillo et al., 2006), whereas neurotrophic PCD involves apoptotic signals, such as caspases

and Bax (for a review, see Valenciano et al., 2009). In the mouse retina, up to 60% of recently born retinal ganglion cells die after birth in a Bcl2 dependent way (Bonfanti et al., 1996; Strettoi and Volpini, 2002; Péquignot et al., 2003). Furthermore, BDNF/trkb controls the dynamic of RGC death after birth (Pollock et al., 2003). Trafficking of apoptotic signals through gap junctions also regulates PCD in INL and GCL (Cusato et al., 2003). There is also a suggestion of caspase-independent cell death mediated by PARP-1 and AIF nuclear translocation during the first postnatal week (Marín-Teva et al., 2011). Several other studies on different species, have demonstrated the important role of neurotransmitters and signaling pathways, such as glutamate, ATP, insulin, integrins, cyclic AMP and nitric oxide in PCD during retinal development (Martins et al., 2005; Valenciano et al., 2009; Cossenza et al., 2014; Ventura et al., 2019a).

In the developing retina, dying cells are phagocyted mainly by microglia, but also by neuroepithelial cells and Müller cells, enabling a clean removal of dead cells (Francisco-Morcillo et al., 2014; Silverman and Wong, 2018). In chick embryo retina (E4), engulfment and lysosomal degradation of apoptotic bodies seem to depend on autophagic cell death (Mellén et al., 2008). Microglia are already present at E11.5, shortly after the onset of retinal neurogenesis (Santos et al., 2008). At E12.5 and E14.5, microglia primarily associate with neurons, especially ganglion cells (Anderson et al., 2019). During this period, a small percentage of microglia contact cleaved-caspase 3-positive cells (15% at E12.5 and 7% at E16.5) (Anderson et al., 2019). Anderson et al. have shown that microglia phagocyte non-apoptotic neurons, in a process called phagoptosis, regulating the elimination of RGCs in the early stage of PCD (Anderson et al., 2019). The PCD of these neurons is also stimulated by Nerve Growth Factor through p75 receptor, in early (E13-15.5) but not later (E17) stages (Frade and Barde, 1999; Harada et al., 2006).

CONGENITAL TORCH DISEASES

The acronym TORCH is globally used to encompass pathogens known for their teratogenic effects, namely ***T**oxoplasma gondii*, ***R**ubella virus*, ***C**ytomegalovirus,* and ***H**erpes virus*. Currently, **O** stands for ***O**thers* and can include syphilis, parvovirus, coxsackievirus, listeriosis, hepatitis virus, varicella-zoster virus, *Trypanosoma cruzi*, enterovirus and human immunodeficiency virus (HIV). Recently, the Zika virus was also included in this list, after the 2015–2016 outbreaks in Latin America, which were correlated with a high number of microcephaly cases (Schwartz, 2017). All these diseases are teratogenic, i.e., can cause disturbances in fetal development, leading to malformations. Neurotropism also occurs among the aforementioned microorganisms. In this topic, we will present the main teratogenic pathogens, their characteristics, and how they affect development, focusing on eye abnormalities, with special focus given to Congenital toxoplasmosis.

The placenta is the first biological barrier that TORCH pathogens must overcome in order to reach fetal tissues. During normal placental development, invasive cytotrophoblasts (CTBs) originating from anchoring chorionic villi invade the maternal decidua. CTBs are specialized epithelial cells of the placenta which leave the basement membrane and differentiate along two independent pathways, depending on their location, to initiate the blood flow to the placenta. A subset of these cells remodels the uterine vasculature in the decidua at the maternal-fetal interface. This process is finely controlled through the coordinated actions of invasion- and angiogenesis-promoting factors. The maternal decidua exhibits a distinctive multicell nature, comprising invasive CTBs and uterine epithelial, stromal, and endothelial cells, as well as immune cells (reviewed by Maltepe et al., 2010).

Trophoblast cells of the human placenta, derived from the outer cell mass of the blastocyst, are at the center of the balance between infection responses and conception tolerance (Heerema-McKenney, 2018). Vertical transmission (mother to fetus) of pathogens can occur by several routes, including the following: infection of endothelial cells in the maternal microvasculature and spread to invasive extravillous trophoblasts, which anchor the villous trees to the uterine wall, trafficking of infected maternal immune cells across the placental barrier, paracellular or transcellular transport from the maternal blood across the villous trees and into the fetal capillaries, damage to the villous tree and breaks in the syncytiotrophoblasts layer, and/or transvaginal ascending infection (Coyne and Lazear, 2016). Most TORCH agents are thought to infect the placenta and fetus from a hematogenous route, although infection from cervical shedding or decidua infection may also occur.

A recent study using single-cell RNA-Seq has demonstrated that placental cells express NRP2, PDFGRA and CD46 receptors, which permit CMV invasion to host cells (Pique-Regi et al., 2020). CMV may cross the placenta via transcytosis of first-trimester syncytiotrophoblast cells and, in an *ex vivo* infection decidual organ culture model, HCMV infects invasive cytotrophoblasts, macrophages, and endothelial, decidual and dendritic cells (Weisblum et al., 2011). ZikV has been shown to infect syncytiotrophoblasts, cytotrophoblasts, decidual, and endothelial cells, leading to increased inflammation response, including CD68 and CD8 cell infiltration and cytokines, chemokines and MMP secretion (Rabelo et al., 2020). Additionally, placental cells at birth (mean gestational age 36 weeks) were shown to express AXL, CD209 and TYRO3, which may serve as preferential receptors for the Zika virus entry (Pique-Regi et al., 2020). Specifically, AXL was found to be expressed in placenta cells and chorioamniotic membranes, whereas CD209 was mostly expressed in maternal and fetal macrophages subsets. In the same study, C1QBP (Complement component 1 Q subcomponent-binding protein) and CALM1, both known Rubella virus interactors (Mohan et al., 2002; Zhou et al., 2010), were expressed in syncytiotrophoblasts throughout the pregnancy, and to a lower extent in decidual, endometrial and cytotrophoblast cells (Pique-Regi et al., 2020). Regarding congenital toxoplasmosis, the *in vivo* mechanisms of human transmission are poorly understood. Using *in vitro* explants of human first trimester villous, Robbins et al. (2012) demonstrated that extravillous trophoblast of anchoring villi are most susceptible to infection, followed by villous cytotrophoblast and

rare *foci* of syncytiotrophoblast infection observed near damage areas. These findings suggested that maternal parasitemia likely leads to decidual tissue seeding, with subsequent spread to extravillous and villous cytotrophoblast through anchoring villi (Robbins et al., 2012). Histopathological examinations have shown that the placenta may exhibit lymphohistiocytic chronic villitis, with severe and diffuse inflammation and granulomas, immature villi and increased Hofbauer cells in the villous stroma, chorion, and Wharton jelly (reviewed by Costa et al., 2020). Although, the teratogenic effects of each TORCH agent is probably caused by different mechanisms, placental inflammation is possibly an important player in a CNS development context, by increasing cytokine production from reactive microglia and astrocytes and altering neurotransmitters expression/activity (al-Haddad et al., 2019).

Congenital Rubella Syndrome

Rubella is a common disease whose etiological agent is the *Rubella* virus (RV). Belonging to the *Togaviridae* family, this single-stranded RNA virus is transmitted by direct contact or by droplets through respiratory secretions. It is of extreme concern when infecting pregnant women, due to its teratogenic ability (Frey, 1994). The rate of congenital infection following maternal rubella has been reported as 85% in the first trimester, 54% at 13 to 16 weeks, 36% at 17 to 22 weeks, 30% at 23 to 30 weeks, and then 60% at 31 to 36 weeks, with an impressive 100% transmission rate in the last month of pregnancy (Freij et al., 1988; Boppana et al., 2017). In addition to causing miscarriages, congenital rubella syndrome is a major cause of blindness, deafness, heart disease and intellectual disability. These clinical manifestations and the ability of RV to cross the placenta, causing development impairment, are similar to those of other TORCH pathogens (Robertson et al., 2003).

Ophthalmic pathologies are commonly found in congenital rubella. Cataract was the first reported teratogenic effect of gestational rubella (Gregg, 1941), as well as retinal defects, iris adherence to the lens, microphthalmia (Töndury and Smith, 1966), subretinal vascularization and glaucoma (Freij et al., 1988). Pigmentary retinopathy and strabismus are additional examples of abnormalities in this condition. Each clinical manifestation mentioned above is closely correlated with the gestational period in which the primary infection occurs (Duszak, 2009), with the first trimester exhibiting the most damage (Boppana et al., 2017). Viral particles were found in the ciliary body and lacrimal glands, which can contribute to cataractogenesis (Nguyen et al., 2015). Studies have shown that RV infection causes changes in actin filaments, which appear as amorphous clusters, presumably due to actin depolymerization (Bowden et al., 1987). This lack of organization of actin cable/bundles can result in cell division inhibition. In fact, decreased mitotic activity has been demonstrated in infected primary embryonic cell cultures, while cell division deceleration has been reported in human fetal cells infected by RV (Rawls and Melnick, 1966; Bowden et al., 1987). The rubella virus non-structural protein, P90, can interact with important cell cycle regulators, retinoblastoma and cytokinesis-regulatory proteins, thus influencing cell cycle and apoptosis (Atreya et al., 2004; for a review, see George et al., 2019). Furthermore, downregulation of genes involved in sensory organs and eye development have also been reported by gene expression profiling of RV-infected human umbilical vein endothelial cells (HUVEC) (Geyer et al., 2016). RV infection can induce apoptosis in several cell types involving classic signaling pathways, leading to the activation of caspases, p53, p21, and Bcl-2 family proteins. However, PCD induced by RV infection is observed only in non-proliferative and differentiated cells (for a review, see George et al., 2019). These data suggest that apoptosis is not involved in the regulation of mitotic rate of progenitor infected cell populations. These alterations may explain why RV infection is associated with loss of eyesight as an ophthalmic sequelae (Geyer et al., 2016). Current studies on congenital rubella indicate that such ophthalmic sequelae may be correlated to the regulation of genes involved in the development of sensory organs and to changes in the host cell cytoskeleton that may lead to changes in mitotic pattern (George et al., 2019). However, the molecular/cellular mechanisms responsible for multiple retinal defects in CRS are still poorly understood. Few studies investigating this topic are available, most focusing on histopathological analyses performed during the autopsy of aborted or dead fetuses.

Congenital Cytomegalovirus Infection

Cytomegalovirus (CMV) is a worldwide widespread member of the *Herpes virus* family. In healthy people it is asymptomatic, thus characterizes as an opportunistic microorganism (Landolfo et al., 2003). Affecting about 60% of the population in developed countries, and reaching 100% in developing countries, CMV behaves similarly to the *Herpes simplex virus* (HSV). After primary infection (symptomatic or not), the virus goes into latency and reactivation can occur in situations of low immunity (Griffiths et al., 2015). Cytomegalovirus can be transmitted through direct or indirect contact with infectious body fluids like saliva, urine, blood, semen, or cervical or vaginal secretions. Maternal CMV infection is mainly acquired through contact with the urine or saliva of infected individuals or sexual contact (Cannon, 2009). Like the other pathogens described in this review, CMV can cross the transplacental barrier, and is one of the most hazardous TORCH pathogens.

Congenital CMV infection is common in humans, since maternal immunity is unable to prevent reactivation of the virus during pregnancy and prevent transmission to the fetus (Alford et al., 1980). Factors influencing fetal transmission rates are the trimester of exposure, maternal age, CMV serological status, maternal immunological status and viral load (Ghekiere et al., 2012). Congenital CMV infection can occur even if the infection occurred before pregnancy (non-primary infection). Forms of transmission to the fetus and baby include the transplacentary route, perinatal route (during delivery) by cervical secretions and blood or by breastfeeding (Malm and Engman, 2007).

The main clinical manifestations of congenital infection commonly found in neonates are thrombocytopenia, jaundice, hepatosplenomegaly, microcephaly and retinochoroiditis (Bale, 2014). Some ophthalmic changes caused by congenital CMV infection may be observed in symptomatic and asymptomatic patients. Among those found in both cases are macular

scars, strabismus, retinochoroiditis and anterior stromal corneal scars. Symptoms found only in symptomatic patients include peripheral retinal scars, optic atrophy, optic nerve hypoplasia, coloboma, microphthalmia, anophthalmia, and incomplete cyclopia (Ghekiere et al., 2012).

Although congenital defects caused by CMV infection are well-recognized, their pathogenesis is still poorly understood. This is due to the fact that it is difficult to establish adequate animal models for this type of study, since the virus exhibits infectivity in a species-dependent manner. Some studies focused on understanding the effects of CMV infection on neurodevelopment and providing a basis for understanding the damage caused to fetuses have been carried out (Cheeran et al., 2009; Kawasaki et al., 2017). It has been demonstrated in a murine model that developmental damage may be associated to the type of embryonic cells susceptible to CMV infection and to the effects of the infection on their cellular functions. Mesenchymal stem cells are infection targets during mid-pregnancy, affecting brain, eye and orofacial region organogenesis (Tsutsui et al., 1993). Using neural precursor cell neurospheres obtained from the forebrain of aborted human fetuses during the first trimester as an *in vitro* model, it was demonstrated that HCMV inhibits neuronal differentiation induction and provokes apoptosis in infected cells (Odeberg et al., 2006). More recently, studies using cerebral organoids derived from human-induced pluripotent stem cells have indicated that CMV infection can lead to severe damage to the organoid structure, in addition to resulting in calcium signaling and neural network activity alterations. The infection dramatically affects organoid neurological development, reaching the developing cortical structure to fully formed ones, with associated changes in architecture organization and lamination depth within these structures. Such changes may be correlated with microcephaly in human fetuses (Brown et al., 2019; Sun et al., 2020).

Congenital Herpes Simplex Infection

The *Herpes simplex virus* (HSV), a member of the family *Herpesviridae* viruses, has an enveloped DNA capable of multiplying in the host cell nucleus (Liesegang, 2001). HSV transmission is dependent on mucosal or injured skin contact between a susceptible seronegative individual and another who excretes HSV. Two herpes simplex virus serotypes are known, HSV-1, correlated with oral lesions, and HSV-2, associated with genital lesions. Both viral serotypes establish latent infection in sensory neurons and, when reactivated, cause lesions near or at the body's entry sites (James and Kimberlin, 2015). Approximately 5% of neonatal HSV infections occur *in utero*, 85% during the peripartum period, and the remaining 10%, postnatally, through direct contact with infectious lesions or secretions (Brown et al., 1997).

Congenital HSV infection is associated with high levels of morbidity and mortality. The most common form of transmission occurs at birth, through direct contact with lesions or by asymptomatic viral shedding (Fa et al., 2020). Transplacental HSV transmission was first reported in 1963, in which the newborn exhibited herpetic lesions at birth. During developmental follow-up, several neurological damages associated with congenital HSV infection were observed, such as strabismus, retinochoroiditis, hyperreflexia, and slow speech development (Mitchell and Mccall, 1963). Additional ocular abnormalities such as chorioretinitis, microphthalmia, keratoconjunctivitis and optic atrophy are also found in congenitally infected individuals (Leung et al., 2020).

Although vertical transmission by HSV is considered rare, like other TORCH pathogens, the greatest risk of infection occurs during early pregnancy (Fa et al., 2020). *In vitro* HSV infection models of neural progenitor cells may give clues that may aid in understanding what occurs in the developing CNS, including the brain. It has been demonstrated *in vitro* that HSV can infect undifferentiated iPS cells, neural precursors cells and iPS-derived differentiated sensory neurons (Lee et al., 2012). Infection by HSV is highly cytotoxic to neural progenitor cells, unlike infection by the Varicella Zoster virus (VZV), which does not infect undifferentiated iPS cells. Similarly, HSV-1 can successfully infect human embryonic stem cells, whereas VZV does not (Dukhovny et al., 2012). In the adult mouse brain, ependymal and neural stem cells express the Herpes virus entry mediator protein (HVEM) and *in vitro* studies concerning the infection of such cells indicate reduced neuronal generation rates, as shown by doublecortin (DCX) immunostaining, which was prevented by microglia-derived IL-6 secretion (Chucair-Elliott et al., 2014). Infection of mouse neural stem cells by HSV in a neurosphere model leads to cell death, with reduction in neurosphere size and the production of IFN-γ mediated by Toll-like receptor 3 activation (Sun et al., 2015). HSV-1 also activates the JNK and p38 MAP kinase signaling pathways, which further contribute to cytolytic host cell effects (Zachos et al., 1999; Diao et al., 2005; Hargett et al., 2005). In turn, p38 and JNK are known apoptosis regulators and may be implicated in neurodegeneration and brain and retina neurogenic defects (Shou et al., 2003; Diao et al., 2005; Dhanasekaran and Reddy, 2008; Shklover et al., 2015; Wang et al., 2018; Kawamura and Kano, 2019; Kovacs et al., 2019; Lei et al., 2020; Pang et al., 2020). Although no direct evidence has indicated direct effects of HSV infection to retinal progenitor cells, either *in vitro*, *in vivo* or in human cases, it is tempting to assume that, similarly to what is observed in cortical progenitor cells, retinal progenitor cells may be susceptible to HSV infection, resulting in similar neurogenesis and apoptosis effects.

Congenital Zika Virus Infection

The *Zika virus* (ZikV) is an arbovirus, displaying a classic human-arthropod-human vector transmission pathway. Belonging to the *Flaviviridae* family, it was first described in 1947 (Dick, 1952). Initially, the pathogenesis of this disease was considered mild, characterized by fever, rash, joint pain and conjunctivitis. However, the relevance of ZikV infection increased after an outbreak in 2015 in northeastern Brazil, where a sudden increase in the birth of neonates with microcephaly was observed (Rasmussen et al., 2016). This increase was correlated with primary maternal ZikV infection during pregnancy after confirmation of viral genetic material in the amniotic fluid of pregnant women with microcephalic fetuses (Calvet et al., 2016; de Araújo et al., 2016). Thus, it has become clear that in addition to classical transmission, ZikV is transmitted sexually

and congenitally and is highly teratogenic (de Araújo et al., 2016). Therefore, ZiKV is considered an important member of the TORCH pathogen group (Musso and Gubler, 2016). Some authors suggest modifying the old acronym TORCH for new TORZiCH to highlight the position of Zika virus due to the serious congenital disorders associated with ZikV infection (Tahotná et al., 2018).

The emerging association of congenital ZikV infection with microcephaly demanded the beginning of research in the area to identify possible damage to the offspring and preventive or curative interventions. Among animal models, the mouse model has been widely applied in several ZikV infection studies (Caine et al., 2018). Among the reported damage from congenital pathogenesis caused by ZikV are primary microcephaly and microphthalmia. Although infection of neural progenitors, neurons and glial cells have been described (Cugola et al., 2016; Gabriel et al., 2017; Büttner et al., 2019; Ferraris et al., 2019), a recent study based on *in vitro* research suggests that the primary targets of ZikV are astrocyte cells (Ledur et al., 2020). Such infection also affects cell migration, neurogenesis, differentiation and cell death, leading to microcephaly in neonates (Russo et al., 2017; Wen et al., 2017; Christian et al., 2019).

Eye abnormalities and visual problems are also observed in neonates congenitally infected with ZikV (Ventura et al., 2019b; Lima et al., 2020). Clinical manifestations include microphthalmia, retinal pigment changes, chorioretinal atrophy, vascular changes and optic nerve hypoplasia (Ventura et al., 2016). Such anomalies opened a precedent for studies on the development of the infected offspring retina. ZikV infection in pregnant mice generated decreased eyeballs, optic nerve thinning, retinal damage and impaired visual projection (Shi et al., 2018) and impaired vascular offspring development (Garcez et al., 2018).

It is still unclear which are the cellular targets of ZikV in the developing human fetus. *In vitro* studies have reported that ZikV infects human embryonic cortical neural progenitor cells (hNPCs), inducing cell cycle dysregulation and increased cell death (Tang et al., 2016). In addition, by studying the mechanisms by which ZikV modulates the cell cycle of hNPCs, it has been observed that the virus induces DNA breaks which, in turn, inhibits cell cycle progression from the S phase, thus preventing host DNA replication completion (Hammack et al., 2019). Using an *in vivo* congenital ZikV infection model, it has been verified that, besides neurogenesis impacts, the infection also affects angiogenesis. When compared to control offspring, ZikV-infected offspring exhibited decreased blood vessels in the vasculature of both the cerebral cortex and the retina (Garcez et al., 2018). Using intrauterine infection as a vertical transmission model, congenital Zika syndrome has been shown to generate mice with smaller eyeballs and smaller optic nerves. Additionally, a reduction in the thickness of GCL, IPL, and ONL and the absence of OPL was also detected, which could be correlated to visual neural connection defects. ZikV infection also decreased the number of ganglion cells in the GCL, which is clearly associated to optic nerve damage (Shi et al., 2018). It is known that retinal endothelial cells, retinal pericytes and retinal pigmented epithelial cells are permissive for lytic ZIKV replication and primary retinal barrier target cells concerning infection (Alcendor, 2019). These data can contribute to elucidate how ZikV affects retina development and the mechanisms involved in the pathogenesis of retina lesions after congenital infection.

Congenital Toxoplasmosis

Toxoplasmosis is a zoonosis of great interest in the context of public health, since it affects a third of the world population, with the protozoan parasite *Toxoplasma gondii* as etiological agent (Tenter et al., 2000). Among the TORCH agents, *T. gondii* is the main protozoan representative, while most display a viral etiology. Toxoplasmosis is widely distributed across the countries, reaching seropositivity rates that vary from <10% to over 90% (Torgerson and Mastroiacovo, 2013). Among the infected population, two groups of medical importance are highlighted, immunocompromised persons and those congenitally infected, in which the most severe forms of the disease are observed (Furtado et al., 2011).

In Brazil, seroprevalence reaches very high numbers, of over 60% (Ozgonul and Besirli, 2016), with the presence of anti-*T. gondii* antibodies present in up to 50% of children in primary school and 50–80% of women in fertile age. The rates of congenitally infected children in Brazil are also high, reaching 5–23 born infected out of 10,000 born alive in Brazil (for review, Dubey et al., 2012). Some factors are determinant for such a high seroprevalence, such as scholarity and low family income. Therefore, social vulnerability may play an important role in high seroprevalence rates (Mareze et al., 2019). Toxoplasmosis is still relevant in Brazil and frequent outbreaks are observed, such as the one that occurred in 2018 in the city of Santa Maria, in which 1,116 cases were reported by public health agents, with another 766 suspect cases (Dal Ponte et al., 2019).

Toxoplasma gondii is an opportunistic protozoan that belongs to the Apicomplexa phylum, first described by Nicolle and Manceaux (1908) in rodents in North Africa (Ferguson, 2009). In that same year, it was described in Brazil in the state of São Paulo by Splendore, thus suggesting that *T. gondii* is a cosmopolitan parasite (Frenkel, 1973).

T. gondii is an intracellular obligate parasite capable of infecting virtually all nucleated cells in the host, thus reaching different tissues, with a preference in forming tissue cysts in muscle and neuronal cells (Dubey, 2004). The ability of the parasite to infect cells and persist in the tissues in a latency state, i.e., tissue cysts, contribute to toxoplasmic retinochoroiditis. Chronic infection reactivation by *T. gondii*, and consequently, the disease, is common in congenitally infected individuals. Different mechanisms are pointed as responsible for recurrent ocular toxoplasmosis (OT): first, the destruction of retinal tissue may be due to the release of parasites from tissue cysts, which in turn invade and promote the lysis of adjacent cells; second, the immune response generated against this parasite may be harmful for the host's tissue (Roberts and McLeod, 1999). The classic clinical aspect observed in patients is an active lesion and a fresh white elevated focus of a necrotizing lesion, proximal to a previous pigmented scar (Pavesio and Lightman, 1996). Retinochoroiditis can be incapacitant, with most cases

observed in young adults, correlated to untreated congenital toxoplasmosis. Because of this, CT has great medical and socio-economic relevance, and is the reason for the creation of pre- and neonatal triage programs (Wong, 2006).

The first reported case of infantile toxoplasmosis with confirmed vertical transmission dates back to 1942 (Cowen et al., 1942). Currently, it is known that the congenital infection is the most severe form of toxoplasmosis and occurs in the offspring of mothers that contracted primary *T. gondii* infection during pregnancy. The diagnosis is made through serological testing for *T. gondii* or based on abnormal ultrasonography examination (Bollani et al., 1967). Around 90% of individuals that acquire toxoplasmosis will not exhibit typical signs and symptoms, which makes the diagnostic even more difficult. In addition, symptoms (fever, nausea and lymphadenopathy) are easily mistaken with those of other non-teratogenic infections (Hampton, 2015).

The incidence and severity of congenital toxoplasmosis infection depend on the gestational period when infection occurs. The risk of vertical transmission increases over the gestational weeks, of 15% in the 13th week, 44% in the 26th and 71% in the 36th, increasing to 90% in the last week of pregnancy. However, severity of the damage to the fetus is inversely proportional to the infection period. Severe manifestations are seen in the offspring of women who acquired the infection during the beginning of the pregnancy whereas it may be subclinical in neonates born to mothers infected at the end of the pregnancy (Hall, 1992). Placenta physiology plays an important role and is closely related to infectivity rates, since it is immunologically responsible for avoiding maternal-fetal rejection and for preventing vertical infection (Wong, 2006).

CT may manifest in the first month of life or be noticeable as long-term ocular and neurological sequela in childhood or even adulthood. The main consequences include spontaneous abortions, neurological disturbances and ocular damage (Randall and Hunter, 2011). Ophthalmological manifestations are among the main sequelae in CT, and retinochoroiditis is the most common, with an estimated incidence of 9–31%. Other possible ocular manifestations include strabismus, microphthalmia, cataracts, retinal detachment, optic atrophy, iridocyclitis, nystagmus and glaucoma. Some of these characteristics are apparently correlated with a retinochoroiditis process that is then applied as a marker of CT severity (Bollani et al., 1967).

Despite ocular lesions being frequently correlated with CT, they can be found after infection even in immunocompetent hosts (Gazzinelli et al., 1994). For example, retinal neovascularization, a rare complication of ocular toxoplasmosis (OT) can be a source of vitreous hemorrhage (Gaynon et al., 1984). Other less common abnormalities may be noticeable, such as vascular occlusion even far from active lesions, thus resulting in hemorrhage. Retinal detachment and subretinal neovascularization have also been reported (Nussenblatt and Belfort, 1994).

The first description of OT was made by Jankû in 1923, followed by Levaditi in 1928. However, the relationship between *T. gondii* infection and retinochoroiditis was only reported in 1952, as reviewed by Kim and Weiss (2004). OT has been widely studied since then, although it still poses many challenges regarding its physiopathology (Maenz et al., 2014). In OT, the first tissue to be affected is the retina, followed by the choroid, the vitreous humor and anterior chamber, which can all be affected, but never before the retina (Nasaré and Tedesco, 2017). Uveitis and retinochoroiditis are clinical aspects characterized by the inflammation of the uveal tract that can occur during the pathogenesis of OT, possibly evolving to irreversible ocular lesions (Holland, 1999).

Although not completely clear, it is thought that *T. gondii* reaches the retinal tissue using a Trojan horse mechanism, being transported by an infected inflammatory cell through the Blood-Retinal Barrier, similarly to described in brain invasion (Kijlstra and Petersen, 2014; Lachenmaier et al., 2014). In experimental models, *T. gondii*-infected THP-1 monocytes have been reported as transmigrating monolayers of human retinal pigmented epithelial cells (ARPE-19) (Song et al., 2017), whereas direct infection of ARPE-19 cells affects their junctional properties, including decreases in Transepithelial (/endothelial) Electrical Resistance (TEER) (Nogueira et al., 2016). Regarding the Blood-Retinal Barrier, Furtado and colleagues have indicated that *T. gondii* can cross through retinal endothelial cells without disturbing the integrity of the monolayer (Furtado et al., 2012), thus penetrating the retinal layers and infecting neuronal and glial cells (Furtado et al., 2013). Similarly, *T. gondii* has been shown to infect cerebral microvascular endothelial cells, which may serve as a niche to gain entry to the brain (Konradt et al., 2016).

It is noteworthy that *T. gondii* utilizes an intricate mechanism to disseminate through the host organism, traveling in infected inflammatory cells, including dendritic cells, monocytes and lymphocytes, that acquire a hypermigratory phenotype (Da Gama et al., 2004; Seipel et al., 2010; Fuks et al., 2012; Kanatani et al., 2015, 2017; Ueno et al., 2015; Ólafsson et al., 2018; Bhandage et al., 2019). This phenomenon also holds true for retinal tissue, since infected dendritic cells have been shown to transmigrate across retinal vascular endothelium through adhesion molecules (ICAM-1, V-CAM and ALCAM) and chemokines (CCL21 and CXCL10) (Furtado et al., 2012). Therefore, increasing evidence has shown that *T. gondii* has developed complex mechanisms to penetrate the CNS, either in the brain or retina.

Once inside the tissue, tachyzoites invade host cells and proliferate, leading either to host cell lysis or to the formation of tissue cysts, composed of bradyzoites (Kijlstra and Petersen, 2014). The preference for retinal tissue may be correlated to a higher susceptibility of the vascular endothelium present in the retina to *T. gondii* infection, and such susceptibility may be related to easy penetration in the host cell, intracellular proliferation rates and/or the cellular response to infection (Smith et al., 2004).

Animal infection models used to study OT must recapitulate aspects of the human pathology from the invasion of the host until the development of disease. The first experimental models had the goal of providing a better description of the disease pathogenesis. In order to analyze the migration of the parasite to the retinal tissue, rabbits and hamsters were infected through distinct routes of infection, including the intracarotid and

intraperitoneal routes, respectively (Frenkel, 1955). However, such approaches do not mimic the natural route of infection. Throughout the years, an increasing number of studies has focused on experimental modeling of Toxoplasma-induced retinochoroiditis, through the use of non-human primates, cats, rabbits, hamsters and mice. A recent review compared mouse strains, parasite genotypes, disease stage and inoculum dosage, reporting that adult C57bl/6 mice were more susceptible to infection via the oral route and developed OT very rapidly (14 to 21 days post infection, dpi), thus becoming the model to more closely mimic natural infection (Dukaczewska et al., 2015). C57bl/6 mice are more susceptible to infection, with higher lethality rates of mothers and offspring. This makes it more difficult to develop a reliable system to be used as an OT/CT animal model. However, the fact that these animals are pigmented animals makes them a more appropriate model to study retinal biology, as retinal development of albino animals is already impaired. Thus, it is worth reinforcing the importance of prioritizing studies with pigmented animals to increase the chances of clinical translation to humans. Up to this moment, very few studies were conducted in order to directly assess the interaction between *T. gondii* and retinal cell types, neither aiming at characterizing the morphological or functional alterations induced by the parasite, nor looking for specific tropisms for retinal cell types. Lahmar et al. (2010) reported that neonatal infection of Swiss Webster albino mice by *T. gondii* can lead to retinal layer disorganization, especially in the GCL. This same group exhibited a discrete, qualitative alteration in immunoreactivity for vimentin and GFAP in the retinas of infected mice. Moreover, a reduction in the number of cells in the ONL was also observed, thus suggesting photoreceptor depletion (Lahmar et al., 2014). *In vitro* infection of retinal cells obtained from chick embryos or retinal explants from adult or chicks embryos demonstrate that *T. gondii* is capable of replicating in these systems and that this is dependent on polyamine production by the host cells (Moraes et al., 2004). Using RPE and Müller cells, isolated from Lewis rats, Delair et al. (2009) indicated that TNF-α and IFN-γ differentially restrict *in vitro T. gondii* infection, thus indicating that RMC are more susceptible to infection than RPE. Finally, it was recently described that *T. gondii* disrupts correct cytokinesis patterns and the formation of the mitotic spindle in bovine endothelial cells (Velásquez et al., 2019). It is known that changes in spindle structure, with or without cell cycle protein alterations, can lead to abnormal retinal and brain cortex development (Uzquiano et al., 2018), which could also explain how CT affects these processes.

Alterations in the profile of the structures of retinal layers, such as detachment of the pigmented epithelium from the ONL and irregularities in the placement of retinal layers, have been described in the literature in congenitally infected mice, where ocular abnormalities were more evident than in acquired infection (Ashour et al., 2018). However, the literature lacks studies systematically describing whether the damage found in congenital OT is derived from alterations that occur during the proliferation and differentiation of retinal progenitor cells during development.

CONCLUDING REMARKS

Congenital infection by TORCH syndrome agents is a relevant public health threat with varying degrees of severity. In the specific case of the Rubella virus, transmission rates were greatly reduced due to vaccination programs in the 1980s−1990s. However, special attention must be given to antivax movement, which has contributed to increasing the number of Measles-Rubella cases (Hotez, 2019; Krishnendhu and George, 2019). In 2019, 1,241 new measles cases were reported in the United States as a result of this movement (Nathala et al., 2019). Regarding CT, this infection comprises a high epidemiologic burden and its ensuing sequelae are irreversible which, combined with the lack of efficient chemotherapeutic schemes represents an important challenge in terms of basic research that aim to understand the molecular and cellular events that lead to these malformations.

All TORCH infections can cause severe but different neurological disabilities and ophthalmic problems. However, the outcome may differ depending on the pathogen infection, as exhibited in **Figure 3**. There is still much left to unravel concerning the mechanisms by which each pathogen affects eye/retinal development. One important interfering determinant is the embryonic stage of the infection. As highlighted for each topic, the infection period can vary greatly depending on the pathogen, with 85% of congenital HSV occurring during labor whereas 85% of congenital rubella infection occurs during the first gestation trimester. Evidently, since different retinal development phenomena occur throughout the gestational period, as well as postnatally, different outcomes are expected depending on the infection period. Nevertheless, these differences *per se* are insufficient to explain the distinct retinal lesions observed among TORCH infections. Target host cells tropism and the specific molecular/cellular alterations that each pathogen induces are probably as important as the infection period. In the context of ocular malformations and altered retinogenesis observed during TORCH agent infection, certain questions remain unanswered and may serve as motivation for further research, as follows:

1. What are the consequences of TOR(Zi)CH infection in retinal development? What is the exact impact on cell proliferation, morphological and neurochemical differentiation of different cell types, synaptogenesis, programmed cell death, and vascularization? Given the similarities found between neural and retinal progenitor cells, including their susceptibility to infections and the role of altered mitosis and apoptotic balance, it seems tempting to speculate that these may be common mechanisms by which TOR(Zi)CH agents affect retinogenesis.
2. What cell types in the retina are affected during CT? Does the parasite present a tropism for a specific cell type?
3. Are cases of strabismus and nystagmus related to *T. gondii* infection of lateral and medial rectus muscle tissue?
4. Is there a correlation between *T. gondii* genotype and clinical outcomes?
5. Finally, since some reports demonstrate that SARS-CoV-2 not only is transmitted vertically, but cause disease in the infected

Toxoplasma gondii

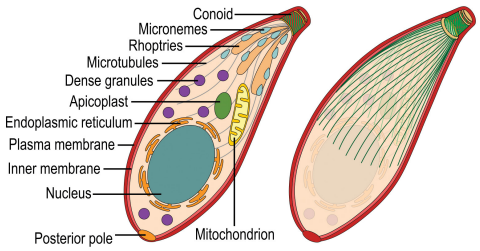

- Retinochoroiditis
- Strabismus
- Microphthalmia
- Cataracts
- Retinal detachment
- Optic atrophy
- Iridocyclitis
- Nystagmus
- Glaucoma
- Retinal neovascularization
- Vitreous hemorrhage

Herpes Simplex Virus

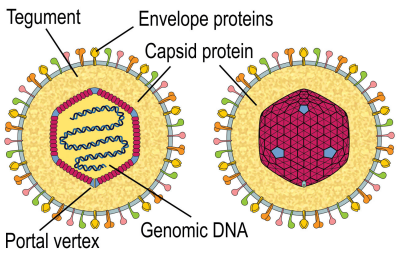

- Strabismus
- Retinochoroiditis
- Hyperreflexia

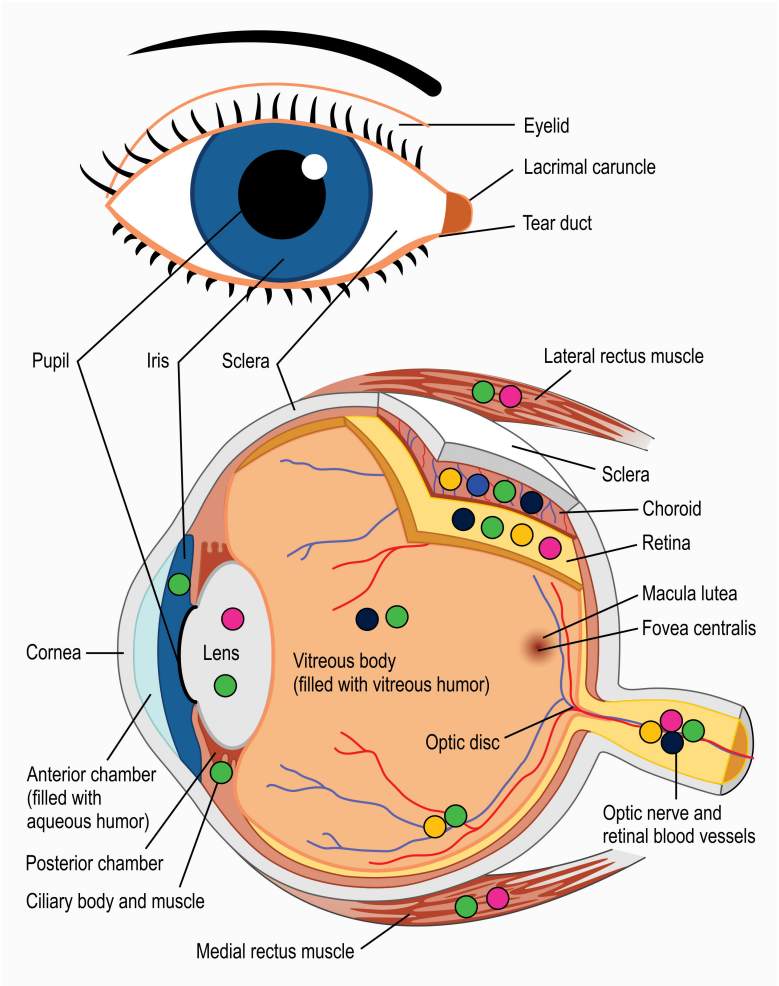

Cytomegalovirus

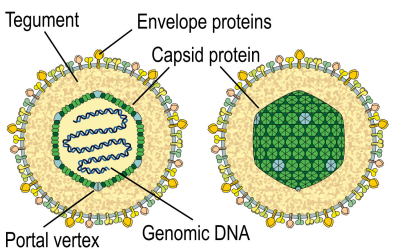

- Retinochoroiditis
- Peripheral retinal scars
- Optic atrophy
- Optic nerve hypoplasia
- Coloboma
- Microphthalmia, Anophthalmia
- Incomplete cyclopia

Rubella Virus

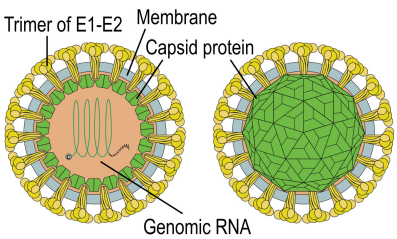

- Cataracts
- Microphthalmia
- Glaucoma
- Pigmentary retinopathy
- Strabismus

Zika Virus

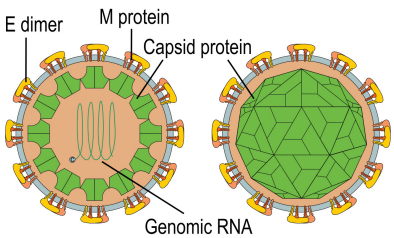

- Optic nerve hypoplasia
- Microphthalmia
- Retinal pigment changes
- Chorioretinal atrophy
- Vascular changes

FIGURE 3 | Main eye structures affected by each TORCH agent during development (indicated by colored circles). Clinical consequences regarding congenital *T. gondii* (green symbols), Herpes simplex virus (blue), Rubella virus (magenta), Zika Virus (orange), and Cytomegalovirus (navy blue) infection are listed besides each pathogen's name. Viral structure representations were based on Hulo et al. (2011).

newborns, future studies will reveal whether this virus could actually be included as a new TORCH pathogen (Muldoon et al., 2020).

AUTHOR CONTRIBUTIONS

VdC wrote the first draft of the manuscript and prepared the figures. KC and DA revised and discussed the manuscript and figures. All authors contributed to the article and approved the submitted version.

FUNDING

This work was supported by: Fundação Oswaldo Cruz (Edital INOVA Geração de Conhecimento 2018, grant no. 3231984391); Conselho Nacional de Pesquisa e Desenvolvimento Tecnológico (CNPq, grant nos. 401772/2015-2 and 444478/2014-0 for DA; INCT/INNT Proc. 465346/2014-6 for KC), Fundação Carlos Chagas Filho de Amparo à Pesquisa do Rio de Janeiro (Faperj, Projetos Temáticos grant no. E-26/010-001199/2015, Redes em Saúde, grant no. E-26-211.570/2019 for DA, Projetos Temáticos grant no. E26/010.101037/201, and Sediadas grant no. E-26/010.001493/2019 for KC). VdC was sponsored with a Ph.D. fellowship from CAPES/Brazil and KC has individual research fellowships from CNPq and Faperj.

ACKNOWLEDGMENTS

The authors thank Mrs. Heloisa Diniz from the Department of Image Production and Processing (Serviço de Produção e Tratamento de Imagem - IOC) at the Oswaldo Cruz Institute for the excellent preparation of the figures. Dr. Rachel Ann Hauser Davis for excellent proof editing of this manuscript.

REFERENCES

Alcendor, D. J. (2019). *Human vascular pericytes and Cytomegalovirus* pathobiology. *Int. J. Mol. Sci.* 20:1456. doi: 10.3390/ijms20061456

Alford, C. A., Stagno, S., Pass, R. F., Britt, W. J., Nakao, T., Chiba, S., et al. (1980). Congenital and perinatal *Cytomegalovirus* infection. *Rev. Infect. Dis.* 24, 274–279. doi: 10.1111/j.1442-200X.1980.tb00519.x

al-Haddad, B. J. S., Oler, E., Armistead, B., Elsayed, N. A., Weinberger, D. R., Bernier, R., et al. (2019). The fetal origins of mental illness. *Am. J. Obstet. Gynecol.* 221, 549–562. doi: 10.1016/j.ajog.2019.06.013

Ambroise-Thomas, P., and Petersen, E. (2000). "Congenital toxoplasmosis: past, present and future," in *Congenital Toxoplasmosis*, eds. P. Ambroise-Thomas and E. Petersen (Berlin: Springer-Verlag France), 1–7. doi: 10.1093/jpids/piu077

Anderson, S. R., Zhang, J., Steele, M. R., Romero, C. O., Kautzman, A. G., Schafer, D. P., et al. (2019). Complement targets newborn retinal ganglion cells for phagocytic elimination by microglia. *J. Neurosci.* 39, 2025–2040. doi: 10.1523/JNEUROSCI.1854-18.2018

Ashour, D. S., Saad, A. E., Bakary, R. H., El Bakary, R. H., and El Barody, M. A. (2018). Can the route of *Toxoplasma gondii* infection affect the ophthalmic outcomes? *Pathog. Dis.* 76, 1–7. doi: 10.1093/femspd/fty056

Atreya, C. D., Mohan, K. V. K., and Kulkarni, S. (2004). *Rubella virus* and birth defects: Molecular insights into the viral teratogenesis at the cellular level. *Birth Defects Res. A Clin. Mol. Teratol.* 70, 431–437. doi: 10.1002/bdra.20045

Bale, J. F. (2014). "Congenital cytomegalovirus infection," in *Handbook of Clinical Neurology*, eds A. C. Tselis and J. Booss (Salt Lake City, UT: Elsevier B.V.), 319–326. doi: 10.1016/B978-0-444-53488-0.00015-8

Bhandage, A. K., Kanatani, S., and Barragan, A. (2019). Toxoplasma-induced hypermigration of primary cortical microglia implicates GABAergic signaling. *Front. Cell. Infect. Microbiol.* 9:53. doi: 10.3389/fcimb.2019.00073

Bollani, L., Strocchio, L., Stronati, M., Kieffer, F., and Wallon, M. (1967). Congenital toxoplasmosis. *J. Paediatr. Child Health* 112, 1099–1101.

Bonfanti, L., Strettoi, E., Chierzi, S., Cenni, M. C., Liu, X. H., Martinou, J. C., et al. (1996). Protection of retinal ganglion cells from natural and axotomy-induced cell death in neonatal transgenic mice overexpressing bcl-2. *J. Neurosci.* 16, 4186–4194. doi: 10.1523/JNEUROSCI.16-13-04186.1996

Boppana, S. B., Britt, W. J., Fowler, K., Hutto, S. C., James, S. H., Kimberlin, D. W., et al. (2017). Pathogenesis of Non-Zika congenital viral infections. *J. Infect. Dis.* 216, S912–S918. doi: 10.1093/infdis/jix431

Bowden, D. S., Pedersen, J. S., Toh, B. H., and Westaway, E. G. (1987). Distribution by immunofluorescence of viral products and actin-containing cytoskeletal filaments in *Rubella virus*-infected cells. *Arch. Virol.* 92, 211–219. doi: 10.1007/BF01317478

Braunger, B. M., Demmer, C., and Tamm, E. R. (2014). Retinal degenerative diseases: isolation and *ex vivo* characterization of the immunophenotype and function of microglia/ macrophage populations in normal dog retina. *Adv. Exp. Med. Biol.* 664, 447–456.

Bringmann, A., and Reichenbach, A. (2001). Role of müller cells in retinal degenerations andreas. *Front. Biosci.* 6, 77–92. doi: 10.2741/Bringman

Brown, R. M., Rana, P. S. J. B., Jaeger, H. K., O'Dowd, J. M., Balemba, O. B., and Fortunato, E. A. (2019). Human *Cytomegalovirus* compromises development of cerebral organoids. *J. Virol.* 93:e00957-19. doi: 10.1128/JVI.00957-19

Brown, Z. A., Selke, S., Zeh, J., Kopelman, J., Maslow, A., Ashley, R. L., et al. (1997). The acquisition of herpes simplex virus during pregnancy. *J. Med.* 25, 509–515. doi: 10.1056/NEJM199708213370801

Büttner, C., Heer, M., Traichel, J., Schwemmle, M., and Heimrich, B. (2019). Zika Virus-mediated death of hippocampal neurons is independent from maturation state. *Front. Cell. Neurosci.* 13:389. doi: 10.3389/fncel.2019.00389

Caine, E. A., Jagger, B. W., and Diamond, M. S. (2018). Animal models of Zika virus infection during pregnancy. *Viruses* 10:598. doi: 10.3390/v10110598

Calvet, G., Aguiar, R. S., Melo, A. S. O., Sampaio, S. A., de Filippis, I., Fabri, A., et al. (2016). Detection and sequencing of Zika virus from amniotic fluid of fetuses with microcephaly in Brazil: a case study. *Lancet Infect. Dis.* 16, 653–660. doi: 10.1016/S1473-3099(16)00095-5

Cannon, M. J. (2009). Congenital *Cytomegalovirus* (CMV) epidemiology and awareness. *J. Clin. Virol.* 46, 6–10. doi: 10.1016/j.jcv.2009.09.002

Carter-Dawson, L. D., and Lavail, M. M. (1979). Rods and cones in the mouse retina. I. Structural analysis using light and electron microscopy. *J. Comp. Neurol.* 188, 245–262. doi: 10.1002/cne.901880204

Cepko, C. L., Austin, C. P., Yang, X., Alexiades, M., and Ezzeddine, D. (1996). Cell fate determination in the vertebrate retina. *Proc. Natl. Acad. Sci. U.S.A.* 93, 589–595. doi: 10.1073/pnas.93.2.589

Chan-Ling, T. (1994). Glial, neuronal and vascular interactions in the mammalian retina. *Prog. Retin. Eye Res.* 13, 357–389. doi: 10.1016/1350-9462(94)90015-9

Chavarría, T., Baleriola, J., Mayordomo, R., De Pablo, F., and De La Rosa, E. J. (2013). Early neural cell death is an extensive, dynamic process in the embryonic chick and mouse retina. *Sci. World J.* 2013:627240. doi: 10.1155/2013/627240

Cheeran, M. C. J., Lokensgard, J. R., and Schleiss, M. R. (2009). Neuropathogenesis of congenital *Cytomegalovirus* infection: disease mechanisms and prospects for intervention. *Clin. Microbiol. Rev.* 22, 99–126. doi: 10.1128/CMR.00023-08

Christian, K. M., Song, H., and Ming, G. (2019). Pathophysiology and mechanisms of Zika virus infection in the nervous system. *Annu. Rev. Neurosci.* 42, 249–269. doi: 10.1146/annurev-neuro-080317-062231

Chucair-Elliott, A. J., Conrady, C., Zheng, M., Kroll, C. M., Lane, T. E., and Carr, D. J. J. (2014). Microglia-induced IL-6 protects against neuronal loss

following HSV-1 infection of neural progenitor cells. *Glia* 62, 1418–1434. doi: 10.1002/glia.22689

Cossenza, M., Socodato, R., Portugal, C. C., Domith, I. C. L., Gladulich, L. F. H., Encarnação, T. G., et al. (2014). Nitric oxide in the nervous system: biochemical, developmental, and neurobiological aspects. *Vitam. Horm.* 96, 79–125. doi: 10.1016/B978-0-12-800254-4.00005-2

Costa, M. L., de Moraes Nobrega, G., and Antolini-Tavares, A. (2020). Key Infections in the Placenta. *Obstet. Gynecol. Clin. North Am*. 47, 133–146. doi: 10.1016/j.ogc.2019.10.003

Cowen, D., Wolf, A., and Paige, B. H. (1942). Toxoplasmic encephalomyelitis. *Arch. Neurol. Psychiatry* 48, 187–214. doi: 10.1001/archneurpsyc.1942.02290110009001

Coyne, C. B., and Lazear, H. M. (2016). Zika virus-reigniting the TORCH. *Nat. Rev. Microbiol*. 14, 707–715. doi: 10.1038/nrmicro.2016.125

Cugola, F. R., Fernandes, I. R., Russo, F. B., Freitas, B. C., Dias, J. L. M., Guimarães, K. P., et al. (2016). The Brazilian Zika virus strain causes birth defects in experimental models. *Nature* 534, 267–271. doi: 10.1038/nature18296

Cusato, K., Bosco, A., Rozental, R., Guimarães, C. A., Reese, B. E., Linden, R., et al. (2003). Gap junctions mediate bystander cell death in developing retina. *J. Neurosci*. 23, 6413–6422. doi: 10.1523/JNEUROSCI.23-16-06413.2003

Da Gama, L. M., Ribeiro-Gomes, F. L., Guimarães, U., and Arnholdt, A. C. V. (2004). Reduction in adhesiveness to extracellular matrix components, modulation of adhesion molecules and *in vivo* migration of murine macrophages infected with *Toxoplasma gondii*. *Microbes Infect*. 6, 1287–1296. doi: 10.1016/j.micinf.2004.07.008

Dal Ponte, S., Burguez, D., and Andrioli, G. (2019). Outbreak of Toxoplasmosis in the city of Santa Maria, Brazil. *Prehosp. Disaster Med*. 34:s74. doi: 10.1017/S1049023X19001602

de Araújo, T. V. B., Rodrigues, L. C., de Alencar Ximenes, R. A., de Barros Miranda-Filho, D., Montarroyos, U. R., de Melo, A. P. L., et al. (2016). Association between Zika virus infection and microcephaly in Brazil, January to May, 2016: preliminary report of a case-control study. *Lancet Infect. Dis*. 16, 1356–1363. doi: 10.1016/S1473-3099(16)30318-8

Delair, E., Creuzet, C., Dupouy-Camet, J., and Roisin, M. P. (2009). *In vitro* effect of TNF-α and IFN-γ in retinal cell infection with *Toxoplasma gondii*. *Investig. Ophthalmol. Vis. Sci*. 50, 1754–1760. doi: 10.1167/iovs.07-1376

Dhanasekaran, D. N., and Reddy, E. P. (2008). JNK signaling in apoptosis. *Oncogene* 27, 6245–6251. doi: 10.1038/onc.2008.301

Diao, L., Zhang, B., Xuan, C., Sun, S., Yang, K., Tang, Y., et al. (2005). Activation of c-Jun N-terminal kinase (JNK) pathway by HSV-1 immediate early protein ICP0. *Exp. Cell Res*. 308, 196–210. doi: 10.1016/j.yexcr.2005.04.016

Dick, G. (1952). Zika isolation and serological specificity. *Trans. R. Soc. Trop. Med. Hyg*. 46, 509–520. doi: 10.1016/0035-9203(52)90042-4

Dräger, U. C. (1985). Birth dates of retinal ganglion cells giving rise to the crossed and uncrossed optic projections in the mouse. *Proc. R. Soc. London - Biol. Sci.* 224, 57–77. doi: 10.1098/rspb.1985.0021

Dubey, J. P. (2004). Toxoplasmosis - a waterborne zoonosis. *Vet. Parasitol*. 126, 57–72. doi: 10.1016/j.vetpar.2004.09.005

Dubey, J. P., Lago, E. G., Gennari, S. M., Su, C., and Jones, J. L. (2012). Toxoplasmosis in humans and animals in Brazil : high prevalence, high burden of disease, and epidemiology. *Parasitology* 139, 1375–1424. doi: 10.1017/S0031182012000765

Dukaczewska, A., Tedesco, R., and Liesenfeld, O. (2015). Experimental models of ocular infection with *Toxoplasma gondii*. *Eur. J. Microbiol. Immunol*. 5, 293–305. doi: 10.1556/1886.2015.00045

Dukhovny, A., Sloutskin, A., Markus, A., Yee, M. B., Kinchington, P. R., and Goldstein, R. S. (2012). Varicella-zoster virus infects human embryonic stem cell-derived neurons and neurospheres but not pluripotent embryonic stem cells or early progenitors. *J. Virol*. 86, 3211–3218. doi: 10.1128/JVI.06810-11

Duszak, R. S. (2009). Congenital rubella syndrome-major review. *Optometry* 80, 36–43. doi: 10.1016/j.optm.2008.03.006

Dyer, M. A., and Cepko, C. L. (2001). Regulating proliferation during retinal development. *Nat. Rev. Neurosci*. 2, 333–342. doi: 10.1038/35072555

Fa, F., Laup, L., Mandelbrot, L., Sibiude, J., and Picone, O. (2020). Fetal and neonatal abnormalities due to congenital herpes simplex virus infection: a literature review. *Prenat. Diagn*. 40, 408–414. doi: 10.1002/pd.5587

Fan, W. J., Li, X., Yao, H. L., Deng, J. X., Liu, H. L., Cui, Z. J., et al. (2016). Neural differentiation and synaptogenesis in retinal development. *Neural Regen. Res*. 11, 312–318. doi: 10.4103/1673-5374.177743

Ferguson, D. J. P. (2009). *Toxoplasma gondii*: 1908-2008, homage to Nicolle, Manceaux and Splendore. *Mem. Inst. Oswaldo Cruz* 104, 133–148. doi: 10.1590/S0074-02762009000200003

Ferraris, P., Yssel, H., and Missé, D. (2019). Zika virus infection: an update. *Microbes Infect*. 21, 353–360. doi: 10.1016/j.micinf.2019.04.005

Fisher, L. J. (1979). Development of synaptic arrays in the inner plexiform layer of neonatal mouse retina. *J. Comp. Neurol*. 187, 359–372. doi: 10.1002/cne.901870207

Frade, J. M., and Barde, Y. A. (1999). Genetic evidence for cell death mediated by nerve growth factor and the neurotrophin receptor p75 in the developing mouse retina and spinal cord. *Development* 126, 683–690.

Francisco-Morcillo, J., Bejarano-Escobar, R., Rodríguez-León, J., Navascués, J., and Martín-Partido, G. (2014). Ontogenetic cell death and phagocytosis in the visual system of vertebrates. *Dev. Dyn*. 243, 1203–1225. doi: 10.1002/dvdy.24174

Francisco-Morcillo, J., Hidalgo-Sánchez, M., and Martín-Partido, G. (2006). Spatial and temporal patterns of proliferation and differentiation in the developing turtle eye. *Brain Res*. 1103, 32–48. doi: 10.1016/j.brainres.2006.05.052

Freij, B. J., South, M. A., and Sever, J. L. (1988). Maternal rubella and the congenital rubella syndrome. *Clin. Perinatol*. 15, 247–257. doi: 10.1016/S0095-5108(18)30710-3

Frenkel, J. K. (1955). Ocular lesions in hamsters; with chronic Toxoplasma and *Besnoitia* infection. *Am. J. Ophthalmol*. 39, 203–225. doi: 10.1016/0002-9394(55)90026-X

Frenkel, J. K. (1973). Toxoplasma in and around us. *Bioscience* 23, 343–352. doi: 10.2307/1296513

Frey, T. K. (1994). Molecular biology of *Rubella virus*. *Adv. Virus Res*. 44, 69–160. doi: 10.1016/S0065-3527(08)60328-0

Fuks, J. M., Arrighi, R. B. G., Weidner, J. M., Kumar Mendu, S., Jin, Z., Wallin, R. P. A., et al. (2012). GABAergic signaling is linked to a hypermigratory phenotype in dendritic cells infected by *Toxoplasma gondii*. *PLoS Pathog*. 8:e1003051. doi: 10.1371/journal.ppat.1003051

Furtado, J., Smith, J., Belfort, R., Gattey, D., and Winthrop, K. (2011). Toxoplasmosis: a global threat. *J. Glob. Infect. Dis*. 3, 281–284. doi: 10.4103/0974-777X.83536

Furtado, J. M., Ashander, L. M., Mohs, K., Chipps, T. J., Appukuttan, B., and Smith, J. R. (2013). *Toxoplasma gondii* migration within and infection of human retina. *PLoS ONE* 8:e54358. doi: 10.1371/journal.pone.0054358

Furtado, J. M., Bharadwaj, A. S., Chipps, T. J., Pan, Y., Ashander, L. M., and Smith, J. R. (2012). *Toxoplasma gondii* tachyzoites cross retinal endothelium assisted by intercellular adhesion molecule-1 *in vitro*. *Immunol. Cell Biol*. 90, 912–915. doi: 10.1038/icb.2012.21

Gabriel, E., Ramani, A., Karow, U., Gottardo, M., Natarajan, K., Gooi, L. M., et al. (2017). Recent Zika virus isolates induce premature differentiation of neural progenitors in human brain organoids. *Cell Stem Cell* 20, 397–406.e5. doi: 10.1016/j.stem.2016.12.005

Garcez, P. P., Stolp, H. B., Sravanam, S., Christoff, R. R., Ferreira, J. C. C. G., Dias, A. A., et al. (2018). Zika virus impairs the development of blood vessels in a mouse model of congenital infection. *Sci. Rep*. 8:12774. doi: 10.1038/s41598-018-31149-3

Gaynon, M. W., Boldrey, E. E., Strahlman, E. R., and Fine, S. L. (1984). Retinal neovascularization and ocular toxoplasmosis. *Am. J. Ophthalmol*. 98, 585–589. doi: 10.1016/0002-9394(84)90244-7

Gazzinelli, R. T., Brézin, A., Li, Q., Nussenblatt, R. B., and Chan, C. C. (1994). *Toxoplasma gondii*: acquired ocular toxoplasmosis in the murine model, protective role of TNF-α and IFN-γ. *Exp. Parasitol*. 78, 217–229. doi: 10.1006/expr.1994.1022

George, S., Viswanathan, R., and Sapkal, G. N. (2019). Molecular aspects of the teratogenesis of *Rubella virus*. *Biol. Res*. 52:47. doi: 10.1186/s40659-019-0254-3

Georges, P., Madigan, M. C., and Provis, J. M. (1999). Apoptosis during development of the human retina: relationship to foveal development and retinal synaptogenesis. *J. Comp. Neurol*. 413, 198–208. doi: 10.1002/(SICI)1096-9861(19991018)413:2<198::AID-CNE2>3.0.CO;2-J

Geyer, H., Bauer, M., Neumann, J., Lüdde, A., Rennert, P., Friedrich, N., et al. (2016). Gene expression profiling of *Rubella virus* infected primary endothelial cells of fetal and adult origin Positive-strand RNA viruses. *Virol. J.* 13, 1–17. doi: 10.1186/s12985-016-0475-9

Ghekiere, S., Allegaert, K., Cossey, V., Van Ranst, M., Cassiman, C., and Casteels, I. (2012). Ophthalmological findings in congenital *Cytomegalovirus* infection: when to screen, when to treat? *J. Pediatr. Ophthalmol. Strabismus* 49, 274–282. doi: 10.3928/01913913-20120710-03

Gregg, N. M. (1941). Congenital cataract following German measles in the mother. Epidemiol. Infect. 107, iii–xiv. doi: 10.1017/S0950268800048627

Griffiths, P., Baraniak, I., and Reeves, M. (2015). The pathogenesis of human *Cytomegalovirus*. *J. Pathol.* 235, 288–297. doi: 10.1002/path.4437

Hall, S. M. (1992). Congenital toxoplasmosis. *BMJ* 305:291. doi: 10.1136/bmj.305.6848.291

Hamburger, V., and Hamilton, H. L. (1951). A series of normal stages in the development of the chick embryo. *J. Morphol.* 88, 49–92. doi: 10.1002/jmor.1050880104

Hammack, C., Ogden, S. C., Madden, J. C., Medina, A., Xu, C., and Phillips, E. (2019). Crossm Zika virus infection induces DNA damage response in human. *J. Virol.* 93:e00638-19. doi: 10.1128/JVI.00638-19

Hampton, M. M. (2015). Congenital toxoplasmosis: a review. *Neonatal Netw.* 34, 274–278. doi: 10.1891/0730-0832.34.5.274

Harada, C., Harada, T., Nakamura, K., Sakai, Y., Tanaka, K., and Parada, L. F. (2006). Effect of p75NTR on the regulation of naturally occurring cell death and retinal ganglion cell number in the mouse eye. *Dev. Biol.* 290, 57–65. doi: 10.1016/j.ydbio.2005.08.051

Hargett, D., McLean, T., and Bachenheimer, S. L. (2005). Herpes simplex virus ICP27 activation of stress kinases JNK and p38. *J. Virol.* 79, 8348–8360. doi: 10.1128/JVI.79.13.8348-8360.2005

Heavner, W., and Pevny, L. (2012). Eye development and retinogenesis. *Cold Spring Harb. Perspect. Biol.* 4:a008391. doi: 10.1101/cshperspect.a008391

Heerema-McKenney, A. (2018). Defense and infection of the human placenta. *Apmis* 126, 570–588. doi: 10.1111/apm.12847

Hendrickson, A. (2016). Development of retinal layers in prenatal human retina. *Physiol. Behav.* 176, 139–148. doi: 10.1016/j.physbeh.2017.03.040

Hendrickson, A., and Zhang, C. (2017). Development of cone photoreceptors and their synapses in the human and monkey fovea. *J. Comp. Neurol.* 527, 38–51. doi: 10.1002/cne.24170

Holland, G. N. (1999). Reconsidering the pathogenesis of ocular toxoplasmosis. *Am. J. Ophthalmol.* 128, 502–505. doi: 10.1016/S0002-9394(99)00263-9

Hollenberg, M. J., and Spira, A. W. (1973). Human retinal development: ultrastructure of the outer retina. *Am. J. Anat.* 137, 357–385. doi: 10.1002/aja.1001370402

Hotez, P. (2019). The physician-scientist: defending vaccines and combating antiscience. *J. Clin. Invest.* 129, 2169–2171. doi: 10.1172/JCI129121

Hughes, S., Yang, H., and Chan-Ling, T. (2000). Vascularization of the human fetal retina: roles of vasculogenesis and angiogenesis. *Investig. Ophthalmol. Vis. Sci.* 41, 1217–1228.

Hulo, C., De Castro, E., Masson, P., Bougueleret, L., Bairoch, A., Xenarios, I., et al. (2011). ViralZone: a knowledge resource to understand virus diversity. *Nucleic Acids Res.* 39, 576–582. doi: 10.1093/nar/gkq901

James, S. H., and Kimberlin, D. W. (2015). Neonatal herpes simplex virus infection: epidemiology and treatment. *Clin. Perinatol.* 42, 47–59. doi: 10.1016/j.clp.2014.10.005

Kanatani, S., Fuks, J. M., Olafsson, E. B., Westermark, L., Chambers, B., Varas-Godoy, M., et al. (2017). Voltage-dependent calcium channel signaling mediates GABAAreceptor-induced migratory activation of dendritic cells infected by *Toxoplasma gondii*. *PLoS Pathog.* 13:e1006739. doi: 10.1371/journal.ppat.1006739

Kanatani, S., Uhlén, P., and Barragan, A. (2015). Infection by *Toxoplasma gondii* induces amoeboid-like migration of dendritic cells in a three-dimensional collagen matrix. *PLoS ONE* 10:e0139104. doi: 10.1371/journal.pone.0139104

Kawamura, K., and Kano, Y. (2019). Electrical stimulation induces neurite outgrowth in PC12m3 cells via the p38 mitogen-activated protein kinase pathway. *Neurosci. Lett.* 698, 81–84. doi: 10.1016/j.neulet.2019.01.015

Kawasaki, H., Kosugi, I., Meguro, S., and Iwashita, T. (2017). Pathogenesis of developmental anomalies of the central nervous system induced by congenital *Cytomegalovirus* infection. *Pathol. Int.* 67, 72–82. doi: 10.1111/pin.12502

Kijlstra, A., and Petersen, E. (2014). Epidemiology, pathophysiology, and the future of ocular toxoplasmosis. *Ocul. Immunol. Inflamm.* 22, 138–147. doi: 10.3109/09273948.2013.823214

Kim, K., and Weiss, L. M. (2004). *Toxoplasma gondii*: the model apicomplexan. *Int. J. Parasitol.* 34, 423–432. doi: 10.1016/j.ijpara.2003.12.009

Kolb, H. (2003). How the retina works. *Am. Sci.* 91:28. doi: 10.1511/2003.1.28

Konradt, C., Ueno, N., Christian, D. A., Delong, J. H., Pritchard, G. H., Herz, J., et al. (2016). Endothelial cells are a replicative niche for entry of *Toxoplasma gondii* to the central nervous system. *Nat. Microbiol.* 1:16001. doi: 10.1038/nmicrobiol.2016.1

Kovacs, K., Vaczy, A., Fekete, K., Petra, K., Atlasz, T., Reglodi, D., et al. (2019). PARP inhibitor protects against chronic hypoxia/ reoxygenation-induced retinal injury by regulation of MAPKs, HIF1α, Nrf2, and NFjB. *Investig. Ophthalmol. Vis. Sci.* 60, 1478–1490. doi: 10.1167/iovs.18-25936

Krishnendhu, V. K., and George, L. S. (2019). Drivers and barriers for measles rubella vaccination campaign: as qualitative study. *J. Fam. Med. Prim. Care* 8, 881–885. doi: 10.4103/jfmpc.jfmpc_73_19

Lachenmaier, S. M., Deli, M. A., Meissner, M., and Liesenfeld, O. (2014). Intracellular transport of *Toxoplasma gondii* through the blood – brain *barrier*. *J. Neuroimmunol.* 232, 119–130. doi: 10.1016/j.jneuroim.2010.10.029

Laemle, L. K., Puszkarczuk, M., and Feinberg, R. N. (1999). Apoptosis in early ocular morphogenesis in the mouse. *Dev. Brain Res.* 112, 129–133. doi: 10.1016/S0165-3806(98)00153-9

Lahmar, I., Guinard, M., Sauer, A., Marcellin, L., Abdelrahman, T., Roux, M., et al. (2010). Murine neonatal infection provides an efficient model for congenital ocular toxoplasmosis. *Exp. Parasitol.* 124, 190–196. doi: 10.1016/j.exppara.2009.09.010

Lahmar, I., Pfaff, A. W., Marcellin, L., Sauer, A., Moussa, A., Babba, H., et al. (2014). Müller cell activation and photoreceptor depletion in a mice model of congenital ocular toxoplasmosis. *Exp. Parasitol.* 144, 22–26. doi: 10.1016/j.exppara.2014.06.006

Landolfo, S., Gariglio, M., Gribaudo, G., and Lembo, D. (2003). The human *Cytomegalovirus*. *Pharmacol. Ther.* 98, 269–297. doi: 10.1016/S0163-7258(03)00034-2

Ledur, P. F., Karmirian, K., Pedrosa, C., da, S. G., Souza, L. R. Q., Assis-de-Lemos, G., Martins, T. M., et al. (2020). Zika virus infection leads to mitochondrial failure, oxidative stress and DNA damage in human iPSC-derived astrocytes. *Sci. Rep.* 10:1218. doi: 10.1038/s41598-020-57914-x

Lee, K. S., Zhou, W., Scott-McKean, J. J., Emmerling, K. L., Cai, G., yun, Krah, D. L., et al. (2012). Human sensory neurons derived from induced pluripotent stem cells support varicella-zoster virus infection. *PLoS ONE* 7:e53010. doi: 10.1371/journal.pone.0053010

Lei, S., Lu, P., Lu, Y., Zheng, J., Li, W., Wang, N., et al. (2020). Dexmedetomidine alleviates neurogenesis damage following neonatal midazolam exposure in rats through JNK and P38 MAPK pathways. *ACS Chem. Neurosci.* 11, 579–591. doi: 10.1021/acschemneuro.9b00611

Leung, K. K. Y., Hon, K. L., Yeung, A., Leung, A. K. C., and Man, E. (2020). Congenital infections in Hong Kong: an overview of TORCH. *Hong Kong Med. J.* 26, 127–138. doi: 10.12809/hkmj198287

Liesegang, T. J. (2001). Herpes simplex virus epidemiology and ocular importance. *Cornea* 20, 1–13. doi: 10.1097/00003226-200101000-00001

Lima, L. D. S., Baran, L. C. P., Hamer, R. D., da Costa, M. F., Vidal, K. S., Damico, F. M., et al. (2020). Longitudinal visual acuity development in ZIKV-exposed children. *J. AAPOS* 24, 23.e1–23.e6. doi: 10.1016/j.jaapos.2019.11.005

Maenz, M., Schlüter, D., Liesenfeld, O., Schares, G., Gross, U., and Pleyer, U. (2014). Progress in retinal and eye research ocular toxoplasmosis past, present and new aspects of an old disease. *Prog. Retin. Eye Res.* 39, 77–106. doi: 10.1016/j.preteyeres.2013.12.005

Malm, G., and Engman, M. L. (2007). Congenital *Cytomegalovirus* infections. *Semin. Fetal Neonatal Med.* 12, 154–159. doi: 10.1016/j.siny.2007.01.012

Maltepe, E., Bakardjiev, A. I., Fisher, S. J., Maltepe, E., Bakardjiev, A. I., and Fisher, S. J. (2010). The placenta : transcriptional, epigenetic, and physiological integration during development Find the latest version : review series the placenta : transcriptional, epigenetic, and physiological integration during development. *J. Clin. Invest.* 120, 1016–1025. doi: 10.1172/JCI41211

Mareze, M., Benitez, N., Pe, A., Pinto-ferreira, F., Miura, A. C., Danyel, F., et al. (2019). Socioeconomic vulnerability associated to *Toxoplasma gondii* exposure in southern Brazil. *PLoS ONE* 14:e0212375. doi: 10.1371/journal.pone.0212375

Marín-Teva, J. L., Cuadros, M. A., Martín-Oliva, D., and Navascués, J. (2011). Microglia and neuronal cell death. *Neuron Glia Biol.* 7, 25–40. doi: 10.1017/S1740925X12000014

Marquardt, T., and Gruss, P. (2002). Generating neuronal diversity in the retina : one for nearly *all*. *Trends Neurosci.* 25, 32–38. doi: 10.1016/S0166-2236(00)02028-2

Martins, R. A. P., and Pearson, R. A. (2008). Control of cell proliferation by neurotransmitters in the developing vertebrate retina. *Brain Res.* 1192, 37–60. doi: 10.1016/j.brainres.2007.04.076

Martins, R. A. P., Silveira, M. S., Curado, M. R., Police, A. I., and Linden, R. (2005). NMDA receptor activation modulates programmed cell death during early post-natal retinal development: A BDNF-dependent mechanism. *J. Neurochem.* 95, 244–253. doi: 10.1111/j.1471-4159.2005.03360.x

Mellén, M. A., de la Rosa, E. J., and Boya, P. (2008). The autophagic machinery is necessary for removal of cell corpses from the developing retinal neuroepithelium. *Cell Death Differ.* 15, 1279–1290. doi: 10.1038/cdd.2008.40

Mitchell, J. O. E. E., and Mccall, F. C. (1963). Transplacental by Herpes. *Am. J. Dis. Child.* 106, 121–123. doi: 10.1001/archpedi.1963.02080050209015

Mohan, K. V. K., Ghebrehiwet, B., and Atreya, C. D. (2002). The N-terminal conserved domain of *Rubella virus* capsid interacts with the C-terminal region of cellular p32 and overexpression of p32 enhances the viral infectivity. *Virus Res.* 85, 151–161. doi: 10.1016/S0168-1702(02)00030-8

Moraes, A. M. M. M., Pessôa, C. N., Vommaro, R. C., De Souza, W., De Mello, F. G., and Hoko,ç, J. N. (2004). Cultured embryonic retina systems as a model for the study of underlying mechanisms of *Toxoplasma gondii* infection. *Investig. Ophthalmol. Vis. Sci.* 45, 2813–2821. doi: 10.1167/iovs.04-0177

Muldoon, K. M., Fowler, K. B., Pesch, M. H., and Schleiss, M. R. (2020). SARS-CoV-2: Is it the newest spark in the TORCH? *J. Clin. Virol.* 127:104372. doi: 10.1016/j.jcv.2020.104372

Musso, D., and Gubler, D. J. (2016). Zika Virus. *Clin. Microbiol. Rev.* 29, 487–524. doi: 10.1128/CMR.00072-15

Nag, T. C., and Wadhwa, S. (2001). Differential expression of syntaxin-1 and synaptophysin in the developing and adult human retina. *J. Biosci.* 26, 179–191. doi: 10.1007/BF02703642

Nasaré, A. M., and Tedesco, R. C. (2017). "*Experimental models of ocular toxoplasmosis*," in *Toxoplasmosis*, ed I. Akyar (São Paulo: IntechOpen), 69–85. doi: 10.5772/67947

Nathala, P., Fatima, S., Sumner, R., and Lippmann, S. (2019). Measles 101. *Postgrad. Med.* 131, 574–575. doi: 10.1080/00325481.2019.1669409

Newman, E. A. (2004). Glial modulation of synaptic transmission in the retina. *Glia* 47, 268–274. doi: 10.1002/glia.20030

Nguyen, T., Van Pham, V. H., and Abe, K. (2015). Pathogenesis of congenital *Rubella virus* infection in human fetuses: viral infection in the ciliary body could play an important role in cataractogenesis. *EBioMedicine* 2, 59–63. doi: 10.1016/j.ebiom.2014.10.021

Nicolle, C., and Manceaux, L. H. (1908). "Sur une infection a coyes de Leishman (ou organismes voisins) du gondi" in *Comptes Rendus Hebdomadaires des Seances de L'Academie des Sciences* (Gauthier-Villars), 763–766.

Nogueira, A. R., Leve, F., Morgado-Diaz, J., Tedesco, R. C., and Pereira, M. C. S. (2016). Effect of *Toxoplasma gondii* infection on the junctional complex of retinal pigment epithelial cells. *Parasitology* 143, 568–575. doi: 10.1017/S0031182015001973

Nussenblatt, R. B., and Belfort, R. (1994). Ocular toxoplasmosis: an old disease revisited. *J. Am. Med. Assoc.* 271, 304–307. doi: 10.1001/jama.1994.03510280066035

Odeberg, J., Wolmer, N., Falci, S., Westgren, M., Seiger, Å., and Söderberg-Nauclér, C. (2006). Human *Cytomegalovirus* inhibits neuronal differentiation and induces apoptosis in human neural precursor cells. *J. Virol.* 80, 8929–8939. doi: 10.1128/JVI.00676-06

Ólafsson, E. B., Varas-Godoy, M., and Barragan, A. (2018). *Toxoplasma gondii* infection shifts dendritic cells into an amoeboid rapid migration mode encompassing podosome dissolution, secretion of TIMP-1, and reduced proteolysis of extracellular matrix. *Cell. Microbiol.* 20, 1–15. doi: 10.1111/cmi.12808

Olney, J. W. (1968). An electron microscopic study of synapse formation, receptor outer segment development, and other aspects of developing mouse retina. *Investig. Ophthalmol.* 7, 251–268.

Ozgonul, C., and Besirli, C. G. (2016). Recent developments in the diagnosis and treatment of ocular toxoplasmosis. *Ophthalmic Res.* 57, 1–12. doi: 10.1159/000449169

Pang, B., Li, M., Song, J., Li, Q. W., Wang, J., Di, S., et al. (2020). Luo Tong formula attenuates retinal inflammation in diabetic rats via inhibition of the p38MAPK/NF-κB pathway. *Chin. Med.* 15:5. doi: 10.1186/s13020-019-0284-3

Pavesio, C. E., and Lightman, S. (1996). *Toxoplasma gondii* and ocular toxoplasmosis: pathogenesis. *Br. J. Ophthalmol.* 80, 1099–1107. doi: 10.1136/bjo.80.12.1099

Péquignot, M. O., Provost, A. C., Sallé, S., Taupin, P., Sainton, K. M., Marchant, D., et al. (2003). Major role of BAX in apoptosis during retinal development and in establishment of a functional postnatal retina. *Dev. Dyn.* 228, 231–238. doi: 10.1002/dvdy.10376

Pique-Regi, R., Romero, R., Tarca, A. L., Luca, F., Xu, Y., Alazizi, A., et al. (2020). Does the human placenta express the canonical cell entry mediators for SARS-CoV-2? *Elife* 9:e58716. doi: 10.7554/eLife.58716

Pollock, G. S., Robichon, R., Boyd, K. A., Kerkel, K. A., Kramer, M., Lyles, J., et al. (2003). TrkB receptor signaling regulates developmental death dynamics, but not final number, of retinal ganglion cells. *J. Neurosci.* 23, 10137–10145. doi: 10.1523/JNEUROSCI.23-31-10137.2003

Prada, C., Puga, J., Perez-Mendez, L., Lopez, R., and Ramirez, G. (1991). Erratum: spatial and temporal patterns of neurogenesis in the chick retina. *Eur. J. Neurosci.* 3, 559–569. doi: 10.1111/j.1460-9568.1991.tb00843.x

Provis, J. M., Van Driel, D., Billson, F. A., and Russell, P. (1985). Development of the human retina: patterns of cell distribution and redistribution in the ganglion cell layer. J. Comp. *Neurol.* 233, 429–451. doi: 10.1002/cne.902330403

Rabelo, K., Souza, L. J., De, Salomão, N. G., Basílio-de-oliveira, R., Barreto, F., and Neves, L. D. (2020). Zika induces human placental damage and *inflammation*. *Front. Immunol.* 11:2146. doi: 10.3389/fimmu.2020.02146

Randall, L. M., and Hunter, C. A. (2011). Parasite dissemination and the pathogenesis of toxoplasmosis. *Eur. J. Microbiol. Immunol.* 1, 3–9. doi: 10.1556/EuJMI.1.2011.1.3

Rasmussen, S. A., Jamieson, D. J., Honein, M. A., and Petersen, L. R. (2016). Zika virus and birth defects - reviewing the evidence for causality. *N. Engl. J. Med.* 374, 1981–1987. doi: 10.1056/NEJMsr1604338

Rawls, W. E., and Melnick, J. L. (1966). *Rubella virus* carrier cultures derived from congenitally infected infants. *J. Exp. Med.* 123, 795–816. doi: 10.1084/jem.123.5.795

Robbins, J. R., Zeldovich, V. B., Poukchanski, A., Boothroyd, J. C., and Bakardjiev, A. I. (2012). Tissue barriers of the human placenta to infection with *Toxoplasma gondii*. *Infect. Immun.* 80, 418–428. doi: 10.1128/IAI.05899-11

Roberts, F., and McLeod, R. (1999). Pathogenesis of toxoplasmic retinochoroiditis. *Parasitol. Today* 15, 51–57. doi: 10.1016/S0169-4758(98)01377-5

Robertson, S. E., Featherstone, D. A., Gacic-Dobo, M., and Hersh, B. S. (2003). Rubella and congenital rubella syndrome: global update. *Rev. Panam. Salud Publica* 14, 306–315. doi: 10.1590/S1020-49892003001000005

Russo, F. B., Jungmann, P., and Beltrão-Braga, P. C. B. (2017). Zika infection and the development of neurological defects. *Cell. Microbiol.* 19, 1–6. doi: 10.1111/cmi.12744

Santos, A. M., Calvente, R., Tassi, M., Carrasco, M.-C., Martín-Oliva, D., Marín-Teva, J. L., et al. (2008). Age-dependent effect of nitric oxide on subventricular zone and olfactory bulb. *J. Comp. Neurol.* 346, 339–346. doi: 10.1002/cne.21556

Schwartz, D. A. (2017). The origins and emergence of Zika virus, the newest torch infection: what's old is new again. *Arch. Pathol. Lab. Med.* 141, 18–24. doi: 10.5858/arpa.2016-0429-ED

Seipel, D., de Lima Oliveira, B. C., Resende, T. L., Schuindt, S. H. S., de Oliveira Pimentel, P. M., Kanashiro, M. M., et al. (2010). *Toxoplasma gondii* infection positively modulates the macrophages migratory molecular complex by increasing matrix metalloproteinases, CD44 and alphavbeta3 integrin. *Vet. Parasitol.* 169, 312–319. doi: 10.1016/j.vetpar.2009.12.042

Shi, Y., Li, S., Wu, Q., Sun, L., Zhang, J., Pan, N., et al. (2018). Vertical transmission of the Zika virus causes neurological disorders in mouse offspring. *Sci. Rep.* 8:3541. doi: 10.1038/s41598-018-21894-w

Shklover, J., Mishnaevski, K., Levy-Adam, F., and Kurant, E. (2015). JNK pathway activation is able to synchronize neuronal death and glial phagocytosis in Drosophila. *Cell Death Dis.* 6, e1649–e1611. doi: 10.1038/cddis.2015.27

Shou, Y., Li, L., Prabhakaran, K., Borowitz, J. L., and Isom, G. E. (2003). P38 mitogen-activated protein kinase regulates bax translocation in cyanide-induced apoptosis. *Toxicol. Sci*. 75, 99–107. doi: 10.1093/toxsci/kfg157

Silverman, S. M., and Wong, W. T. (2018). Microglia in the retina: roles in development, maturity, and disease. *Annu. Rev. Vis. Sci*. 4, 45–77. doi: 10.1146/annurev-vision-091517-034425

Smirnov, E. B., and Puchkov, V. F. (2004). Characteristics of cellular proliferation in the developing human retina. *Neurosci. Behav. Physiol*. 34, 643–648. doi: 10.1023/B:NEAB.0000028299.76009.1c

Smith, J. R., Franc, D. T., Carter, N. S., Zamora, D., Planck, S. R., and Rosenbaum, J. T. (2004). Susceptibility of retinal vascular endothelium to infection with *Toxoplasma gondii* tachyzoites. *Investig. Opthalmol. Vis. Sci*. 45, 1157–1161. doi: 10.1167/iovs.03-1105

Song, H. B., Jun, H. O., Kim, J. H., Lee, Y. H., Choi, M. H., and Kim, J. H. (2017). Disruption of outer blood-retinal barrier by *Toxoplasma gondii*-infected monocytes is mediated by paracrinely activated FAK signaling. *PLoS ONE* 12:e0175159. doi: 10.1371/journal.pone.0175159

Stone, J., and Dreher, Z. (1987). Relationship between astrocytes, ganglion cells and vasculature of the retina. *J. Comp. Neurol*. 255, 35–49. doi: 10.1002/cne.902550104

Strauss, O. (2005). The retinal pigment epithelium in visual function. *Physiol. Rev*. 85, 845–881. doi: 10.1152/physrev.00021.2004

Strettoi, E., and Volpini, M. (2002). Retinal organization in the bcl-2-overexpressing transgenic mouse. *J. Comp. Neurol*. 446, 1–10. doi: 10.1002/cne.10177

Strongin, A. C., and Guillery, R. W. (1981). The distribution of melanin in the developing optic cup and stalk and its relation to cellular degeneration. *J. Neurosci*. 1, 1193–1204. doi: 10.1523/JNEUROSCI.01-11-01193.1981

Sun, G., Chiuppesi, F., Chen, X., Wang, C., Tian, E., Nguyen, J., et al. (2020). *Modeling human Cytomegalovirus-induced microcephaly in Human iPSC-derived brain* organoids. *Cell Rep. Med*. 1:100002. doi: 10.1016/j.xcrm.2020.100002

Sun, X., Shi, L., Zhang, H., Li, R., Liang, R., and Liu, Z. (2015). Effects of toll-like receptor 3 on herpes simplex virus type-1-infected mouse neural stem cells. *Can. J. Microbiol*. 61, 201–208. doi: 10.1139/cjm-2014-0540

Tahotná, A., Brucknerová, J., and Brucknerová, I. (2018). Zika virus infection from a newborn point of view. TORCH or TORZiCH? *Interdiscip. Toxicol*. 11, 241–246. doi: 10.2478/intox-2018-0023

Tang, H., Hammack, C., Ogden, S. C., Wen, Z., Qian, X., Li, Y., et al. (2016). Zika virus infects human cortical neural precursors and attenuates their growth. *Cell Stem Cell* 18, 1067–1073. doi: 10.1016/j.stem.2016.02.016

Tenter, A. M., Heckeroth, A. R., and Weiss, L. M. (2000). *Toxoplasma gondii* : from animals to *humans*. *Int. J. Parasitol*. 30, 1217–1258. doi: 10.1016/S0020-7519(00)00124-7

Töndury, G., and Smith, D. W. (1966). Fetal rubella pathology. *J. Pediatr*. 68, 867–879. doi: 10.1016/S0022-3476(66)80204-4

Torgerson, P. R., and Mastroiacovo, P. (2013). The global burden of congenital toxoplasmosis: a systematic review. *Bull. World Health Organ*. 91, 501–508. doi: 10.2471/BLT.12.111732

Tsutsui, Y., Kashiwai, A., Kawamura, N., and Kadota, C. (1993). Microphthalmia and cerebral atrophy induced in mouse embryos by infection with murine *Cytomegalovirus* in midgestation. *Am. J. Pathol*. 143, 804–812.

Turner, D. L., and Cepko, C. L. (1987). A common progenitor for neurons and glia persists in rat retina late in development. *Nature* 328, 131–136. doi: 10.1038/328131a0

Ueno, N., Lodoen, M. B., Hickey, G. L., Robey, E. A., and Coombes, J. L. (2015). *Toxoplasma gondii*-infected natural killer cells display a hypermotility phenotype *in vivo*. *Immunol. Cell Biol*. 93, 508–513. doi: 10.1038/icb.2014.106

Uzquiano, A., Gladwyn-Ng, I., Nguyen, L., Reiner, O., Götz, M., Matsuzaki, F., et al. (2018). Cortical progenitor biology: key features mediating proliferation versus differentiation. *J. Neurochem*. 146, 500–525. doi: 10.1111/jnc.14338

Valenciano, A. I., Boya, P., and De La Rosa, E. J. (2009). Early neural cell death: numbers and cues from the developing neuroretina. *Int. J. Dev. Biol*. 53, 1515–1528. doi: 10.1387/ijdb.072446av

Vecino, E., and Acera, A. (2015). Development and programed cell death in the mammalian eye. *Int. J. Dev. Biol*. 59, 63–71. doi: 10.1387/ijdb.150070ev

Vecino, E., Hernández, M., and García, M. (2004). Cell death in the developing vertebrate retina. *Int. J. Dev. Biol*. 48, 965–974. doi: 10.1387/ijdb.041891ev

Velásquez, Z. D., Conejeros, I., Larrazabal, C., Kerner, K., Hermosilla, C., and Taubert, A. (2019). *Toxoplasma gondii*-induced host cellular cell cycle dysregulation is linked to chromosome missegregation and cytokinesis failure in primary endothelial host cells. *Sci. Rep*. 9:12496. doi: 10.1038/s41598-019-48961-0

Ventura, A. L. M., dos Santos-Rodrigues, A., Mitchell, C. H., and Faillace, M. P. (2019a). Purinergic signaling in the retina: from development to disease. *Brain Res. Bull*. 151, 92–108. doi: 10.1016/j.brainresbull.2018.10.016

Ventura, C. V., Maia, M., Bravo-Filho, V., Góis, A. L., and Belfort, R. (2016). Zika virus in Brazil and macular atrophy in a child with microcephaly. *Lancet* 387:228. doi: 10.1016/S0140-6736(16)00006-4

Ventura, C. V., Ventura Filho, M. C., and Ventura, L. O. (2019b). Ocular manifestations and visual outcome in children with congenital Zika syndrome. *Top. Magn. Reson. Imaging* 28, 23–27. doi: 10.1097/RMR.0000000000000192

Voinescu, P. E., Kay, J. N., and Sanes, J. R. (2009). Birthdays of retinal amacrine cell subtypes are systematically related to their molecular identity and soma position. *J. Comp. Neurol*. 517, 737–750. doi: 10.1002/cne.22200

Wang, Z., Dou, M., Liu, F., Jiang, P., Ye, S., Ma, L., et al. (2018). GDF11 induces differentiation and apoptosis and inhibits migration of C17.2 neural stem cells via modulating MAPK signaling pathway. *PeerJ* 6:e5524. doi: 10.7287/peerj.preprints.27003

Weisblum, Y., Panet, A., Zakay-Rones, Z., Haimov-Kochman, R., Goldman-Wohl, D., Ariel, I., et al. (2011). Modeling of human *Cytomegalovirus* maternal-fetal transmission in a novel decidual organ culture. *J. Virol*. 85, 13204–13213. doi: 10.1128/JVI.05749-11

Wen, Z., Song, H., and Ming, G. L. (2017). How does Zika virus cause microcephaly? *Genes Dev*. 31, 849–861. doi: 10.1101/gad.298216.117

Wetts, R., and Fraser, S. E. (1988). Multipotent precursors can give rise to all major cell types of the frog retina. *Science* 239, 1142–1145. doi: 10.1126/science.2449732

Wong, R. (2006). "Chapter 1: Introduction - from eye field to eyesight," in *Retinal Development*, eds E. Sernagor, S. Eglen, B. Harris, and R. Wong (Cambridge: Cambridge University Press), 1–7. doi: 10.1017/CBO9781107415324.004

Wu, L. Y., Li, M., Hinton, D. R., Guo, L., Jiang, S., Wang, J. T., et al. (2003). Microphthalmia resulting from Msx2-induced apoptosis in the optic vesicle. *Investig. Ophthalmol. Vis. Sci*. 44, 2404–2412. doi: 10.1167/iovs.02-0317

Yang, X.-J. (2004). Roles of cell-extrinsic growth factors in vertebrate eye pattern formation and retinogenesis. *Semin. Cell Dev. Biol*. 15, 91–103. doi: 10.1016/j.semcdb.2003.09.004

Young, R. W. (1984). Cell death during differentiation of the retina in the mouse. *J. Comp. Neurol*. 229, 362–373. doi: 10.1002/cne.902290307

Young, R. W. (1985). Cell differentiation in the retina of the mouse. *Anat. Rec*. 212, 199–205. doi: 10.1002/ar.1092120215

Zachos, G., Clements, B., and Conner, J. (1999). Herpes simplex virus type I infection stimulates p38/c-Jun N-terminal mitogen-activated protein kinase pathways and activates transcription factor AP-1. *J. Biol. Chem*. 274, 5097–5103. doi: 10.1074/jbc.274.8.5097

Zhang, H. R. (1994). Scanning electron-microscopic study of corrosion casts on retinal and choroidal angioarchitecture in man and animals. *Prog. Retin. Eye Res*. 13, 243–270. doi: 10.1016/1350-9462(94)90012-4

Zhou, Y., Tzeng, W. P., Wong, H. C., Ye, Y., Jiang, J., Chen, Y., et al. (2010). Calcium-dependent association of calmodulin with the *Rubella virus* nonstructural protease domain. *J. Biol. Chem*. 285, 8855–8868. doi: 10.1074/jbc.M109.097063

Conflict of Interest: The authors declare that the research was conducted in the absence of any commercial or financial relationships that could be construed as a potential conflict of interest.

frontiers in Cellular and Infection Microbiology

ORIGINAL RESEARCH
published: 30 November 2020
doi: 10.3389/fcimb.2020.586946

ROP18-Mediated Transcriptional Reprogramming of HEK293T Cell Reveals New Roles of ROP18 in the Interplay Between *Toxoplasma gondii* and the Host Cell

Jie-Xi Li[1], *Jun-Jun He*[1]*, *Hany M. Elsheikha*[2], *Jun Ma*[1], *Xiao-Pei Xu*[1,3] *and Xing-Quan Zhu*[1,4]

[1] State Key Laboratory of Veterinary Etiological Biology, Key Laboratory of Veterinary Parasitology of Gansu Province, Lanzhou Veterinary Research Institute, Chinese Academy of Agricultural Sciences, Lanzhou, China, [2] Faculty of Medicine and Health Sciences, School of Veterinary Medicine and Science, University of Nottingham, Loughborough, United Kingdom, [3] Heilongjiang Key Laboratory for Zoonosis, College of Veterinary Medicine, Northeast Agricultural University, Harbin, China, [4] College of Veterinary Medicine, Shanxi Agricultural University, Taigu, China

OPEN ACCESS

Edited by:
Jorge Enrique Gómez Marín, University of Quindío, Colombia

Reviewed by:
Robson De Queiroz Monteiro, Federal University of Rio de Janeiro, Brazil
Daniel Adesse, Oswaldo Cruz Foundation (Fiocruz), Brazil

***Correspondence:**
Jun-Jun He
hejunjun617@163.com

Specialty section:
This article was submitted to Parasite and Host, a section of the journal Frontiers in Cellular and Infection Microbiology

Received: *24 July 2020*
Accepted: *30 October 2020*
Published: *30 November 2020*

Citation:
Li J-X, He J-J, Elsheikha HM, Ma J, Xu X-P and Zhu X-Q (2020) ROP18-Mediated Transcriptional Reprogramming of HEK293T Cell Reveals New Roles of ROP18 in the Interplay Between Toxoplasma gondii and the Host Cell. Front. Cell. Infect. Microbiol. 10:586946. doi: 10.3389/fcimb.2020.586946

Toxoplasma gondii secretes a number of virulence-related effector proteins, such as the rhoptry protein 18 (ROP18). To further broaden our understanding of the molecular functions of ROP18, we examined the transcriptional response of human embryonic kidney cells (HEK293T) to ROP18 of type I *T. gondii* RH strain. Using RNA-sequencing, we compared the transcriptome of ROP18-expressing HEK293T cells to control HEK293T cells. Our analysis revealed that ROP18 altered the expression of 750 genes (467 upregulated genes and 283 downregulated genes) in HEK293T cells. Gene ontology (GO) and pathway enrichment analyses showed that differentially expressed genes (DEGs) were significantly enriched in extracellular matrix– and immune–related GO terms and pathways. KEGG pathway enrichment analysis revealed that DEGs were involved in several disease-related pathways, such as nervous system diseases and eye disease. ROP18 significantly increased the alternative splicing pattern "retained intron" and altered the expression of 144 transcription factors (TFs). These results provide new insight into how ROP18 may influence biological processes in the host cells *via* altering the expression of genes, TFs, and pathways. More *in vitro* and *in vivo* studies are required to substantiate these findings.

Keywords: ROP18, transcriptome, *Toxoplasma gondii*, differentially expressed genes, transcription factors

INTRODUCTION

Toxoplasma gondii is an opportunistic and obligate intracellular protozoan, which can establish a persistent infection (Sibley, 2003). *T. gondii* infects nearly one third of the world's human population (Tenter et al., 2000). Strains of *T. gondii* are categorized into three major genotypes based on their virulence in mice into types I, II, and III. Genotype I strains are highly virulent, whereas strains of genotypes II and III are less virulent (Saeij et al., 2006). In general, infection of immunocompetent

individuals is either asymptomatic or causes mild flu-like symptoms (Beazley and Egerman, 1998; Schneider et al., 2013). High risks of encephalitis and even death due to reactivation of a latent infection can occur in immuno-compromised individuals (Dubey, 2004; Weiss and Dubey, 2009; Kaye, 2011; An et al., 2018). *T. gondii* can also result in adverse health consequences in congenitally infected fetuses (Elsheikha, 2008).

In order to establish an infection, *T. gondii* manipulates the host cells *via* altering the cellular metabolism (Ma et al., 2019), dysregulating the gene expression (He et al., 2016), and subverting the immune response (Yarovinsky, 2014). Infection of *T. gondii* elicits the production of interferon gamma (IFN-γ), tumor necrosis factor (TNF), interleukin 10 (IL-10), IL-12, and several cytokine receptors (Gazzinelli et al., 1996; He et al., 2016), while reduces production of nitric oxide (Rozenfeld et al., 2005). The parasite performs these functions by secreting a number of effector molecules into host cell, such as dense granule proteins (GRAs) and rhoptry proteins (ROPs) (Bradley and Sibley, 2007) that play important roles in the regulation of immune responses (Fox et al., 2016) and gene expression (Rastogi et al., 2020). For example, GRA15 regulates the expression of genes in the NF-κB pathway (Sangare et al., 2019); ROP17 inhibits the expression of innate immune response genes (Li et al., 2019). ROP18 induces apoptosis in mouse neuroblastoma Neuro2a cells *via* endoplasmic reticulum stress-mediated apoptosis pathway (Wan et al., 2015) and inhibits the differentiation of cultured murine neural stem cells *via* inhibiting the activity of the Wnt/β-catenin signaling pathway (Zhang et al., 2017).

ROP18 is serine/threonine phosphokinase and contributes to the virulence of *T. gondii* (Hunter and Sibley, 2012). The expression of ROP18 is higher in *T. gondii* genotype I strain than in genotype III strain (Taylor et al., 2006). Deletion of ROP18 significantly increases the survival of infected mouse (Behnke et al., 2015). *T. gondii* utilizes ROP18 to prevent disruption of parasitophorous vacuole membrane (PVM) *via* phosphorylating the immunity-related GTPases (IRGs) of host cell, and to regulate the biological processes of neurocytes (Steinfeldt et al., 2010; Fleckenstein et al., 2012; Wan et al., 2015; Zhang et al., 2017). Also, ROP18 *via* degradation of the transcription factor (TF) p65 inhibits the NF-κB pathway and suppresses the inflammatory responses to promote its own survival and growth (Du et al., 2014). Besides p65, ROP18 also targets other TFs, such as p53 and Smad1 (Yang et al., 2017).

These diverse functions of ROP18 have led us to hypothesize that ROP18 exerts its multiple effects *via* reprogramming host cell transcriptome. In the present study, we investigated the molecular involvement and significance of ROP18 in the pathogenesis of *T. gondii* infection by investigating the influence of ROP18 on the transcriptome of HEK293T cells using RNA sequencing (RNA-Seq).

MATERIALS AND METHODS

Cell Culture and Parasite

HEK293T (human embryonic kidney) cells were purchased from the American Type Culture Collection (ATCC, Manassas, VA) and were cultured in high glucose Dulbecco's modified Eagle's medium (Sigma-Aldrich, USA), containing 2 mM l-glutamine, 100 U/ml penicillin and 10 mg/mL streptomycin, and 10% (vol/vol) fetal bovine serum (Gibco, New Zealand). The cultured HEK293T cells were incubated at 37°C in humidified air with 5% CO_2. HEK293T cell line was chosen in this study due to its high efficiency for transfection and expression of exogenous genes. *T. gondii* RH strain was maintained *via* passage in human foreskin fibroblast (HFF) cells. Total RNA of the *T. gondii* RH tachyzoites was extracted using TRIzol reagent (Invitrogen, USA) according to the manufacturer's protocol. The residual genomic DNA of *T. gondii* was removed using RNase-Free DNase (Ambion, Shanghai, China).

Plasmid Construction

The coding sequence (CDS) of ROP18 of *T. gondii* RH strain (GenBank No. JX045330) was amplified from total RNA extracted from tachyzoite of *T. gondii* RH strain using the primers: ROP18-F (5'-GGGGGATCCATGACACTTGGTC CTTCAAAACTCG-3') and ROP18-R (5'-GGGGTCGACTT CTGTGTGGAGATGTTCCTGCTGTTC-3'). The PCR conditions were set as follows: pre-denaturation for 5 min at 98°C followed by 35 cycles of 98°C for 20 s, 56°C for 18 s, and 72°C for 30 s; 72°C for 5 min and hold at 4°C. The PCR product was purified using Gel Extraction kit (OMEGA, China). The purified ROP18 CDS was cloned into PCMV-N-HA vector using BamHI and SalI restriction enzymes (NEB, USA), according to the manufacturer's instructions. The constructed plasmid (PCMV-N-HA-ROP18) was transformed into *E. coli* DH5α competent cells (TIANGEN, China). Single bacterial colony was randomly selected and identified using PCR primers ROP18-F and ROP18-R. Positive colonies were sequenced by Genscript Corporation (Nanjing, China). The plasmid of PCMV-N-HA-ROP18 bacterial colony was extracted using Endofree Plasmid Kit (TIANGEN, China) following the manufacturer's instructions, and the extracted plasmid was stored at −20°C until use.

Transfection of HEK293T Cells

The HEK293T cells were cultured in T-25cm^2 cell culture flasks (NEST, China). When the monolayers reached 70%–80% confluence, transfection was performed using Xfect™ Transfection Reagent (Takara, China). Briefly, 30 μg PCMV-N-HA-ROP18 and PCMV-N-HA (empty control vector) were diluted separately in 300 μl Xfect™ transfection buffer. Then, 10 μl Xfect™ polymer was added and vortexed for 5 s at high speed, followed by incubation for 10 min at room temperature. The mixture was then added into the supernatant of the cultured cells and incubated for 4 h. Following the incubation, the DMEM of transfected cell was replaced with 5 ml fresh DMEM supplemented with 10% FBS. Forty-eight hours post transfection, transfected cells were collected and used for Western blotting, indirect immunofluorescence and transcriptome analysis as described below.

Western Blotting

We examined whether ROP18 was correctly expressed in HEK293T cells using Western blotting analysis. Briefly, total

protein was extracted using ProteinExt™ Mammalian Total Protein Extraction Kit (TRAN, China). Then, 20 μg of the extracted protein and 10 μl PageRuler™ Prestained Protein Ladder (Thermo Scientific, USA) were electrophoresed on 12% ExpressplusTM PAGE Gels (GenScript, China) under 120V and then electrotransferred to PVDF membrane (Thermo, Germany). The PVDF blotting membrane was incubated with anti-HA tag antibody (Abcam, UK) overnight at 4°C. Then, the PVDF membrane was washed three times with 1× TBS (Solarbio, China) and the PVDF membrane was incubated with secondary antibody, goat anti-mouse IgG H&L (HRP) (Abcam, UK), for 1 h at 37°C. The PVDF membrane was washed three times by 1× TBS. The ECL reagent (Solarbio, China) was used to detect the targeted protein (Solarbio, China). The Western blot image was recorded by Gel DocTM XR+ with image lab™ Software (BIO-RAD, USA).

Indirect Immunofluorescence Assay

The transfected cells were washed three times with phosphate buffered saline (PBS) and fixed with 4% paraformaldehyde (Solarbio, China) for 10 min. The paraformaldehyde was discarded and the fixed cells were washed three times with PBS, permeabilized using 0.1% Triton X-100 (Beyotime, China), and blocked with 5% bovine serum albumin for 1 h. Following three times washing with PBS, primary mouse anti-HA tag antibody (Abcam, UK) was used to recognize HA tag of ROP18 protein. After incubation with the anti-HA tag antibody at 4°C overnight, the residue HA-tag antibody was discarded and the fixed cells were washed three times with PBS, and then incubated with goat anti-mouse IgG H&L conjugated with Alexa Fluor®555 (Abcam, UK) at 37°C for 1 h. Nucleus was counter-stained with 10 μg/ml DAPI (Solarbio, China). Before the immunofluorescence detection, the goat anti-mouse IgG H&L antibody and DAPI were discarded by washing three times with PBS. The immunofluorescence images were recorded using a Fluorescence microscope Axiovert 100TV (Zeiss, Germany).

Total RNA Extraction and RNA Sequencing of HEK293T Cells

Total RNA of HEK293T cells was extracted by using TRIzol Reagent (Invitrogen China Ltd, Beijing, China) according to the manufacturer's instructions. All extracted RNA samples were treated with RNase-Free DNase (Ambion, Shanghai, China) to remove residual genomic DNA. The concentration and quality of RNA were detected using the Agilent 2100 Bioanalyzer (Agilent Technologies, Palo Alto, Calif.). mRNA was isolated from total RNA using Poly-T oligo-conjugated magnetic beads, and then mRNA was reversely transcribed into cDNA with PrimerScriptTMRT reagent kit with gDNA Eraser (Takara, China) following the manufacturer's instructions. Construction of transcriptomic libraries and RNA-Seq were performed by BGI-Shenzhen (Shenzhen, China).

Sequencing Quality and Mapping of Sequencing Reads

Reads were trimmed to remove the adaptor primers, low-quality reads, and very short (<50 nt) reads. The quality of RNA-Seq was checked by using the quality scores Q20 and Q30. The clean reads were mapped against the human reference genome (ftp://ftp.ncbi.nlm.nih.gov/genomes/H_sapiens/current/GCF_000001405.39_GRCh38.p13/) using SOAPaligner/SOAP2 software. Reads per kilobase per million mapped reads (RPKM) method was used for calculation of the relative gene expression (Mortazavi et al., 2008). rMATS software was used to detect gene alternative splicing (AS) events among samples, including skipped exon (SE), alternative 5' splicing site (A5SS), alternative 3' splicing site (A3SS), mutually exclusive exons (MXE) and retained intron (RI).

Bioinformatic Analysis of the Differentially Expressed Genes

DESeq2 software was used to determine gene expression and identify differentially expressed genes (DEGs) between the PCMV-N-HA-ROP18 transfected cells and PCMV-N-HA transfected (control) cells. The Benjamini and Hochberg false discovery rate (FDR) was used to correct multiple hypothesis testing *P* values. Genes with FDR adjusted *P* values of Fisher's exact test ≤ 0.05 and $|\log_2(\text{fold change})| \geq 1$ were deemed as DEGs. The fold change (FC) = gene RPKM value of ROP18-expressing HEK293T cells/gene RPKM value of control-HEK293T cells. The gene expression data were clustered using Euclidean distance. The functional annotation and pathways involving the DEGs were analyzed using Gene Ontology (GO), Reactome, and KEGG (http://www.kegg.jp/) pathway enrichment analyses. Fisher's exact test adjusted with FDR was used to identify significantly enriched GO terms or pathways. The FDR adjusted *P* value ≤ 0.05 was used to identify the significantly enriched GO terms or pathways. TRRUST database was used to identify the relationship between TFs and their target genes. Cytoscape software was used to visualize the relationship between DEGs, GO terms, and pathways.

Real-Time Quantitative PCR (qRT-PCR) Validation

We examined the reliability of RNA-seq results by using qRT-PCR. Twenty DEGs were chosen, including *WNK4*, *TNC*, *TNFRSF9*, *IL6R*, *PCK1*, *FRMD1*, *TES1*, *INHBA*, *CD44*, *LINC01599*, *LOC400710*, *EIF4EBP3*, *LOC101929181*, *OR2B6*, *LRRC46*, *FGF21*, *KRTAP5-2*, *KCNN4*, *SEZ6*, and *RNU1-2*. *GAPDH* was included as a reference gene. The details of all the primers are shown in **Supplementary Table S1**. Briefly, total RNA was extracted from the transfected cells, and reverse transcribed into cDNA using PrimerScriptTMRT reagent kit with gDNA Eraser (Takara, China). The cDNA was stored at –80°C until use. The following qRT-PCR conditions were used for gene amplification: 95°C for 10 min, followed by 40 cycles of denaturing at 94°C for 15 s and 60°C for 1 min. The melt curve analysis ranged from 72°C to 95°C to ensure that specific product was amplified in each qRT-PCR reaction. The $2^{-\Delta\Delta CT}$ relative expression calculation method was used to calculate the relative gene expression levels of the examined genes (Livak and Schmittgen, 2001).

RESULTS

Confirmation of ROP18 Expression in HEK293T Cell

Sequencing of PCMV-N-HA-ROP18 showed that the CDS of ROP18 of *T. gondii* RH strain had been correctly cloned into the PCMV-N-HA plasmid. The results of Western blotting demonstrated that ROP18 protein was correctly expressed in HEK293T cells; however, no protein was detected in the HEK293T cells transfected with PCMV-N-HA (**Figure S1**). The efficiency of transfection was examined using indirect immunofluorescence analysis, which demonstrated the high expression of ROP18 in HEK293T cells. As expected, no fluorescent signal was detected in HEK293T cells transfected with PCMV-N-HA (**Figure 1**).

RNA-Sequencing and Identification of Differentially Expressed Genes

Each sequenced sample had > 119 million raw reads and 110 to 111 million clean reads. Also, 98% and 92% clean reads have met the sequencing quality standards of Q20 and Q30, respectively, demonstrating the high quality of RNA-seq data. Approximately 85%–86% clean reads were mapped to reference human genome (Version: hg38) and 71%–72% clean reads were aligned against reference human genes. A total of 22,460 genes were detected in the HEK293T cells, of which 283 and 467 genes had decreased and increased expression, respectively (**Figure 2A**). Details of the DEGs are shown in **Supplementary Table S2**. Clustering analysis of gene expression clearly separated the data into two clusters (ROP18-expressing cell cluster and control cell cluster), showing the distinct transcriptomic profiles between ROP18 expressing cells and non-ROP18 expressing cells (**Figure 2B**). The RNA-seq data were validated by examining the level of expression of 20 DEGs using qRT-PCR and the results obtained by qRT-PCR and RNA-seq were consistent (**Figure 2C**). Analysis of AS events showed that ROP18 had no significant impact on the SE, A5SS, A3SS, and MXE; however, RI event was significantly increased in ROP18-expressing cells (**Table 1**).

Pathway Enrichment Analysis of DEGs

To further investigate the the cellular functions that were significantly altered by ROP18 of *T. gondii* RH strain, pathway enrichment analysis was performed. As shown in **Supplementary Table S3**, the DEGs were significantly enriched in 129 pathways. The top 30 enriched pathways were extracellular matrix (ECM) organization, ECM-receptor interaction, ECM proteoglycans, integrin cell surface interactions, degradation of the ECM, focal adhesion, laminin interactions, integrin signalling pathway, non-integrin membrane-ECM interactions, immune system, PI3K-Akt signaling pathway, collagen formation, protein digestion and absorption, assembly of collagen fibrils and other multimeric structures, collagen chain trimerization, cytokine-cytokine receptor interaction, collagen degradation, amoebiasis, hematopoietic cell lineage, binding and uptake of ligands by scavenger receptors, MET activates PTK2 signaling, elastic fibre formation, human papillomavirus infection, small cell lung cancer, molecules associated with elastic fibres, collagen biosynthesis and

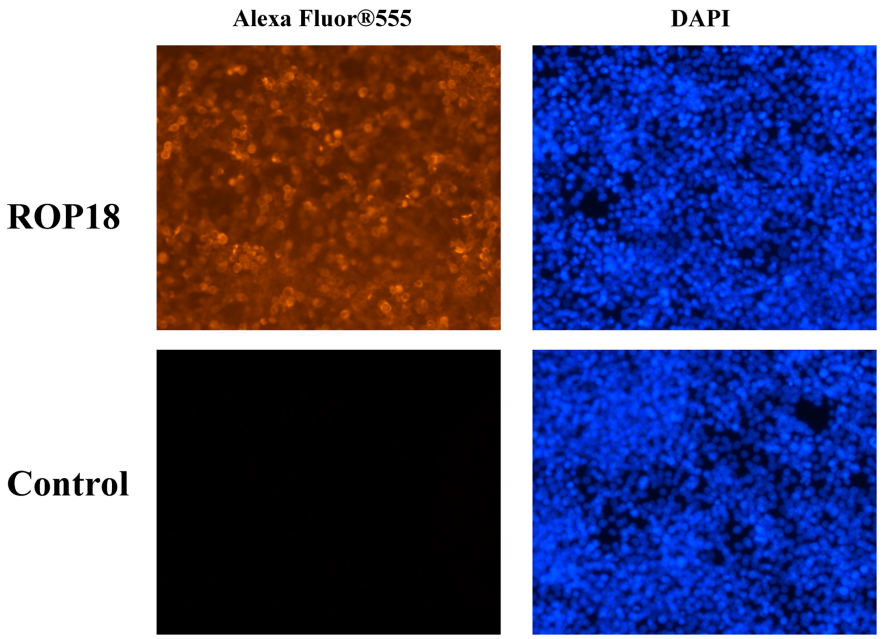

FIGURE 1 | Indirect immunofluorescence of the transfected HEK293T cells. The ROP18 protein tagged with HA was stained with AlexaFluor 555 (Orange) and the nucleus was counterstained with DAPI (Blue). The HEK293T cells transfected with PCMV-N-HA-ROP18 showed high density of orange signal, whereas HEK293T cells transfected with PCMV-N-HA did not show any fluorescent signal.

modifying enzymes, MET promotes cell motility, neuroactive ligand-receptor interaction, GPCR ligand binding, and signaling by receptor tyrosine kinases. All the top 30 pahtways were upregulated by ROP18. The details of the relationship between the DEGs and the top 30 pathways are shown in **Figure 3** and **Supplementary Table S3**.

Disease Pathway Enrichment Analysis of DEGs

The significantly enriched disease pathways were congenital malformations, congenital malformations of the musculoskeletal system, cardiovascular diseases, immune system diseases, nervous system diseases, eye disease, vascular diseases, epidermolysis bullosa, junctional, atypical hemolytic uremic syndrome, congenital malformations of skin, hematologic diseases, inherited thrombophilia, musculoskeletal diseases, and primary immunodeficiency. Most of these disease related pathways were dominated by upregulated genes. The relationships between DEGs and disease-related pathways are shown in **Supplementary Table S4**.

GO Enrichment and Transcripton Factor Analysis of DEGs

A total of 264 GO terms were significantly enriched by DEGs. The top 30 enriched GO terms included twenty-three biological process GO terms (response to external stimulus, regulation of multicellular organismal process, system development, positive regulation of multicellular organismal process, collagen metabolic process, cell adhesion, locomotion, cell surface receptor signaling pathway, cellular response to cytokine stimulus, cellular process, angiogenesis, positive regulation of cell population proliferation, ECM organization, blood vessel development, biological adhesion, regulation of transport, positive regulation of biological process, response to stimulus, cell migration, tissue migration, cell population proliferation, regulation of cell communication, and metabolic process), five cellular component GO terms (integral component of membrane, cell periphery, extracellular region, extracellular vesicle, and cell surface), and two molecular function GO terms (ECM structural constituent and calcium ion binding) (**Figure 4** and **Supplementary Table S5**). We also identifed 144 differentially expressed TFs (DETFs), including 75 upregulated TFs and 69 down-regulated TFs. As shown in **Figure 5**, the DETFs were classed into 29 families. zf-C2H2, Homeobox and HMGI/HMGY were the top 3 families that contained most DETFs altered by ROP18 of *T. gondii*. We identified the target DEGs of DETFs in the TRRUST database, where 16, 4, 2, and 1 DEGs are targeted by ETS1, RUNX2, NFATC2, and IRF9, respectively (**Figure 6**).

DISCUSSION

In this study, we expressed ROP18 of RH strain in HEK293T cells and studied the resultant effects on the cell transcriptome by using RNA-seq approach. Sequencing of PCMV-N-HA-ROP18 plasmid showed that ROP18 eukaryotic expression plasmid has been successfully constructed, and Western blotting showed that ROP18 was correctly expressed in HEK293T cell (**Figure S1**). As shown in **Figure 1**, no HA-tagged protein was detected in the control cells, however a strong fluorescent signal was detected in HEK293T cells transfected with PCMV-N-HA-ROP18. RNA-seq showed that ROP18 of RH strain decreased the expression of 283 gene but increased the expressions of 467 genes of HEK293T cells (**Figure 2A** and **Supplementary Table S2**). ROP18-expressing cell cluster and control cell cluster were clearly separated into two clusters, indicating the distinct transcriptomic profiles between ROP18 expressing cells and non-ROP18 expressing cells (**Figure 2B**). The qRT-PCR validation showed an agreement between the results obtained by qRT-PCR and RNA-seq (**Figure 2C**), demonstrating the reliability of the RNA-seq data.

The GO enrichment and pathway analyses showed that DEGs were significantly enriched in 129 pathways (**Supplementary Table S3**), and 115 DEGs were linked to 14 KEGG disease pathways (**Supplementary Table S4**). Most of the top 30 enriched pathways were involved in ECM, cell binding and immune response (**Figure 3**). Consistent with the KEGG analysis, most of the top 30 enriched GO terms were also related to ECM, cell binding and immune response (**Figure 4** and **Supplementary Table S5**). These data clearly showed that a large number of ECM-related pathways and GO terms were significantly enriched (**Figures 3** and **4**). These findings are expected because HEK293 cells are frequently used as a model for ECM-interaction studies because they express several β1 integrin containing subunits on their cell surface, which allow them to adhere to a range of ECM proteins (Bodary and McLean, 1990). ECM components are critical scaffolds for adhesive cells, and regulate proliferation, differentiation, and fate of the cells. All these crucial processes contribute to cell migration, cellular communication, inflammation, and histopathology. Alterations in ECM composition, structure, abundance, or expression of ECM genes have been shown to cause or underpin sevreal diseases (Lamande and Bateman, 2020). Given these highly versatile functions of ECM, it is not surprising to see significant alterations in multiple disease-related processes enriched by DEGs. Also, ECM plays a key role in the morphogenesis and regulation of the neural progenitor behavior (Long and Huttner, 2019). We also found that ECM organization and congenital malformation processes were significantly enriched by 47 DEGs (**Figure 3**) and 47 DEGs (**Supplementary Table S4**), respectively. Most of the DEGs were upregulated by ROP18. Whether alterations in the expression of genes related to ECM or tissue defects caused by ROP18 contribute to the prenatal congenital pathologies that occur in the fetus who become infected during pregnancy remains to be investigated.

ECM modulates the activities of growth factors and cytokines (Schonherr and Hausser, 2000). Also, upregulation of ECM components has been linked to inflammatory responses (Sorokin, 2010; Herrera et al., 2018). We identified 88 immune-related DEGs in ROP18-expressing cells, including 61

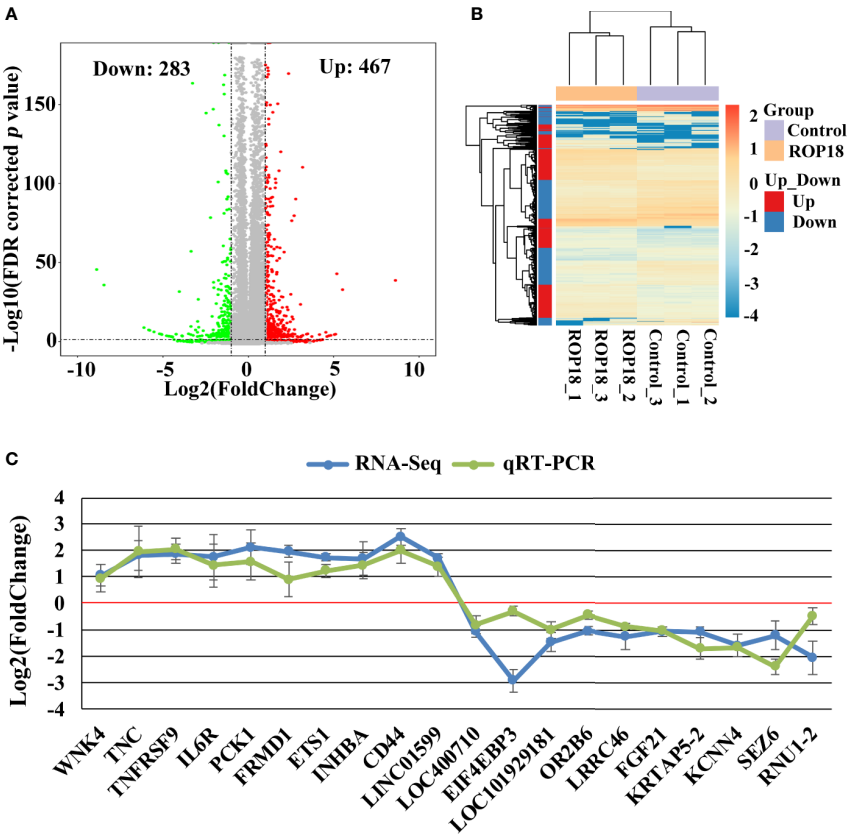

FIGURE 2 | Differentially expressed genes (DEGs) and qRT-PCR validation. **(A)** Volcano plot showing gene expression changes in ROP18-expressing HEK293T cells, including 467 upregulated genes and 283 downregulated genes. Red and green colors represent upregulated and downregulated genes, respectively. **(B)** Clustering analysis of DEGs and samples. The color scale bar for heat intensity indicates Log_2(Fold Change); up and down indicate upregulated and downregulated genes in ROP18-expressing cells, respectively. Columns, samples; rows, DEGs. The samples were grouped into two distinct clusters: ROP18-expressing group and control group. **(C)** qRT-PCR validation of the RNA-seq results. The expressional trends of the examined DEGs were similar between qRT-PCR and RNA-seq results. Blue and green colors represent the result of RNA-seq and qRT-PCR, respectively.

TABLE 1 | The number of alternative splicing events in ROP18-expressing compared to non-expressing (control) HEK239T cells.

Sample	SE	MXE	A5SS	A3SS	RI
Control_1	56,027	12,900	5,283	5,419	5,992
Control_2	55,326	12,675	5,215	5,401	5,954
Control_3	50,519	11,138	5,167	5,285	5,985
ROP18_1	52,504	11,444	5,161	5,349	6,043
ROP18_2	55,771	12,523	5,274	5,485	6,100
ROP18_3	50,314	10,772	5,142	5,296	6,036
P value of T test	0.665	0.431	0.611	0.911	0.024

SE, skipped exon; A5SS, alternative 5' splicing site; A3SS, alternative 3' splicing site; MXE, mutually exclusive exons; RI, retained intron.

upregulated and 27 downregulated genes (**Figure 3**). The enriched innate immune system pathway was alterd by 28 upregulated genes (*CR2*, *LPCAT1*, *IFIH1*, *LGALS3*, *AMPD3*, *HPSE*, *CLU*, *PLD1*, *PROS1*, *CFB*, *NLRP1*, *TXK*, *MGAM*, *PLAU*, *PTX3*, *PLPP5*, *NFATC2*, *CFI*, *PTPRB*, *ANPEP*, *CD68*, *HP*, *GNLY*, *PRG2*, *ATP6V0D2*, *S100P*, *C3AR1*, and *CD44*) and 11 downregulated genes (*LCK*, *CLEC7A*, *MB21D1*, *PRSS3*, *TICAM2*, *C4B*, *ZBP1*, *LYZ*, *TLR7*, *LAIR1*, and *CEACAM8*) (**Supplementary Table S3**). Also, 24 genes of cytokine-cytokine receptor interaction pathway were significantly altered (**Figure 3** and **Supplementary Table S3**), including 17 upregulated genes (*GDF7*, *ACVR1C*, *TGFBR2*, *CNTF*, *IL18R1*, *IL1RAP*, *TNFSF13B*, *IL32*, *TNFSF4*, *TNFRSF13C*, *CXCL8*, *INHBA*, *IL6R*, *TNFSF11*, *TNFRSF9*, *CX3CL1*, and *IL7*) and 7 downregulated genes (*TNFRSF25*, *IL17C*, *IL31*, *CCR4*, *CCL5*, *IL15*, and *IL12RB1*). In these differentially expressed cytokine-related genes, four of them regulate the chemotaxis of immune cells, including *CXCL8*, *CXCL1*, *CCR4*, and *CCL5*. These chemotaxis-related genes have several biological and immunological functions. Maintaining a balanced immune response during *T. gondii* infection is essential in order to limit the parasite proliferation, while at the same time protects the host from the adverse effects of excessive inflammatory pathologies (Chousterman et al., 2017). The CCL5 which regulates the migration of eosinophils and regulatory T cells (Griffith et al., 2014) was downregulated by ROP18. However,

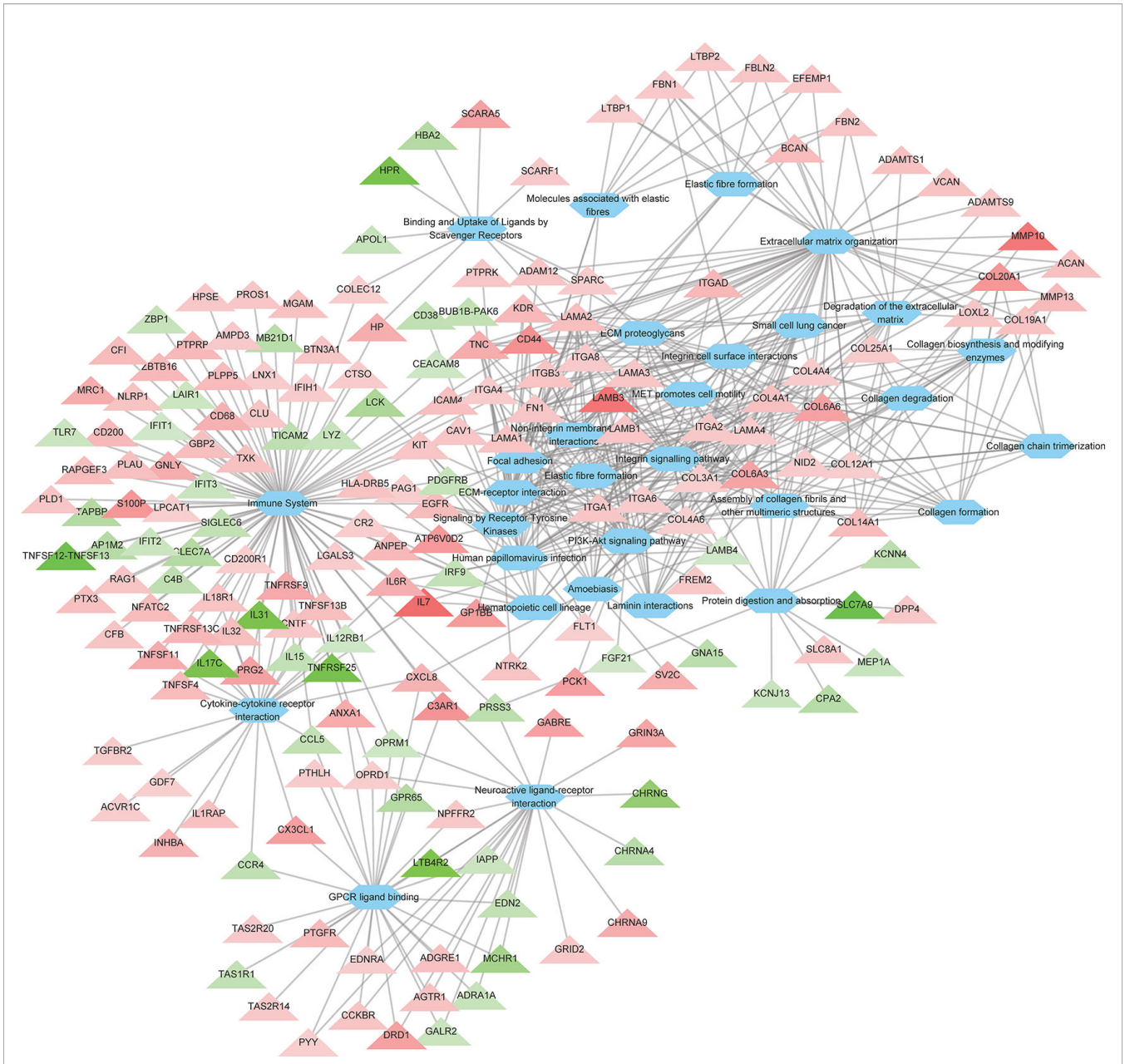

FIGURE 3 | The relationship between the DEGs and the top 30 enriched pathways. A total of 186 DEGs were linked to the top 30 pathways. Triangles represent the DEGs and ovals represent the pathways. Red and green triangles represent upregulated and downregulated DEGs, respectively. The details of DEGs are listed in **Supplementary Table S2**.

CXCL8 and CXCL1 that regulate the chemotaxis of $CD8^+$ effector T cells, resident monocytes, microglia, $CD8^+$ effector-memory T cells, and T cells were significantly upregulated by ROP18. Thus, it is possible that ROP18 contributes to the recruitment of host immune cells to the infection site.

We also found that DEGs were enriched in several disease pathways. Chorioretinitis is a common manifestation in ocular toxoplasmosis, and a correlation exists between ROP18 allele type and the severity of ocular inflammatory response (Sanchez et al., 2014). As shown in **Supplementary Table S4**, ROP18 altered the expressions of 15 eye disease-related genes, including *EFEMP1*, *SLC7A14*, *MIP* (major intrinsic protein of lens fibe), *COL25A1*, *CFB*, *SLC38A8*, *CFI*, *RIMS1*, *CABP4*, *RP1L1*, *CRYAB*, *PROM1*, *CRX*, *KCNJ13*, and *VCAN*. Previous studies showed that *EFEMP1* (Lin et al., 2018; Thompson et al., 2019), *SLC7A14* (Jin et al., 2014), and *RP1L1* (Albarry et al., 2019) are linked to macular degeneration or retinitis pigmentosa; *COL25A1*, which encodes a membrane associated collagen, is associated with oculomotor neuron development (Shinwari et al., 2015). Also, *RP1L1* (Fujinami-Yokokawa et al., 2019), *PROM1*

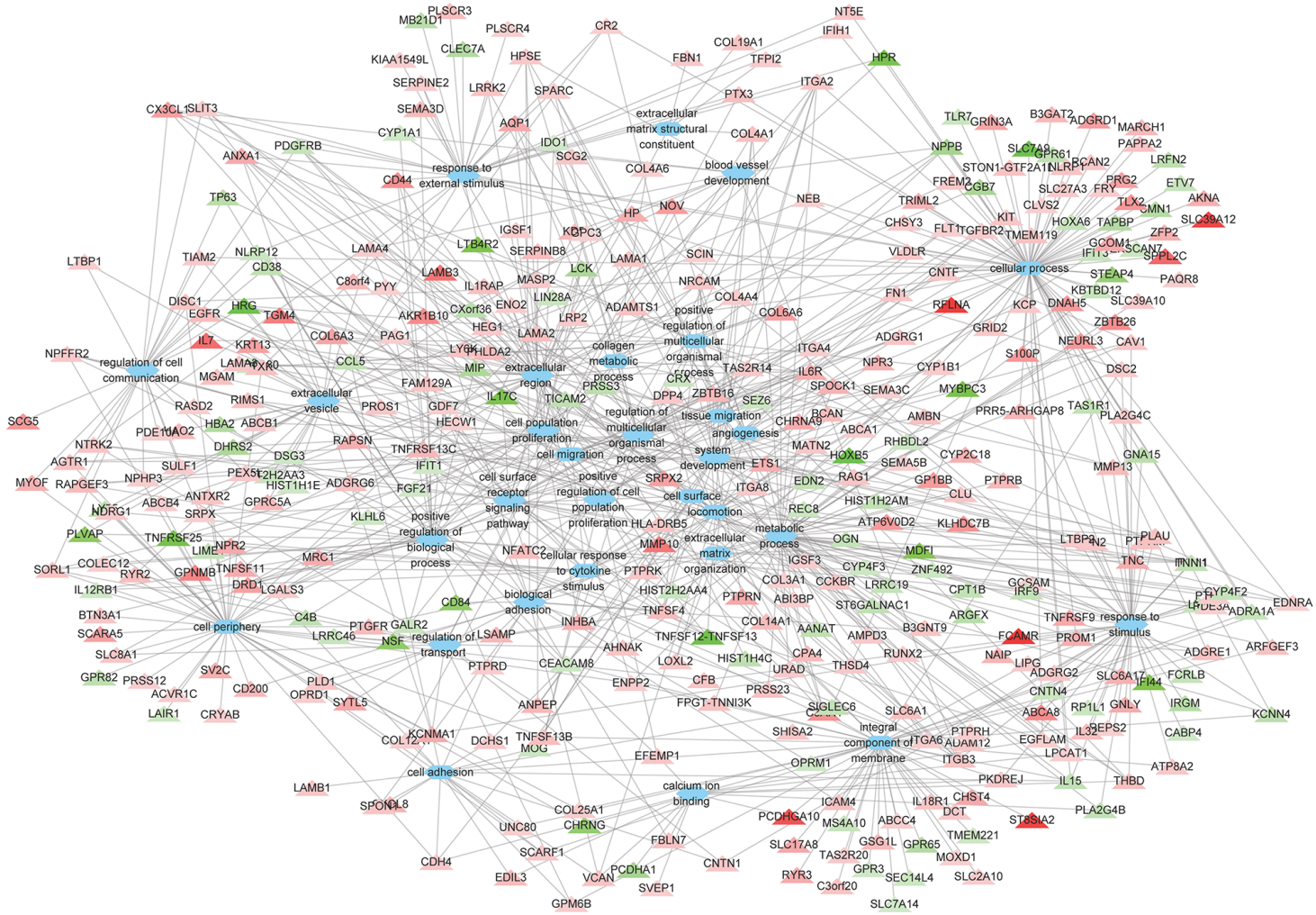

FIGURE 4 | The relationships between the DEGs and the top 30 enriched GO terms. The 373 DEGs were enriched in the top 30 enriched GO terms. Triangles represent the DEGs and ovals represent the GO terms. Red and green triangles represent upregulated and downregulated DEGs, respectively. The details of DEGs are listed in **Supplementary Table S2**.

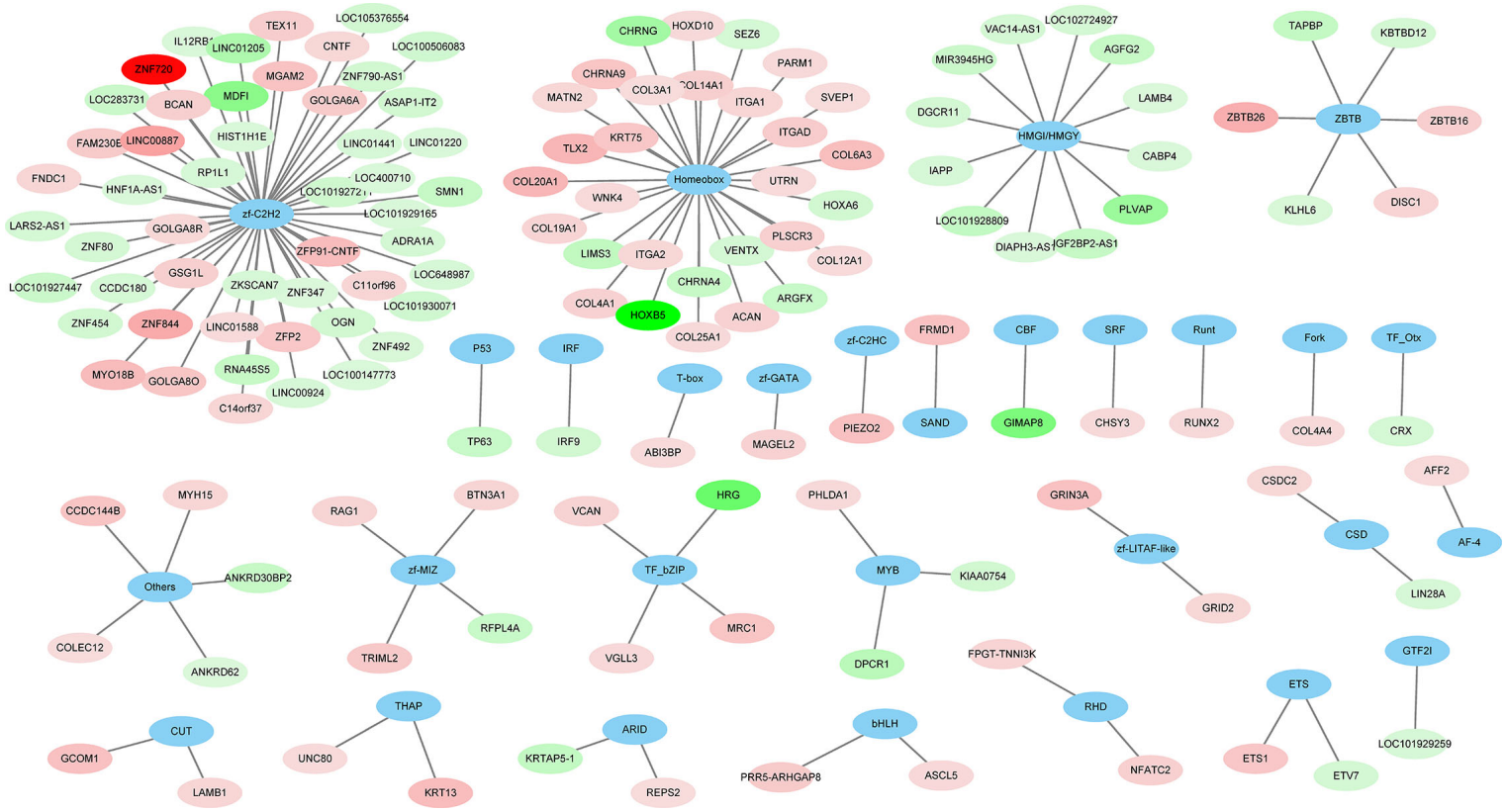

FIGURE 5 | The families of differentially expressed transcription factors (DETFs). A total of 144 DETFs were categorized into 29 transcription families. Blue ovals represent the TF family. Red and green ovals represent TF with increased and decreased expression, respectively. The details of DETFs are listed in **Supplementary Table S2**.

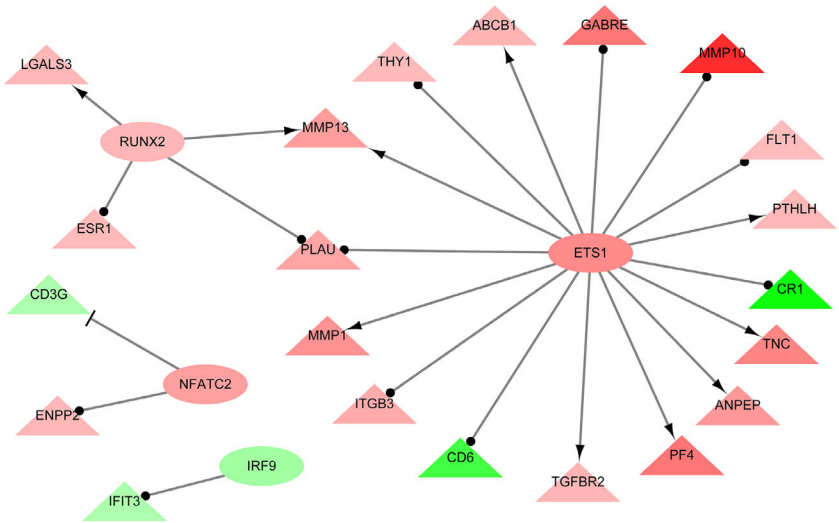

FIGURE 6 | The interaction network showing the relationships between differentially expressed transcription factors (DETFs) and their corresponding target genes. Ovals and triangles represent DETFs and their target genes, respectively. Red and green denote genes with increased and decreased expression, respectively. Arrows with a T-shaped end represent inhibition or repression of gene expression, arrows with a delta-shaped end represent gene activation, and arrows with a dot-shaped end represent unknown regulatory type. Network was constructed using Cytoscape and TRRUST database. The details of DEGs are listed in **Supplementary Table S2**.

(Fujinami et al., 2020), *CRX* (Fujinami-Yokokawa et al., 2020), *CFI* and *CFB* (Rathi et al., 2017; Shahulhameed et al., 2020), and *KCNJ13* (Toms et al., 2019) have been linked to retinopathy. Additionally, *SLC38A8* contributes to congenital nystagmus (Weiner et al., 2020), and *RIMS1* and *CABP4* are associated with dystrophy (Sisodiya et al., 2007) and synaptic disorder of cone-rod (Littink et al., 2009), respectively. Furthermore, alteration of *CRYAB* is associated with cataract (Molnar et al., 2019), and *VCAN* is associated with vitreoretinal degeneration (Tang et al., 2019). Most of these eye disease-related genes were upregulated in HEK293T cells by ROP18 (**Supplementary Table S3**). Whether the same genes are also altered in other cell lines such as occular cell types remains to be determined. A previous study showed that the expression of IFN-γ and IL-1β was not significantly influenced by ROP18 in peripheral blood mononuclear cells collected from patients with ocular toxoplasmosis (Hernandez-de-Los-Rios et al., 2019). Our results also showed that the expression of IFN-γ and IL-1β was not significantly influenced by the expression of ROP18 protein in HEK293T cells.

Recent studies show that *T. gondii* infection can induce significant structural, functional and metabolic changes in the brain microvascular endotehlial cells (Al-Sandaqchi et al., 2018; Hu et al., 2018; Ma et al., 2019; Al-Sandaqchi et al., 2020; Harun et al., 2020a; Harun et al., 2020b) and can change the neuron subpopulations (Odorizzi et al., 2010). However, the exact mechanisms of behavioral abnormalities and change in the subpopulations of neurons induced by *T. gondii* infection remains to be clearly defined. A previous study revealed a role for ROP18 in increased neural apoptosis and encephalitis during *T. gondii* infection (An et al., 2018). Although HEK293T cells are not drieved from brain, our transcriptomic analysis showed that ROP18 can alter the expressions of genes involved in several neural activity-related pathways, neuron differentiation and development processes. We found that the neural activity-related pathways/GO terms were significantly enriched in HEK293T cells following expression of ROP18 protein. Neuroactive ligand-receptor interaction was enriched by 23 DEGs, including 13 upregulated genes and 10 downregulated genes (**Figure 5** and **Table Supplementary S3**). Nervous system diseases were also enriched by 23 upregulated genes and 13 downregulated genes (**Supplementary Table S4**). GO enrichment analysis showed that neuronal cell body and neuron differentiation process were significantly altered by 10 DEGs and 13 DEGs, respectively; cell morphogenesis involved in neuron differentiation was significantly altered by 6 upregulated genes and 3 downregulated genes; and regulation of neuron differentiation was significantly altered by 5 upergulated genes and 1 downregulated genes (**Supplementary Table S5**). Although the impact of ROP18 on neurons remains to be determined, our results offer preliminary results for further investigation of the effect of ROP18 on the neurobiology of cerebral toxoplasmosis.

RNA-seq analysis has been used to detect AS events (Filichkin et al., 2010; Feng et al., 2013; Shen et al., 2014). Our previous study showed that ROP17 of *T. gondii* can modify host AS events (Li et al., 2019) which have significant roles in various biological processes (Blencowe, 2006; Baralle and Giudice, 2017). We investigated the role of ROP18 in the regulation of host AS events by comparing five AS events, including SE, A5SS, A3SS, MXE, and RI, in ROP18-expressing and control cells. As shown

in **Table 1**, RI event was significantly increased in ROP18-expressing cells. RI is a type of AS envent that can introduce functional elements to the protein (Buckley et al., 2011) or results in the degradation of mRNA by RNA surveillance mechanism (Belgrader et al., 1994). This result suggests that ROP18 can influence host biological processes *via* altering the RI event within the host cells. The exact mechanism by which ROP18 alters RI event is unknown, however, we found that U2 small nuclear RNA auxiliary factor 1 like 5 (U2AF1L5) was significanlty downregulated ($Log_2FC = -1.135$, FDR corrected *P* value = 0) in ROP18-expressioning cells. The U2AF1L5 seems to participate in mRNA splicing according to annotation in NCBI database.

Analysis of the regulatory networks between DEGs and TFs is important for elucidating the role of ROP18 in regulating the host biological processes. ROP18 protein upregulated the expressions of 75 TFs, but downregulated the expressions of other 69 TFs in HEK293T cells, showing the significant impact of ROP18 on the expression of TFs. The TFs altered by ROP18 were classed into 29 families, and the zf-C2H2, Homeobox and HMGI/HMGY families were the top families with the most DETFs (**Figure 6**). These results suggest a marked influence of ROP18 on the expression of TFs belonging to these three TF families. Most DETFs of Homeobox family were upregulated, however all DETFs of HMGI/HMGY family were downregulated (**Figure 5**), suggesting that ROP18 could have a suppressive effect on members of the HMGI/HMGY family. By searching TRRUST database, we identified four DETFs, including ETS1, RUNX2, NFATC2, and IRF9, which target 16, 4, 2, and 1 DEGs, respectively (**Figure 6**). ETS1 induces the expression of *MMP13* (Ghosh et al., 2012), *ABCB1* (Kars et al., 2010), *PTHLH* (Dittmer et al., 1994), *TNC* (Jinnin et al., 2004), *ANPEP* (Petrovic et al., 2003), *PF4* (Okada et al., 2003), *TGFBR2* (Kopp et al., 2004), and *MMP1* (Mix et al., 2007). RUNX2 enhances the expression of *LGALS3* (Zhang et al., 2009) and *MMP13* (Wang et al., 2004). NFATC2 suppresses the expression of *CD3G*. The expression of these target genes is consistent with the regulatory functions of the DETFs, suggesting that ROP18 modifies host gene expression *via* altering the expression of TFs. Analysis of the interaction between ROP18 and host TFs may elucidate the interplay between ROP18 and cellular processes. Previous studies showed that ROP18 interacts with several TFs, including SOX6, SPDEF, HMGN1, ATF3, MLLT10, DNMT3L, MYCN, MXD4, TAF12, EPAS1, CNBP, HMGA1, ATM, TBX3, ZNF148, p65, p53, ATF6B, and SMAD1 (Cheng et al., 2012; Du et al., 2014; Yang et al., 2017; Xia et al., 2018). Interestingly, the expressions of these interacting TFs were not significantly altered by ROP18. However, by searching TRRUST database, we found that MYCN activates the expressions of CD44 and NDRG1, EPAS1 activates the expression of FLT1, and HMGA1 activates the expression of CD44. In this study, CD44 (Log2FC = 2.5, FDR corrected *P*-value = 1.23E-30), NDRG1 (Log2FC = 1.1, FDR corrected *P*-value = 0) and FLT1 (Log2FC = 1, FDR corrected *P*-value = 1.16E-36) were upregulated by ROP18 stimulation. The expression of these target genes is consistent with the regulatory functions of the MYCN, EPAS1, and HMGA1. Whether these regulatory effects depend on the phosphokinase activity of ROP18 remains to be elucidated.

In our study, the cell cycle process was not significantly affected by ROP18 at the gene transcriptional level. However, another effector protein, ROP16, plays a significant role in host cell cycle (Chang et al., 2015). The difference between these two virulence-associated proteins (ROP16 and ROP18) in the effect on host cell cycle may be attributed to differences in their host target genes. In a previous study, ROP18 of RH strain was found to interact with 492 host proteins (Xia et al., 2018). In our study, only a few of these interacting proteins (including upregulated DDX60, COL6A3, PTPRK, and RCAN2; downregulated LYPD5, KIR3DX1, NPPB, and TNNI1) were significantly altered at the gene expression level. This difference might be attributed to variations in the behavior of the transfected host cells. Both ROP17 and ROP18 are secretory proteins of the ROP2 family (El Hajj et al., 2006) and have a similar location within the host cell (Etheridge et al., 2014). By comparing the host transcriptional responses to ROP17 (Li et al., 2019) and ROP18 in the present study, we identified 110 and 276 genes whose expression was decreased or increased, respectively, in both ROP17 and ROP18. This similarity in the location inside the host cell and in the effect on host cell transcriptome is consistent with the fact that ROP17 and ROP18 share some host cell targets (Etheridge et al., 2014). ROP5 forms complexes with ROP18 and ROP17 to mediate the parasite survival in mice (Etheridge et al., 2014). A link between ROP18 allele type and virulence in mice has been reported (Sanchez et al., 2014) and the combination of ROP18/ROP5 allele types was found to be even more predictive of *T. gondii* virulence in mice (Shwab et al., 2016). Given the interaction and overlap between the functions of ROP proteins, studying the effect of simultaneous expression of ROP5, ROP16, ROP17, and ROP18 on the host cell transcriptional reprogramming may improve the understanding of the virulence mechanism of *T. gondii*.

CONCLUSION

This study presents the first RNA-Seq-based analysis of the transcriptomic responses of HEK239T cells to ROP18 expression. We identified 22,460 host genes, and the expression of 750 genes was significantly altered by ROP18, including 467 upregulated genes and 283 downregulated genes. The functions of significantly altered genes were mainly involved in ECM organization, immune responses and disease processes. ROP18 also alters the expression of 144 TFs belonging to 29 TF families and increased the RI pattern of AS. Our data revealed several potential new roles of ROP18 in the transcriptional regulation of host cells. Further investigations of the effects of a catalytic inactive mutant of ROP18 on the host cell transcriptome and using different cell lines (e.g. neurons and immune cells) will deepen our understanding of *T. gondii* interactions with the host cell processes. Also, using methods such as siRNA and gene editing to alter ROP18 protein

expression can improve the evaluation of the effects of ROP18 protein with the concomitant entry of live parasites.

DATA AVAILABILITY STATEMENT

The datasets presented in this study can be found in online repositories. The names of the repository/repositories and accession number(s) can be found at https://www.ncbi.nlm.nih.gov/ (SRR7825256), https://www.ncbi.nlm.nih.gov/ (SRR7825257), https://www.ncbi.nlm.nih.gov/ (SRR7825258), https://www.ncbi.nlm.nih.gov/ (SRR12130694), https://www.ncbi.nlm.nih.gov/ (SRR12130695), and https://www.ncbi.nlm.nih.gov/ (SRR12130696).

AUTHOR CONTRIBUTIONS

J-JH, HME, and X-QZ conceived and designed the study and critically revised the manuscript. J-XL and J-JH performed the experiment, analyzed the transcriptomic data, and drafted the manuscript. JM and X-PX helped in data analysis and manuscript revision. All authors contributed to the article and approved the submitted version.

FUNDING

Project support was provided by the National Key Research and Development Program of China (Grant No. 2017YFD0500403), the National Natural Science Foundation of China (Grant No. 31902291), and the International Science and Technology Cooperation Project of Gansu Provincial Key Research and Development Program (Grant No. 17JR7WA031).

ACKNOWLEDGMENTS

The authors are thankful for the technical assistance provided by BGI-Shenzhen, China.

SUPPLEMENTARY MATERIAL

The Supplementary Material for this article can be found online at: https://www.frontiersin.org/articles/10.3389/fcimb.2020.586946/full#supplementary-material

SUPPLEMENTARY TABLE 1 | The primers used in the qRT-PCR analysis.

SUPPLEMENTARY TABLE 2 | Differentially expressed genes altered by ROP18 of *T. gondii* RH strain.

SUPPLEMENTARY TABLE 3 | Pathway enrichment analysis of the differentially expressed genes altered by ROP18 of *T. gondii* RH strain.

SUPPLEMENTARY TABLE 4 | Analysis of KEGG disease related pathway involving the differentially expressed genes altered by ROP18 of *T. gondii* RH strain.

SUPPLEMENTARY TABLE 5 | GO enrichment analysis of the differentially expressed genes altered by ROP18 of *T. gondii* RH strain.

SUPPLEMENTARY FIGURE 1 | Western blotting analysis using anti-HA tag antibody detects the ROP18 protein in HEK293 cells transfected with PCMV-N-HA-ROP18. PL, PageRuler™ Prestained Protein Ladder; C, Extract of control HEK293 transfected with the plasmid PCMV-N-HA; 18, Extract of HEK293 transfected with the plasmid PCMV-N-HA-ROP18.

REFERENCES

Albarry, M. A., Hashmi, J. A., Alreheli, A. Q., Albalawi, A. M., Khan, B., Ramzan, K., et al. (2019). Novel homozygous loss-of-function mutations in RP1 and RP1L1 genes in retinitis pigmentosa patients. *Ophthalmic Genet.* 40, 507–513. doi: 10.1080/13816810.2019.1703014

Al-Sandaqchi, A. T., Brignell, C., Collingwood, J. F., Geraki, K., Mirkes, E. M., Kong, K., et al. (2018). Metallome of cerebrovascular endothelial cells infected with *Toxoplasma gondii* using mu-XRF imaging and inductively coupled plasma mass spectrometry. *Metallomics* 10, 1401–1414. doi: 10.1039/c8mt00136g

Al-Sandaqchi, A. T., Marsh, V., Williams, H. E. L., Stevenson, C. W., and Elsheikha, H. M. (2020). Structural, functional, and metabolic alterations in human cerebrovascular endothelial cells during *Toxoplasma gondii* infection and amelioration by verapamil in vitro. *Microorganisms* 8, 1386. doi: 10.3390/microorganisms8091386

An, R., Tang, Y., Chen, L., Cai, H., Lai, D. H., Liu, K., et al. (2018). Encephalitis is mediated by ROP18 of *Toxoplasma gondii*, a severe pathogen in AIDS patients. *Proc. Natl. Acad. Sci. U.S.A.* 115, E5344–E5352. doi: 10.1073/pnas.1801118115

Baralle, F. E., and Giudice, J. (2017). Alternative splicing as a regulator of development and tissue identity. *Nat. Rev. Mol. Cell Biol.* 18, 437–451. doi: 10.1038/nrm.2017.27

Beazley, D. M., and Egerman, R. S. (1998). Toxoplasmosis. *Semin. Perinatol.* 22, 332–338. doi: 10.1016/s0146-0005(98)80022-0

Behnke, M. S., Khan, A., Lauron, E. J., Jimah, J. R., Wang, Q., Tolia, N. H., et al. (2015). Rhoptry proteins ROP5 and ROP18 are major murine virulence factors in genetically divergent South American strains of *Toxoplasma gondii*. *PloS Genet.* 11, e1005434. doi: 10.1371/journal.pgen.1005434

Belgrader, P., Cheng, J., Zhou, X., Stephenson, L. S., and Maquat, L. E. (1994). Mammalian nonsense codons can be cis effectors of nuclear mRNA half-life. *Mol. Cell Biol.* 14, 8219–8228. doi: 10.1128/mcb.14.12.8219

Blencowe, B. J. (2006). Alternative splicing: new insights from global analyses. *Cell* 126, 37–47. doi: 10.1016/j.cell.2006.06.023

Bodary, S. C., and McLean, J. W. (1990). The integrin beta 1 subunit associates with the vitronectin receptor alpha v subunit to form a novel vitronectin receptor in a human embryonic kidney cell line. *J. Biol. Chem.* 265, 5938–5941. doi: 10.1016/0006-291X(90)91719-9

Bradley, P. J., and Sibley, L. D. (2007). Rhoptries: an arsenal of secreted virulence factors. *Curr. Opin. Microbiol.* 10, 582–587. doi: 10.1016/j.mib.2007.09.013

Buckley, P. T., Lee, M. T., Sul, J. Y., Miyashiro, K. Y., Bell, T. J., Fisher, S. A., et al. (2011). Cytoplasmic intron sequence-retaining transcripts can be dendritically targeted via ID element retrotransposons. *Neuron* 69, 877–884. doi: 10.1016/j.neuron.2011.02.028

Chang, S., Shan, X., Li, X., Fan, W., Zhang, S. Q., Zhang, J., et al. (2015). *Toxoplasma gondii* rhoptry protein ROP16 mediates partially SH-SY5Y cells apoptosis and cell cycle arrest by directing Ser15/37 phosphorylation of p53. *Int. J. Biol. Sci.* 11, 1215–1225. doi: 10.7150/ijbs.10516

Cheng, L., Chen, Y., Chen, L., Shen, Y., Shen, J., An, R., et al. (2012). Interactions between the ROP18 kinase and host cell proteins that aid in the parasitism of *Toxoplasma gondii*. *Acta Trop.* 122, 255–260. doi: 10.1016/j.actatropica.2012.02.001

Chousterman, B. G., Swirski, F. K., and Weber, G. F. (2017). Cytokine storm and sepsis disease pathogenesis. *Semin. Immunopathol.* 39, 517–528. doi: 10.1007/s00281-017-0639-8

Dittmer, J., Gegonne, A., Gitlin, S. D., Ghysdael, J., and Brady, J. N. (1994). Regulation of parathyroid hormone-related protein (PTHrP) gene expression.

Sp1 binds through an inverted CACCC motif and regulates promoter activity in cooperation with Ets1. *J. Biol. Chem.* 269, 21428–21434.

Du, J., An, R., Chen, L., Shen, Y., Chen, Y., Cheng, L., et al. (2014). Toxoplasma gondii virulence factor ROP18 inhibits the host NF-kappaB pathway by promoting p65 degradation. *J. Biol. Chem.* 289, 12578–12592. doi: 10.1074/jbc.M113.544718

Dubey, J. P. (2004). Toxoplasmosis – a waterborne zoonosis. *Vet. Parasitol.* 126, 57–72. doi: 10.1016/j.vetpar.2004.09.005

El Hajj, H., Demey, E., Poncet, J., Lebrun, M., Wu, B., Galeotti, N., et al. (2006). The ROP2 family of *Toxoplasma gondii* rhoptry proteins: proteomic and genomic characterization and molecular modeling. *Proteomics* 6, 5773–5784. doi: 10.1002/pmic.200600187

Elsheikha, H. M. (2008). Congenital toxoplasmosis: priorities for further health promotion action. *Public Health* 122, 335–353. doi: 10.1016/j.puhe.2007.08.009

Etheridge, R. D., Alaganan, A., Tang, K., Lou, H. J., Turk, B. E., and Sibley, L. D. (2014). The *Toxoplasma* pseudokinase ROP5 forms complexes with ROP18 and ROP17 kinases that synergize to control acute virulence in mice. *Cell Host Microbe* 15, 537–550. doi: 10.1016/j.chom.2014.04.002

Feng, H., Qin, Z., and Zhang, X. (2013). Opportunities and methods for studying alternative splicing in cancer with RNA-Seq. *Cancer Lett.* 340, 179–191. doi: 10.1016/j.canlet.2012.11.010

Filichkin, S. A., Priest, H. D., Givan, S. A., Shen, R., Bryant, D. W., Fox, S. E., et al. (2010). Genome-wide mapping of alternative splicing in *Arabidopsis thaliana*. *Genome Res.* 20, 45–58. doi: 10.1101/gr.093302.109

Fleckenstein, M. C., Reese, M. L., Konen-Waisman, S., Boothroyd, J. C., Howard, J. C., and Steinfeldt, T. (2012). A *Toxoplasma gondii* pseudokinase inhibits host IRG resistance proteins. *PloS Biol.* 10, e1001358. doi: 10.1371/journal.pbio.1001358

Fox, B. A., Rommereim, L. M., Guevara, R. B., Falla, A., Hortua Triana, M. A., Sun, Y., et al. (2016). The *Toxoplasma gondii* rhoptry kinome is essential for chronic infection. *mBio* 7, e00193–e00116. doi: 10.1128/mBio.00193-16

Fujinami, K., Oishi, A., Yang, L., Arno, G., Pontikos, N., Yoshitake, K., et al. (2020). Clinical and genetic characteristics of 10 Japanese patients with PROM1-associated retinal disorder: A report of the phenotype spectrum and a literature review in the Japanese population. *Am. J. Med. Genet. C Semin. Med. Genet.* 184, 656–674. doi: 10.1002/ajmg.c.31826

Fujinami-Yokokawa, Y., Pontikos, N., Yang, L., Tsunoda, K., Yoshitake, K., Iwata, T., et al. (2019). Prediction of causative genes in inherited retinal disorders from spectral-domain optical coherence tomography utilizing deep learning techniques. *J. Ophthalmol.* 2019, 1691064. doi: 10.1155/2019/1691064

Fujinami-Yokokawa, Y., Fujinami, K., Kuniyoshi, K., Hayashi, T., Ueno, S., Mizota, A., et al. (2020). Clinical and genetic characteristics of 18 patients from 13 Japanese families with CRX-associated retinal disorder: identification of genotype-phenotype association. *Sci. Rep.* 10, 9531. doi: 10.1038/s41598-020-65737-z

Gazzinelli, R. T., Amichay, D., Sharton-Kersten, T., Grunwald, E., Farber, J. M., and Sher, A. (1996). Role of macrophage-derived cytokines in the induction and regulation of cell-mediated immunity to *Toxoplasma gondii*. *Curr. Top. Microbiol. Immunol.* 219, 127–139. doi: 10.1007/978-3-642-51014-4_12

Ghosh, S., Basu, M., and Roy, S. S. (2012). ETS-1 protein regulates vascular endothelial growth factor-induced matrix metalloproteinase-9 and matrix metalloproteinase-13 expression in human ovarian carcinoma cell line SKOV-3. *J. Biol. Chem.* 287, 15001–15015. doi: 10.1074/jbc.M111.284034

Griffith, J. W., Sokol, C. L., and Luster, A. D. (2014). Chemokines and chemokine receptors: positioning cells for host defense and immunity. *Annu. Rev. Immunol.* 32, 659–702. doi: 10.1146/annurev-immunol-032713-120145

Harun, M. S. R., Marsh, V., Elsaied, N. A., Webb, K. F., and Elsheikha, H. M. (2020a). Effects of *Toxoplasma gondii* infection on the function and integrity of human cerebrovascular endothelial cells and the influence of verapamil treatment in vitro. *Brain Res.* 1746, 147002. doi: 10.1016/j.brainres.2020.147002

Harun, M. S. R., Taylor, M., Zhu, X. Q., and Elsheikha, H. M. (2020b). Transcriptome profiling of *Toxoplasma gondii*-infected human cerebromicrovascular endothelial cell response to treatment with monensin. *Microorganisms* 8, 842. doi: 10.3390/microorganisms8060842

He, J. J., Ma, J., Elsheikha, H. M., Song, H. Q., Huang, S. Y., and Zhu, X. Q. (2016). Transcriptomic analysis of mouse liver reveals a potential hepato-enteric pathogenic mechanism in acute *Toxoplasma gondii* infection. *Parasit. Vectors* 9, 427. doi: 10.1186/s13071-016-1716-x

Hernandez-de-Los-Rios, A., Murillo-Leon, M., Mantilla-Muriel, L. E., Arenas, A. F., Vargas-Montes, M., Cardona, N., et al. (2019). Influence of two major *Toxoplasma gondii* virulence factors (ROP16 and ROP18) on the immune response of peripheral blood mononuclear cells to human Toxoplasmosis infection. *Front. Cell Infect. Microbiol.* 9:413. doi: 10.3389/fcimb.2019.00413

Herrera, J., Henke, C. A., and Bitterman, P. B. (2018). Extracellular matrix as a driver of progressive fibrosis. *J. Clin. Invest.* 128, 45–53. doi: 10.1172/JCI93557

Hu, R. S., He, J. J., Elsheikha, H. M., Zhang, F. K., Zou, Y., Zhao, G. H., et al. (2018). Differential brain microRNA expression profiles after acute and chronic infection of mice with *Toxoplasma gondii* oocysts. *Front. Microbiol.* 9:2316. doi: 10.3389/fmicb.2018.02316

Hunter, C. A., and Sibley, L. D. (2012). Modulation of innate immunity by *Toxoplasma gondii* virulence effectors. *Nat. Rev. Microbiol.* 10, 766–778. doi: 10.1038/nrmicro2858

Jin, Z. B., Huang, X. F., Lv, J. N., Xiang, L., Li, D. Q., Chen, J., et al. (2014). SLC7A14 linked to autosomal recessive retinitis pigmentosa. *Nat. Commun.* 5, 3517. doi: 10.1038/ncomms4517

Jinnin, M., Ihn, H., Asano, Y., Yamane, K., Trojanowska, M., and Tamaki, K. (2004). Tenascin-C upregulation by transforming growth factor-beta in human dermal fibroblasts involves Smad3, Sp1, and Ets1. *Oncogene* 23, 1656–1667. doi: 10.1038/sj.onc.1207064

Kars, M. D., Iseri, O. D., and Gunduz, U. (2010). Drug resistant breast cancer cells overexpress ETS1 gene. *BioMed. Pharmacother.* 64, 458–462. doi: 10.1016/j.biopha.2010.01.008

Kaye, A. (2011). Toxoplasmosis: Diagnosis, Treatment, and Prevention in Congenitally Exposed Infants. *J. Pediatr. Health Care* 25, 355–364. doi: 10.1016/j.pedhc.2010.04.008

Kopp, J. L., Wilder, P. J., Desler, M., Kim, J. H., Hou, J., Nowling, T., et al. (2004). Unique and selective effects of five Ets family members, Elf3, Ets1, Ets2, PEA3, and PU.1, on the promoter of the type II transforming growth factor-beta receptor gene. *J. Biol. Chem.* 279, 19407–19420. doi: 10.1074/jbc.M314115200

Lamande, S. R., and Bateman, J. F. (2020). Genetic disorders of the extracellular matrix. *Anat. Rec. (Hoboken)* 303, 1527–1542. doi: 10.1002/ar.24086

Li, J. X., He, J. J., Elsheikha, H. M., Chen, D., Zhai, B. T., Zhu, X. Q., et al. (2019). *Toxoplasma gondii* ROP17 inhibits the innate immune response of HEK293T cells to promote its survival. *Parasitol. Res.* 118, 783–792. doi: 10.1007/s00436-019-06215-y

Lin, M. K., Yang, J., Hsu, C. W., Gore, A., Bassuk, A. G., Brown, L. M., et al. (2018). HTRA1, an age-related macular degeneration protease, processes extracellular matrix proteins EFEMP1 and TSP1. *Aging Cell* 17, e12710. doi: 10.1111/acel.12710

Littink, K. W., van Genderen, M. M., Collin, R. W., Roosing, S., de Brouwer, A. P., Riemslag, F. C., et al. (2009). A novel homozygous nonsense mutation in CABP4 causes congenital cone-rod synaptic disorder. *Invest. Ophthalmol. Vis. Sci.* 50, 2344–2350. doi: 10.1167/iovs.08-2553

Livak, K. J., and Schmittgen, T. D. (2001). Analysis of relative gene expression data using real-time quantitative PCR and the 2(-Delta Delta C(T)) Method. *Methods* 25, 402–408. doi: 10.1006/meth.2001.1262

Long, K. R., and Huttner, W. B. (2019). How the extracellular matrix shapes neural development. *Open Biol.* 9:180216. doi: 10.1098/rsob.180216

Ma, J., He, J. J., Hou, J. L., Zhou, C. X., Zhang, F. K., Elsheikha, H. M., et al. (2019). Metabolomic signature of mouse cerebral cortex following *Toxoplasma gondii* infection. *Parasit. Vectors* 12, 373. doi: 10.1186/s13071-019-3623-4

Mix, K. S., Attur, M. G., Al-Mussawir, H., Abramson, S. B., Brinckerhoff, C. E., and Murphy, E. P. (2007). Transcriptional repression of matrix metalloproteinase gene expression by the orphan nuclear receptor NURR1 in cartilage. *J. Biol. Chem.* 282, 9492–9504. doi: 10.1074/jbc.M608327200

Molnar, K. S., Dunyak, B. M., Su, B., Izrayelit, Y., McGlasson-Naumann, B., Hamilton, P. D., et al. (2019). Mechanism of action of VP1-001 in cryAB (R120G)-associated and age-related cataracts. *Invest. Ophthalmol. Vis. Sci.* 60, 3320–3331. doi: 10.1167/iovs.18-25647

Mortazavi, A., Williams, B. A., McCue, K., Schaeffer, L., and Wold, B. (2008). Mapping and quantifying mammalian transcriptomes by RNA-Seq. *Nat. Methods* 5, 621–628. doi: 10.1038/nmeth.1226

Odorizzi, L., Moreira, N. M., Goncalves, G. F., da Silva, A. V., Sant'ana Dde, M., and Araujo, E. J. (2010). Quantitative and morphometric changes of subpopulations of myenteric neurons in swines with toxoplasmosis. *Auton. Neurosci.* 155, 68–72. doi: 10.1016/j.autneu.2010.01.012

Okada, Y., Nagai, R., Sato, T., Matsuura, E., Minami, T., Morita, I., et al. (2003). Homeodomain proteins MEIS1 and PBXs regulate the lineage-specific transcription of the platelet factor 4 gene. *Blood* 101, 4748–4756. doi: 10.1182/blood-2002-02-0380

Petrovic, N., Bhagwat, S. V., Ratzan, W. J., Ostrowski, M. C., and Shapiro, L. H. (2003). CD13/APN transcription is induced by RAS/MAPK-mediated phosphorylation of Ets-2 in activated endothelial cells. *J. Biol. Chem.* 278, 49358–49368. doi: 10.1074/jbc.M308071200

Rastogi, S., Xue, Y., Quake, S. R., and Boothroyd, J. C. (2020). Differential impacts on host transcription by ROP and GRA effectors from the intracellular parasite *Toxoplasma gondii*. *mBio* 11, e00182-20. doi: 10.1128/mBio.00182-20

Rathi, S., Jalali, S., Patnaik, S., Shahulhameed, S., Musada, G. R., Balakrishnan, D., et al. (2017). Abnormal complement activation and inflammation in the pathogenesis of retinopathy of prematurity. *Front. Immunol.* 8, 1868. doi: 10.3389/fimmu.2017.01868

Rozenfeld, C., Martinez, R., Seabra, S., Sant'anna, C., Goncalves, J. G., Bozza, M., et al. (2005). *Toxoplasma gondii* prevents neuron degeneration by interferon-gamma-activated microglia in a mechanism involving inhibition of inducible nitric oxide synthase and transforming growth factor-beta1 production by infected microglia. *Am. J. Pathol.* 167, 1021–1031. doi: 10.1016/s0002-9440(10)61191-1

Saeij, J., Boyle, J., Coller, S., Taylor, S., Sibley, L., Brooke-Powell, E., et al. (2006). Polymorphic secreted kinases are key virulence factors in toxoplasmosis. *Science* 314, 1780–1783. doi: 10.1126/science.1133690

Sanchez, V., de-la-Torre, A., and Gomez-Marin, J. E. (2014). Characterization of ROP18 alleles in human toxoplasmosis. *Parasitol. Int.* 63, 463–469. doi: 10.1016/j.parint.2013.10.012

Sangare, L. O., Yang, N., Konstantinou, E. K., Lu, D., Mukhopadhyay, D., Young, L. H., et al. (2019). *Toxoplasma* GRA15 activates the NF-kappaB pathway through interactions with TNF receptor-associated factors. *mBio* 10. doi: 10.1128/mBio.00808-19

Schneider, A. G., Abi Abdallah, D. S., Butcher, B. A., and Denkers, E. Y. (2013). *Toxoplasma gondii* triggers phosphorylation and nuclear translocation of dendritic cell STAT1 while simultaneously blocking IFNgamma-induced STAT1 transcriptional activity. *PloS One* 8, e60215. doi: 10.1371/journal.pone.0060215

Schonherr, E., and Hausser, H. J. (2000). Extracellular matrix and cytokines: a functional unit. *Dev. Immunol.* 7, 89–101. doi: 10.1155/2000/31748

Shahulhameed, S., Vishwakarma, S., Chhablani, J., Tyagi, M., Pappuru, R. R., Jakati, S., et al. (2020). A systematic investigation on complement pathway activation in diabetic retinopathy. *Front. Immunol.* 11, 154. doi: 10.3389/fimmu.2020.00154

Shen, S., Park, J. W., Lu, Z. X., Lin, L., Henry, M. D., Wu, Y. N., et al. (2014). rMATS: robust and flexible detection of differential alternative splicing from replicate RNA-Seq data. *Proc. Natl. Acad. Sci. U.S.A.* 111, E5593–E5601. doi: 10.1073/pnas.1419161111

Shinwari, J. M., Khan, A., Awad, S., Shinwari, Z., Alaiya, A., Alanazi, M., et al. (2015). Recessive mutations in COL25A1 are a cause of congenital cranial dysinnervation disorder. *Am. J. Hum. Genet.* 96, 147–152. doi: 10.1016/j.ajhg.2014.11.006

Shwab, E. K., Jiang, T., Pena, H. F., Gennari, S. M., Dubey, J. P., and Su, C. (2016). The ROP18 and ROP5 gene allele types are highly predictive of virulence in mice across globally distributed strains of *Toxoplasma gondii*. *Int. J. Parasitol.* 46, 141–146. doi: 10.1016/j.ijpara.2015.10.005

Sibley, L. D. (2003). *Toxoplasma gondii*: perfecting an intracellular life style. *Traffic* 4, 581–586. doi: 10.1034/j.1600-0854.2003.00117.x

Sisodiya, S. M., Thompson, P. J., Need, A., Harris, S. E., Weale, M. E., Wilkie, S. E., et al. (2007). Genetic enhancement of cognition in a kindred with cone-rod dystrophy due to RIMS1 mutation. *J. Med. Genet.* 44, 373–380. doi: 10.1136/jmg.2006.047407

Sorokin, L. (2010). The impact of the extracellular matrix on inflammation. *Nat. Rev. Immunol.* 10, 712–723. doi: 10.1038/nri2852

Steinfeldt, T., Konen-Waisman, S., Tong, L., Pawlowski, N., Lamkemeyer, T., Sibley, L. D., et al. (2010). Phosphorylation of mouse immunity-related GTPase (IRG) resistance proteins is an evasion strategy for virulent Toxoplasma gondii. *PloS Biol.* 8, e1000576. doi: 10.1371/journal.pbio.1000576

Tang, P. H., Velez, G., Tsang, S. H., Bassuk, A. G., and Mahajan, V. B. (2019). VCAN canonical splice site mutation is associated with vitreoretinal degeneration and disrupts an MMP proteolytic site. *Invest. Ophthalmol. Vis. Sci.* 60, 282–293. doi: 10.1167/iovs.18-25624

Taylor, S., Barragan, A., Su, C., Fux, B., Fentress, S. J., Tang, K., et al. (2006). A secreted serine-threonine kinase determines virulence in the eukaryotic pathogen *Toxoplasma gondii*. *Science* 314, 1776–1780. doi: 10.1126/science.1133643

Tenter, A. M., Heckeroth, A. R., and Weiss, L. M. (2000). *Toxoplasma gondii*: from animals to humans. *Int. J. Parasitol.* 30, 1217–1258. doi: 10.1016/S0020-7519(00)00124-7

Thompson, S., Blodi, F. R., Larson, D. R., Anderson, M. G., and Stasheff, S. F. (2019). The Efemp1R345W macular dystrophy mutation causes amplified circadian and photophobic responses to light in mice. *Invest. Ophthalmol. Vis. Sci.* 60, 2110–2117. doi: 10.1167/iovs.19-26881

Toms, M., Burgoyne, T., Tracey-White, D., Richardson, R., Dubis, A. M., Webster, A. R., et al. (2019). Phagosomal and mitochondrial alterations in RPE may contribute to KCNJ13 retinopathy. *Sci. Rep.* 9, 3793. doi: 10.1038/s41598-019-40507-8

Wan, L., Gong, L., Wang, W., An, R., Zheng, M., Jiang, Z., et al. (2015). *T. gondii* rhoptry protein ROP18 induces apoptosis of neural cells via endoplasmic reticulum stress pathway. *Parasit. Vectors* 8, 554. doi: 10.1186/s13071-015-1103-z

Wang, X., Manner, P. A., Horner, A., Shum, L., Tuan, R. S., and Nuckolls, G. H. (2004). Regulation of MMP-13 expression by RUNX2 and FGF2 in osteoarthritic cartilage. *Osteoarthritis Cartilage* 12, 963–973. doi: 10.1016/j.joca.2004.08.008

Weiner, C., Hecht, I., Rotenstreich, Y., Guttman, S., Or, L., Morad, Y., et al. (2020). The pathogenicity of SLC38A8 in five families with foveal hypoplasia and congenital nystagmus. *Exp. Eye Res.* 193:107958. doi: 10.1016/j.exer.2020.107958

Weiss, L. M., and Dubey, J. P. (2009). Toxoplasmosis: A history of clinical observations. *Int. J. Parasitol.* 39, 895–901. doi: 10.1016/j.ijpara.2009.02.004

Xia, J., Kong, L., Zhou, L. J., Wu, S. Z., Yao, L. J., He, C., et al. (2018). Genome-wide bimolecular fluorescence complementation-based proteomic analysis of *Toxoplasma gondii* ROP18's human interactome shows its key role in regulation of cell immunity and apoptosis. *Front. Immunol.* 9:61. doi: 10.3389/fimmu.2018.00061

Yang, Z., Hou, Y., Hao, T., Rho, H. S., Wan, J., Luan, Y., et al. (2017). A human proteome array approach to identifying key host proteins targeted by *Toxoplasma* kinase ROP18. *Mol. Cell Proteomics* 16, 469–484. doi: 10.1074/mcp.M116.063602

Yarovinsky, F. (2014). Innate immunity to *Toxoplasma gondii* infection. *Nat. Rev. Immunol.* 14, 109–121. doi: 10.1038/nri3598

Zhang, H. Y., Jin, L., Stilling, G. A., Ruebel, K. H., Coonse, K., Tanizaki, Y., et al. (2009). RUNX1 and RUNX2 upregulate Galectin-3 expression in human pituitary tumors. *Endocrine* 35, 101–111. doi: 10.1007/s12020-008-9129-z

Zhang, X., Su, R., Cheng, Z., Zhu, W., Li, Y., Wang, Y., et al. (2017). A mechanistic study of *Toxoplasma gondii* ROP18 inhibiting differentiation of C17.2 neural stem cells. *Parasit. Vectors* 10, 585. doi: 10.1186/s13071-017-2529-2

Conflict of Interest: The authors declare that the research was conducted in the absence of any commercial or financial relationships that could be construed as a potential conflict of interest.

Advantages of publishing in Frontiers

OPEN ACCESS
Articles are free to read for greatest visibility and readership

FAST PUBLICATION
Around 90 days from submission to decision

HIGH QUALITY PEER-REVIEW
Rigorous, collaborative, and constructive peer-review

TRANSPARENT PEER-REVIEW
Editors and reviewers acknowledged by name on published articles

Frontiers
Avenue du Tribunal-Fédéral 34
1005 Lausanne | Switzerland

Visit us: www.frontiersin.org
Contact us: frontiersin.org/about/contact

REPRODUCIBILITY OF RESEARCH
Support open data and methods to enhance research reproducibility

DIGITAL PUBLISHING
Articles designed for optimal readership across devices

FOLLOW US
@frontiersin

IMPACT METRICS
Advanced article metrics track visibility across digital media

EXTENSIVE PROMOTION
Marketing and promotion of impactful research

LOOP RESEARCH NETWORK
Our network increases your article's readership